Springer Theses
Recognizing Outstanding Ph.D. Research

Paul R. Eizenhöfer

Subduction and Closure of the Palaeo-Asian Ocean along the Solonker Suture Zone: Constraints from an Integrated Sedimentary Provenance Analysis

Springer

Springer Theses

Recognizing Outstanding Ph.D. Research

Aims and Scope

The series "Springer Theses" brings together a selection of the very best Ph.D. theses from around the world and across the physical sciences. Nominated and endorsed by two recognized specialists, each published volume has been selected for its scientific excellence and the high impact of its contents for the pertinent field of research. For greater accessibility to non-specialists, the published versions include an extended introduction, as well as a foreword by the student's supervisor explaining the special relevance of the work for the field. As a whole, the series will provide a valuable resource both for newcomers to the research fields described, and for other scientists seeking detailed background information on special questions. Finally, it provides an accredited documentation of the valuable contributions made by today's younger generation of scientists.

Theses are accepted into the series by invited nomination only and must fulfill all of the following criteria

- They must be written in good English.
- The topic should fall within the confines of Chemistry, Physics, Earth Sciences, Engineering and related interdisciplinary fields such as Materials, Nanoscience, Chemical Engineering, Complex Systems and Biophysics.
- The work reported in the thesis must represent a significant scientific advance.
- If the thesis includes previously published material, permission to reproduce this must be gained from the respective copyright holder.
- They must have been examined and passed during the 12 months prior to nomination.
- Each thesis should include a foreword by the supervisor outlining the significance of its content.
- The theses should have a clearly defined structure including an introduction accessible to scientists not expert in that particular field.

More information about this series at http://www.springer.com/series/8790

Paul R. Eizenhöfer

Subduction and Closure of the Palaeo-Asian Ocean along the Solonker Suture Zone: Constraints from an Integrated Sedimentary Provenance Analysis

Doctoral Thesis accepted by
the University of Hong Kong, Pokfulam,
Hong Kong

Springer

Author
Dr. Paul R. Eizenhöfer
Department of Geosciences
University of Tübingen
Tübingen, Baden-Württemberg, Germany

Supervisor
Prof. Guochun Zhao
Department of Earth Sciences
The University of Hong Kong
Pokfulam, Hong Kong

ISSN 2190-5053 ISSN 2190-5061 (electronic)
Springer Theses
ISBN 978-981-32-9199-7 ISBN 978-981-32-9200-0 (eBook)
https://doi.org/10.1007/978-981-32-9200-0

This Springer imprint is published by the registered company Springer Nature Singapore Pte Ltd.
The registered company address is: 152 Beach Road, #21-01/04 Gateway East, Singapore 189721, Singapore

Daß ich erkenne, was die Welt
Im Innersten zusammenhält,
Schau alle Wirkenskraft und Samen,
Und tu nicht mehr in Worten kramen.

To grant me a vision of Nature's forces
That bind the world, all its seeds and sources
And innermost life—all this I shall see,
And stop peddling in words that mean nothing to me.

Johann Wolfgang von Goethe, Faust, lines 382–5.

For my Parents

Supervisor's Foreword

The Central Asian Orogenic Belt represents one of the largest tectonic accretionary collages on Earth, tracing its origins from the Neoproterozoic breakup of the supercontinent Rodinia. It stretches over most of northern Central Asia from the Urals to the Japanese Islands, occupying the area between the Siberian Craton, Tarim Craton, and North China Craton. However, the role of East Asian blocks, among which the aforementioned cratons, during the late Palaeozoic to early Mesozoic assembly of Pangaea remained enigmatic until recently. Early palaeo-biogeographic studies revealed a broad mixing zone of Angaran (i.e., Siberian) and Cathaysian (i.e., Asian) faunas along the southern Mongolian Terranes implying the presence of a major tectonic suture in East Asia. Subsequent studies identified remnants of a vast Palaeozoic ocean having left footprints in subduction-related igneous rocks, accretionary wedges, and ophiolithic material. This ocean is known today as the Palaeo-Asian Ocean and occupied the area north of the Tarim and North China cratons during most of the Palaeozoic. The location of its final disappearance in East Asia took place along the cryptic Solonker Suture Zone broadly traced through the present-day low-relief Mongolian steppes, and infamous for the absence of typical collision-related features such as high-grade metamorphic rocks, regional-scale ophiolite belts, tectonic mélanges, or fold-thrust structures, in stark contrast to more traditional sutures such as the Indus-Yarlung Suture separating the Eurasian and Indian plates. Thus, attempts to constrain the exact location and timing of suturing along the Solonker Suture Zone have not reached a satisfying consensus yet. The dissertation by Dr. Paul R. Eizenhöfer aimed to shed new light on this issue through an in-depth study of Palaeozoic sedimentary and volcanic rocks across the suture. During his studies, he carried out extensive field geological investigations followed by a detailed integration of geochemical and geochronological analyses in order to pinpoint the locus and timing of the final closure of the Palaeo-Asian Ocean.

This Ph.D. research is manifested in important contributions to better understanding the Palaeozoic to early Mesozoic tectonic evolution of the Palaeo-Asian Ocean along the Solonker Suture Zone and the role of East Asian blocks during the assembly of Pangaea, for example, (i) the exact determination of the sedimentary provenance of Late Permian sedimentary strata across the suture, e.g., the North China Craton to the south and the Mongolian Terranes to the north, (ii) the geochemical and geochronologic characterisation of major tectonic belts across the suture, e.g., the Northern and Southern Accretionary Orogens, and the Hegenshan Ophiolite Belt, (iii) the identification of two distinct periods (ca. 269 Ma and 436 Ma) of active subduction beneath the northern margin of the North China Craton as opposed to continuous subduction (ca. 429-328 Ma) activity beneath the Mongolian Terranes concurrent with the opening of the Hegenshan Back-Arc Basin at ca. 314 Ma, and (iv) constraining the final closure of the Palaeo-Asian Ocean to the Late Permian to Early Triassic. Reconstructions of the tectonic events taking into account palaeo-geographic geometries during the Palaeozoic closure of the Palaeo-Asian Ocean required the formulation of a "soft-collision" model that involves concurrent subduction beneath two opposing active continental margins and the collision of two accretionary wedges. Such collision would not involve continental deep subduction and, thus, predicts the absence of typical collision-related lithological, structural and tectonic features as is the case across the present-day Solonker Suture Zone.

The conclusions of this Ph.D. thesis invoked a new interest in double-sided subduction at a much larger scale involving the closure of major oceans, whereas in the past such geometries were attributed to smaller-scaled present-day scenarios located, for example, along the Molucca Sea and the Adriatic Sea. Following, double-sided subduction geometries have been proposed, for example, for the formation of the Neoproterozoic Jiangnan Orogen in South China and are now being intensely studied in geodynamic numerical models. This Ph.D. thesis and the publications that resulted from it provide a new cornerstone for future studies on the evolution of the Central Asian Orogenic Belt and the demystification of cryptic suture zones in similar tectonic environments. The absence of large-scale present-day examples of double-sided divergent subduction geometries places additional weight on the importance of the closure of the Palaeo-Asian Ocean along the Solonker Suture as a potential blueprint for similar, yet undiscovered tectonic geometries in Earth's past. In light of its achievements, I am certain publication of this dissertation will provide an important piece of literature on the Palaeozoic geology and tectonic evolution of East Asia and will represent a significant contribution to the international geoscientific community deciphering the formation of the vast Central Asian Orogenic Belt.

Hong Kong, China
June 2019

Prof. Guochun Zhao

Abstract

The Central Asian Orogenic Belt formed by accretion subsequent to the contraction of the Palaeo-Asian Ocean that ultimately disappeared along the Solonker Suture Zone in East Asia. Since typical regional collisional features are absent, the tectonic evolution of the suture remains speculative. Integrated sedimentary provenance analyses across the accretionary collision zone between the Mongolian Arcs and the North China Craton place new constraints on the events that led to final suturing. An investigation on the geochronological and geochemical variability in Permian strata along a southeast-northwest transect revealed distinct differences across the Solonker Suture Zone: northern basins carry a broad Mesoproterozoic to latest Precambrian age signature, and their provenance terranes are of mixed juvenile to crustal magmatic origin. In contrast, southern basins contain detritus from the North China Craton, and their sources are of dominantly crustal contaminated magmatic origin. Provenance analysis suggests that in the Early Palaeozoic (ca. 429 Ma) the Palaeo-Asian Ocean was consumed along the Uliastai Arc and the North China Craton, initiating the formation of the Northern and Southern Accretionary Orogens, respectively. By the end of the Middle Carboniferous, the Mongolian Arcs consolidated after accretion of the Uliastai Arc. In the Late Carboniferous (ca. 314 Ma), the Hegenshan back-arc basin opened, detaching the Northern Accretionary Orogen. While subduction continued there, it may have temporarily ceased along the Southern Accretionary Orogen after accretion of a microcontinent (ca. 300 Ma). During the Middle Permian, back-arc basin closure led to the formation and obduction of the Hegenshan supra-subduction zone ophiolite. Eventually, the Palaeo-Asian Ocean closed after wedge-wedge collision, which would not involve continental deep subduction, thus leading to cryptic suturing from the Late Permian to Early Triassic. Statistical analyses on the heterogeneity and similarity of the age probability density functions require a complex Permian palaeo-geographic setting, involving a variety of arc basins, which received sediments dependent on the contemporary arc geometry. Early stages of the sequence likely resembled a Pacific-type scenario, including Japan-type back-arc basin opening, whereas the late stages were similar to the archipelago-type setting of present-day Southeast Asia.

Parts of this thesis have been published in the following international peer-reviewed journals:

Eizenhöfer, P. R., & Zhao, G. (2018). Solonker Suture in East Asia and its bearing on the final closure of the eastern segment of the Palaeo-Asian Ocean. *Earth-Science Reviews*, *186*, 153–172.

Eizenhöfer, P. R., Zhao, G., Zhang, J., Han, Y., Hou, W., Liu, D., & Wang, B. (2015). Geochemical characteristics of the Permian basins and their provenances across the Solonker Suture Zone: assessment of net crustal growth during the closure of the Palaeo-Asian Ocean. *Lithos*, *224*, 240–255.

Eizenhöfer, P. R., Zhao, G., Sun, M., Zhang, J., Han, Y., & Hou, W. (2015). Geochronological and Hf isotopic variability of detrital zircons in Paleozoic strata across the accretionary collision zone between the North China craton and Mongolian arcs and tectonic implications. *GSA Bulletin*, *127*(9-10), 1422–1436.

Eizenhöfer, P. R., Zhao, G., Zhang, J., & Sun, M. (2014). Final closure of the Paleo-Asian Ocean along the Solonker suture zone: Constraints from geochronological and geochemical data of Permian volcanic and sedimentary rocks. *Tectonics*, *33*(4), 441–463.

Declaration

I declare that this dissertation represents my own work, except where due acknowledgement is made, and that it has not been previously included in a thesis, dissertation, or report submitted to this University or to any other institution for a degree, diploma, or other qualifications.

Paul R. Eizenhöfer

Acknowledgements

First, and foremost, I owe my highest gratitude to my supervisor Prof. Guochun Zhao, who supported me in every aspect, academically as well as personally, to the best of his knowledge and abilities. Furthermore, he gave me the unique chance to gain such a rich, intense, and valuable understanding of Chinese culture and science, I believe, rarely any other foreign student has enjoyed.

Without my research group fellows, I would have been lost during my trips to China. My sincerest thanks especially to: Zhang Jian, whom together with I went to my first fieldwork. Liu Chaohui for helping me obtaining my very first U-Pb zircon data. Han Yigui for simply being the good and always helping soul of the group. Hou Wenzhu for her very open-minded and honest character. Liu Dongxing and Wang Bo for their around-the-clock availability. Last, but not least, Driver Zhao, who took me tirelessly on these epic journeys from eastern- to westernmost China.

Thanks also go to The University of Hong Kong for providing such excellent academic infrastructure, represented also by the Staff of the Department of Earth Sciences. My special thanks go to: Lillian Ng and Joanne Ko for being so caring. Mike Chio, Terence Lam, and Lily Chiu for the enjoyable corridor chats.

Four years in one office would not have been as bearable without my most dearest office mates, Diane Chung and Teng Teng Yang: together we went through all kinds of ups and downs. There will be these moments stuck in memory, when thinking back of those good old times in Hong Kong.

Being so far away from Germany I sometimes forgot where my roots are. For reminding me that, I like to thank Kono Lemke and Petra Bach for being inspiring mentors and simply good friends.

Before being crucified, I better do not forgot the “Hong Kong Gang”. They are proof that Hong Kong has a face, and the Department of Earth Sciences a heart and soul. I thank all of you for welcoming me right from the beginning, joining our yum cha’s, BBQ’s, field trips, KTV’s, 207 parties, dinners, weddings, movies, writing poems, and so much more: Prof. Lung Chan, Jean Wong, Tammy Tam, Wu Meiling, Zuo Xuran, all three Panda’s, Helen Geng, Steve Ng, George Ma, Samuel Ng, Jay Tung, Haz Cheung, Brad Chum, Hon Chim Chiu, Philip Wu, and Kevin Tse.

I would regret ending this list without the people who helped maintaining my mental balance during my studies: my best man and true friend Raja Arumugam. Yang Xiao for being the nerd among friends I was always looking for. My Taichi Master Chung, for teaching me, that mind is over body. Jan Kretzschmar, who came all the way to join my wedding. Matthias Herzog, together with whom I still philosophy about the meaning of life. Clemens Wiedemann, for unforgettable football moments. Joachim Fillauer, for pushing me back on track, when doubts arose.

It keeps someone's mind at peace to have certain constants in life, despite the changes that may occur. I would not be the person I am today without my family: my brother Rudolf and sister Viktoria Eizenhöfer, my wonderful wife Li Yanli and my daughter Lena Eizenhöfer. I will not forget the sacrifices my parents made to guide me on my way until today, wherever they are watching over me now, Jörg and Magdalena Eizenhöfer.

Contents

Abbreviations

AAC	Arc-accretion complex
AC	Accretion complex
AFM	Na_2O + K_2O (A), FeO + Fe_2O_3 (F), MgO (M)
BGMRIM	Bureau of Geology and Mineral Resources of Inner Mongolia
CAOB	Central Asian Orogenic Belt
CL	Cathodoluminescence
Cr	Cretaceous *(mostly in geological maps)*
D	Devonian *(mostly in geological maps)*
Dipl. Geol.	*(German)* Diplom Geologe, *(English)* Diploma Geologist (German M.Phil. degree)
DZHf	Zircon Hf analysis
DZUPb	Zircon U–Pb analysis
EP	Early Palaeozoic arc
F	Fold plane *(in geological cross sections)*
Fig., Figs.	Figure(s)
Ga	Billion years
HfNd	Whole-rock Hf and Nd isotope analysis
HO	Hegenshan Ophiolite Complex
ICP-MS	Inductively coupled mass spectrometry
J	Jurassic *(mostly in geological maps)*
LA-ICPMS	Laser-ablation inductively coupled mass spectrometry
LP	Late Palaeozoic arc
Ma	Million years
MA	Mongolian arcs
MaTE	Whole-rock major and trace element analysis
MSWD	Mean standard weighted deviation
Mz	Mesozoic *(mostly in geological maps)*
NAO	Northern Accretionary Orogen
NCC	North China Craton
N-MORB	Normal mid-ocean ridge basalt

P	Permian *(mostly in geological maps)*
PA	Palaeozoic arcs
PDF	Probability density function
QFL	Quartz-Feldspar-Lithic Fragments
SAC	Subduction-accretion complex
SAO	Southern Accretionary Orogen
SC	South China Craton
SPOCS	Spectroscopic properties of cool stars
SSZ	Solonker Suture Zone *OR* supra-subduction zone *(refer to context)*
Tab., Tabs.	Table(s)
TAS	Total alkali silica
TSS	Tian Shan Suture
XRF	X-ray fluorescence

List of Figures

List of Tables

Chapter 1
Introduction

1.1 The Central Asian Orogenic Belt

The Central Asian Orogenic Belt (CAOB), situated between the East European Platform, the Siberian Craton, and the combined Tarim and North China Cratons (Fig. 1.1), is one of the largest Phanerozoic orogenic systems on Earth [4, 8, 21, 42]. Despite numerous investigations (e.g. [1, 24, 37, 41, 42], and references therein), however, it perhaps still remains the least understood tectonic belt on the Eurasian continent. It formed as a result of accretionary events induced by the Palaeozoic subduction of the Palaeo-Asian Ocean, which separated the Tarim and North China Cratons from the growing accretionary front encircling the Siberian Craton and East European Platform until the Late Permian to Early Triassic. The entire variety of convergent plate tectonics are involved in the accretionary processes: (1) accretion of accretionary wedges, island arcs, terranes or microcontinents, and oceanic seamounts, and (2) continental collision, subduction, subduction roll-back, and back-arc spreading. Based on distinct isotopic geochemical differences the CAOB has also been termed an "internal" orogen in contrast to the circum-Pacific "external" orogens. Whereas "external" orogens are formed at the boundary of large mantle convection cells, "internal" orogens form within a single long-lived mantle convection supercell [8]. Moreover, accretionary orogens are considered as the dominant contributor of continental lithospheric growth through Earth's history [4]. However, net crustal growth can only be achieved when juvenile crustal addition outweighs crustal reworking. Since the evolution of the CAOB included numerous already existing lithospheric crustal units, such as Precambrian blocks of various scales, this has become the focus of reignited debates (e.g. [24]).

The characterisation and identification of terranes within the CAOB still remains challenging (e.g. [11, 19]), and the relationship between major tectonic blocks involved in the formation of the CAOB is often controversial and hypothetical. For example, the existence of blocks that rifted from the northern margins of Gondwana, or possibly from the Siberian Craton, in the Precambrian is still debated (e.g. [33, 41]). The extent of volcanic arc chains situated in the open oceans between major tectonic units, such as the Palaeo-Asian Ocean between the North China and Siberian Cratons, is unknown. Final disappearance of the Palaeo-Asian Ocean terminated the

P. R. Eizenhöfer, *Subduction and Closure of the Palaeo-Asian Ocean along the Solonker Suture Zone: Constraints from an Integrated Sedimentary Provenance Analysis*, Springer Theses, https://doi.org/10.1007/978-981-32-9200-0_1

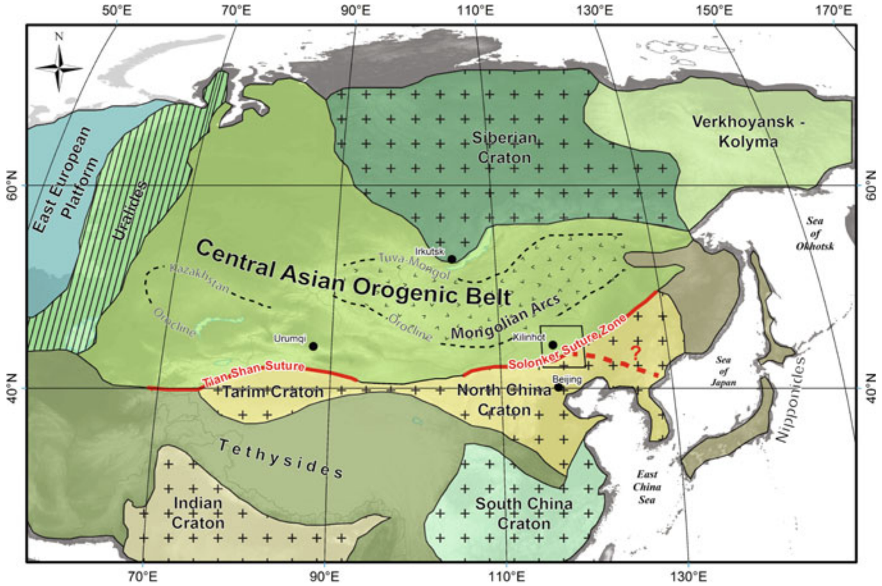

Fig. 1.1 Tectonic subdivision of Central and East Asia (modified after [37]). The study area across the Solonker Suture Zone is outlined as box around the city of Xilinhot

formation of the CAOB, leading to collision between the combined Tarim and North China Cratons and the wider accretionary disk encircling the Siberian Craton to its south (also known as the Mongolian Arcs) in the Late Palaeozoic and/or Early Mesozoic. This ultimately formed two major regional lineaments: the nearly east-west trending Tian Shan Suture located in Central Asia and the Solonker Suture Zone in East Asia (Fig. 1.1, [44]).

Sedimentary provenance studies can assist in the reconstruction of palaeo-geographic positions and the tectonic evolution of a region [20]. Thus, the analysis of arc basins and their potential sedimentary provenance terranes can provide important insights into the architecture of arc systems, which are the predominant tectonic building block of the CAOB [5, 13, 33]. This approach is particularly applicable across cryptic suture zones [35, 46], such as the Solonker Suture Zone [22, 23, 47], where suture-typical features appear to be largely absent or not exposed.

Several tectonic models have been proposed to explain the formation and evolution of the CAOB (Fig. 1.2). The classic, and repeatedly modified (e.g. [36, 49]), single-arc model was initially proposed by Şengör [37]. It suggests that the main elements of the CAOB were derived from the successive roll-back, accretion, strike-slip faulting and oroclinal bending of a global, single (or multiple) ocean spanning, arc system, also known as the Kipchak-Tuva-Mongol arc. However, more recent palaeomagnetic data constraining the palaeo-geographic positions of the Siberian Craton and the East European Platform in Neoproterozoic time [32, 40], and more recent structural studies [25] have challenged this model. Instead, an archipelago-type model has been brought forward [42, 44, 45, 47], which shares more resemblance with modern-day

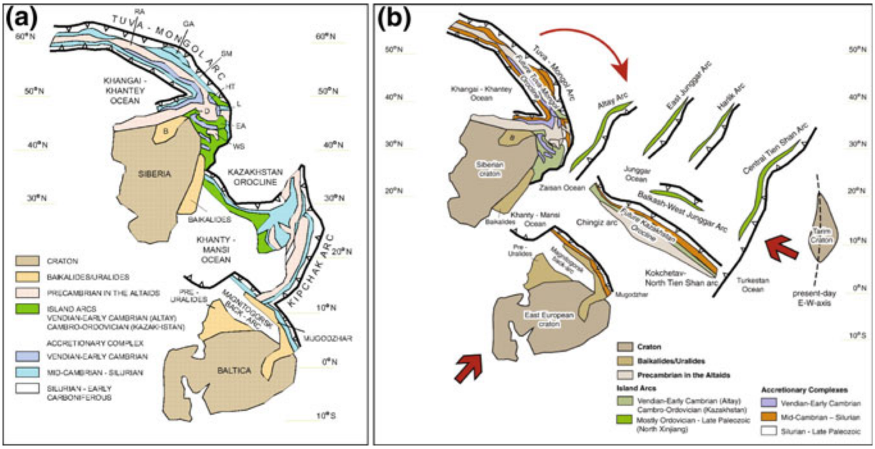

Fig. 1.2 Proposed tectonic models for the evolution of the CAOB. **a** single-arc model for the period 420–390 Ma [36, 37]; figure from and abbreviations in Windley et al. [42]; **b** archipelago-type model during the Middle Palaeozoic [42, 44, 45, 47]

Southeast Asia [18]. In this model, distinct volcanic arcs and terranes were accreted onto the active margins of the Siberian Craton and the East European Platform from the Early Palaeozoic to the Late Permian to Early Triassic. Lehmann et al. [25] modified the archipelago-type model by postulating initial east-west, followed by north-south directed shortening, based on their extensive structural analyses. The extent to which accretion occurred along the northern margins of the Tarim and North China Cratons prior to the formation of the Solonker Suture Zone, however, remains a matter of debate (e.g. [22, 47]).

A large number of issues related to the palaeo-geographic geometry and origins of major tectonic units in the CAOB have not been satisfactorily resolved yet. A more detailed understanding is needed with respect to the development of volcanic arcs, the relative palaeo-geographic locations of terranes prior to the final closure of the Palaeo-Asian Ocean. Additionally, the current definition of major tectonic units in the eastern segment of the CAOB by different workers (e.g. [22, 23, 47]) is still confusing due to inconsistent nomenclatures and definitions of tectonic units and their location. Thus, this dissertation aims to solve these issues based on a combination of literature review (e.g. [2, 22, 23, 47]) and the results of integrated sedimentary provenance analyses during this four-year doctoral study.

1.2 Closure of the Palaeo-Asian Ocean Along the Solonker Suture Zone

The Late Permian to Early Triassic Solonker Suture Zone along the southeast part of the CAOB is generally interpreted as the locus of the final closure of the Palaeo-Asian Ocean, which separated the Siberian Craton and Mongolian Arcs to the northwest from the North China Craton to the southeast during the Palaeozoic (Fig. 1.1, [26, 47], this study). However, geologically it still remains ill-defined. Its tectonic evolution, exact location and the time of final suturing are contended (e.g. [48, 54]), although there is an overall consensus with respect to its approximate east/northeast-west strike. Its tectonic nature remarkably differs from many other typical continent-collisional sutures (e.g. the Himalayan, Alpine or Dabie-Sulu collisional belts), which impedes tectonic reconstructions of the accretionary collision zone between the Mongolian Arcs and the North China Craton. Ophiolite slivers occur erratically in a hundreds of kilometres broad southwest-northeast trending corridor (Fig. 1.3, [3]). Regional metamorphism, distinct mountain ranges, and large-scale thrust features appear to be absent or are not exposed. Similar lithologies and tectonic architectures of the arc terranes across the suture makes the suture in the field barely recognisable. In addition, complex Palaeozoic arc geometries and processes might have affected the preservation of and access to key tectonic elements [12]. Later Mesozoic plutonic and volcanic activity further overprinted the region (e.g. [30]). Hence, the tectonic interpretations and geographical extent of such an important regional lineament are often controversial and hypothetical.

Palaeo-biogeographical studies [29, 39] identified a broad mixing zone of Angaran and Cathaysian marine facies along the present-day border between Mongolia and China. Earlier works [31, 37] suggest that the suture zone is located far to the north of the Xar Moron River linking the Solonker (Solon Obo) ophiolite at the southernmost border between Mongolia and China to the Hegenshan ophiolite to the northeast. Alternatively, [22, 23, 47] argue that the suture lies about 500 km further south following the course of the Xar Moron River. It has been contested whether the suture zone eventually branches into two separate sutures to the east, namely the northern Solonker-Heihe and southern Solonker-Chanchun suture (Fig. 1.3, e.g. [43, 55]). The results and interpretations in this study favour a broad cryptic suture zone to the point where it reaches the Songliao block to the east and branches into the two above mentioned subordinate sutures (Fig. 1.3). Cryptic sutures in similar tectonic settings were also documented in other parts of the CAOB, such as the Tian Shan [46], and in the Bohemian Massif in the Variscides [35].

Most recent studies (e.g. [27, 28, 47, 50]), including this work, confirmed a Late Permian to Early Triassic collision of two accretionary orogens via double-sided southward and northward dipping subduction beneath the North China Craton and the Mongolian Arcs, respectively. Subsequently, the resulting suture was termed a cryptic suture, since typical suture-related and collisional features could not be observed. Other studies (e.g. [22, 23]) prefer a single-sided southward dipping subduction beneath the North China Craton that led to ocean closure. Despite the long established Late Palaeozoic to Early Mesozoic closure time of the Palaeo-Asian Ocean [27, 28, 37, 41, 42, 47, 50], and confirmed in this study, some researchers still argue for a different timing of suturing, e.g. pre-Late Devonian [54] or Mesozoic [31].

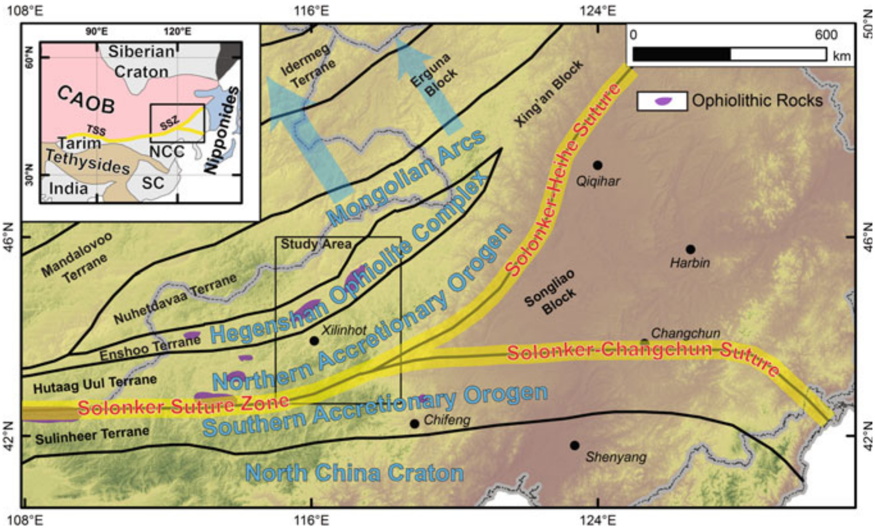

Fig. 1.3 Tectonic framework, its subdivision and proposed course of the Solonker Suture Zone in the study area including its continuation into Mongolia and East-Northeast China based on the results and interpretation in this work. TSS: Tian Shan Suture; SSZ: Solonker Suture Zone; NCC: North China Craton; SC: South China Craton; CAOB: Central Asian Orogenic Belt. The locations of ophiolithic rock assemblages outside the study area are taken from Xiao et al. ([44], and references therein). Tectonic subdivision modified after Xiao et al. [47], Jian et al. [22, 23]

1.3 General Geological Background of the Study Area

Unlike classic continent-continent collisions, the Palaeo-Asian Ocean closed as a result of complex Palaeozoic accretionary processes and arc geometries, which involved a number of independent tectonic units (Fig. 1.3). The study area can be generally subdivided from north to south into the Mongolian Arcs, representing an entire collage of arc terranes, the Hegenshan Ophiolite Complex, the Northern Accretionary Orogen, the Southern Accretionary Orogen and the North China Craton ([22, 23, 47], this work), which are separated by the Linxi, the Erenhot and Uliastai faults, respectively (see also Fig. 2.1). Among these units, the Mongolian Arcs and the North China Craton are confirmed to contain Precambrian basement (e.g. [9, 52, 53]). Each of the accretionary belts can be traced westwards into Mongolia as Nuhetdavaa, Enshoo, Hutaag Uul and Sulinheer terrane, respectively [1]. To the east/northeast the Mongolian Arcs and the Northern Accretionary Orogen are represented as the Erguna and Xing'an blocks in China, while the Hegenshan Ophiolite Complex is assumed to thin out to the northeast. The Songliao block, the origin of which claimed by some authors to be Gondwanan because of the occurrence of Pan-African ages [55], is framed to the north and south by the east/northeast continuation of aforementioned accretionary orogens. The tectonic and lithological similarities between the belts in the study area impedes a clear identification of the

Solonker Suture Zone, assumed to be located between the Northern and Southern Accretionary Orogen according to the interpretations in this work.

The Permian lithologies in the study region reflect the subduction and active arc tectonic environment during the Palaeozoic closure of the Palaeo-Asian Ocean. Thus, volcano-clastic sedimentary rocks represent the predominant arc basin fills, and basaltic to andesitic volcanic rocks typify the active volcanic arc chains at shallow crustal levels. Their deeper crustal plutonic equivalents, however, only crop out at key locations, such as the villages of Bainaimiao (e.g. [51]) or Baolidao (e.g. [6, 7]), along the Southern and Northern Accretionary Orogens, respectively. Isolated low- to medium degree metamorphic complexes, such as the Xilinhot and Shuangjing metamorphic complexes and small-scaled ophiolithic slivers occur only within the accretionary wedges attached along the subduction fronts of the orogens (Fig. 2.1). The kilometre-scaled Hegenshan Ophiolite Complex represents and exception to this, and is prominently featured in the northern parts of the study area.

1.4 Research Objectives and Methodology

High-strain zones, ophiolite remnants, blueschist melanges, or two dissimilar continental terranes, all of which indicators for the most fundamental type of sutures [10] that would aid in the identification of the closure of a major ocean, do not occur in the study region. Consequently, the geological background of the region is far from being entirely understood. The overarching aim of this doctoral study is to systematically decipher the tectonic evolution of the accretionary collision zone between the Siberian and North China Cratons, and the spatiotemporal accretionary architecture that led to subduction and ultimately disappearance of the Palaeo-Asian Ocean during the Palaeozoic.

The integration of multiple approaches in this sedimentary provenance analysis of arc basins across the entire accretionary collision zone between the Mongolian Arcs and the North China Craton, thus, represents a powerful tool that would go beyond a potentially restricted local scope, while assessing the tectonic evolution of the area at a regional scale [20]. Amongst the large variety of analytical methods available, this study predominantly adopted detrital zircon U–Pb geochronology, detrital zircon Lu–Hf isotopic, whole-rock geochemical, and statistical analyses, all of which complemented by fundamental petrographic, structural and field investigations.

Detrital zircon U–Pb geochronology of Late Palaeozoic sedimentary arc basins located in the Palaeo-Asian Ocean is able to quantitatively evaluate issues of when and how the Palaeo-Asian Ocean was closed to form the Solonker Suture Zone. It provides information on sedimentary and tectonic relationships between major tectonic blocks, such as their relative palaeo-geographic positions during the Palaeozoic, or relative contribution of sedimentary material to the basins [20]. Major tectonic units can be identified by comparing measured age distributions to well-defined "age-fingerprints" of potential sedimentary provenance terranes. The variability of contemporaneous detrital age distributions across the accretionary collision zone can serve as an indicator for subduction polarities and important regional lineaments, such as cryptic sutures.

The study of detrital zircon Lu–Hf isotopes, tied to respective U–Pb ages, provides important insights into the magmatic composition of the sedimentary provenance terranes, and thus, into the accretionary and collisional processes that were operative during the subduction of the Palaeo-Asian Ocean. Areas can be demarcated, which involved reworked material, such as that from Precambrian crust, and juvenile material, such as that from young intra-oceanic island arcs. This information proves itself especially valuable for the reconstruction of ancient and complex accretionary tectonic environments such as the CAOB. On a more global perspective, the regional evolution of lithospheric crust, and the amount of crustal addition and reworking can be assessed, and compared with existing evaluations (e.g. [8, 24]).

Whole-rock geochemical analyses of clastic sedimentary rocks can better characterise their respective provenance terranes and the environment, in which the source formed and its respective detritus was deposited [16, 17, 34]. Source and basin relationships can be determined by comparing the geochemical signature of immobile elements of potential provenance terranes with that of the sedimentary rocks. Differences in basins across a cryptic suture, hence, can assist in better defining the latter. Furthermore, these geochemical fingerprints reflect on the depositional environment and the tectonic setting. Since clastic sedimentary rocks represent the eroded end-product of exposed crust, they can also serve as an alternative measure to estimate the contribution to net crustal growth in the catchment area of the sedimentary system. Thus, the analysis of whole-rock Hf and Nd isotopic compositions in clastic sedimentary rocks can be utilised to assess, in combination with the detrital zircon Hf isotopic record, the net addition of lithospheric crust during the formation of the sedimentary provenance terranes.

The large amount of geochronological data collected in this study inevitably opened ground for an intensive statistical review of the measured detrital age distributions. When geochronological age data are seen from an information theoretical point of view, that these are generated by a source, transferred through a noisy channel and analysed by a receiver, then the mathematical tools provided by the groundbreaking treatise on information theory by Shannon and Weaver [38], in geochronology barely recognised, can readily be adopted. These enable a simple quantitative description of an age probability distribution function, a classification of geochronological systems, and an alternative approach in estimating required sample sizes in geochronological provenance studies. Thus, the reconstruction of depositional environments and tectonic settings can be supplemented by a more robust statistical foundation, which also can test existing tectonic models, or even potentially lead to their revision.

The results in this study identify major sedimentary provenance terranes of the Permian arc basins across the accretionary collision zone between the Mongolian Arcs and the North China Craton, outlines the depositional environment and the tectonic setting, in which the Permian sedimentary rocks were formed, evaluates the net crustal Palaeozoic growth in the eastern segment of the CAOB during the closure of the Palaeo-Asian Ocean, and gives an updated definition of the cryptic Solonker Suture Zone. This integrated sedimentary provenance analysis ultimately leads to the development of a tectonic model for the Palaeozoic subduction and closure of the Palaeo-Asian Ocean, which may further impact the current view on east Asian blocks during the assembly of the supercontinent Pangaea.

1.5 Dissertation Overview

This doctoral study comprises the results of four years research at the *Department of Earth Sciences* of *The University of Hong Kong* in cooperation with the *Collaborative Innovation Centre of Continental Tectonics* at *Northwest University Xi'an*, and other Chinese research institutions. Three field excursions in Inner Mongolia and north China, as well as several laboratory visits in China were conducted. The dissertation in its current form reflects the content of four independent manuscripts, of which two are published [14, 15], another in press,[1] and one to be submitted after the final submission of this thesis.[2] Parts of this work have been presented as poster during the *AGU Fall Meeting 2013* in San Francisco, and as oral presentations during a joint conference between the *Guangzhou Institute of Geochemistry, Chinese Academy of Sciences* and the *Department of Earth Sciences* of *The University of Hong Kong* in 2012 (being awarded the best student presentation), during annual meetings of the major NSFC program *Reconstruction of East Asian Blocks in Pangea* in Sanya 2012 and Qingdao 2013, and the *GSA Annual Meeting 2014* in Vancouver. The dissertation is divided into seven chapters, including this introduction, a detailed description of the regional geology of the study area, the applied methodology, the analytical results, the interpretation of the data, and the final conclusions made during the research.

Chapter 2, *Regional Geology across the Solonker Suture Zone*, introduces the geology of the study area in detail, characterises the current subdivision of tectonic units, and outlines controversies surrounding the tectonic evolution of the region.

Chapter 3, *Methodology*, describes in more depth the analytical techniques applied to conduct the sedimentary provenance study. These include detrital zircon U–Pb geochronology, detrital zircon Lu–Hf isotope, whole-rock major, trace element, Nd and Hf isotope analyses, and the statistical tools used to quantitatively evaluate age distributions, of which the latter will be more elaborated in Chap. 5.

Chapter 4, *Results*, presents the detrital zircon U–Pb geochronological, Lu–Hf isotopic, whole-rock major, trace element, Hf, Nd isotopic and statistical results within the context of their respective tectonic unit in the study area.

Chapter 5, *Geochronological Entropy and its Relevance to Age Measurements*, introduces a new perspective in estimating sample sizes in sedimentary provenance studies by adopting principles of information theory. The new term "Geochronological Entropy" will be defined, and its geological implications outlined. The study

[1] Eizenhöfer, P.R., Zhao, G., Sun, M., Zhang, J., Han, Y. & Hou, W. (*in press*). Geochronological and Hf isotopic variability of detrital zircons across the North China Craton and the Mongolian Arcs, and its implications. *Geological Society of America Bulletin*, https://doi.org/10.1130/B31175.1.

[2] Eizenhöfer et al. (*in prep.*). Geochronological entropy and its relevance to age provenance studies.

area across the Solonker Suture Zone serves as a case study to demonstrate the applicability of this statistical approach.

Chapter 6, *Accretionary Collision between the Mongolian Arcs and the North China Craton*, integrates, combined with previous studies, the geochronological, geochemical and statistical results, and interpretations of the sedimentary provenance analyses into a single coherent tectonic model. This model is then being compared with existing models and present-day tectonic analogues. Focus is on the identification of sedimentary provenance terranes, the overall accretionary tectonic and depositional setting during formation of the sedimentary rocks in their respective lithotectonic belts, the characterisation of the Solonker Suture Zone and the integration of the outcomes in this study into an overall tectonic model.

A summary of all findings is given in Chap. 7, *Conclusions*.

The Appendices A, B, C, D, E and F generally contain all analytical results obtained during the entire four-year study period at The University of Hong Kong in table form, which include zircon U–Pb, zircon Hf, whole-rock major and trace element, Hf and Nd isotopic, and thin section point-counting data. In addition, the during the study period developed Matlab© Mathworks data reduction software package "RatSuite" is briefly introduced, with which a significant number of U–Pb and Hf data were extracted for this thesis.

References

1. Badarch G, Cunningham WD, Windley BF (2002) A new terrane subdivision for Mongolia: implications for the Phanerozoic crustal growth of Central Asia. J Asian Earth Sci 21(1):87–110
2. BGMRIM (1991) Regional Geology of Nei Mongol (Inner Mongolia) autonomous region (in Chinese with English summary), vol 25. Geological memoirs series 2. Geological Publishing House, Beijing
3. Cao C (1989) The ophiolite belts of northeastern China. J Southeast Asian Earth Sci 3(1–4):233–236
4. Cawood PA, Kröner A, Collins WJ, Kusky TM, Mooney WD, Windley BF (2009) Accretionary orogens through Earth history. Geol Soc Lond Spec Publ 318(1):1–36
5. Cawood P, Hawkesworth C, Dhuime B (2012) Detrital zircon record and tectonic setting. Geology 40(10):875–878
6. Chen B, Jahn B, Wilde S, Xu B (2000) Two contrasting paleozoic magmatic belts in northern Inner Mongolia, China: petrogenesis and tectonic implications. Tectonophysics 328(1–2):157–182
7. Chen B, Jahn B, Tian W (2009) Evolution of the Solonker suture zone: Constraints from zircon U-Pb ages, Hf isotopic ratios and whole-rock Nd-Sr isotope compositions of subduction- and collision-related magmas and forearc sediments. J Asian Earth Sci 34(3):245–257
8. Collins WJ, Belousova EA, Kemp AIS, Murphy JB (2011) Two contrasting Phanerozoic orogenic systems revealed by hafnium isotope data. Nat Geosci 4(5):333–337
9. Demoux A, Kröner A, Liu D, Badarch G (2009) Precambrian crystalline basement in southern Mongolia as revealed by SHRIMP zircon dating. Int J Earth Sci 98(6):1365–1380
10. Dewey JF (1977) Suture zone complexities: a review. Tectonophysics 40(1–2):53–67
11. Dobretsov N, Buslov M, Yu U (2004) Fragments of oceanic islands in accretion-collision areas of Gorny Altai and Salair, southern Siberia, Russia: early stages of continental crustal growth of the Siberian continent in Vendian-Early Cambrian time. J Asian Earth Sci 23(5):673–690 (Phanerozoic Continental Growth in Central Asia)

12. Draut AE, Clift PD (2013) Differential preservation in the geologic record of intraoceanic arc sedimentary and tectonic processes. Earth Sci Rev 116:57–84
13. Dumitru TA, Ernst W, Wright JE, Wooden JL, Wells RE, Farmer LP, Kent AJ, Graham SA (2013) Eocene extension in Idaho generated massive sediment floods into the Franciscan trench and into the Tyee, Great Valley, and Green River basins. Geology 41(2):187–190
14. Eizenhöfer PR, Zhao G, Zhang J, Sun M (2014) Final closure of the Paleo-Asian Ocean along the Solonker Suture Zone: Constraints from geochronological and geochemical data of Permian volcanic and sedimentary rocks. Tectonics 33(4):441–463
15. Eizenhöfer PR, Zhao G, Zhang J, Han Y, Hou W, Liu D, Wang B (2015) Geochemical characteristics of the Permian basins and their provenances across the Solonker Suture Zone: assessment of net crustal growth during the closure of the Palaeo-Asian Ocean. Lithos 224–225:240–255
16. Fralick P (2003) Geochemistry of clastic sedimentary rocks: ratio techniques. In: Lentz D (ed) Geochemistry of sediments and sedimentary rocks. Geological Association of Canada, St. John's, pp 85–103
17. Fralick P, Kronberg B (1997) Geochemical discrimination of clastic sedimentary rock sources. Sediment Geol 113(1–2):111–124
18. Hall R (2009) Southeast Asia's changing palaeogeography. Blumea Biodivers Evol Biogeogr Plants 54(1–1):148–161
19. Han G, Liu Y, Neubauer F, Jin W, Genser J, Ren S, Li W, Wen Q, Zhao Y, Liang C (2012) LA-ICP-MS U–Pb dating and Hf isotopic compositions of detrital zircons from the Permian sandstones in Da Xing'an Mountains, NE China: new evidence for the eastern extension of the Erenhot-Hegenshan suture zone. J Asian Earth Sci 49(0):249–271 (Orogenic Belts in Central Asia: Correlations and connections)
20. Haughton PDW, Todd SP, Morton AC (1991) Sedimentary provenance studies. Geol Soc Lond Spec Publ 57(1):1–11
21. Jahn B-M, Wu F, Chen B (2000) Granitoids of the central Asian Orogenic Belt and continental growth in the Phanerozoic. Geol Soc Am Special Papers 350:181–193
22. Jian P, Liu D, Kröner A, Windley BF, Shi Y, Zhang F, Shi G, Miao L, Zhang W, Zhang Q, Zhang L, Ren J (2008) Time scale of an early to mid-Paleozoic orogenic cycle of the long-lived Central Asian Orogenic Belt, Inner Mongolia of China: implications for continental growth. Lithos 101(3–4):233–259
23. Jian P, Liu D, Kröner A, Windley BF, Shi Y, Zhang W, Zhang F, Miao L, Zhang L, Tomurhuu D (2010) Evolution of a Permian intraoceanic arc-trench system in the Solonker suture zone, Central Asian Orogenic Belt China and Mongolia. Lithos 118(1–2):169–190
24. Kröner A, Kovach V, Belousova E, Hegner E, Armstrong R, Dolgopolova A, Seltmann R, Alexeiev DV, Hoffmann JE, Wong J, Sun M, Cai K, Wang T, Tong Y, Wilde SA, Degtyarev KE, Rytsk E (2014) Reassessment of continental growth during the accretionary history of the Central Asian Orogenic Belt. Gondwana Res 25(1):103–125
25. Lehmann J, Schulmann K, Lexa O, Corsini M, Kröner A, Štípská P, Tomurhuu D, Otgonbator D (2010) Structural constraints on the evolution of the Central Asian Orogenic Belt in SW Mongolia. Am J Sci 310(7):575–628
26. Li J-Y (2006) Permian geodynamic setting of Northeast China and adjacent regions: closure of the Paleo-Asian Ocean and subduction of the Paleo-Pacific Plate. J Asian Earth Sci 26(3–4):207–224
27. Li Y, Zhou H, Brouwer F, Xiao W, Wijbrans J, Zhao J, Zhong Z, Liu H (2014a) Nature and timing of the Solonker suture of the Central Asian Orogenic Belt: insights from geochronology and geochemistry of basic intrusions in the Xilin Gol Complex, Inner Mongolia China. Int J Earth Sci 103(1):41–60
28. Li Y, Zhou H, Brouwer FM, Xiao W, Wijbrans JR, Zhong Z (2014b) Early Paleozoic to Middle Triassic bivergent accretion in the Central Asian Orogenic Belt: insights from zircon U-Pb dating of ductile shear zones in central Inner Mongolia China. Lithos 205:84–111
29. Manankov I, Shi G, Shen S (2006) An overview of Permian marine stratigraphy and biostratigraphy of Mongolia. J Asian Earth Sci 26(3–4):294–303 (Permian of East and Northeast Asia)

30. Meng Q-R (2003) What drove late Mesozoic extension of the northern China-Mongolia tract? Tectonophysics 369(3–4):155–174
31. Nozaka T, Liu Y (2002) Petrology of the Hegenshan ophiolite and its implication for the tectonic evolution of northern China. Earth Planet Sci Lett 202(1):89–104
32. Popov V, Khramov A, Bachtadse V (2005) Palaeomagnetism, magnetic stratigraphy, and petromagnetism of the Upper Vendian sedimentary rocks in the sections of the Zolotitsa River and in the Verkhotina Hole, Winter Coast of the White Sea Russia. Russ J Earth Sci 7(2):1–29
33. Rojas-Agramonte Y, Kröner A, Demoux A, Xia X, Wang W, Donskaya T, Liu D, Sun M (2011) Detrital and xenocrystic zircon ages from Neoproterozoic to Palaeozoic arc terranes of Mongolia: Significance for the origin of crustal fragments in the Central Asian Orogenic Belt. Gondwana Res 19(3):751–763 (Island Arcs: Their role in growth of accretionary orogens and mineral endowment)
34. Sawyer E (1986) The influence of source rock type, chemical weathering and sorting on the geochemistry of clastic sediments from the Quetico Metasedimentary Belt, Superior Province Canada. Chem Geol 55(1–2):77–95
35. Schulmann K, Lexa O, Janoušek V, Lardeaux JM, Edel JB (2014) Anatomy of a diffuse cryptic suture zone: an example from the Bohemian Massif European Variscides. Geology 42(4):275–278
36. Şengör A, Natal'In B (2004) Phanerozoic analogues of Archaean oceanic basement fragments: altaid ophiolites and ophirags. In: Kusky T (ed) Precambrian ophiolites and related rocks. Elsevier, Amsterdam
37. Şengör AMC, Natal'in BA, Burtman VS (1993) Evolution of the Altaid tectonic collage and Palaeozoic crustal growth in Eurasia. Nature 364(6435):299–307
38. Shannon CE, Weaver W (1971) The mathematical theory of communication. University of Illinois Press, Illinois
39. Shi G (2006) The marine Permian of East and Northeast Asia: an overview of biostratigraphy, palaeobiogeography and palaeogeographical implications. J Asian Earth Sci 26(3–4):175–206 (Permian of East and Northeast Asia)
40. Smethurst MA, Khramov AN, Torsvik TH (1998) The Neoproterozoic and Palaeozoic palaeomagnetic data for the Siberian platform: from Rodinia to Pangea. Earth Sci Rev 43(1–2):1–24
41. Wilhem C, Windley BF, Stampfli GM (2012) The Altaids of Central Asia: a tectonic and evolutionary innovative review. Earth Sci Rev 113(3–4):303–341
42. Windley BF, Alexeiev D, Xiao W, Kröner A, Badarch G (2007) Tectonic models for accretion of the Central Asian Orogenic Belt. J Geol Soc Lond 164(1):31–47
43. Wu F, Zhao G-C, Sun D-Y, Wilde SA, Yang J-H (2007) The Hulan group: its role in the evolution of the Central Asian Orogenic Belt of NE China. J Asian Earth Sci 30(3–4):542–556
44. Xiao WJ, Windley BF, Huang BC, Han CM, Yuan C, Chen HL, Sun M, Sun S, Li JL (2009) End-Permian to mid-Triassic termination of the accretionary processes of the southern Altaids: implications for the geodynamic evolution, Phanerozoic continental growth, and metallogeny of Central Asia. Int J Earth Sci 98(6):1189–1217
45. Xiao W, Huang B, Han C, Sun S, Li J (2010) A review of the western part of the Altaids: a key to understanding the architecture of accretionary orogens. Gondwana Res 18(2–3):253–273
46. Xiao W, Windley BF, Allen MB, Han C (2013) Paleozoic multiple accretionary and collisional tectonics of the Chinese Tianshan orogenic collage. Gondwana Res 23(4):1316–1341
47. Xiao W, Windley BF, Hao J, Zhai M (2003) Accretion leading to collision and the Permian Solonker suture, Inner Mongolia, China: termination of the central Asian Orogenic Belt. Tectonics 22(6)
48. Xu B, Charvet J, Chen Y, Zhao P, Shi G (2013) Middle Paleozoic convergent orogenic belts in western Inner Mongolia (China): framework, kinematics, geochronology and implications for tectonic evolution of the Central Asian Orogenic Belt. Gondwana Res 23(4):1342–1364
49. Yakubchuk A (2008) Re-deciphering the tectonic jigsaw puzzle of northern Eurasia. J Asian Earth Sci 32(2–4):82–101 (Geodynamics and Metallogeny of the Altaid Orogen)
50. Zhang S, Gao R, Li H, Hou H, Wu H, Li Q, Yang K, Li C, Li W, Zhang J, Yang T, Keller G, Liu M (2014a) Crustal structures revealed from a deep seismic reflection profile across

the Solonker suture zone of the Central Asian Orogenic Belt, northern China: An integrated interpretation. Tectonophysics 612–613:26–39
51. Zhang S-H, Zhao Y, Ye H, Liu J-M, Hu Z-C (2014b) Origin and evolution of the Bainaimiao arc belt: implications for crustal growth in the southern Central Asian orogenic belt. Geol Soc Am Bull 126(9–10):1275–1300
52. Zhao G, Wilde SA, Cawood PA, Sun M (2001) Archean blocks and their boundaries in the North China Craton: lithological, geochemical, structural and P-T path constraints and tectonic evolution. Precambrian Res 107(1–2):45–73
53. Zhao G, Sun M, Wilde SA, Sanzhong L (2005) Late Archean to Paleoproterozoic evolution of the North China Craton: key issues revisited. Precambrian Res 136(2):177–202
54. Zhao P, Chen Y, Xu B, Faure M, Shi G, Choulet F (2013) Did the Paleo-Asian Ocean between North China block and Mongolia block exist during the late Paleozoic? First paleomagnetic evidence from central-eastern Inner Mongolia, China. J Geophys Res Solid Earth 118(5):1873–1894
55. Zhou J-B, Wilde SA, Zhang X-Z, Liu F-L, Liu J-H (2012) Detrital zircons from phanerozoic rocks of the Songliao block, NE China: evidence and tectonic implications. J Asian Earth Sci 47:21–34

Chapter 2
Regional Geology Across the Solonker Suture Zone

The study area is situated in the southeastern segment of the Central Asian Orogenic Belt (CAOB) across the more than 500 km wide accretionary collision zone between the Mongolian Arcs to the north and the North China Craton to the south (Figs. 1.3 and 2.1). Its central position provides an ideal opportunity to ascertain the exact location and timing of the formation of the cryptic Solonker Suture Zone, and evaluate existing suggestions [23]. It further represents an ideal testing ground for the assessment and refinement, or erection of new tectonic models for the Palaeozoic closure of the Palaeo-Asian Ocean.

Embedded to the southeastern end of the wider accretionary framework produced by the enclosing Palaeozoic relative movements of the Siberian and North China Cratons [38, 51, 58], the study area can be generally divided from north to south into four first-order lithotectonic belts: the Chinese southern sections of the Mongolian Arcs (also known as Uliastai active continental margin, [66]), the Hegenshan Ophiolite Complex, the Northern Accretionary Orogen and the Southern Accretionary Orogen, all of which separated by the regional Uliastai, Erenhot, and Linxi faults, respectively (Fig. 2.1). Each of the belts are further subdivided into smaller-scaled tectonic subunits, which correspond to their respective arc geometry (e.g. volcanic arc-accretion and their attached subduction-accretion complexes), and will be prominently highlighted in each of the following sections. There is much controversy on the actual existence of Precambrian basement within the accretionary collision zone, whereas the existence of such rocks is confirmed for the southern Mongolian Arcs [10], and trivial for the North China Craton [75, 76].

P. R. Eizenhöfer, *Subduction and Closure of the Palaeo-Asian Ocean along the Solonker Suture Zone: Constraints from an Integrated Sedimentary Provenance Analysis*, Springer Theses, https://doi.org/10.1007/978-981-32-9200-0_2

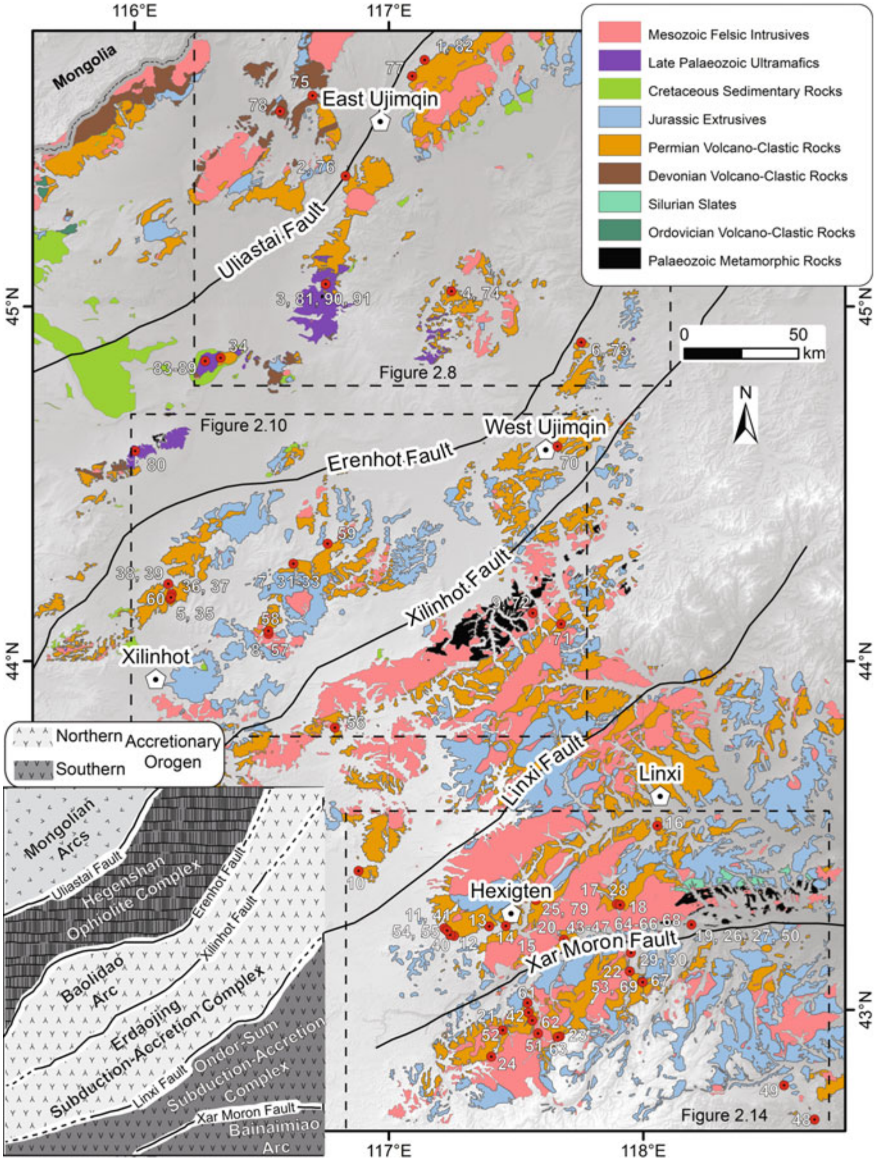

Fig. 2.1 Regional geological map of Palaeozoic and Mesozoic rocks, and sample locations, in the accretionary collision zone between the southern Mongolian Arcs to the north and the North China Craton to the south. For a more detailed description of the samples see Table 3.1. The distribution of geological units is based on BGMRIM [2], whereas the tectonic subdivision of the region broadly follows [18, 19, 66] and the results of this work. Legend entries refer to the predominant rock type, and do not necessarily represent all occurring rock types. Inlayer (bottom left) depicts the tectonic subdivision of the map extent

2.1 Tectonic Framework of the Accretionary Collision Zone

2.1.1 The Mongolian Arcs

The Mongolian Arcs (Figs. 1.1, 1.3 and 2.2) represent an assemblage of Palaeozoic arcs, microcontinents and Precambrian nuclei, which successively accreted onto the growing accretionary front of the Siberian Craton during the Palaeozoic northward subduction of the Palaeo-Asian Ocean [1, 58]. Their individual origin, e.g. potentially dispersed fragments of Gondwana, the Siberian, Tarim, and North China Cratons, or independent microcontinents, often remains disputed. Consequently, the Mongolian Arcs constitute a large variety of sub-terranes of variable geochronological, geochemical and tectonic character. Determined rock formation ages range from the Palaeoproterozoic to Late Palaeozoic [41], and zircon Hf isotopic compositions indicate different degrees of juvenile addition and reworking of crust during the accretionary processes [21]. Their evolution terminated with the arrival of the North China Craton in the Late Permian to Early Triassic ([58, 66], this work).

Sub-terranes of the southern Mongolian Arcs likely influenced arc basins to their south across the accretionary collision zone with the North China Craton. These southern terranes are composed of Precambrian cratonic blocks, Palaeozoic island arcs, accretionary wedges and backarc/forearc basin deposits [1]. Lamb and Badarch

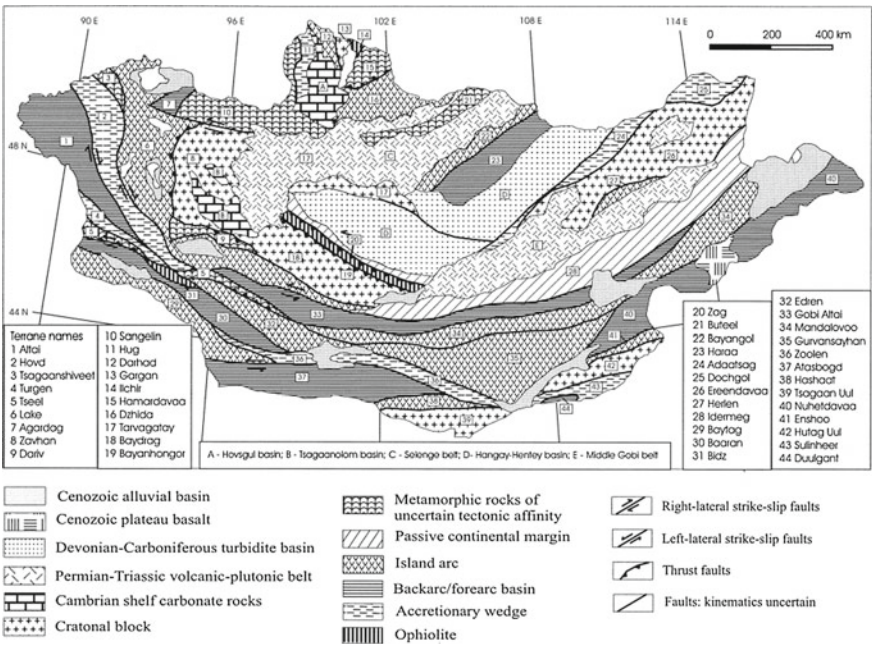

Fig. 2.2 Tectonic subdivision of Mongolia according to Badarch et al. [1]

[22] and Demoux et al. [10] proposed a mature island arc terrane (Uliastai Arc), probably atop an ancient microcontinent, which may have rifted from the Tarim Craton before it accreted onto the Mongolian Arcs [41]. The existence of such an island arc is further supported by the identification of mafic to felsic volcanic rocks as principal source for lower Mesozoic sedimentary strata in the southern Mongolian Noyon Uul syncline [14]. In addition, [15] concluded that detrital zircons from sedimentary sequences in southern Mongolia at Bulgan Uul and Nomgon along the border with China are derived from Carboniferous and Ordovician-Silurian arcs. A variety of ages, all of which potential age provenances, were reported for southern Mongolia: ca. 1.5 Ga, ca. 950 Ma and ca. 500 Ma for the emplacement of gneiss protoliths [10], ca. 916 Ma for a granitoid gneiss [56], ca. 770 Ma for an aplite in a gneiss of the southern Mongolian Tsagaan Uul Terrane [1], and ca. 330–300 Ma for granites [3, 20].

2.1.2 The North China Craton

The North China Craton (Fig. 2.3) can be generally subdivided into an eastern and a western block, separated by the Palaeoproterozoic Trans-North China Orogen. The craton is characterised by two age populations with distinct zircon Hf compositions [13, 75, 76]. A Neoarchean (ca. 2.5 Ga) craton-wide tectono-thermal event produced

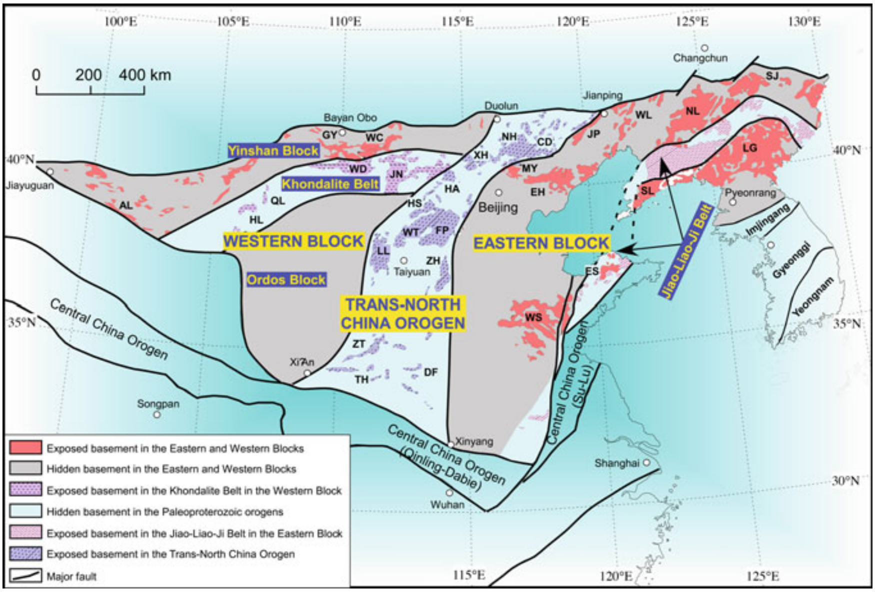

Fig. 2.3 Tectonic subdivision of the North China Craton according to Zhao et al. [75, 76]

zircons with overall positive *e*Hf values. The Palaeoproterozoic (ca. 1.85 Ga) consolidation of the craton, involving a significant reworking of older crust, formed zircons with largely negative *e*Hf values. The absence of any other ages, e.g. in Neoproterozoic to Cambrian sedimentary strata studied by Darby and Gehrels [8], signalises that the craton and its margins remained largely isolated and passive since then.

An active Andean-type continental margin developed along its northern edge, when subduction of the Palaeo-Asian Ocean was initiated in the Early Palaeozoic ([7, 32, 52, 53, 63, 66], this work). Thus, arc basins likely received eroded material from its Precambrian basement. Subsequently, the North China Craton collided with the Mongolian Arcs in the Late Permian to Early Triassic.

2.1.3 The Songliao Block

Several studies suggest that the Songliao block, located to the east of the study area (Fig. 1.3) and mostly covered by undeformed Mesozoic sedimentary rocks, contains Precambrian basement. Gneisses from drill cores yielded ages of ca. 1.8 Ga [37, 57]. Others rule out the existence of Precambrian basement [62]. Besides presenting evidence for Precambrian basement in form of such aged detrital zircons, [78] proposes that all of the tectonic units in northeast China were affected by a Pan-African event at ca. 500 Ma. However, no significant influence of the Songliao block on the arc basins in the study area was observed during this study, suggesting that it probably did not significantly affect detrital zircon age and Hf populations in the study area until the disappearance of the Palaeo-Asian Ocean.

2.2 Tectonic Subdivision of the Accretionary Collision Zone

2.2.1 The Chinese Southern Mongolian Arcs

The Chinese southern Mongolian Arcs (Fig. 2.8; also known as Uliastai active continental margin, [66]) mainly consist of Devonian to Permian arc volcanic rocks and their associated volcano-clastic sedimentary strata (Fig. 2.4). Studies indicated that these originated from an active Andean-type continental margin during both periods [44, 54]. Xiao et al. [66], corroborated by a recent deep-seismic reflection profile [74], suggest northward dipping subduction of the Palaeo-Asian Ocean from the Devonian to Late Permian. In contrast to the Hegenshan Ophiolite Complex to the south, the Permian rocks here are intercalated by or contain lenses of fossiliferous limestones, which, together with several kilometres thick clastic sedimentary strata, originate from a continental to shallow marine environment [44]. A shift from cold-water to warm-water facies in Early Permian sedimentary rocks [17] provides evidence for the general southward drift of the Mongolian Arcs during the Late Palaeozoic [66].

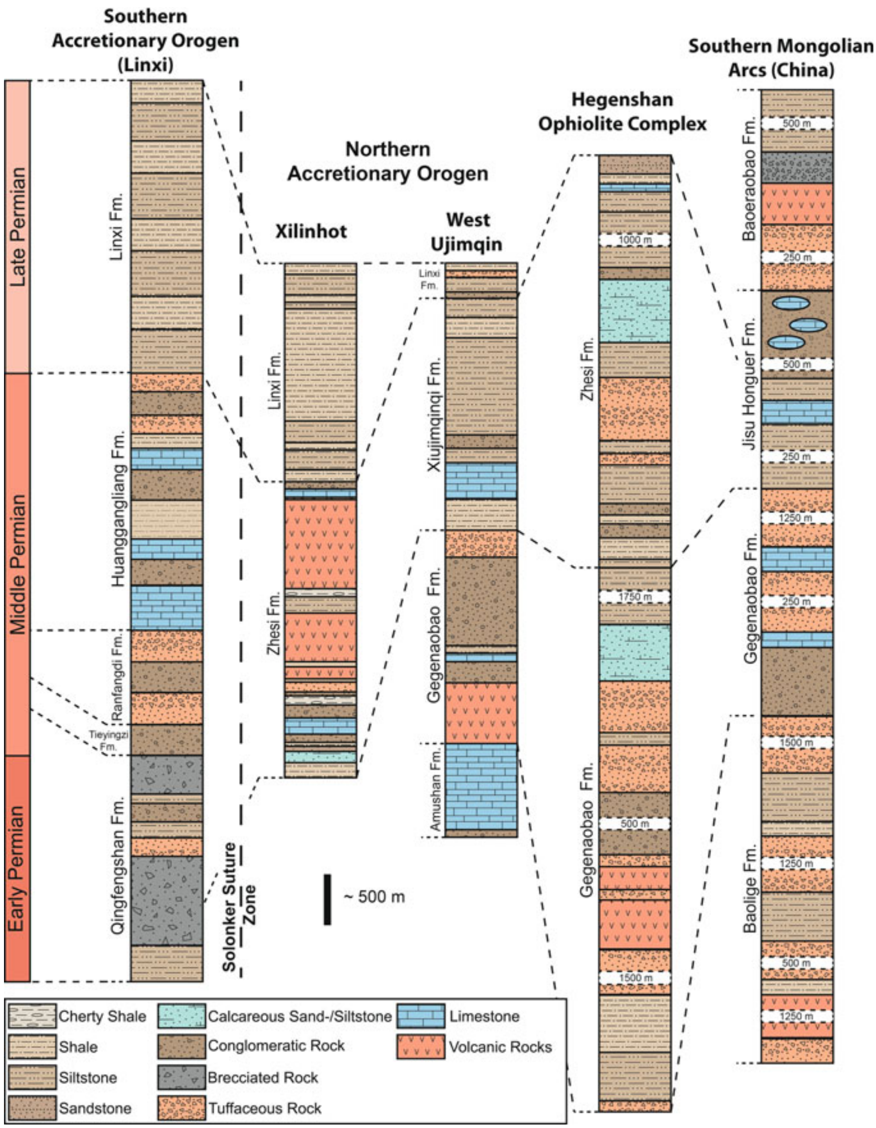

Fig. 2.4 Permian stratigraphic columns for the lithotectonic belts of the accretionary collision zone between the North China Craton and the Mongolian Arcs (modified after [2, 45]). Photographs of selected formations can be found in Figs. 2.5 and 2.6

Carboniferous rocks are not known in the study area. The accretionary processes, induced by the closure of the Palaeo-Asian Ocean, are likely responsible for the mostly sub-vertically dip of the sedimentary strata.

A Permian stratigraphic column recorded near the town of East Ujimqin (Fig. 2.4; [2, 45]) comprises from bottom to top the Baolige, the Gegenaobao, the Jisu Honguer and Baoeraobao formations, all of which dominantly consisting of volcano-clastic sedimentary strata (e.g. Fig. 2.5a). Intervals of carbonate rocks and mature sandstones may indicate several periods, during which the depositional setting resembled a temporary stable passive continental margin. Most of the sedimentary strata are interpreted as turbiditic in origin and tilted to variable degrees. Regional high-degree metamorphism does not occur or is not exposed.

The Early Permian ca. 8 km thick Baolige formation is dominated by several layers of tuffaceous rocks, interrupted by a section of volcanic rocks at its base and several intervals of brecciated rocks and finer clastic sedimentary strata. This suggests an overall volcanically active depositional environment during the Early Permian.

The Baolige formation is conformably overlain by the Early to Middle Permian ca. 3.5 km thick Gegenaobao formation, which also occurs to the south in the Hegenshan Ophiolite Complex and the Northern Accretionary Orogen. The Gegenaobao formation here contains at its base conglomerates followed by fossiliferous carbonate layers and tuffaceous breccias, and finer clastic strata towards the top (Figs. 2.5a and 2.6a). The depositional environment may have shifted from a comparatively inactive to an active volcanic setting.

The about 2.5 km thick Middle to Late Permian Jisu Honguer formation unconformably overlies the Gegenaobao formation, and is very characteristic for the absence of volcano-clastic and volcanic rocks. At its base mudstones are followed by intervals of fossiliferous limestones (Fig. 2.7), and finer to coarser grained clastic strata dotted by fossiliferous carbonate lenses. The depositional environment might have resembled a temporary passive continental margin setting.

The Permian stratigraphic column is capped by the ca. 2.5 km thick Late Permian Baoeraobao formation, which is characterised by a strong volcanic character. Brecciated volcanic rocks at the base are followed by a section of volcanic rocks, which may appear reworked within the overlying volcano-clastic breccias. The latest deposits are represented as finer clastic strata. The overall depositional environment returned to an active volcanic setting until quieter conditions concluded sediment deposition during the latest Permian.

2.2.2 The Hegenshan Ophiolite Complex

The Hegenshan Ophiolite Complex located north of the Northern Accretionary Orogen and continuing into eastern Mongolia as Enshoo terrane, while assumed to thin out further to the east (Figs. 1.3, 2.1 and 2.8), is characterised by a ca. 150 km long southwest-northeast striking belt of ophiolithic rocks (not depicted in the stratigraphic columns; Fig. 2.9a), and a several kilometres thick succession of Permian clastic sedimentary rocks. Some sections of the ophiolite are covered by fossiliferous Middle to Late Devonian limestones and Late Devonian cherts, which again are locally unconformably overlain by Permian conglomerates and breccias [17, 55]. Hence,

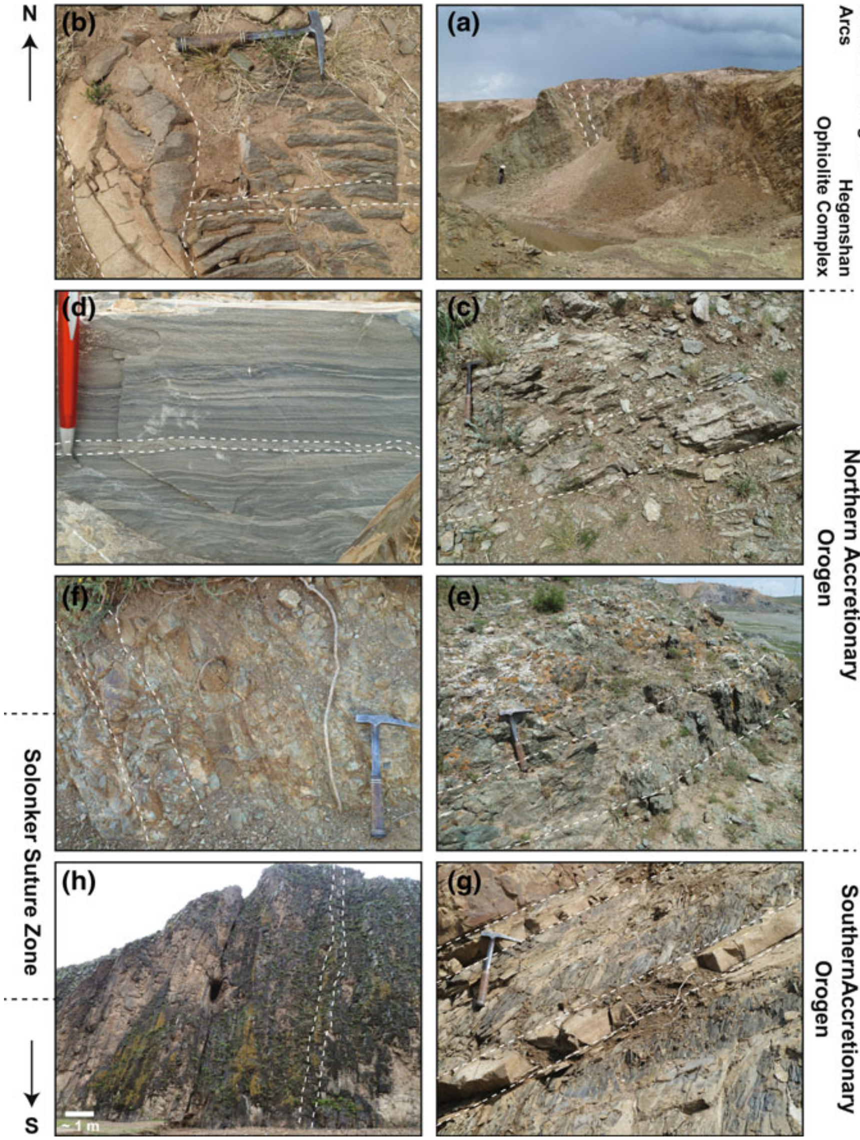

Fig. 2.5 Photographs of representative outcrops across the accretionary collision zone between the North China Craton and the Mongolian Arcs (slate 1) **a** Massive sub-vertically dipping volcano-clastic strata of the Gegenaobao formation, southern Mongolian Arcs; **b** Sandstone of the Gegenaobao formation, Hegenshan Ophiolite Complex; **c** Slightly metamorphosed and foliated volcano-clastic strata of the Gegenaobao formation, Northern Accretionary Orogen; **d** Fine-laminated siltstone of the Xiujimqinqi formation, Northern Accretionary Orogen; **e** Slightly metamorphosed volcano-clastic strata of the Zhesi formation, Northern Accretionary Orogen; **f** Volcano-clastic beds of the Linxi formation, Southern Accretionary Orogen; **g** Sandstones with intercalated mudstones of the Huanggangliang formation, Southern Accretionary Orogen; **h** Vertically dipping massive turbiditic volcano-clastic strata of the Linxi formation, Southern Accretionary Orogen

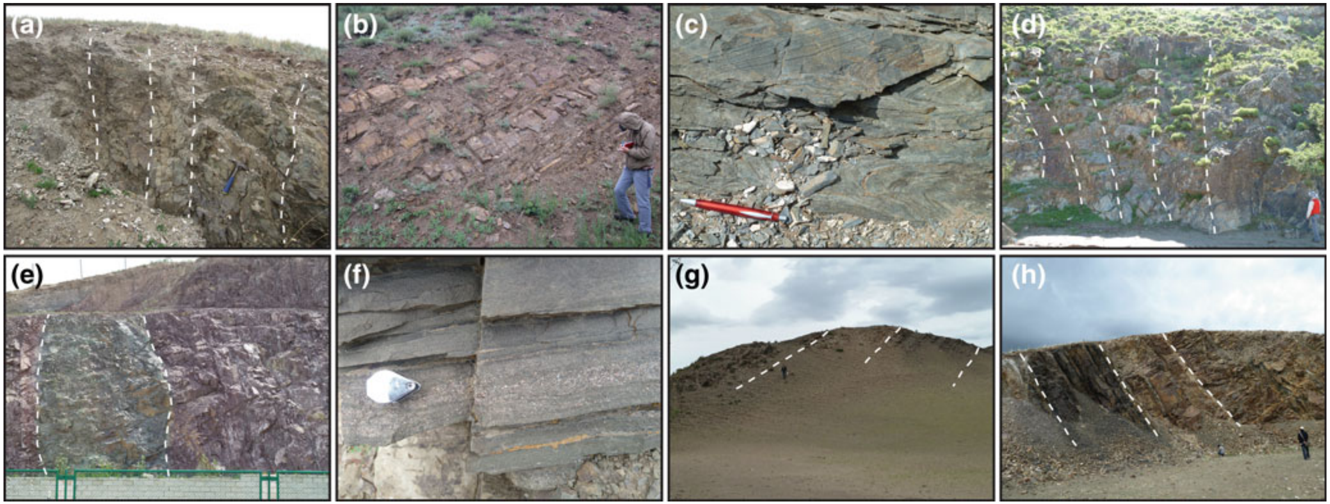

Fig. 2.6 Photographs of representative outcrops across the accretionary collision zone between the North China Craton and the Mongolian Arcs (slate 2) **a** Volcano-clastic strata and diabase intrusion in the Gegenaobao formation, Northern Accretionary Orogen; **b** Turbiditic volcano-clastic strata of the Huanggangliang formation, Southern Accretionary Orogen; **c** Folded laminated sediments of the Gegenaobao formation, Northern Accretionary Orogen; **d** Volcano-clastic succession in the Linxi formation, Southern Accretionary Orogen; **e** Slightly metamorphosed volcano-clastic strata of the Zhesi formation, Northern Accretionary Orogen; **f** Massive felsic volcanic rocks of the Huanggangliang formation, Southern Accretionary Orogen; **g** Sand-/siltstone interlayering in the Ranfangdi formation, Southern Accretionary Orogen; **h** Volcano-clastic succession within the Ranfangdi formation, Southern Accretionary Orogen; **i** Vertically dipping massive turbiditic volcano-clastic strata of the Linxi formation, Southern Accretionary Orogen

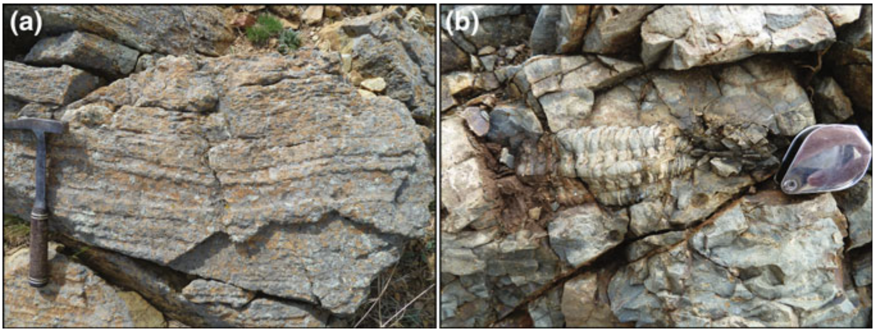

Fig. 2.7 Middle to Late Permian fossiliferous limestones of the Jisu Honguer formation. **a** Laminated limestone; **b** Trilobite in limestone

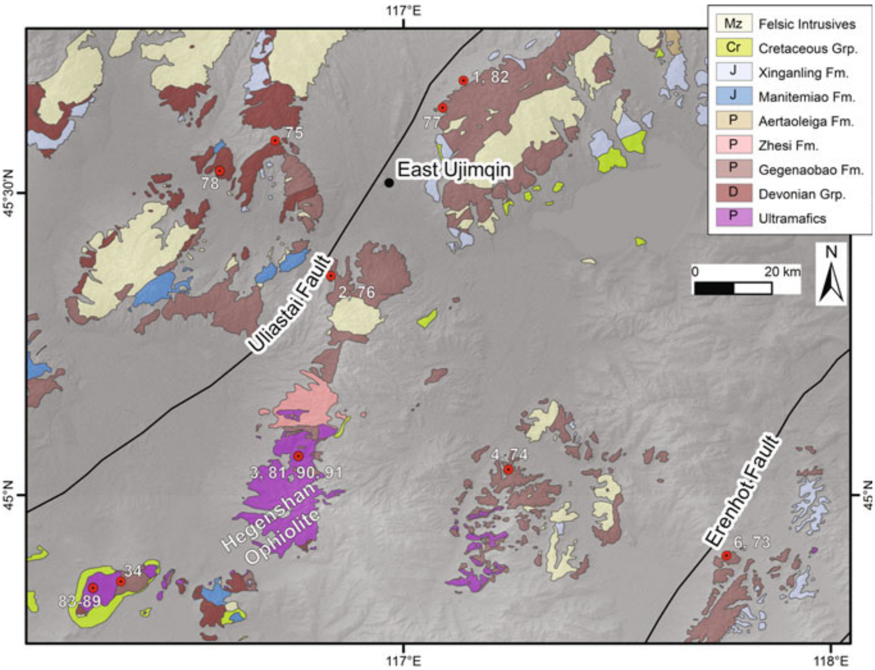

Fig. 2.8 High-resolution geological map of the Chinese southern Mongolian Arcs and the Hegenshan Ophiolite Complex, and sample locations. D: Devonian, P: Permian, J: Jurassic, Cr: Cretaceous, Mz: Mesozoic

[66] concluded, based on previous structural studies [52], that the ophiolite formed during the Middle Devonian, and was thrust onto an arc-accretion complex located to the south of the active southern Mongolian Arcs in the Late Permian to Early Triassic. However, geochemical analyses led [39, 40] to propose a back-arc basin or island arc—marginal basin origin, respectively. Miao et al. [33] further suggests

that the back-arc basin opening took place ca. 295 Ma, and, thus, the ophiolite rocks formed later as supra-subduction zone ophiolites. Bimodal volcanic rock suites southeast of the Hegenshan Ophiolite, located in the Northern Accretionary Orogen and dated at ca. 280 Ma, support this scenario [71]. Another more controversial study concluded a Mesozoic mid-ocean ridge origin for the ophiolite [36]. Consequently, the Northern Accretionary Orogen to the south may have been part of the Mongolian Arcs during the early stages of its formation, before back-arc basin opening took place in the Early Permian.

The stratigraphic column recorded across the ophiolite belt features more than 10 km of mostly clastic sedimentary strata (Fig. 2.4), making it one of the thickest across the entire accretionary collision zone between the North China Craton and the Mongolian Arcs [2, 45]. Its thickness, thus, marks the existence of a major sedimentary basin, such as a back-arc basin. It comprises the relatively homogenous Early to Middle Gegenaobao and the Middle to Late Permian Zhesi formations. The absence of distinct Permian carbonaceous strata, except for a single latest Permian layer, distinguishes it from the other tectonic units across the study area.

The Gegenaobao formation in this belt comprises at its base carbonaceous finer clastic sediments, such as siltstones and slates, overlain by arcosic sandstones and breccias. After an interval of andesites and tuffs, carbonaceous sandstones and conglomerates follow atop (Fig. 2.5b). Sandstones and slates, intercalated by breccias, are then followed by carbonaceous arcosic sand-, and siltstones at its top.

The Zhesi formation, in contrast, does not contain distinct intervals of volcanic rocks. Its strata are dominated by sand-, siltstones and slates, occasionally intercalated by fossiliferous limestones and interrupted by breccias. The top of the formation comprises the only well developed fossiliferous limestone horizon in the entire Permian stratigraphic column, which is capped by arcosic sandstones (Fig. 2.9b). This suggests that a shallow marine environment existed only during the Late Permian, when the back-arc basin was either filled and/or nearly closed.

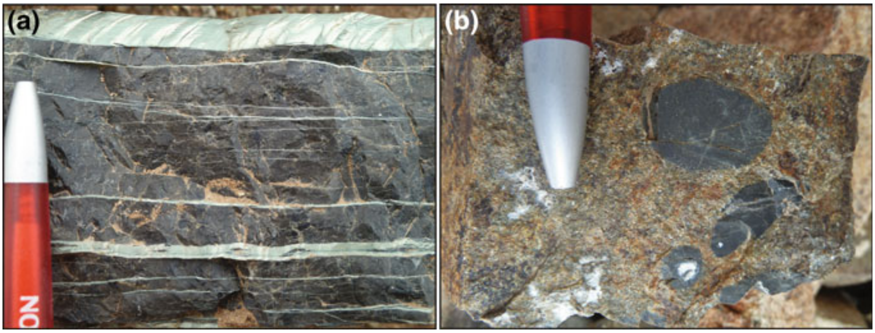

Fig. 2.9 **a** Fine-grained massive chromitite with distinct serpentinite laminae from the Hegenshan ophiolite. **b** Permian conglomeratic arcose containing well rounded chert pebbles observed near the Hegenshan ophiolite

The Permian sedimentary strata across the ophiolite belt do not share the same dominantly volcano-clastic lithology as those to the north or south. Nevertheless, the Middle Permian section contains volcanic rocks pointing at some volcanic activity, which appears to have ceased towards the Late Permian. The degree of sedimentary maturity also increases from base to top. The often carbonaceous clastic strata, especially in the Gegenaobao formation, may be derived from the rift shoulders, namely the Northern Accretionary Orogen and the southern Mongolian Arcs, where several well developed limestone intervals occur.

2.2.3 The Northern Accretionary Orogen

Situated to the south of the Hegenshan Ophiolite Complex and the Erenhot fault (Figs. 1.3, 2.1 and 2.10), the Northern Accretionary Orogen is subdivided by the Xilinhot fault into the northern Baolidao arc and the southern Erdaojing subduction-accretion complex [6, 18, 19, 66], both of which striking southeast-northwest. The lithology in both belts is dominated by Late Palaeozoic volcanic arc rocks and turbiditic volcano-clastic strata (Fig. 2.5c), which makes their distinction in the field difficult. Isolated low-grade metamorphic complexes, such as the Xilinhot complex,

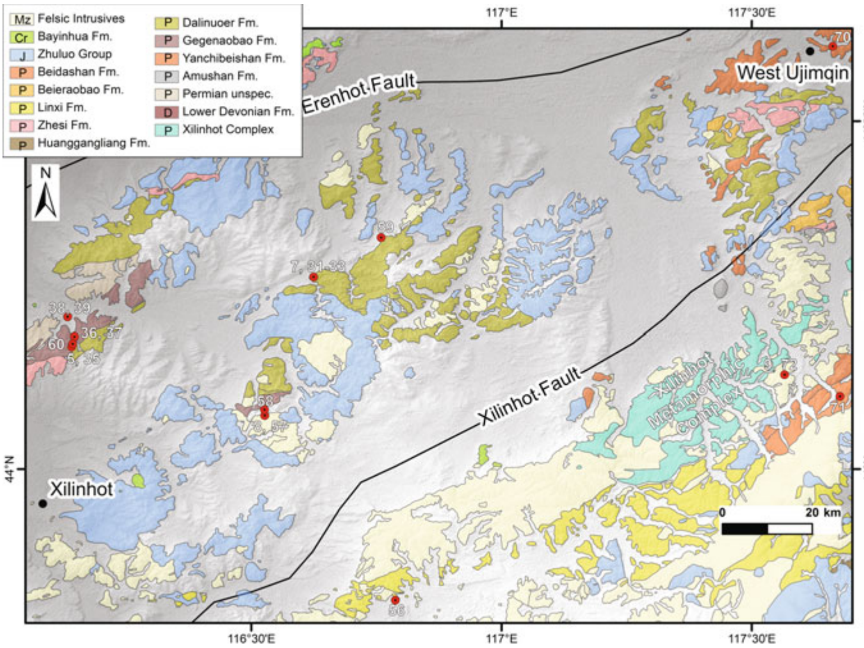

Fig. 2.10 High-resolution geological map of the Northern Accretionary Orogen, and sample locations. D: Devonian, P: Permian, J: Jurassic, Cr: Cretaceous, Mz: Mesozoic

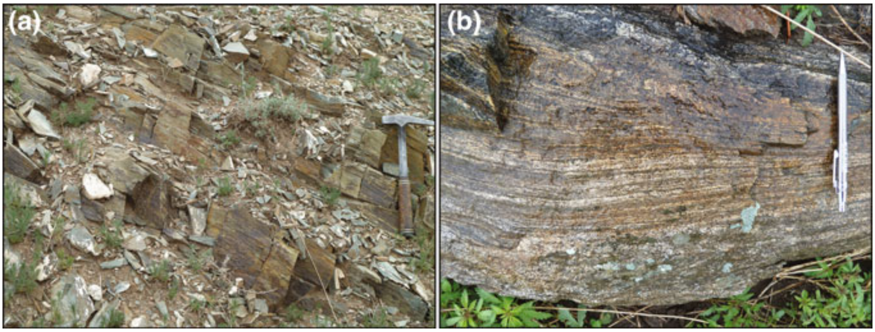

Fig. 2.11 **a** Fine-grained Permian siltstones slightly metamorphosed to low-degree greenschist facies. **b** Biotite-plagioclase paragneiss of the Xilinhot metamorphic complex

and ophiolite slivers, however, appear to only occur in the Erdaojing subduction-accretion complex. In the Permian intercalations of fossiliferous limestones (Fig. 2.4; [2]) are common, in contrast to the neighbouring Hegenshan ophiolite complex to the north, suggesting a relatively stable shallow marine environment along the orogen. Sections of distant turbidites can appear as fine laminated siltstones (Fig. 2.5d). However, most of the turbidites crop out as slightly metamorphosed (Fig. 2.11a) or undeformed decimetre-scaled, tilted beds of mud-, silt- and sandstones (Figs. 2.12, 2.5e and f). These observations suggest that the Permian accretionary processes were not accompanied by regional medium- to high grade metamorphism or deformation, similar to the Southern Accretionary Orogen. Nan and Guo [34] concluded that the volcano-clastic strata to the north formed in an island arc to back-arc basin setting, which is consistent with the back-arc basin scenario for the evolution of Hegenshan Ophiolite Complex situated to the north.

Unresolved controversies surround the nature of the Northern Accretionary Orogen, which developed along the northern margin of the Palaeo-Asian Ocean during the Palaeozoic ([18, 19], this work). Some researchers argue that it contains Precambrian basement extending into the Huutag Uul terrane in eastern Mongolia ([1, 25, 26, 28], Fig. 1.3). Others explain the occurrence of Precambrian ages as detrital, originating from the Mongolian Precambrian blocks to the north [6]. One group of studies favours an Early Palaeozoic consolidation of the orogen followed by a Late Palaeozoic extension within the orogen [18, 19, 71], while others suggest a continuous northward dipping subduction of the Palaeo-Asian Ocean throughout the Palaeozoic [29, 66].

The timing of arc magmatism in the Baolidao arc has not been well constrained until recently. Chen et al. [5, 6] obtained a zircon U-Pb age of 310 ± 5 Ma for a subduction-related gabbroic diorite, and zircon e_{Hf}—values (0 to +18.3) indicate a mixed juvenile and crustal source during magma production supported by respective e_{Nd} values (+2.5 to +5.6). However, a crustal component requires a certain degree of arc maturity, which needs to be clarified in subsequent studies. Similar to the Bainaimiao arc in the Southern Accretionary Orogen, plutonic arc rocks do not occur in the study region, but their shallow crustal volcanic equivalents and respective arc basins. The duration of arc activity still remains unclear. However, there is a general consensus that it lasted either continuously or episodically during the Palaeozoic [18, 19, 66].

The Erdaojing subduction-accretion complex comprises a variety of ages, which further substantiate its accretionary character and the similar tectonic nature in comparison to the Ondor-Sum subduction accretion complex in the Southern Accretionary Orogen (see Sect. 2.2.4). Thus, several studies concluded that it formed during the northward dipping subduction of the Palaeo-Asian Ocean, thus facing southwards to the open ocean. Among the dated ophiolite slivers in the belt are the Solonker (Solon Obo) ophiolite along the Chinese-Mongolian border (279 ± 10 Ma; [33, 66]), the Jiaoqier ophiolite (ca. 279 Ma; [32, 33]) and the Sonidzuoqi ophiolite (Late Silurian to Early Devonian; [73]). Plagioclase-biotite paragneisses from the Xilinhot complex (Fig. 2.11b) yielded magmatic and metamorphic U-Pb ages of 452 ± 4 Ma, and 339 ± 4 Ma [26], respectively, while [47] obtained the upper and lower intercept ages of 437 ± 3 Ma and 316 ± 3 Ma for the same gneisses. Most studies [2, 26, 47] suggest its of Precambrian origin. However, field observations during this study and other works [6] indicate that it may represent a low- to medium degree metamorphic equivalent to the predominantly volcanic and volcano-clastic lithology in the Northern Accretionary Orogen, which had been incorporated into the Erdaojing subduction-accretion complex during the Palaeozoic accretionary processes.

In comparison to the Permian sedimentary record to the north and south, the stratigraphic columns across the Northern Accretionary Orogen [2, 45] are only a few kilometres thick, comprising the Zhesi and Linxi formations in the area around Xilinhot, and the Amushan, Gegenaobao, Xiujimqinqi and Linxi formations in the area around West Ujimqin (Fig. 2.4). This may indicate that sediment deposition took place in major arc basins adjacent to, and not within, the Northern Accretionary Orogen.

The ca. 2.5 km thick Early to Middle Permian Zhesi formation can be subdivided into a lower clastic, an intermediate volcanic to volcano-clastic, and an upper carbonaceous clastic section. These strata are locally metamorphosed up to greenschist facies degree (Fig. 2.6e). The lower section contains tuffaceous slates, sandstones, and conglomerates intercalated by fossiliferous limestones. The intermediate section contains dominantly andesites and rhyolites, with intervals of fossiliferous slates. The upper section is dominated by sandstones and conglomerates, intercalated by fossiliferous limestones.

The ca. 2 km thick Late Permian Linxi formation shares much resemblance with that of the Southern Accretionary Orogen, and is likely to be of turbiditic origin. It is dominated by finer grained volcano-clastic strata, such as shales and siltstones, occasionally intercalated by sandstones and volcanic rocks. The formation thins out towards north, where it disappears in the Hegenshan Ophiolite Complex, suggesting that it represents the latest sedimentary deposit before the Late Permian to Early Triassic closure of the Palaeo-Asian Ocean.

The ca. 1 km thick Early Permian carbonaceous Amushan formation contains at its base a carbonaceous clastic section followed by fossiliferous limestone beds.

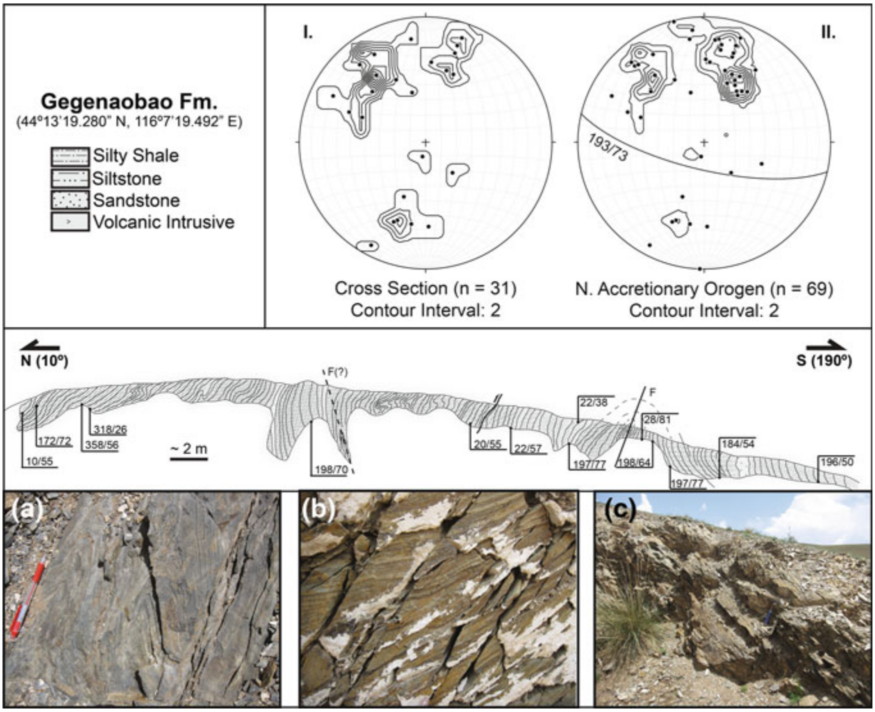

Fig. 2.12 A cross section of turbiditic sequences, slightly metamorphosed, with structural attitudes (dip azimuth/dip) in the Gegenaobao formation. Photographs show **a** isoclinal folding of fine-laminated siltstones, **b** well preserved bedding structures penetrated by angled early stages of schistosity, and **c** low-degree metamorphic turbiditic schists. Stereonets show (I.) measurements of S_0 from the cross section and S_0 for the entire Northern Accretionary Orogen. The average of all measurements is projected as dashed great circle. F: fold plane

The ca. 2 km thick Early to Middle Permian Gegenaobao formation (Fig. 2.12) contains at its base dominantly volcanic rocks, such as andesites and tuffs, occasionally intercalated by slates and conglomeratic sandstones (Fig. 2.6a). The section is overlain by volcano-clastic, often arcosic sand- and siltstones (Fig. 2.6c), and layers of conglomeratic sandstones. Fossiliferous limestone lenses may occur locally.

The ca. 2 km thick Middle to Late Permian Xiujimqinqi formation mainly comprises finer grained volcano-clastic strata, such as shales and siltstones. The formation contains interlayers of limestones and conglomeratic sandstones.

Similar to the Southern Accretionary Orogen, the sedimentary strata have a strong active arc affinity, but also a recycled orogenic character (Fig. 2.13). Carbonaceous intervals may indicate periods of relative tectonic quiescence and a stable bathymetry

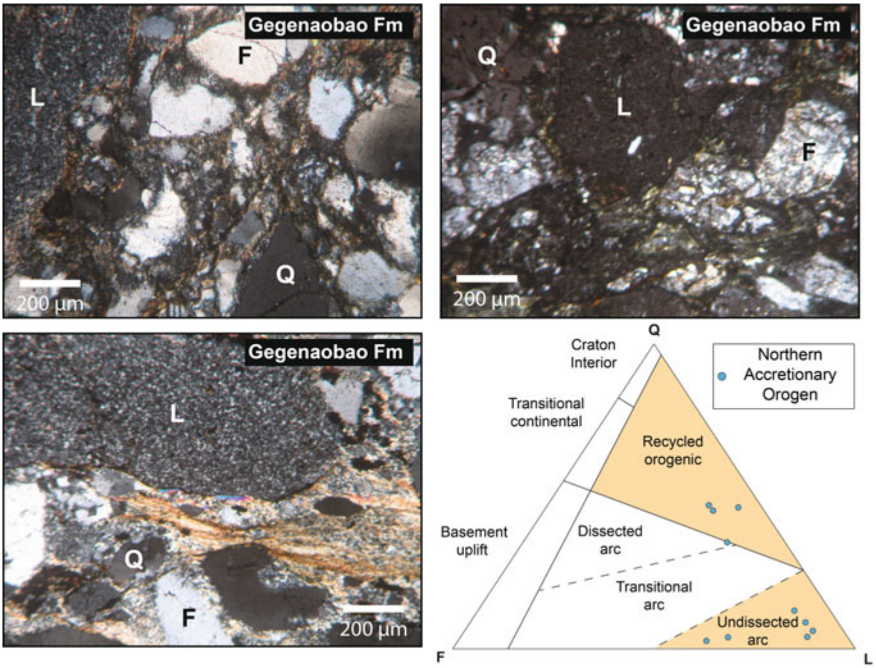

Fig. 2.13 Photomicrographs showing representative textures of sandstones from the Gegenaobao formation, and quartz-feldspar-lithics (QFL) diagram [11, 12] with point-counting results for the Northern Accretionary Orogen

along the accretionary orogen. The Linxi formation may represent the latest finer-clastic sedimentary deposits under relatively stable conditions before eventual ocean closure.

2.2.4 The Southern Accretionary Orogen

The Southern Accretionary Orogen is regarded as a Palaeozoic Andean-type continental margin along the northern edge of the North China Craton [7, 9, 32, 52, 53, 63, 66]. Situated to the south of the Northern Accretionary Orogen and the southwest-northeast striking Linxi fault, it comprises the northern Ondor-Sum subduction-accretion complex and the southern Bainaimiao arc, both of which separated by the west-southwest-east-northeast striking Xar Moron fault (Figs. 1.3, 2.1 and 2.14). While the Bainaimiao arc stretches along the northern edge of the North China Craton, it remains unclear whether the Ondor-Sum subduction accretion complex disappears, broadens or branches along the margin of the Songliao block to the east [60, 78].

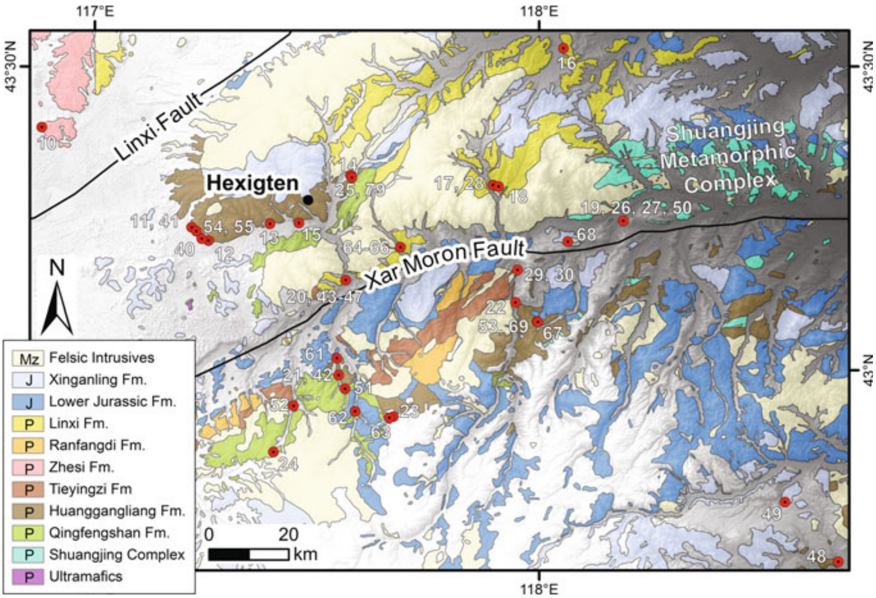

Fig. 2.14 High-resolution geological map of the Southern Accretionary Orogen, and sample locations. P: Permian, J: Jurassic, Mz: Mesozoic

The overall lithology along the accretionary orogen is dominated by Permian volcanic rocks and volcano-clastic sedimentary rocks intercalated during Middle Permian time by fossiliferous limestones (Fig. 2.4; [2]). The turbiditic strata are generally well developed, compared to their counterparts in the lithotectonic belts further north, such as well-defined alternating sandstone-mudstone beds in the Gegenaobao formation (Fig. 2.5g) and massive sub-vertically dipping turbiditic strata of the Linxi formation along the Xar Moron River (Fig. 2.5h). Intercalated limestone beds in the Huanggangliang formation followed by fine grained Late Permian clastic strata of the Linxi formation immediately prior to the closure of the Palaeo-Asian Ocean may indicate an overall shallowing upwards trend in the arc basins during the Permian.

Similar in tectonic nature to the adjacent Erdaojing subduction-accretion complex to the north, the Ondor-Sum subduction-accretion complex contains isolated metamorphic complexes and slivers of ophiolithic rocks, but also Silurian slates, all of which largely absent along the Bainaimiao arc right to its south. It is thus interpreted as the accretionary wedge/melange, which developed along the Bainaimiao arc during the southward dipping subduction of the Palaeo-Asian Ocean beneath the North China Craton [66]. Ages of ophiolithic rock slivers summarised by Xiao et al. ([63], and references therein) are ca. 260 Ma for the Ondor-Sum ophiolite and ca. 256 Ma for the Banlashan ophiolite, of which the latter crops out near the Kedanshan ophiolite near the town of Linxi [52]. The Tulinkai ophiolite yielded ages between 497 Ma and 477 Ma [18]. Jong et al. [9] reported ^{40}Ar/^{39}Ar—ages of 453.2 ± 1.8 Ma and 449.4 ± 1.8 Ma for phengites from blueschist metamorphic quartzite mylonites to the west of the study area (see also [68]). Analyses of magmatic zircons in greenschists of the Shuangjing metamorphic complex, which crops out along the northern banks of the Xar Moron River, returned an age of 298 ± 2 Ma. A granite intruded into the greenschists, is 272 ± 2 Ma old. Based on these data and their own observations [24, 27] assume that the Shuangjing metamorphic complex is a greenschist metamorphic equivalent to the volcanic rocks and volcano-clastic strata in the region, formed in the Late Carboniferous to Middle Permian, similar to the Xilinhot metamorphic complex in the Northern Accretionary Orogen during the Palaeozoic accretionary processes.

Magmatic activity in the Bainaimiao arc lasted throughout the Palaeozoic, although it possibly ceased for a short period of time subsequent to the accretion of the Hunshandake microcontinent [50, 67] at ca. 300 Ma [66]. Tang and Yan [53] report a zircon U-Pb age of 466 Ma for a granodiorite porphyry near the village of Bainaimiao, while [69] obtained a muscovite K-Ar age of 430 Ma for a muscovite granite. Cope et al. [7] propose that the arc existed from ca. 400 Ma to 275 Ma. Nie and Bjørlykke [35] concluded that arc magmas were derived by mixing of mantle derived and crustal rocks.

A Late Palaeozoic stratigraphy of the region is relatively well established (Fig. 2.4; [23, 31, 45, 46, 49]). The Permian lithology across the Xar Moron River near Hexigten is dominated by the Linxi and Huangganliang formations, and undeformed Mesozoic granitic intrusions (Figs. 2.1 and 2.4). Most of the volcano-clastic strata are sub-vertical without any signs of higher-grade metamorphism. Horizontally bedded Jurassic volcanic strata unconformably overlie the entire region (Fig. 2.15). A several kilometres thick Permian stratigraphic column near the town of Linxi [2, 45] comprises from Early to Late Permian the volcano-clastic Qingfengshan, Ranfangdi, Huanggangliang and Linxi formations. Each of the formations contain intervals of volcanic rocks, although not always depicted as such in the stratigraphic column (Fig. 2.4). Most sedimentary strata are interpreted to be of turbiditic origin.

The upper section of the ca. 2 km thick Early Permian Qingfengshan formation constitutes a larger fraction of lava flows, andesites and diabases. The volcano-clastic sedimentary rocks appear overall coarser grained as breccias and conglomerates, intercalated by shales, silt- and sandstones.

The only ca. 400 m thick Tieyingzi formation consists dominantly of fossiliferous conglomeratic sandstones, which can be intercalated by tuffs.

Fig. 2.15 **a** Permian sedimentary strata unconformably overlain by horizontal Jurassic basalts on the southern bank of the Xar Moron River. **b** Felsic dikes cross-cutting the Huanggangliang formation

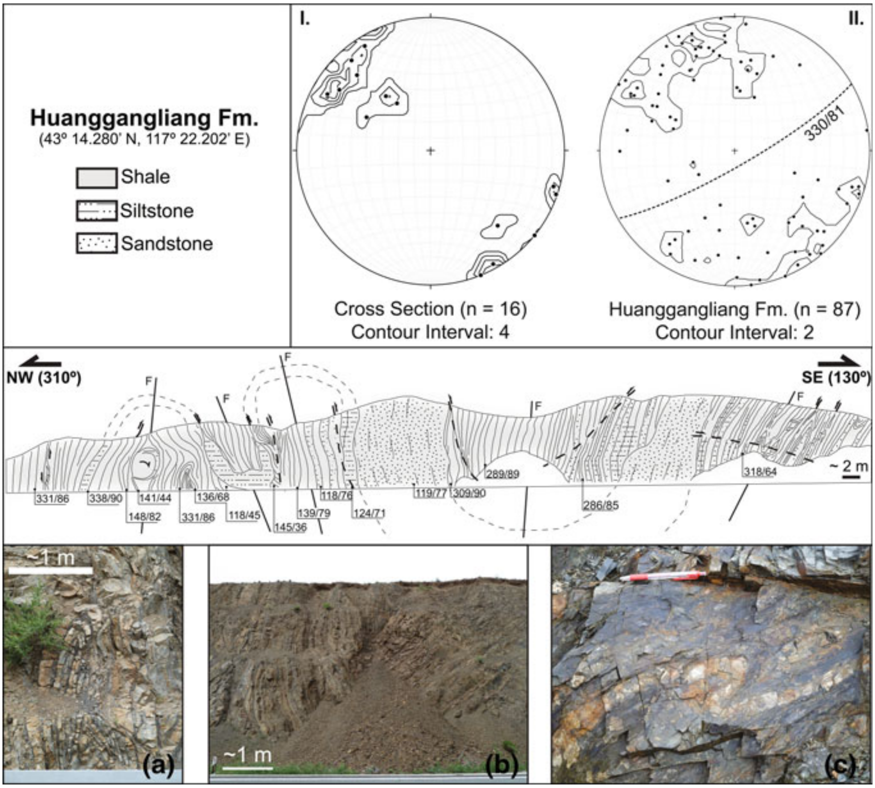

Fig. 2.16 A cross section of turbiditic sequences with structural attitudes (dip azimuth/dip) in the Huanggangliang formation. Photographs show **a** isoclinal fold, **b** open upright fold, and **c** shear fold. Stereonets show (I.) measurements of S_0 from the cross section and S_0 for the formation in the entire study area. The average of all measurements is projected as dashed great circle. F: fold plane

A comparatively higher degree of volcanic activity is recorded in the ca. 1 km thick Middle Permian Ranfangdi formation, in which tuffs, andesites and rhyolites crop out next to non-fossiliferous conglomeratic sandstones, tuffaceous rocks and breccias (Fig. 2.6g and h).

The ca. 3 km thick Middle Permian Huanggangliang formation is divided into a lower fossiliferous and an upper non-fossiliferous section. The lower section comprises andesites (Fig. 2.6f), slates, tuffaceous sandstones, conglomerates, and thick layers of carbonate rocks, whereas the upper section is exclusively represented by sedimentary rocks, e.g. conglomerates, sand-, siltstones, and slates (Fig. 2.6b). Cross-sections show open upright folding, thrust directions generally towards southeast or northwest, while shear folding, probably related to syn-sedimentary compression, can be observed as well (Fig. 2.16).

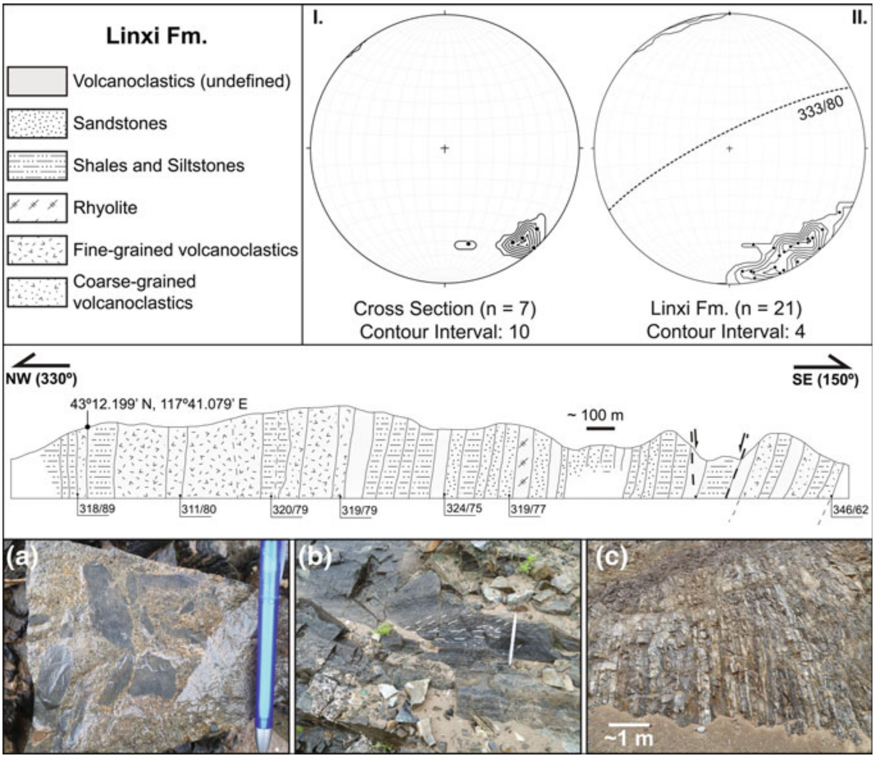

Fig. 2.17 A cross section of turbiditic sequences with structural attitudes (dip azimuth/dip) in the Linxi formation. Photographs show **a** conglomeratic arcose, **b** signs of cross-stratification in greywackes, and **c** vertical bedding of fine-grained turbiditic succession. Stereonets show (I.) measurements of S_0 from the cross section and S_0 for the formation in the entire study area. The average of all measurements is projected as dashed great circle

The ca. 3 km thick Late Permian Linxi formation is characterised by fine grained volcano-clastic strata including slates and siltstones, intercalated occasionally by sandstones and andesites (Fig. 2.6d and i). Although typical turbiditic patterns (e.g. cross-stratification, graded or convolute bedding) are rare, a turbiditic origin on a regional scale is assumed. In comparison to the Huanggangliang formation, thrust faults are rare, if not absent (Fig. 2.17). Some authors [45] propose a terrestrial origin. Since this formation recorded the final closure of the Palaeo-Asian Ocean, a marine origin deems more likely.

The overall volcano-clastic character, interrupted by carbonate production during the Middle Permian, suggest an active arc setting in a comparatively shallow marine depositional environment throughout the Permian (Fig. 2.18). The homogenous finer-clastic Linxi formation to the top may be indicative for a stabilised tectonic

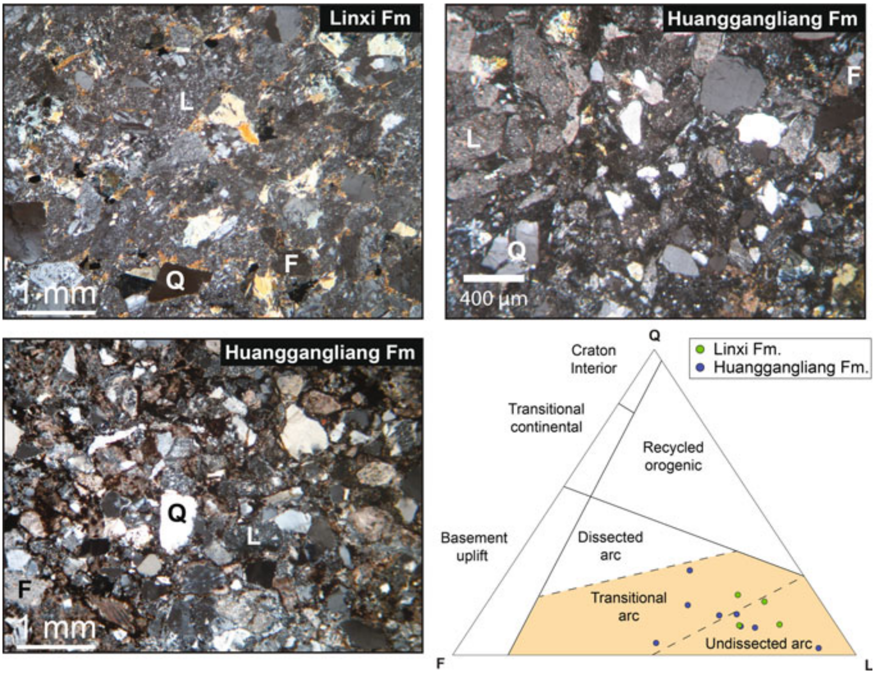

Fig. 2.18 Photomicrographs showing representative textures of greywackes from the Linxi and Huanggangliang formations, and quartz-feldspar-lithics (QFL) diagram [11, 12] with point-counting results for the Southern Accretionary Orogen

environment, in comparison to the coarser-grained base of the stratigraphic column, probably due to the successive cessation of volcanic arc activity during the final stages of ocean closure.

2.3 Formation of the Solonker Suture Zone and Closure of the Palaeo-Asian Ocean—A Review

Many controversies surround the formation of the Solonker Suture Zone, which is interpreted as the eastward continuation of the Tian Shan Suture in the central southern part of the Central Asian Orogenic Belt (Fig. 1.1; [58, 64, 66]). In contrast to many other sutures (e.g. in the Alpine, Dabie-Sulu, Himalayan collisional belts) it is not characterised by a continuous ophiolite belt. Instead, displaced ophiolithic rocks occur relatively randomly (Fig. 1.3), integrated into subduction-accretion complexes ranging in size from a single outcrop (e.g. the Kedanshan ophiolite) to kilometre-sized bodies (e.g. the Hegenshan ophiolite). The situation is further complicated by a Palaeozoic archipelago-type tectonic setting (Fig. 1.2b; [58, 66]), comparable only to present-day Southeast Asia or the Cordilleran and Andean continental arcs. Hence, some authors [42, 65] coined the term "Cryptic Sutures" for such broad and diffuse accretionary collision belts.

There has been much debate on whether the Solonker Suture Zone was formed by episodic [18, 19] or continuous [5, 6, 66] tectonic activity caused by subduction of oceanic lithosphere. The question of whether the final collision took place by southward dipping subduction beneath the northern margin of the North China Craton or northward subduction beneath the southward growing accretionary margin of the Siberian Craton (e.g. the Mongolian Arcs), as well as the actual subduction type (continental or oceanic) and its geometry (one-sided, double-sided, multiple), remain unresolved. Most researchers [6, 9, 18, 19, 23, 30, 59, 61, 66, 70, 72, 73], locate the final closure of the Palaeo-Asian Ocean along the banks of the Xar Moron River. Wu et al. [59, 61] traced it farther towards the far east, where it was offset by several major fault systems (the Yitong-Yilan fault and the Dunhua-Mishan fault), away from the Xar Moron River. However, some authors (e.g. [36, 44, 52]) assume that the final collision took place further north near the Hegenshan ophiolite complex [33, 39, 40]. Proposed ages for the final suturing vary from the Late Devonian to the middle Mesozoic. In summary, many past models are temporally and spatially contrary to the most recent ones, of which the two most widely accepted will be elaborated below.

According to the tectonic model proposed by Li [23], Jian et al. [18, 19] (Fig. 2.19a and b) the Solonker Suture Zone is located along the northern bank of the Xar Moron River. Northwards it is bound by the northeast trending Linxi fault and southwards by the northeast oriented Xar Moron fault. The Linxi fault separates the Solonker Suture Zone from an accretionary belt, named the Northern Orogen (equal to the Northern Accretionary Orogen in this study; [18]), which comprises accretionary and metamorphic complexes such as the Xilinhot complex along the Xilinhot fault [6, 47]. Situated south of the Solonker Suture Zone defined by Jian et al. [18] is the Southern Orogen (equal to the Southern Accretionary Orogen in this study), which is considered to have successively developed along the northern margin of the North China Craton during the Palaeozoic. The orogen comprises subduction-accretion complexes including the Ondor-Sum subduction-accretion complex [6, 9, 68], whereas earlier outdated studies assumed the existence of an east-west trending "Wendur-Miao—Xar Moron Ophiolite Belt" (see [4]). Jian et al. [18, 19] argued that the North China and Siberian Cratons were separated by the Palaeo-Asian Ocean and a microcontinent during the Cambrian. By the end of the Cambrian intra-oceanic southward dipping subduction led to arc volcanism and ophiolite formation, while northward dipping subduction occurred beneath a microcontinent. Subsequently, concurrent ridge subduction beneath the volcanic arcs in the south and north caused high-grade metamorphism in the Ordovician and the Silurian. The end-Silurian collision of several microcontinents eventually terminated subduction on both sides by forming the Southern and Northern Orogens, while they were still separated by the Palaeo-Asian Ocean. During Early Permian time, tectonic activity continued with subduction, arc formation and ridge-trench collision along the Southern Orogen. By then, the Southern Orogen was amalgamated with the northern margin of North

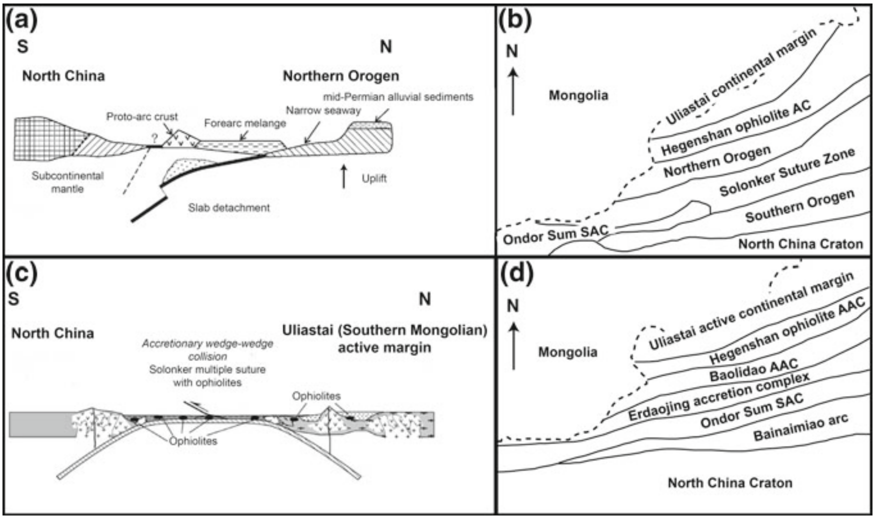

Fig. 2.19 Previous tectonic models for the formation of the Solonker Suture Zone during the Late Permian. **a** single-sided subduction model according to Jian et al. [18, 19] with its tectonic subdivision (**b**), and **c** double-sided subduction model according to Xiao et al. [63, 66] with its tectonic subdivision (**d**). AAC: arc-accretion complex; SAC: subduction-accretion complex; AC: accretion complex

China. Meanwhile, bimodal volcanism occurred in the Northern Orogen. The final closure of the Palaeo-Asian Ocean in the Late Permian led to the formation of the Solonker Suture Zone.

Xiao et al. [63, 66] (Fig. 2.19c and d), however, proposed a model with a slightly different subdivision of tectonic units in the region. In this model the Solonker Suture Zone is represented by the Erdaojing accretion complex. Thus, it is shifted to the north and narrower. The Erdaojing accretion complex is juxtaposed towards north against the Baolidao arc-accretion complex [6], and towards south against the Ondor-Sum subduction-accretion complex [9, 68]. Closure of the Palaeo-Asian Ocean started with north-directed intra-oceanic subduction, forming the Ulan arc and the attached Ondor-Sum subduction-accretion complex. In the Ordovician—Silurian the Ulan arc and the Ondor-Sum subduction accretion complex were accreted onto the northern margin of north China, while subduction took place southward beneath the North China Craton. Meanwhile, subduction had also been initiated along the southern margin of the Mongolian arc terranes (the southernmost extent of the accretionary disk encircling the Siberian Craton), forming the Uliastai active continental margin north of the Hegenshan ophiolite arc-accretion complex. The contemporary double-sided subduction beneath the North China Craton and the Mongolian arc terranes, as well as simultaneous intra-oceanic subduction, led to a “soft-collision” of two opposing accretionary wedges [43] and the final closure of the Palaeo-Asian Ocean in the Late Permian. This model would explain the absence of continental deep subduction, regional medium- to high-grade metamorphism, large-scale thrust faults and distinct mountain topology. The detachment of the oceanic from continental crust, as a result of such subduction geometry, may promote the emplacement of post-collisional A-type granitic plutons. Such post-collisional granites were identified in the southern Mongolian Arcs [16], and in the Xilinhot complex [48]. As will be outlined in the following chapters, the conclusions made in this thesis favour this model.

The above outlined two tectonic models [18, 19, 63, 66] are different in their subduction geometries and definition of tectonic units that were involved during the closure of the Palaeo-Asian Ocean. Both models need to be improved with respect to the continuation of the lithotectonic belts to the east and west. Notably, the suggested tectonic relationships between the tectonic units prior to the formation of the Solonker Suture Zone remain inconsistent. Like most authors (e.g. [28, 29, 58, 66]) both models support a Late Permian to Early Triassic ocean closure. However, proposed ages for the timing of final suturing range from the Devonian [52, 77], through Carboniferous [67], to the Mesozoic [36]. Geometry, timing and tectonic evolution of the Solonker Suture Zone are all issues to be addressed in this dissertation.

References

1. Badarch G, Cunningham WD, Windley BF (2002) A new terrane subdivision for Mongolia: implications for the Phanerozoic crustal growth of Central Asia. J Asian Earth Sci 21(1):87–110
2. BGMRIM (1991) Regional geology of Nei Mongol (Inner Mongolia) autonomous region (in Chinese with English summary). Geological memoirs series 2, vol 25. Geological Publishing House, Beijing
3. Blight JH, Crowley QG, Petterson MG, Cunningham D (2010) Granites of the Southern Mongolia Carboniferous Arc: new geochronological and geochemical constraints. Lithos 116(1–2):35–52
4. Cao C (1989) The ophiolite belts of northeastern China. J Southeast Asian Earth Sci 3(1–4):233–236
5. Chen B, Jahn B, Wilde S, Xu B (2000) Two contrasting paleozoic magmatic belts in northern Inner Mongolia, China: petrogenesis and tectonic implications. Tectonophysics 328(1–2):157–182
6. Chen B, Jahn B, Tian W (2009) Evolution of the Solonker suture zone: constraints from zircon U-Pb ages, Hf isotopic ratios and whole-rock Nd-Sr isotope compositions of subduction- and collision-related magmas and forearc sediments. J Asian Earth Sci 34(3):245–257
7. Cope T, Ritts BD, Darby BJ, Fildani A, Graham SA (2005) Late Paleozoic sedimentation on the Northern margin of the North China block: implications for regional tectonics and climate change. Int Geol Rev 47(3):270–296
8. Darby BJ, Gehrels G (2006) Detrital zircon reference for the North China block. J Asian Earth Sci 26(6):637–648
9. de Jong K, Xiao W, Windley BF, Masago H, Lo C-H (2006) Ordovician 40Ar/39Ar phengite ages from the blueschist-facies Ondor Sum subduction-accretion complex (Inner Mongolia) and implications for the early Paleozoic history of continental blocks in China and adjacent areas. Am J Sci 306(10):799–845
10. Demoux A, Kröner A, Liu D, Badarch G (2009) Precambrian crystalline basement in southern Mongolia as revealed by SHRIMP zircon dating. Int J Earth Sci 98(6):1365–1380

11. Dickinson W (1985) Interpreting provenance relations from detrital modes of sandstones. In: Zuffa G (ed) Provenance of arenites, vol 148. Springer, Netherlands, pp 333–361
12. Dickinson W, Beard L, Brakenridge G, Erjavec J, Ferguson R, Inman K, Knepp R, Lindberg F, Ryberg P (1983) Provenance of North American Phanerozoic sandstones in relation to tectonic setting. Geol Soc Am Bull 94(2):222–235
13. Geng Y, Du L, Ren L (2012) Growth and reworking of the early Precambrian continental crust in the North China Craton: constraints from zircon Hf isotopes. Gondwana Res 21(2–3):517–529 (Special Issue: Western Gondwana)
14. Hendrix MS, Graham SA, Amory JY, Badarch G (1996) Noyon Uul syncline, southern Mongolia: lower Mesozoic sedimentary record of the tectonic amalgamation of central Asia. Geol Soc Am Bull 108(10):1256–1274
15. Heumann MJ, Johnson CL, Webb LE, Taylor JP, Jalbaa U, Minjin C (2012) Paleogeographic reconstruction of a late Paleozoic arc collision zone, southern Mongolia. Geol Soc Am Bull 124(9–10):1514–1534
16. Hong D, Chang W, Huang H, Xiao Y, Xu H, Jin M (1994) The Permian alkaline granites in Central Inner Mongolia and their geodynamic significance. J Southeast Asian Earth Sci 10(3–4):169–176
17. Hsu KJ, Wang Q, Li L, Hao J (1991) Geologic evolution of the Neimonides: a working hypothesis. Eclogae geologicae helvetiae 84(1):31
18. Jian P, Liu D, Kröner A, Windley BF, Shi Y, Zhang F, Shi G, Miao L, Zhang W, Zhang Q, Zhang L, Ren J (2008) Time scale of an early to mid-Paleozoic orogenic cycle of the long-lived Central Asian Orogenic Belt, Inner Mongolia of China: implications for continental growth. Lithos 101(3–4):233–259
19. Jian P, Liu D, Kröner A, Windley BF, Shi Y, Zhang W, Zhang F, Miao L, Zhang L, Tomurhuu D (2010) Evolution of a Permian intraoceanic arc-trench system in the Solonker suture zone, Central Asian Orogenic Belt, China and Mongolia. Lithos 118(1–2):169–190
20. Kovalenko VI, Yarmoluyk VV, Sal'nikova EB, Kozlovsky AM, Kotov AB, Kovach VP, Savatenkov VM, Vladykin NV, Ponomarchuk VA (2006) Geology, Geochronology, and Geodynamics of the Khan Bogd alkali granite pluton in southern Mongolia. Geotectonics 40(6):450–466
21. Kröner A, Kovach V, Belousova E, Hegner E, Armstrong R, Dolgopolova A, Seltmann R, Alexeiev DV, Hoffmann JE, Wong J, Sun M, Cai K, Wang T, Tong Y, Wilde SA, Degtyarev KE, Rytsk E (2014) Reassessment of continental growth during the accretionary history of the Central Asian Orogenic Belt. Gondwana Res 25(1):103–125
22. Lamb MA, Badarch G (1997) Paleozoic sedimentary basins and volcanic-arc systems of southern mongolia: new stratigraphic and sedimentologic constraints. Int Geol Rev 39(6):542–576
23. Li J-Y (2006) Permian geodynamic setting of Northeast China and adjacent regions: closure of the Paleo-Asian Ocean and subduction of the Paleo-Pacific Plate. J Asian Earth Sci 26(3–4):207–224
24. Li J, Gao L, Sun G, Li Y, Wang Y (2007) Shuangjingzi middle Triassic syn-collisional crust-derived granite in the east Inner Mongolia and its constraint on the timing of collision between Siberian and Sino-Korean paleo-plates. Acta Petrol Sin 23(3):565–582
25. Li D, Chen Y, Wang Z, Hou K, Liu C (2011) Detrital zircon U-Pb ages, Hf isotopes and tectonic implications for Palaeozoic sedimentary rocks from the Xing-Meng orogenic belt, middle-east part of inner Mongolia China. Geol J 46(1):63–81
26. Li Y, Zhou H, Brouwer FM, Wijbrans JR, Zhong Z, Liu H (2011) Tectonic significance of the Xilin Gol Complex, Inner Mongolia, China: petrological, geochemical and U-Pb zircon age constraints. J Asian Earth Sci 42(5):1018–1029
27. Li Y, Zhou H, Brouwer FM, Xiao W, Zhong Z, Wijbrans JR (2011) Late Carboniferous-Middle Permian arc/forearc-related basin in Central Asian Orogenic Belt: insights from the petrology and geochemistry of the Shuangjing Schist in Inner Mongolia, China. Isl Arc 20(4):535–549
28. Li Y, Zhou H, Brouwer F, Xiao W, Wijbrans J, Zhao J, Zhong Z, Liu H (2014) Nature and timing of the Solonker suture of the Central Asian Orogenic Belt: insights from geochronology and geochemistry of basic intrusions in the Xilin Gol Complex, Inner Mongolia China. Int J Earth Sci 103(1):41–60

29. Li Y, Zhou H, Brouwer FM, Xiao W, Wijbrans JR, Zhong Z (2014) Early Paleozoic to Middle Triassic bivergent accretion in the Central Asian Orogenic Belt: insights from zircon U-Pb dating of ductile shear zones in central Inner Mongolia China. Lithos 205:84–111
30. Lin W, Faure M, Nomade S, Shang Q, Renne PR (2008) Permian-Triassic amalgamation of Asia: insights from Northeast China sutures and their place in the final collision of North China and Siberia. C R Geosci 340(2–3):190–201
31. Manankov I, Shi G, Shen S (2006) An overview of Permian marine stratigraphy and biostratigraphy of Mongolia. J Asian Earth Sci 26(3–4):294–303 (Permian of East and Northeast Asia)
32. Miao L, Zhang F, Fan W-M, Liu D (2007) Phanerozoic evolution of the Inner Mongolia-Daxinganling orogenic belt in North China: constraints from geochronology of ophiolites and associated formations. Geol Soc Lond Spec Publ 280(1):223–237
33. Miao L, Fan W, Liu D, Zhang F, Shi Y, Guo F (2008) Geochronology and geochemistry of the Hegenshan ophiolitic complex: implications for late-stage tectonic evolution of the Inner Mongolia-Daxinganling Orogenic Belt China. J Asian Earth Sci 32(5–6):348–370
34. Nan R, Guo S (1992) Paleozoic biostratigraphy and palaeo-geography in the geosynclinal region of Nei Mongol and Northeast China. Geological Publishing House, Beijing
35. Nie F, Bjørlykke A (1999) Nd and Sr isotope constraints on the age and origin of Proterozoic meta-mafic volcanic rocks in the Bainaimiao-Wenduermiao district, south-central Inner Mongolia, China. Cont Dyn 4:1–14
36. Nozaka T, Liu Y (2002) Petrology of the Hegenshan ophiolite and its implication for the tectonic evolution of northern China. Earth Planet Sci Lett 202(1):89–104
37. Pei F, Xu W, Yang D, Zhao Q, Liu X, Hu Z (2007) Zircon U-Pb geochronology of basement metamorphic rocks in the Songliao Basin. Chin Sci Bull 52(7):942–948
38. Popov V, Khramov A, Bachtadse V (2005) Palaeomagnetism, magnetic stratigraphy, and petromagnetism of the Upper Vendian sedimentary rocks in the sections of the Zolotitsa River and in the Verkhotina Hole, Winter Coast of the White Sea, Russia. Russ J Earth Sci 7(2):1–29
39. Robinson P, Zhou M, Hu X, Reynolds P, Bai W, Yang J (1995) Geochemical constraints on petrogenesis and crustal accretion of the Hegenshan ophiolite, Northern China. Acta Petrol Sin 11:112–124
40. Robinson P, Zhou M-F, Hu X-F, Reynolds P, Wenji B, Yang J (1999) Geochemical constraints on the origin of the Hegenshan Ophiolite, Inner Mongolia. China. J Asian Earth Sci 17(4):423–442
41. Rojas-Agramonte Y, Kröner A, Demoux A, Xia X, Wang W, Donskaya T, Liu D, Sun M (2011) Detrital and xenocrystic zircon ages from Neoproterozoic to Palaeozoic arc terranes of Mongolia: Significance for the origin of crustal fragments in the Central Asian Orogenic Belt. Gondwana Res 19(3):751–763 (Island Arcs: Their role in growth of accretionary orogens and mineral endowment)
42. Schulmann K, Lexa O, Janoušek V, Lardeaux JM, Edel JB (2014) Anatomy of a diffuse cryptic suture zone: An example from the Bohemian Massif, European Variscides. Geology 42(4):275–278
43. Şengör A, Okurogullari A (1991) The role of accretionary wedges in the growth of continents-asiatic examples from argand to plate-tectonics. Eclogae Geologicae Helvetica 84:535–597
44. Shao J (1989) Continental crust accretion and tectono-magmatic activity at the northern margin of the Sino-Korean plate. J Southeast Asian Earth Sci 3(1–4):57–62
45. Shen S-Z, Zhang H, Shang Q, Li W-Z (2006) Permian stratigraphy and correlation of Northeast China: a review. J Asian Earth Sci 26(3–4):304–326 (Permian of East and Northeast Asia)
46. Shi G (2006) The marine Permian of East and Northeast Asia: an overview of biostratigraphy, palaeobiogeography and palaeogeographical implications. J Asian Earth Sci 26(3–4):175–206 (Permian of East and Northeast Asia)
47. Shi G, Liu D, Zhang F, Jian P, Miao L, Shi Y, Tao H (2003) SHRIMP U-Pb zircon geochronology and its implications on the Xilin Gol Complex Inner Mongolia, China. Chin Sci Bull 48(24):2742–2748

48. Shi G, Miao L, Zhang F, Jian P, Fan W, Liu D (2004) Emplacement age and tectonic implications of the Xilinhot A-type granite in Inner Mongolia China. Chin Sci Bull 49(7):723–729
49. Shi G, Campi MJ, Shen S (2006) The permian of east and Northeast Asia. J Asian Earth Sci 26(3):173–174
50. Shi G, Faure M, Xu B, Zhao P, Chen Y (2013) Structural and kinematic analysis of the Early Paleozoic Ondor Sum-Hongqi melange belt, eastern part of the Altaids (CAOB) in Inner Mongolia, China. J Asian Earth Sci 66:123–139
51. Smethurst MA, Khramov AN, Torsvik TH (1998) The Neoproterozoic and Palaeozoic palaeomagnetic data for the Siberian Platform: from Rodinia to Pangea. Earth Sci Rev 43(1–2):1–24
52. Tang K (1990) Tectonic development of Paleozoic foldbelts at the north margin of the Sino-Korean Craton. Tectonics 9(2):249–260
53. Tang K, Yan Z (1993) Regional metamorphism and tectonic evolution of the Inner Mongolian suture zone. J Metamorph Geol 11(4):511–522
54. Wang Y (1996) Tectonic evolutional processes of inner Mongolia-Yanshan Orogenic Belt in Eastern China during the Late Paleozoic-Mesozoic. Geological Publishing House, Beijing
55. Wang Q, Liu X (1986) Paleoplate tectonics between Cathaysia and Angaraland in inner Mongolia of China. Tectonics 5(7):1073–1088
56. Wang T, Zheng Y, Gehrels GE, Mu Z (2001) Geochronological evidence for existence of South Mongolian microcontinent-A zircon U-Pb age of grantoid gneisses from the Yagan-Onch Hayrhan metamorphic core complex. Chin Sci Bull 46(23):2005–2008
57. Wang Y, Zhang F, Zhang D, Miao L, Li T, Xie H, Meng Q, Liu D (2006) Zircon SHRIMP U-Pb dating of meta-diorite from the basement of the Songliao Basin and its geological significance. Chin Sci Bull 51(15):1877–1883
58. Windley BF, Alexeiev D, Xiao W, Kröner A, Badarch G (2007) Tectonic models for accretion of the Central Asian Orogenic Belt. J Geol Soc Lond 164(1):31–47
59. Wu F, Jahn B, Wilde SA, Sun D (2000) Phanerozoic crustal growth: U-Pb and Sr-Nd isotopic evidence from the granites in northeastern China. Tectonophysics 328(1–2):89–113
60. Wu F, Sun D, Li H, Jahn B, Wilde S (2002) A-type granites in northeastern China: age and geochemical constraints on their petrogenesis. Chem Geol 187(1–2):143–173
61. Wu F, Zhao G-C, Sun D-Y, Wilde SA, Yang J-H (2007) The Hulan Group: its role in the evolution of the Central Asian Orogenic Belt of NE China. J Asian Earth Sci 30(3–4):542–556
62. Wu F, Sun D-Y, Ge W-C, Zhang Y-B, Grant ML, Wilde SA, Jahn B-M (2011) Geochronology of the Phanerozoic granitoids in northeastern China. J Asian Earth Sci 41(1):1–30
63. Xiao WJ, Windley BF, Huang BC, Han CM, Yuan C, Chen HL, Sun M, Sun S, Li JL (2009) End-Permian to mid-Triassic termination of the accretionary processes of the southern Altaids: implications for the geodynamic evolution, Phanerozoic continental growth, and metallogeny of Central Asia. Int J Earth Sci 98(6):1189–1217
64. Xiao W, Huang B, Han C, Sun S, Li J (2010) A review of the western part of the Altaids: a key to understanding the architecture of accretionary orogens. Gondwana Res 18(2–3):253–273
65. Xiao W, Windley BF, Allen MB, Han C (2013) Paleozoic multiple accretionary and collisional tectonics of the Chinese Tianshan orogenic collage. Gondwana Res 23(4):1316–1341
66. Xiao W, Windley BF, Hao J, Zhai M (2003) Accretion leading to collision and the Permian Solonker suture, Inner Mongolia, China: termination of the central Asian orogenic belt. Tectonics 22(6)
67. Xu B, Charvet J, Chen Y, Zhao P, Shi G (2013) Middle Paleozoic convergent orogenic belts in western Inner Mongolia (China): framework, kinematics, geochronology and implications for tectonic evolution of the Central Asian Orogenic Belt. Gondwana Res 23(4):1342–1364
68. Yan Z, Tang K, Bai J, Mo Y (1989) High pressure metamorphic rocks and their tectonic environment in northeastern China. J Southeast Asian Earth Sci 3(1–4):303–313
69. Zhang Y, Tang K (1989) Pre-Jurassic tectonic evolution of intercontinental region and the suture zone between the North China and Siberian platforms. J Southeast Asian Earth Sci 3(1–4):47–55
70. Zhang S-H, Zhao Y, Song B, Yang Z-Y, Hu J-M, Wu H (2007) Carboniferous granitic plutons from the northern margin of the North China block: implications for a late Palaeozoic active continental margin. J Geol Soc 164(2):451–463

71. Zhang X, Zhang H, Tang Y, Wilde SA, Hu Z (2008) Geochemistry of Permian bimodal volcanic rocks from central Inner Mongolia, North China: implication for tectonic setting and Phanerozoic continental growth in Central Asian Orogenic Belt. Chem Geol 249(3–4):262–281
72. Zhang S-H, Zhao Y, Kröner A, Liu X-M, Xie L-W, Chen F-K (2009) Early Permian plutons from the northern North China Block: constraints on continental arc evolution and convergent margin magmatism related to the Central Asian Orogenic Belt. Int J Earth Sci 98(6):1441–1467
73. Zhang X, Wilde SA, Zhang H, Tang Y, Zhai M (2009) Geochemistry of hornblende gabbros from Sonidzuoqi, Inner Mongolia, North China: implications for magmatism during the final stage of suprasubduction-zone ophiolite formation. Int Geol Rev 51(4):345–373
74. Zhang S, Gao R, Li H, Hou H, Wu H, Li Q, Yang K, Li C, Li W, Zhang J, Yang T, Keller G, Liu M (2014) Crustal structures revealed from a deep seismic reflection profile across the Solonker suture zone of the Central Asian Orogenic Belt, northern China: an integrated interpretation. Tectonophysics 612–613:26–39
75. Zhao G, Wilde SA, Cawood PA, Sun M (2001) Archean blocks and their boundaries in the North China Craton: lithological, geochemical, structural and P-T path constraints and tectonic evolution. Precambrian Res 107(1–2):45–73
76. Zhao G, Sun M, Wilde SA, Sanzhong L (2005) Late Archean to Paleoproterozoic evolution of the North China Craton: key issues revisited. Precambrian Res 136(2):177–202
77. Zhao P, Chen Y, Xu B, Faure M, Shi G, Choulet F (2013) Did the Paleo-Asian Ocean between North China Block and Mongolia Block exist during the late Paleozoic? First paleomagnetic evidence from central-eastern Inner Mongolia, China. J Geophys Res Solid Earth 118(5):1873–1894
78. Zhou J-B, Wilde SA, Zhang X-Z, Liu F-L, Liu J-H (2012) Detrital zircons from phanerozoic rocks of the Songliao Block, NE China: evidence and tectonic implications. J Asian Earth Sci 47:21–34

Chapter 3
Methodology

3.1 Integrated Sedimentary Provenance Analysis

Clastic sedimentary rocks are a unique geological archive, which contain crucial geological information on the sedimentary depositional environment, the tectonic setting, the sedimentary provenance terranes, and the relative palaeo-geographic positions of sedimentary basins and their respective catchments. The broad field of sedimentary provenance analysis integrates a large variety of analytical tools to reconstruct the geological framework of sedimentary rock formation. Thus, it combines several branches of geology and the broader field of earth sciences, such as geochronology, geochemistry, mineralogy, petrology, and statistics [12]. A broad selection of which will be applied in this dissertation, which aims to provide a more complete understanding of the geometry, timing and tectonic evolution of the Solonker Suture Zone. The advent and maturity of sophisticated analytical techniques, such as laser-ablation inductively coupled plasma mass spectrometry (LA-ICPMS, see also [28]) and X-ray fluorescence analysis (XRF, see also [7, 8]) led to faster and more efficient analytical procedures, which enabled access to large data sets. As a result, modern sedimentary provenance analyses are able to answer geological questions from local to global scales.

During three field excursions in Summer 2011, 2012 and 2013, 91 samples of Devonian and Permian sedimentary (mostly volcano-clastic) and volcanic rocks collected along a broad northwest-southeast transect across the accretionary collision zone between the Mongolian Arcs and the North China Craton (Table 3.1; Fig. 2.1) were analysed. Field work also included structural analyses of macroscopic rock deformation, and general geological observations, such as outcrop descriptions and relationships between different rock types. The regional scale of this study is

P. R. Eizenhöfer, *Subduction and Closure of the Palaeo-Asian Ocean along the Solonker Suture Zone: Constraints from an Integrated Sedimentary Provenance Analysis*, Springer Theses, https://doi.org/10.1007/978-981-32-9200-0_3

Table 3.1 List of samples, their respective rock type (incl. formation) and undertaken analyses. DZUPb: zircon U–Pb analysis; DZHf: zircon Hf analysis, MaTE: whole-rock major and trace element analysis, HfNd: whole-rock Hf and Nd isotope analysis

Sample	Rock (Formation)	Analyses
1 (12XL18-3)	Arcose (Gegenaobao Fm.)	DZUPb
2 (12XL16-1)	Greywacke (Gegenaobao Fm.)	DZUPb
3 (11XL42-1)	Greywacke (Gegenaobao Fm.)	DZUPb, DZHf, MaTE
4 (12XL19-1)	Arcose (Gegenaobao Fm.)	DZUPb
5 (11XL45-1)	Conglomerate (Gegenaobao Fm.)	DZUPb, DZHf
6 (12XL21-1)	Sandstone (Gegenaobao Fm.)	DZUPb
7 (11XL41-2)	Sandstone (Dalinuoer Fm.)	DZUPb, DZHf, MaTE
8 (11XL37-1)	Volcano-clast (Gegenaobao Fm.)	DZUPb, DZHf
9 (12XL24-1)	(meta-) Sandstone (Xilinhot Complex)	DZUPb
10 (11XL29-1)	Greenschist (Zhesi Fm.)	DZUPb, DZHf
11 (11XL51-1)	Greywacke (Huanggangliang Fm.)	DZUPb, DZHf
12 (11XL27)	Greywacke (Huanggangliang Fm.)	DZUPb, DZHf, MaTE
13 (11XL26)	Greywacke (Huanggangliang Fm.)	DZUPb, DZHf
14 (11XL13)	Arcose (Huanggangliang Fm.)	DZUPb, DZHf
15 (11XL25)	Siltstone (Huanggangliang Fm.)	DZUPb, DZHf, MaTE
16 (11XL20)	Sandstone (Linxi Fm.)	DZUPb, DZHf
17 (11XL17-2)	Greywacke (Linxi Fm.)	DZUPb, DZHf
18 (11XL16-1)	Brecciated conglomerate (Linxi Fm.)	DZUPb, DZHf
19 (11XL15-1)	Arcose (Linxi Fm.)	DZUPb, DZHf, MaTE
20 (11XL7-2)	Conglomeratic greywacke (Linxi Fm.)	DZUPb, DZHf
21 (11XL54-1)	Arcose (Huanggangliang Fm.)	DZUPb, DZHf
22 (11XL23)	Greywacke (Huanggangliang Fm.)	DZUPb, DZHf, MaTE, HfNd
23 (11XL57)	Conglomerate (Huanggangliang Fm.)	DZUPb, DZHf
24 (11XL12)	Volcano-clast (Qingfengshan Fm.)	MaTE
25 (11XL14-1)	Shale (Huanggangliang Fm.)	MaTE
26 (11XL15-2)	Arcose (Linxi Fm.)	MaTE, HfNd
27 (11XL15-3)	Arcose (Linxi Fm.)	MaTE
28 (11XL17-1)	Greywacke (Linxi Fm.)	MaTE, HfNd
29 (11XL21-2)	Arcosic sandstone (Tieyingzi Fm.)	MaTE
30 (11XL21-3)	Siltstone (Tieyingzi Fm.)	MaTE
31 (11XL41-3)	Sandstone (Dalinuoer Fm.)	MaTE
32 (11XL41-4)	Siltstone (Dalinuoer Fm.)	MaTE
33 (11XL41-5)	Siltstone (Dalinuoer Fm.)	MaTE
34 (11XL42-4)	Greywacke (Gegenaobao Fm.)	MaTE, HfNd
35 (11XL45-2)	Sandstone (Gegenaobao Fm.)	MaTE,
36 (11XL47-1)	Greywacke (Gegenaobao Fm.)	MaTE, HfNd
37 (11XL47-2)	Greywacke (Gegenaobao Fm.)	MaTE
38 (11XL48-1)	Arcose (Gegenaobao Fm.)	MaTE

(continued)

Table 3.1 (continued)

Sample	Rock (Formation)	Analyses
39 (11XL48-2)	Arcose (Gegenaobao Fm.)	MaTE
40 (11XL50-2)	Sandstone (Huanggangliang Fm.)	MaTE
41 (11XL51-2)	Greywacke (Huanggangliang Fm.)	MaTE, HfNd
42 (11XL54-2)	Arcose (Huanggangliang Fm.)	MaTE, HfNd
43 (11XL7-3)	Greywacke (Linxi Fm.)	MaTE
44 (11XL7-4)	Greywacke (Linxi Fm.)	MaTE
45 (11XL7-5)	Greywacke (Linxi Fm.)	MaTE
46 (11XL7-6)	Greywacke (Linxi Fm.)	MaTE
47 (11XL7-7)	Greywacke (Linxi Fm.)	MaTE
48 (11XL001)	Dacite (Huanggangliang Fm.)	MaTE
49 (11XL002-1)	Dolerite (Huanggangliang Fm.)	MaTE
50 (11XL5-2)	Basalt (Shuangjing Complex)	MaTE
51 (11XL9)	Basalt (Qingfengshan Fm.)	MaTE
52 (11XL11)	Basalt (Qingfengshan Fm.)	MaTE
53 (11XL24-2)	Andesite (Huanggangliang Fm.)	MaTE
54 (11XL28-2)	Andesite (Huanggangliang Fm.)	MaTE
55 (11XL28-3)	Andesite (Huanggangliang Fm.)	MaTE, HfNd
56 (11XL31)	Pyroclastic andesite (Linxi Fm.)	DZUPb, MaTE, HfNd
57 (11XL37-2)	Rhyolithic pyroclast (Gegenaobao Fm.)	MaTE, HfNd
58 (11XL38-1)	Rhyolithic pyroclast (Gegenaobao Fm.)	MaTE
59 (11XL39-1)	Andesite/Rhyolite (Dalinuoer Fm.)	MaTE, HfNd
60 (11XL46-1)	Dolerite (Gegenaobao Fm.)	MaTE
61 (11XL52-2)	Andesite (Huanggangliang Fm.)	MaTE, HfNd
62 (11XL55)	Rhyolite (Qingfengshan Fm.)	MaTE
63 (11XL56-2)	Basalt (Huanggangliang Fm.)	MaTE
64 (11XL58-1)	Andesite/Rhyolite (Linxi Fm.)	MaTE, HfNd
65 (11XL58-2)	Tuff (Linxi Fm.)	MaTE
66 (11XL58-3)	Tuff (Linxi Fm.)	MaTE
67 (11XL59-1)	Andesite (Huanggangliang Fm.)	MaTE
68 (11XL63-1)	Andesite (Huanggangliang Fm. (?))	MaTE
69 (11XL24-1)	Pyroclastic andesite (Huanggangliang Fm.)	DZUPb, MaTE, HfNd
70 (12XL22)	Mudstone (Yanchibeishan Fm.)	HfNd
71 (12XL23-4)	Mudstone (Beidashan Fm.)	HfNd
72 (12XL24-2)	(meta-) Sandstone (Xilinhot Complex)	HfNd
73 (12XL21-2)	Sandstone (Gegenaobao Fm.)	HfNd
74 (12XL19-2)	Sandstone (Gegenaobao Fm.)	HfNd
75 (12XL14-2)	Siltstone (Devonian Grp.)	DZUPb, HfNd
76 (12XL16-3)	Greywacke (Gegenaobao Fm.)	HfNd
77 (12XL17-2)	Quartzite (Devonian Grp.)	DZUPb, HfNd
78 (12XL15-1)	Sandstone (Devonian Grp.)	DZUPb

(continued)

Table 3.1 (continued)

Sample	Rock (Formation)	Analyses
79 (11XL14-2)	Felsic dike (Huanggangliang Fm.)	DZUPb
80 (11XL36-1)	Dunite/Serpentinite (Hegenshan Ophiolite)	HfNd
81 (11XL44-1)	Peridotite (Hegenshan Ophiolite)	MaTE, HfNd
82 (12XL18-2)	Andesite (Gegenaobao Fm.)	HfNd
83 (11XL43-1)	Chromite Hegenshan Ophiolite	MaTE
84 (11XL43-10)	Ultramafic rock (Hegenshan Ophiolite)	MaTE
85 (11XL43-11)	Ultramafic rock (Hegenshan Ophiolite)	MaTE
86 (11XL43-3)	Chromite (Hegenshan Ophiolite)	MaTE
87 (11XL43-4)	Chromite (Hegenshan Ophiolite)	MaTE
88 (11XL43-5)	Chromite (Hegenshan Ophiolite)	MaTE
89 (11XL43-7)	Chromite (Hegenshan Ophiolite)	MaTE
90 (11XL44-2)	Pyroxenite (Hegenshan Ophiolite)	MaTE
91 (11XL44-3)	Ultramafic rock (Hegenshan Ophiolite)	MaTE

unprecedented in the literature available for the region, which allows in combination with previous studies a more thorough and complete reconstruction of the Palaeozoic tectonic evolution of the study area at a high resolution. Selected samples were geochronologically, geochemically and statistically analysed, as described in more detail in the following sections.

Each of the following sections will describe the analytical procedures and the technical equipment used. The section on the statistical analysis will describe the statistical tools and basic mathematical formula applied to quantitatively evaluate detrital age probability functions. A more elaborate discourse on statistical methods adopted from an information theoretical point of view will be given in Chap. 5.

3.2 Detrital Zircon U–Pb Geochronology

Rock samples were first crushed, sieved and milled, and then separated by standard heavy liquid and electromagnetic techniques, followed by handpicking of zircons from the heavy liquid residue. Individual grains were randomly selected and mounted on double-sided adhesive tape under a binocular microscope. Grains were then embedded in epoxy resin and polished down to about half a grain size to reveal internal grain surfaces and structures. Sample mounts were photographed in reflected and transmitted light. In order to guide laser ablation U–Pb isotope analyses, grain growth structures were revealed by cathodoluminescence (CL) imaging.

Zircon U–Pb ages were obtained from three laboratories: (1) The State Key Laboratory of Ore Deposit Geochemistry, Institute of Geochemistry, Chinese Academy of Sciences, Guiyang operates a LA-ICP-MS. A GeoLasPro laser ablation system

(Lamda Physik, Göttingen) and an Agilent 7700x ICP-MS (Agilent Technologies, Tokyo, Japan) were combined for the experiments. The 193 nm ArF excimer laser, homogenised by a set of beam delivery systems, was focused on the zircon surface with an energy flux of 10 J/cm^2. Ablation protocol employed a spot diameter of 32 μm at 6 Hz repetition rate for 40 s (equating to 200 pulses) for most samples. A few zircons were ablated with a spot diameter of 40 μm. Helium was used as a carrier gas to efficiently transport aerosol to the ICP-MS. (2) The Northwest University Xi'an maintains a LA-ICP-MS with a GeoLas 2005 ArF (MICROLAS) laser ablation system combined with an Agilent 7700 Series ICP-MS (Agilent Technologies, Tokyo, Japan). The laser system was operated at 28 kV corresponding to an energy transmission of 100 mJ/m^2. 300 laser pulses were directed to most analysis spots of 40 μm diameter equal to 50 s of acquisition time and a 6 Hz repetition rate. Background was measured for 40 s amounting to a total of 90 s analysis time per grain. Nitrogen served as carrier gas within the ICP-MS system. (3) The Department of Earth Sciences at the University of Hong Kong houses a multi-collector LA-ICP-MS. A Nu Instruments multi collector ICP-MS is attached to a Resonetics RESOlution M-50-HR excimer laser ablation system. Analyses were performed with a beam diameter of 30 μm and 6 Hz repetition rate, which yielded a signal intensity of 0.03 V at ^{238}U for the standard 91500. Typical ablation time was 40 s for each measurement, resulting in pits of 30–40 μm depth. Masses 232, 208-204 were simultaneously measured in static-collection mode.

A minimum of 90 zircons were analysed for most samples. Zircon 91500 (^{207}Pb/^{206}Pb age of 1065.4 $\pm$ 0.3 Ma, ^{206}Pb/^{238}U age of 1062.4 $\pm$ 0.4 Ma, Wiedenbeck et al. [30]) was used as an external standard to correct for elemental fractionation, while zircon GJ-1 (^{207}Pb/^{206}Pb age of 608.53 $\pm$ 0.37 Ma, Jackson et al. [14]) and Plešovice (^{206}Pb/^{238}U age of 337.13 $\pm$ 0.37 Ma, Sláma et al. [25]) were, either of which or both, used as quality control. Lead concentration in zircon was externally calibrated, where required, against NIST SRM 610 with Si as an internal standard, whereas Zr served as an internal standard for other trace elements [13]. Data reduction and single age calculation were performed off-line by ICPMSDataCal [16, 17] or the in-house developed RatSuite software package (see Appendix A). Weighted mean average ages, when necessary, were calculated using Isoplot version 3.75 [18]. All results are summarised in Appendix B.

Age histograms and concordia plots were produced by the in-house developed RatSuite software package within the Matlab® code environment provided by Mathworks (see Appendix A). The total age probability density function of each sedimentary rock sample was calculated by assuming a Gaussian error distribution for each single age and its respective 1σ error. Single age probability density functions were summed to obtain the detrital probability density function of the entire sample, and then normalised by the number of total analyses for each rock sample. If ages are higher than 1 Ga, the age recorded by the ^{207}Pb/^{206}Pb decay system was selected, otherwise, the ^{206}Pb/^{238}U was used (see for comparison also [10]). The concordia plots use a log-log scale in order to adequately visualise the entire detrital age spectrum of a sample in a single plot. The unlikeliness that errors of each of the two isotope ratios reach simultaneously their maximum value has been taken into account by drawing error ellipses based on a 95% confidence level (2σ), instead of error hexagons (for a review see e.g. [9]).

3.3 Detrital Zircon Hf Isotope Analysis

Only zircon grains with concordant U–Pb ages were selected for further Hf isotope analysis. 30 single grain analyses were undertaken for each sample upon availability of grains sufficing strict quality requirements.

Zircon Hf isotope analyses were carried out by employing a Nu Instruments multi-collector ICP-MS, attached to a Resonetics RESOlution M-50-HR excimer laser ablation system, at the Department of Earth Sciences of The University of Hong Kong. Analyses were performed with a beam diameter of 55 μm and 6 Hz repetition rate on laser ablation spots, above which prior in-situ U–Pb analyses were performed (see previous Sect. 3.2) to ensure an accurate correlation between U–Pb and Hf isotopic compositions. Measurement of standard 91500 yielded a signal intensity of 0.04 V for ^{179}Hf. Typical ablation time was 40 s for each measurement, resulting in pits of 30–40 μm depth. Masses 172–179 were simultaneously measured in static-collection mode. External corrections were applied to all unknowns, and standard zircons 91500 (^{176}Lu/^{177}Hf = 0.000311 and ^{176}Hf/^{177}Hf = 0.282306; Woodhead et al. [31]) and GJ-1 (^{176}Lu/^{177}Hf = 0.00025 and ^{176}Hf/^{177}Hf = 0.282000; Morel et al. [20]) were used as external standards and were analysed twice before and after every ten analyses. Data were normalised to ^{179}Hf/^{177}Hf = 0.7325, using exponential correction for mass bias. Interference of ^{176}Lu on ^{176}Hf was corrected by measuring the intensity of the interference-free ^{175}Lu isotope and using the newly recommended ^{176}Lu/^{175}Lu ratio of 0.02655 [19]. The ^{176}Lu decay constant of 1.867×10^{-5} per million years was used to calculate initial ^{176}Lu/^{177}Hf ratios [27]. The chrondritic values of ^{176}Hf/^{177}Hf = 0.282772 and ^{176}Lu/^{177}Hf = 0.0332 reported by Blichert-Toft and Albarède [2] were adopted for the calculation of εHf values. The evolution of the depleted mantle was calculated from present-day MORB values of ^{176}Lu/^{177}Hf = 0.0384 and ^{176}Hf/^{177}Hf = 0.283250, resulting in an initial depleted mantle reservoir ratio of ^{176}Hf/^{177}Hf = 0.279718 assuming a linear isotopic growth [11]. Data reduction was performed by the in-house developed RatSuite software package (see Appendix A). All results are summarised in Appendix C.

3.4 Whole-Rock Geochemical Analysis

Rock samples were first crushed, sieved and milled to obtain sample powder for whole-rock geochemical analyses.

Major oxide and trace elements were measured by standard wavelength-dispersive X-ray fluorescence spectrometry (XRF) at the Guangzhou Institute of Geochemistry, Chinese Academy of Sciences. Calibration lines used in quantification were produced by bivariate regression of data from 36 reference materials encompassing a wide range of silicate compositions [15]. Analytical uncertainties are in the range 1–5%. All results are summarised in Appendix D.

Nd and Hf isotopic compositions were measured at the Northwest University Xi'an. Rock powder for each sample was digested in a two-step process: First, single samples were dissolved in a HNO_3–HF–$HClO_4$ acid solution using high-temperature teflon bombs sealed in PTFE coated stainless steel. Second, Nd and Hf isotopes were separated from the matrix applying a combination of AG1-X8, AG50W-X8 and Ln-spec ion exchange columns. Recovery of the isotopes reached more than 95%. The isotope purification was monitored by the AGV-2, BCR-2, BHVO-2 and JMC475 (for Hf)/Jndi-1 (for Nd) rock standards. Purified solutions were then analysed by multi-collector ICP-MS. Two sample analyses were bracketed by standard measurements, which yielded, out of eleven, mean isotope ratios agreeing well with the recommended literature values ($^{176}Hf/^{177}Hf$: 0.282949 ± 7, 0.282877 ± 4, 0.283111 ± 8 and 0.282173 ± 8, respectively. $^{143}Nd/^{144}Nd$: 0.512611 ± 6, 0.512386 ± 7, 0.512386 ± 9, 0.512116 ± 6, respectively). The following chondritic values were adopted for the ε(0) notation: $(^{176}Hf/^{177}Hf)_{CHUR} = 0.282785 \pm 11$ and $(^{143}Nd/^{144}Nd)_{CHUR} = 0.512630 \pm 11$ [3]. All results are summarised in Appendix E.

3.5 Statistical Quantification of Geochronological Data

In most cases U–Pb ages for more than 90 detrital zircon grains were analysed for each clastic sedimentary rock sample. As outlined by Vermeesch [29] 117 concordant ages per sample are required to identify at a 95% confidence level every age component comprising more than 5% of the entire age population. According to Andersen [1], 60 concordant ages are sufficient to identify on a 95% confidence level a single age component representing more than 5% of the entire age population based on the standard binomial probability formula [6]. As will be outlined in Chap. 5, 97 analyses are sufficient to reach a similarity index of 0.95 with respect to a reasonably complex ideal age probability density function based on information theory. The total number of concordant detrital zircon ages amounts to 1694, therefore, indicating that the probability of missing a significant age population across the Solonker Suture Zone tends statistically towards zero, assuming an entirely random selection process [1].

In order to provide an additional measure to quantitatively compare different probability density functions (PDF's), a heterogeneity value (H_{rel}) has been calculated for each sample [21, 24, 26]. PDF's with lower relative heterogeneity values tend to be dominated by fewer age peaks, and vice versa. The relative heterogeneity H_{rel} is defined as follows:

$$H_{rel} = 100 \cdot \frac{H}{H_{max}} \tag{3.1}$$

with H describing the absolute value of heterogeneity using the information function [21, 23] for a data set consisting of n components and probability p_i of the i-th age component:

$$H = \sum_{i=1}^{n} p_i \cdot ln(p_i) \tag{3.2}$$

and H_{max} describing the maximum value of H assuming equal probability of each occurring age component [21, 26]:

$$H_{max} = -n(\frac{1}{n}) \cdot ln(\frac{1}{n}) \tag{3.3}$$

The heterogeneity values calculated in this dissertation are either based on a 4000 or 4500 component system for each sample, referring to an age range of 0–4000 or 4500 Ma, respectively, in 1 Ma steps. The large number of analyses taken in this study may indicate that significant changes of relative heterogeneity calculated for large data sets (e.g. all ages obtained in a rock formation) reflect changes in the sedimentary depositional environment.

Another statistical measure has been adopted to quantitatively compare two age probability density functions. Similarity, or fidelity as described among other statistical distance measures in Cha [4], describes the distance of one probability density function to another taking values between 0 and 1. Higher values indicate greater similarity, identity if PDF's are identical, and 0 if PDF's are dissimilar (see also [22]). The similarity statistic adopted in this dissertation is defined as follows (also known as Bhattacharyya coefficient or Hellinger affinity, see also [4, 5]):

$$s = \sum_{i=1}^{n} \sqrt{(p_i \cdot q_i)} \tag{3.4}$$

with s = similarity index, n = maximum hypothetically possible age components, p_i = probability of the i-th age component in age distribution function p, q_i = probability of the i-th age component in age distribution function q.

References

1. Andersen T (2005) Detrital zircons as tracers of sedimentary provenance: limiting conditions from statistics and numerical simulation. Chem Geol 216(3–4):249–270
2. Blichert-Toft J, Albarède F (1997) The Lu-Hf isotope geochemistry of chondrites and the evolution of the mantle-crust system. Earth Planet Sci Lett 148(1–2):243–258
3. Bouvier A, Vervoort JD, Patchett PJ (2008) The Lu-Hf and Sm-Nd isotopic composition of CHUR: constraints from unequilibrated chondrites and implications for the bulk composition of terrestrial planets. Earth Planet Sci Lett 273(1–2):48–57
4. Cha S (2007) Comprehensive survey on distance/similarity measures between probability/density functions. Int J Math Model Methods Appl Sci 1(4):300–307

5. Deza M-M, Deza E (2006) Dictionary of distances. Elsevier BV
6. Dodson MH, Compston W, Williams IS, Wilson JF (1988) A search for ancient detrital zircons in Zimbabwean sediments. J Geol Soc 145(6):977–983
7. Fralick P (2003) Geochemistry of clastic sedimentary rocks: ratio techniques. In: Lentz D (ed) Geochemistry of sediments and sedimentary rocks. Geological Association of Canada, St. John's, pp 85–103
8. Fralick P, Kronberg B (1997) Geochemical discrimination of clastic sedimentary rock sources. Sediment Geol 113(1–2):111–124
9. Gehrels G (2011) Detrital zircon U-Pb geochronology: current methods and new opportunities. In: Busby C, Azor A (eds) Tectonics of sedimentary basins: recent advances. Wiley, Chichester, UK, pp 45–62
10. Gehrels GE, Valencia VA, Ruiz J (2008) Enhanced precision, accuracy, efficiency, and spatial resolution of U-Pb ages by laser ablation-multicollector-inductively coupled plasma-mass spectrometry. Geochem Geophys Geosyst 9(3):1–13
11. Griffin W, Pearson N, Belousova E, Jackson S, van Achterbergh E, O'Reilly SY, Shee S (2000) The Hf isotope composition of cratonic mantle: LAM-MC-ICPMS analysis of zircon megacrysts in kimberlites. Geochim Cosmochim Acta 64(1):133–147
12. Haughton PDW, Todd SP, Morton AC (1991) Sedimentary provenance studies. Geol Soc Lond Spec Publ 57(1):1–11
13. Hu Z, Liu Y, Chen L, Zhou L, Li M, Zong K, Zhu L, Gao S (2011) Contrasting matrix induced elemental fractionation in NIST SRM and rock glasses during laser ablation ICP-MS analysis at high spatial resolution. J Anal AtIc Spectrom 26:425–430
14. Jackson SE, Pearson NJ, Griffin WL, Belousova EA (2004) The application of laser ablation-inductively coupled plasma-mass spectrometry to in situ U-Pb zircon geochronology. Chem Geol 211(1–2):47–69
15. Li X-H, Li Z-X, Wingate MT, Chung S-L, Liu Y, Lin G-C, Li W-X (2006) Geochemistry of the 755 Ma Mundine Well dyke swarm, Northwestern Australia: part of a Neoproterozoic mantle superplume beneath Rodinia? Precambrian Res 146(1–2):1–15
16. Liu Y, Gao S, Hu Z, Gao C, Zong K, Wang D (2009) Continental and Oceanic Crust Recycling-induced Melt-Peridotite Interactions in the Trans-North China Orogen: U-Pb Dating, Hf Isotopes and Trace Elements in Zircons from Mantle Xenoliths. J Petrol 51(1–2):537–571
17. Liu Y, Hu Z, Zong K, Gao C, Gao S, Xu J, Chen H (2010) Reappraisement and refinement of zircon U-Pb isotope and trace element analyses by LA-ICP-MS. Chin Sci Bull 55(15):1535–1546
18. Ludwig K (2008) Manual for Isoplot 3.7. Berkeley Geochronology Center, Berkeley
19. Machado N, Simonetti A (2001) U-Pb dating and Hf isotopic composition of zircons by laser ablation-MC-ICP-MS. In: Sylvester P (ed) Laser ablation-ICP-MS in the earth sciences: principles and applications, vol 29. Mineralogical Association of Canada, pp. 121–146
20. Morel M, Nebel O, Nebel-Jacobsen Y, Miller J, Vroon P (2008) Hafnium isotope characterization of the GJ-1 zircon reference material by solution and laser-ablation MC-ICPMS. Chem Geol 255(1–2):231–235
21. Pelto CR (1954) Mapping of multicomponent systems. J Geol 62:501–511
22. Satkoski AM, Wilkinson BH, Hietpas J, Samson SD (2013) Likeness among detrital zircon populations—an approach to the comparison of age frequency data in time and space. Geol Soc Am Bull 125(11–12):1783–1799
23. Shannon CE, Weaver W (1971) The mathematical theory of communication. University of Illinois Press, Illinois
24. Sircombe KN (2004) AgeDisplay: an EXCEL workbook to evaluate and display univariate geochronological data using binned frequency histograms and probability density distributions. Comput Geosci 30(1):21–31
25. Sláma J, Košler J, Condon DJ, Crowley JL, Gerdes A, Hanchar JM, Horstwood MSA, Morris GA, Nasdala L, Norberg N, Schaltegger U, Schoene B, Tubrett MN, Whitehouse MJ (2008) Plešovice zircon—a new natural reference material for U-Pb and Hf isotopic microanalysis. Chem Geol 249(1–2):1–35

26. Smosna R, Bruner KR, Burns A (1999) Numerical analysis of sandstone composition, provenance, and paleogeography. J Sediment Res 69(5):1063–1070
27. Söderlund U, Patchett PJ, Vervoort JD, Isachsen CE (2004) The 176Lu decay constant determined by Lu-Hf and U-Pb isotope systematics of Precambrian mafic intrusions. Earth Planet Sci Lett 219(3–4):311–324
28. Sylvester PJ (2008) Laser ablation-ICP-MS in the earth sciences: current practices and outstanding issues, vol 40. Mineralogical Association of Canada
29. Vermeesch P (2004) How many grains are needed for a provenance study? Earth Planet Sci Lett 224(3–4):441–451
30. Wiedenbeck M, Alle P, Corfu F, Griffin W, Meier M, Oberli F, von Quadt A, Roddick J, Spiegel W (1995) Three natural zircon standards for U-Th-Pb, Lu-Hf, trace element and REE analyses. Geostand Newsl 19(1):1–23
31. Woodhead J, Hergt J, Shelley M, Eggins S, Kemp R (2004) Zircon Hf-isotope analysis with an excimer laser, depth profiling, ablation of complex geometries, and concomitant age estimation. Chem Geol 209(1–2):121–135

Chapter 4
Results

4.1 Detrital Zircon U–Pb Age Data

The 1694 U–Pb ages of detrital zircons from Permian arc basins of the accretionary collision zone between the Mongolian Arcs and the North China Craton exhibit a wide age range, from Neoarchean (ca. 2.5 Ga) to Late Permian (ca. 269 Ma), with major age populations around ca. 2.5 Ga, ca. 1.8 Ga, ca. 436 Ma, ca. 314 Ma and ca. 269 Ma (Figs. 4.1 and 4.2a). Each of the lithotectonic belts yielded a characteristic age distribution. All ages can be divided into three groups, approximately corresponding to their proposed respective sedimentary provenance terranes: (i) Neoarchean to Palaeoproterozoic (North China Craton), (ii) Mesoproterozoic to the latest Precambrian (Mongolian Arcs), and (iii) Palaeozoic (Palaeozoic arcs). Relative abundances of these age groups for each sample are illustrated as pie charts in Fig. 4.1. Except for Fig. 4.2, concordant ages (>0.9 concordance between the $^{206}Pb^{*}/^{238}U$ and $^{207}Pb^{*}/^{235}U$; Figs. 4.4, 4.8 and 4.11) were plotted as combined histograms/probability density functions (PDF's; Figs. 4.5, 4.6, 4.9 and 4.12).

In order to better understand the Palaeozoic evolution of the Mongolian Arcs as a sedimentary provenance terrane, 308 detrital zircon U–Pb ages were obtained from Devonian clastic sedimentary rocks of the Chinese southern Mongolian Arcs (Fig. 4.2b). They show major age populations at ca. 409 Ma, ca. 511 Ma and ca. 965 Ma. Late subduction-related volcanic rocks were additionally dated to provide a better minimum depositional age, and, thus, in combination with the maximum depositional age a more robust age range for the final closure of the Palaeo-Asian Ocean (see Sects. 4.1.1 and 4.1.3).

P. R. Eizenhöfer, *Subduction and Closure of the Palaeo-Asian Ocean along the Solonker Suture Zone: Constraints from an Integrated Sedimentary Provenance Analysis*, Springer Theses, https://doi.org/10.1007/978-981-32-9200-0_4

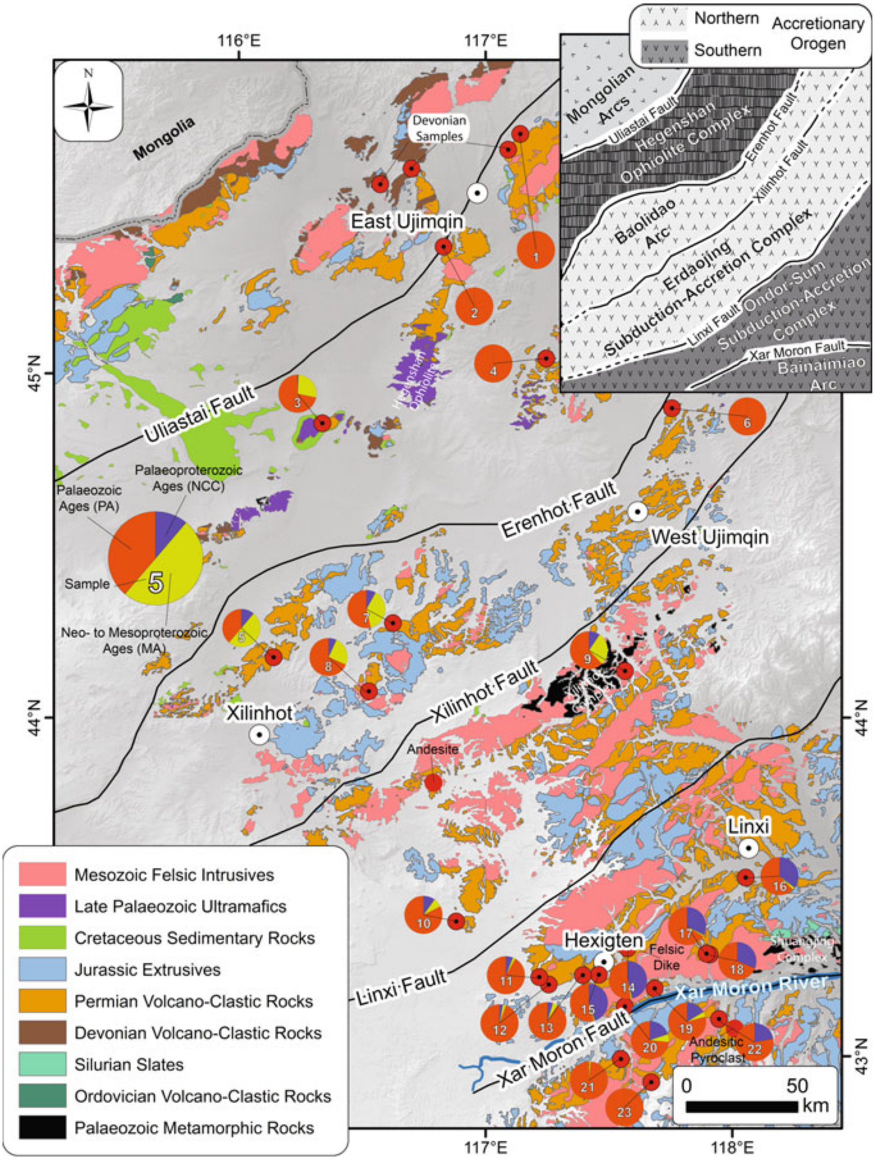

Fig. 4.1 Geological map of the study area, and locations of dated clastic sedimentary rock samples, supplemented with pie charts illustrating the contribution of each of the three age groups defined in the text (not applied for the Devonian sedimentary and Permian volcanic rocks). NCC: North China Craton; MA: Mongolian Arcs; PA: Palaeozoic arcs

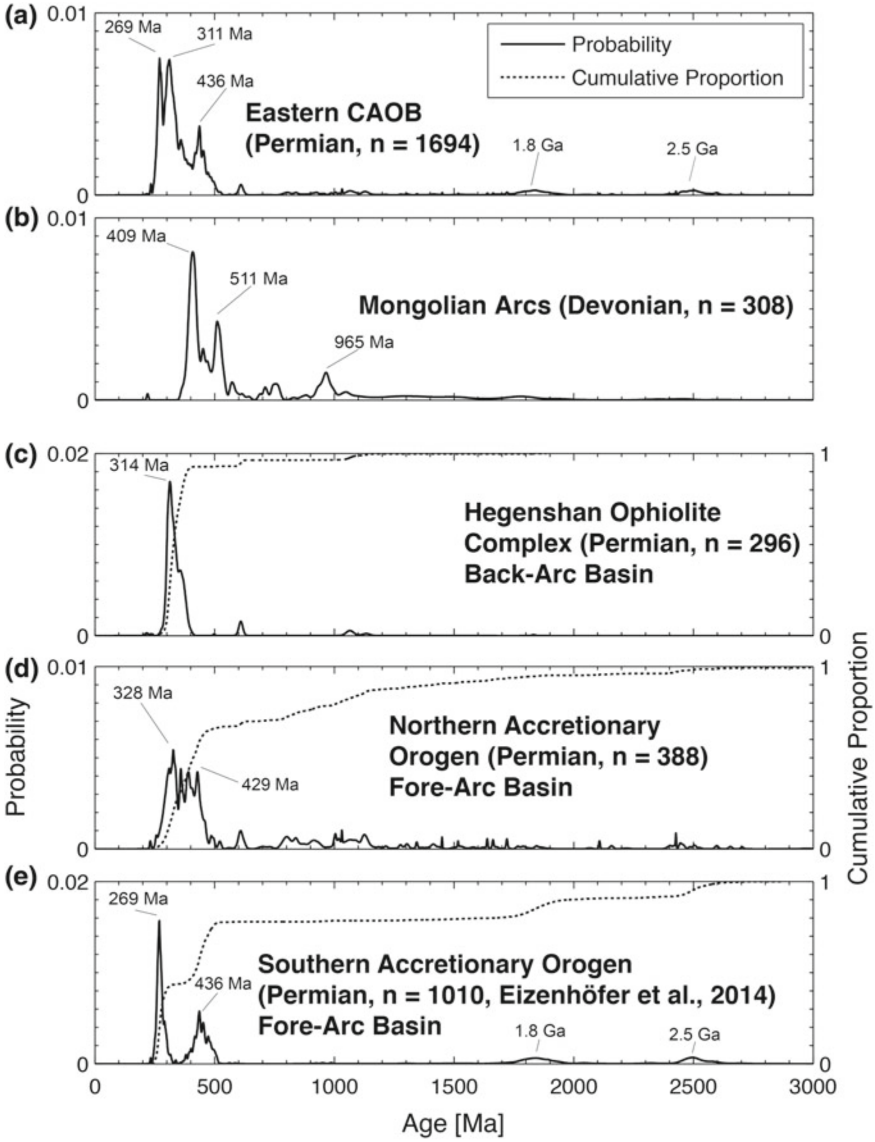

Fig. 4.2 **a**, **b** Summarised age probability density functions of **a** the entire accretionary collision zone between the Mongolian Arcs and the North China Craton, and **b** Devonian strata of the southern Mongolian Arcs; **c**–**e** Summarised age probability density functions and cumulative age proportions of Permian strata in the **c** Hegenshan Ophiolite Complex, **d** Northern Accretionary Orogen, and **e** Southern Accretionary Orogen

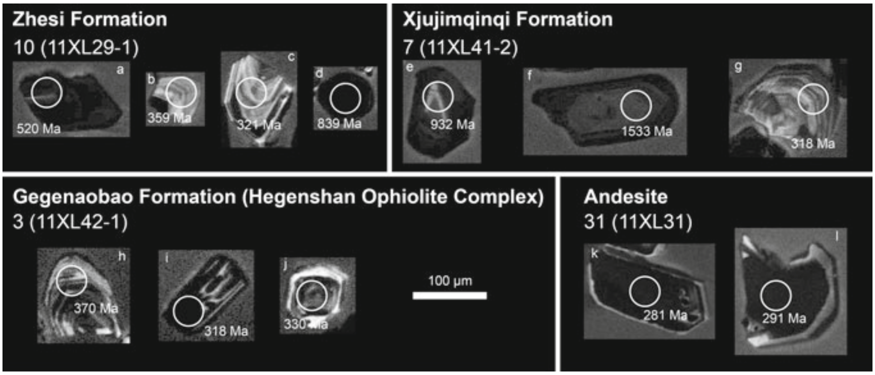

Fig. 4.3 Representative CL images of zircons from samples of the Hegenshan Ophiolite Complex and the Northern Accretionary Orogen. Open circles mark laser ablation sites, labeled with their individual $^{206}Pb^{*}/^{238}U$ or $^{207}Pb^{*}/^{206}Pb^{*}$ age, respectively

4.1.1 The Hegenshan Ophiolite Complex and Northern Accretionary Orogen

Internal structures of detrital zircons from the Hegenshan Ophiolite Complex are dominated by concentric, mostly well developed, oscillatory zoning (Fig. 4.3). In most cases zircons are eu- to subhedral, indicating relatively short transport distances. While most of the samples appear to contain zircons of different provenances, sample 1 seems to be dominated by a single zircon provenance despite its sedimentary origin. None of the laser ablation sites show Th/U values below 0.07, thus corroborating a magmatic origin of the detrital zircons in the Hegenshan Ophiolite Complex.

Growth structures of zircons from the Northern Accretionary Orogen reveal a much larger variety (Fig. 4.3). Concentric oscillatory zoning defines the majority of grains, although developed to different degrees, most likely due to their derivation from different magmatic sources. Some grains show patchy growth structures. The zircon grains have eu- to subhedral shapes corroborating the immature state of most of the volcano-clastic sedimentary rocks. Similar to the zircon grains of the Hegenshan Ophiolite Complex, none of the zircons have Th/U values indicative of a metamorphic origin.

As expected, zircon grains extracted from an andesite (sample 56) are homogenous in growth structure, texture and shape. Concentric oscillatory zoning is poorly developed, often merely indicated by a dark interior and a thin bright rim. All zircons are euhedral.

Age spectra for four samples (samples 1–4, two arcosic sandstones and two greywacke samples from the Gegenaobao formation), containing 296 concordant ages (Fig. 4.4) from the Hegenshan Ophiolite Complex, are consistently dominated by a single age population centred at ca. 314 Ma (Figs. 4.2 and 4.5). Their age PDF's

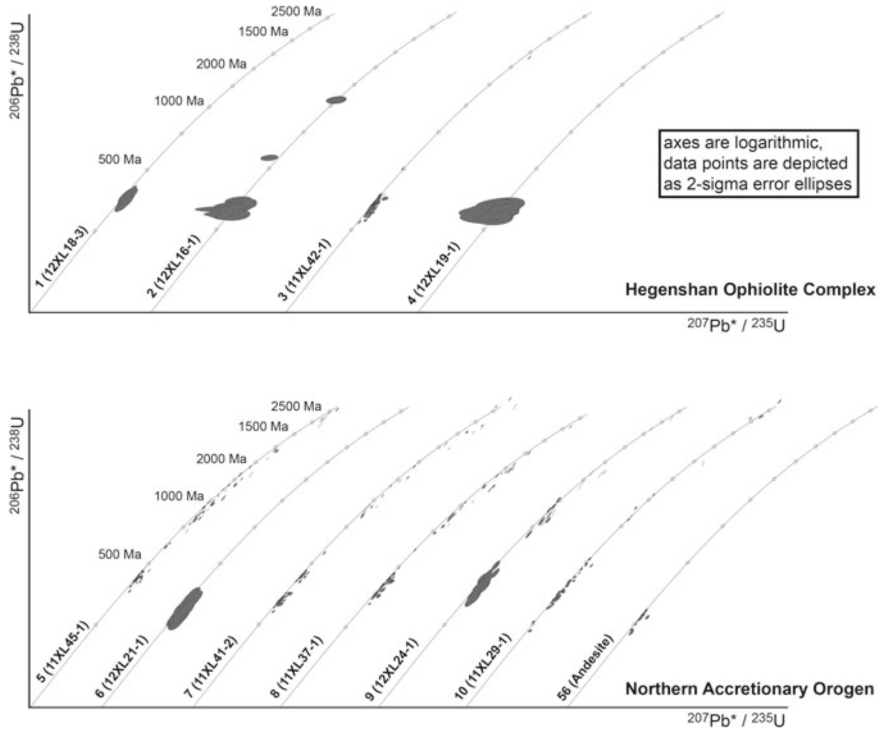

Fig. 4.4 U–Pb concordia diagrams for zircons from the Northern Accretionary Orogen and the Hegenshan Ophiolite Complex

also yield low relative heterogeneity values (50–66%). Sample 3 also contains ages at ca. 610 Ma and ca. 1066 Ma, thus being the most heterogenous in this group of samples.

Three samples of Permian sedimentary rocks (samples 5–7, one conglomerate of the Gegenaobao formation, one volcano-clastic sandstone of the Gegenaobao formation, and one sandstone of the Dalinuoer/Xiujimqinqi formation; Fig. 2.4) and two samples of Permian greenschist metamorphic meta-sedimentary schists from the Xilinhot complex (sample 8) and Zhesi formation (sample 9), respectively, exhibit very heterogenous ($H_{rel} = 72$–81%) age distributions (Figs. 4.4 and 4.5). A single sandstone sample of the Xiujimqinqi formation, however, is dominated by a single age peak ($H_{rel} = 57\%$). About 70% of all ages fall within ca. 328–429 Ma (Fig. 4.2), while other ages are broadly distributed in the Mesoproterozoic to latest Precambrian age range.

The andesite yielded a weighted mean age of 270 ± 2 Ma (MSWD $= 6.7$) for the ages occurring in the interval 260–280 Ma (Fig. 4.6).

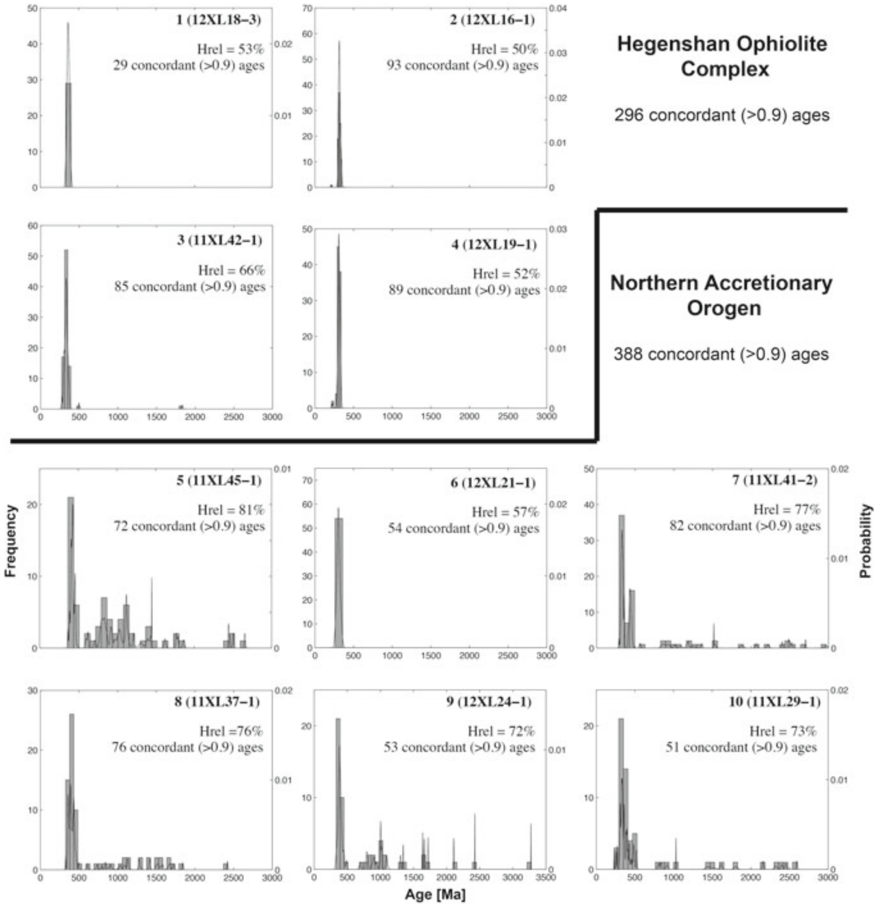

Fig. 4.5 Combined age histograms and probability density functions for samples from the Hegenshan Ophiolite Complex and the Northern Accretionary Orogen

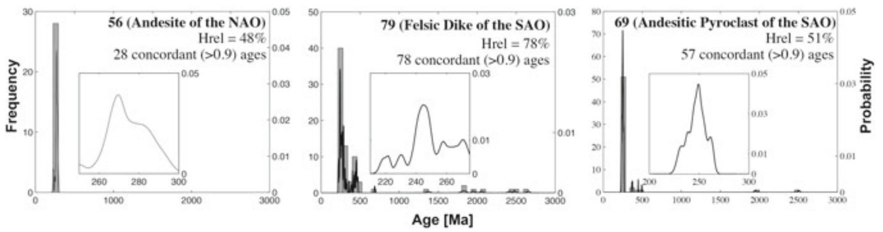

Fig. 4.6 Combined age histograms and probability density functions for samples from Permian volcanic rocks in the Northern and Southern Accretionary Orogens. NAO: Northern Accretionary Orogen; SAO: Southern Accretionary Orogen

4.1.2 Devonian Sedimentary Rocks from the Chinese Southern Mongolian Arcs

Growth structures of sedimentary rocks from Devonian strata are dominantly concentric oscillatory (Fig. 4.7). A few grains do not show any oscillatory zoning, and are under CL either single coloured or show bright overgrowth rims, which suggests either a metamorphic origin or overgrowth. However, laser ablation sites do not show Th/U ratios characteristic for metamorphic zircons, thus suggesting that such zircons were either not analysed or are not related to metamorphism. Most grains have a sub- to anhedral and well-rounded shape, implying a higher degree of maturity for the respective clastic sedimentary rock sample.

Ages of Devonian sedimentary rock samples, two of which sandstones and one quartzite, comprise three major age groups: ca. 965 Ma, ca. 511 Ma and ca. 409 Ma (Figs. 4.8 and 4.9). However, age spectra of single samples vary considerably, despite having to variable degrees all age groups represented. This is also reflected in their wide range of relative heterogeneity values between 67 and 85%. Thus, sedimentary provenance terranes may not necessarily be identical for each sample.

4.1.3 The Southern Accretionary Orogen

In the Huanggangliang formation concentric oscillatory zoning dominates the growth structure of most zircons throughout the samples (Fig. 4.10). Metamorphic overgrowths are rare but occur in sample 15. Few zircon grains contain inherited Precambrian aged cores with younger oscillatory rims. Zircons without any visible internal structures occur, but are rare and can be explained by either a comparatively high U-content or a metamorphic origin. However, the relatively low CL image quality should be taken into account. Zircon grains are generally euhedral to subhedral, with a few subrounded grains indicating a higher degree of reworking, particularly in sample 15. Analytical sites show a range of Th/U ratios from 0.03 to 0.65; most,

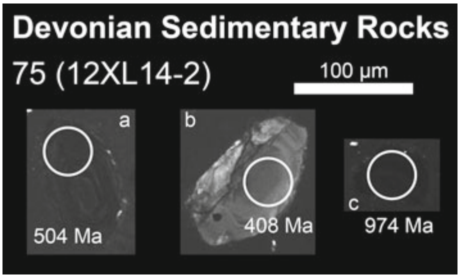

Fig. 4.7 Representative CL images of zircons from Devonian sedimentary strata in the Chinese southern Mongolian Arcs

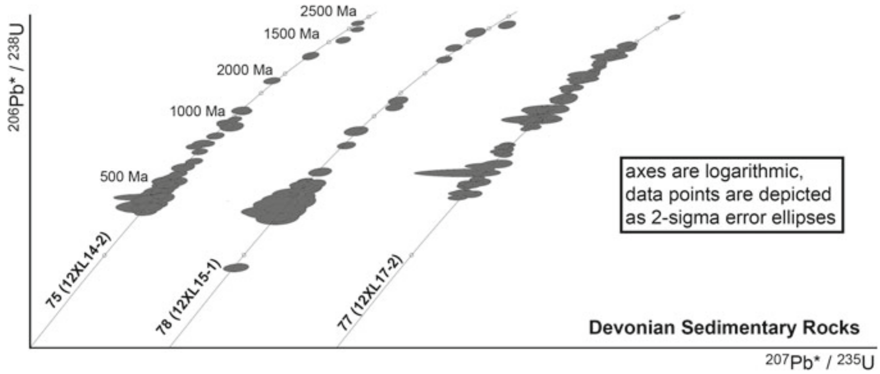

Fig. 4.8 U–Pb concordia diagrams for zircons from Devonian sedimentary strata in the Chinese southern Mongolian Arcs

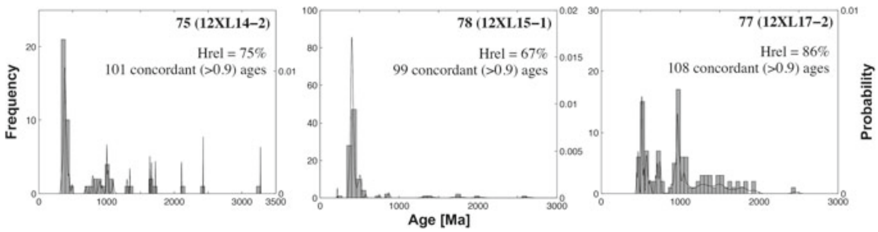

Fig. 4.9 Combined age histograms and probability density functions for samples from Devonian strata in the Chinese southern Mongolian Arcs

however, are above 0.07. The majority of zircons are, therefore, of magmatic origin, and only a few experienced metamorphism or reworking.

In the Linxi formation zircons generally exhibit concentric oscillatory zoning (Fig. 4.10). A significant number of grains have metamorphic overgrowth rims. Few do not have any visible internal structures and are either light coloured or dark under CL. However, the CL image quality is relatively poor and might lead to some bias. The degree of rounding is highly variable ranging from euhedral crystals to well rounded grains. A small number of grains show striped zoning originating either from (a) reworking of larger concentric oscillatory grains or (b) from crystallisation from mafic magma. All laser ablation sites show a large range of Th/U ratios from 0.03 to 2.02, with most above 0.07. This indicates that most zircons are of magmatic origin, though a small number of grains underwent metamorphic growth either as rims or single zircons.

Zircons from the andesitic pyroclast are generally euhedral to subhedral and predominantly exhibit concentric oscillatory zoning (Fig. 4.10). A significant amount of zircon grains show patchy zoning. Laser ablation sites show a range of Th/U ratios from 0.10 to 1.65, with an average value of 0.58. Analysed zircons are, therefore, of magmatic origin.

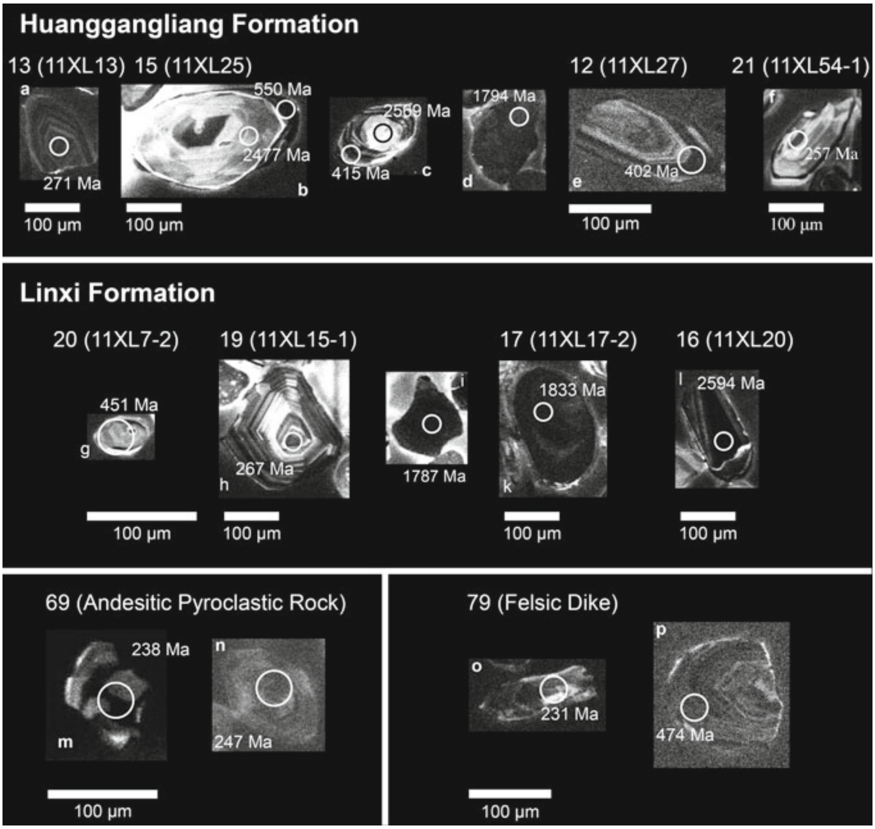

Fig. 4.10 Representative CL images of zircons from the Southern Accretionary Orogen

Zircons from a felsic dike, which intruded the Huanggangliang formation turbidites, are generally euhedral to subhedral with mostly concentric oscillatory zoning (Fig. 4.10). Laser ablation sites show Th/U ratios from 0.16 to 1.13, with an average value of 0.83. The grains are, thus, considered to be of magmatic origin. However, a few grains do not show any zoning or are slightly rounded, and interpreted to be xenocrysts captured either (a) from the host rock or (b) during magma ascent.

Overall, four age groups can be observed in the Huanggangliang formation (Figs. 4.11 and 4.12): ca. 2.50 Ga, ca. 1.80 Ga, ca. 437 Ma and ca. 268 Ma. A relative heterogeneity value of 72% for the entire formation indicates the dominance of several age groups; however, they are not consistently present throughout the formation. Samples 23 and 21 are dominated by a single age peak at ca. 268 Ma, which is also reflected in low relative heterogeneity values of 43–49%, indicating the dominance of the one age group. Samples 11–13 mainly contain the ca. 268 Ma and ca. 437 Ma age groups, with minor Precambrian ages, if any at all. Subsequently, the relative heterogeneity values are higher ($H_{rel} = 65\%$, $H_{rel} = 63\%$ and

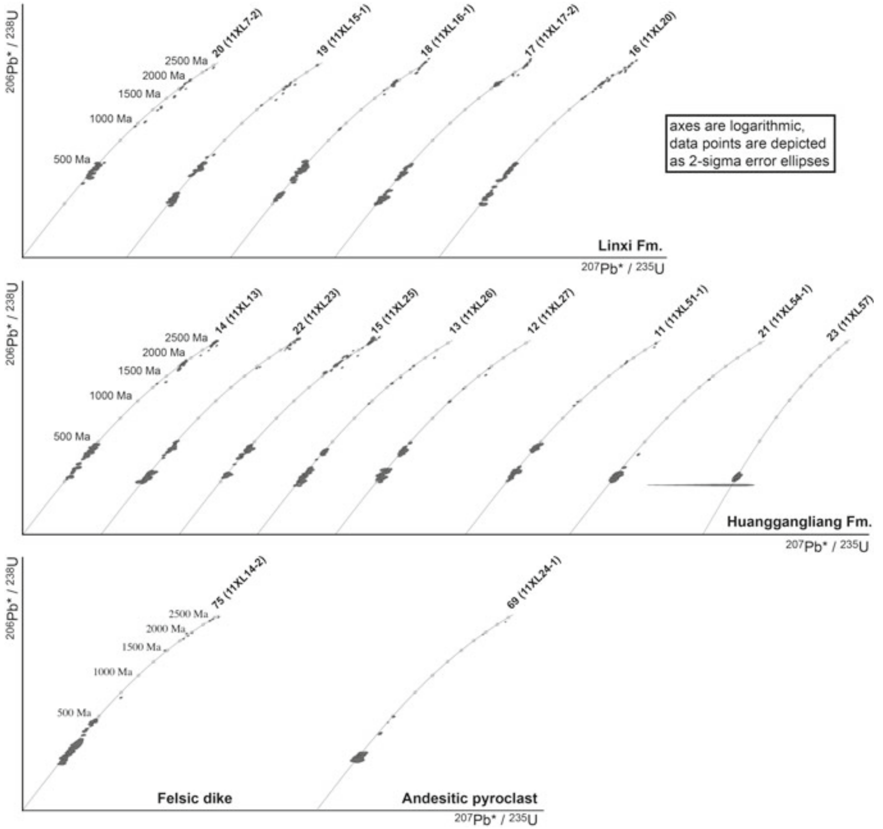

Fig. 4.11 U–Pb concordia diagrams for zircons from the Southern Accretionary Orogen

$H_{rel} = 64\%$). In contrast, samples 14, 15 and 22 contain all age groups. Their values of relative heterogeneity are the highest, with $H_{rel} = 79\%$ $H_{rel} = 71\%$ and $H_{rel} = 78\%$, respectively.

Age populations recognised in the Linxi formation are similar to those of the Huanggangliang formation (Figs. 4.11 and 4.12): ca. 2.49 Ga, ca. 1.85 Ga, ca. 455 Ma and ca. 270 Ma. These age groups are relatively well represented in all samples, in contrast to the Huanggangliang formation. The overall value of relative heterogeneity ($H_{rel} = 79\%$) is higher as well. The four age groups are all present in samples 16–18 as also indicated by the highest values of relative heterogeneity ($H_{rel} = 73\%$, $H_{rel} = 80\%$ and $H_{rel} = 76\%$, respectively). In comparison, Precambrian zircons are less represented in sample 19 but still occur, as also demonstrated by a lower value of relative heterogeneity ($H_{rel} = 68\%$). Sample 20 is the only sample with no pronounced Permian age peak ($H_{rel} = 72\%$), although a few discordant zircons around ca. 270 Ma were measured.

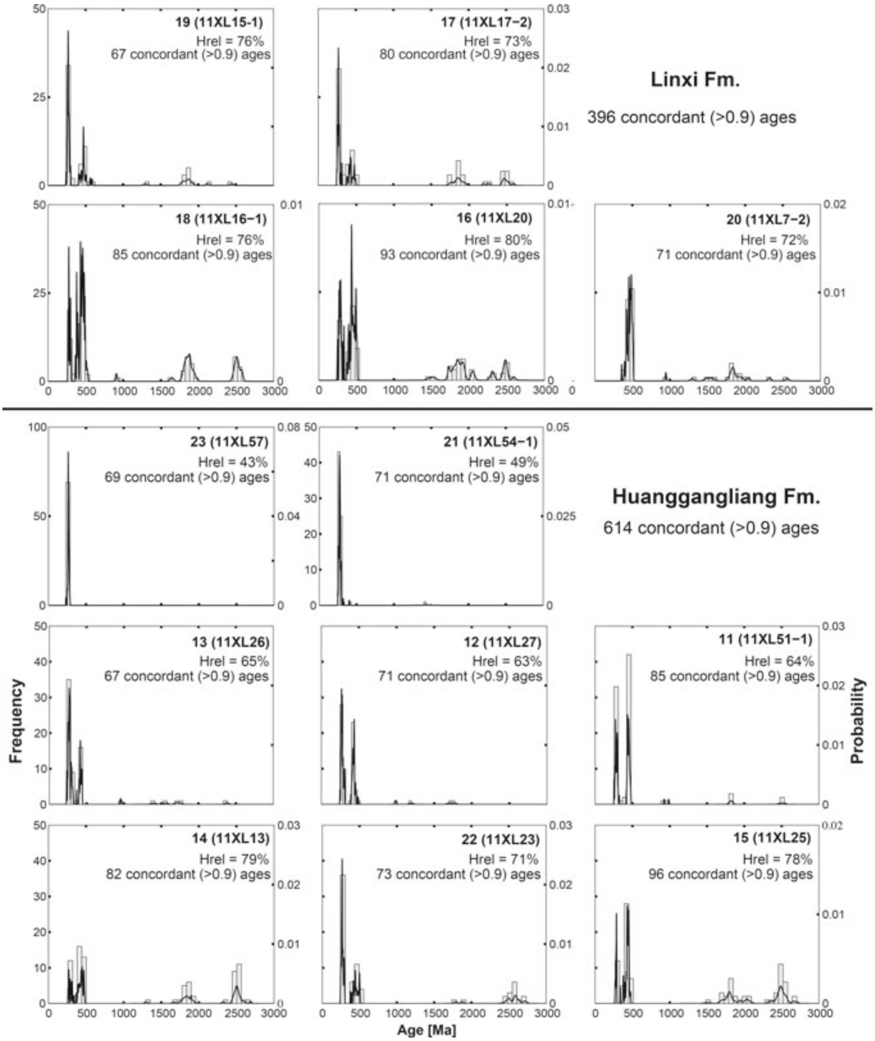

Fig. 4.12 Combined age histograms and PDF's for samples from the Southern Accretionary Orogen

A dominant single age peak in the andesitic pyroclast (sample 69) is located between ca. 225 Ma and ca. 275 Ma (Figs. 4.9 and 4.11), which yielded an unrealistically precise weighted mean average age of 249 ± 2 Ma (MSWD = 12). The high MSWD indicates a large component of geological scatter in the data, most likely due to the presence of several similar age populations. The sample might have been multiply reworked, and pyroclastic material successively added before final deposition. The older zircon grains are considered to be xenocrysts captured either from the nearby Permian volcanic arc rocks or volcano-clastic strata during magma ascent. Thus, the weighted mean age has to be taken with caution. The majority of the youngest ages suggests that the andesitic pyroclastic rock formed at a later time, most likely between the Early to Middle Triassic.

The felsic dike (sample 79) shows a dominant age group between ca. 255 Ma and ca. 245 Ma (Figs. 4.9 and 4.11), which gave a weighted mean average age of 242 ± 3 Ma (MSWD = 9.6), slightly younger than that calculated for the andesitic pyroclastic rock. The high MSWD indicates a large component of geological scatter and probably the presence of several similar age populations. This can be understood by assuming that captured zircons form nearby volcanic rocks and sedimentary strata were added during dike emplacement, thus possibly tapping several age reservoirs. As discussed above, the Huanggangliang formation, in where the dike intruded, is characterised by age peaks at ca. 2.49 Ga, ca. 1.85 Ga, ca. 455 Ma and ca. 270 Ma. These ages all occur in the age population of the felsic dike. Other zircons mostly yielded ages around ca. 451 Ma, with a few yielding Precambrian ages ranging from 2656 ± 19 Ma to 1376 ± 23 Ma. The Early to Middle Triassic volcanic activity, evidenced by the andesitic pyroclastic rock, also contributed zircons, adding to the complexity of the age distribution. Since these ages are not considered in the calculation of the weighted mean average age, the latter only can serve as a general age reference for the location of the major age population in the dike. Based on the youngest zircon age groups, it is, thus, assumed that dike emplacement occurred later, between the Early to Middle Triassic.

4.2 Detrital Zircon Hf Isotope Compositions

Hf isotopic compositions were measured for 487 detrital zircon grains from Permian sedimentary strata covering all three major age groups from the Neoarchaean to Late Palaeozoic across the accretionary collision zone between the Mongolian Arcs and the North China Craton. εHf values, dominantly ranging from ca. −20 to +15, indicate that these zircons were formed in a broad range of magma compositions from juvenile to crustal contaminated. Similar to the geochronological data set, each lithotectonic belt is characterised by a distinct distribution of εHf values (Fig. 4.13).

4.2.1 The Hegenshan Ophiolite Complex and Northern Accretionary Orogen

εHf values north of the Solonker Suture Zone generally produce a fanning array ranging from ca. −15 to ca. +15 when reaching the Late Palaeozoic. The initial trend towards negative εHf values shifts during the Early Palaeozoic to dominantly positive values (Fig. 4.14; for a summarised plot see also Fig. 6.6). Two samples (samples 3 and 10), one of which from the Hegenshan Ophiolite Complex, exhibit

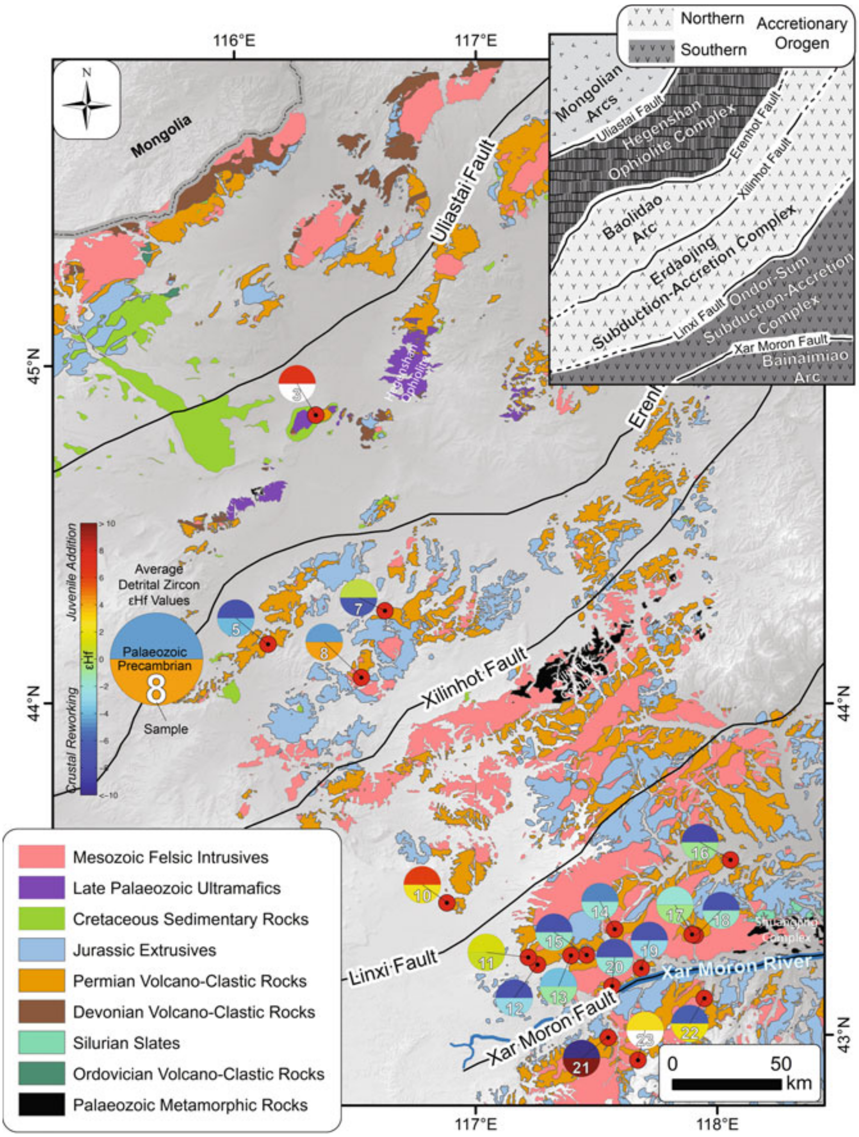

Fig. 4.13 Geological map and locations of samples analysed for zircon Hf isotopic compositions. Colours in circles correspond to the average detrital zircon εHf values recorded in the Precambrian and Palaeozoic

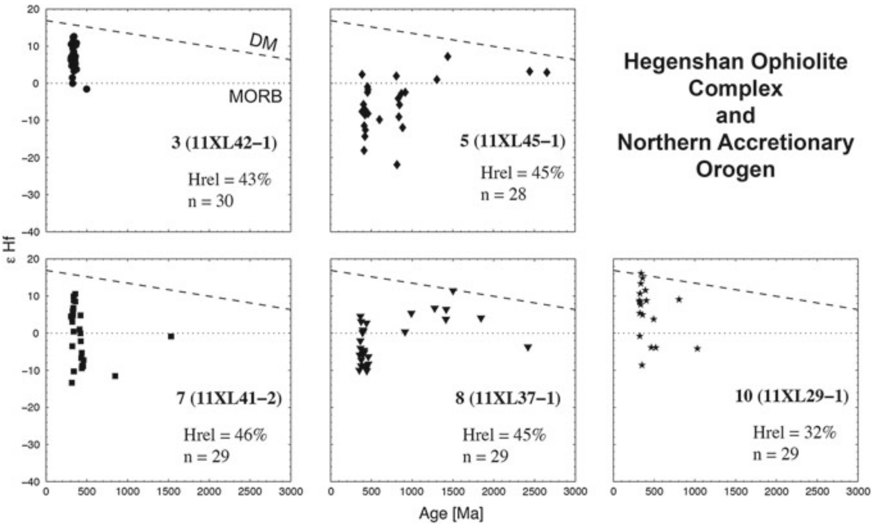

Fig. 4.14 Detrital zircon εHf versus age diagrams for single samples of the Hegenshan Ophiolite Complex and the Northern Accretionary Orogen

strong positive εHf values (ca. +15 to ca. +3) during Carboniferous time, sample 7 (Fig. 4.14) follows the overall mixed trend (ca. +10 to ca. −10), and two samples (samples 5 and 8) develop to moderately negative εHf values (ca. +5 to ca. −15).

These observations imply that different local provenance terranes delivered, either independently or as a coherent assemblage, detritus to the sedimentary basins: those consisting of a considerable amount of reworked crust, whereas others were comprised of an exclusively juvenile source, likely to have appeared in the Carboniferous.

4.2.2 The Southern Accretionary Orogen

The development of εHf values to the south of the Solonker Suture Zone stands in stark contrast to the north. The fanning array follows an overall trend that broadens towards negative values reaching a range of ca. +10 to −15 in the Palaeozoic. In the Early Palaeozoic a strong shift towards positive values is again followed by a broadening trend towards negative values in the Late Palaeozoic (Fig. 6.6). Eight samples (samples 12, 13, 16, 18–22; Fig. 4.15) comply with the overall trend. The remaining five samples (samples 11, 14, 15, 17, 23) display stronger shifts towards positive εHf values either in the Early or Late Palaeozoic, or both. The εHf values for the ca. 1.8 Ga and 2.5 Ga old zircons are consistent with those reported for the North China Craton [4].

These relative homogenous results indicate that the arc basins in the Southern Accretionary Orogen were dominated by detritus from well defined provenance terranes, that are comprised of a considerable amount of reworked crust, but were supplemented by juvenile material in the Early and Late Palaeozoic.

4.3 Whole-Rock Geochemical Data

Major and trace element geochemical analyses were performed for 23 volcanic and 30 sedimentary rock samples collected across the entire accretionary collision zone from the Mongolian Arcs to the North China Craton (Fig. 4.16). The sampled formations cover the Permian Qingfengshan, Ranfangdi, Huanggangliang, Linxi, Zhesi and Gegenaobao formations (Fig. 2.4).

4.3.1 Major Element Oxide Content

The sedimentary rocks in the Northern Accretionary Orogen have bimodal SiO_2 compositions with one group having a range of 54.8–61.1 wt.% and the other 79.9–81.7 wt.% (Fig. 4.17). Negative correlations can be observed with respect to TiO_2 (from ca. 0.3 to 1.2 wt.%), Al_2O_3 (from ca. 8.1 to 16.3 wt.%), Fe_2O_3 (from ca. 1.8 to 8.8 wt.%), MnO (from ca. 0.02 to 0.12 wt.%), MgO (from ca. 0.5 to 5.2 wt.%) and CaO (from ca. 9.8 to 0.2 wt.%). Na_2O (ca. 1.6–2.7 wt.%), K_2O (ca. 1.3–2.0 wt.%) and P_2O_5 (ca. 0.1–0.2 wt.%) appear to be independent from the SiO_2 content.

Volcanic rocks (Fig. 4.17) in the Northern Accretionary Orogen have SiO_2 values of 50.1–71.2 wt.%, not reflecting the bimodal character as well as the sedimentary rocks. In most cases negative, but weak, correlations can be assumed with respect to TiO_2 (from ca. 0.6 to 1.8 wt.%), Al_2O_3 (from ca. 12.3 to 16.5 wt.%), Fe_2O_3 (from ca. 3.9 to 10.2 wt.%), MnO (from ca. 0.06 to 0.14 wt.%), MgO (from ca. 2.5 to 6.3 wt.%) and CaO (from ca. 1.9 to 8.7 wt.%). Weight percentages of aforementioned oxides are on average higher than those in the sedimentary rocks. Na_2O (ca. 2.6–4.6 wt.%) and P_2O_5 (ca. 0.1–0.2 wt.%) appear to be largely independent from the SiO_2 content. K_2O (ca. 0.2–3.1 wt.%), however, shows a weak positive correlation.

In contrast, the sedimentary rocks of the Southern Accretionary Orogen exhibit a continuous distribution of SiO_2 content from ca. 48.7 to 70.0 wt.%. However, negative correlations, similar to the Northern Accretionary Orogen, can be observed for TiO_2 (from ca. 0.4 to 1.9 wt.%), Al_2O_3 (from ca. 9.6 to 16.9 wt.%), Fe_2O_3 (from ca. 2.1 to 13.0 wt.%), MnO (from ca. 0.03 to 0.2 wt.%) and MgO (from ca. 1.1 to 3.8 wt.%), whereas the negative trend is not as clear for CaO (from ca. 1.5 to 7.4 wt.%) and Na_2O (from ca. 0.1 to 4.5 wt.%). A slight positive correlation is visible for K_2O (from ca. 0.7 to 5.38 wt.%). The correlation between SiO_2 and P_2O_5 appears to be slightly negative (from ca. 0.1 to 0.2 wt.%).

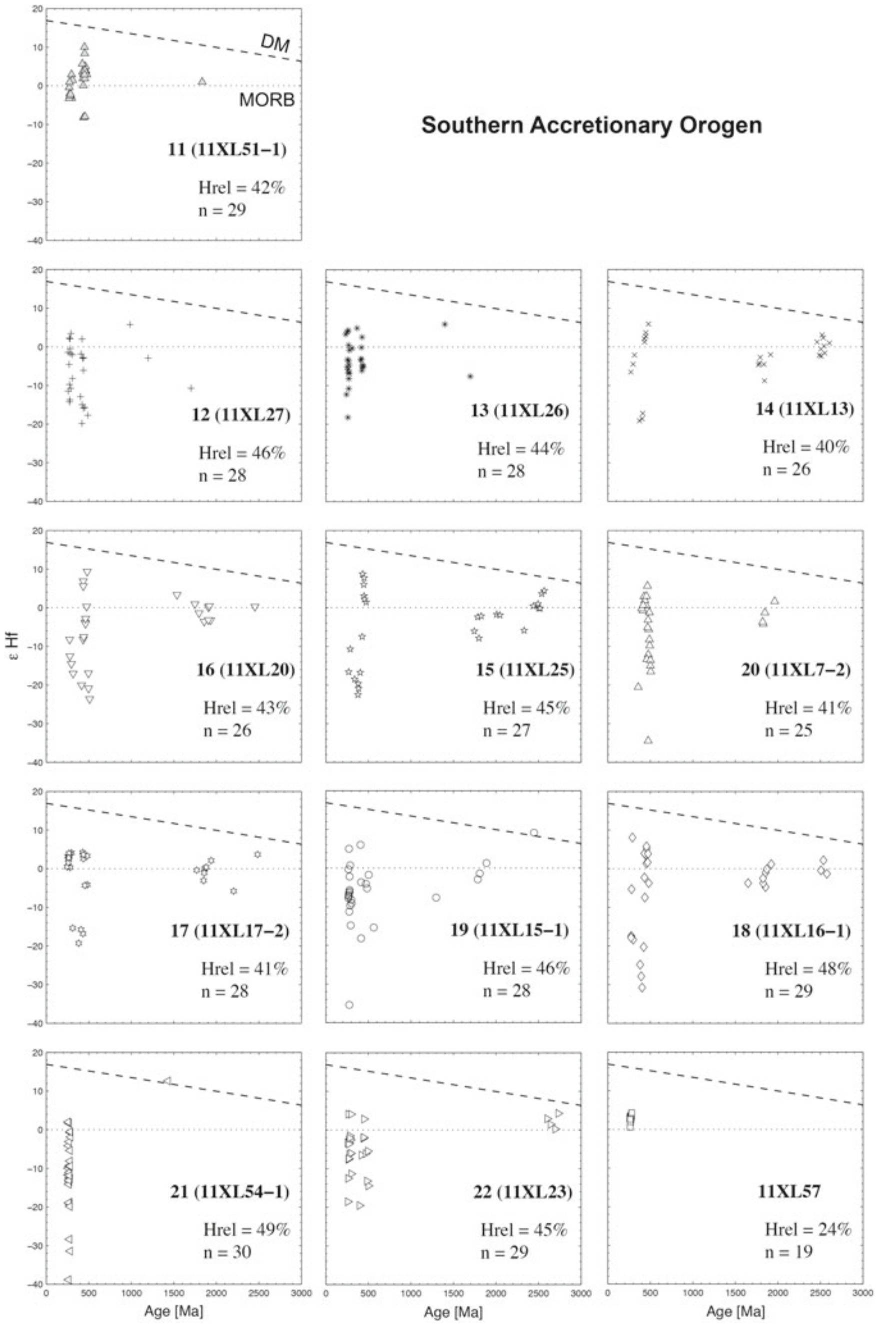

Fig. 4.15 Detrital zircon εHf versus age diagrams for samples of the Southern Accretionary Orogen

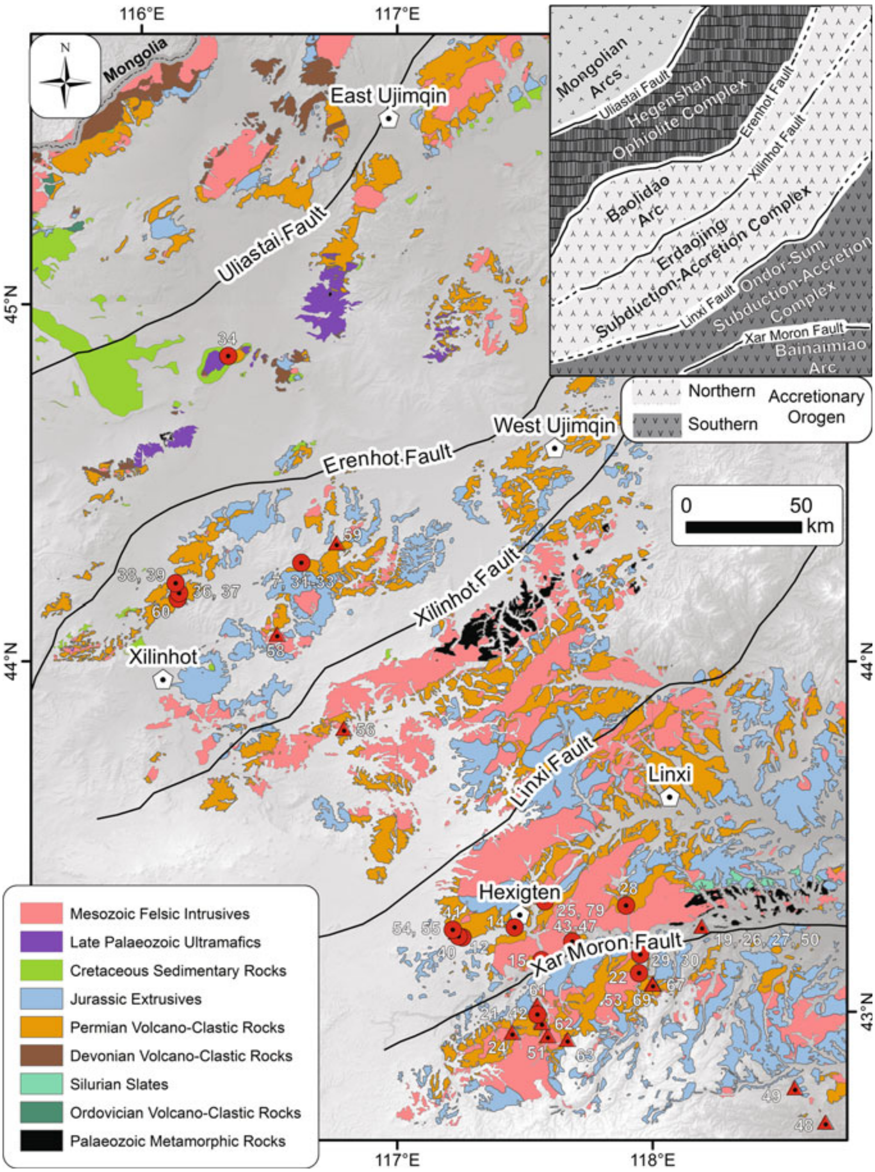

Fig. 4.16 Sample locations of sedimentary (circles) and volcanic rocks (triangles) analysed for whole-rock major and trace element compositions

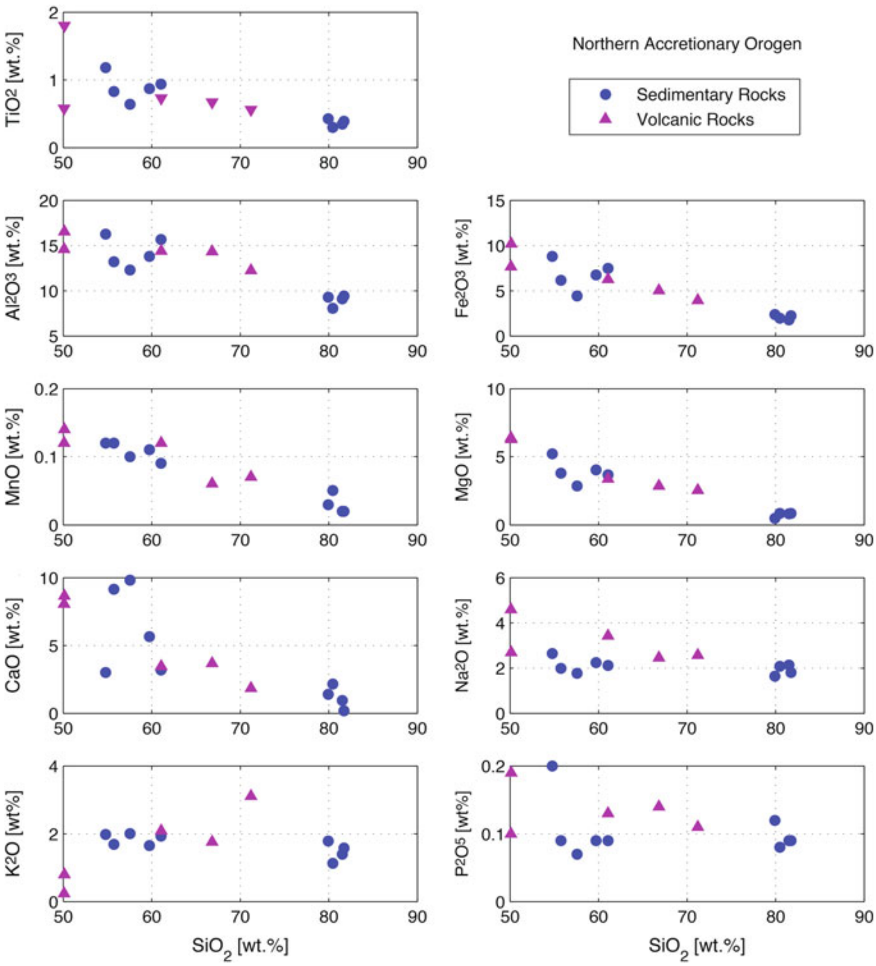

Fig. 4.17 Harker diagrams for volcano-clastic sedimentary and volcanic rocks of the Northern Accretionary Orogen

Volcanic rocks in the Southern Accretionary Orogen have SiO_2 contents ranging from 48.7 to 67.0 wt.%, overall lower than their equivalents to the north (Fig. 4.18). Strong negative correlations with respect to SiO_2 content can be observed for Fe_2O_3 (from ca. 4.1 to 12.2 wt.%), MgO (from ca. 1.6 to 8.5 wt.%) and CaO (from ca. 1.8 to 10.7 wt.%), which most likely reflect successive fractionation of minerals such as pyroxenes and plagioclase with higher silica content. Weak negative correlations with respect to increasingly felsic compositions might exist for TiO_2 (from ca. 0.5 to 2.1 wt.%), Al_2O_3 (from ca. 15.1 to 16.4 wt.%) and MnO (from ca. 0.1 to 0.3 wt.%). No obvious correlations are observed for Na_2O (ca. 1.8–5.4 wt.%), K_2O (ca. 0.2–4.2 wt.%) and P_2O_5 (ca. 0.1–0.8 wt.%).

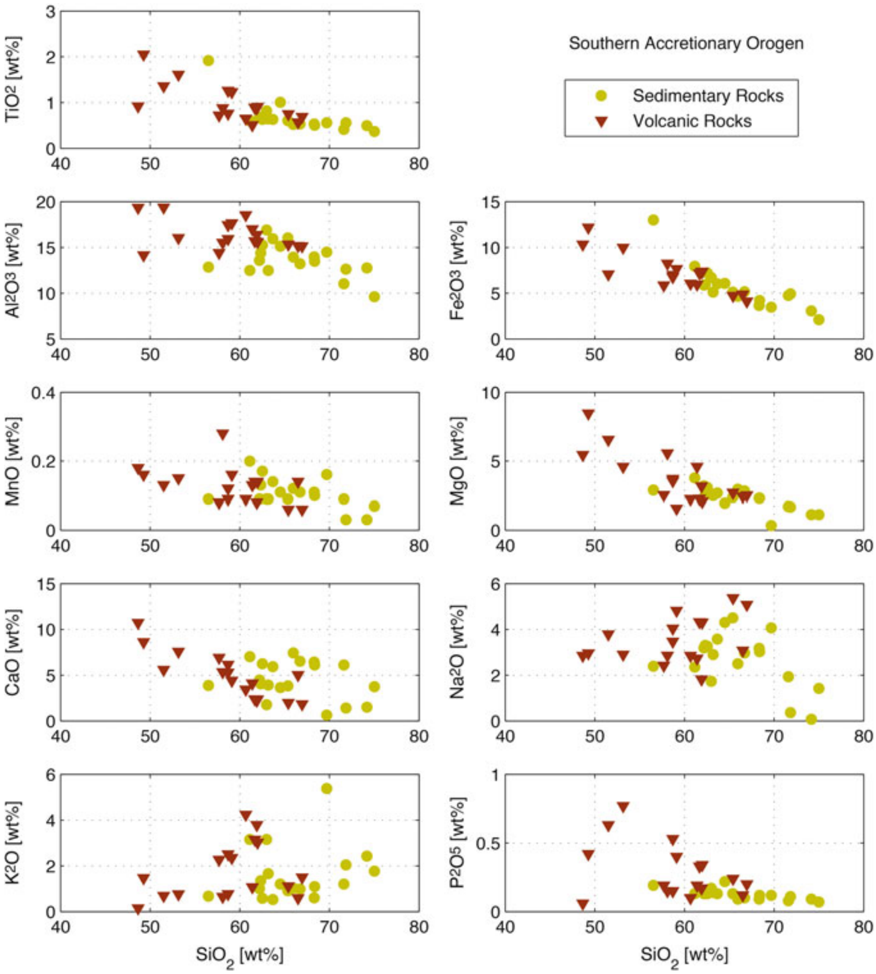

Fig. 4.18 Harker diagrams for volcano-clastic sedimentary and volcanic rocks of the Southern Accretionary Orogen

Under the assumption that SiO_2 increases with higher textural maturity of the clastic sedimentary rocks, TiO_2 and Al_2O_3 seem to be largely immobile during sediment deposition in both orogens, and, thus, can be used as tracers for sedimentary provenance (see also [2, 3]). Although P_2O_5 is likely to be immobile as well, it was excluded as a tracer for provenance analysis due to its differing behaviour in the two accretionary orogens as will be further elaborated below.

P_2O_5 in the volcanic rocks is slightly enriched compared to average N-MORB compositions in the Northern Accretionary Orogen, whereas in the Southern Accretionary Orogen it is slightly depleted (Fig. 4.19). Compared to average continental crust P_2O_5 in the clastic sedimentary rocks is slightly depleted in both orogens. K_2O

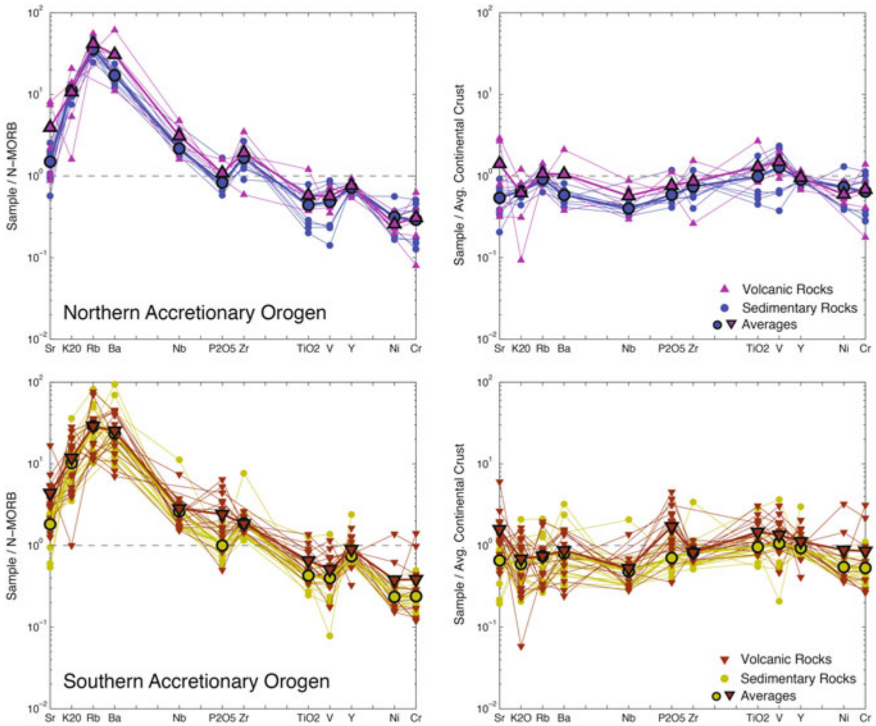

Fig. 4.19 N-MORB and average continental crust normalised extended spider diagrams of major and trace elements (according to [2, 7, 11]) for the Northern and Southern Accretionary Orogen. N-MORB compositions are from Rollinson [9], average continental crust from Wedepohl [14]

is enriched in both orogens with respect to N-MORB compositions, but shows values close to average continental crust. TiO_2 is in both orogens slightly depleted with respect to N-MORB, but closely resembles average continental crust.

Provenance discrimination diagrams by Roser and Korsch [10] indicate that the clastic sedimentary rocks of the Southern Accretionary Orogen plot dominantly in the intermediate to mafic igneous provenance fields, whereas those of the Northern Accretionary Orogen are distinctly located in the quartzose to felsic igneous provenance fields. In tectonic discrimination diagrams by Bhatia [1] sedimentary rocks of the Southern Accretionary Orogen plot in a wide range of active arc settings, whereas those of the Northern Accretionary Orogen are located either in the passive margin, which partly overlaps with the active continental margin field, or the oceanic arc field.

In the TAS diagram the volcanic rocks of both orogens plot at relatively low total alkali contents ranging from basic to acidic compositions. The volcanic rocks in the Northern Accretionary Orogen point to a weak bimodal character. In the AFM diagram most volcanic rocks plot in the calc-alkaline series field, implying an overall convergent plate tectonic setting (Figs. 4.20 and 4.21).

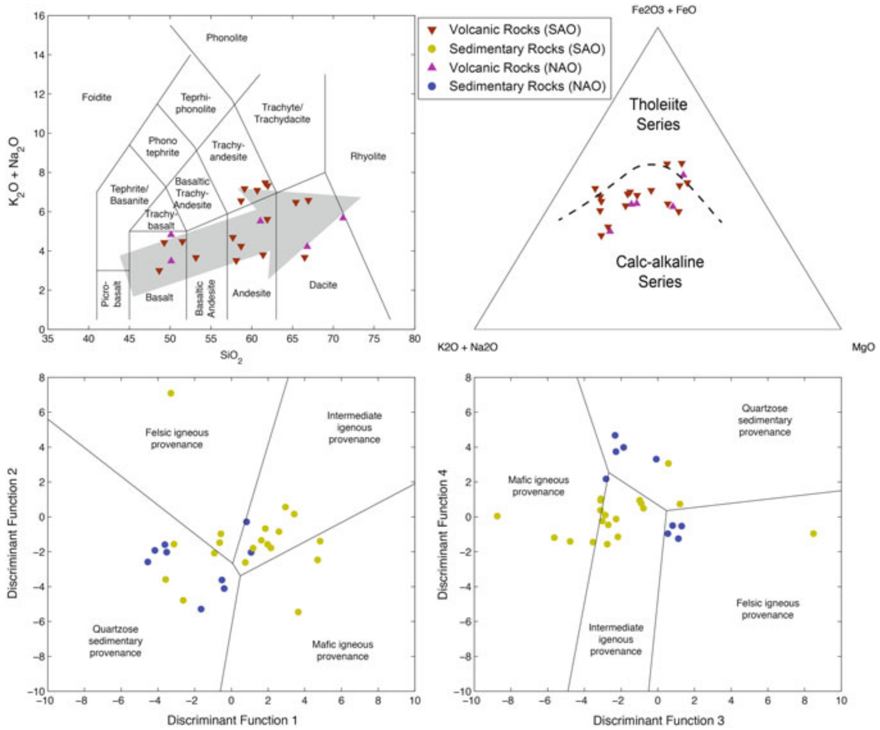

Fig. 4.20 TAS (top left), AFM (top right) and sedimentary provenance discrimination diagrams for major element oxide compositions of sedimentary and volcanic rocks (bottom row; after [5, 6, 10]) of the Northern and Southern Accretionary Orogens. Discrimination function 1 = −1.773 TiO_2 + 0.607 Al_2O_3 + 0.76 Fe_2O_3 − 1.5 MgO + 0.616 CaO + 0.509 Na_2O − 1.224 K_2O − 9.09; discrimination function 2 = 0.445 TiO_2 + 0.07 Al_2O_3 − 0.25 Fe_2O_3 − 1.142 MgO + 0.438 CaO + 1.475 Na_2O + 1.426 K_2O − 6.861; discrimination function 3 = 30.638 TiO_2/Al_2O_3 − 12.541 Fe_2O_3/Al_2O_3 + 7.329 MgO/Al_2O_3 + 12.031 Na_2O/Al_2O_3 + 35.402 $K2O/Al_2O_3$ − 6.382; discrimination function 4 = 56.500 TiO_2/Al_2O_3 − 10.879 Fe_2O_3/Al_2O_3 + 30.875 MgO/Al_2O_3 − 5.404 Na_2O/Al_2O_3 + 11.112 K_2O/Al_2O_3 − 3.89

4.3.2 Trace Element Concentrations

Trace element concentrations of V, Cr, Co, Ni, Cu, Zn, Rb, Sr, Zr, Ba, Y and Nb were measured, and plotted over SiO_2 content (Figs. 4.22 and 4.23). Concentrations were only plotted when they were above the detection limit. Limited sample numbers and/or concentrations below the detection limit may impede statements on any correlative behaviour, especially in the Northern Accretionary Orogen. However, weak trends are observable and will be described below, but should be taken with caution. Concentrations given in brackets behind the respective element represent the absolute range, which does not necessarily reflect the positive or negative correlation. The weak character of the correlations may also indicate nearly constant

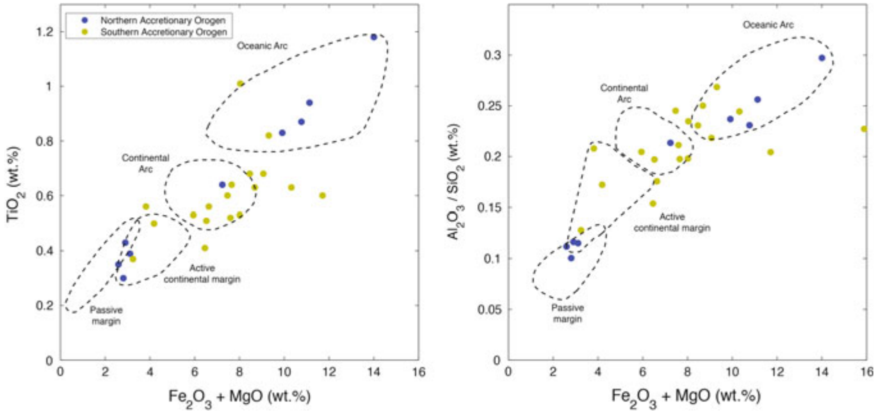

Fig. 4.21 Tectonic discrimination diagrams for major element oxide compositions of sandstones in the Northern and Southern Accretionary Orogen (after [1])

concentrations of most trace elements in the sedimentary rocks. Real positive and negative correlations are most likely linked to the increased textural maturity of the clastic sedimentary rock, causing, for example, the "zircon effect".

Analyses of sedimentary rocks of the Northern Accretionary Orogen (Fig. 4.22) reveal relatively scattered data points for concentrations of V (ca. 60–228 ppm), Cr (ca. 48–143 ppm), Co (ca. 24–27 ppm), Cu (ca. 22–73 ppm), and Y (ca. 17–25 ppm), and thus no visible correlation. Results for Ni (ca. 22–73 ppm), Zn (ca. 35–85 ppm), Rb (ca. 64–96 ppm) and Sr (ca. 113–305 ppm) may suggest weak negative correlations with increasing silica content. Concentrations for Zr (ca. 81–240 ppm), Ba (ca. 243–473 ppm) and Nb (ca. 6–9 ppm) show a slight positive correlation with higher SiO_2 content.

Results for the volcanic rocks do in many, but not all, cases correspond to the pattern seen in the sedimentary rocks (Fig. 4.22). No clear correlations with increasing SiO_2 content are observed for Cr (ca. 22–228 ppm), Co (ca. 26–28 ppm), Ni (ca. 26–48 ppm), Sr (ca. 106–966 ppm), Y (ca. 16–28 ppm) and Nb (ca. 6–17 ppm). Weak negative correlations can be inferred for Zn (ca. 56–112 ppm), Zr (ca. 53–313 ppm) and Ba (ca. 221–1229 ppm). Weak positive correlations can be observed for V (ca. 91–193 ppm), Cu (ca. 23–41 ppm) and Rb (ca. 67–111 ppm).

A higher number of analytical results for the sedimentary rocks of the Southern Accretionary Orogen is able to better identify possible trends with respect to silica content (Fig. 4.23). Measurements for V (ca. 20–358 ppm), Zn (ca. 56–152 ppm) and Sr (ca. 65–354 ppm) yielded weak to moderate negative correlations. No clear positive correlations were observed, although Rb (ca. 24–165 ppm) might increase with higher silica content. Concentrations for Cr (ca. 36–139 ppm), Ni (ca. 22–51 ppm), Zr (ca. 104–234 ppm), Ba (ca. 187–840 ppm), Y (ca. 17–72 ppm) and Nb (ca. 6–39 ppm) appear to be largely constant, and thus independent from the SiO_2 content. Only a single data point was retrieved for Co (ca. 24 ppm).

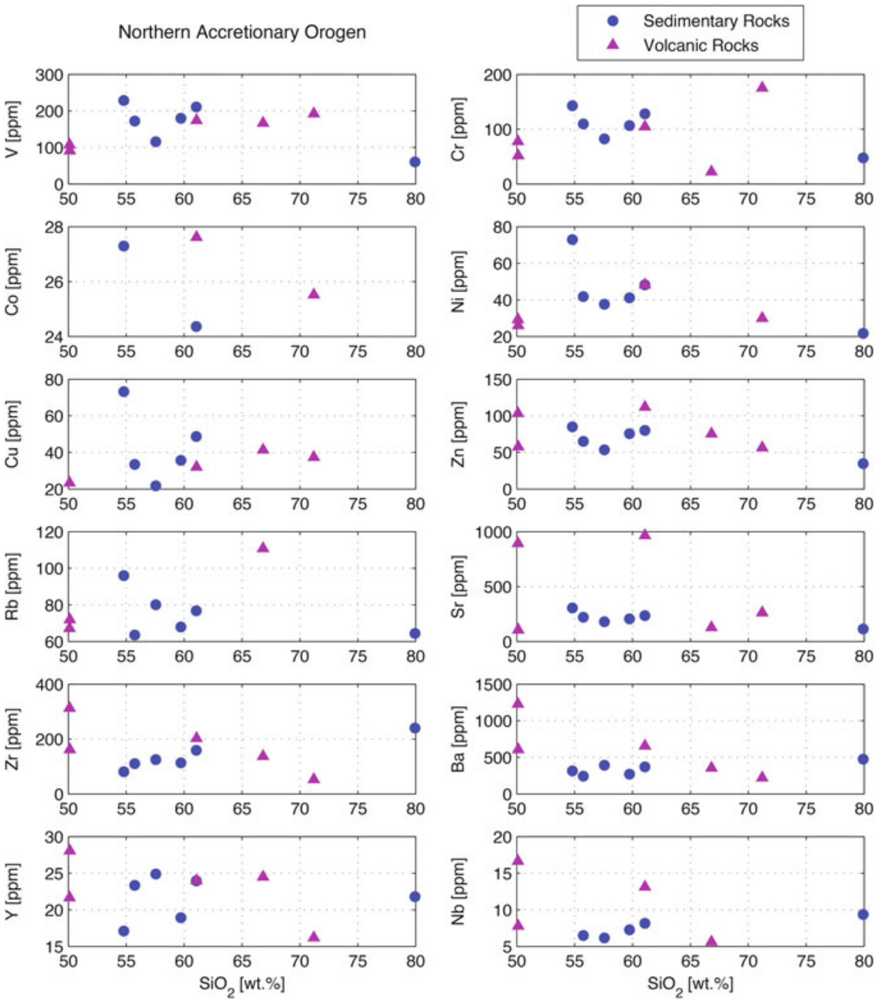

Fig. 4.22 Trace element concentrations with respect to SiO_2 content for clastic sedimentary and volcanic rocks of the Northern Accretionary Orogen

Trace element compositions of volcanic rocks in the Southern Accretionary Orogen are mostly scattered with respect to SiO_2 content (Fig. 4.23), such as for V (ca. 46–299 ppm), Cr (ca. 34–123 ppm), Co (ca. 21–48 ppm), Zn (ca. 34–152 ppm), Rb (ca. 23–152 ppm) and Ba (ca. 140–913 ppm). Weak negative correlations may be inferred for Ni (ca. 20–180 ppm), Cu (ca. 11–44 ppm) and Sr (ca. 151–880 ppm). Concentrations for Zr (ca. 134–235 ppm), Y (ca. 10–49 ppm) and Nb (ca. 5–26 ppm) are largely constant with increasing SiO_2 content.

Zr, Y and Nb appear largely independent from silica content in the sedimentary rocks, which suggests that these elements behaved immobile during sedimentary

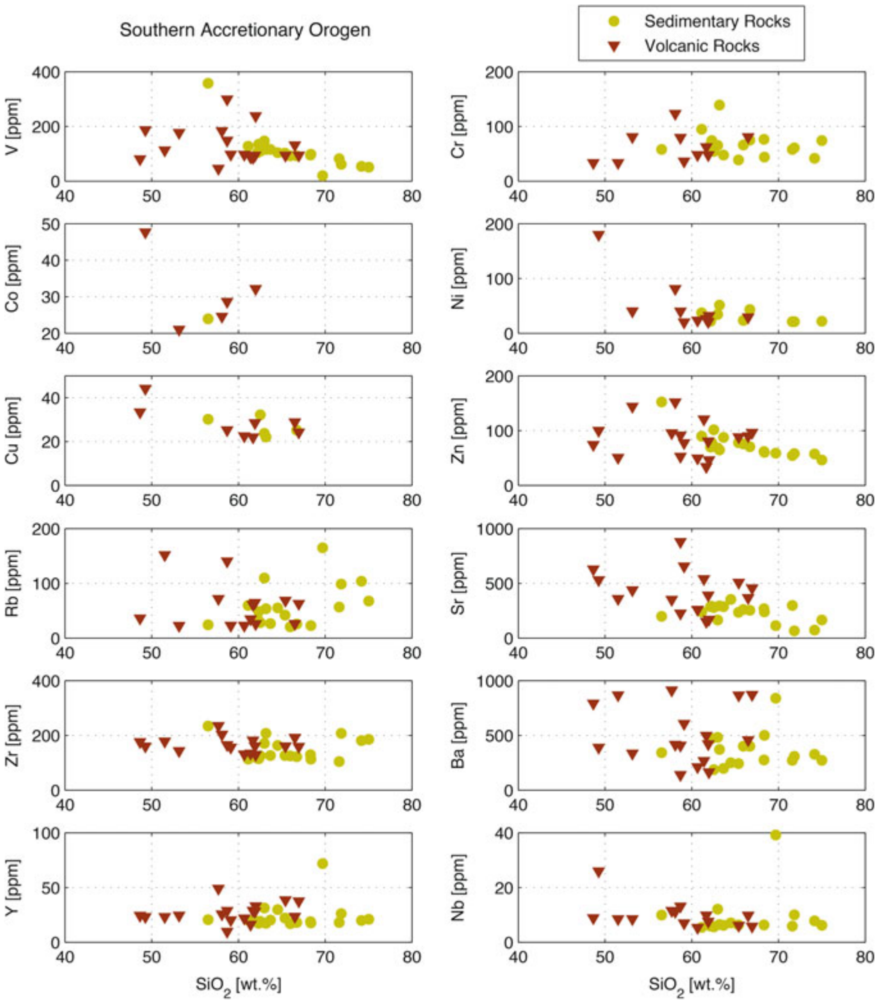

Fig. 4.23 Trace element concentrations with respect to SiO_2 content for clastic sedimentary and volcanic rocks of the Southern Accretionary Orogen

processes. They are, thus, used as tracers for further geochemical provenance analyses (see also [2, 3]). Sr, Nb and Zr in both orogens are on average slightly enriched with respect to N-MORB, and slightly depleted with respect to average continental crust (Fig. 4.19). V, Ni, and Cr are slightly to moderately depleted with respect to N-MORB, and slightly depleted with respect to continental crust. Y in both orogens appears to closely match the compositions of N-MORB and average continental crust, thus underlining its immobile character.

Spider diagrams for the volcanic rocks broadly follow the pattern observed for the sedimentary rocks in both orogens (Fig. 4.19). Sr is slightly enriched with respect to

N-MORB and average continental crust. Nb and Zr are slightly enriched with respect to N-MORB, but slightly depleted with respect to average continental crust. Rb and Ba in both orogens are enriched with respect to N-MORB, but correspond well to average continental crust. V, Ni and Cr are slightly to moderately depleted with respect to N-MORB, but only slightly depleted with respect to average continental crust. Y closely matches both standard compositions similar to the sedimentary rocks.

4.4 Whole-Rock Nd and Hf Isotope Compositions

εHf_{today} and εNd_{today} values across the accretionary collision zone between the Mongolian Arcs and the North China Craton (Fig. 4.24) have a very narrow range of ca. −2 to 0 and −2 to +2, respectively, for both sedimentary and igenous rocks (Fig. 4.25). They are positively correlated and well in agreement with the terrestrial array defined by Vervoort et al. [12, 13]. It appears that both isotopic compositions are also positively correlated with latitude from south to north. Isotopic compositions of the Southern Accretionary Orogen are overall negative, those of the Northern Accretionary Orogen mixed, and those of the Hegenshan Ophiolite Belt largely positive. These observations imply that crustal reworked magmatic material in the south is about equal to juvenile controlled magma production to the north.

The sedimentary rock samples of the Hegenshan Ophiolite Complex yielded, except for a single sample, positive εHf_{today} values (ca. −0.7 to +1.5), while all εNd_{today} values (ca. −0.04 to −1.1) are negative. The volcanic rock samples show throughout positive εHf_{today} values (ca. +0.6 to +1.4). εNd_{today} values are dominantly negative, except for one sample (ca. −0.5 to +0.3).

Whole-rock εHf_{today} values for sedimentary rocks of the Northern Accretionary Orogen exhibit a relatively large range (ca. −1.8 to +1.0) with a slight dominance of negative values. εNd_{today} values are in the range ca. −1.8 to +0.5 and, except for a single data point, all negative. Both analysed volcanic rocks have slightly positive εHf_{today} values (ca. +0.1 to +0.3), thus close to chondrite isotopic compositions, whereas εNd_{today} values are negative (ca. −0.7 to −0.9).

For both, sedimentary and volcanic rocks in the Southern Accretionary Orogen, εHf_{today} values (ca. −1.0 to −0.02 and ca. −0.7 to −0.1, respectively) and εNd_{today} values (ca. −1.8 to −0.6 and ca. −1.2 to −1.0, respectively) are throughout negative.

4.5 Relative Heterogeneity and Similarity Statistics

Similarity of the detrital age PDF's (see Sect. 4.1) with that of the North China Craton (Fig. 4.26), taken from Rojas-Agramonte et al. [8], reaches fairly high values (up to 0.6) in the Southern Accretionary Orogen, which dramatically decreases towards the Northern Accretionary Orogen (down to ca. 0.2) and diminishes in the Hegenshan Ophiolite Complex (ca. zero).

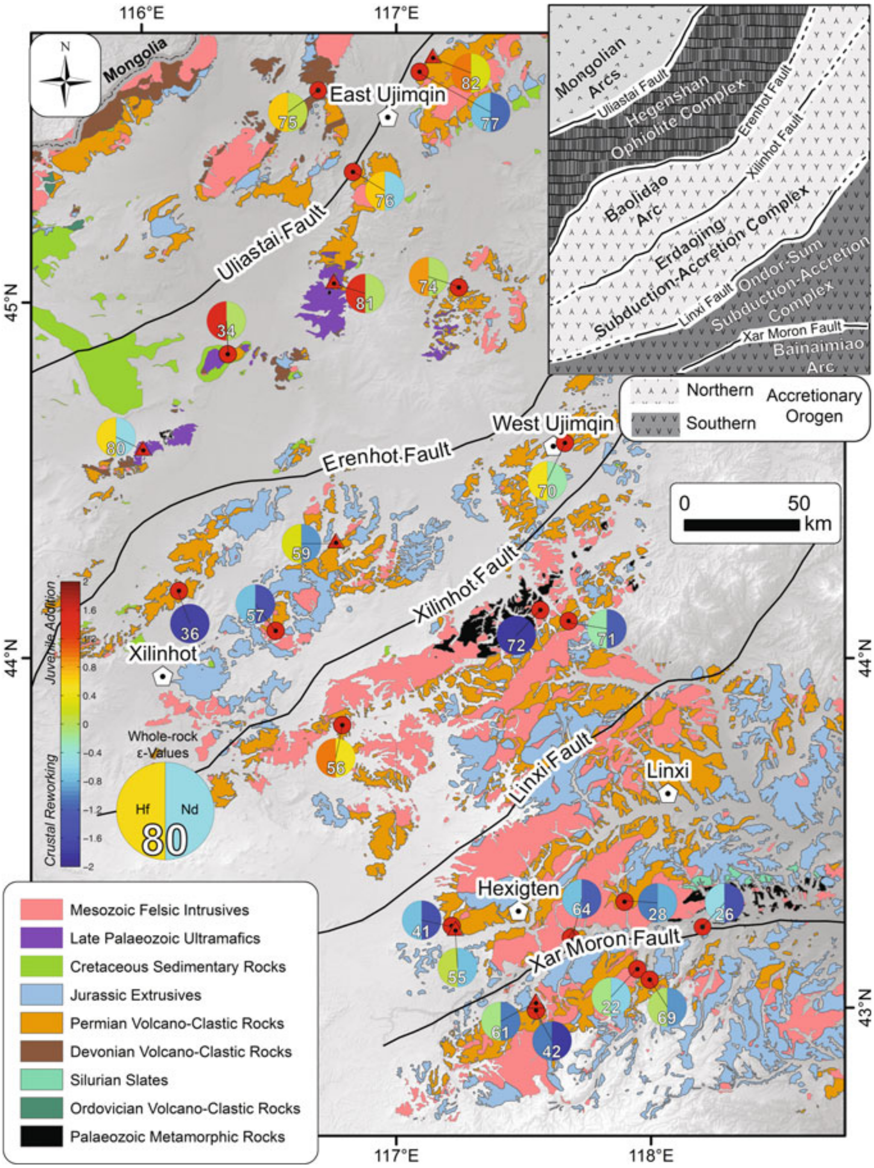

Fig. 4.24 Sample locations of sedimentary (circles) and volcanic rocks (triangles) analysed for Hf and Nd isotopic compositions. Colours in circles correspond to the whole-rock εHf and Nd values of the samples

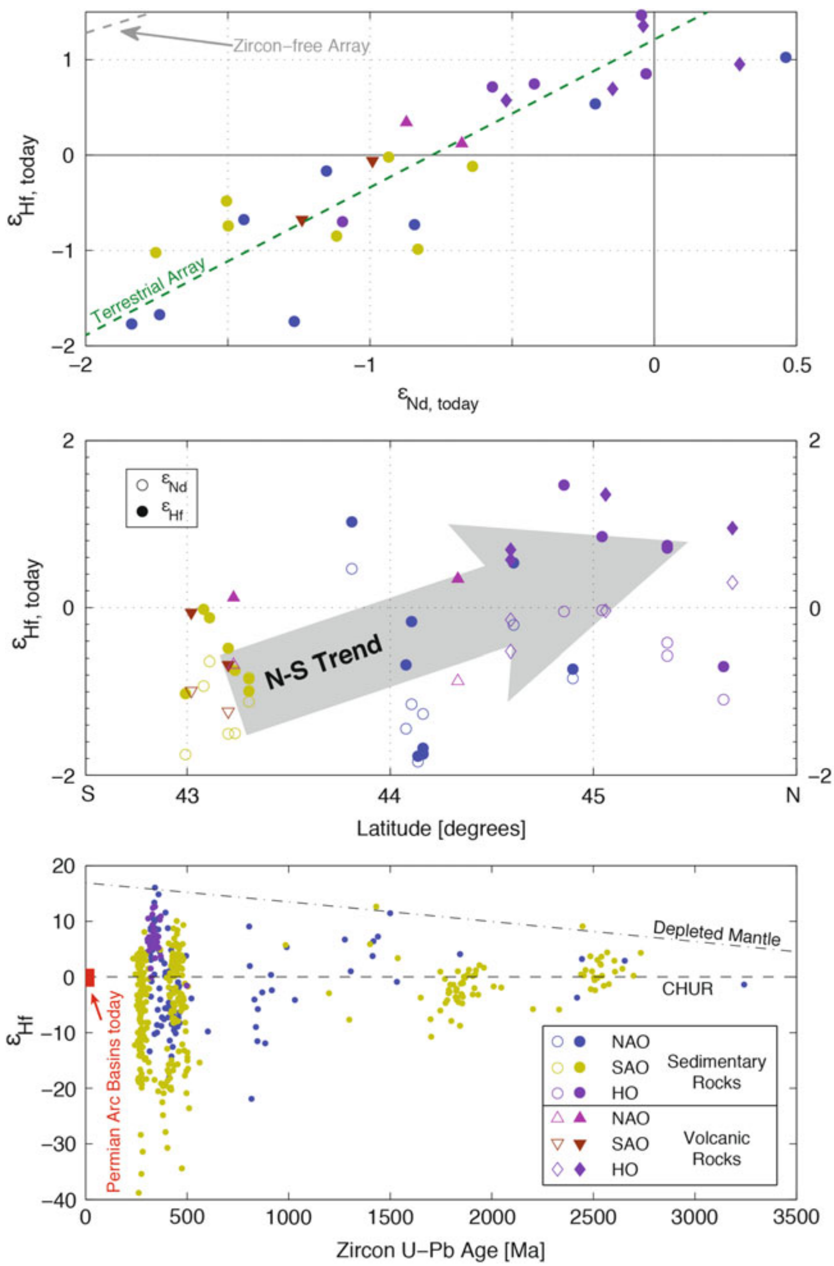

Fig. 4.25 εHf_{today} values with respect to εNd_{today} values (top), latitude (middle) and detrital zircon U–Pb ages (bottom). NAO: Northern Accretionary Orogen; SAO: Southern Accretionary Orogen; HO: Hegenshan Ophiolite Complex; zircon-free array after Vervoort et al. [13]

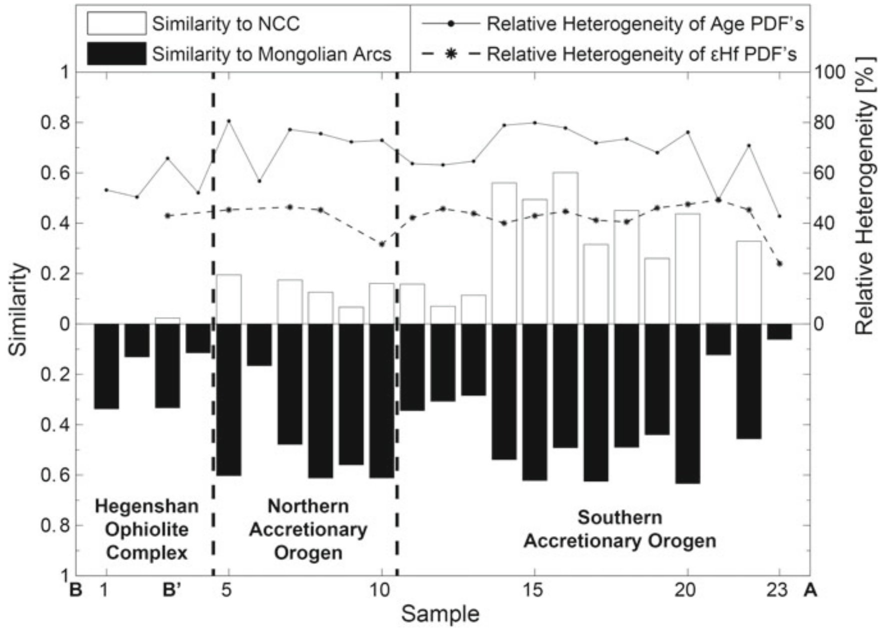

Fig. 4.26 Similarity and heterogeneity statistics for detrital age and εHf values across the accretionary collision zone between the Mongolian Arcs and the North China Craton. NCC: North China Craton; PDF: probability density function

Similarity with the Mongolian Arcs, the PDF of which taken from Rojas-Agramonte et al. [8], is not as indicative, showing high values in both, the Southern and Northern Accretionary Orogens (up to ca. 0.6), and yielding relatively low values (up to ca. 0.3) in the Hegenshan Ophiolite Complex. However, the increased similarity indices across the Southern Accretionary Orogen likely represent a statistical artefact. Ages in the North China Craton also occur with lower intensity in the Mongolian Arcs. Thus, samples which are clearly affiliated with the North China Craton, yield higher similarity indices for the Mongolian Arcs, although without geological meaning.

The heterogeneity values (Fig. 4.26) for the detrital age and εHf probability density functions (see also Sects. 4.1 and 4.2) are comparatively low when single age or εHf populations are dominant. Values for the εHf distributions remain overall constant, except for a few samples, in which εHf strongly shifts towards positive values. The low heterogeneity values for the age probability density functions characterise fairly well the Hegenshan Ophiolite Complex, but vary in the other tectonic belts. A sharp drop, however, can be observed, where the similarity with the North China Craton in the Southern Accretionary Orogen diminishes towards north.

References

1. Bhatia MR (1983) Plate tectonics and geochemical composition of sandstones. J Geol 91(6):611–627
2. Fralick P (2003) Geochemistry of clastic sedimentary rocks: ratio techniques. In: Lentz D (ed) Geochemistry of sediments and sedimentary rocks. Geological Association of Canada, St. John's, pp 85–103
3. Fralick P, Kronberg B (1997) Geochemical discrimination of clastic sedimentary rock sources. Sediment Geol 113(1–2):111–124
4. Geng Y, Du L, Ren L (2012) Growth and reworking of the early Precambrian continental crust in the North China Craton: constraints from zircon Hf isotopes. Gondwana Res 21(2–3):517–529. Special Issue: Western Gondwana
5. Irvine TN, Baragar WRA (1971) A guide to the chemical classification of the common volcanic rocks. Can J Earth Sci 8(5):523–548
6. Le Maitre RW, Bateman P, Dudek A, Keller J, Lameyre J, Le Bas M, Sabine P, Schmid R, Sorensen H, Streckeisen A (1989) A classification of igneous rocks and glossary of terms: recommendations of the international union of geological sciences subcommission on the systematics of igneous rocks, vol 193. Blackwell, Oxford
7. Pearce J (1983) Role of the sub-continental lithosphere in magma genesis at active continental margins. In: Hawkesworth C, Norry M (eds) Continental basalts and mantle xenoliths. Shiva Publications, Nantwich, Cheshire, pp 230–249
8. Rojas-Agramonte Y, Kröner A, Demoux A, Xia X, Wang W, Donskaya T, Liu D, Sun M (2011) Detrital and xenocrystic zircon ages from Neoproterozoic to Palaeozoic arc terranes of Mongolia: significance for the origin of crustal fragments in the Central Asian Orogenic Belt. Gondwana Res 19(3):751–763. Island Arcs: Their role in growth of accretionary orogens and mineral endowment
9. Rollinson HR (1993) Using geochemical data: evaluation, presentation, interpretation. Longman geochemistry series. Routledge, New York
10. Roser B, Korsch R (1988) Provenance signatures of sandstone-mudstone suites determined using discriminant function analysis of major-element data. Chem Geol 67(1–2):119–139
11. Sun S, McDonough WF (1989) Chemical and isotopic systematics of oceanic basalts: implications for mantle composition and processes. Geol Soc Lond Spec Publ 42(1):313–345
12. Vervoort JD, Patchett P, Blichert-Toft J, Albarède F (1999) Relationships between Lu-Hf and Sm-Nd isotopic systems in the global sedimentary system. Earth Planet Sci Lett 168(1–2):79–99
13. Vervoort JD, Plank T, Prytulak J (2011) The Hf-Nd isotopic composition of marine sediments. Geochim Cosmochim Acta 75(20):5903–5926
14. Wedepohl K (1995) The composition of the continental crust. Geochim Cosmochim Acta 59(7):1217–1232

Chapter 5
Geochronological Entropy, and Its Relevance to Age Measurements

5.1 Introduction

The maturity of geochronological techniques in recent years, e.g. (semi-)automated fission-track analysis [1] and laser-ablation systems [2], made large data sets more effectively available in shorter analyses times at an acceptable cost of precision and accuracy. Complex geological systems harbouring multiple age populations, typical in sedimentary provenance studies, instinctively require statistically robust large numbers of single geochronological analyses per sample in order to approximate the ideal age distribution. Prior to each sample analysis, for which multiple age populations are expected, questions arise on how many age dates are required to detect each age population, and how close will the results be to the ideal age probability density function (PDF)? The answers to these have a significant impact in different aspects: (i) the geological interpretation, and (ii) analysis time, resources and costs. Current sample size recommendations based on combinatoric approaches range from 35–70 analyses per sample [3] through 60 [4] to 117 [5]. Emphasis in these is laid on effectively detecting every single significant age population, but less on the quality of accurately representing the ideal age source PDF by the measured age PDF. Naturally, more complex age source PDF's should require larger sample sizes relative to simpler ones. Thus, are existing sample size recommendations universal in depicting the ideal age source PDF?

A long-lasting shortfall in geochronological provenance studies had been the rather qualitative presentation of analytical results. Most commonly, detrital age data are illustrated in histograms of mostly arbitrary bin widths in combination with age PDF's. Comparisons between different PDF's are often performed visually by simple stacking of age PDF's in question, followed by visually highlighting the absence or presence of characteristic age populations. Several attempts have been made to provide a more quantitative description of and comparison between age PDF's. Sircombe [6] elaborated a method to evaluate required bin widths for age histograms, and a quantitative description (relative heterogeneity) for age PDF's.

P. R. Eizenhöfer, *Subduction and Closure of the Palaeo-Asian Ocean along the Solonker Suture Zone: Constraints from an Integrated Sedimentary Provenance Analysis*, Springer Theses, https://doi.org/10.1007/978-981-32-9200-0_5

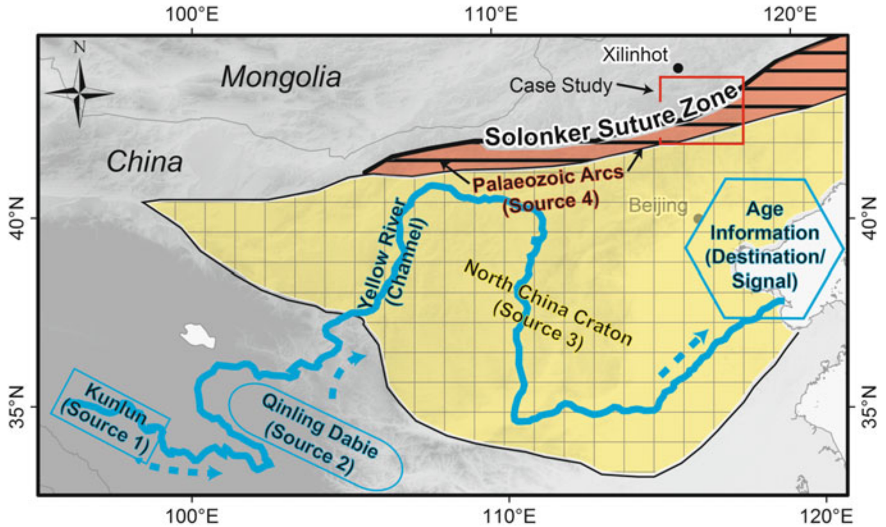

Fig. 5.1 Simplified illustration of the principle behind the generation of age information within a geological context: from origin through transmission to identification of age information with respect to information theoretical aspects exemplified for the Yellow River in China, and location of the case study area within the wider regional tectonic framework. For a detailed sedimentary provenance analysis of the Yellow River see e.g. [9]

Gehrels [7, 8] apply overlap, similarity and Kolmogorow–Smirnov (K–S) statistics to quantitatively compare age PDF's. These tools can be used and further supplemented by information theoretical aspects in order to provide more robust statistical handles to constrain sample sizes and accurate age source PDF representations in age provenance studies.

When age information per se, e.g. a set of geochronological age dates, is scaffolded within an information theoretical framework, that it is generated by a source, transferred through a noisy channel and analysed by a receiver (Fig. 5.1), then we can readily adopt the, in geochronology barely recognised, mathematical tools developed in the groundbreaking treatise on information theory by Shannon and Weaver [10]. These provide additional means to quantitatively characterise age information, categorise types of geochronological systems, which ultimately will lead to an alternative approach in estimating required sample sizes in age provenance studies. The new information theoretical aspects will be first evaluated by a synthetic age data set, and then applied to the detrital zircon U–Pb results of Permian turbiditic strata of the Southern Accretionary Orogen presented in Sect. 4.1.3.

5.2 Geochronological Entropy

In provenance studies geochronological data are often presented, combined with age histograms, as age PDF's, of which the latter constitute the finite mixture distribution of all, usually, but not necessarily, Gaussian distributed, measured single ages (e.g. [6, 11, 12]). Such derived age PDF's solely are defined by the density of measured single age data and their uncertainties, e.g. their mean μ_i and their variances σ^2 (or uncertainties σ), along a fixed time range:

$$p(x) = \frac{1}{n} \sum_{i=1}^{n} \frac{1}{\sigma_1 \sqrt{2\pi}} * e^{-\frac{(x-\mu_i)^2}{2\sigma_i^2}} \tag{5.1}$$

This form of geochronological data presentation eventually inherits a certain bias since measurements of variable precision yield differently shaped age PDF's despite being derived from the same sample. Different attempts have been made to remove this bias. Sambridge and Compston [13] applied principles of finite mixture distribution analyses (e.g. [11]) to model age PDF's from an estimated finite number of enveloping weighted distributions for a measured set of ages. This approach would remove the bias from single age uncertainties by solely observing densities of single age means. However, this approach would assume an infinite precision of the measured mean single age dates. Thus, reasonable mixture distributions would only be achieved by age measurements of similar precision such as an age data set obtained from a single laboratory. Nevertheless, mixture modelling is able to identify higher-order geochronological events and reduce over-interpretation of small age populations, the latter of which often the result of a limited number of analyses within a broader normal distributed age group. Vermeesch [14] proposes a kernel density estimation to normalise any instrumental bias. In this approach a finite number of single age PDF's with fixed uncertainty parameters, which equals the total number of measurements, is summed and normalised to obtain the final age PDF. Its advantage is, that instrumental uncertainties, given age data of similar precision, are accounted for and standardised. Both methods are analytically complex, hence, less practical, and information on single age uncertainties lost, while age populations can be artificially over- or underrepresented.

Problems still arise when attempts are made to quantitatively characterise age PDF's of a single sample without relating it to a reference PDF. Commonly, age PDF's are qualitatively described by stating the number of ages measured, and by pointing out the presence or absence of characteristic age populations, which is visually often aided by stacking age PDF's atop each other. Information theory allows us to add another quantitative measure to describe finite mixture PDF's without relating it to a reference PDF, such as an age PDF measured for a single sample, utilising the information function (see also [6]). Let x be the single mean age in question, p(x) its normal distributed uncertainty or single age PDF (Eq. 5.1), and n the total number of available age dates, then (see also Eq. 3.2):

$$H = \sum_{i}^{n} p(x) ln(p(x)) \tag{5.2}$$

Within a geochronological context, the scalar H represents a quantitative measure to estimate the size of age information, the potential choices available to generate age information, and the probability that a particular age information occurs. Thus, in analogue to Boltzmann's thermodynamic H-theorem [15], which attempts to describe the energy distribution of molecules, and applications of statistical mechanics, e.g. quantum statistical mechanics (see also [16]), H will be defined here as the geochronological entropy. High geochronological entropies correspond to large age information sizes, a larger variety of potentially measurable age data, and lower probabilities that an explicit single age would be measured.

The geochronological entropy is controlled by the total number of potential age components and their respective probabilities of occurring in a defined geochronological system. Age PDF's comprising a single dominant age peak resemble age information with low geochronological entropy, whereas age PDF's constituting several age peaks have a higher entropy within the same system. Moreover, large age uncertainties increase the number of potential age components and, thus, the total geochronological entropy of the system (Fig. 5.2). However, the geological entropy as such is firmly anchored to the geochronological system, which is defined by its maximum number of components and their respective (conventionally equal) probabilities of being detected. Accordingly, the geochronological entropy can be normalised by the maximum entropy that can be reached in the geochronological system (see Eq. 3.1; [6]). This approach ensures the comparability between similar geochronological systems by adopting relative geochronological entropies. For example, the maximum potential number of age components (assuming one 1 Ma increments) that can occur on Earth is 4540, corresponding to a maximum entropy

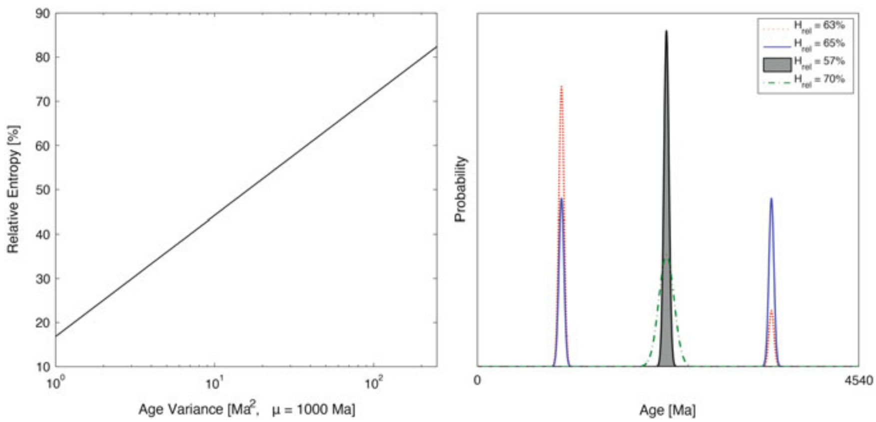

Fig. 5.2 Behaviour of geochronological entropy with respect to increasing age uncertainty (left) and variable numbers of age populations (right)

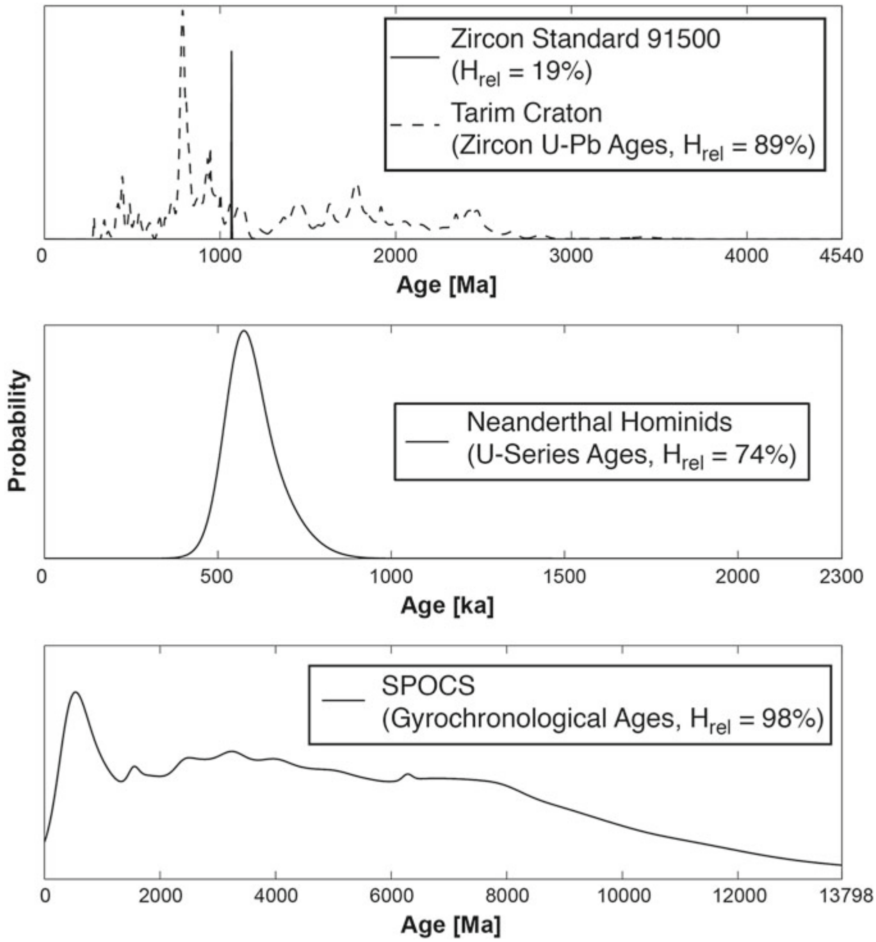

Fig. 5.3 Geochronological Entropy for different geochronological systems: zircon U–Pb ages on Earth ([19, 20], top), U-series ages of Neanderthal hominids ([17], middle), and gyrochronological ages of stars from the SPOCS catalogue ([18], bottom). Maximum analytical uncertainties were assumed for the construction of all presented PDF's

of 8.42 (given that every age date would be measured with equal probability; Eq. 5.2; see also Sect. 3.5). Geochronological systems can be readily extended to different types of geochronological systems, such as the U-series ages of early hominids [17] or gyrochronological ages of nearby cool stars ([18], Fig. 5.3 and Table 5.1) to name a few rather exotic examples. As will be discussed below, estimating the entropy of an age source dictates the number of analyses required to adequately represent the age source with respect to the desired accuracy.

Table 5.1 Comparison of different geochronological systems. Age of the Earth according to Patterson [21] and Dalrymple [22]; appearance of *Homo Habilis* according to Jones et al. [23] and Ruse and Travis [24]; age of the Universe according to Planck Collaboration [25] and Bennett et al. [26]

	Zircon U–Pb ages on earth	U-series ages of hominids	Stellar gyrochronological ages
Maximum geochronological entropy	8.42	7.74	9.53
Referred maximum age	ca. 4.54 Ga; *Age of the Earth*	ca. 2.3 Ma; *Appearance of Homo Habilis*	ca. 13.798 Ga; *Age of the Universe*
No. of age components	4540	2300	13798

5.3 Types of Geochronological Systems

Information theoretical principles can only be adopted for geochronological systems if the age source, the medium through which the age information is carried and its destination are well defined. Within a geological context, for example, sedimentary provenance terranes resemble age sources, the sedimentary system (e.g. turbidity currents in a fore-arc basin) the medium through which the age information is carried, and the sedimentary basin the destination of the age information. Geochronological systems can generally be divided into three categories, which shall be defined here as open, restricted and locked (Table 5.2). Open systems are usually of global character allowing any age information of the defined set of age components to occur (in simplified ideal cases at equal probabilities). Restricted systems are embedded within open systems, such as Earth, and correspond to more natural scenarios, for example river systems, which only tap a limited number of ages (e.g. sedimentary provenance terranes), and not the entire range of the open global geochronological system. Locked systems only host a single age date originating from a single age source (e.g. a volcanic dike). However, such subdivision depends on the prior definition of the age information per se, which can also be defined, for example, as an entire set of ages summarised in a distinct age PDF (thus, a single information is given by a PDF), instead as, more commonly, a single age, which for both types of age information would then be regarded as a single information of certain probability of occurring (see case study in Sect. 5.5). Thus, the character and type of the age information should be clearly defined prior to any geochronological analysis adopting information theoretical principles.

Let T be the number of ideal analyses (a single analysis being able to detect multiple age dates), each of arbitrarily long time, needed to measure all possible age information (defined either as single age data or age PDF’s), which per definition

Table 5.2 Examples for locked, restricted and open geochronological systems and their age information capacities

Examples of geochronological systems	Capacity
Locked	
Grain and debris flow deposits, igneous rocks, dikes, single turbidite layers, short lived river mouths, alluvial fans, small-scale lake deposits	0
Restricted	
Regional active arc basins, large-scale magmatic provinces, regional river deltas, regional glacier systems, global sedimentary systems, large-scale lakes and ocean basins, continental shelves	$0 < C < C_{max}$
Open	
Earth, universe, existence of hominids	C_{max}

would be one, and N(T) the number of all possible age information that can be registered during T, then a capacity C of a noiseless geochronological channel can mathematically be described as follows:

$$C = \lim_{T \to 0} \frac{ln(N(T))}{T} \tag{5.3}$$

Assuming the open U–Pb geochronological system of Earth, a hypothetically perfect methodology at hand able to detect every single potentially occurring age in a single analysis (T = 1), and N(T) = 4540 age components that potentially can occur corresponding to the age of the Earth, then the maximum capacity in this geochronological system amounts to $C_{max} = H_{max} = 8.42$ (see also Table 5.1). This result is in accordance with a fundamental information theoretical theorem that states translated into the geochronological context, that when the geochronological entropy of an age source exceeds the capacity of the geochronological channel, age information in the geochronological system will be lost, which defines the restricted geochronological system. Thus, every geochronological system has a maximum, commonly during a single analysis fixed, capacity equal or smaller than H_{max}. Geochronological capacity may be best paraphrased as the degree of freedom a geochronological system possesses. Systems with only one degree of freedom (locked geochronological systems) consist only of a single age component, in contrast to restricted systems (limited age components) and open systems (all possible age components; Table 5.2). Locked geochronological systems within a geological context are often short-lived and/or spatially well confined, whereas restricted geological systems tend to be usually long-lived, complex and spatially and/or temporally large-scaled. It should be noted for the latter case, that the geochronological entropy of the age source may potentially be subject to geological changes, which subsequently changes the degree of information loss. Open geochronological systems refer to a more universal, general scale that addresses every potential age information within the geochronological system.

In addition to limitations imposed by the capacity of a geochronological channel, geochronological noise is induced by various processes, e.g. (a) the accessibility of the age source in sedimentary systems resulting in weighted age populations, (b) chemical compositions/processes restricting the formation of the required minerals (mafic magmas produce less zircons than felsic ones), (c) rock type, (d) the random addition of insignificant ages (dike intrusions unrelated to the regional geology), (e) insufficient resolution of the applied methodology, (f) natural filter processes (e.g. heavy mineral enrichment with increasing textural maturity of a clastic sedimentary rock), (g) random systematic errors and uncertainties, (h) sample processing, (i) sample size, etc. Certainly, this list is far from being complete, and only a few parameters, such as sample size, methodological resolution and random noise can be statistically addressed in terms of information theory, whereas many more factors are beyond direct analytical control. Thus, restricted geochronological systems originated from open ones after introduction of various types of entropic noise.

Let H_{ideal} be the geochronological entropy of the ideal age source and H_{meas} be the age information measured, then the effective entropic noise H_{noise}, causing the difference between both age PDF's, can be expressed as follows:

$$H_{noise} = |H_{ideal} - H_{meas}| \tag{5.4}$$

which describes the effective rate of correct transmission of age information, and should be minimised. It should be noted that the introduction of noise is a purely random process. Thus, noise may result in positive and negative feedback with respect to the ideal age PDF, and may potentially be compensated, despite the fact that effective entropic noise is still present in the system (see Fig. 5.4).

In case of an ideal noiseless geochronological channel, the required capacity to transmit the complete age information is equal to the geochronological entropy H of the age source. In a noisy channel, however, the capacity of transmitting correct information is reduced since it is occupied to a certain degree by incorrect age information, while the overall capacity of the geochronological system remains unchanged. Since the overall capacity of the geochronological channel is constant, noise needs to be instinctively reduced. This can be achieved by increasing the amount of age

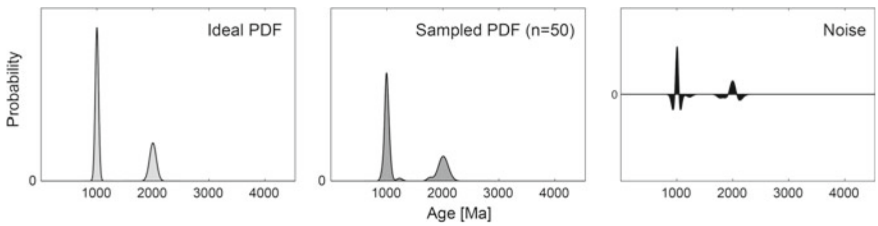

Fig. 5.4 Illustration of entropic noise introduced during the transmission of age information. The sampled PDF also included a random 1% chance of obtaining incorrect results, due to, for example, systematic errors during the analysis

information to be measured (e.g. the number of age dates obtained from a sandstone) during the analysis, while keeping the loss of age information due to noise at an acceptable level, which will be discussed in the following section.

5.4 Sample Sizes

Current sample size recommendations [3–5] are all based on combinatoric approaches, all of which placing emphasis on the identification of either single major or all age accumulations. However, the identification of every single age population may not necessarily impact regional-scale geologic interpretations, or the detection of major age provenances. In a worst-case scenario additional age populations may be attributed to unrelated random noise. Nevertheless, conclusions made from peripheral age fractions, e.g. occasionally used to determine maximum depositional ages of sedimentary basins, should be taken with care [3, 27]. Information theory may shed new light on the selection of sample sizes by treating the age information and its respective probabilities as such by linking the geochronological entropy of the measured age PDF with that of the ideal age source. A major advantage of this approach is the complete independence from the size and locations of age populations in age PDF's.

In order to investigate the relationship between age source geochronological entropy and that of the measured PDF with variable sample size, multiple sampling situations were numerically simulated in this work. Sample age PDF's were extracted from constructed ideal age source PDF's by varying the number of age dates measured as well as the geochronological entropy of the age source (Fig. 5.5). Random 2–4% uncertainties were assigned to each measured age date, typical for present-day detrital zircon U–Pb analyses measured by LA-ICPMS (e.g. this work, Appendix B). The effective entropic noise was then calculated according to Eq. 5.4, and the similarity between measured and ideal age PDF monitored by adopting the Bhattacharyya coefficient/Hellinger affinity (Eq. 3.4; see also [28]). In order to achieve a more robust estimate of the development of similarity indices and effective noise, their averages were taken from a set of ten simulation runs without changing sampling parameters. The possibility of potential systematic errors was not implemented during the simulations.

The results (Fig. 5.5) of the sampling simulations clearly indicate that increasing sample sizes in each analysis reduces the effective entropic noise, while increasing the similarity with the ideal age source PDF, which is trivial. Not as trivial, however, is that the simulations demonstrate that the effects of increasing sample sizes become marginal when a certain degree of similarity or effective noise reduction is reached. Most significantly, the results indicate that the sample size is dependent on the entropy of the ideal age PDF by retaining the same levels of noise and similarity. Thus, previous sample size recommendations merely represent a special case, e.g. the sampling of a universal age PDF of fixed geochronological entropy, and need to be extended with respect to different age source geochronological entropies.

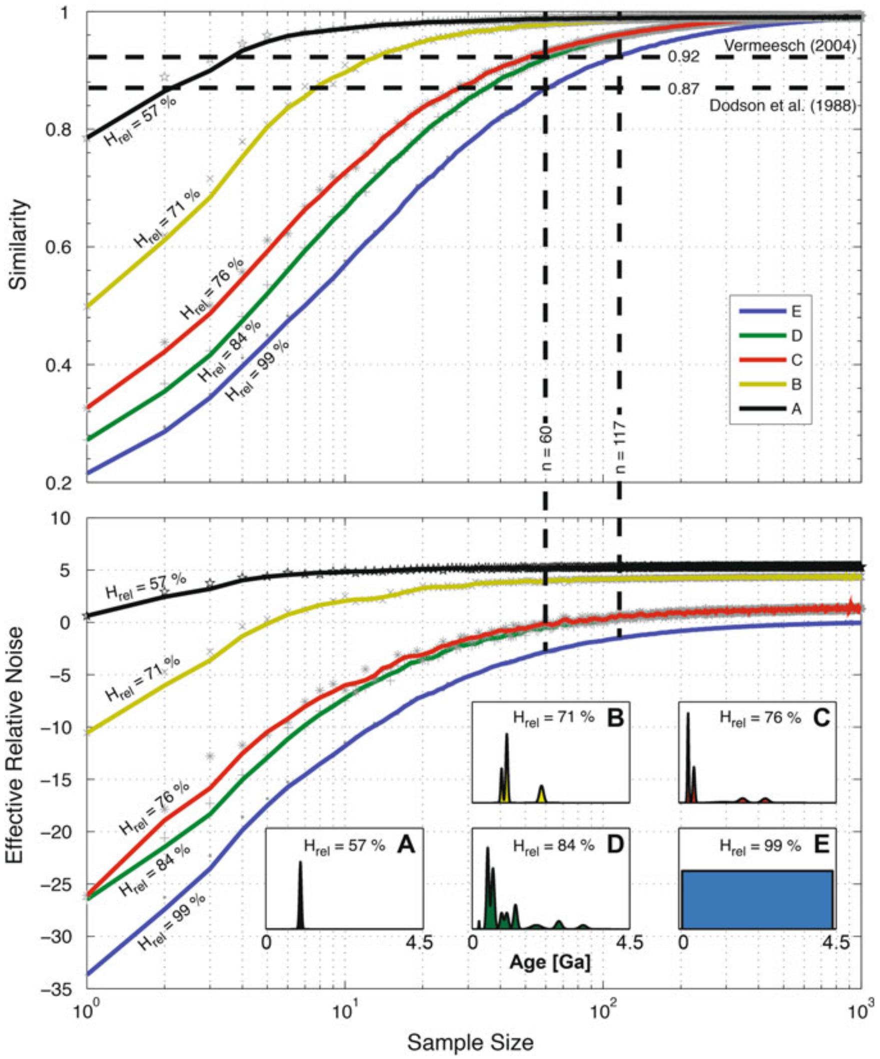

Fig. 5.5 Numerical simulations on the effects of increasing sample sizes on similarity indices and effective relative noise of sample age PDF's of variable geochronological entropy with respect to ideal age source PDF's. Similarity index increase and effective relative noise reduction become marginal with very large sample sizes. Age uncertainties of 2–4% were assumed for simulated single age measurements, typical for detrital zircon U–Pb analyses with LA-ICPMS

Table 5.3 Sample size recommendations for detrital zircon U–Pb provenance analyses for different age source geochronological entropies. Rec.: Recommended; Eff.: Effective

$H_{rel}(\%)$	Similarity index			
	0.9		0.95	
	Rec. sample size	Eff. relative noise	Rec. sample size	Eff. relative noise
57 (single mode)	3	3.2	5	4.4
71 (three modes)	10	2.1	21	3.3
76 (four modes)	39	0.8	88	0.2
84 (complex modes)	49	0.9	97	0.2
99 (block)	83	2.0	183	0.9

For example, a sample size of 117 [5], ensures similarity levels >0.92 and effective relative entropic noise levels of <0.027 on average for each sample. A sample size of 60 [4], guarantees similarity levels of >0.87, and noise levels of <0.047 on average for each sample. However, the results presented here recommend a prior estimate of the age source entropy by maintaining equal levels of similarity and noise reduction, in order to increase analytical efficiency (e.g. analysis time, costs and resources). Thus, this study refrains from recommending a fixed sample size, and instead urges the analyst to decide, what degree of similarity and noise, in other words age information loss, deems acceptable within the respective geochronological study. As a "rule-of-thumb", similarity levels >0.95 and effective noise levels <5 approximate the ideal age PDF fairly well, despite the low probability of missing a minor age group (for details see [3]). Table 5.3 lists up recommended sample sizes for similarity indices of 0.9 and 0.95 and effective relative noise reductions of <5 for a number of examples. Figure 5.6 illustrates exemplified the accuracy on ideal age source representation for different sample size recommendations: the recommendation by Dodson et al. [4] appears to be slightly inferior in comparison to the others, but reflects the ideal age PDF fairly well, and should be considered for geochronological studies, in which minor age populations are of minor importance. Barely any quality difference can be observed between the higher recommended sample size by Vermeesch [5] and this study, despite a ca. 20% difference in sample size, and thus analysis time and cost.

5.5 Geological Implications and Case Study

Detrital zircon U–Pb data from Permian sedimentary strata across the Solonker Suture Zone (see Sect. 4.1), particularly from the Southern Accretionary Orogen, are used as a case study to demonstrate the applicability and geological implications of the information theoretical principles introduced in the previous section. Measured age PDF's in Middle Permian strata of the Southern Accretionary Orogen are

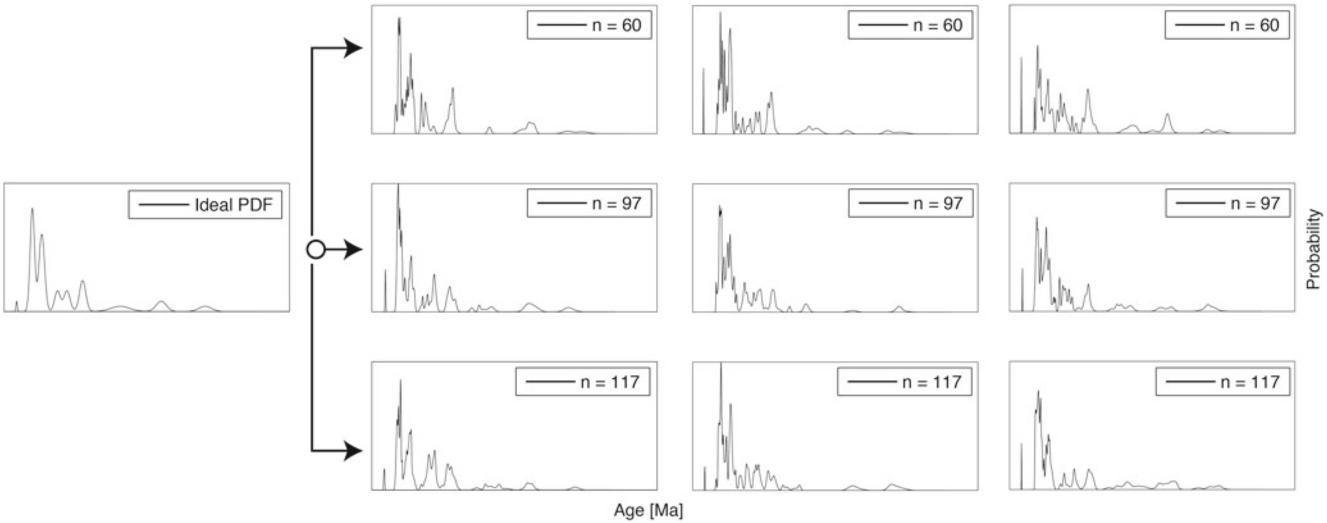

Fig. 5.6 Qualitative assessment of variable sample size recommendations on the accuracy of representing the age source PDF by the measured age PDF exemplified for random samples of sample sizes 60 [4], 97 (this study) and 117 [5]. Analytical uncertainties during simulated random sampling are 2–4%, typical for detrital zircon U–Pb studies

remarkably inconsistent in their appearance, which led to the conclusion in this work that the Middle Permian sedimentary system was very complex (see also the following Chap. 6). However, most authors agree that an active Andean-type arc existed along the northern margin of the North China Craton throughout the Palaeozoic [29–32], while some propose an island arc origin (e.g. [33]). Taking into account the information theoretical aspects introduced in this study, then the aforementioned geological conclusions made in this dissertation are corroborated by statistically postulating the existence of multiple independent arc basins, e.g. involving the opening of an immature back-arc basin followed by its closure contemporaneous to final suturing.

1010 concordant ages were determined within the Southern Accretionary Orogen in this study, which statistically suggests, that every significant age population had been identified on a 95% confidence level [3]. Thus, the summarised age PDF for the entire Southern Accretionary Orogen is assumed to approximate reasonably well the ideal age PDF. In order to minimise any bias originating from single age measurement uncertainties, a mixture distribution model, which places more emphasis on age densities, has been erected (Fig. 5.7; [11]) following the approach by Sambridge and Compston [13]. Both, measured and modelled, age PDF's (H_{rel} = 72% and H_{rel} = 74%, respectively) are composed by the contribution of three age provenances: the Precambrian North China Craton (ca. 2.5 and 1.8 Ga), the Early Palaeozoic (ca. 430 Ma) and Late Palaeozoic (ca. 260 Ma) arcs (see also the following Chap. 6).

A similarity index >0.95 and an effective relative entropic noise reduction of <0.2 when approximating the ideal age source of having a relative entropy of 76% can be statistically achieved by measuring on average 88 single age dates. Since the mixture distribution model for the Southern Accretionary Orogen reaches a relative entropy of ca. 74%, it is likely that either even higher similarity levels and better noise reductions can be accomplished by adopting this sample size, or that slightly fewer ages may lead to comparable similarity levels and noise reductions. Thus, sample sizes of the selected representative samples for this case study (Fig. 5.7; n = 71, 85 and 95), can be considered sufficient to approximate reasonably well the modelled age PDF. It should be noted, that age source representation even improves should the age source comprise less then the number of age populations in the modelled age PDF.

The measured age PDF's for the Southern Accretionary Orogen can be generally subdivided into four groups, of which one representative sample for each was selected in this case study (Fig. 5.7): (I) age PDF's with a dominant Late Palaeozoic age population, (II) age PDF's with a dominantly Early and Late Palaeozoic age populations, (III) age PDF's with dominantly Precambrian and Early Palaeozoic age populations, and (IV) age PDF's showing Precambrian, Early and Late Palaeozoic age populations.

Measured age PDF's of group IV reflect the ideal age PDF fairly well, whereas age PDF's of group I, II and III show the least similarity with the modelled age PDF (Table 5.4). At a global scale, the Middle Permian sedimentary system across the Southern Accretionary Orogen can be regarded as a restricted geochronological system, since only those ages occur, which are related to the sedimentary provenance terranes of the region. However, additional natural noise, besides the entropic noise

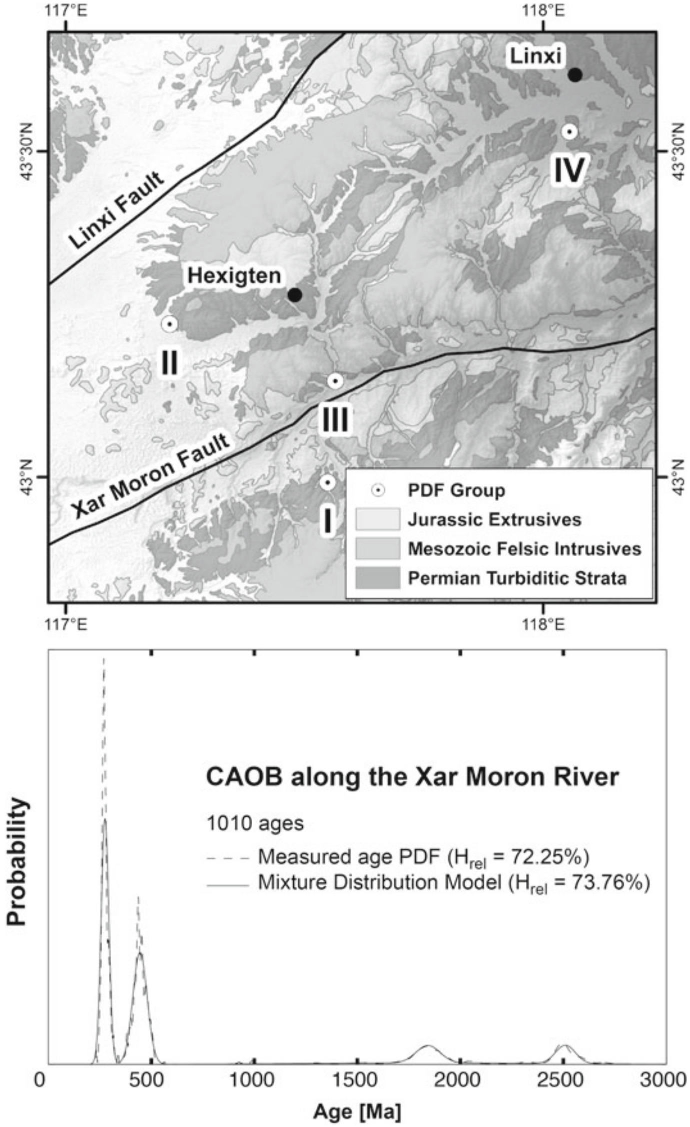

Fig. 5.7 Simplified geological map of the Southern Accretionary Orogen (top) including representative locations of age PDF groups and their summarised measured and modelled age PDF's (bottom)

Table 5.4 Similarity indices (see also Fig. 4.26) and effective relative noise for representative samples of the Southern Accretionary Orogen

Age group	Similarity index	Effective relative noise	Possible depositional environment; Fig. 5.8
Group I	0.6	26	Trench, fore-arc basin, seaward back-arc basin
Group II	0.8	13	Trench, fore-arc basin, seaward and central back-arc basin
Group III	0.6	5	Trench, continent-facing back-arc basin
Group IV	0.9	2.7	Trench, fore-arc basin, central back-arc basin

caused by sample size and analytical uncertainty, has been added to age groups I, II and III, which inhibits a complete representation of the ideal modelled age PDF of the region. The additional effective entropic noise is assumed to be systematic and attributed to geological features, such as sedimentary barriers, which restrict access to all sedimentary provenance terranes. Within a geological context this can be achieved, for example, by a sedimentary system that involves multiple independent arc basins.

Typical active continental arc cross-sections comprise (starting seawards): an oceanic basin, an accretionary prism, the fore-arc basin fill separated from the former by a trench slope break, and a volcanic arc massif. Often, back-arc basins may separate the arc-massif from ancient arcs or continental crust in the hinterland (Fig. 5.8; [34–36]). Besides direct products of the volcanic arc, such as volcanic ash falls and pyroclastic flows, turbidity currents represent a major contributor to sedimentary detritus to the accretionary prism, the fore-arc and back-arc basin fill, in which terrigneous sediments are more likely to be found in the latter two. Catastrophic events, such as seismic activity and/or slope instability, are the main causes, which trigger these density flows. Depending on the scale and location of these catastrophic disturbances, detritus sources may differ, which offers a possible explanation for the inconsistent appearance of the measured age PDF groups. Combining these sedimentary characteristics with a possible back-arc basin scenario (Fig. 5.8), the occurrence of different age PDF's can be well explained by the complex sedimentary system of a temporarily seawards retreating subduction zone in an active arc environment. Possible depositional settings for each age PDF group are listed in Table 5.4 and illustrated in Fig. 2.5. Thus, the statistically sufficient large sample size requires a tectonic and depositional setting that enables the introduction of effective entropic noise and age information filter into the restricted geochronological systems, such as a back-arc basin, while ensuring the simultaneous occurrence of different age PDF's.

Alternatively, the Permian sedimentary system may also be defined as an open geochronological system, in which the actual age information is not represented as a single age date, but as a set of age dates summarised in an age PDF. Thus, up to three different types of age information ($n = 3$), e.g. age PDF's (the Early and Late Palaeozoic age groups, and the Precambrian age group), can potentially occur combined in a measured age information. Assuming a simplified scenario in

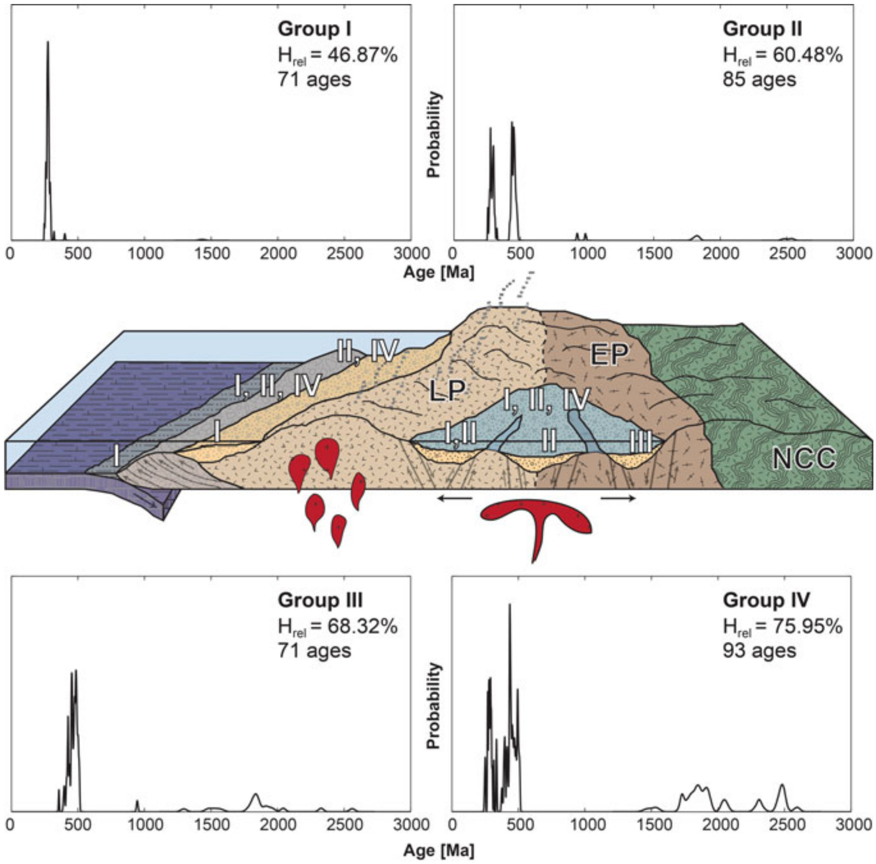

Fig. 5.8 Possible depositional setting explaining the variable appearance of measured age PDF's in the Southern Accretionary Orogen. LP: Late Palaeozoic arc; EP: Early Palaeozoic arc; NCC: North China Craton

which the probability of each such defined age information to occur is equal (H_{max} = C_{max} = 1.10; Eq. 5.3), then the sample size needs to be increased to suffice a reasonably high similarity index and effective noise reduction in order to approximate the ideal age information source. In other words, a single measurement may not be representative for the entire Middle Permian sedimentary system, but multiple measurements. Provenance analyses in similarly complex tectonic and depositional environments based on a single or very few samples, may thus require careful re-examination and—evaluation.

The case study demonstrates that the mathematical tools provided by information theory [10] can be readily adopted to geological problems, where geochronological analyses are involved, and furthermore to any type of geochronological analysis. Geochronological entropy can be used to characterise in a geochronological system quantitatively different possible choices of age information as well as the uncertainty representing the ideal age information. By applying the information theoretical channel principles, it is not only possible to estimate the amount of age information loss due to entropic noise, but also categorise geochronological systems in open, restricted and locked, of which the first two usually require multiple analyses in order to sufficiently approximate the ideal age information source in a geochronological system within certain accuracy. The application of information theoretical principles further demonstrated that existing sample size recommendations for detrital zircon U–Pb sedimentary provenance analyses merely represent special cases of age information sources of fixed entropy. Thus, it is strongly recommended, especially with respect to analysis time and costs, to estimate the maximum entropy of a geochronological system upon which sample sizes will be individually chosen dependant on the accepted degree of information loss.

References

1. Dumitru TA (1993) A new computer-automated microscope stage system for fission-track analysis. Nucl Tracks Radiat Meas 21(4):575–580
2. Sylvester PJ (2008) Laser ablation-ICP-MS in the earth sciences: current practices and outstanding issues, vol. 40. Mineralogical Association of Canada
3. Andersen T (2005) Detrital zircons as tracers of sedimentary provenance: limiting conditions from statistics and numerical simulation. Chem Geol 216(3–4):249–270
4. Dodson MH, Compston W, Williams IS, Wilson JF (1988) A search for ancient detrital zircons in Zimbabwean sediments. J Geol Soc 145(6):977–983
5. Vermeesch P (2004) How many grains are needed for a provenance study? Earth Planet Sci Lett 224(3–4):441–451
6. Sircombe KN (2004) AgeDisplay: an EXCEL workbook to evaluate and display univariate geochronological data using binned frequency histograms and probability density distributions. Comput Geosci 30(1):21–31
7. Gehrels GE (2000) Introduction to detrital zircon studies of Paleozoic and Triassic strata in Western Nevada and Northern California. Geol Soc Am Spec Pap 347:1–17
8. Gehrels GE, Blakey R, Karlstrom KE, Timmons JM, Dickinson B, Pecha M (2011) Detrital zircon U–Pb geochronology of Paleozoic strata in the Grand Canyon, Arizona. Lithosphere 3(3):183–200
9. Yang J, Gao S, Chen C, Tang Y, Yuan H, Gong H, Xie S, Wang J (2009) Episodic crustal growth of North China as revealed by U–Pb age and Hf isotopes of detrital zircons from modern rivers. Geochim Cosmochim Acta 73(9):2660–2673
10. Shannon CE, Weaver W (1971) The mathematical theory of communication. University of Illinois Press, Illinois
11. Titterington DM, Smith AF, Makov UE (1985) Statistical analysis of finite mixture distributions, vol 7. Wiley, New York
12. Ludwig K (2008) Manual for Isoplot 3.7. Berkeley Geochronology Center, Berkeley
13. Sambridge M, Compston W (1994) Mixture modeling of multi-component data sets with application to ion-probe zircon ages. Earth Planet Sci Lett 128(3–4):373–390
14. Vermeesch P (2013) Multi-sample comparison of detrital age distributions. Chem Geol 341:140–146
15. Boltzmann L (1872) Weitere studien über das wärmegleichgewicht unter gasmolekülen, (pp. 270–370). Number 66. Sitzungsberichte Akademie der Wissenschaften: Wien

16. Tolman R (1938) The principles of statistical mechanics. Courier Dover Publications, New York
17. Bischoff JL, Williams RW, Rosenbauer RJ, Aramburu A, Arsuaga JL, García N, Cuenca-Bescós G (2007) High-resolution U-series dates from the Sima de los Huesos hominids yields: implications for the evolution of the early Neanderthal lineage. J Archaeol Sci 34(5):763–770
18. Valenti JA, Fischer DA (2005) Spectroscopic properties of cool stars (SPOCS). I. 1040 F, G, and K dwarfs from Keck, Lick, and AAT planet search programs. Astrophys J Suppl Ser 159(1):141
19. Rojas-Agramonte Y, Kröner A, Demoux A, Xia X, Wang W, Donskaya T, Liu D, Sun M (2011) Detrital and xenocrystic zircon ages from Neoproterozoic to Palaeozoic arc terranes of Mongolia: Significance for the origin of crustal fragments in the Central Asian Orogenic Belt. Gondwana Res 19(3):751–763. Their role in growth of accretionary orogens and mineral endowment, Island Arcs
20. Wiedenbeck M, Alle P, Corfu F, Griffin W, Meier M, Oberli F, Quadt AV, Roddick J, Spiegel W (1995) Three natural zircon standards for U–Th–Pb, Lu–Hf, trace element and REE analyses. Geostand Newsl 19(1):1–23
21. Patterson C (1956) Age of meteorites and the earth. Geochim Cosmochim Acta 10(4):230–237
22. Dalrymple GB (2001) The age of the Earth in the twentieth century: a problem (mostly) solved. Geol Soc, Lond, Spec Publ 190(1):205–221
23. Jones S, Martin RD, Pilbeam D, Bunney S, Dawkins R (1992) The Cambridge encyclopedia of human evolution. Cambridge University Press, Cambridge
24. Ruse M, Travis JX (2009) Evolution: the first four billion years. Harvard University Press, Cambrigde, Massachusetts
25. Planck Collaboration (2014) Planck 2013 results. I. Overview of products and scientific results. Astron Astrophys 571:A1
26. Bennett C, Larson D, Weiland J, Jarosik N, Hinshaw G, Odegard N, Smith K, Hill R, Gold B, Halpern M (2013) Nine-year Wilkinson Microwave Anisotropy Probe (WMAP) observations: final maps and results. Astrophys J Suppl Ser 208(2):20
27. Dickinson WR, Gehrels GE (2009) Use of U–Pb ages of detrital zircons to infer maximum depositional ages of strata: a test against a Colorado Plateau Mesozoic database. Earth Planet Sci Lett 288(1–2):115–125
28. Cha S (2007) Comprehensive survey on distance/similarity measures between probability/density functions. Int J Math Model Methods Appl Sci 1(4):300–307
29. Xiao W, Windley BF, Hao J, Zhai M (2003) Accretion leading to collision and the Permian Solonker suture, Inner Mongolia, China: Termination of the central Asian orogenic belt. Tectonics 22(6)
30. Cope T, Ritts BD, Darby BJ, Fildani A, Graham SA (2005) Late Paleozoic sedimentation on the northern margin of the North China Block: implications for regional tectonics and climate change. Int Geol Rev 47(3):270–296
31. Jian P, Liu D, Kröner A, Windley BF, Shi Y, Zhang F, Shi G, Miao L, Zhang W, Zhang Q, Zhang L, Ren J (2008) Time scale of an early to mid-Paleozoic orogenic cycle of the long-lived Central Asian Orogenic Belt, Inner Mongolia of China: Implications for continental growth. Lithos 101(3–4):233–259
32. Jian P, Liu D, Kröner A, Windley BF, Shi Y, Zhang W, Zhang F, Miao L, Zhang L, Tomurhuu D (2010) Evolution of a Permian intraoceanic arc-trench system in the Solonker suture zone, Central Asian Orogenic Belt, China and Mongolia. Lithos 118(1–2):169–190
33. Zhang S-H, Zhao Y, Ye H, Liu J-M, Hu Z-C (2014b) Origin and evolution of the Bainaimiao arc belt: Implications for crustal growth in the southern Central Asian orogenic belt. Geol Soc Am Bull 126(9–10):1275–1300
34. Dickinson W (1995) Forearc basins. Tectonics of sedimentary basins. Blackwell Science, Oxford, pp 221–261
35. Underwood M, Moore G (1995) Trenches and trench-slope basins. Tectonics Sediment Basins 179–219
36. Leeder MR (2001) Sedimentology and sedimentary basins: from turbulence to tectonics. Blackwell Science, Oxford

Chapter 6
Accretionary Collision Between the Mongolian Arcs and North China Craton

6.1 Sedimentary Provenance Terranes of the Permian Arc Basins

The sedimentary provenance analysis of Palaeozoic arc basins across the Solonker Suture Zone can provide important insights into the role of major tectonic units as sedimentary provenance terranes during the final closure of the Palaeo–Asian Ocean. Their relative contributions can be identified and defined by their characteristic age spectrum [1, 2]. Their palaeo-geographic locations, as an indirect measure for the direction of regional sediment transport toward the arc basins, may also serve as an indicator for subduction polarities in convergent tectonic settings.

The North China Craton to the south and the Mongolian Arcs to the north represent the most likely sedimentary provenance terranes due to their close geographic location to the study region. Other major tectonic units such as the Siberian craton, the Tarim craton, Gondwana-derived fragments within the CAOB, and a potential pan-African orogenic terrane located in northeast China [3] are less likely to have influenced the sedimentary systems in the study region, and will only be briefly discussed here. A detailed geochronological summary and discussion of most of these potential provenance terranes have been provided by Rojas-Agramonte et al. ([4], and references therein).

6.1.1 Geochemical Relationships Between Arc Basins and Their Provenance Terranes

Geochemical compositions of volcanic rocks in the Southern Accretionary Orogen range from mafic to felsic compositions, and are then continued by the higher silicic sedimentary rocks as a result of increasing textural maturity with prolonged sedimentary transport. Most major oxides decrease with increasing SiO_2, for example

P. R. Eizenhöfer, *Subduction and Closure of the Palaeo-Asian Ocean along the Solonker Suture Zone: Constraints from an Integrated Sedimentary Provenance Analysis*, Springer Theses, https://doi.org/10.1007/978-981-32-9200-0_6

TiO_2. In combination with the identification of immobile elements (Figs. 4.18 and 4.23), it becomes apparent that in the Southern Accretionary Orogen the clastic sedimentary rocks deposited in the arc basins are closely related to the local volcanic rocks, although most trace element concentrations seem generally independent from silica content. Generally applied to sedimentary rocks, a change in slope or a scatter of data points in respective bivariate diagrams indicate the mobility of the respective element as a result of varying degrees of chemical alteration [5–7]. Adopting this feature to the sampled volcanic rocks, suggests that some major element oxides, such as TiO_2 and P_2O_5 were mobile at the interface of erosion and deposition, but not during hydraulic sorting and diagenetic chemical alteration of the clastic sediments. The close relationship between the volcanic and sedimentary rocks is further corroborated by the similar enrichment and depletion of mobile and immobile elements and oxides, except for P_2O_5, with respect to N-MORB and average continental crust (Fig. 4.19).

The Bainaimiao arc forms an essential part of the Southern Accretionary Orogen, and, thus, is likely to be a major source of detritus [8–10]. Plotting immobile elements and ratios against each other indicates that the sedimentary rocks cannot be derived by the sampled Permian volcanic rocks alone (Fig. 6.1). In addition, not all volcanic rocks appear to be the sources for the clastic sedimentary rocks. The clastic sedimentary rocks seem to be also sourced by the Bainaimiao arc, which contains significant Early Palaeozoic basement. This interpretation would explain the intermediate position of the sedimentary rocks in the plots. Low Cr/V and comparatively high Y/Ni ratios suggest that ultramafic, ophiolithic material was not involved during sediment deposition (Fig. 6.2). Consequently, the Hegenshan Ophiolite was either not exposed to erosion, or, more likely, stood in no relation to the sedimentary system in the Southern Accretionary Orogen.

These lines of evidence suggest that the arc basins in the Southern Accretionary Orogen were predominantly sourced by the Early and Late Palaeozoic Bainaimiao arc rocks. Geochemical similarities between the volcanic and sedimentary rocks can be explained by short transport distances typical for active arc depositional environments, consistent also with the derivation from dominantly mafic to intermediate sedimentary provenances (Fig. 4.20).

In the Northern Accretionary Orogen geochemical relationships between the clastic sedimentary rocks and their provenance terranes appear to be more complex. Both, volcanic and clastic sedimentary rock samples, exhibit a bimodal character (Fig. 4.17), similar to observations made by Zhang et al. [11] in the same accretionary belt, although not as pronounced as in the latter. This suggests that the sedimentary rocks were dominantly derived either from two different provenance terranes, or a single provenance terrane with bimodal geochemical character, of which the latter appears more likely since the volcanic rocks, analysed in this work and those in literature, are bimodal in the region. The overall continuous trend from low to high silicious compositions, while rock types alternate between volcanic and sedimentary, further substantiates the idea that the volcanic rocks originated from the same magma suite during different stages of differentiation. Elements tested for immobility either follow a linear trend, or remain approximately constant in their concentrations with

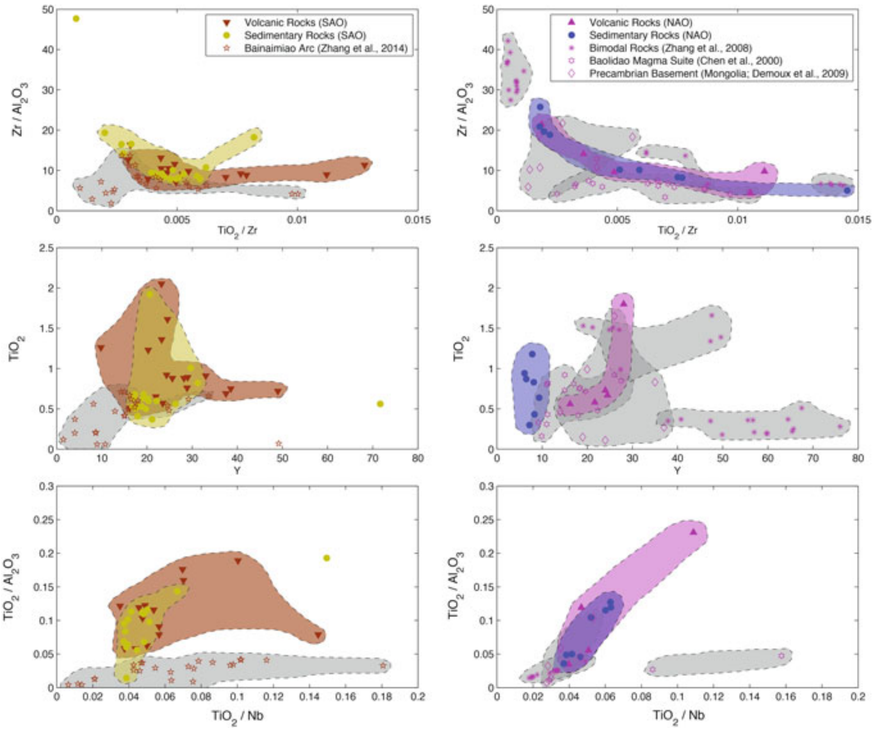

Fig. 6.1 Immobile element relationships between potential sedimentary provenance terranes and clastic sedimentary rocks of the Southern Accretionary Orogen (left column) and the Northern Accretionary Orogen (right column). Shaded areas demarcate the assumed compositional variability of the rock suites

higher silica content independent from rock type (Figs. 4.17 and 4.22). This feature implies the overall immobility of the tested elements from erosion to deposition [6], although a slight mobility can be inferred for TiO_2 at the transition from erosion to deposition. The comparison to N-MORB and average continental crust confirms a close relationship of the clastic sedimentary with the volcanic rocks in the Northern Accretionary Orogen (Fig. 4.19).

Based on the geographic location of the Northern Accretionary Orogen, several potential provenance terranes need to be considered as source for the Permian clastic sedimentary rocks: (a) a bimodal volcanic rock suite investigated in an area near Xilinhot [11], (b) the Baolidao magma suite as representative of the Baolidao arc rocks [12], and (c) the Precambrian basement of the southern Mongolian Arcs [13]. However, the identification of explicit sources using immobile elements (Fig. 6.1) emerges to be more difficult in comparison to the Southern Accretionary Orogen, since none of the candidates directly overlap with the geochemical composition of the clastic sedimentary rocks when plotting Zr/Al_2O_3 over TiO_2/Zr and TiO_2 over Y, respectively. Both plots may suggest an unknown, variably weighted, mixture of the

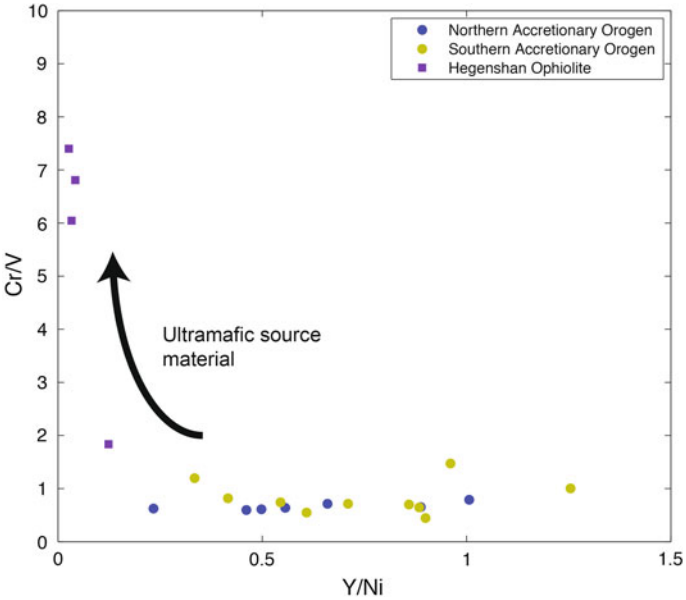

Fig. 6.2 Cr/V versus Y/Ni diagram as indicator for potential contribution of ultramafic material (e.g. the Hegenshan Ophiolite) to arc basins in the Southern and Northern Accretionary Orogens

potential provenance terranes, or an unidentified terrane, the latter of which rather unlikely. The positive correlation in the TiO_2/Al_2O_3 versus TiO_2/Nb diagram may be supportive of this interpretation. Again, an ophiolithic source can be excluded (Fig. 6.2), suggesting that the Hegenshan ophiolite either had not been formed or was not yet exposed to erosion during the Permian.

The heterogenous tectonic nature of the Northern Accretionary Orogen and its proximity to the Precambrian basement of the Mongolian Arcs may be the reason why a clear relationship between the clastic sedimentary rocks and their provenance terranes cannot be found. Provenance discrimination plots equally suggest both, a quartzose sedimentary and a felsic igneous provenance (Fig. 4.20). In the most likely case, the sedimentary rocks were derived from a mixture of bimodal volcanic and plutonic rock suites, and probably influenced by Precambrian basement of the southern Mongolian Arcs.

6.1.2 *Geochronological Relationships Between Arc Basins and Their Provenance Terranes*

The Palaeoproterozoic age peaks (ca. 2.5 and ca. 1.8 Ga) detected across the Southern Accretionary Orogen (Fig. 4.2) are similar to those from the North China Craton [14]. According to Rojas-Agramonte et al. [4] zircon U–Pb ages originating from the North China Craton generally range from ca. 3.8 to 1.6 Ga, with major age peaks at ca 2.8–2.6, 2.4–2.35 and 2.1–1.85 Ga (Fig. 6.3). Taking into account the proximity to the study region, the North China Craton is identified as a significant, although minor, provider of sedimentary detritus to the Permian clastic sedimentary strata in the Southern Accretionary Orogen, e.g. the Huanggangliang and Linxi formations (Fig. 2.4).

The Mongolian Arcs comprise a large variety of Palaeoproterozoic to Palaeozoic zircon U–Pb ages. Major age peaks are around 2710–2182, 950–760, 580–460 and 400–340 Ma (Fig. 6.3). These ages were sourced from the arc terranes themselves and the Tarim craton, while the North China Craton is not considered as a contributor [4]. The large value of relative age heterogeneity of the Mongolian Arcs (H_{rel} = 87%) cannot be observed in the age populations in this study. Prominent Mongolian age populations were detected at variable extent, only in the Northern Accretionary Orogen, such as a broad range of Neoproterozoic ages. The dominant earliest Palaeozoic Mongolian age population (ca. 515 Ma), however, is clearly represented only in the Devonian samples (Fig. 2.4). Therefore, the Mongolian Arcs as a whole can only be accounted as a very dynamic sedimentary provenance terrane, that exerts its influence at a variable degree until the Late Palaeozoic.

The Siberian craton is characterised by a larger population of Archean to Early Palaeoproterozoic ages (Fig. 6.3; [4]). Taking into account the palaeo-geographic distance and the late final eastern attachment to the CAOB after the Late Jurassic to Early Cretaceous closure of the Mongol-Okhotsk Ocean (e.g. [15]), the Siberian craton is unlikely to have contributed detritus to the study region. The Tarim craton reveals a very heterogenous age distribution (ca. H_{rel} = 95%) with a distinct Neoproterozoic age population (ca. 788 Ma), neither of which is observed in the study region. Recently, Ge et al. [16] reported abundant 2.5 Ga and 1.85 Ga ages, similar to those in the North China Craton. However, the Tarim craton is discarded as an age source, although [4] suggest that it was an important contributor of detrital material to the Palaeozoic basins in Mongolia. Large-scale northeastern Gondwana-derived fragments in the eastern CAOB, which could have provided detritus to the study region, are not reported so far. As pointed out by Rojas-Agramonte et al. [4], Gondwanan fragments are generally characterised by a Pan-African age peak (ca. 650–550 Ma) and a Mesoproterozoic age gap (ca. 1.75–1.0 Ga). These age peak and gap are absent in the analysed samples in this study. They are, thus, not considered as provenance sources of the Permian sedimentary basins across the accretionary collision zone between the North China Craton and the Mongolian Arcs. Zhou et al. [3] and Han et al. [17], proposed that the Erguna, Xing'an, Jiamusi-Khanka and Songliao blocks in northeast China have Pan-African basement (Fig. 6.3) and resemble fragments that rifted from northern Gondwana, which may have influenced sedimentary systems in the region during the Late Palaeozoic.

Therefore, additional sedimentary provenance terranes need to be considered to explain the dominant occurrence of Early and Late Palaeozoic, and broad Palaeozoic age populations in the Southern Accretionary Orogen and Northern Accretionary Orogen, respectively. An Early Palaeozoic arc along the northern margin of north China has been proposed (e.g. [9]), termed the Southern Orogen by Jian et al. [18, 19].

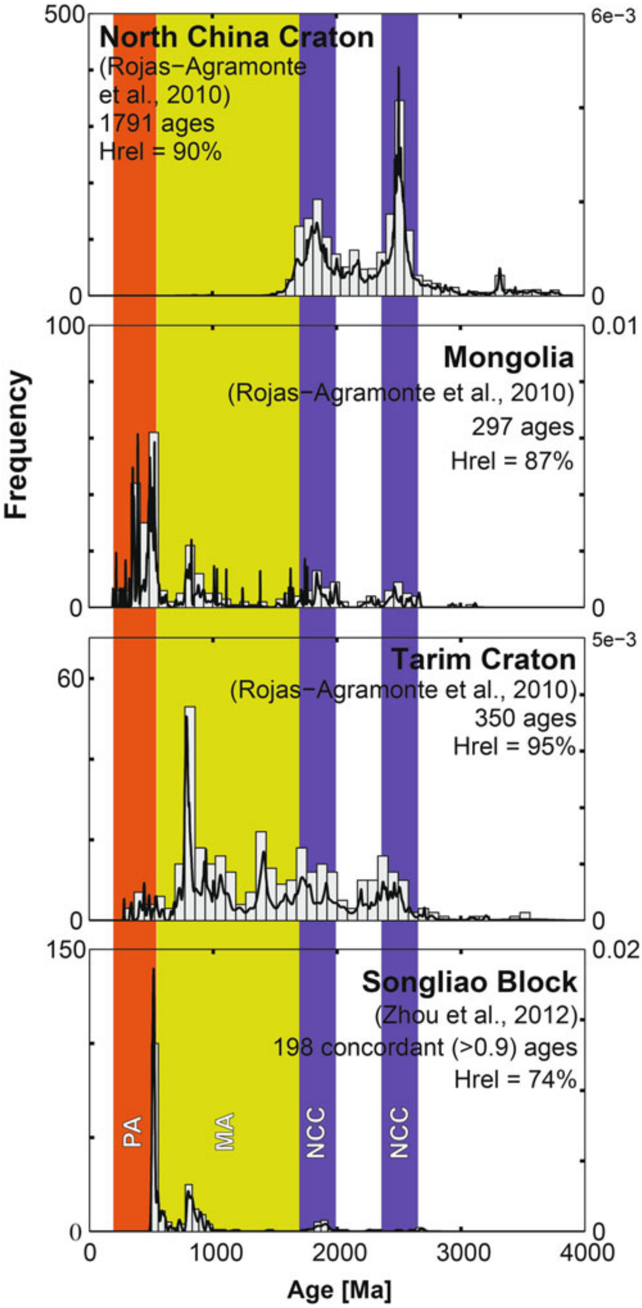

Fig. 6.3 Zircon U–Pb age spectra for potential sedimentary provenance terranes in the study region. PA: Palaeozoic arcs; MA: Mongolian Arcs; NCC: North China Craton

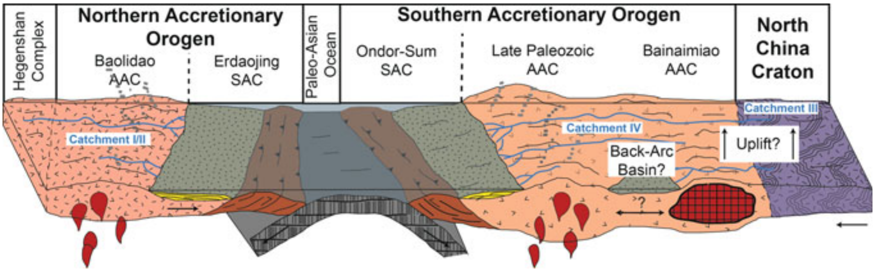

Fig. 6.4 Tectonic sketch map of potential sedimentary provenances and their basin relationships during the closure of the Palaeo–Asian Ocean in Late Permian time. AAC: arc-accretion complex; SAC: subduction-accretion complex; catchment I/II: Mongolian Arcs (located further north, not depicted in this sketch) and Northern Accretionary Orogen; catchment III: North China Craton; catchment IV: Southern Accretionary Orogen

Early Palaeozoic activity and collision with a microcontinent (Hunshandake microcontinent) along the Ondor-Sum subduction-accretion complex were recently reported by Shi et al. [20] and Xu et al. [21]. Phengites in blueschists from the Ondor-Sum subduction-accretion complex gave $^{40}Ar/^{39}Ar$ ages of 453 ± 1.8 Ma and 449.4 ± 1.8 Ma [22]. Additionally, Cope et al. [23] considered that a continental arc existed along the northern margin of the North China Craton from ca. 400 Ma to ca. 275 Ma based on a detrital zircon analysis of Carboniferous to Permian non-marine strata. These lines of evidence suggest that the Early and Late Palaeozoic zircons in the arc basins of the Southern Accretionary Orogen originated most likely from a major provenance terrane along the northern margin of north China, not from the Mongolian Arcs, which were on the opposite side of the Palaeo–Asian Ocean (Fig. 6.4) during sediment deposition in the Permian.

A number of studies proposed the existence of an active Palaeozoic arc along the southern edge of the Mongolian Arcs [9, 13, 18, 19, 24–27]. Zircons from a biotite-plagioclase gneiss sample collected from the Xilinhot complex in the Northern Accretionary Orogen yielded upper and lower intercept ages of 437 ± 3 Ma and 316 ± 3 Ma, respectively [28]. The Baolidao magma suite was emplaced at ca. 310 Ma [12]. This implies that the broad Palaeozoic age range likely originated from an active arc to the north of the Palaeo–Asian Ocean. However, its tectonic nature, continental or ensialic, remains unresolved.

In summary, the results of this thesis imply that at least four different sedimentary provenance terranes contributed to the arc basins across the accretionary collision zone between the North China Craton and the Mongolian Arcs (Figs. 6.4 and 6.5): To the north, arc basins received sedimentary material from the (I) Precambrian basement of the southern Mongolian Arcs and (II) an active Palaeozoic arc, e.g. the Northern Accretionary Orogen. (b) To the south, the (III) Precambrian basement of the North China Craton and the (IV) Early and Late Palaeozoic active continental arc, e.g. the Southern Accretionary Orogen. Minor age contributions of unknown origin may indicate the influence of less well constrained, and locally restricted, tectonic units such as the Hunshandake microcontinent [20, 21]. Mixture of detritus of all four sedimentary provenance terranes may have occurred during the latest stages of ocean closure and formation of the Solonker Suture Zone.

6.2 Accretionary Tectonic and Depositional Settings

The geochronological and Hf isotopic record in detrital zircons of Devonian and Permian arc basins (Figs. 6.5 and 6.6) combined with previous studies, allows for a comprehensive outline of the tectonic setting of each tectonic unit across the accretionary collision zone between the North China Craton and the Mongolian Arcs.

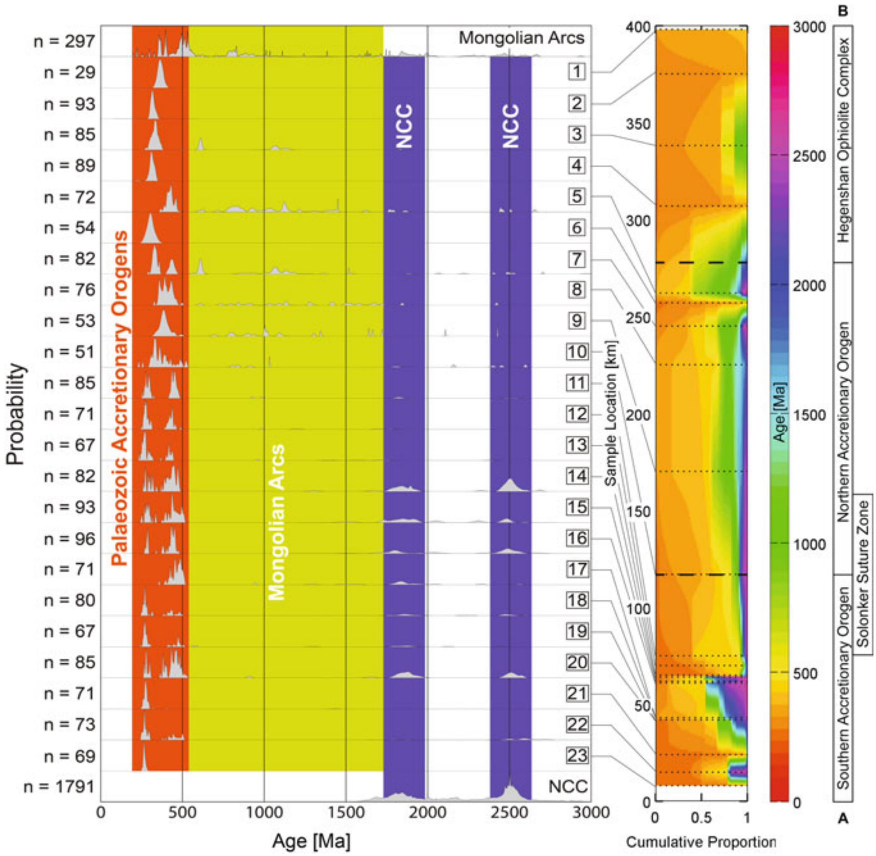

Fig. 6.5 Zircon U–Pb age probability density functions and cumulative age distributions across the accretionary collision zone. NCC: North China Craton; A, B northwest-southeast transect (see Fig. 4.1 for sample locations)

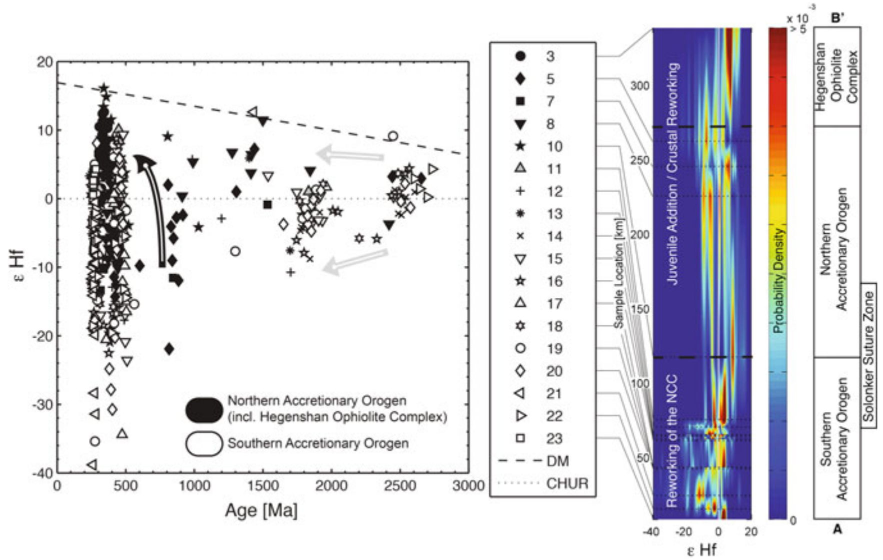

Fig. 6.6 Detrital zircon ϵHf versus age diagram for the Southern and Northern Accretionary Orogens (left). Spatial linear interpolation of ϵHf probability density functions along a NE-SW transect (see Fig. 4.13 for sample locations)

Geochemical characteristics further constrain the overall depositional environment, and answer questions on the net amount of crustal growth during the closure of the Palaeo–Asian Ocean across the Solonker Suture Zone.

6.2.1 *The Chinese Southern Mongolian Arcs*

The detrital age distributions in Devonian strata in the Chinese southern Mongolian Arcs (Figs. 4.9 and 4.2) broadly agree with those reported for a hypothetical matured Early Palaeozoic southern Mongolian island arc terrane atop an ancient microcontinent (Uliastai arc [9, 13, 26, 27, 29]). However, its origin, probably a fragment rifted from the Tarim craton [4], is debatable, even though it shares a major age population at ca. 966 Ma with the latter. Sedimentary access to other tectonic units of the Mongolian Arcs, if any, seemed limited since other ages do not occur in the Devonian strata, suggesting that the Mongolian Arcs as a coherent terrane still did not exist in the Devonian, but an archipelago of independent tectonic units [30].

Active arc volcanism, likely associated with the southward accretionary growth of the Siberian craton and the Mongolian Arcs and/or subduction beneath the Uliastai arc, continued in the Carboniferous [31], as also evidenced by such aged zircons in the Permian strata of the Northern Accretionary Orogen (see following section). The broader range of Precambrian ages detected in the Permian basins of the Northern

Accretionary Orogen may be interpreted as a result of a consolidation of the Mongolian Arcs as a coherent sedimentary provenance terrane in the Permian. This suggests that in the Permian, in contrast to the Devonian, a larger variety of sediment, and thus age sources, were available. Likely, the Uliastai arc had accreted onto the Mongolian Arcs before the Permian.

6.2.2 The Northern Accretionary Orogen and Hegenshan Ophiolite Complex

Several authors [9, 18, 19, 24, 25, 27, 32] argue that northward dipping subduction of the Palaeo–Asian Ocean beneath the Mongolian Arcs took place along an Andean-type active continental margin from the Devonian to Late Permian, initiating the formation of the Northern Accretionary Orogen. However, a subtle change in sedimentary provenance from the Devonian to Permian (Fig. 4.2) suggests that a fully developed continental margin existed only in the Permian, when the Mongolian Arcs as a terrane were consolidated, whereas in the Devonian subduction took place beneath the isolated Uliastai arc [9, 13, 26].

The Hegenshan Ophiolite Complex, separating the Northern Accretionary Orogen from the Mongolian Arcs today, may play a crucial role in understanding the tectonic setting from the Carboniferous to Late Permian. The geochronological and Hf isotopic data in this work (Figs. 6.5 and 6.6) imply that its basins received sedimentary material from a single juvenile Carboniferous source. The Northern Accretionary Orogen, on the other hand, contains clastic sedimentary rocks from juvenile, crustal and mixed sources from the Palaeozoic arcs and the Mongolian Arcs, consistent with the findings for subduction-related gabbroic diorites [12, 33]. The Permian strata in the Northern Accretionary Orogen and the southern Mongolian Arcs are intercalated by limestones, indicative for a relatively stable shallow marine environment except for the Hegenshan Ophiolite Complex in between (Fig. 2.4). All these features, including the overall bimodal geochemical and textural character of the sedimentary and volcanic rocks observed in this study, can be explained by the opening of a back-arc basin in the Late Carboniferous followed by its closure before the Late Permian, as already proposed by several other authors [34–36], largely consistent with Zhang et al. [11] and Jian et al. [19], but contrary to the model of Xiao et al. [9]. Opening of the back-arc basin would have caused the Northern Accretionary Orogen to drift away from the assemblage of Precambrian crustal material of the Mongolian Arcs, which may have successively supported the addition of juvenile magma sources by continued subduction beneath the now disconnected accretionary orogen. During back-arc basin closure, the Hegenshan ophiolite formed subsequent to subduction of the back-arc oceanic crust at ca. 295 Ma [36]. Eventually it was obducted onto the Mongolian Arcs shortly before the closure of the Palaeo–Asian Ocean further south, where the youngest Early Triassic subduction-related arc activity is recorded. In comparison, the youngest volcanic activity recorded in the Northern Accretionary

Orogen took place in the Permian, as evidenced by a ca. 270 Ma old andesite dated in this study (e.g. Fig. 4.6). After the closure of the back-arc basin sediment from the Mongolian Arcs would again be able to reach the arc basins of the Northern Accretionary Orogen until the final ocean closure (Fig. 6.4).

6.2.3 The Southern Accretionary Orogen

Whole-rock geochemical data suggest a tectonic convergent (oceanic subduction and continental collision) setting across the Solonker Suture Zone during the Permian (Figs. 4.20 and 4.21). The location of the detected provenance terranes implies southward directed oceanic subduction beneath the Southern Accretionary Orogen and the North China Craton. The major Permian age population (ca. 269 Ma) coincides with the age of the stratigraphic host formations. The overall detrital zircon U–Pb age distribution of the study area (Fig. 4.2) resembles that of a convergent tectonic setting as recently characterised by Cawood et al. [37], thus representing a basin environment within or near an active arc system. This is supported by arc-related volcanic rocks along the Xar Moron River, which are characterised by calc-alkaline compositions [17, 38–41]. Previous sections outlined that the Permian clastic sedimentary and volcanic rock suites are geochemically closely related. The sedimentary rock suite is geochemically characteristic of a higher quartzose but less detrital content compared to the volcanic rock suite. Nevertheless, a continuous geochemical trend toward higher silica content can be observed between both rock types (Fig. 4.18). Geochemically, a mafic to intermediate sedimentary provenance is suggested (Fig. 4.20), consistent with an overall active arc setting in the Permian (Fig. 4.21). These observations suggest short transport distances from the major source regions to the sedimentary basins, with a certain degree of sedimentary reworking. This is further supported by the textural immaturity of the sedimentary (volcano-clastic) rocks (Fig. 2.18). Further evidence for an arc and/or collisional environment is the presence of paired metamorphic belts farther west of the study area, of which the high-pressure belt is represented by blueschists in the Ondor-Sum subduction-accretion complex [22]. Point-counting results in this study indicate a transitional to undissected arc setting (Fig. 2.18). Distinction between different arc settings within the QFL-diagram is not clear, which supports the idea of a complex convergent tectonic setting during the Permian as also sufficed by investigating the geochronological entropy of the geochronological system (Chap. 5). In summary, a subduction and collisional tectonic environment is inferred across the present Xar Moron River area during the Late Palaeozoic.

The above conclusion, that the fore-arc basins in the Southern Accretionary Orogen were accessed by the Early and Late Palaeozoic continental arcs and the North China Craton, is widely accepted [9, 18, 19], and further corroborated by the new Hf data presented in this study (Fig. 6.6). Precambrian crust of the North China Craton appears to had been reworked by the southward dipping subduction of the Palaeo–Asian Ocean during the Early Palaeozoic, but with a significant addition of juvenile sources, visible in a slight shift to positive εHf values. The second, Late Permian subduction phase most probably reworked crustal material from both, the North China Craton and the Early Palaeozoic arc. Addition of juvenile material at this time, if any, seemed minor. In general, the data presented in this thesis indicate a relatively stable Andean-type continental margin along the North China Craton throughout the Palaeozoic. However, arc activity was possibly interrupted for a short period of time during the accretion of the Hunshandake microcontinent in the Late Carboniferous or Early Permian [20, 21], and an overall dynamic subduction regime (e.g. a temporary immature back-arc basin opening; Fig. 6.4) may have caused a more complex arc basin geometry.

6.2.4 General Depositional Setting

The conclusions in the previous section agree with the overall consensus that southward dipping subduction of the Palaeo–Asian Ocean took place beneath the North China Craton throughout the Palaeozoic [8, 9, 18, 19, 23, 32]. This gave rise to the formation of the Southern Accretionary Orogen, of which the Bainaimiao arc is an essential component. This tectonic scenario is consistent with the geochemical results presented in this work. The volcanic rocks in the Southern Accretionary Orogen have all calc-alkaline mafic to felsic compositions, indicative for a collisional tectonic setting (Fig. 4.20). The close relationship to the sedimentary rocks does not only identify them, next to the Bainaimiao arc per se, as a major sedimentary provenance terrane, but also imply short transport distances, typical for active arc basin settings, and consistent with the geochronological data. Geochemical discrimination plots for tectonic settings of sedimentary rocks (Fig. 4.21) support this conclusion, although a dynamic accretionary setting, such as a temporary extensional environment in the hinterland cannot be excluded, since some data points fall into the oceanic arc field (Fig. 6.4).

The depositional environment in the Northern Accretionary Orogen appears to be more complex. In general, two scenarios have been proposed, one of which suggesting that the orogen consolidated during the Early Palaeozoic and experienced bimodal volcanism due to extension in the Late Palaeozoic [11, 18, 19]. However, it does not provide any comprehensible explanation for the emplacement of the Hegenshan ophiolite. An alternative scenario involves northward dipping subduction beneath the orogen throughout the Palaeozoic, during which back-arc basin opening and closure led to the formation and obduction of the Hegenshan ophiolite [9]. Both scenarios are consistent with the occurrence of geochemically bimodal volcanic and clastic sedimentary rocks across the orogen (Fig. 4.17), as well as their close mutual geochemical affinity (Figs. 4.17 and 4.19). This implies short transport distances and identifies the volcanic rocks as a major contributor to detritus, albeit not the only one. Likely, arc basins in the Northern Accretionary Orogen were also sourced by multiple provenances, such as the Baolidao magma suite plutons and Precambrian basement rocks of southern Mongolia (Fig. 6.1). Nonetheless, the back-arc basin scenario is favoured, since it would explain the simultaneous occurrence of mature sedimentary rocks deposited in a passive continental margin setting facing the open back-arc basin, as well as the oceanic arc affinity of immature sedimentary rocks deposited in a fore-arc basin facing a northward dipping subduction (Figs. 2.13 and 4.21). Minor, but significant, amounts of detritus was derived from the Precambrian basement of southern Mongolia after its consolidation as a consistent sedimentary provenance terrane in the Permian.

6.3 Identification and Location of the Solonker Suture Zone

The cryptic nature of the Solonker Suture Zone impedes its unambiguous identification. The overall geochemical and geochronological similarities across the suture further suggest a similar tectonic and depositional environment. However, a significant variability across the accretionary collision zone between the North China Craton and the Mongolian Arcs is able to reveal its tectonic nature and location.

Arc basins of the Southern Accretionary Orogen have recorded the youngest major age peak at ca. 270 Ma among all clastic sedimentary rock samples in the study area (Fig. 4.2), which defines the maximum depositional age of the Huanggangliang and Linxi formations. An andesitic pyroclastic rock collected from the southern shoreline of the Xar Moron River formed between the Early and Middle Triassic, interpreted as the timing of the latest volcanic activity related to the southward subduction of oceanic lithosphere of the Palaeo–Asian Ocean. An undeformed felsic dike intruding the Huanggangliang formation is interpreted to have recorded a period of latest magmatic activity and thus giving a constraint on the minimum depositional age of the Huanggangliang formation. The dominant age peaks in both igneous rocks, however, are located in the Early Triassic (ca. 240–250 Ma; Fig. 4.6). In comparison, the youngest volcanic activity in the Northern Accretionary Orogen was recorded by a ca. 270 Ma old andesitic dike. Taken together, the geochronological data suggest that the final closure of the Palaeo–Asian Ocean along the Solonker Suture Zone most likely occurred in the Xar Moron River region (Fig. 6.7) in the period between ca. 240–270 Ma. This is consistent with previous data obtained in the Xar Moron River area (e.g. [41, 42]). For example, magmatic zircons from a biotite-plagioclase schist and an intrusive syncollisional granite of the Shuangjing metamorphic complex located along the northern banks of the Xar Moron River yielded ages of 298 ± 2 Ma and 272 ± 2 Ma, respectively, suggesting that the final closure of the Palaeo–Asian Ocean occurred some time after, not in the Early Palaeozoic. In addition, previous structural, sedimentary and geochronological data from other areas in vicinity of the Xar Moron River region also suggested that the Solonker Suture Zone developed in the Late Palaeozoic or Early Triassic (e.g. [9, 18, 19, 30, 38, 43]), in accordance with the results in this study.

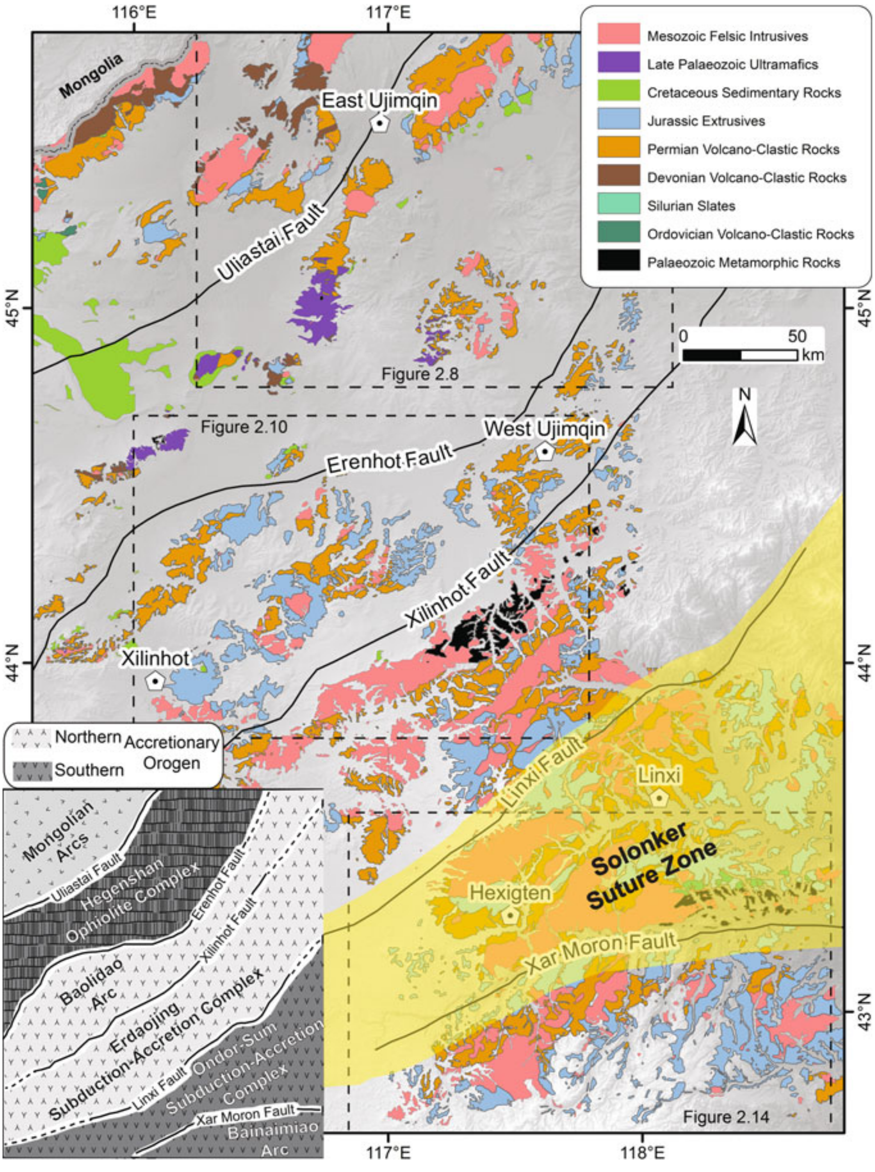

Fig. 6.7 Proposed location of the cryptic Solonker Suture Zone in the study area based on the results presented in this dissertation

An overall increased, but variably, P_2O_5 concentration in the volcanic rocks can only be observed in the Southern Accretionary Orogen (Fig. 4.19), while Zr appears to be positively correlated with increasing silica content only in the clastic sedimentary rocks of the Northern Accretionary Orogen. This suggests that phosphate minerals (e.g. apatite) played an important role during the formation of the volcanic rocks of the Southern Accretionary Orogen, but not after their erosion. The increased Zr concentrations are likely related to the "zircon effect", which becomes more apparent in texturally mature clastic sedimentary rocks, which implies that the depositional environment of the Northern Accretionary Orogen has not been as homogenous as that to the south. However, the overall enrichment and depletion of mobile and immobile elements with respect to N-MORB and average continental crust remain similar, and may indicate an overall similar depositional environment despite the slight differences.

Major differences are observed in the geochemical and geochronological character of the sedimentary source terranes north and south of the Solonker Suture Zone. Arc basins of the Southern Accretionary Orogen originated dominantly from a fairly homogenous mafic to intermediate provenance terrane, e.g. the Early and Late Palaeozoic arcs (ca. 436 and 269 Ma, respectively), while they were significantly accessed by the North China Craton (ca. 1.8 and 2.5 Ga). Detrital zircon Hf results further indicate a higher degree of crustal contaminated magma formation during subduction of the Palaeo–Asian Ocean. Arc basins of the Northern Accretionary Orogen appear to be derived from a more heterogeneous mixture of different felsic to quartzose sedimentary provenances, e.g. a Palaeozoic active arc system (ca. 328–429 Ma) as well as the Precambrian aged accretionary assemblage of the Mongolian Arcs. This is also corroborated by an overall bimodal geochemical distribution of volcanic and clastic sedimentary rocks. Despite the proximity of the Northern Accretionary Orogen to the Hegenshan Ophiolite Complex, no influence of ultramafic material was observed in both accretionary orogens. Hence, exposure of the Hegenshan ophiolite must have taken place after the formation of the Permian arc basins. In contrast to the Southern Accretionary Orogen, more juvenile magma sources were involved during the subduction of the Palaeo–Asian Ocean beneath the Northern Accretionary Orogen.

In summary, the Solonker Suture Zone (Fig. 6.7) delineates from south to north the transition from (a) a more homogenous to a more heterogeneous assemblage of sedimentary provenance terranes, (b) a subduction regime with significant involvement of crustal contaminated magma sources to a more juvenile crustal character and (c) the Southern Accretionary Orogen and the North China Craton as primary sedimentary provenance terranes to the Northern Accretionary Orogen and the Mongolian Arcs.

6.4 Tectonic Model for the Accretionary Collision Between the Mongolian Arcs and the North China Craton

6.4.1 *Early to Middle Palaeozoic (Fig. 6.8)*

During the Late Ordovician to Devonian the Palaeo–Asian Ocean was involved in subduction beneath the northern margin of the North China Craton to the south and the Uliastai arc to the north, which initiated the formation of the Southern and Northern Accretionary Orogens, respectively. The Devonian strata likely were deposited on either sides of the Uliastai arc receiveing material from the arc. A large number of studies have confirmed the existence of such symmetric Early Palaeozoic arc geometry along both sides of the ocean [9, 23, 36, 43–46], which is further supported by recent deep-seismic images [32]. Major Ordovician to Devonian age populations in the Devonian and Permian basins across both accretionary orogens are consistent with this conclusion.

From the Early to Middle Carboniferous the Uliastai arc accreted onto the Mongolian Arcs sensu lato, consolidating the Mongolian Arcs sensu stricto as the Permian sedimentary provenance terrane of arc basins in the Northern Accretionary Orogen. Subduction polarity of this accretionary event is debatable. Since then the Palaeo–Asian Ocean remained the only open ocean, further contracting as a result of subduction beneath the Mongolian Arcs and the North China Craton. Active arc volcanism along both sides of the ocean is again supported by a large number of ages during this period.

In the Late Carboniferous back-arc basin opening separated the Mongolian Arcs from the Northern Accretionary Orogen as indicated by a significant shift from mixed to positive εHf values, and the absence of Precambrian ages in Permian sedimentary strata of the Hegenshan Ophiolite Complex. The occurrence of a bimodal volcanic rock suite near Xilinhot further supports this conclusion [11]. Subduction beneath the isolated Northern Accretionary Orogen continued, evidenced by such aged zircons in basins north of the Solonker Suture Zone. Subduction and/or magma production may have temporarily ceased due to the accretion of the Hunshandake microcontinent [20, 21], since such aged zircons are absent in Permian basins south of the Solonker Suture Zone. A back-arc basin scenario is supported by most researchers [34–36], although opposed by some [9, 47].

6.4.2 *Late Palaeozoic to Early Mesozoic (Fig. 6.8)*

From the Early to Middle Permian the consumption of the Palaeo–Asian Ocean continued, while the Hegenshan back-arc basin began to close. The initiation of subduction, supposedly northward dipping beneath the Mongolian Arcs according to fault attitudes in deep-seismic profiles [32], led to the formation of the supra-subduction zone Hegenshan ophiolite at ca. 295 Ma [36]. The results in this dissertation

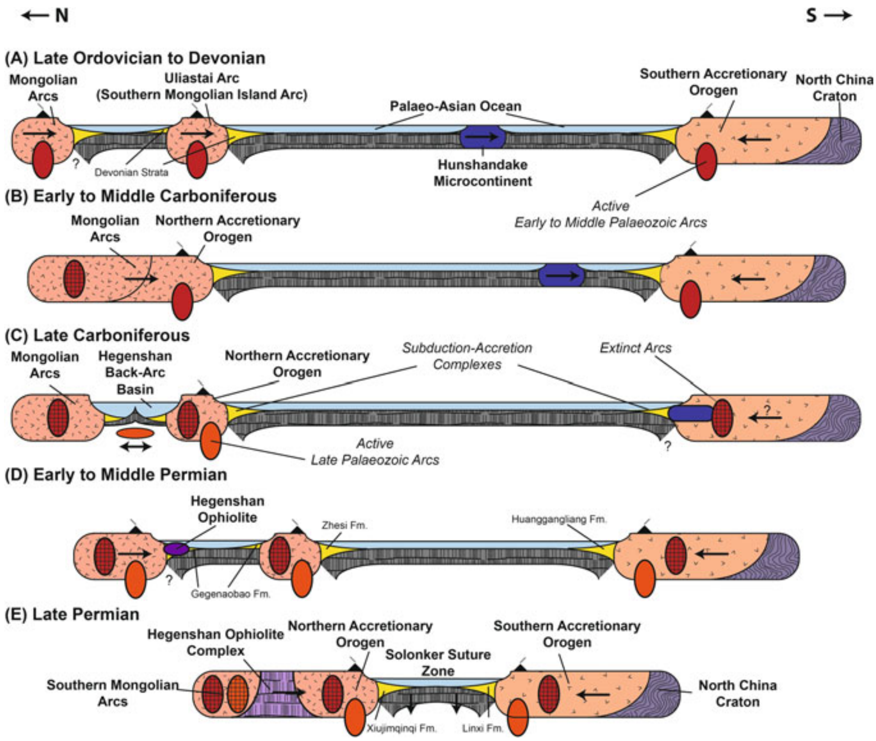

Fig. 6.8 Proposed Palaeozoic tectonic evolution of the Palaeo–Asian Ocean between the Mongolian Arcs and the North China Craton. **A** Late Ordovician to Devonian, double-sided subduction of the Palaeo–Asian Ocean along the Uliastai arc and Southern Accretionary Orogen; **B** Early to Middle Carboniferous, consolidation of the Mongolian Arcs and double-sided subduction beneath the Northern and Southern Accretionary Orogen; **C** Late Carboniferous, opening of the Hegenshan back-arc basin, subduction beneath the Northern Accretionary Orogen and accretion of the Hunshandake microcontinent onto the Southern Accretionary Orogen; **D** Early to Middle Permian, closure of the Hegenshan back-arc basin, formation of the supra-subduction zone Hegenshan ophiolite and double-sided subduction beneath the Northern and Southern Accretionary Orogens; **E** Late Permian, obduction of the Hegenshan ophiolite and imminent closure of the Palaeo–Asian Ocean

suggest that northward dipping subduction beneath the Northern Accretionary Orogen continued, while southward dipping subduction beneath the Southern Accretionary Orogen resumed to full-scale [9]. The Gegenaobao formation, which occurs in the southern Mongolian Arcs, the Hegenshan Ophiolite Complex and the Northern Accretionary Orogen, likely represents the back-arc basin fill comprising sediment from the Bainaimiao arc and the Mongolian Arcs. The Zhesi and Huanggangliang formations likely formed as fore-arc basin deposits in the Northern and Southern Accretionary Orogens, respectively.

In the Late Permian the Hegenshan ophiolite was obducted onto the Mongolian Arcs during the closure of the Hegenshan back-arc basin [36]. During this time the

Late Permian Xiujimqinqi and Linxi formations were deposited, likely as fore-arc basin fills receiving sediment from the active arcs, and the Mongolian Arcs and North China Craton, respectively. The Linxi formation likely represents the latest basin deposits as it conformably overlies the Xiujimqinqi formation and the earlier Zhesi formation, dominantly comprising sediment from the, during the Early and Late Palaeozoic active, Bainaimiao arc and the North China Craton.

By the end of the Early Triassic the Palaeo–Asian Ocean closed following a bipolar subduction geometry, leading to a “soft” collision of the accretionary wedges of the Northern and Southern Accretionary Orogens. A distinct change of the detrital age, εHf distributions and geochemical characteristics observed between the opposing accretionary orogens clearly demarcates the location of the cryptic Solonker Suture Zone. The latest arc activity in the region (ca. 270–240 Ma) also identifies it as the final one.

Following the closure of the Palaeo–Asian Ocean, A-type post-collisional plutons were emplaced across the accretionary collision zone [12, 48], probably stimulated by the detachment of oceanic crust in the region as a result of the bipolar subduction geometry. This interpretation is consistent with the absence of remnants of oceanic crust in recent deep-seismic profiles [32]. However, Jian et al. [19] suggests that A-type granites were a result of a Permian rifting event in the Northern Accretionary Orogen.

6.5 Net Crustal Growth and Present-Day Tectonic Analogues

Most studies concluded that juvenile crustal growth surpassed crustal reworking during the closure of the Palaeo–Asian Ocean and the CAOB as a whole [12, 49–52]. Projected average $\varepsilon\mathrm{Hf}_{\mathrm{today}}$ and $\varepsilon\mathrm{Nd}_{\mathrm{today}}$ values should tend to more radiogenic values, or vice versa if crustal contamination was dominant during the accretionary events leading to the closure of the Palaeo–Asian Ocean. $\varepsilon\mathrm{Hf}_{\mathrm{today}}$ and $\varepsilon\mathrm{Nd}_{\mathrm{today}}$ of bulk sedimentary and volcanic rocks (Fig. 4.25) indeed shift to more radiogenic compositions in the Northern Accretionary Orogen and the Hegenshan Ophiolite Complex, or north of the Solonker Suture Zone, which indicates predominant juvenile crustal addition. To its south in the Southern Accretionary Orogen, however, whole-rock Hf and Nd isotopic compositions are less radiogenic, thus, crustal reworking played a more dominant role there during the subduction of the Palaeo–Asian Ocean. However, the overall range of compositions settles around $\varepsilon\mathrm{Hf}_{\mathrm{today}} = 0$, slightly less for $\varepsilon\mathrm{Nd}_{\mathrm{today}}$, implying that overall juvenile addition and crustal reworking were kept at balance, averaging CHUR compositions, which would not contradict projected, hypothetical crustal development paths based on detrital zircon εHf compositions across the accretionary collision zone. This conclusion is in accordance to the definition of “internal” orogens by Collins et al. [53], although the results in this study point out that the Northern Accretionary Orogen shares, in contrast to the Southern Accretionary Orogen, more resemblance to an "external" orogen. Hence, net juvenile addition in the study region, and probably throughout the CAOB, remains questionable [54]. This study indicates that dominantly crustal contaminated or juvenile magmas can be locally restricted depending on the local setting. Conclusions drawn from one location, thus, do not necessarily apply to an entire region, especially within very complex accretionary environments such as the CAOB.

Collins et al. [53] defined two contrasting Phanerozoic global orogenic systems based on zircon Hf data: external orogens, which form by accretionary processes due to the subduction of dominantly oceanic lithosphere (e.g. along the Pacific "Ring-of-Fire"), and internal orogens, which involve the accretion of numerous large-scale continental fragments (e.g. in the CAOB). However, such definition only represents two end-members of orogenic belts, and many collisional belts may have involved both subduction-related accretion and continent-continent or arc-continent collision, as is the case in the accretionary collision zone between the Mongolian Arcs and the North China Craton. The broadening of negative εHf values in detrital zircons in the Southern Accretionary Orogen (Fig. 4.14) resembles more that of an internal orogen, reflecting the crustal contamination induced by the continued southward dipping subduction beneath the North China Craton. The Northern Accretionary Orogen, on the other hand, corresponds more to an external orogen, with significant occurrences of positive εHf values in detrital zircons as a result of juvenile addition and simultaneous crustal reworking by the continued northward dipping subduction of the Palaeo–Asian Ocean, and back-arc spreading similar to the opening of the Japanese Sea (see also Hf data for Japan in Collins et al. [53]).

Cryptic suturing subsequent to "soft" collision of two opposing accretionary wedges might be common in accretionary tectonic environments, such as the CAOB [9, 54], Southeast Asia, the Arabian-Nubian shield [55, 56], and the circum-Pacific. The absence of regional metamorphism and large-scale thrust features can be explained by a bipolar subduction geometry, where oceanic crust is largely detached from continental crust. Continental deep subduction would, thus, not occur, and collision reduced to a mere docking of tectonic blocks. Accretionary tectonic settings, especially in archipelago-type tectonic environments [30] share many common features, which may support such collision type. The results of this dissertation demonstrated that the analysis of the isotopic geochemical variability of detrital zircons and whole-rock geochemical features in arc basins in accretionary collision zones can be an important tool to identify these cryptic sutures.

The Pacific Ocean may serve as a present-day analogue to the Palaeozoic development of the Palaeo–Asian Ocean. The opening of the Japanese Sea [57] and the spreading of the Izu-Bonin-Mariana arc system [58] may be similar to the opening of the Hegenshan back-arc basin. The Permian environment may resemble Southeast Asia, where multiple subduction geometries are common, such as the situation in the Molucca or the Philippine Sea [59]. The imminent collision of mature arc-systems along the islands of Papua New Guinea and Solomon with the Australian craton [60] may produce an analoguous geochronological and Hf isotopic detrital zircon record to that in the accretionary collision zone between the Mongolian Arcs and the North China Craton, although northward dipping subduction is dominant in the present-day example.

References

1. Sircombe KN (2004) AgeDisplay: an EXCEL workbook to evaluate and display univariate geochronological data using binned frequency histograms and probability density distributions. Comput Geosci 30(1):21–31
2. Gehrels GE, Blakey R, Karlstrom KE, Timmons JM, Dickinson B, Pecha M (2011) Detrital zircon U-Pb geochronology of Paleozoic strata in the Grand Canyon, Arizona. Lithosphere 3(3):183–200
3. Zhou J-B, Wilde SA, Zhang X-Z, Liu F-L, Liu J-H (2012) Detrital zircons from phanerozoic rocks of the Songliao Block, NE China: evidence and tectonic implications. J Asian Earth Sci 47:21–34
4. Rojas-Agramonte Y, Kröner A, Demoux A, Xia X, Wang W, Donskaya T, Liu D, Sun M (2011) Detrital and xenocrystic zircon ages from Neoproterozoic to Palaeozoic arc terranes of Mongolia: significance for the origin of crustal fragments in the Central Asian Orogenic Belt. Gondwana Res 19(3):751–763. Their role in growth of accretionary orogens and mineral endowment, Island Arcs
5. Sawyer E (1986) The influence of source rock type, chemical weathering and sorting on the geochemistry of clastic sediments from the Quetico Metasedimentary Belt, Superior Province Canada. Chem Geol 55(1–2):77–95
6. Fralick P, Kronberg B (1997) Geochemical discrimination of clastic sedimentary rock sources. Sediment Geol 113(1–2):111–124
7. Fralick P (2003) Geochemistry of clastic sedimentary rocks: ratio techniques. In: Lentz D (ed) Geochemistry of Sediments and sedimentary rocks. Geological Association of Canada, St. John's, pp 85–103
8. Nie F, Bjørlykke A (1999) Nd and Sr isotope constraints on the age and origin of Proterozoic meta-mafic volcanic rocks in the Bainaimiao-Wenduermiao district, south-central Inner Mongolia, China. Cont Dyn 4:1–14
9. Xiao W, Windley BF, Hao J, Zhai M (2003) Accretion leading to collision and the Permian Solonker suture, Inner Mongolia, China: Termination of the central Asian orogenic belt. Tectonics 22(6)
10. Zhang S-H, Zhao Y, Ye H, Liu J-M, Hu Z-C (2014b) Origin and evolution of the Bainaimiao arc belt: implications for crustal growth in the southern Central Asian orogenic belt. Geol Soc Am Bull 126(9–10):1275–1300
11. Zhang X, Zhang H, Tang Y, Wilde SA, Hu Z (2008) Geochemistry of Permian bimodal volcanic rocks from central inner Mongolia, North China: implication for tectonic setting and Phanerozoic continental growth in Central Asian Orogenic Belt. Chem Geol 249(3–4):262–281
12. Chen B, Jahn B, Wilde S, Xu B (2000) Two contrasting paleozoic magmatic belts in northern Inner Mongolia, China: petrogenesis and tectonic implications. Tectonophysics 328(1–2):157–182
13. Demoux A, Kröner A, Liu D, Badarch G (2009) Precambrian crystalline basement in southern Mongolia as revealed by SHRIMP zircon dating. Int J Earth Sci 98(6):1365–1380
14. Darby BJ, Gehrels G (2006) Detrital zircon reference for the North China block. J Asian Earth Sci 26(6):637–648
15. Cogné J-P, Kravchinsky VA, Halim N, Hankard F (2005) Late Jurassic-Early Cretaceous closure of the Mongol-Okhotsk Ocean demonstrated by new Mesozoic palaeomagnetic results from the Trans-Baïkal area (SE Siberia). Geophys J Int 163(2):813–832
16. Ge R, Zhu W, Wu H, He J, Zheng B (2013) Zircon U–Pb ages and Lu–Hf isotopes of Paleoproterozoic metasedimentary rocks in the Korla Complex, NW China: implications for metamorphic zircon formation and geological evolution of the Tarim Craton. Precambrian Res 231:1–18

17. Han G, Liu Y, Neubauer F, Jin W, Genser J, Ren S, Li W, Wen Q, Zhao Y, Liang C (2012) LA-ICP-MS U-Pb dating and Hf isotopic compositions of detrital zircons from the Permian sandstones in Da Xing'an Mountains, NE China: New evidence for the eastern extension of the Erenhot-Hegenshan suture zone. J Asian Earth Sci 49(0):249–271. Orogenic Belts in Central Asia: Correlations and connections
18. Jian P, Liu D, Kröner A, Windley BF, Shi Y, Zhang F, Shi G, Miao L, Zhang W, Zhang Q, Zhang L, Ren J (2008) Time scale of an early to mid-Paleozoic orogenic cycle of the long-lived Central Asian Orogenic Belt, Inner Mongolia of China: implications for continental growth. Lithos 101(3–4):233–259
19. Jian P, Liu D, Kröner A, Windley BF, Shi Y, Zhang W, Zhang F, Miao L, Zhang L, Tomurhuu D (2010) Evolution of a Permian intraoceanic arc-trench system in the Solonker suture zone, Central Asian Orogenic Belt, China and Mongolia. Lithos 118(1–2):169–190
20. Shi G, Faure M, Xu B, Zhao P, Chen Y (2013) Structural and kinematic analysis of the Early Paleozoic Ondor Sum-Hongqi melange belt, eastern part of the Altaids (CAOB) in Inner Mongolia, China. J Asian Earth Sci 66:123–139
21. Xu B, Charvet J, Chen Y, Zhao P, Shi G (2013) Middle Paleozoic convergent orogenic belts in western Inner Mongolia (China): framework, kinematics, geochronology and implications for tectonic evolution of the Central Asian Orogenic Belt. Gondwana Res 23(4):1342–1364
22. de Jong K, Xiao W, Windley BF, Masago H, Lo C-H (2006) Ordovician 40Ar/39Ar phengite ages from the blueschist-facies Ondor Sum subduction-accretion complex (Inner Mongolia) and implications for the early Paleozoic history of continental blocks in China and adjacent areas. Am J Sci 306(10):799–845
23. Cope T, Ritts BD, Darby BJ, Fildani A, Graham SA (2005) Late Paleozoic Sedimentation on the Northern Margin of the North China Block: implications for regional tectonics and climate change. Int Geol Rev 47(3):270–296
24. Shao J (1989) Continental crust accretion and tectono-magmatic activity at the northern margin of the Sino-Korean plate. J Southeast Asian Earth Sci 3(1–4):57–62
25. Wang Y (1996) Tectonic evolutional processes of Inner Mongolia-Yanshan Orogenic Belt in Eastern China during the Late Paleozoic-Mesozoic. Geological Publishing House, Beijing
26. Lamb MA, Badarch G (1997) Paleozoic sedimentary basins and volcanic-arc systems of southern mongolia: new stratigraphic and sedimentologic constraints. Int Geol Rev 39(6):542–576
27. Badarch G, Cunningham WD, Windley BF (2002) A new terrane subdivision for Mongolia: implications for the Phanerozoic crustal growth of Central Asia. J Asian Earth Sci 21(1):87–110
28. Shi G, Liu D, Zhang F, Jian P, Miao L, Shi Y, Tao H (2003) SHRIMP U–Pb zircon geochronology and its implications on the Xilin Gol Complex, Inner Mongolia, China. Chin Sci Bull 48(24):2742–2748
29. Wang T, Zheng Y, Gehrels GE, Mu Z (2001) Geochronological evidence for existence of South Mongolian microcontinent—a zircon U–Pb age of grantoid gneisses from the Yagan-Onch Hayrhan metamorphic core complex. Chin Sci Bull 46(23):2005–2008
30. Windley BF, Alexeiev D, Xiao W, Kröner A, Badarch G (2007) Tectonic models for accretion of the Central Asian Orogenic Belt. J Geol Soc Lond 164(1):31–47
31. Heumann MJ, Johnson CL, Webb LE, Taylor JP, Jalbaa U, Minjin C (2012) Paleogeographic reconstruction of a late Paleozoic arc collision zone, southern Mongolia. Geol Soc Am Bull 124(9–10):1514–1534
32. Zhang S, Gao R, Li H, Hou H, Wu H, Li Q, Yang K, Li C, Li W, Zhang J, Yang T, Keller G, Liu M (2014a) Crustal structures revealed from a deep seismic reflection profile across the Solonker suture zone of the Central Asian Orogenic Belt, northern China: an integrated interpretation. Tectonophysics 612–613:26–39
33. Chen B, Jahn B, Tian W (2009) Evolution of the Solonker suture zone: constraints from zircon U–Pb ages, Hf isotopic ratios and whole-rock Nd–Sr isotope compositions of subduction—and collision-related magmas and forearc sediments. J Asian Earth Sci 34(3):245–257
34. Robinson P, Zhou M, Hu X, Reynolds P, Bai W, Yang J (1995) Geochemical constraints on petrogenesis and crustal accretion of the Hegenshan ophiolite, Northern China. Acta Petrol Sin 11:112–124

35. Robinson P, Zhou MF, Hu X-F, Reynolds P, Wenji B, Yang J (1999) Geochemical constraints on the origin of the Hegenshan Ophiolite, Inner Mongolia, China. J Asian Earth Sci 17(4):423–442
36. Miao L, Fan W, Liu D, Zhang F, Shi Y, Guo F (2008) Geochronology and geochemistry of the Hegenshan ophiolitic complex: implications for late-stage tectonic evolution of the Inner Mongolia-Daxinganling Orogenic Belt, China. J Asian Earth Sci 32(5–6):348–370
37. Cawood P, Hawkesworth C, Dhuime B (2012) Detrital zircon record and tectonic setting. Geology 40(10):875–878
38. Li J-Y (2006) Permian geodynamic setting of Northeast China and adjacent regions: closure of the Paleo-Asian Ocean and subduction of the Paleo-Pacific Plate. J Asian Earth Sci 26(3–4):207–224
39. Zhang S-H, Zhao Y, Song B, Yang Z-Y, Hu J-M, Wu H (2007) Carboniferous granitic plutons from the northern margin of the North China block: implications for a late Palaeozoic active continental margin. J Geol Soc 164(2):451–463
40. Li D, Chen Y, Wang Z, Hou K, Liu C (2011a) Detrital zircon U–Pb ages, Hf isotopes and tectonic implications for Palaeozoic sedimentary rocks from the Xing-Meng orogenic belt, middle-east part of inner Mongolia, China. Geol J 46(1):63–81
41. Li Y, Zhou H, Brouwer FM, Xiao W, Zhong Z, Wijbrans JR (2011c) Late Carboniferous—Middle Permian arc/forearc-related basin in Central Asian Orogenic Belt: insights from the petrology and geochemistry of the Shuangjing Schist in Inner Mongolia, China. Isl Arc 20(4):535–549
42. Li J, Gao L, Sun G, Li Y, Wang Y (2007) Shuangjingzi middle Triassic syn-collisional crust-derived granite in the east Inner Mongolia and its constraint on the timing of collision between Siberian and Sino-Korean paleo-plates. Acta Petrol Sin 23(3):565–582
43. Xiao WJ, Windley BF, Huang BC, Han CM, Yuan C, Chen HL, Sun M, Sun S, Li JL (2009) End-Permian to mid-Triassic termination of the accretionary processes of the southern Altaids: implications for the geodynamic evolution, Phanerozoic continental growth, and metallogeny of Central Asia. Int J Earth Sci 98(6):1189–1217
44. Tang K (1990) Tectonic development of Paleozoic foldbelts at the north margin of the Sino-Korean Craton. Tectonics 9(2):249–260
45. Tang K, Yan Z (1993) Regional metamorphism and tectonic evolution of the Inner Mongolian suture zone. J Metamorph Geol 11(4):511–522
46. Miao L, Zhang F, Fan W-M, Liu D (2007) Phanerozoic evolution of the Inner Mongolia-Daxinganling orogenic belt in North China: constraints from geochronology of ophiolites and associated formations. Geol Soc, Lond, Spec Publ 280(1):223–237
47. Nozaka T, Liu Y (2002) Petrology of the Hegenshan ophiolite and its implication for the tectonic evolution of northern China. Earth Planet Sci Lett 202(1):89–104
48. Shi G, Miao L, Zhang F, Jian P, Fan W, Liu D (2004) Emplacement age and tectonic implications of the Xilinhot A-type granite in Inner Mongolia, China. Chin Sci Bull 49(7):723–729
49. Wu F, Jahn B, Wilde SA, Sun D (2000) Phanerozoic crustal growth: U–Pb and Sr–Nd isotopic evidence from the granites in northeastern China. Tectonophysics 328(1–2):89–113
50. Jahn B-M (2004) The Central Asian Orogenic Belt and growth of the continental crust in the Phanerozoic. Geol Soc, Lond, Spec Publ 226(1):73–100
51. Wang T, Zheng Y, Li T, Gao Y (2004) Mesozoic granitic magmatism in extensional tectonics near the Mongolian border in China and its implications for crustal growth. J Asian Earth Sci 23(5):715–729
52. Cawood PA, Kröner A, Collins WJ, Kusky TM, Mooney WD, Windley BF (2009) Accretionary orogens through earth history. Geol Soc, Lond, Spec Publ 318(1):1–36
53. Collins WJ, Belousova EA, Kemp AIS, Murphy JB (2011) Two contrasting Phanerozoic orogenic systems revealed by hafnium isotope data. Nat Geosci 4(5):333–337
54. Kröner A, Kovach V, Belousova E, Hegner E, Armstrong R, Dolgopolova A, Seltmann R, Alexeiev DV, Hoffmann JE, Wong J, Sun M, Cai K, Wang T, Tong Y, Wilde SA, Degtyarev KE, Rytsk E (2014) Reassessment of continental growth during the accretionary history of the Central Asian Orogenic Belt. Gondwana Res 25(1):103–125

55. Kröner A, Windley B, Badarch G, Tomurtogoo O, Hegner E, Jahn B, Gruschka S, Khain E, Demoux A, Wingate M (2007) Accretionary growth and crust formation in the Central Asian Orogenic Belt and comparison with the Arabian-Nubian shield. Geol Soc Am Memoirs 200:181–209
56. Johnson P, Andresen A, Collins A, Fowler A, Fritz H, Ghebreab W, Kusky T, Stern R (2011) Late Cryogenian–Ediacaran history of the Arabian–Nubian Shield: a review of depositional, plutonic, structural, and tectonic events in the closing stages of the northern East African Orogen. J Afr Earth Sci 61(3):167–232
57. Celaya M, McCabe R (1987) Kinematic model for the opening of the Sea of Japan and the bending of the Japanese islands. Geology 15(1):53–57
58. Crawford AJ, Beccaluva L, Serri G (1981) Tectono-magmatic evolution of the West Philippine–Mariana region and the origin of boninites. Earth Planet Sci Lett 54(2):346–356
59. Cardwell RK, Isaacks BL, Karig DE (1980) The spatial distribution of earthquakes, focal mechanism solutions, and subducted lithosphere in the Philippine and Northeastern Indonesian Islands. The tectonic and geologic evolution of Southeast Asian seas and islands. American Geophysical Union, Washington, D. C., pp 1–35
60. Abers GA, McCaffrey R (1994) Active arc-continent collision: Earthquakes, gravity anomalies, and fault kinematics in the Huon-Finisterre collision zone, Papua New Guinea. Tectonics 13(2):227–245

Chapter 7
Conclusions

An unambiguous identification and description of the cryptic Solonker Suture Zone remains a major challenge, since typical collisional features, such as regional metamorphism, large-scale thrust features, a continuous ophiolite belt and characteristic mountain topography, are absent. Consequently, tectonic models describing its evolution are often controversial and speculative (e.g. [1–4]). The geochronological, geochemical and statistical analyses, and their interpretation presented in this dissertation, favour a bipolar subduction geometry for the consumption of the Palaeo-Asian Ocean beneath the Mongolian Arcs and the North China Craton during the Palaeozoic, including back-arc basin opening to the north of the suture during Permian time.

The strong geochemical affinity between the Permian volcanic and clastic sedimentary rocks in the study region indicates overall short transport distances, and identified the volcanic rocks, the shallow crustal representatives of the Permian arc chains, as a significant sedimentary provenance terrane. Enrichment and depletions patterns of analysed major and trace element in both rock-types with respect to N-MORB and average continental crust are strikingly similar. Sedimentary rocks to the south of the Solonker Suture Zone are predominantly derived from the active Palaeozoic continental northern margin of the North China Craton, whereas sedimentary rocks north of the suture are sourced from mixed sedimentary provenances, such as the Baolidao arc and the heterogenous Precambrian basement of southern Mongolia. A generally similar collisional tectonic setting, arc activity subsequent to the subduction of the Palaeo-Asian Ocean, is suggested across the suture, although bimodal compositions to the north of it are interpreted to be the result of a Permian back-arc basin opening.

Sedimentary and volcanic rocks tend to have more radiogenic whole-rock Hf and Nd isotopic compositions to the north of the Solonker Suture Zone, whereas to its south they are less radiogenic. Hence, sedimentary provenance terranes to the north appear to be more juvenile in composition, whereas to the south of the suture these are characterised by reworking of crust. However, it appears that net juvenile crustal

P. R. Eizenhöfer, *Subduction and Closure of the Palaeo-Asian Ocean along the Solonker Suture Zone: Constraints from an Integrated Sedimentary Provenance Analysis*, Springer Theses, https://doi.org/10.1007/978-981-32-9200-0_7

addition was equally balanced by crustal reworking during the closure of the Palaeo-Asian Ocean, resulting in a zero net production of crust across the Solonker Suture Zone during the Palaeozoic.

The spatial analysis of geochronological and Hf isotope data revealed a distinct variability in detrital zircons of the arc basins across the accretionary collision zone between the Mongolian Arcs and the North China Craton, which independently confirm the results from whole-rock geochemical analyses. The Hegenshan Ophiolite Complex is characterised by a single age population at ca. 314 Ma and positive ϵHf values. The Northern Accretionary Orogen has a strong affinity with the Mongolian Arcs expressed as a broad distribution of Precambrian ages, and mixed juvenile and crustal reworked sedimentary provenances. Neoarchean and Palaeoproterozoic ages (ca. 1.8 Ga and 2.5 Ga) in arc basins of the Southern Accretionary Orogen indicate a significant contribution of the North China Craton. The latter had been reworked by the Early and Late Palaeozoic southward dipping subduction of the Palaeo-Asian Ocean, which resulted in Hf isotopic ratios developing to successively less radiogenic compositions. The stark geochronological and Hf isotopic contrast between both accretionary orogens clearly outlines the location of the cryptic Solonker Suture Zone along the present-day Xar Moron River, and the locus of the final closure of the Palaeo-Asian Ocean, hosting the youngest major age population of ca. 269 Ma in the collision zone. However, the course of the suture zone further east of the study area beyond the Songliao block [5] remains open to question.

A statistical excursion utilising the mathematical tools of information theory [6] demonstrated that these can be readily adopted in the geochronological data set of this thesis. Its results provide a solid quantitative foundation to justify the very complex and dynamic geochronological systems in the study region, e.g. the existence of multiple types of arc basins (e.g. back-arc, fore-arc and trench basins) with variable access to their respective sedimentary provenances. In addition, statistical similarity and heterogeneity measures were generally able to confirm the location of the Solonker Suture Zone, and characterise the tectonic units involved in this study.

These observations combined with existing studies, enabled an updated tectonic reconstruction of the Palaeozoic evolution of the Palaeo-Asian Ocean and assembly of east Asia in the eastern section of the Central Asian Orogenic Belt. In the Late Ordovician to Devonian, subduction took place beneath a matured southern Mongolian island arc to the north (Uliastai arc) and the North China Craton to the south. In the Carboniferous the Hegenshan back-arc basin opened between the Northern Accretionary Orogen and the then consolidated Mongolian Arcs. From the Early to Middle Permian the Hegenshan back-arc basin closed by northward dipping subduction beneath the Mongolian Arcs, initiating the formation of the supra-subduction zone Hegenshan ophiolite. Meanwhile, continued subduction along both sides of the ocean further narrowed the Palaeo-Asian Ocean. In the Late Permian the Hegenshan Ophiolite was obducted during the closure of the Hegenshan back-arc basin. By the end of the Early Triassic the Palaeo-Asian Ocean closed after the collision between the opposing accretionary wedges of the Northern and Southern Accretionary Orogens, leading to the formation of the cryptic Solonker Suture Zone. Production of

A-type collisional plutons was promoted by the detachment of the oceanic from continental crust, subsequent to such type of bipolar subduction geometry.

This proposed tectonic scenario may be analogue to the modern-day east-west contraction of the Pacific at early stages, including Japan-type back-arc basin opening, whereas in later stages it shares more resemblance with the present tectonic situation in Southeast Asia. Thus, a better understanding of present-day accretionary collision zones may be the key in understanding past ones.

References

1. Xiao W, Windley BF, Hao J, Zhai M (2003) Accretion leading to collision and the Permian Solonker suture, Inner Mongolia, China: termination of the Central Asian Orogenic Belt. Tectonics 22(6)
2. Jian P, Liu D, Kröner A, Windley BF, Shi Y, Zhang W, Zhang F, Miao L, Zhang L, Tomurhuu D (2010) Evolution of a Permian intraoceanic arc-trench system in the Solonker suture zone, Central Asian Orogenic Belt China and Mongolia. Lithos 118(1–2):169–190
3. Jian P, Liu D, Kröner A, Windley BF, Shi Y, Zhang F, Shi G, Miao L, Zhang W, Zhang Q, Zhang L, Ren J (2008) Time scale of an early to mid-Paleozoic orogenic cycle of the long-lived Central Asian Orogenic Belt, Inner Mongolia of China: implications for continental growth. Lithos 101(3–4):233–259
4. Zhang S, Gao R, Li H, Hou H, Wu H, Li Q, Yang K, Li C, Li W, Zhang J, Yang T, Keller G, Liu M (2014a) Crustal structures revealed from a deep seismic reflection profile across the Solonker suture zone of the Central Asian Orogenic Belt, northern China: An integrated interpretation. Tectonophysics 612–613:26–39
5. Zhou J-B, Wilde SA, Zhang X-Z, Liu F-L, Liu J-H (2012) Detrital zircons from phanerozoic rocks of the Songliao block, NE China: evidence and tectonic implications. J Asian Earth Sci 47:21–34
6. Shannon CE, Weaver W (1971) The mathematical theory of communication. University of Illinois Press, Illinois

Appendix A
RatSuite Data Reduction

The Matlab© Mathworks software package "RatSuite" had been specifically designed for data reduction of in-situ Hf and U–Pb isotopic analyses of detrital zircons using (MC-)LA-ICPMS data output. The original purpose of its development was of solely educational nature: understanding in detail how raw Hf and U–Pb isotopic data were transformed into meaningful isotopic ratios and ages. The Matlab code environment operates across operating systems (e.g. Mac, PC, Linux), which gives it a major advantage over other commonly available data reduction codes, such as ICPMSDataCal [1, 2] and GLITTER (e.g. [3]). Although Iolite [4] operates similarly across operating systems, it offers only temporarily free trial usage, after which it needs to be commercially purchased. RatSuite may serve as a full-scale equivalent to alternative isotope data reduction softwares in future versions. Since it does not form an essential part of this dissertation, only a very brief introduction will be presented here. Upon request the author can provide copies of the Matlab code and more specific details on its operation and mathematical solutions to ratio and age calculation, including their respective uncertainties. RatSuite currently operates only within the Matlab code environment, and thus requires an installed version of Matlab (preferably version 7 and above). It comprises the graphical user interfaces IsoRat, AgeRat and HafRat (Figs. A.2, A.3, A.4). RatSuite does not intend to serve as an alternative for, or even replace, well established and highly sophisticated age calculation routines such as those implemented into ISOPLOT [5]. It is currently solely designed for basic age and uncertainty calculations required for detrital zircon U–Pb analyses.

Figure A.1 illustrates the general work flow when reducing Hf and U–Pb isotope data in RatSuite. RatSuite currently accommodates raw ICPMS data from laboratories in Xi'an Northwest University China and The University of Hong Kong (for detailed laboratory descriptions see Sects. 3.2 and 3.3). Data reduction involves two steps: (a) Raw data are introduced into IsoRat, which extracts isotopic ratios including

P. R. Eizenhöfer, *Subduction and Closure of the Palaeo-Asian Ocean along the Solonker Suture Zone: Constraints from an Integrated Sedimentary Provenance Analysis*, Springer Theses, https://doi.org/10.1007/978-981-32-9200-0

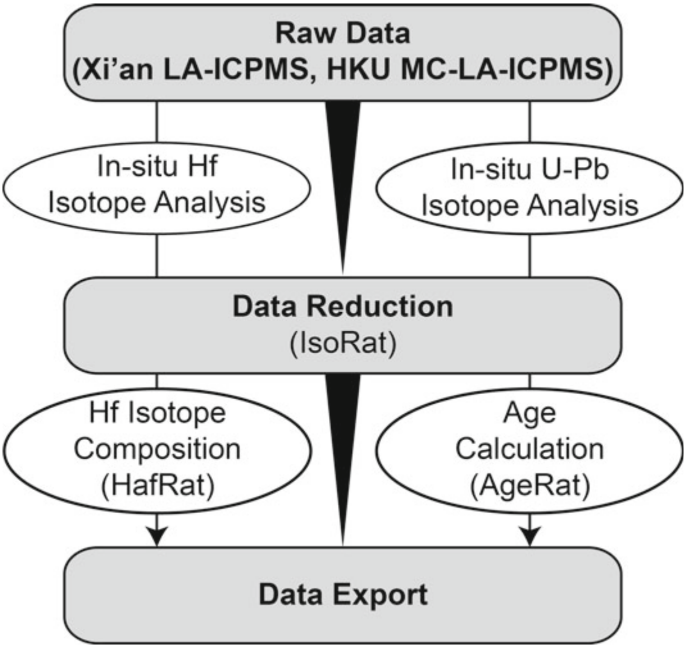

Fig. A.1 Work flow for in-situ Hf and U–Pb data reduction using RatSuite

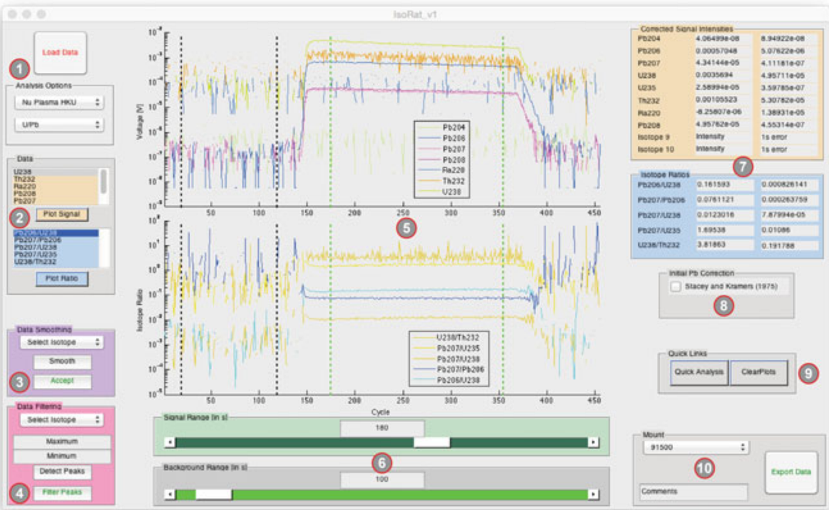

Fig. A.2 IsoRat graphical user-interface: **1** data import; **2** available isotopes and ratios for plotting; **3** data smoothing; **4** peak detection and filtering; **5** plots for measured isotope intensities and ratios; **6** signal and background selection; **7** reduced isotope intensities and values; **8** Optional common Pb correction according to [6]; **9** quick tabs; **10** sample description and data export

Fig. A.3 AgeRat graphical user-interface: **1** data import and export; **2** isotope ratios and calculated ages; **3** concordia plot and histogram of calculated ages and corrected ratios; **4** record of applied standard calibration factors per single grain analysis; **5** plotting options; **6** age calculations with optional selection of concordance range and bin width

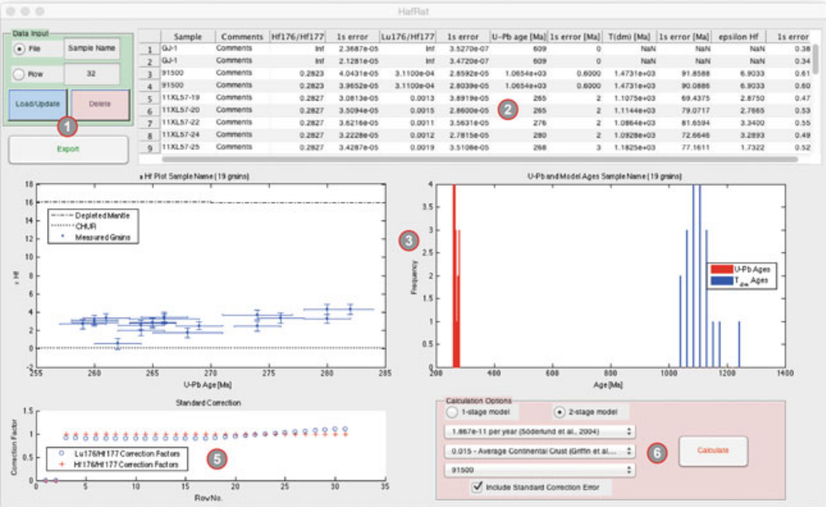

Fig. A.4 HafRat graphical user-interface. **1** Data import and export; **2** isotope ratios and calculated CHUR deviations; **3** ϵHf(t) versus age plot, and formation and model age histogram; **4** record of applied standard calibration factors per single grain analysis; **2** model age and ϵHf(t) calculations uncertainties. This step is followed by (b) zircon standard correction in HafRat for Hf isotope data or AgeRat for U–Pb isotope data, which also performs age calculation. Ultimately, the reduced data are exported (Figs. A.2, A.3, A.4).

References

1. Liu Y, Gao S, Hu Z, Gao C, Zong K, Wang D (2009) Continental and oceanic crust recycling inducedmelt-peridotite interactions in the Trans-North China Orogen: U–Pb dating, Hf isotopes and trace elements in zircons from Mantle Xenoliths. J Petrol 51(1–2):537–571
2. Liu Y, Hu Z, Zong K, Gao C, Gao S, Xu J, Chen H (2010) Reappraisement and refinement of zircon U–Pb isotope and trace element analyses by LA-ICP-MS. Chin Sci Bull 55(15):1535–1546
3. Knudsen T-L, Griffin W, Hartz E, Andresen A, Jackson S (2001) In-situ hafniumand lead isotope analyses of detrital zircons from the Devonian sedimentary basin of NE Greenland: a record of repeated crustal reworking. Contrib Miner Petrol 141(1):83–94
4. Paton C, Hellstrom J, Paul B, Woodhead J, Hergt J (2011) Iolite: freeware for the visualisation and processing of mass spectrometric data. J Anal At Spectrom 26:2508–2518
5. Ludwig K (2008) Manual for isoplot 3.7. Berkeley Geochronology Center, Berkeley
6. Stacey J, Kramers J (1975) Approximation of terrestrial lead isotope evolution by a two-stage model. Earth Planet Sci Lett 26(2):207–221

Appendix B
Zircon U–Pb Data

The data tables on the following pages comprise the results of all single zircon grain U–Pb analyses after data reduction. All analyses were performed during the four-year Ph.D. study period at The University of Hong Kong in laboratories at the Chinese Academy of Sciences in Guiyang, Northwest University Xi'an and The University of Hong Kong. Uncertainties are given at a 1σ level. Table columns correspond to laser-ablation spots, U/Th ratios, $^{206}Pb^{*}/^{207}Pb^{*}$ ratios and their uncertainties, $^{206}Pb^{*}/^{238}U$ ratios and their uncertainties, $^{206}Pb^{*}/^{207}Pb^{*}$-age in Ma and their uncertainties, $^{238}U/^{206}Pb$ age in Ma and their uncertainties, and concordance values. For detailed methodological procedures please refer to Sect. 3.2 of this dissertation (Table B.1).

P. R. Eizenhöfer, *Subduction and Closure of the Palaeo-Asian Ocean along the Solonker Suture Zone: Constraints from an Integrated Sedimentary Provenance Analysis*, Springer Theses, https://doi.org/10.1007/978-981-32-9200-0

Table B.1 Zircon U–Pb data

Sample	U/Th	$^{206}Pb^*/^{207}Pb^*$	$^{206}Pb^*/^{238}U$	$^{207}Pb^*/^{235}U$	$^{206}Pb^*/^{207}Pb^* - Age$ [Ma]	$^{238}U/^{206}Pb - Age$ [Ma]	Concordance [%]
11XL13-01	0.99	0.0577 ± 0.0015	0.0620 ± 0.0007	0.4917 ± 0.0132	520 ± 57	388 ± 4	95
11XL13-02	2.18	0.0546 ± 0.0011	0.0718 ± 0.0005	0.5419 ± 0.0101	394 ± 44	447 ± 3	98
11XL13-03	1.15	0.0523 ± 0.0010	0.0473 ± 0.0004	0.3423 ± 0.0063	298 ± 44	298 ± 2	99
11XL13-04	1.76	0.0548 ± 0.0015	0.0436 ± 0.0004	0.3289 ± 0.0088	406 ± 61	275 ± 2	95
11XL13-05	0.84	0.1645 ± 0.0017	0.4521 ± 0.0026	10.3251 ± 0.1109	2502 ± 18	2404 ± 12	97
11XL13-06	1.59	0.0508 ± 0.0009	0.0429 ± 0.0003	0.3014 ± 0.0053	232 ± 41	271 ± 2	98
11XL13-07	1.35	0.0521 ± 0.0009	0.0413 ± 0.0003	0.2976 ± 0.0051	300 ± 39	261 ± 2	98
11XL13-08	1.08	0.1122 ± 0.0014	0.3314 ± 0.0021	5.1584 ± 0.0649	1836 ± 22	1845 ± 10	99
11XL13-09	1.47	0.1172 ± 0.0020	0.3393 ± 0.0029	5.4844 ± 0.0903	1914 ± 30	1883 ± 14	99
11XL13-10	2.37	0.0573 ± 0.0012	0.0706 ± 0.0005	0.5577 ± 0.0110	502 ± 44	440 ± 3	97
11XL13-11	0.87	0.0573 ± 0.0022	0.0508 ± 0.0006	0.3925 ± 0.0141	502 ± 85	319 ± 4	94
11XL13-12	0.79	0.1693 ± 0.0022	0.4729 ± 0.0035	11.0635 ± 0.1478	2551 ± 22	2496 ± 15	98
11XL13-13	1.62	0.1683 ± 0.0019	0.4764 ± 0.0032	11.1111 ± 0.1256	2543 ± 20	2511 ± 14	99
11XL13-14	1.93	0.0583 ± 0.0024	0.0626 ± 0.0009	0.4800 ± 0.0175	539 ± 89	392 ± 6	98
11XL13-15	2.57	0.0544 ± 0.0013	0.0593 ± 0.0004	0.4437 ± 0.0101	387 ± 49	372 ± 3	99
11XL13-16	1.27	0.0535 ± 0.0012	0.0461 ± 0.0004	0.3397 ± 0.0075	350 ± 50	290 ± 2	97
11XL13-17	0.90	0.1677 ± 0.0018	0.4952 ± 0.0028	11.5178 ± 0.1263	2534 ± 18	2593 ± 12	98
11XL13-18	1.80	0.1650 ± 0.0019	0.4780 ± 0.0031	10.9360 ± 0.1331	2509 ± 19	2518 ± 14	99
11XL13-19	1.63	0.1126 ± 0.0016	0.3208 ± 0.0023	5.0043 ± 0.0727	1843 ± 25	1794 ± 11	98
11XL13-20	1.52	0.1706 ± 0.0021	0.4845 ± 0.0030	11.4615 ± 0.1413	2565 ± 20	2547 ± 13	99
11XL13-21	3.09	0.0548 ± 0.0014	0.0690 ± 0.0008	0.5177 ± 0.0130	467 ± 56	430 ± 5	98
11XL13-22	1.46	0.1647 ± 0.0017	0.4917 ± 0.0029	11.2410 ± 0.1229	2506 ± 18	2578 ± 13	98
11XL13-23	1.71	0.1127 ± 0.0015	0.3357 ± 0.0023	5.2328 ± 0.0676	1843 ± 23	1866 ± 11	99

(continued)

Table B.1 (continued)

Sample	U/Th	$^{206}Pb^*/^{207}Pb^*$	$^{206}Pb^*/^{238}U$	$^{207}Pb^*/^{235}U$	$^{206}Pb^*/^{207}Pb^* - Age$ [Ma]	$^{238}U/^{206}Pb - Age$ [Ma]	Concordance [%]
11XL13-24	1.46	0.1084 ± 0.0016	0.3235 ± 0.0024	4.8529 ± 0.0696	1773 ± 26	1807 ± 12	99
11XL13-25	1.22	0.0555 ± 0.0014	0.0770 ± 0.0007	0.5889 ± 0.0139	432 ± 56	478 ± 4	98
11XL13-26	1.91	0.0550 ± 0.0011	0.0733 ± 0.0006	0.5567 ± 0.0110	413 ± 44	456 ± 4	98
11XL13-27	2.83	0.0533 ± 0.0016	0.0542 ± 0.0006	0.3968 ± 0.0120	343 ± 69	340 ± 4	99
11XL13-28	1.27	0.1089 ± 0.0014	0.3135 ± 0.0022	4.7377 ± 0.0621	1781 ± 19	1758 ± 11	99
11XL13-29	0.85	0.1095 ± 0.0016	0.3325 ± 0.0027	5.0278 ± 0.0678	1792 ± 26	1851 ± 13	98
11XL13-30	0.75	0.1137 ± 0.0031	0.2963 ± 0.0044	4.6315 ± 0.1094	1861 ± 49	1673 ± 22	95
11XL13-31	1.93	0.1629 ± 0.0021	0.4702 ± 0.0034	10.6190 ± 0.1362	2487 ± 22	2484 ± 15	99
11XL13-32	1.68	0.0521 ± 0.0011	0.0731 ± 0.0006	0.5273 ± 0.0115	300 ± 50	455 ± 3	94
11XL13-33	1.91	0.0581 ± 0.0016	0.0681 ± 0.0007	0.5398 ± 0.0144	600 ± 61	425 ± 4	96
11XL13-34	1.44	0.0576 ± 0.0017	0.0661 ± 0.0007	0.5159 ± 0.0142	522 ± 67	413 ± 4	97
11XL13-35	0.91	0.0605 ± 0.0012	0.0706 ± 0.0005	0.5884 ± 0.0111	620 ± 44	440 ± 3	93
11XL13-36	1.68	0.0589 ± 0.0015	0.0701 ± 0.0006	0.5676 ± 0.0142	565 ± 57	437 ± 4	95
11XL13-37	1.12	0.0540 ± 0.0013	0.0647 ± 0.0006	0.4796 ± 0.0114	369 ± 56	404 ± 4	98
11XL13-38	1.38	0.0580 ± 0.0011	0.0712 ± 0.0005	0.5726 ± 0.0104	532 ± 36	443 ± 3	96
11XL13-39	1.56	0.1107 ± 0.0013	0.2931 ± 0.0017	4.5024 ± 0.0508	1810 ± 22	1657 ± 8	95
11XL13-40	3.53	0.1025 ± 0.0016	0.2354 ± 0.0016	3.3452 ± 0.0514	1672 ± 28	1363 ± 8	90
11XL13-41	1.57	0.1652 ± 0.0017	0.4145 ± 0.0026	9.5122 ± 0.1044	2510 ± 18	2235 ± 12	93
11XL13-42	2.51	0.1159 ± 0.0017	0.3261 ± 0.0025	5.2271 ± 0.0762	1894 ± 7	1819 ± 12	97
11XL13-43	7.65	0.1141 ± 0.0019	0.1586 ± 0.0014	2.5134 ± 0.0441	1865 ± 30	949 ± 8	70
11XL13-44	1.30	0.0602 ± 0.0015	0.0763 ± 0.0007	0.6320 ± 0.0156	609 ± 56	474 ± 4	95
11XL13-45	1.08	0.0567 ± 0.0013	0.0675 ± 0.0006	0.5271 ± 0.0117	480 ± 50	421 ± 4	97
11XL13-46	2.72	0.1177 ± 0.0014	0.3169 ± 0.0020	0.0014 ± 5.1860	1921 ± 20	1774 ± 10	95

(continued)

Table B.1 (continued)

Sample	U/Th	$^{206}Pb^*/^{207}Pb^*$	$^{206}Pb^*/^{238}U$	$^{207}Pb^*/^{235}U$	$^{206}Pb^*/^{207}Pb^* - Age$ [Ma]	$^{238}U/^{206}Pb - Age$ [Ma]	Concordance [%]
11XL13-47	2.10	0.0576 ± 0.0010	0.0755 ± 0.0005	0.0010 ± 0.6017	522 ± 37	469 ± 3	98
11XL13-48	2.32	0.1750 ± 0.0018	0.4900 ± 0.0034	0.0018 ± 11.9168	2606 ± 18	2571 ± 15	98
11XL13-49	2.94	0.0583 ± 0.0013	0.0753 ± 0.0007	0.0013 ± 0.6067	539 ± 44	468 ± 4	97
11XL13-50	1.66	0.0546 ± 0.0019	0.0657 ± 0.0008	0.0019 ± 0.4874	394 ± 75	410 ± 5	98
11XL13-51	2.76	0.0671 ± 0.0028	0.0714 ± 0.0012	0.0028 ± 0.6505	843 ± 86	444 ± 7	86
11XL13-52	1.58	0.0562 ± 0.0014	0.0692 ± 0.0007	0.0014 ± 0.5396	461 ± 56	432 ± 4	98
11XL13-53	1.48	0.1662 ± 0.0021	0.4817 ± 0.0039	0.0021 ± 11.1419	2520 ± 21	2535 ± 17	99
11XL13-54	3.20	0.1843 ± 0.0058	0.0468 ± 0.0010	0.0058 ± 1.1876	2692 ± 52	295 ± 6	8
11XL13-55	1.12	0.0604 ± 0.0011	0.0723 ± 0.0006	0.0011 ± 0.6050	617 ± 34	450 ± 4	93
11XL13-56	1.54	0.0525 ± 0.0015	0.0498 ± 0.0005	0.0015 ± 0.3588	309 ± 65	314 ± 3	99
11XL13-57	1.67	0.0529 ± 0.0012	0.0501 ± 0.0004	0.0012 ± 0.3662	324 ± 52	315 ± 3	99
11XL13-58	2.49	0.0845 ± 0.0011	0.2286 ± 0.0018	0.0011 ± 2.6884	1303 ± 24	1327 ± 10	99
11XL13-59	1.74	0.0558 ± 0.0011	0.0719 ± 0.0006	0.0011 ± 0.5571	456 ± 10	447 ± 4	99
11XL13-60	3.99	0.1605 ± 0.0017	0.4774 ± 0.0031	0.0017 ± 10.6952	2461 ± 18	2516 ± 13	99
11XL13-61	1.73	0.1649 ± 0.0020	0.4804 ± 0.0034	0.0020 ± 11.0501	2506 ± 19	2529 ± 15	99
11XL13-62	1.26	0.0537 ± 0.0012	0.0643 ± 0.0006	0.0012 ± 0.4768	361 ± 50	401 ± 3	98
11XL13-63	1.41	0.0553 ± 0.0015	0.0433 ± 0.0005	0.0015 ± 0.3290	433 ± 61	273 ± 3	94
11XL13-64	1.81	0.0643 ± 0.0012	0.0409 ± 0.0003	0.0012 ± 0.3665	750 ± 41	258 ± 2	79
11XL13-65	1.23	0.0528 ± 0.0013	0.0477 ± 0.0004	0.0013 ± 0.3498	317 ± 54	301 ± 3	98
11XL13-66	1.05	0.0688 ± 0.0020	0.0455 ± 0.0006	0.0020 ± 0.4267	894 ± 58	287 ± 4	77
11XL13-67	2.09	0.1836 ± 0.0021	0.4523 ± 0.0038	0.0021 ± 11.5597	2687 ± 14	2406 ± 17	93
11XL13-68	3.66	0.1590 ± 0.0016	0.4582 ± 0.0032	0.0016 ± 10.1680	2456 ± 18	2432 ± 14	99
11XL13-69	2.29	0.1640 ± 0.0018	0.4610 ± 0.0033	0.0018 ± 10.5474	2498 ± 19	2444 ± 14	98

(continued)

Table B.1 (continued)

Sample	U/Th	$^{206}Pb^{*}/^{207}Pb^{*}$	$^{206}Pb^{*}/^{238}U$	$^{207}Pb^{*}/^{235}U$	$^{206}Pb^{*}/^{207}Pb^{*} - Age$ [Ma]	$^{238}U/^{206}Pb - Age$ [Ma]	Concordance [%]
11XL13-70	1.96	0.1622 ± 0.0020	0.4596 ± 0.0035	0.0020 ± 10.3960	2479 ± 21	2438 ± 16	98
11XL13-71	2.23	0.1120 ± 0.0015	0.3460 ± 0.0031	0.0015 ± 5.3995	1832 ± 24	1916 ± 15	98
11XL13-72	1.95	0.1153 ± 0.0016	0.3287 ± 0.0026	0.0016 ± 5.2793	1884 ± 24	1832 ± 13	98
11XL13-73	0.92	0.1648 ± 0.0024	0.4720 ± 0.0040	0.0024 ± 10.8383	2506 ± 24	2492 ± 18	99
11XL13-74	1.60	0.1626 ± 0.0021	0.4655 ± 0.0036	0.0021 ± 10.5437	2483 ± 22	2464 ± 16	99
11XL13-75	1.77	0.1600 ± 0.0022	0.4513 ± 0.0039	0.0022 ± 10.0173	2457 ± 24	2401 ± 17	98
11XL13-76	1.51	0.0604 ± 0.0013	0.0721 ± 0.0005	0.0013 ± 0.6075	620 ± 46	449 ± 3	92
11XL13-77	1.98	0.0548 ± 0.0011	0.0757 ± 0.0007	0.0011 ± 0.5727	467 ± 44	471 ± 4	97
11XL13-78	3.35	0.1135 ± 0.0013	0.3224 ± 0.0030	0.0013 ± 5.0813	1857 ± 21	1802 ± 15	98
11XL13-79	0.82	0.0597 ± 0.0012	0.0541 ± 0.0005	0.0012 ± 0.4491	594 ± 43	340 ± 3	89
11XL13-80	6.79	0.1168 ± 0.0015	0.2455 ± 0.0018	0.0015 ± 3.9860	1907 ± 24	1415 ± 9	85
11XL13-81	1.39	0.0536 ± 0.0010	0.0462 ± 0.0004	0.0010 ± 0.3431	367 ± 38	291 ± 2	97
11XL13-82	0.67	0.0565 ± 0.0014	0.0426 ± 0.0004	0.0014 ± 0.3339	472 ± 52	269 ± 2	91
11XL13-83	1.57	0.1628 ± 0.0020	0.4526 ± 0.0028	0.0020 ± 10.2412	2485 ± 21	2407 ± 12	97
11XL13-84	11.84	0.1483 ± 0.0017	0.3796 ± 0.0021	0.0017 ± 7.8308	2326 ± 20	2074 ± 10	93
11XL13-85	1.77	0.0606 ± 0.0016	0.0662 ± 0.0007	0.0016 ± 0.5504	633 ± 58	413 ± 4	92
11XL13-86	1.10	0.1074 ± 0.0061	0.0433 ± 0.0011	0.0061 ± 0.5619	1755 ± 105	273 ± 7	50
11XL13-87	1.00	0.0577 ± 0.0014	0.0759 ± 0.0008	0.0014 ± 0.6017	517 ± 54	472 ± 5	98
11XL13-88	3.96	0.0579 ± 0.0011	0.0697 ± 0.0005	0.0011 ± 0.5577	528 ± 41	434 ± 3	96
11XL13-89	2.24	0.1653 ± 0.0021	0.4476 ± 0.0056	0.0021 ± 10.2953	2511 ± 16	2385 ± 25	96
11XL13-90	1.34	0.0555 ± 0.0010	0.0626 ± 0.0005	0.0010 ± 0.4815	432 ± 42	392 ± 3	98
11XL23-01	1.82	0.1746 ± 0.0025	0.5078 ± 0.0035	12.3435 ± 0.1729	2603 ± 23	2647 ± 15	99
11XL23-02	3.12	0.1642 ± 0.0020	0.4528 ± 0.0025	10.3513 ± 0.1256	2499 ± 20	2408 ± 11	97

(continued)

Table B.1 (continued)

Sample	U/Th	$^{206}Pb^*/^{207}Pb^*$	$^{206}Pb^*/^{238}U$	$^{207}Pb^*/^{235}U$	$^{206}Pb^*/^{207}Pb^* - Age$ [Ma]	$^{238}U/^{206}Pb - Age$ [Ma]	Concordance [%]
11XL23-03	1.27	0.0607 ± 0.0016	0.0736 ± 0.0006	0.6105 ± 0.0148	628 ± 57	458 ± 4	94
11XL23-04	1.57	0.0588 ± 0.0021	0.0468 ± 0.0005	0.3779 ± 0.0128	561 ± 76	295 ± 3	90
11XL23-05	2.76	0.0634 ± 0.0013	0.0641 ± 0.0004	0.5651 ± 0.0122	720 ± 44	401 ± 3	87
11XL23-06	1.74	0.0522 ± 0.0016	0.0448 ± 0.0005	0.3199 ± 0.0095	295 ± 66	282 ± 3	99
11XL23-07	2.95	0.0565 ± 0.0016	0.0709 ± 0.0008	0.5490 ± 0.0157	478 ± 97	442 ± 5	99
11XL23-08	1.10	0.0573 ± 0.0014	0.0427 ± 0.0004	0.3393 ± 0.0085	502 ± 58	270 ± 2	90
11XL23-09	1.30	0.0516 ± 0.0018	0.0402 ± 0.0005	0.2852 ± 0.0094	333 ± 78	254 ± 3	99
11XL23-10	1.45	0.1341 ± 0.0159	0.0437 ± 0.0006	0.8443 ± 0.0985	2154 ± 207	276 ± 4	23
11XL23-11	1.72	0.1093 ± 0.0012	0.3018 ± 0.0021	4.5779 ± 0.0532	1789 ± 20	1700 ± 11	97
11XL23-12	1.96	0.0570 ± 0.0010	0.0809 ± 0.0006	0.6383 ± 0.0111	500 ± 37	501 ± 3	99
11XL23-13	2.64	0.0534 ± 0.0012	0.0405 ± 0.0003	0.2972 ± 0.0066	346 ± 49	256 ± 2	96
11XL23-14	2.49	0.0564 ± 0.0008	0.0805 ± 0.0006	0.6306 ± 0.0097	478 ± 33	499 ± 3	99
11XL23-15	0.93	0.0514 ± 0.0009	0.0421 ± 0.0003	0.2988 ± 0.0052	261 ± 41	266 ± 2	99
11XL23-16	1.40	0.1144 ± 0.0020	0.0448 ± 0.0003	0.7097 ± 0.0123	1870 ± 31	283 ± 2	36
11XL23-17	1.34	0.0539 ± 0.0008	0.0425 ± 0.0003	0.3175 ± 0.0049	365 ± 33	268 ± 2	95
11XL23-18	1.82	0.0515 ± 0.0012	0.0409 ± 0.0003	0.2914 ± 0.0065	265 ± 52	259 ± 2	99
11XL23-19	2.93	0.0527 ± 0.0010	0.0424 ± 0.0003	0.3097 ± 0.0056	322 ± 47	268 ± 2	97
11XL23-20	0.97	0.0539 ± 0.0012	0.0633 ± 0.0005	0.4721 ± 0.0100	369 ± 50	396 ± 3	99
11XL23-21	2.02	0.0570 ± 0.0017	0.0675 ± 0.0006	0.5262 ± 0.0148	500 ± 67	421 ± 4	98
11XL23-22	2.06	0.1788 ± 0.0018	0.5020 ± 0.0025	12.4747 ± 0.1229	2643 ± 17	2622 ± 11	99
11XL23-23	1.67	0.0583 ± 0.0012	0.0767 ± 0.0006	0.6156 ± 0.0123	539 ± 44	477 ± 4	97
11XL23-24	1.34	0.0528 ± 0.0011	0.0421 ± 0.0003	0.3055 ± 0.0058	320 ± 46	266 ± 2	98
11XL23-25	2.32	0.0507 ± 0.0013	0.0420 ± 0.0003	0.2938 ± 0.0071	228 ± 57	265 ± 2	98

(continued)

Table B.1 (continued)

Sample	U/Th	$^{206}Pb^*/^{207}Pb^*$	$^{206}Pb^*/^{238}U$	$^{207}Pb^*/^{235}U$	$^{206}Pb^*/^{207}Pb^* - Age$ [Ma]	$^{238}U/^{206}Pb - Age$ [Ma]	Concordance [%]
11XL23-26	1.73	0.0512 ± 0.0013	0.0430 ± 0.0004	0.3033 ± 0.0077	250 ± 59	271 ± 2	99
11XL23-27	0.81	0.0569 ± 0.0019	0.0456 ± 0.0005	0.3561 ± 0.0117	487 ± 76	287 ± 3	92
11XL23-28	1.63	0.0576 ± 0.0010	0.0782 ± 0.0005	0.6245 ± 0.0102	522 ± 35	485 ± 3	98
11XL23-29	0.04	0.1064 ± 0.0023	0.2324 ± 0.0029	3.4318 ± 0.0830	1739 ± 45	1347 ± 15	88
11XL23-30	2.72	0.0541 ± 0.0012	0.0422 ± 0.0003	0.3142 ± 0.0067	372 ± 48	266 ± 2	95
11XL23-31	1.35	0.0648 ± 0.0015	0.0685 ± 0.0006	0.6115 ± 0.0138	769 ± 48	427 ± 3	87
11XL23-32	1.51	0.0585 ± 0.0015	0.0709 ± 0.0007	0.5685 ± 0.0143	550 ± 56	441 ± 4	96
11XL23-33	1.37	0.0537 ± 0.0017	0.0471 ± 0.0005	0.3444 ± 0.0108	367 ± 72	297 ± 3	98
11XL23-34	1.83	0.0572 ± 0.0010	0.0668 ± 0.0005	0.5291 ± 0.0092	498 ± 41	417 ± 3	96
11XL23-35	1.58	0.0565 ± 0.0019	0.0415 ± 0.0004	0.3248 ± 0.0112	472 ± 74	262 ± 3	91
11XL23-36	1.54	0.0544 ± 0.0016	0.0397 ± 0.0005	0.2959 ± 0.0084	391 ± 67	251 ± 3	95
11XL23-37	1.70	0.1739 ± 0.0023	0.4262 ± 0.0029	10.2985 ± 0.1349	2596 ± 22	2289 ± 13	92
11XL23-38	1.55	0.1848 ± 0.0023	0.5074 ± 0.0035	13.0178 ± 0.1609	2698 ± 20	2646 ± 15	98
11XL23-39	1.16	0.0526 ± 0.0013	0.0439 ± 0.0004	0.3188 ± 0.0074	322 ± 54	277 ± 2	98
11XL23-40	1.13	0.0642 ± 0.0018	0.0422 ± 0.0004	0.3755 ± 0.0104	748 ± 53	267 ± 3	80
11XL23-41	1.55	0.0575 ± 0.0011	0.0756 ± 0.0006	0.6019 ± 0.0113	509 ± 38	470 ± 3	98
11XL23-42	1.92	0.1769 ± 0.0031	0.0685 ± 0.0006	1.6773 ± 0.0278	2624 ± 29	427 ± 4	19
11XL23-43	1.41	0.0514 ± 0.0013	0.0461 ± 0.0005	0.3263 ± 0.0081	261 ± 55	291 ± 3	98
11XL23-44	1.12	0.0630 ± 0.0014	0.0709 ± 0.0007	0.6170 ± 0.0131	709 ± 46	442 ± 4	90
11XL23-45	1.81	0.0579 ± 0.0011	0.0687 ± 0.0005	0.5539 ± 0.0101	524 ± 41	429 ± 3	95
11XL23-46	1.77	0.0774 ± 0.0016	0.0750 ± 0.0007	0.8047 ± 0.0159	1131 ± 36	466 ± 4	74
11XL23-47	1.23	0.0731 ± 0.0022	0.0604 ± 0.0008	0.6089 ± 0.0179	1017 ± 61	378 ± 5	75
11XL23-48	1.54	0.0537 ± 0.0010	0.0437 ± 0.0003	0.3266 ± 0.0063	367 ± 38	275 ± 2	95

(continued)

Table B.1 (continued)

Sample	U/Th	$^{206}Pb^*/^{207}Pb^*$	$^{206}Pb^*/^{238}U$	$^{207}Pb^*/^{235}U$	$^{206}Pb^*/^{207}Pb^* - Age$ [Ma]	$^{238}U/^{206}Pb - Age$ [Ma]	Concordance [%]
11XL23-49	1.82	0.0510 ± 0.0009	0.0434 ± 0.0003	0.3074 ± 0.0054	239 ± 41	274 ± 2	99
11XL23-50	1.25	0.0527 ± 0.0012	0.0475 ± 0.0005	0.3466 ± 0.0079	322 ± 52	299 ± 3	99
11XL23-51	1.70	0.0694 ± 0.0021	0.0671 ± 0.0007	0.6452 ± 0.0194	922 ± 58	419 ± 4	81
11XL23-52	1.17	0.0522 ± 0.0012	0.0426 ± 0.0003	0.3074 ± 0.0065	295 ± 52	269 ± 2	98
11XL23-53	2.19	0.1141 ± 0.0033	0.0719 ± 0.0009	1.1162 ± 0.0308	1866 ± 52	448 ± 6	48
11XL23-54	1.05	0.0561 ± 0.0013	0.0796 ± 0.0007	0.6188 ± 0.0144	454 ± 19	494 ± 4	99
11XL23-55	1.46	0.0527 ± 0.0016	0.0389 ± 0.0004	0.2819 ± 0.0080	322 ± 73	246 ± 3	97
11XL23-56	2.35	0.1720 ± 0.0022	0.5127 ± 0.0035	12.2948 ± 0.1573	2577 ± 16	2668 ± 15	98
11XL23-57	1.76	0.0602 ± 0.0017	0.0738 ± 0.0008	0.6089 ± 0.0167	609 ± 94	459 ± 5	94
11XL23-58	14.84	0.1642 ± 0.0018	0.4329 ± 0.0023	9.8933 ± 0.1094	2499 ± 19	2319 ± 10	95
11XL23-59	2.42	0.0847 ± 0.0020	0.0505 ± 0.0004	0.5992 ± 0.0157	1309 ± 47	317 ± 2	59
11XL23-60	1.22	0.0531 ± 0.0019	0.0395 ± 0.0005	0.2891 ± 0.0105	345 ± 81	250 ± 3	96
11XL23-61	1.44	0.1613 ± 0.0021	0.4635 ± 0.0031	10.3831 ± 0.1385	2469 ± 22	2455 ± 14	99
11XL23-62	1.84	0.0546 ± 0.0011	0.0443 ± 0.0003	0.3330 ± 0.0068	394 ± 44	279 ± 2	95
11XL23-63	1.67	0.0535 ± 0.0010	0.0413 ± 0.0003	0.3060 ± 0.0061	350 ± 44	261 ± 2	96
11XL23-64	2.15	0.0516 ± 0.0011	0.0442 ± 0.0003	0.3137 ± 0.0066	333 ± 48	279 ± 2	99
11XL23-65	1.12	0.0523 ± 0.0013	0.0426 ± 0.0004	0.3065 ± 0.0074	302 ± 49	269 ± 2	98
11XL23-66	1.88	0.1815 ± 0.0023	0.5140 ± 0.0035	12.9329 ± 0.1746	2733 ± 21	2674 ± 15	99
11XL23-67	2.13	0.0563 ± 0.0013	0.0721 ± 0.0006	0.5580 ± 0.0123	465 ± 53	449 ± 3	99
11XL23-68	1.31	0.0515 ± 0.0010	0.0416 ± 0.0003	0.2956 ± 0.0057	261 ± 46	263 ± 2	99
11XL23-69	1.48	0.0535 ± 0.0019	0.0466 ± 0.0006	0.3361 ± 0.0104	350 ± 50	294 ± 4	99
11XL23-70	1.82	0.0892 ± 0.0022	0.0412 ± 0.0003	0.5034 ± 0.0117	1409 ± 47	260 ± 2	54
11XL23-71	2.81	0.0557 ± 0.0012	0.0711 ± 0.0006	0.5455 ± 0.0113	439 ± 48	443 ± 4	99

(continued)

Table B.1 (continued)

Sample	U/Th	$^{206}Pb^*/^{207}Pb^*$	$^{206}Pb^*/^{238}U$	$^{207}Pb^*/^{235}U$	$^{206}Pb^*/^{207}Pb^* - Age$ [Ma]	$^{238}U/^{206}Pb - Age$ [Ma]	Concordance [%]
11XL23-72	2.27	0.0474 ± 0.0018	0.0394 ± 0.0005	0.2578 ± 0.0099	78 ± 89	249 ± 3	93
11XL23-73	1.71	0.0513 ± 0.0012	0.0426 ± 0.0004	0.3032 ± 0.0072	257 ± 47	269 ± 3	99
11XL23-74	1.75	0.1357 ± 0.0024	0.0796 ± 0.0006	1.5022 ± 0.0277	2174 ± 31	494 ± 4	38
11XL23-75	1.48	0.0556 ± 0.0010	0.0604 ± 0.0004	0.4654 ± 0.0086	435 ± 41	378 ± 3	97
11XL23-76	1.52	0.0516 ± 0.0012	0.0462 ± 0.0004	0.3289 ± 0.0077	333 ± 56	291 ± 2	99
11XL23-77	2.05	0.1657 ± 0.0018	0.4881 ± 0.0042	11.2200 ± 0.1294	2517 ± 17	2562 ± 18	99
11XL23-78	1.15	0.0595 ± 0.0014	0.0499 ± 0.0005	0.4108 ± 0.0093	587 ± 18	314 ± 3	89
11XL23-79	1.71	0.0768 ± 0.0037	0.0399 ± 0.0007	0.4192 ± 0.0217	1117 ± 96	252 ± 4	65
11XL23-80	1.18	0.0553 ± 0.0011	0.0426 ± 0.0004	0.3255 ± 0.0063	433 ± 44	269 ± 2	93
11XL23-81	1.51	0.0586 ± 0.0010	0.0817 ± 0.0007	0.6662 ± 0.0109	554 ± 37	506 ± 4	97
11XL23-82	0.36	0.1587 ± 0.0047	0.4417 ± 0.0139	9.6381 ± 0.3056	2442 ± 50	2358 ± 62	98
11XL23-83	1.49	0.1747 ± 0.0022	0.4764 ± 0.0034	11.5930 ± 0.1418	2603 ± 21	2512 ± 15	97
11XL23-84	3.04	0.1149 ± 0.0014	0.3077 ± 0.0021	4.9288 ± 0.0587	1877 ± 21	1729 ± 10	95
11XL23-85	1.66	0.0578 ± 0.0011	0.0806 ± 0.0007	0.6445 ± 0.0114	524 ± 40	499 ± 4	98
11XL23-86	1.15	0.1724 ± 0.0020	0.5086 ± 0.0036	12.2234 ± 0.1414	2583 ± 25	2650 ± 15	98
11XL23-87	1.57	0.0587 ± 0.0021	0.0416 ± 0.0005	0.3327 ± 0.0123	554 ± 80	263 ± 3	89
11XL23-88	1.51	0.1726 ± 0.0023	0.4992 ± 0.0038	12.0033 ± 0.1562	2583 ± 22	2610 ± 16	99
11XL23-89	1.56	0.0549 ± 0.0010	0.0663 ± 0.0005	0.5058 ± 0.0092	409 ± 43	414 ± 3	99
11XL23-90	2.07	0.0536 ± 0.0014	0.0419 ± 0.0004	0.3101 ± 0.0077	354 ± 57	265 ± 2	96
11XL25-01	2.45	0.0683 ± 0.0013	0.0698 ± 0.0005	0.6638 ± 0.0126	876 ± 38	435 ± 3	82
11XL25-02	1.26	0.0675 ± 0.0011	0.0637 ± 0.0005	0.5961 ± 0.0098	854 ± 35	398 ± 3	82
11XL25-03	1.70	0.0536 ± 0.0011	0.0707 ± 0.0005	0.5229 ± 0.0107	354 ± 81	440 ± 3	97
11XL25-04	1.54	0.0538 ± 0.0013	0.0444 ± 0.0004	0.3290 ± 0.0082	361 ± 56	280 ± 2	97

(continued)

Table B.1 (continued)

Sample	U/Th	$^{206}Pb^*/^{207}Pb^*$	$^{206}Pb^*/^{238}U$	$^{207}Pb^*/^{235}U$	$^{206}Pb^*/^{207}Pb^* - Age$ [Ma]	$^{238}U/^{206}Pb - Age$ [Ma]	Concordance [%]
11XL25-05	1.10	0.0527 ± 0.0010	0.0539 ± 0.0004	0.3935 ± 0.0076	322 ± 17	339 ± 2	99
11XL25-06	1.14	0.0561 ± 0.0012	0.0694 ± 0.0005	0.5377 ± 0.0104	457 ± 44	433 ± 3	99
11XL25-07	1.75	0.1250 ± 0.0014	0.4126 ± 0.0023	7.1604 ± 0.0785	2029 ± 20	2227 ± 11	95
11XL25-08	1.67	0.0572 ± 0.0013	0.0685 ± 0.0005	0.5409 ± 0.0119	498 ± 45	427 ± 3	97
11XL25-09	2.90	0.0547 ± 0.0013	0.0698 ± 0.0006	0.5240 ± 0.0116	398 ± 54	435 ± 4	98
11XL25-10	1.11	0.1627 ± 0.0019	0.4835 ± 0.0033	10.9171 ± 0.1355	2484 ± 20	2542 ± 14	98
11XL25-11	1.42	0.1620 ± 0.0018	0.4820 ± 0.0030	10.8433 ± 0.1249	2477 ± 19	2536 ± 13	98
11XL25-12	30.62	0.0586 ± 0.0009	0.0671 ± 0.0004	0.5456 ± 0.0082	550 ± 33	419 ± 2	94
11XL25-13	2.17	0.1136 ± 0.0013	0.3466 ± 0.0020	5.4701 ± 0.0614	1858 ± 20	1918 ± 10	98
11XL25-14	8.15	0.1199 ± 0.0012	0.3730 ± 0.0026	6.2109 ± 0.0688	1955 ± 19	2044 ± 12	98
11XL25-15	1.22	0.1646 ± 0.0018	0.4741 ± 0.0028	10.8364 ± 0.1170	2503 ± 18	2501 ± 12	99
11XL25-16	1.74	0.0558 ± 0.0011	0.0764 ± 0.0006	0.5907 ± 0.0113	456 ± 10	475 ± 3	99
11XL25-17	4.23	0.1098 ± 0.0014	0.3628 ± 0.0021	5.5411 ± 0.0675	1796 ± 23	1996 ± 10	95
11XL25-18	2.06	0.0551 ± 0.0013	0.0722 ± 0.0006	0.5505 ± 0.0130	417 ± 58	449 ± 4	99
11XL25-19	1.58	0.0566 ± 0.0017	0.0694 ± 0.0007	0.5380 ± 0.0154	476 ± 65	432 ± 4	98
11XL25-20	0.56	0.1629 ± 0.0028	0.4909 ± 0.0048	11.0345 ± 0.1815	2486 ± 30	2575 ± 21	98
11XL25-21	0.51	0.1619 ± 0.0036	0.5198 ± 0.0067	11.5339 ± 0.2412	2476 ± 37	2698 ± 29	95
11XL25-22	2.48	0.1589 ± 0.0022	0.4786 ± 0.0035	10.5670 ± 0.1495	2444 ± 29	2521 ± 15	98
11XL25-23	1.37	0.0504 ± 0.0012	0.0454 ± 0.0004	0.3153 ± 0.0070	217 ± 86	286 ± 2	97
11XL25-24	2.14	0.0538 ± 0.0010	0.0689 ± 0.0005	0.5124 ± 0.0093	361 ± 73	429 ± 3	97
11XL25-25	1.05	0.1170 ± 0.0017	0.3769 ± 0.0031	6.1065 ± 0.0915	1910 ± 27	2062 ± 15	96
11XL25-26	1.36	0.1626 ± 0.0020	0.4977 ± 0.0035	11.2430 ± 0.1386	2483 ± 21	2604 ± 15	97
11XL25-27	1.05	0.0939 ± 0.0024	0.2791 ± 0.0034	3.6044 ± 0.0915	1506 ± 48	1587 ± 17	97

(continued)

Table B.1 (continued)

Sample	U/Th	$^{206}Pb^*/^{207}Pb^*$	$^{206}Pb^*/^{238}U$	$^{207}Pb^*/^{235}U$	$^{206}Pb^*/^{207}Pb^*-Age$ [Ma]	$^{238}U/^{206}Pb - Age$ [Ma]	Concordance [%]
11XL25-28	1.13	0.0532 ± 0.0016	0.0642 ± 0.0007	0.4682 ± 0.0140	339 ± 38	401 ± 4	97
11XL25-29	0.93	0.1584 ± 0.0019	0.4770 ± 0.0033	10.5093 ± 0.1303	2439 ± 19	2514 ± 14	98
11XL25-30	2.27	0.0553 ± 0.0018	0.0746 ± 0.0009	0.5689 ± 0.0190	433 ± 74	464 ± 5	98
11XL25-31	1.87	0.0599 ± 0.0017	0.0671 ± 0.0007	0.5512 ± 0.0151	611 ± 61	419 ± 4	93
11XL25-32	1.18	0.0548 ± 0.0013	0.0615 ± 0.0005	0.4654 ± 0.0108	406 ± 52	385 ± 3	99
11XL25-33	1.76	0.1100 ± 0.0015	0.3310 ± 0.0028	5.0487 ± 0.0723	1800 ± 25	1843 ± 13	99
11XL25-34	3.75	0.1291 ± 0.0017	0.3050 ± 0.0021	5.4669 ± 0.0691	2087 ± 23	1716 ± 11	90
11XL25-35	2.98	0.1525 ± 0.0017	0.3770 ± 0.0023	8.0015 ± 0.0939	2376 ± 20	2062 ± 11	92
11XL25-36	2.57	0.1681 ± 0.0023	0.4942 ± 0.0038	11.5075 ± 0.1584	2539 ± 23	2589 ± 16	99
11XL25-37	1.30	0.1583 ± 0.0021	0.4637 ± 0.0036	10.2107 ± 0.1434	2439 ± 23	2456 ± 16	99
11XL25-38	1.89	0.0583 ± 0.0016	0.0446 ± 0.0004	0.3581 ± 0.0094	543 ± 59	281 ± 3	90
11XL25-39	1.17	0.1634 ± 0.0020	0.4623 ± 0.0030	10.4932 ± 0.1265	2491 ± 26	2450 ± 13	98
11XL25-40	1.25	0.0570 ± 0.0013	0.0706 ± 0.0006	0.5554 ± 0.0123	500 ± 50	439 ± 4	97
11XL25-41	1.07	0.1637 ± 0.0023	0.4822 ± 0.0040	10.9258 ± 0.1502	2494 ± 24	2537 ± 18	99
11XL25-42	1.90	0.0542 ± 0.0010	0.0729 ± 0.0006	0.5466 ± 0.0095	389 ± 41	453 ± 4	97
11XL25-43	1.68	0.0555 ± 0.0014	0.0733 ± 0.0007	0.5607 ± 0.0137	435 ± 56	456 ± 4	99
11XL25-44	1.71	0.1853 ± 0.0025	0.5251 ± 0.0044	13.5186 ± 0.1777	2702 ± 22	2721 ± 19	99
11XL25-45	1.03	0.0525 ± 0.0012	0.0456 ± 0.0006	0.3314 ± 0.0078	309 ± 54	288 ± 4	98
11XL25-46	1.02	0.1630 ± 0.0024	0.4779 ± 0.0049	10.7867 ± 0.1551	2487 ± 30	2518 ± 22	99
11XL25-47	1.80	0.0562 ± 0.0011	0.0689 ± 0.0007	0.5378 ± 0.0106	457 ± 41	430 ± 4	98
11XL25-48	1.35	0.1049 ± 0.0015	0.2899 ± 0.0027	4.2052 ± 0.0603	1722 ± 27	1641 ± 14	97
11XL25-49	1.87	0.0510 ± 0.0012	0.0427 ± 0.0005	0.3016 ± 0.0076	243 ± 56	269 ± 3	99
11XL25-50	1.56	0.1096 ± 0.0016	0.3325 ± 0.0032	5.0410 ± 0.0725	1794 ± 27	1850 ± 15	98

(continued)

Table B.1 (continued)

Sample	U/Th	$^{206}Pb^{*}/^{207}Pb^{*}$	$^{206}Pb^{*}/^{238}U$	$^{207}Pb^{*}/^{235}U$	$^{206}Pb^{*}/^{207}Pb^{*}-Age$ [Ma]	$^{238}U/^{206}Pb-Age$ [Ma]	Concordance [%]
11XL25-51	2.08	0.0547 ± 0.0013	0.0693 ± 0.0009	0.5181 ± 0.0121	398 ± 56	432 ± 5	98
11XL25-52	1.99	0.1033 ± 0.0015	0.3140 ± 0.0027	4.4989 ± 0.0656	1684 ± 26	1761 ± 13	98
11XL25-53	2.24	0.1636 ± 0.0020	0.4948 ± 0.0043	11.2374 ± 0.1460	2494 ± 21	2591 ± 18	98
11XL25-54	1.38	0.1621 ± 0.0023	0.5054 ± 0.0059	11.3073 ± 0.1680	2480 ± 24	2637 ± 25	96
11XL25-55	1.91	0.1235 ± 0.0017	0.3689 ± 0.0032	6.3381 ± 0.0947	2009 ± 25	2024 ± 15	99
11XL25-56	1.38	0.0557 ± 0.0013	0.0723 ± 0.0007	0.5523 ± 0.0123	439 ± 54	450 ± 4	99
11XL25-57	1.07	0.1711 ± 0.0027	0.4873 ± 0.0060	11.4809 ± 0.1795	2568 ± 26	2559 ± 26	99
11XL25-58	1.14	0.1053 ± 0.0023	0.3213 ± 0.0039	4.6893 ± 0.1008	1720 ± 39	1796 ± 19	98
11XL25-59	1.19	0.1263 ± 0.0014	0.3804 ± 0.0024	6.6970 ± 0.0772	2047 ± 19	2078 ± 11	99
11XL25-60	1.54	0.0549 ± 0.0012	0.0456 ± 0.0004	0.3460 ± 0.0074	406 ± 44	288 ± 2	95
11XL25-61	1.88	0.0545 ± 0.0014	0.0700 ± 0.0007	0.5286 ± 0.0144	391 ± 61	436 ± 4	98
11XL25-62	1.74	0.0552 ± 0.0012	0.0702 ± 0.0006	0.5371 ± 0.0111	420 ± 53	437 ± 3	99
11XL25-63	4.04	0.0564 ± 0.0017	0.0716 ± 0.0008	0.5578 ± 0.0173	478 ± 101	446 ± 5	99
11XL25-64	2.98	0.0610 ± 0.0015	0.0468 ± 0.0004	0.3967 ± 0.0098	639 ± 56	295 ± 3	86
11XL25-65	0.89	0.1093 ± 0.0016	0.3272 ± 0.0023	4.9739 ± 0.0684	1788 ± 27	1825 ± 11	99
11XL25-66	1.57	0.0572 ± 0.0015	0.0718 ± 0.0006	0.5679 ± 0.0137	498 ± 56	447 ± 4	97
11XL25-67	1.78	0.1663 ± 0.0020	0.4842 ± 0.0030	11.2185 ± 0.1276	2521 ± 19	2545 ± 13	99
11XL25-68	1.91	0.0543 ± 0.0009	0.0692 ± 0.0005	0.5220 ± 0.0088	383 ± 37	431 ± 3	98
11XL25-69	17.07	0.1096 ± 0.0012	0.3157 ± 0.0023	4.8285 ± 0.0580	1794 ± 20	1769 ± 11	98
11XL25-70	1.27	0.1487 ± 0.0018	0.4333 ± 0.0028	8.9643 ± 0.1058	2331 ± 21	2321 ± 13	99
11XL25-71	1.44	0.0539 ± 0.0016	0.0609 ± 0.0006	0.4516 ± 0.0128	365 ± 65	381 ± 4	99
11XL25-72	1.27	0.1068 ± 0.0020	0.3157 ± 0.0028	4.6765 ± 0.0868	1746 ± 33	1769 ± 14	99
11XL25-73	3.23	0.0559 ± 0.0011	0.0731 ± 0.0006	0.5654 ± 0.0104	456 ± 17	455 ± 3	99

(continued)

Table B.1 (continued)

Sample	U/Th	$^{206}Pb^*/^{207}Pb^*$	$^{206}Pb^*/^{238}U$	$^{207}Pb^*/^{235}U$	$^{206}Pb^*/^{207}Pb^* - Age$ [Ma]	$^{238}U/^{206}Pb - Age$ [Ma]	Concordance [%]
11XL25-74	1.87	0.1116 ± 0.0016	0.3382 ± 0.0025	5.2437 ± 0.0752	1826 ± 27	1878 ± 12	99
11XL25-75	2.44	0.1102 ± 0.0014	0.3717 ± 0.0028	5.7073 ± 0.0761	1803 ± 23	2037 ± 13	94
11XL25-76	1.95	0.0546 ± 0.0010	0.0728 ± 0.0006	0.5510 ± 0.0097	398 ± 34	453 ± 3	98
11XL25-77	1.50	0.0579 ± 0.0012	0.0722 ± 0.0006	0.5775 ± 0.0115	524 ± 44	449 ± 4	97
11XL25-78	0.82	0.0541 ± 0.0019	0.0604 ± 0.0007	0.4462 ± 0.0146	372 ± 78	378 ± 4	99
11XL25-79	1.51	0.0518 ± 0.0013	0.0600 ± 0.0006	0.4300 ± 0.0108	276 ± 57	376 ± 4	96
11XL25-80	2.02	0.0527 ± 0.0015	0.0442 ± 0.0005	0.3199 ± 0.0091	322 ± 60	279 ± 3	98
11XL25-81	1.04	0.0617 ± 0.0018	0.0710 ± 0.0008	0.6105 ± 0.0187	665 ± 65	442 ± 5	90
11XL25-82	1.56	0.0545 ± 0.0010	0.0686 ± 0.0005	0.5193 ± 0.0095	391 ± 41	428 ± 3	99
11XL25-83	1.60	0.0546 ± 0.0011	0.0646 ± 0.0004	0.4902 ± 0.0093	398 ± 43	404 ± 3	99
11XL25-84	2.83	0.0524 ± 0.0015	0.0461 ± 0.0004	0.3318 ± 0.0092	302 ± 67	290 ± 3	99
11XL25-85	3.29	0.0546 ± 0.0016	0.0430 ± 0.0004	0.3232 ± 0.0087	398 ± 65	272 ± 3	95
11XL25-86	1.96	0.1696 ± 0.0022	0.5138 ± 0.0038	12.0902 ± 0.1522	2554 ± 22	2673 ± 16	97
11XL25-87	2.52	0.0609 ± 0.0029	0.0702 ± 0.0010	0.5725 ± 0.0234	635 ± 108	438 ± 6	95
11XL25-88	1.89	0.0553 ± 0.0009	0.0725 ± 0.0005	0.5560 ± 0.0089	433 ± 37	451 ± 3	99
11XL25-89	1.87	0.0564 ± 0.0010	0.0728 ± 0.0006	0.5728 ± 0.0104	478 ± 37	453 ± 4	98
11XL25-90	1.57	0.0586 ± 0.0014	0.0718 ± 0.0007	0.5787 ± 0.0129	550 ± 55	447 ± 4	96
11XL25-91	2.58	0.1712 ± 0.0025	0.4958 ± 0.0039	11.7732 ± 0.1638	2569 ± 24	2596 ± 17	99
11XL25-92	6.06	0.0579 ± 0.0011	0.0665 ± 0.0005	0.5330 ± 0.0102	524 ± 43	415 ± 3	95
11XL25-93	1.37	0.1802 ± 0.0020	0.5025 ± 0.0033	12.5971 ± 0.1416	2655 ± 18	2625 ± 14	99
11XL25-94	1.47	0.1108 ± 0.0013	0.3413 ± 0.0023	5.2444 ± 0.0620	1813 ± 22	1893 ± 11	98
11XL25-95	0.84	0.1690 ± 0.0019	0.4836 ± 0.0035	11.3480 ± 0.1349	2548 ± 20	2543 ± 15	99
11XL25-96	3.14	0.0506 ± 0.0009	0.0452 ± 0.0003	0.3164 ± 0.0054	233 ± 38	285 ± 2	97

(continued)

Table B.1 (continued)

Sample	U/Th	$^{206}Pb^*/^{207}Pb^*$	$^{206}Pb^*/^{238}U$	$^{207}Pb^*/^{235}U$	$^{206}Pb^*/^{207}Pb^* - Age$ [Ma]	$^{238}U/^{206}Pb - Age$ [Ma]	Concordance [%]
11XL25-97	1.05	0.0531 ± 0.0020	0.0451 ± 0.0005	0.3281 ± 0.0121	332 ± 79	284 ± 3	98
11XL25-98	1.23	0.0502 ± 0.0009	0.0454 ± 0.0004	0.3161 ± 0.0060	206 ± 47	286 ± 2	97
11XL25-99	1.79	0.0535 ± 0.0010	0.0691 ± 0.0005	0.5115 ± 0.0095	350 ± 43	431 ± 3	97
11XL26-01	1.62	0.0965 ± 0.0011	0.2542 ± 0.0015	3.3924 ± 0.0402	1567 ± 27	1460 ± 8	97
11XL26-02	1.25	0.0728 ± 0.0017	0.0383 ± 0.0003	0.3795 ± 0.0079	1009 ± 46	242 ± 2	70
11XL26-03	2.02	0.0563 ± 0.0010	0.0694 ± 0.0005	0.5396 ± 0.0096	461 ± 34	433 ± 3	98
11XL26-04	2.62	0.0543 ± 0.0012	0.0670 ± 0.0006	0.5000 ± 0.0110	383 ± 52	418 ± 4	98
11XL26-05	1.19	0.0812 ± 0.0019	0.0467 ± 0.0004	0.5214 ± 0.0121	1228 ± 42	294 ± 2	63
11XL26-06	1.99	0.0514 ± 0.0010	0.0423 ± 0.0003	0.2997 ± 0.0060	257 ± 44	267 ± 2	99
11XL26-07	1.72	0.0546 ± 0.0009	0.0669 ± 0.0005	0.5032 ± 0.0078	394 ± 32	418 ± 3	99
11XL26-08	2.52	0.0520 ± 0.0011	0.0412 ± 0.0003	0.2943 ± 0.0059	283 ± 48	260 ± 2	99
11XL26-09	4.07	0.1533 ± 0.0020	0.3645 ± 0.0026	7.7255 ± 0.0934	2383 ± 22	2003 ± 12	90
11XL26-10	0.98	0.0544 ± 0.0018	0.0503 ± 0.0006	0.3724 ± 0.0112	387 ± 68	316 ± 4	98
11XL26-11	1.10	0.0561 ± 0.0014	0.0368 ± 0.0003	0.2868 ± 0.0072	457 ± 28	233 ± 2	90
11XL26-12	1.56	0.0943 ± 0.0014	0.0682 ± 0.0005	0.8904 ± 0.0125	1515 ± 28	425 ± 3	58
11XL26-13	1.60	0.0558 ± 0.0016	0.0694 ± 0.0007	0.5309 ± 0.0145	443 ± 58	432 ± 4	99
11XL26-14	0.70	0.0510 ± 0.0013	0.0434 ± 0.0004	0.3044 ± 0.0073	239 ± 56	274 ± 2	98
11XL26-15	0.74	0.1146 ± 0.0024	0.0324 ± 0.0003	0.5137 ± 0.0096	1874 ± 37	206 ± 2	31
11XL26-16	1.45	0.0527 ± 0.0012	0.0437 ± 0.0003	0.3182 ± 0.0072	317 ± 54	276 ± 2	98
11XL26-17	0.83	0.0703 ± 0.0010	0.1599 ± 0.0011	1.5612 ± 0.0225	939 ± 28	956 ± 6	99
11XL26-18	1.65	0.0549 ± 0.0008	0.0660 ± 0.0005	0.5014 ± 0.0074	409 ± 35	412 ± 3	99
11XL26-19	1.23	0.0566 ± 0.0019	0.0682 ± 0.0008	0.5288 ± 0.0174	476 ± 42	426 ± 5	98
11XL26-20	1.78	0.0564 ± 0.0018	0.0654 ± 0.0008	0.5050 ± 0.0159	478 ± 72	408 ± 5	98

(continued)

Table B.1 (continued)

Sample	U/Th	$^{206}Pb^*/^{207}Pb^*$	$^{206}Pb^*/^{238}U$	$^{207}Pb^*/^{235}U$	$^{206}Pb^*/^{207}Pb^* - Age$ [Ma]	$^{238}U/^{206}Pb - Age$ [Ma]	Concordance [%]
11XL26-21	0.94	0.0715 ± 0.0014	0.0397 ± 0.0003	0.3905 ± 0.0074	972 ± 42	251 ± 2	71
11XL26-22	2.75	0.0580 ± 0.0012	0.0438 ± 0.0003	0.3519 ± 0.0072	532 ± 46	277 ± 2	89
11XL26-23	2.87	0.0586 ± 0.0010	0.0387 ± 0.0002	0.3143 ± 0.0053	554 ± 34	245 ± 1	87
11XL26-24	1.00	0.0821 ± 0.0020	0.0409 ± 0.0004	0.4657 ± 0.0109	1248 ± 49	259 ± 2	59
11XL26-25	1.91	0.0523 ± 0.0012	0.0426 ± 0.0008	0.3021 ± 0.0067	298 ± 54	269 ± 5	99
11XL26-26	3.78	0.0578 ± 0.0011	0.0702 ± 0.0006	0.5636 ± 0.0103	524 ± 39	438 ± 3	96
11XL26-27	0.98	0.0502 ± 0.0013	0.0433 ± 0.0004	0.3005 ± 0.0078	206 ± 61	273 ± 3	97
11XL26-28	1.71	0.0515 ± 0.0012	0.0402 ± 0.0003	0.2862 ± 0.0063	265 ± 56	254 ± 2	99
11XL26-29	1.74	0.0698 ± 0.0017	0.0416 ± 0.0003	0.4011 ± 0.0095	922 ± 51	263 ± 2	73
11XL26-30	1.13	0.0541 ± 0.0012	0.0438 ± 0.0004	0.3275 ± 0.0073	376 ± 56	276 ± 2	95
11XL26-31	1.47	0.0531 ± 0.0009	0.0586 ± 0.0004	0.4318 ± 0.0070	332 ± 37	367 ± 2	99
11XL26-32	2.60	0.1933 ± 0.0038	0.0521 ± 0.0004	1.4111 ± 0.0290	2772 ± 32	328 ± 2	7
11XL26-33	1.85	0.0509 ± 0.0009	0.0430 ± 0.0003	0.3037 ± 0.0054	239 ± 43	271 ± 2	99
11XL26-34	1.58	0.0527 ± 0.0010	0.0410 ± 0.0003	0.2995 ± 0.0054	317 ± 47	259 ± 2	97
11XL26-35	6.29	0.0710 ± 0.0013	0.0729 ± 0.0006	0.7200 ± 0.0128	967 ± 37	454 ± 3	80
11XL26-36	2.29	0.0556 ± 0.0020	0.0434 ± 0.0005	0.3276 ± 0.0110	435 ± 78	274 ± 3	95
11XL26-41	1.41	0.0795 ± 0.0014	0.0364 ± 0.0003	0.3986 ± 0.0068	1185 ± 35	230 ± 2	61
11XL26-42	1.56	0.0520 ± 0.0010	0.0424 ± 0.0003	0.3045 ± 0.0059	287 ± 44	268 ± 2	99
11XL26-43	1.72	0.0556 ± 0.0012	0.0421 ± 0.0003	0.3229 ± 0.0065	435 ± 46	266 ± 2	93
11XL26-44	1.59	0.0567 ± 0.0016	0.0463 ± 0.0005	0.3599 ± 0.0097	480 ± 61	292 ± 3	93
11XL26-45	2.28	0.0569 ± 0.0012	0.0704 ± 0.0006	0.5506 ± 0.0118	500 ± 81	439 ± 3	98
11XL26-46	1.82	0.0504 ± 0.0012	0.0369 ± 0.0003	0.2581 ± 0.0059	213 ± 83	234 ± 2	99
11XL26-47	1.73	0.0517 ± 0.0011	0.0418 ± 0.0003	0.2978 ± 0.0058	333 ± 42	264 ± 2	99

(continued)

Table B.1 (continued)

Sample	U/Th	$^{206}Pb^*/^{207}Pb^*$	$^{206}Pb^*/^{238}U$	$^{207}Pb^*/^{235}U$	$^{206}Pb^*/^{207}Pb^* - Age$ [Ma]	$^{238}U/^{206}Pb - Age$ [Ma]	Concordance [%]
11XL26-48	1.88	0.0504 ± 0.0010	0.0403 ± 0.0003	0.2814 ± 0.0056	213 ± 44	255 ± 2	98
11XL26-49	3.43	0.0550 ± 0.0010	0.0680 ± 0.0005	0.5185 ± 0.0094	413 ± 41	424 ± 3	99
11XL26-50	2.02	0.0577 ± 0.0015	0.0639 ± 0.0006	0.5121 ± 0.0138	517 ± 59	399 ± 4	95
11XL26-51	1.58	0.0519 ± 0.0010	0.0384 ± 0.0003	0.2752 ± 0.0050	283 ± 44	243 ± 2	98
11XL26-52	2.05	0.0511 ± 0.0010	0.0398 ± 0.0003	0.2819 ± 0.0056	256 ± 51	252 ± 2	99
11XL26-53	2.04	0.1040 ± 0.0013	0.2951 ± 0.0019	4.2637 ± 0.0522	1698 ± 22	1667 ± 9	98
11XL26-54	2.26	0.0951 ± 0.0014	0.0586 ± 0.0004	0.7736 ± 0.0111	1529 ± 32	367 ± 2	54
11XL26-55	1.72	0.0554 ± 0.0017	0.0466 ± 0.0005	0.3516 ± 0.0102	428 ± 64	294 ± 3	95
11XL26-56	0.98	0.0515 ± 0.0010	0.0409 ± 0.0003	0.2914 ± 0.0057	265 ± 44	258 ± 2	99
11XL26-57	1.07	0.0534 ± 0.0012	0.0427 ± 0.0004	0.3160 ± 0.0072	346 ± 52	270 ± 2	96
11XL26-58	1.66	0.0507 ± 0.0012	0.0454 ± 0.0004	0.3180 ± 0.0073	228 ± 56	286 ± 2	97
11XL26-59	1.24	0.0599 ± 0.0017	0.0448 ± 0.0004	0.3715 ± 0.0104	598 ± 61	282 ± 2	87
11XL26-60	3.92	0.0518 ± 0.0010	0.0429 ± 0.0003	0.3075 ± 0.0059	276 ± 44	271 ± 2	99
11XL26-61	3.09	0.0572 ± 0.0016	0.0388 ± 0.0004	0.3058 ± 0.0080	498 ± 61	245 ± 3	90
11XL26-62	1.79	0.0535 ± 0.0014	0.0476 ± 0.0004	0.3519 ± 0.0093	350 ± 61	300 ± 3	97
11XL26-63	1.10	0.0569 ± 0.0019	0.0461 ± 0.0006	0.3601 ± 0.0117	487 ± 74	291 ± 3	92
11XL26-64	3.00	0.0535 ± 0.0008	0.0478 ± 0.0003	0.3548 ± 0.0054	350 ± 33	301 ± 2	97
11XL26-65	1.83	0.0534 ± 0.0014	0.0495 ± 0.0005	0.3624 ± 0.0093	346 ± 90	311 ± 3	99
11XL26-66	5.94	0.0987 ± 0.0013	0.2021 ± 0.0013	2.7726 ± 0.0344	1600 ± 29	1187 ± 7	87
11XL26-67	1.04	0.0521 ± 0.0021	0.0428 ± 0.0006	0.3073 ± 0.0123	287 ± 97	270 ± 4	99
11XL26-68	2.05	0.0565 ± 0.0010	0.0666 ± 0.0005	0.5215 ± 0.0092	472 ± 39	416 ± 3	97
11XL26-69	2.62	0.0542 ± 0.0010	0.0666 ± 0.0005	0.4992 ± 0.0096	389 ± 38	416 ± 3	98
11XL26-70	1.85	0.0859 ± 0.0015	0.2298 ± 0.0019	2.7400 ± 0.0493	1400 ± 33	1333 ± 10	99

(continued)

Table B.1 (continued)

Sample	U/Th	$^{206}Pb^*/^{207}Pb^*$	$^{206}Pb^*/^{238}U$	$^{207}Pb^*/^{235}U$	$^{206}Pb^*/^{207}Pb^*-Age$ [Ma]	$^{238}U/^{206}Pb - Age$ [Ma]	Concordance [%]
11XL26-71	1.14	0.0763 ± 0.0036	0.0425 ± 0.0006	0.4443 ± 0.0202	1103 ± 94	268 ± 4	67
11XL26-72	1.62	0.0579 ± 0.0014	0.0485 ± 0.0004	0.3888 ± 0.0097	524 ± 56	306 ± 3	91
11XL26-73	2.29	0.0679 ± 0.0018	0.0453 ± 0.0003	0.4250 ± 0.0116	865 ± 56	286 ± 2	77
11XL26-74	1.99	0.1070 ± 0.0035	0.0388 ± 0.0004	0.5408 ± 0.0135	1750 ± 59	246 ± 3	43
11XL26-75	3.50	0.1070 ± 0.0013	0.3156 ± 0.0021	4.6775 ± 0.0603	1750 ± 24	1768 ± 10	99
11XL26-76	2.35	0.0550 ± 0.0016	0.0465 ± 0.0006	0.3534 ± 0.0100	413 ± 65	293 ± 4	95
11XL26-77	1.53	0.0534 ± 0.0013	0.0423 ± 0.0004	0.3106 ± 0.0075	346 ± 83	267 ± 3	97
11XL26-78	1.98	0.0558 ± 0.0011	0.0398 ± 0.0003	0.3076 ± 0.0058	456 ± 10	251 ± 2	92
11XL26-79	0.78	0.0580 ± 0.0024	0.0398 ± 0.0005	0.3139 ± 0.0123	528 ± 89	251 ± 3	90
11XL26-80	2.17	0.0517 ± 0.0009	0.0414 ± 0.0003	0.2961 ± 0.0050	276 ± 44	261 ± 2	99
11XL26-81	2.07	0.0522 ± 0.0009	0.0417 ± 0.0003	0.3016 ± 0.0050	295 ± 39	263 ± 2	98
11XL26-82	1.59	0.0531 ± 0.0013	0.0415 ± 0.0004	0.3034 ± 0.0074	345 ± 57	262 ± 3	97
11XL26-83	1.33	0.0515 ± 0.0014	0.0395 ± 0.0004	0.2812 ± 0.0073	265 ± 56	250 ± 2	99
11XL26-84	1.59	0.0543 ± 0.0016	0.0405 ± 0.0004	0.3029 ± 0.0082	383 ± 69	256 ± 2	95
11XL26-85	3.09	0.0877 ± 0.0014	0.0618 ± 0.0004	0.7537 ± 0.0112	1377 ± 30	386 ± 3	61
11XL26-86	1.91	0.0517 ± 0.0010	0.0436 ± 0.0003	0.3122 ± 0.0056	272 ± 47	275 ± 2	99
11XL26-87	2.71	0.0588 ± 0.0011	0.0669 ± 0.0004	0.5451 ± 0.0100	567 ± 41	417 ± 3	94
11XL26-88	1.88	0.0715 ± 0.0015	0.0569 ± 0.0004	0.5651 ± 0.0112	972 ± 43	357 ± 2	75
11XL26-89	6.48	0.1167 ± 0.0046	0.0706 ± 0.0042	1.0185 ± 0.0835	1906 ± 71	440 ± 25	52
11XL26-90	2.88	0.0840 ± 0.0012	0.1133 ± 0.0017	1.3280 ± 0.0266	1292 ± 28	692 ± 10	78
11XL26-91	3.64	0.0558 ± 0.0010	0.0707 ± 0.0005	0.5460 ± 0.0091	456 ± 39	440 ± 3	99
11XL26-92	1.73	0.0724 ± 0.0017	0.0521 ± 0.0005	0.5221 ± 0.0123	998 ± 55	327 ± 3	73
11XL26-93	2.52	0.0507 ± 0.0014	0.0421 ± 0.0003	0.2960 ± 0.0078	228 ± 61	266 ± 2	99
11XL26-94	4.04	0.0580 ± 0.0011	0.0641 ± 0.0004	0.5163 ± 0.0091	532 ± 36	401 ± 2	94

(continued)

Table B.1 (continued)

Sample	U/Th	$^{206}Pb^*/^{207}Pb^*$	$^{206}Pb^*/^{238}U$	$^{207}Pb^*/^{235}U$	$^{206}Pb^*/^{207}Pb^* - Age$ [Ma]	$^{238}U/^{206}Pb - Age$ [Ma]	Concordance [%]
11XL27-01	1.90	0.0523 ± 0.0012	0.0441 ± 0.0004	0.3190 ± 0.0071	298 ± 47	278 ± 2	98
11XL27-02	1.77	0.0515 ± 0.0010	0.0442 ± 0.0003	0.3138 ± 0.0059	265 ± 44	279 ± 2	99
11XL27-03	2.05	0.0520 ± 0.0012	0.0437 ± 0.0003	0.3134 ± 0.0071	287 ± 54	275 ± 2	99
11XL27-04	1.77	0.0529 ± 0.0016	0.0490 ± 0.0005	0.3540 ± 0.0104	324 ± 67	308 ± 3	99
11XL27-05	1.17	0.0543 ± 0.0010	0.0660 ± 0.0005	0.4942 ± 0.0088	383 ± 43	412 ± 3	98
11XL27-06	2.39	0.0551 ± 0.0009	0.0644 ± 0.0004	0.4917 ± 0.0080	417 ± 32	402 ± 3	99
11XL27-07	1.22	0.0521 ± 0.0029	0.0489 ± 0.0006	0.3484 ± 0.0197	287 ± 130	308 ± 4	98
11XL27-08	2.31	0.0543 ± 0.0011	0.0415 ± 0.0003	0.3119 ± 0.0066	383 ± 44	262 ± 2	94
11XL27-09	1.77	0.0568 ± 0.0014	0.0628 ± 0.0005	0.4935 ± 0.0122	483 ± 53	393 ± 3	96
11XL27-10	2.26	0.0521 ± 0.0012	0.0409 ± 0.0004	0.2961 ± 0.0071	287 ± 54	259 ± 2	98
11XL27-11	1.74	0.0617 ± 0.0013	0.0415 ± 0.0003	0.3550 ± 0.0072	661 ± 44	262 ± 2	83
11XL27-12	1.91	0.0555 ± 0.0018	0.0463 ± 0.0005	0.3525 ± 0.0108	432 ± 69	292 ± 3	95
11XL27-13	1.25	0.0604 ± 0.0011	0.0648 ± 0.0005	0.5416 ± 0.0095	617 ± 39	405 ± 3	91
11XL27-14	2.09	0.0557 ± 0.0008	0.0677 ± 0.0004	0.5230 ± 0.0074	443 ± 31	423 ± 3	98
11XL27-15	1.31	0.0524 ± 0.0014	0.0439 ± 0.0004	0.3175 ± 0.0079	302 ± 62	277 ± 2	98
11XL27-16	1.77	0.0808 ± 0.0017	0.0448 ± 0.0005	0.4996 ± 0.0097	1218 ± 41	282 ± 3	62
11XL27-17	1.38	0.0521 ± 0.0014	0.0448 ± 0.0004	0.3216 ± 0.0088	300 ± 63	282 ± 3	99
11XL27-18	1.21	0.0563 ± 0.0016	0.0468 ± 0.0005	0.3654 ± 0.0104	465 ± 65	295 ± 3	93
11XL27-19	0.91	0.0550 ± 0.0019	0.0426 ± 0.0005	0.3174 ± 0.0102	413 ± 71	269 ± 3	95
11XL27-20	1.21	0.0992 ± 0.0026	0.0365 ± 0.0004	0.4968 ± 0.0120	1610 ± 49	231 ± 2	44
11XL27-21	1.59	0.0529 ± 0.0010	0.0683 ± 0.0005	0.5005 ± 0.0096	324 ± 44	426 ± 3	96
11XL27-22	1.36	0.0585 ± 0.0023	0.0426 ± 0.0005	0.3376 ± 0.0127	550 ± 85	269 ± 3	90
11XL27-23	1.54	0.0486 ± 0.0016	0.0443 ± 0.0005	0.2959 ± 0.0102	128 ± 78	279 ± 3	94

(continued)

Table B.1 (continued)

Sample	U/Th	$^{206}Pb^*/^{207}Pb^*$	$^{206}Pb^*/^{238}U$	$^{207}Pb^*/^{235}U$	$^{206}Pb^*/^{207}Pb^* - Age$ [Ma]	$^{238}U/^{206}Pb - Age$ [Ma]	Concordance [%]
11XL27-24	1.93	0.0566 ± 0.0011	0.0663 ± 0.0006	0.5202 ± 0.0093	476 ± 41	414 ± 3	97
11XL27-25	1.62	0.0514 ± 0.0012	0.0431 ± 0.0003	0.3042 ± 0.0068	257 ± 49	272 ± 2	99
11XL27-26	1.21	0.0527 ± 0.0015	0.0426 ± 0.0004	0.3101 ± 0.0084	322 ± 63	269 ± 2	97
11XL27-27	0.96	0.0786 ± 0.0014	0.0448 ± 0.0003	0.4875 ± 0.0084	1161 ± 36	282 ± 2	64
11XL27-28	1.06	0.0524 ± 0.0013	0.0455 ± 0.0004	0.3288 ± 0.0083	302 ± 62	287 ± 3	99
11XL27-29	2.34	0.0500 ± 0.0009	0.0443 ± 0.0003	0.3077 ± 0.0055	195 ± 41	280 ± 2	97
11XL27-30	2.34	0.0542 ± 0.0011	0.0703 ± 0.0006	0.5261 ± 0.0108	376 ± 51	438 ± 4	97
11XL27-31	1.91	0.0546 ± 0.0010	0.0727 ± 0.0005	0.5510 ± 0.0101	398 ± 34	453 ± 3	98
11XL27-32	1.20	0.0794 ± 0.0016	0.0551 ± 0.0005	0.5985 ± 0.0109	1183 ± 45	346 ± 3	68
11XL27-33	2.55	0.0534 ± 0.0009	0.0690 ± 0.0006	0.5098 ± 0.0090	346 ± 39	430 ± 3	97
11XL27-34	1.21	0.1081 ± 0.0021	0.0417 ± 0.0004	0.6220 ± 0.0114	1769 ± 35	263 ± 2	39
11XL27-35	1.63	0.0561 ± 0.0011	0.0701 ± 0.0006	0.5396 ± 0.0098	457 ± 44	437 ± 3	99
11XL27-36	1.69	0.0656 ± 0.0015	0.0498 ± 0.0004	0.4508 ± 0.0099	794 ± 48	313 ± 2	81
11XL27-37	1.08	0.0559 ± 0.0015	0.0479 ± 0.0005	0.3704 ± 0.0104	456 ± 59	301 ± 3	94
11XL27-38	1.10	0.0571 ± 0.0016	0.0413 ± 0.0005	0.3216 ± 0.0089	494 ± 68	261 ± 3	91
11XL27-39	1.27	0.0603 ± 0.0016	0.0677 ± 0.0006	0.5607 ± 0.0145	613 ± 83	422 ± 4	93
11XL27-40	2.30	0.0554 ± 0.0010	0.0701 ± 0.0005	0.5390 ± 0.0096	432 ± 44	437 ± 3	99
11XL27-41	4.87	0.0668 ± 0.0010	0.0601 ± 0.0003	0.5586 ± 0.0078	833 ± −169	376 ± 2	82
11XL27-42	1.25	0.1043 ± 0.0015	0.3003 ± 0.0019	4.3570 ± 0.0618	1702 ± 26	1693 ± 10	99
11XL27-43	2.39	0.0508 ± 0.0011	0.0442 ± 0.0004	0.3090 ± 0.0065	232 ± 47	279 ± 2	97
11XL27-44	2.77	0.0507 ± 0.0013	0.0408 ± 0.0004	0.2873 ± 0.0073	233 ± 59	258 ± 2	99
11XL27-45	1.10	0.0513 ± 0.0011	0.0435 ± 0.0004	0.3098 ± 0.0063	254 ± 46	274 ± 2	99
11XL27-46	2.18	0.0897 ± 0.0036	0.0376 ± 0.0004	0.4593 ± 0.0173	1420 ± 77	238 ± 3	53

(continued)

Table B.1 (continued)

Sample	U/Th	$^{206}Pb^{*}/^{207}Pb^{*}$	$^{206}Pb^{*}/^{238}U$	$^{207}Pb^{*}/^{235}U$	$^{206}Pb^{*}/^{207}Pb^{*}-Age$ [Ma]	$^{238}U/^{206}Pb-Age$ [Ma]	Concordance [%]
11XL27 -47	2.05	0.0554 ± 0.0014	0.0675 ± 0.0006	0.5169 ± 0.0132	428 ± 59	421 ± 4	99
11XL27-48	2.16	0.0800 ± 0.0010	0.2082 ± 0.0013	2.3214 ± 0.0275	1198 ± 24	1219 ± 7	99
11XL27-49	1.38	0.0616 ± 0.0009	0.0692 ± 0.0004	0.5936 ± 0.0082	661 ± 36	432 ± 3	90
11XL27-50	1.35	0.0516 ± 0.0010	0.0426 ± 0.0003	0.3048 ± 0.0061	333 ± 51	269 ± 2	99
11XL27-51	1.82	0.0551 ± 0.0011	0.0703 ± 0.0005	0.5378 ± 0.0103	417 ± 43	438 ± 3	99
11XL27-52	1.75	0.0542 ± 0.0011	0.0701 ± 0.0005	0.5270 ± 0.0101	389 ± 51	437 ± 3	98
11XL27-53	1.62	0.0550 ± 0.0011	0.0738 ± 0.0006	0.5632 ± 0.0107	413 ± 43	459 ± 4	98
11XL27-54	1.42	0.0642 ± 0.0019	0.0410 ± 0.0005	0.3636 ± 0.0099	750 ± 61	259 ± 3	80
11XL27-55	0.68	0.0979 ± 0.0024	0.0419 ± 0.0004	0.5698 ± 0.0135	1584 ± 46	265 ± 2	46
11XL27-56	0.84	0.0564 ± 0.0015	0.0393 ± 0.0004	0.3069 ± 0.0081	465 ± 59	248 ± 2	91
11XL27-57	1.75	0.0554 ± 0.0012	0.0418 ± 0.0004	0.3216 ± 0.0069	428 ± 45	264 ± 2	93
11XL27-58	1.08	0.4190 ± 0.0171	0.1701 ± 0.0091	14.5355 ± 1.0643	3979 ± 61	1013 ± 50	6
11XL27-59	2.61	0.0750 ± 0.0017	0.0665 ± 0.0006	0.7042 ± 0.0187	1133 ± 50	415 ± 4	73
11XL27-60	5.19	0.0715 ± 0.0013	0.0898 ± 0.0007	0.8963 ± 0.0166	972 ± 5	555 ± 4	84
11XL27-61	1.73	0.0724 ± 0.0014	0.1651 ± 0.0015	1.6520 ± 0.0304	996 ± 34	985 ± 8	99
11XL27-62	2.29	0.0657 ± 0.0014	0.0396 ± 0.0003	0.3617 ± 0.0076	798 ± 45	250 ± 2	77
11XL27-63	1.25	0.0523 ± 0.0013	0.0454 ± 0.0004	0.3292 ± 0.0083	302 ± 62	286 ± 3	99
11XL27-64	2.25	0.0559 ± 0.0011	0.0673 ± 0.0006	0.5222 ± 0.0102	456 ± 17	420 ± 4	98
11XL27-65	2.49	0.0535 ± 0.0012	0.0460 ± 0.0004	0.3413 ± 0.0073	350 ± 50	290 ± 3	97
11XL27-66	6.36	0.0580 ± 0.0013	0.0788 ± 0.0007	0.6327 ± 0.0143	528 ± 55	489 ± 4	98
11XL27-67	2.23	0.0536 ± 0.0009	0.0700 ± 0.0005	0.5214 ± 0.0090	354 ± 34	436 ± 3	97
11XL27-68	1.34	0.0497 ± 0.0010	0.0427 ± 0.0003	0.2952 ± 0.0056	189 ± 17	270 ± 2	97
11XL27-69	1.65	0.0563 ± 0.0014	0.0690 ± 0.0007	0.5363 ± 0.0133	465 ± 57	430 ± 4	98

(continued)

Table B.1 (continued)

Sample	U/Th	^{206}Pb*/^{207}Pb*	^{206}Pb*/^{238}U	^{207}Pb*/^{235}U	^{206}Pb*/^{207}Pb*−*Age* [Ma]	^{238}U/^{206}Pb − *Age* [Ma]	Concordance [%]
11XL27-70	1.64	0.0525 ± 0.0021	0.0459 ± 0.0005	0.3273 ± 0.0127	309 ± 93	290 ± 3	99
11XL27-71	1.23	0.0620 ± 0.0019	0.0420 ± 0.0005	0.3610 ± 0.0114	672 ± 67	265 ± 3	83
11XL27-72	1.80	0.0572 ± 0.0015	0.0490 ± 0.0005	0.3853 ± 0.0098	498 ± 64	308 ± 3	92
11XL27-73	1.52	0.0588 ± 0.0013	0.0703 ± 0.0006	0.5712 ± 0.0123	561 ± 44	438 ± 4	95
11XL27-74	1.92	0.0537 ± 0.0010	0.0730 ± 0.0006	0.5442 ± 0.0106	361 ± 75	454 ± 4	97
11XL27-75	3.09	0.0537 ± 0.0010	0.0429 ± 0.0003	0.3191 ± 0.0056	367 ± 41	271 ± 2	96
11XL27-76	1.33	0.0540 ± 0.0012	0.0655 ± 0.0005	0.4884 ± 0.0105	372 ± 50	409 ± 3	98
11XL27-77	1.94	0.0659 ± 0.0021	0.0423 ± 0.0004	0.3817 ± 0.0114	1200 ± 73	267 ± 3	79
11XL27-78	1.36	0.0556 ± 0.0015	0.0423 ± 0.0004	0.3237 ± 0.0084	435 ± 63	267 ± 2	93
11XL27-79	1.21	0.0515 ± 0.0015	0.0436 ± 0.0004	0.3065 ± 0.0083	261 ± 65	275 ± 3	98
11XL27-80	1.81	0.0521 ± 0.0019	0.0421 ± 0.0005	0.3002 ± 0.0106	300 ± 83	266 ± 3	99
11XL27-81	1.12	0.0624 ± 0.0016	0.0403 ± 0.0004	0.3465 ± 0.0085	689 ± 54	255 ± 2	82
11XL27-82	0.89	0.0562 ± 0.0019	0.0426 ± 0.0005	0.3245 ± 0.0104	457 ± 74	269 ± 3	94
11XL27-83	2.51	0.0547 ± 0.0012	0.0676 ± 0.0006	0.5108 ± 0.0107	467 ± 48	422 ± 4	99
11XL27-84	2.43	0.0568 ± 0.0010	0.0711 ± 0.0006	0.5597 ± 0.0097	483 ± 32	443 ± 3	98
11XL27-85	2.92	0.0584 ± 0.0010	0.0670 ± 0.0004	0.5410 ± 0.0086	546 ± 40	418 ± 3	95
11XL27-86	11.77	0.0703 ± 0.0013	0.0594 ± 0.0004	0.5782 ± 0.0105	939 ± 38	372 ± 3	78
11XL27-87	1.47	0.0525 ± 0.0011	0.0438 ± 0.0004	0.3163 ± 0.0062	309 ± 46	276 ± 3	99
11XL27-88	1.77	0.1084 ± 0.0014	0.2670 ± 0.0019	4.0135 ± 0.0542	1773 ± 24	1525 ± 10	92
11XL27-89	2.70	0.0545 ± 0.0008	0.0705 ± 0.0006	0.5316 ± 0.0085	391 ± 40	439 ± 3	98
11XL27-90	2.20	0.0518 ± 0.0011	0.0482 ± 0.0004	0.3449 ± 0.0073	276 ± 46	303 ± 2	99
11XL51-1-01	3.37	0.0566 ± 0.0011	0.0690 ± 0.0005	0.5443 ± 0.0105	476 ± 43	430 ± 3	97
11XL51-1-02	1.59	0.0563 ± 0.0011	0.0697 ± 0.0006	0.5456 ± 0.0101	465 ± 36	434 ± 3	98

(continued)

Table B.1 (continued)

Sample	U/Th	$^{206}Pb^*/^{207}Pb^*$	$^{206}Pb^*/^{238}U$	$^{207}Pb^*/^{235}U$	$^{206}Pb^*/^{207}Pb^* - Age$ [Ma]	$^{238}U/^{206}Pb - Age$ [Ma]	Concordance [%]
11XL51-1-03	1.55	0.0551 ± 0.0015	0.0698 ± 0.0007	0.5255 ± 0.0138	417 ± 63	435 ± 4	98
11XL51-1-04	1.32	0.0528 ± 0.0016	0.0432 ± 0.0004	0.3112 ± 0.0085	320 ± 67	273 ± 2	99
11XL51-1-05	2.71	0.0551 ± 0.0008	0.0704 ± 0.0005	0.5400 ± 0.0077	417 ± 33	439 ± 3	99
11XL51-1-06	1.79	0.0527 ± 0.0012	0.0460 ± 0.0004	0.3343 ± 0.0077	322 ± 54	290 ± 3	98
11XL51-1-07	1.36	0.0547 ± 0.0009	0.0700 ± 0.0005	0.5332 ± 0.0088	398 ± 35	436 ± 3	99
11XL51-1-08	1.76	0.0598 ± 0.0012	0.0452 ± 0.0004	0.3748 ± 0.0074	594 ± 44	285 ± 2	87
11XL51-1-09	1.56	0.0523 ± 0.0012	0.0405 ± 0.0004	0.2930 ± 0.0063	298 ± 45	256 ± 2	97
11XL51-1-10	1.75	0.0566 ± 0.0010	0.0697 ± 0.0005	0.5477 ± 0.0097	476 ± 41	435 ± 3	97
11XL51-1-11	2.98	0.0528 ± 0.0011	0.0436 ± 0.0003	0.3189 ± 0.0061	320 ± 46	275 ± 2	97
11XL51-1-12	2.45	0.0560 ± 0.0010	0.0690 ± 0.0005	0.5347 ± 0.0095	454 ± 41	430 ± 3	98
11XL51-1-13	2.28	0.0545 ± 0.0014	0.0691 ± 0.0005	0.5226 ± 0.0145	391 ± 62	431 ± 3	99
11XL51-1-14	1.50	0.0575 ± 0.0018	0.0479 ± 0.0005	0.3783 ± 0.0113	522 ± 73	301 ± 3	92
11XL51-1-15	1.67	0.0556 ± 0.0016	0.0467 ± 0.0004	0.3555 ± 0.0097	435 ± 65	294 ± 3	95
11XL51-1-16	1.76	0.0573 ± 0.0015	0.0730 ± 0.0007	0.5730 ± 0.0140	502 ± 59	454 ± 4	98
11XL51-1-17	1.17	0.0579 ± 0.0014	0.0699 ± 0.0006	0.5596 ± 0.0134	524 ± 56	436 ± 3	96
11XL51-1-18	1.29	0.0563 ± 0.0010	0.0732 ± 0.0005	0.5735 ± 0.0097	465 ± 34	455 ± 3	98
11XL51-1-19	1.79	0.0571 ± 0.0015	0.0728 ± 0.0007	0.5725 ± 0.0141	494 ± 56	453 ± 4	98
11XL51-1-20	2.21	0.0564 ± 0.0011	0.0742 ± 0.0006	0.5816 ± 0.0111	478 ± 38	461 ± 3	99
11XL51-1-21	2.66	0.0572 ± 0.0011	0.0757 ± 0.0005	0.6006 ± 0.0109	498 ± 41	471 ± 3	98
11XL51-1-22	2.88	0.0580 ± 0.0015	0.0724 ± 0.0006	0.5803 ± 0.0145	532 ± 56	451 ± 4	96
11XL51-1-23	1.37	0.0559 ± 0.0014	0.0717 ± 0.0006	0.5529 ± 0.0136	456 ± 56	447 ± 4	99
11XL51-1-24	1.71	0.0574 ± 0.0013	0.0718 ± 0.0006	0.5685 ± 0.0125	506 ± 56	447 ± 4	97
11XL51-1-25	1.51	0.0525 ± 0.0015	0.0444 ± 0.0004	0.3201 ± 0.0088	306 ± 63	280 ± 3	99

(continued)

Table B.1 (continued)

Sample	U/Th	$^{206}Pb^*/^{207}Pb^*$	$^{206}Pb^*/^{238}U$	$^{207}Pb^*/^{235}U$	$^{206}Pb^*/^{207}Pb^*-Age$ [Ma]	$^{238}U/^{206}Pb - Age$ [Ma]	Concordance [%]
11XL51-1-26	1.05	0.0509 ± 0.0012	0.0434 ± 0.0003	0.3046 ± 0.0068	239 ± 58	274 ± 2	98
11XL51-1-27	1.10	0.0526 ± 0.0010	0.0420 ± 0.0003	0.3067 ± 0.0060	322 ± 44	265 ± 2	97
11XL51-1-28	1.64	0.0531 ± 0.0009	0.0477 ± 0.0003	0.3510 ± 0.0058	332 ± 37	300 ± 2	98
11XL51-1-29	2.03	0.0566 ± 0.0018	0.0745 ± 0.0008	0.5766 ± 0.0180	476 ± 70	463 ± 5	99
11XL51-1-30	1.65	0.0521 ± 0.0010	0.0472 ± 0.0003	0.3405 ± 0.0068	300 ± 51	297 ± 2	99
11XL51-1-31	1.58	0.0553 ± 0.0009	0.0723 ± 0.0005	0.5549 ± 0.0090	428 ± 35	450 ± 3	99
11XL51-1-32	2.42	0.0585 ± 0.0019	0.0464 ± 0.0005	0.3722 ± 0.0117	546 ± 70	293 ± 3	90
11XL51-1-33	2.92	0.0529 ± 0.0016	0.0453 ± 0.0004	0.3288 ± 0.0097	324 ± 70	286 ± 3	98
11XL51-1-34	0.68	0.0511 ± 0.0010	0.0426 ± 0.0003	0.3026 ± 0.0058	256 ± 44	269 ± 2	99
11XL51-1-35	1.05	0.0538 ± 0.0013	0.0491 ± 0.0004	0.3639 ± 0.0083	361 ± 54	309 ± 3	98
11XL51-1-36	4.24	0.0503 ± 0.0009	0.0425 ± 0.0003	0.2973 ± 0.0053	206 ± 43	269 ± 2	98
11XL51-1-37	2.88	0.0533 ± 0.0010	0.0436 ± 0.0003	0.3233 ± 0.0056	339 ± 45	275 ± 2	96
11XL51-1-38	3.76	0.1114 ± 0.0013	0.3350 ± 0.0021	5.2116 ± 0.0619	1833 ± 17	1862 ± 10	99
11XL51-1-39	1.45	0.0559 ± 0.0018	0.0476 ± 0.0005	0.3630 ± 0.0113	456 ± 72	300 ± 3	95
11XL51-1-40	0.95	0.0519 ± 0.0012	0.0440 ± 0.0004	0.3152 ± 0.0070	280 ± 49	278 ± 2	99
11XL51-1-41	1.46	0.0507 ± 0.0012	0.0460 ± 0.0004	0.3219 ± 0.0076	228 ± 57	290 ± 2	97
11XL51-1-42	2.12	0.0563 ± 0.0010	0.0671 ± 0.0005	0.5260 ± 0.0097	465 ± 36	418 ± 3	97
11XL51-1-43	1.23	0.0514 ± 0.0010	0.0402 ± 0.0003	0.2875 ± 0.0054	257 ± 44	254 ± 2	98
11XL51-1-44	1.35	0.0609 ± 0.0014	0.0708 ± 0.0006	0.5953 ± 0.0126	635 ± 48	441 ± 3	92
11XL51-1-45	0.79	0.0919 ± 0.0019	0.0439 ± 0.0003	0.5629 ± 0.0117	1465 ± 40	277 ± 2	51
11XL51-1-46	1.33	0.0567 ± 0.0015	0.0742 ± 0.0007	0.5816 ± 0.0152	483 ± 53	461 ± 4	99
11XL51-1-47	2.49	0.0580 ± 0.0014	0.0738 ± 0.0007	0.5915 ± 0.0143	528 ± 58	459 ± 4	97
11XL51-1-48	2.28	0.0554 ± 0.0014	0.0722 ± 0.0006	0.5533 ± 0.0136	428 ± 56	449 ± 4	99

(continued)

Table B.1 (continued)

Sample	U/Th	$^{206}Pb^*/^{207}Pb^*$	$^{206}Pb^*/^{238}U$	$^{207}Pb^*/^{235}U$	$^{206}Pb^*/^{207}Pb^*-Age$ [Ma]	$^{238}U/^{206}Pb-Age$ [Ma]	Concordance [%]
11XL51-1-49	2.08	0.0536 ± 0.0009	0.0733 ± 0.0005	0.5429 ± 0.0088	354 ± 37	456 ± 3	96
11XL51-1-50	1.21	0.0559 ± 0.0014	0.0685 ± 0.0007	0.5242 ± 0.0121	456 ± 54	427 ± 4	99
11XL51-1-51	4.21	0.0540 ± 0.0007	0.0700 ± 0.0004	0.5249 ± 0.0072	372 ± 64	436 ± 2	98
11XL51-1-52	2.61	0.0686 ± 0.0009	0.1654 ± 0.0010	1.5744 ± 0.0216	887 ± 29	987 ± 5	97
11XL51-1-53	6.48	0.0675 ± 0.0010	0.1545 ± 0.0009	1.4455 ± 0.0219	854 ± 31	926 ± 5	98
11XL51-1-54	2.02	0.0509 ± 0.0012	0.0442 ± 0.0003	0.3100 ± 0.0073	235 ± 56	279 ± 2	98
11XL51-1-55	1.84	0.0509 ± 0.0012	0.0462 ± 0.0004	0.3246 ± 0.0074	239 ± 58	291 ± 2	98
11XL51-1-56	0.82	0.0785 ± 0.0078	0.0441 ± 0.0008	0.4617 ± 0.0463	1161 ± 199	278 ± 5	67
11XL51-1-57	1.83	0.0568 ± 0.0011	0.0717 ± 0.0005	0.5632 ± 0.0105	483 ± 41	446 ± 3	98
11XL51-1-58	6.90	0.0542 ± 0.0008	0.0721 ± 0.0005	0.5436 ± 0.0087	389 ± 31	449 ± 3	98
11XL51-1-59	3.29	0.1109 ± 0.0014	0.3279 ± 0.0023	5.0461 ± 0.0652	1817 ± 24	1828 ± 11	99
11XL51-1-60	3.02	0.1101 ± 0.0013	0.3429 ± 0.0020	5.2501 ± 0.0633	1811 ± 22	1901 ± 9	97
11XL51-1-61	2.03	0.0654 ± 0.0010	0.0435 ± 0.0003	0.3956 ± 0.0061	787 ± 33	274 ± 2	79
11XL51-1-62	3.51	0.0567 ± 0.0017	0.0700 ± 0.0007	0.5472 ± 0.0160	480 ± 65	436 ± 4	98
11XL51-1-63	2.22	0.0566 ± 0.0012	0.0734 ± 0.0007	0.5756 ± 0.0123	476 ± 48	457 ± 4	98
11XL51-1-64	2.31	0.0532 ± 0.0011	0.0471 ± 0.0004	0.3487 ± 0.0073	339 ± 44	297 ± 2	97
11XL51-1-65	1.77	0.0517 ± 0.0016	0.0470 ± 0.0005	0.3293 ± 0.0094	333 ± 70	296 ± 3	97
11XL51-1-66	1.55	0.0556 ± 0.0010	0.0767 ± 0.0006	0.5923 ± 0.0105	435 ± 41	477 ± 3	99
11XL51-1-67	9.85	0.1678 ± 0.0019	0.4395 ± 0.0025	10.2864 ± 0.1181	2536 ± 19	2348 ± 11	95
11XL51-1-68	2.17	0.0563 ± 0.0010	0.0699 ± 0.0006	0.5449 ± 0.0092	465 ± 34	435 ± 3	98
11XL51-1-69	1.51	0.0503 ± 0.0013	0.0487 ± 0.0005	0.3357 ± 0.0081	206 ± 59	306 ± 3	95
11XL51-1-70	2.26	0.0526 ± 0.0009	0.0435 ± 0.0003	0.3174 ± 0.0049	322 ± 37	274 ± 2	98
11XL51-1-71	1.74	0.0514 ± 0.0011	0.0435 ± 0.0003	0.3101 ± 0.0064	261 ± 50	274 ± 2	99

(continued)

Table B.1 (continued)

Sample	U/Th	$^{206}Pb^*/^{207}Pb^*$	$^{206}Pb^*/^{238}U$	$^{207}Pb^*/^{235}U$	$^{206}Pb^*/^{207}Pb^* - Age$ [Ma]	$^{238}U/^{206}Pb - Age$ [Ma]	Concordance [%]
11XL51-1-72	1.60	0.0555 ± 0.0012	0.0680 ± 0.0005	0.5223 ± 0.0106	432 ± 48	424 ± 3	99
11XL51-1-73	1.57	0.0562 ± 0.0016	0.0726 ± 0.0009	0.5584 ± 0.0151	461 ± 61	452 ± 5	99
11XL51-1-74	2.10	0.0575 ± 0.0012	0.0718 ± 0.0006	0.5709 ± 0.0119	509 ± 53	447 ± 4	97
11XL51-1-75	1.75	0.0522 ± 0.0010	0.0452 ± 0.0003	0.3274 ± 0.0061	295 ± 44	285 ± 2	99
11XL51-1-76	1.69	0.0533 ± 0.0010	0.0446 ± 0.0003	0.3294 ± 0.0061	343 ± 44	281 ± 2	97
11XL51-1-77	1.52	0.0590 ± 0.0019	0.0703 ± 0.0008	0.5631 ± 0.0168	569 ± 70	438 ± 5	96
11XL51-1-78	1.63	0.0556 ± 0.0022	0.0703 ± 0.0009	0.5351 ± 0.0207	439 ± 89	438 ± 5	99
11XL51-1-79	1.74	0.0562 ± 0.0019	0.0730 ± 0.0008	0.5602 ± 0.0183	461 ± 108	454 ± 5	99
11XL51-1-80	1.50	0.0561 ± 0.0019	0.0743 ± 0.0009	0.5634 ± 0.0173	457 ± 69	462 ± 5	98
11XL51-1-81	2.96	0.0589 ± 0.0016	0.0755 ± 0.0008	0.6116 ± 0.0159	565 ± 57	469 ± 5	96
11XL51-1-82	1.53	0.0608 ± 0.0019	0.0769 ± 0.0009	0.6414 ± 0.0189	632 ± 69	478 ± 5	94
11XL51-1-83	1.58	0.0525 ± 0.0017	0.0467 ± 0.0006	0.3316 ± 0.0097	309 ± 77	294 ± 4	98
11XL51-1-84	1.85	0.0511 ± 0.0012	0.0469 ± 0.0004	0.3313 ± 0.0077	256 ± 56	296 ± 2	98
11XL51-1-85	1.96	0.0559 ± 0.0012	0.0723 ± 0.0006	0.5573 ± 0.0113	456 ± 48	450 ± 4	99
11XL51-1-86	1.14	0.0601 ± 0.0018	0.0423 ± 0.0005	0.3494 ± 0.0099	606 ± 97	267 ± 3	87
11XL51-1-87	1.87	0.0561 ± 0.0016	0.0751 ± 0.0008	0.5811 ± 0.0167	457 ± 63	467 ± 5	99
11XL51-1-88	1.33	0.1623 ± 0.0021	0.4690 ± 0.0032	10.6284 ± 0.1324	2480 ± 22	2479 ± 14	99
11XL51-1-89	1.79	0.0543 ± 0.0012	0.0418 ± 0.0004	0.3162 ± 0.0067	383 ± 44	264 ± 2	94
11XL51-1-90	1.08	0.0530 ± 0.0012	0.0513 ± 0.0005	0.3787 ± 0.0087	332 ± 56	323 ± 3	98
11XL54-1-01	5.78	0.0543 ± 0.0010	0.0444 ± 0.0004	0.3333 ± 0.0064	383 ± 47	280 ± 2	95
11XL54-1-02	2.21	0.0522 ± 0.0011	0.0435 ± 0.0004	0.3127 ± 0.0065	295 ± 44	275 ± 2	99
11XL54-1-03	1.35	0.0553 ± 0.0012	0.0439 ± 0.0004	0.3350 ± 0.0070	433 ± 51	277 ± 2	94
11XL54-1-04	3.15	0.0496 ± 0.0010	0.0457 ± 0.0004	0.3129 ± 0.0060	176 ± 46	288 ± 2	95

(continued)

Table B.1 (continued)

Sample	U/Th	$^{206}Pb^*/^{207}Pb^*$	$^{206}Pb^*/^{238}U$	$^{207}Pb^*/^{235}U$	$^{206}Pb^*/^{207}Pb^* - Age$ [Ma]	$^{238}U/^{206}Pb - Age$ [Ma]	Concordance [%]
11XL54-1-05	3.16	0.0534 ± 0.0015	0.0430 ± 0.0004	0.3179 ± 0.0089	346 ± 65	272 ± 3	96
11XL54-1-06	4.00	0.0637 ± 0.0015	0.0408 ± 0.0004	0.3606 ± 0.0086	731 ± 55	258 ± 2	80
11XL54-1-07	6.06	0.0545 ± 0.0011	0.0470 ± 0.0003	0.3542 ± 0.0070	391 ± 46	296 ± 2	95
11XL54-1-08	1.93	0.0524 ± 0.0014	0.0423 ± 0.0004	0.3057 ± 0.0077	302 ± 59	267 ± 2	98
11XL54-1-09	1.91	0.0530 ± 0.0012	0.0405 ± 0.0003	0.2969 ± 0.0065	328 ± 56	256 ± 2	96
11XL54-1-10	0.89	0.0547 ± 0.0023	0.0423 ± 0.0005	0.3133 ± 0.0121	398 ± 99	267 ± 3	96
11XL54-1-11	4.16	0.0571 ± 0.0008	0.0411 ± 0.0003	0.3262 ± 0.0046	494 ± 31	260 ± 2	90
11XL54-1-12	2.35	0.0536 ± 0.0010	0.0430 ± 0.0004	0.3181 ± 0.0058	354 ± 43	272 ± 2	96
11XL54-1-13	1.60	0.0545 ± 0.0021	0.0449 ± 0.0006	0.3315 ± 0.0120	394 ± 85	283 ± 4	97
11XL54-1-14	1.73	0.0511 ± 0.0010	0.0432 ± 0.0003	0.3067 ± 0.0059	256 ± 44	272 ± 2	99
11XL54-1-15	3.83	0.0505 ± 0.0010	0.0426 ± 0.0003	0.2983 ± 0.0057	217 ± 44	269 ± 2	98
11XL54-1-16	1.92	0.0519 ± 0.0010	0.0428 ± 0.0003	0.3068 ± 0.0059	280 ± 46	270 ± 2	99
11XL54-1-17	3.12	0.0554 ± 0.0010	0.0424 ± 0.0003	0.3255 ± 0.0058	428 ± 45	268 ± 2	93
11XL54-1-18	1.83	0.0514 ± 0.0012	0.0445 ± 0.0004	0.3161 ± 0.0074	261 ± 58	281 ± 3	99
11XL54-1-19	1.37	0.0492 ± 0.0013	0.0424 ± 0.0004	0.2874 ± 0.0074	167 ± 61	268 ± 3	95
11XL54-1-20	2.59	0.0555 ± 0.0014	0.0399 ± 0.0004	0.3035 ± 0.0074	435 ± 62	252 ± 2	93
11XL54-1-21	2.74	0.0523 ± 0.0011	0.0414 ± 0.0004	0.2992 ± 0.0062	298 ± 44	261 ± 2	98
11XL54-1-22	2.30	0.0501 ± 0.0011	0.0409 ± 0.0003	0.2834 ± 0.0058	198 ± 53	258 ± 2	97
11XL54-1-23	3.32	0.0665 ± 0.0013	0.0366 ± 0.0003	0.3311 ± 0.0052	822 ± 39	232 ± 2	77
11XL54-1-24	1.27	0.0516 ± 0.0017	0.0440 ± 0.0005	0.3087 ± 0.0097	265 ± 74	277 ± 3	98
11XL54-1-25	4.16	0.0598 ± 0.0011	0.0412 ± 0.0003	0.3434 ± 0.0068	598 ± 36	261 ± 2	86
11XL54-1-26	1.83	0.0509 ± 0.0012	0.0416 ± 0.0003	0.2918 ± 0.0067	239 ± 58	263 ± 2	99
11XL54-1-27	3.00	0.0522 ± 0.0010	0.0406 ± 0.0003	0.2930 ± 0.0053	295 ± 47	256 ± 2	98

(continued)

Table B.1 (continued)

Sample	U/Th	$^{206}Pb^*/^{207}Pb^*$	$^{206}Pb^*/^{238}U$	$^{207}Pb^*/^{235}U$	$^{206}Pb^*/^{207}Pb^*-Age$ [Ma]	$^{238}U/^{206}Pb-Age$ [Ma]	Concordance [%]
11XL54-1-28	4.62	0.0569 ± 0.0010	0.0434 ± 0.0003	0.3411 ± 0.0061	487 ± 34	274 ± 2	91
11XL54-1-29	2.34	0.0523 ± 0.0013	0.0431 ± 0.0005	0.3088 ± 0.0077	298 ± 56	272 ± 3	99
11XL54-1-30	2.11	0.0520 ± 0.0010	0.0407 ± 0.0003	0.2929 ± 0.0054	287 ± 43	257 ± 2	98
11XL54-1-31	1.58	0.0516 ± 0.0014	0.0423 ± 0.0004	0.2991 ± 0.0080	333 ± 60	267 ± 2	99
11XL54-1-32	3.26	0.0534 ± 0.0013	0.0426 ± 0.0004	0.3152 ± 0.0075	346 ± 49	269 ± 2	96
11XL54-1-33	3.04	0.0496 ± 0.0010	0.0434 ± 0.0004	0.2980 ± 0.0059	176 ± 46	274 ± 2	96
11XL54-1-34	5.57	0.0520 ± 0.0009	0.0425 ± 0.0003	0.3066 ± 0.0052	287 ± 34	269 ± 2	98
11XL54-1-35	2.58	0.0543 ± 0.0015	0.0457 ± 0.0006	0.3391 ± 0.0091	383 ± 68	288 ± 4	97
11XL54-1-36	1.43	0.0645 ± 0.0015	0.0455 ± 0.0004	0.4073 ± 0.0095	759 ± 49	287 ± 2	80
11XL54-1-37	2.18	0.0518 ± 0.0012	0.0439 ± 0.0003	0.3147 ± 0.0070	276 ± 54	277 ± 2	99
11XL54-1-38	1.47	0.0500 ± 0.0010	0.0428 ± 0.0003	0.2968 ± 0.0057	195 ± 46	270 ± 2	97
11XL54-1-39	2.31	0.0577 ± 0.0009	0.0446 ± 0.0003	0.3578 ± 0.0056	517 ± 33	282 ± 2	90
11XL54-1-40	1.94	0.0541 ± 0.0015	0.0439 ± 0.0004	0.3266 ± 0.0080	376 ± 56	277 ± 2	96
11XL54-1-41	2.39	0.0513 ± 0.0010	0.0446 ± 0.0003	0.3170 ± 0.0062	254 ± 44	281 ± 2	99
11XL54-1-42	2.29	0.0618 ± 0.0018	0.0455 ± 0.0005	0.3853 ± 0.0112	733 ± 58	287 ± 3	85
11XL54-1-43	2.47	0.0506 ± 0.0010	0.0435 ± 0.0004	0.3030 ± 0.0057	220 ± 44	274 ± 2	97
11XL54-1-44	4.22	0.0523 ± 0.0008	0.0415 ± 0.0003	0.3009 ± 0.0046	298 ± 40	262 ± 2	98
11XL54-1-45	1.74	0.0512 ± 0.0014	0.0422 ± 0.0004	0.2967 ± 0.0080	250 ± 68	266 ± 3	99
11XL54-1-46	1.65	0.0541 ± 0.0015	0.0428 ± 0.0004	0.3171 ± 0.0086	376 ± 58	270 ± 3	96
11XL54-1-47	1.47	0.0805 ± 0.0017	0.0464 ± 0.0004	0.5183 ± 0.0114	1209 ± 42	292 ± 3	63
11XL54-1-48	0.94	0.0508 ± 0.0012	0.0452 ± 0.0004	0.3150 ± 0.0076	232 ± 56	285 ± 3	97
11XL54-1-49	3.09	0.0543 ± 0.0013	0.0508 ± 0.0005	0.3858 ± 0.0101	383 ± 52	320 ± 3	96
11XL54-1-50	2.40	0.0649 ± 0.0010	0.0712 ± 0.0009	0.6489 ± 0.0134	772 ± 33	443 ± 5	86

(continued)

Table B.1 (continued)

Sample	U/Th	$^{206}Pb^*/^{207}Pb^*$	$^{206}Pb^*/^{238}U$	$^{207}Pb^*/^{235}U$	$^{206}Pb^*/^{207}Pb^*-Age$ [Ma]	$^{238}U/^{206}Pb - Age$ [Ma]	Concordance [%]
11XL54-1-51	1.57	0.0553 ± 0.0014	0.0466 ± 0.0005	0.3522 ± 0.0085	433 ± 56	293 ± 3	95
11XL54-1-52	1.18	0.0577 ± 0.0022	0.0444 ± 0.0005	0.3486 ± 0.0132	517 ± 92	280 ± 3	91
11XL54-1-53	3.73	0.0514 ± 0.0012	0.0429 ± 0.0003	0.3056 ± 0.0067	257 ± 52	271 ± 2	99
11XL54-1-54	1.04	0.0518 ± 0.0019	0.0406 ± 0.0004	0.2879 ± 0.0105	276 ± 88	257 ± 3	99
11XL54-1-55	2.90	0.0518 ± 0.0011	0.0438 ± 0.0004	0.3143 ± 0.0066	276 ± 45	276 ± 2	99
11XL54-1-56	1.87	0.0573 ± 0.0011	0.0462 ± 0.0004	0.3665 ± 0.0065	502 ± 41	291 ± 2	91
11XL54-1-57	3.00	0.0611 ± 0.0009	0.0642 ± 0.0006	0.5455 ± 0.0094	643 ± 31	401 ± 4	90
11XL54-1-58	1.57	0.0529 ± 0.0011	0.0437 ± 0.0005	0.3183 ± 0.0069	324 ± 48	276 ± 3	98
11XL54-1-59	5.54	0.0701 ± 0.0010	0.0422 ± 0.0004	0.4089 ± 0.0060	931 ± 29	266 ± 2	73
11XL54-1-60	0.95	0.0512 ± 0.0011	0.0463 ± 0.0004	0.3254 ± 0.0069	256 ± 50	292 ± 2	98
11XL54-1-61	2.73	0.0731 ± 0.0014	0.0786 ± 0.0007	0.7952 ± 0.0151	1017 ± 38	488 ± 4	80
11XL54-1-62	4.15	0.0630 ± 0.0009	0.0423 ± 0.0003	0.3693 ± 0.0053	706 ± 34	267 ± 2	82
11XL54-1-63	0.87	0.0903 ± 0.0013	0.2457 ± 0.0017	3.0776 ± 0.0472	1431 ± 26	1416 ± 9	99
11XL54-1-64	2.11	0.0598 ± 0.0009	0.0425 ± 0.0003	0.3522 ± 0.0058	598 ± 35	269 ± 2	86
11XL54-1-65	3.09	0.0600 ± 0.0016	0.0533 ± 0.0005	0.4408 ± 0.0110	606 ± 56	335 ± 3	89
11XL54-1-66	1.16	0.0524 ± 0.0013	0.0443 ± 0.0004	0.3191 ± 0.0078	306 ± 56	279 ± 2	99
11XL54-1-67	1.91	0.0515 ± 0.0020	0.0446 ± 0.0004	0.3157 ± 0.0120	261 ± 87	281 ± 2	99
11XL54-1-68	3.41	0.0516 ± 0.0009	0.0438 ± 0.0006	0.3104 ± 0.0054	333 ± 41	276 ± 4	99
11XL54-1-69	1.57	0.0549 ± 0.0009	0.0447 ± 0.0004	0.3388 ± 0.0058	409 ± 44	282 ± 2	95
11XL54-1-70	6.82	0.0604 ± 0.0025	0.0443 ± 0.0026	0.3560 ± 0.0148	620 ± 93	279 ± 16	89
11XL54-1-71	3.16	0.0593 ± 0.0011	0.0436 ± 0.0003	0.3563 ± 0.0060	589 ± 39	275 ± 2	88
11XL54-1-72	2.15	0.0718 ± 0.0012	0.0378 ± 0.0002	0.3758 ± 0.0060	989 ± 33	239 ± 2	69
11XL54-1-73	1.49	0.0544 ± 0.0014	0.0433 ± 0.0004	0.3248 ± 0.0085	387 ± 59	274 ± 3	95

(continued)

Table B.1 (continued)

Sample	U/Th	$^{206}Pb^*/^{207}Pb^*$	$^{206}Pb^*/^{238}U$	$^{207}Pb^*/^{235}U$	$^{206}Pb^*/^{207}Pb^* - Age$ [Ma]	$^{238}U/^{206}Pb - Age$ [Ma]	Concordance [%]
11XL54-1-74	1.70	0.0531 ± 0.0010	0.0421 ± 0.0003	0.3098 ± 0.0059	332 ± 44	266 ± 2	97
11XL54-1-75	1.74	0.0530 ± 0.0011	0.0391 ± 0.0003	0.2867 ± 0.0058	332 ± 48	247 ± 2	96
11XL54-1-76	1.70	0.0554 ± 0.0013	0.0411 ± 0.0003	0.3167 ± 0.0073	428 ± 52	260 ± 2	92
11XL54-1-77	2.13	0.1595 ± 0.0019	0.3634 ± 0.0021	8.0615 ± 0.0923	2451 ± 20	1998 ± 10	88
11XL54-1-78	2.06	0.0535 ± 0.0023	0.0434 ± 0.0007	0.3109 ± 0.0120	350 ± 96	274 ± 4	99
11XL54-1-79	2.37	0.0551 ± 0.0014	0.0443 ± 0.0004	0.3372 ± 0.0084	417 ± 53	280 ± 3	94
11XL54-1-80	1.85	0.0504 ± 0.0013	0.0434 ± 0.0004	0.3021 ± 0.0077	213 ± 92	274 ± 3	97
11XL54-1-81	3.17	0.0650 ± 0.0012	0.0385 ± 0.0003	0.3461 ± 0.0058	776 ± 34	244 ± 2	78
11XL54-1-82	1.75	0.0538 ± 0.0012	0.0439 ± 0.0004	0.3281 ± 0.0074	365 ± 45	277 ± 2	95
11XL54-1-83	2.19	0.0537 ± 0.0017	0.0466 ± 0.0006	0.3464 ± 0.0111	367 ± 74	293 ± 3	97
11XL54-1-84	1.79	0.0500 ± 0.0010	0.0462 ± 0.0004	0.3192 ± 0.0061	195 ± 46	291 ± 2	96
11XL54-1-85	1.54	0.0542 ± 0.0011	0.0435 ± 0.0003	0.3262 ± 0.0062	389 ± 44	274 ± 2	95
11XL54-1-86	3.84	0.0513 ± 0.0008	0.0439 ± 0.0003	0.3122 ± 0.0051	254 ± 44	277 ± 2	99
11XL54-1-87	1.76	0.0582 ± 0.0023	0.0428 ± 0.0005	0.3437 ± 0.0140	539 ± 92	270 ± 3	89
11XL54-1-88	1.43	0.0519 ± 0.0012	0.0434 ± 0.0003	0.3103 ± 0.0068	283 ± 56	274 ± 2	99
11XL54-1-89	1.84	0.0561 ± 0.0016	0.0449 ± 0.0005	0.3445 ± 0.0097	454 ± 65	283 ± 3	94
11XL54-1-90	1.93	0.0657 ± 0.0017	0.0434 ± 0.0005	0.3891 ± 0.0099	796 ± 56	274 ± 3	80
11XL57-19	1.37	0.0516 ± 0.0012	0.0420 ± 0.0003	0.3000 ± 0.0066	333 ± 54	265 ± 2	99
11XL57-20	1.23	0.0517 ± 0.0011	0.0419 ± 0.0003	0.3014 ± 0.0063	272 ± 44	265 ± 2	98
11XL57-21	0.91	0.0611 ± 0.0020	0.0406 ± 0.0004	0.3406 ± 0.0111	643 ± 75	256 ± 3	85
11XL57-22	1.31	0.0511 ± 0.0011	0.0437 ± 0.0003	0.3088 ± 0.0068	256 ± 52	276 ± 2	99
11XL57-23	1.44	0.0502 ± 0.0011	0.0424 ± 0.0003	0.2940 ± 0.0066	206 ± 52	267 ± 2	97
11XL57-24	1.07	0.0524 ± 0.0011	0.0443 ± 0.0003	0.3221 ± 0.0066	302 ± 48	280 ± 2	98

(continued)

Table B.1 (continued)

Sample	U/Th	$^{206}Pb^*/^{207}Pb^*$	$^{206}Pb^*/^{238}U$	$^{207}Pb^*/^{235}U$	$^{206}Pb^*/^{207}Pb^* - Age$ [Ma]	$^{238}U/^{206}Pb - Age$ [Ma]	Concordance [%]
11XL57-25	1.29	0.0522 ± 0.0016	0.0425 ± 0.0004	0.3045 ± 0.0092	295 ± 64	268 ± 3	99
11XL57-26	1.42	0.0506 ± 0.0018	0.0428 ± 0.0005	0.2972 ± 0.0107	220 ± 51	270 ± 3	97
11XL57-27	1.36	0.0638 ± 0.0030	0.0443 ± 0.0007	0.3741 ± 0.0162	744 ± 98	279 ± 4	85
11XL57-28	0.74	0.0546 ± 0.0014	0.0418 ± 0.0004	0.3144 ± 0.0079	394 ± 53	264 ± 2	94
11XL57-29	0.88	0.0612 ± 0.0027	0.0436 ± 0.0007	0.3559 ± 0.0143	656 ± 94	275 ± 4	88
11XL57-30	0.83	0.0512 ± 0.0011	0.0413 ± 0.0003	0.2925 ± 0.0063	250 ± 45	261 ± 2	99
11XL57-31	1.59	0.0600 ± 0.0015	0.0434 ± 0.0004	0.3612 ± 0.0094	611 ± 54	274 ± 2	86
11XL57-32	1.04	0.0536 ± 0.0018	0.0421 ± 0.0005	0.3059 ± 0.0101	354 ± 76	266 ± 3	98
11XL57-33	0.74	0.0531 ± 0.0011	0.0428 ± 0.0003	0.3140 ± 0.0066	332 ± 53	270 ± 2	97
11XL57-34	0.41	0.0540 ± 0.0026	0.0435 ± 0.0006	0.3129 ± 0.0139	369 ± 107	274 ± 4	99
11XL57-35	1.32	0.0628 ± 0.0029	0.0400 ± 0.0006	0.3356 ± 0.0149	702 ± 100	253 ± 4	85
11XL57-36	1.75	0.0534 ± 0.0012	0.0434 ± 0.0003	0.3198 ± 0.0069	346 ± 50	274 ± 2	97
11XL57-37	0.94	0.0509 ± 0.0013	0.0412 ± 0.0004	0.2897 ± 0.0074	235 ± 59	260 ± 2	99
11XL57-38	1.39	0.0532 ± 0.0012	0.0413 ± 0.0003	0.3037 ± 0.0068	339 ± 52	261 ± 2	96
11XL57-39	1.40	0.0510 ± 0.0012	0.0411 ± 0.0004	0.2891 ± 0.0066	243 ± 54	260 ± 2	99
11XL57-40	1.55	0.0525 ± 0.0011	0.0396 ± 0.0003	0.2870 ± 0.0056	306 ± 46	250 ± 2	97
11XL57-41	1.24	0.0547 ± 0.0012	0.0424 ± 0.0003	0.3193 ± 0.0066	398 ± 53	268 ± 2	94
11XL57-42	0.37	0.0510 ± 0.0011	0.0414 ± 0.0003	0.2918 ± 0.0064	239 ± 56	262 ± 2	99
11XL57-43	1.10	0.0518 ± 0.0012	0.0426 ± 0.0003	0.3047 ± 0.0070	276 ± 47	269 ± 2	99
11XL57-44	0.37	0.0564 ± 0.0011	0.0418 ± 0.0003	0.3280 ± 0.0066	478 ± 44	264 ± 2	91
11XL57-45	0.85	0.0525 ± 0.0014	0.0445 ± 0.0004	0.3203 ± 0.0084	306 ± 63	280 ± 2	99
11XL57-46	1.19	0.0511 ± 0.0009	0.0418 ± 0.0003	0.2949 ± 0.0049	256 ± 41	264 ± 2	99
11XL57-47	1.43	0.0538 ± 0.0012	0.0438 ± 0.0004	0.3245 ± 0.0070	361 ± 50	276 ± 2	96

(continued)

Table B.1 (continued)

Sample	U/Th	$^{206}Pb^*/^{207}Pb^*$	$^{206}Pb^*/^{238}U$	$^{207}Pb^*/^{235}U$	$^{206}Pb^*/^{207}Pb^* - Age$ [Ma]	$^{238}U/^{206}Pb - Age$ [Ma]	Concordance [%]
11XL57-48	1.68	0.0505 ± 0.0011	0.0409 ± 0.0003	0.2853 ± 0.0060	217 ± 84	259 ± 2	98
11XL57-49	0.98	0.0520 ± 0.0015	0.0421 ± 0.0004	0.3009 ± 0.0084	283 ± 67	266 ± 2	99
11XL57-50	1.33	0.0495 ± 0.0018	0.0417 ± 0.0004	0.2859 ± 0.0102	172 ± 83	263 ± 3	96
11XL57-51	1.27	0.0500 ± 0.0010	0.0417 ± 0.0003	0.2884 ± 0.0054	195 ± 46	264 ± 2	97
11XL57-52	1.16	0.0526 ± 0.0020	0.0435 ± 0.0005	0.3093 ± 0.0112	322 ± 81	274 ± 3	99
11XL57-53	0.84	0.0515 ± 0.0014	0.0448 ± 0.0004	0.3164 ± 0.0083	265 ± 65	282 ± 2	98
11XL57-54	0.86	0.0509 ± 0.0011	0.0417 ± 0.0003	0.2945 ± 0.0066	239 ± 58	264 ± 2	99
11XL57-55	0.91	0.0510 ± 0.0014	0.0407 ± 0.0004	0.2857 ± 0.0079	239 ± 65	257 ± 2	99
11XL57-56	1.62	0.0496 ± 0.0010	0.0433 ± 0.0003	0.2972 ± 0.0061	189 ± 53	273 ± 2	96
11XL57-57	1.64	0.0499 ± 0.0011	0.0426 ± 0.0003	0.2950 ± 0.0066	191 ± 52	269 ± 2	97
11XL57-58	1.80	0.0505 ± 0.0010	0.0412 ± 0.0003	0.2885 ± 0.0055	217 ± 44	260 ± 2	98
11XL57-59	0.84	0.0520 ± 0.0009	0.0415 ± 0.0003	0.3005 ± 0.0051	287 ± 36	262 ± 2	98
11XL57-60	0.44	0.0513 ± 0.0009	0.0395 ± 0.0003	0.2816 ± 0.0050	254 ± 43	250 ± 2	99
11XL57-61	0.80	0.0526 ± 0.0015	0.0413 ± 0.0004	0.2975 ± 0.0083	322 ± 67	261 ± 3	98
11XL57-62	0.70	0.0533 ± 0.0015	0.0410 ± 0.0004	0.3011 ± 0.0086	343 ± 65	259 ± 2	96
11XL57-63	1.01	0.0549 ± 0.0018	0.0409 ± 0.0005	0.3040 ± 0.0098	409 ± 76	259 ± 3	95
11XL57-64	1.36	0.0529 ± 0.0022	0.0428 ± 0.0006	0.3064 ± 0.0122	324 ± 92	270 ± 4	99
11XL57-65	1.39	0.0548 ± 0.0017	0.0412 ± 0.0004	0.3120 ± 0.0090	406 ± 64	260 ± 2	94
11XL57-66	1.42	0.0531 ± 0.0019	0.0416 ± 0.0006	0.2971 ± 0.0100	332 ± 80	263 ± 4	99
11XL57-67	0.76	0.0527 ± 0.0011	0.0411 ± 0.0003	0.3002 ± 0.0058	317 ± 14	260 ± 2	97
11XL57-68	1.51	0.0520 ± 0.0014	0.0435 ± 0.0004	0.3109 ± 0.0084	287 ± 63	274 ± 2	99
11XL57-69	1.82	0.0528 ± 0.0013	0.0423 ± 0.0006	0.3042 ± 0.0074	320 ± 57	267 ± 4	99
11XL57-70	1.50	0.0487 ± 0.0012	0.0407 ± 0.0003	0.2757 ± 0.0070	200 ± 57	257 ± 2	96

(continued)

Table B.1 (continued)

Sample	U/Th	$^{206}Pb^*/^{207}Pb^*$	$^{206}Pb^*/^{238}U$	$^{207}Pb^*/^{235}U$	$^{206}Pb^*/^{207}Pb^*-Age$ [Ma]	$^{238}U/^{206}Pb-Age$ [Ma]	Concordance [%]
11XL57-71	0.93	0.0511 ± 0.0010	0.0421 ± 0.0003	0.2989 ± 0.0055	256 ± 44	266 ± 2	99
11XL57-72	1.00	0.0528 ± 0.0014	0.0414 ± 0.0004	0.3016 ± 0.0077	320 ± 66	262 ± 2	97
11XL57-73	0.98	0.0570 ± 0.0018	0.0436 ± 0.0005	0.3410 ± 0.0105	500 ± 70	275 ± 3	92
11XL57-74	0.83	0.0546 ± 0.0018	0.0426 ± 0.0004	0.3190 ± 0.0107	398 ± 79	269 ± 3	95
11XL57-75	0.39	0.0521 ± 0.0010	0.0424 ± 0.0003	0.3058 ± 0.0058	300 ± 51	268 ± 2	98
11XL57-76	1.39	0.0628 ± 0.0039	0.0409 ± 0.0008	0.3320 ± 0.0182	702 ± 133	259 ± 5	88
11XL57-77	1.01	0.0544 ± 0.0016	0.0430 ± 0.0004	0.3189 ± 0.0089	387 ± 67	271 ± 2	96
11XL57-78	1.08	0.0526 ± 0.0016	0.0411 ± 0.0004	0.2949 ± 0.0084	322 ± 73	260 ± 2	98
11XL57-79	1.37	0.0550 ± 0.0011	0.0418 ± 0.0003	0.3184 ± 0.0066	413 ± 46	264 ± 2	93
11XL57-80	0.82	0.0519 ± 0.0017	0.0421 ± 0.0004	0.2982 ± 0.0093	280 ± 72	266 ± 3	99
11XL57-81	0.56	0.0526 ± 0.0013	0.0415 ± 0.0004	0.3004 ± 0.0071	322 ± 56	262 ± 2	98
11XL57-82	0.78	0.0530 ± 0.0012	0.0417 ± 0.0003	0.3044 ± 0.0067	328 ± 56	263 ± 2	97
11XL57-83	1.24	0.0545 ± 0.0012	0.0418 ± 0.0003	0.3136 ± 0.0068	391 ± 50	264 ± 2	95
11XL57-84	1.58	0.0540 ± 0.0010	0.0417 ± 0.0003	0.3114 ± 0.0055	372 ± 41	263 ± 2	95
11XL57-85	1.82	0.0511 ± 0.0010	0.0421 ± 0.0003	0.2968 ± 0.0059	243 ± 44	266 ± 2	99
11XL57-86	1.27	0.0521 ± 0.0011	0.0419 ± 0.0003	0.3021 ± 0.0063	287 ± 53	265 ± 2	98
11XL57-87	1.14	0.0523 ± 0.0014	0.0454 ± 0.0004	0.3239 ± 0.0082	298 ± 66	286 ± 3	99
11XL57-88	1.08	0.0541 ± 0.0018	0.0427 ± 0.0005	0.3146 ± 0.0100	372 ± 79	269 ± 3	96
11XL57-89	1.13	0.0494 ± 0.0012	0.0425 ± 0.0003	0.2888 ± 0.0068	165 ± 62	268 ± 2	95
11XL57-90	1.29	0.0500 ± 0.0012	0.0420 ± 0.0004	0.2891 ± 0.0067	195 ± 58	265 ± 2	97
11XL7-2-01	8.37	0.1333 ± 0.0019	0.3037 ± 0.0025	5.6103 ± 0.0824	2143 ± 26	1710 ± 12	88
11XL7-2-02	2.87	0.0573 ± 0.0011	0.0766 ± 0.0006	0.6059 ± 0.0110	502 ± 41	476 ± 4	98
11XL7-2-03	2.94	0.1164 ± 0.0013	0.3492 ± 0.0019	5.6446 ± 0.0630	1902 ± 20	1931 ± 9	99

(continued)

Table B.1 (continued)

Sample	U/Th	$^{206}Pb^*/^{207}Pb^*$	$^{206}Pb^*/^{238}U$	$^{207}Pb^*/^{235}U$	$^{206}Pb^*/^{207}Pb^* - Age$ [Ma]	$^{238}U/^{206}Pb - Age$ [Ma]	Concordance [%]
11XL7-2-04	3.09	0.1179 ± 0.0015	0.3660 ± 0.0029	6.0016 ± 0.0837	1924 ± 22	2011 ± 14	98
11XL7-2-05	2.20	0.0608 ± 0.0009	0.0763 ± 0.0005	0.6443 ± 0.0092	632 ± 27	474 ± 3	93
11XL7-2-06	1.16	0.0607 ± 0.0018	0.0776 ± 0.0009	0.6487 ± 0.0173	632 ± 68	482 ± 5	94
11XL7-2-07	14.06	0.1135 ± 0.0012	0.3204 ± 0.0024	5.0683 ± 0.0593	1857 ± 19	1792 ± 12	97
11XL7-2-08	3.02	0.0575 ± 0.0009	0.0790 ± 0.0006	0.6305 ± 0.0097	509 ± 33	490 ± 4	98
11XL7-2-09	1.10	0.0575 ± 0.0012	0.0727 ± 0.0007	0.5757 ± 0.0115	509 ± 51	452 ± 4	97
11XL7-2-10	3.32	0.0540 ± 0.0014	0.0820 ± 0.0008	0.6157 ± 0.0158	372 ± 53	508 ± 5	95
11XL7-2-11	2.34	0.0622 ± 0.0013	0.0781 ± 0.0007	0.6690 ± 0.0132	680 ± 44	485 ± 4	93
11XL7-2-12	0.58	0.1124 ± 0.0013	0.3358 ± 0.0022	5.2570 ± 0.0615	1839 ± 21	1866 ± 11	99
11XL7-2-13	1.64	0.0581 ± 0.0008	0.0786 ± 0.0005	0.6365 ± 0.0084	600 ± 28	488 ± 3	97
11XL7-2-14	1.41	0.1117 ± 0.0014	0.3420 ± 0.0022	5.3170 ± 0.0671	1828 ± 23	1896 ± 11	98
11XL7-2-15	2.41	0.1129 ± 0.0012	0.3415 ± 0.0022	5.3723 ± 0.0563	1847 ± 19	1894 ± 11	99
11XL7-2-16	1.89	0.1445 ± 0.0017	0.2403 ± 0.0027	4.8925 ± 0.0867	2281 ± 20	1388 ± 14	74
11XL7-2-17	2.57	0.0645 ± 0.0011	0.0824 ± 0.0005	0.7392 ± 0.0123	767 ± 37	511 ± 3	90
11XL7-2-18	3.01	0.0566 ± 0.0011	0.0750 ± 0.0006	0.5904 ± 0.0117	476 ± 44	466 ± 4	98
11XL7-2-19	1.15	0.0550 ± 0.0010	0.0684 ± 0.0006	0.5225 ± 0.0092	413 ± 41	426 ± 4	99
11XL7-2-20	1.73	0.0580 ± 0.0011	0.0775 ± 0.0006	0.6250 ± 0.0114	532 ± 36	481 ± 4	97
11XL7-2-21	1.89	0.0925 ± 0.0012	0.2115 ± 0.0015	2.7253 ± 0.0367	1477 ± 24	1237 ± 8	92
11XL7-2-22	1.84	0.1484 ± 0.0016	0.4362 ± 0.0025	9.0146 ± 0.0980	2327 ± 19	2334 ± 11	99
11XL7-2-23	2.28	0.1118 ± 0.0013	0.3063 ± 0.0021	4.7579 ± 0.0572	1828 ± 22	1723 ± 10	96
11XL7-2-24	3.14	0.1260 ± 0.0013	0.3106 ± 0.0016	5.4457 ± 0.0562	2043 ± 19	1744 ± 8	91
11XL7-2-25	3.36	0.0717 ± 0.0011	0.1580 ± 0.0011	1.5739 ± 0.0241	976 ± 33	946 ± 6	98
11XL7-2-26	1.92	0.0601 ± 0.0011	0.0730 ± 0.0005	0.6080 ± 0.0105	609 ± 44	454 ± 3	93

(continued)

Table B.1 (continued)

Sample	U/Th	$^{206}Pb^*/^{207}Pb^*$	$^{206}Pb^*/^{238}U$	$^{207}Pb^*/^{235}U$	$^{206}Pb^*/^{207}Pb^* - Age$ [Ma]	$^{238}U/^{206}Pb - Age$ [Ma]	Concordance [%]
11XL7-2-27	12.48	0.1204 ± 0.0015	0.3558 ± 0.0026	5.9582 ± 0.0770	1962 ± 22	1962 ± 12	99
11XL7-2-28	2.53	0.0612 ± 0.0013	0.0781 ± 0.0007	0.6618 ± 0.0133	656 ± 44	485 ± 4	93
11XL7-2-29	2.07	0.1107 ± 0.0020	0.2682 ± 0.0021	4.1180 ± 0.0671	1811 ± 33	1532 ± 11	92
11XL7-2-30	3.85	0.0770 ± 0.0014	0.0439 ± 0.0003	0.4695 ± 0.0081	1121 ± 40	277 ± 2	65
11XL7-2-31	1.68	0.0564 ± 0.0017	0.0725 ± 0.0007	0.5649 ± 0.0174	478 ± 67	451 ± 4	99
11XL7-2-32	1.49	0.0750 ± 0.0028	0.0650 ± 0.0009	0.6718 ± 0.0242	1133 ± 75	406 ± 5	74
11XL7-2-33	2.43	0.0614 ± 0.0008	0.0722 ± 0.0005	0.6144 ± 0.0073	654 ± 28	449 ± 3	92
11XL7-2-34	2.65	0.0580 ± 0.0008	0.0738 ± 0.0004	0.5940 ± 0.0076	528 ± 34	459 ± 3	96
11XL7-2-35	1.83	0.0613 ± 0.0009	0.0738 ± 0.0007	0.6295 ± 0.0107	650 ± 33	459 ± 4	92
11XL7-2-36	1.79	0.0655 ± 0.0016	0.0666 ± 0.0006	0.6042 ± 0.0142	791 ± 51	416 ± 4	85
11XL7-2-37	3.05	0.0557 ± 0.0012	0.0569 ± 0.0005	0.4399 ± 0.0092	439 ± 46	357 ± 3	96
11XL7-2-38	2.40	0.0580 ± 0.0014	0.0663 ± 0.0007	0.5249 ± 0.0120	528 ± 56	414 ± 4	96
11XL7-2-39	3.38	0.0575 ± 0.0013	0.0784 ± 0.0007	0.6193 ± 0.0140	509 ± 52	487 ± 4	99
11XL7-2-40	1.32	0.0554 ± 0.0011	0.0638 ± 0.0006	0.4882 ± 0.0093	428 ± 47	399 ± 4	98
11XL7-2-41	1.00	0.0612 ± 0.0013	0.0683 ± 0.0007	0.5791 ± 0.0121	656 ± 44	426 ± 4	91
11XL7-2-42	37.95	0.1125 ± 0.0013	0.2362 ± 0.0015	3.6999 ± 0.0414	1840 ± 21	1367 ± 8	86
11XL7-2-43	2.85	0.0594 ± 0.0008	0.0800 ± 0.0005	0.6593 ± 0.0091	581 ± 31	496 ± 3	96
11XL7-2-44	3.83	0.1702 ± 0.0022	0.4525 ± 0.0037	10.7022 ± 0.1404	2561 ± 21	2406 ± 17	96
11XL7-2-45	2.98	0.0698 ± 0.0013	0.0656 ± 0.0006	0.6390 ± 0.0129	922 ± 39	410 ± 4	79
11XL7-2-46	2.25	0.0560 ± 0.0009	0.0697 ± 0.0005	0.5409 ± 0.0080	450 ± 33	435 ± 3	98
11XL7-2-47	2.02	0.0735 ± 0.0015	0.0706 ± 0.0006	0.7125 ± 0.0139	1028 ± 43	440 ± 4	78
11XL7-2-48	1.32	0.0560 ± 0.0014	0.0755 ± 0.0007	0.5818 ± 0.0136	454 ± 54	469 ± 4	99
11XL7-2-49	2.11	0.0575 ± 0.0011	0.0736 ± 0.0006	0.5832 ± 0.0104	509 ± 36	458 ± 3	98

(continued)

Table B.1 (continued)

Sample	U/Th	$^{206}Pb^*/^{207}Pb^*$	$^{206}Pb^*/^{238}U$	$^{207}Pb^*/^{235}U$	$^{206}Pb^*/^{207}Pb^*-Age$ [Ma]	$^{238}U/^{206}Pb - Age$ [Ma]	Concordance [%]
11XL7-2-50	1.84	0.0577 ± 0.0009	0.0808 ± 0.0006	0.6454 ± 0.0102	520 ± 35	501 ± 4	99
11XL7-2-51	2.52	0.0596 ± 0.0012	0.0762 ± 0.0006	0.6282 ± 0.0122	589 ± 43	473 ± 3	95
11XL7-2-52	2.01	0.0554 ± 0.0010	0.0731 ± 0.0006	0.5615 ± 0.0101	428 ± 44	455 ± 4	99
11XL7-2-53	2.66	0.0586 ± 0.0011	0.0727 ± 0.0006	0.5892 ± 0.0106	554 ± 36	453 ± 3	96
11XL7-2-54	2.05	0.0591 ± 0.0012	0.0782 ± 0.0007	0.6377 ± 0.0134	572 ± 46	485 ± 4	96
11XL7-2-55	4.33	0.0616 ± 0.0011	0.0734 ± 0.0006	0.6259 ± 0.0109	661 ± 39	457 ± 4	92
11XL7-2-56	2.02	0.0580 ± 0.0009	0.0809 ± 0.0007	0.6519 ± 0.0111	532 ± 35	501 ± 4	98
11XL7-2-57	2.09	0.0583 ± 0.0009	0.0814 ± 0.0008	0.6566 ± 0.0111	539 ± 35	504 ± 5	98
11XL7-2-58	2.92	0.0583 ± 0.0009	0.0796 ± 0.0006	0.6468 ± 0.0108	539 ± 33	493 ± 4	97
11XL7-2-59	1.48	0.0613 ± 0.0011	0.0678 ± 0.0005	0.5786 ± 0.0103	650 ± 37	423 ± 3	90
11XL7-2-60	1.87	0.0612 ± 0.0018	0.0438 ± 0.0005	0.3693 ± 0.0109	656 ± 63	276 ± 3	85
11XL7-2-61	2.07	0.0740 ± 0.0025	0.0423 ± 0.0005	0.4264 ± 0.0134	1043 ± 69	267 ± 3	70
11XL7-2-62	1.46	0.0570 ± 0.0014	0.0762 ± 0.0007	0.5972 ± 0.0143	500 ± 54	473 ± 4	99
11XL7-2-63	2.74	0.0607 ± 0.0023	0.0629 ± 0.0008	0.5315 ± 0.0205	632 ± 81	393 ± 5	90
11XL7-2-64	2.00	0.0701 ± 0.0018	0.0724 ± 0.0007	0.7070 ± 0.0185	931 ± 55	451 ± 4	81
11XL7-2-65	1.34	0.0972 ± 0.0014	0.2205 ± 0.0018	2.9812 ± 0.0424	1572 ± 28	1285 ± 9	91
11XL7-2-66	2.69	0.0658 ± 0.0015	0.0734 ± 0.0007	0.6696 ± 0.0148	1200 ± 49	457 ± 4	86
11XL7-2-67	2.62	0.0557 ± 0.0010	0.0682 ± 0.0005	0.5274 ± 0.0097	439 ± 41	425 ± 3	98
11XL7-2-68	1.26	0.0559 ± 0.0017	0.0666 ± 0.0007	0.5129 ± 0.0150	456 ± 67	416 ± 4	98
11XL7-2-69	1.45	0.0674 ± 0.0019	0.0682 ± 0.0008	0.6306 ± 0.0167	850 ± 59	426 ± 5	84
11XL7-2-70	3.21	0.0984 ± 0.0015	0.0620 ± 0.0005	0.8480 ± 0.0125	1595 ± 34	388 ± 3	53
11XL7-2-71	1.79	0.1087 ± 0.0014	0.2731 ± 0.0020	4.1260 ± 0.0527	1789 ± 24	1557 ± 10	93
11XL7-2-72	1.07	0.0948 ± 0.0013	0.2251 ± 0.0017	2.9670 ± 0.0408	1524 ± 26	1309 ± 9	93

(continued)

Table B.1 (continued)

Sample	U/Th	$^{206}Pb^*/^{207}Pb^*$	$^{206}Pb^*/^{238}U$	$^{207}Pb^*/^{235}U$	$^{206}Pb^*/^{207}Pb^* - Age$ [Ma]	$^{238}U/^{206}Pb - Age$ [Ma]	Concordance [%]
11XL7-2-73	3.12	0.0841 ± 0.0012	0.1718 ± 0.0018	2.0145 ± 0.0335	1295 ± 23	1022 ± 10	90
11XL7-2-74	2.37	0.0780 ± 0.0031	0.0631 ± 0.0010	0.6637 ± 0.0244	1146 ± 84	395 ± 6	73
11XL7-2-75	0.86	0.1113 ± 0.0014	0.3167 ± 0.0024	4.8981 ± 0.0625	1821 ± 22	1773 ± 12	98
11XL7-2-76	1.71	0.0583 ± 0.0009	0.0748 ± 0.0005	0.6040 ± 0.0088	543 ± 31	465 ± 3	96
11XL7-2-77	1.58	0.0566 ± 0.0019	0.0707 ± 0.0008	0.5383 ± 0.0166	476 ± 40	440 ± 5	99
11XL7-2-78	1.15	0.0580 ± 0.0012	0.0724 ± 0.0005	0.5822 ± 0.0122	528 ± 44	451 ± 3	96
11XL7-2-79	1.60	0.0564 ± 0.0012	0.0760 ± 0.0006	0.5923 ± 0.0124	478 ± 42	472 ± 4	99
11XL7-2-80	2.77	0.0561 ± 0.0008	0.0793 ± 0.0005	0.6159 ± 0.0088	454 ± 27	492 ± 3	99
11XL7-2-81	3.33	0.0598 ± 0.0010	0.0772 ± 0.0006	0.6395 ± 0.0103	594 ± 35	479 ± 4	95
11XL7-2-82	1.59	0.0573 ± 0.0012	0.0810 ± 0.0007	0.6412 ± 0.0131	502 ± 44	502 ± 4	99
11XL7-2-83	2.59	0.0692 ± 0.0012	0.0811 ± 0.0006	0.7783 ± 0.0136	906 ± 31	503 ± 3	84
11XL7-2-84	1.16	0.0630 ± 0.0014	0.0785 ± 0.0008	0.6764 ± 0.0146	709 ± 48	487 ± 5	92
11XL7-2-85	1.61	0.0604 ± 0.0010	0.0778 ± 0.0005	0.6487 ± 0.0102	617 ± 35	483 ± 3	94
11XL7-2-86	2.69	0.0657 ± 0.0018	0.0766 ± 0.0009	0.6924 ± 0.0185	798 ± 57	476 ± 6	88
11XL7-2-87	1.32	0.0679 ± 0.0013	0.0666 ± 0.0005	0.6235 ± 0.0119	865 ± 36	416 ± 3	83
11XL7-2-88	1.82	0.0727 ± 0.0019	0.0758 ± 0.0007	0.7537 ± 0.0190	1006 ± 54	471 ± 4	80
11XL7-2-89	1.61	0.0541 ± 0.0009	0.0704 ± 0.0005	0.5270 ± 0.0089	376 ± 39	438 ± 3	98
11XL7-2-90	2.15	0.0540 ± 0.0008	0.0684 ± 0.0004	0.5121 ± 0.0071	372 ± 64	426 ± 3	98
11XL15-1-01	3.03	0.0807 ± 0.0015	0.1323 ± 0.0018	1.4831 ± 0.0323	1214 ± 37	801 ± 10	85
11XL15-1-02	2.50	0.0907 ± 0.0020	0.0821 ± 0.0008	1.0368 ± 0.0232	1440 ± 42	509 ± 5	65
11XL15-1-03	1.14	0.0538 ± 0.0010	0.0453 ± 0.0004	0.3391 ± 0.0061	365 ± 41	286 ± 3	96
11XL15-1-04	1.28	0.1138 ± 0.0036	0.0456 ± 0.0005	0.7254 ± 0.0232	1861 ± 57	288 ± 3	36
11XL15-1-05	1.49	0.0567 ± 0.0012	0.0813 ± 0.0012	0.6359 ± 0.0140	480 ± 46	504 ± 7	99

(continued)

Table B.1 (continued)

Sample	U/Th	$^{206}Pb^*/^{207}Pb^*$	$^{206}Pb^*/^{238}U$	$^{207}Pb^*/^{235}U$	$^{206}Pb^*/^{207}Pb^* - Age$ [Ma]	$^{238}U/^{206}Pb - Age$ [Ma]	Concordance [%]
11XL15-1-06	2.14	0.0533 ± 0.0012	0.0720 ± 0.0007	0.5338 ± 0.0126	343 ± 54	448 ± 4	96
11XL15-1-07	2.80	0.0704 ± 0.0014	0.0833 ± 0.0010	0.8162 ± 0.0160	939 ± 45	516 ± 6	83
11XL15-1-08	1.70	0.0550 ± 0.0022	0.0434 ± 0.0008	0.3192 ± 0.0117	413 ± 89	274 ± 5	97
11XL15-1-09	3.76	0.0524 ± 0.0014	0.0436 ± 0.0005	0.3156 ± 0.0079	306 ± 61	275 ± 3	98
11XL15-1-10	0.95	0.1591 ± 0.0026	0.4755 ± 0.0041	10.5362 ± 0.1512	2447 ± 27	2508 ± 18	99
11XL15-1-11	3.54	0.0514 ± 0.0011	0.0446 ± 0.0005	0.3197 ± 0.0069	257 ± 48	281 ± 3	99
11XL15-1-12	2.05	0.0534 ± 0.0017	0.0463 ± 0.0006	0.3350 ± 0.0103	346 ± 42	292 ± 4	99
11XL15-1-13	1.62	0.0530 ± 0.0012	0.0430 ± 0.0004	0.3165 ± 0.0070	332 ± 55	272 ± 2	97
11XL15-1-14	3.34	0.0726 ± 0.0013	0.0452 ± 0.0004	0.4589 ± 0.0085	1011 ± 37	285 ± 2	70
11XL15-1-15	2.66	0.0502 ± 0.0010	0.0451 ± 0.0005	0.3134 ± 0.0062	211 ± 44	284 ± 3	97
11XL15-1-16	2.98	0.0542 ± 0.0008	0.0430 ± 0.0003	0.3239 ± 0.0046	389 ± 33	271 ± 2	95
11XL15-1-17	0.87	0.0704 ± 0.0013	0.0791 ± 0.0007	0.7731 ± 0.0137	943 ± 37	491 ± 4	83
11XL15-1-18	2.20	0.0565 ± 0.0010	0.0911 ± 0.0008	0.7153 ± 0.0133	472 ± 45	562 ± 5	97
11XL15-1-19	2.10	0.0800 ± 0.0015	0.0813 ± 0.0006	0.9025 ± 0.0165	1198 ± 37	504 ± 4	74
11XL15-1-20	3.80	0.0492 ± 0.0012	0.0407 ± 0.0004	0.2767 ± 0.0066	167 ± 57	257 ± 2	96
11XL15-1-21	3.58	0.0545 ± 0.0008	0.0417 ± 0.0003	0.3162 ± 0.0048	391 ± 33	263 ± 2	94
11XL15-1-22	2.98	0.0560 ± 0.0017	0.0385 ± 0.0004	0.2979 ± 0.0088	454 ± 69	243 ± 3	91
11XL15-1-23	2.68	0.1151 ± 0.0014	0.2861 ± 0.0019	4.5907 ± 0.0584	1881 ± 21	1622 ± 10	92
11XL15-1-24	2.18	0.0655 ± 0.0013	0.0462 ± 0.0003	0.4192 ± 0.0083	791 ± 43	291 ± 2	80
11XL15-1-25	1.91	0.0548 ± 0.0015	0.0666 ± 0.0006	0.5023 ± 0.0129	406 ± 61	416 ± 4	99
11XL15-1-26	1.96	0.0597 ± 0.0018	0.0449 ± 0.0006	0.3696 ± 0.0108	591 ± 67	283 ± 4	87
11XL15-1-27	2.04	0.0539 ± 0.0014	0.0431 ± 0.0004	0.3211 ± 0.0082	369 ± 62	272 ± 2	96
11XL15-1-28	1.46	0.0552 ± 0.0016	0.0417 ± 0.0005	0.3177 ± 0.0090	420 ± 58	264 ± 3	93

(continued)

Table B.1 (continued)

Sample	U/Th	$^{206}Pb^*/^{207}Pb^*$	$^{206}Pb^*/^{238}U$	$^{207}Pb^*/^{235}U$	$^{206}Pb^*/^{207}Pb^* - Age$ [Ma]	$^{238}U/^{206}Pb - Age$ [Ma]	Concordance [%]
11XL15-1-29	1.83	0.0843 ± 0.0012	0.2316 ± 0.0017	2.7163 ± 0.0403	1298 ± 28	1343 ± 9	99
11XL15-1-30	1.37	0.0584 ± 0.0010	0.0407 ± 0.0003	0.3286 ± 0.0055	546 ± 39	257 ± 2	88
11XL15-1-31	2.11	0.0562 ± 0.0014	0.0420 ± 0.0004	0.3254 ± 0.0078	461 ± 58	265 ± 2	92
11XL15-1-32	1.56	0.0528 ± 0.0011	0.0441 ± 0.0004	0.3229 ± 0.0067	320 ± 48	278 ± 2	97
11XL15-1-33	2.67	0.0566 ± 0.0008	0.0761 ± 0.0005	0.6005 ± 0.0081	476 ± 25	473 ± 3	99
11XL15-1-34	0.97	0.0573 ± 0.0013	0.0757 ± 0.0007	0.6019 ± 0.0136	502 ± 52	470 ± 4	98
11XL15-1-35	3.08	0.2911 ± 0.0060	0.0527 ± 0.0005	2.1349 ± 0.0442	3423 ± 32	331 ± 3	-12
11XL15-1-36	1.64	0.0554 ± 0.0009	0.0418 ± 0.0004	0.3220 ± 0.0053	428 ± 37	264 ± 2	92
11XL15-1-37	2.80	0.2543 ± 0.0126	0.0467 ± 0.0012	1.4928 ± 0.0566	3212 ± 78	294 ± 7	-4
11XL15-1-38	1.69	0.0596 ± 0.0010	0.0764 ± 0.0006	0.6346 ± 0.0110	591 ± 39	475 ± 4	94
11XL15-1-39	2.62	0.1101 ± 0.0016	0.3071 ± 0.0024	4.7051 ± 0.0666	1811 ± 26	1726 ± 12	97
11XL15-1-40	1.91	0.0684 ± 0.0012	0.0777 ± 0.0007	0.7363 ± 0.0130	880 ± 37	482 ± 4	85
11XL15-1-41	1.63	0.0742 ± 0.0012	0.0427 ± 0.0004	0.4436 ± 0.0080	1056 ± 32	270 ± 2	67
11XL15-1-42	2.29	0.0522 ± 0.0011	0.0421 ± 0.0004	0.3036 ± 0.0062	300 ± 48	266 ± 2	98
11XL15-1-43	2.24	0.1319 ± 0.0017	0.3349 ± 0.0022	6.1568 ± 0.0825	2124 ± 22	1862 ± 11	92
11XL15-1-44	1.26	0.0526 ± 0.0022	0.0474 ± 0.0006	0.3387 ± 0.0130	322 ± 96	298 ± 4	99
11XL15-1-45	1.79	0.1051 ± 0.0032	0.0466 ± 0.0006	0.6724 ± 0.0193	1717 ± 56	294 ± 4	44
11XL15-1-46	2.79	0.0559 ± 0.0019	0.0421 ± 0.0005	0.3191 ± 0.0103	456 ± 76	266 ± 3	94
11XL15-1-47	2.00	0.0666 ± 0.0013	0.0422 ± 0.0003	0.3914 ± 0.0082	833 ± 41	266 ± 2	77
11XL15-1-48	1.83	0.0567 ± 0.0011	0.0758 ± 0.0006	0.5950 ± 0.0114	480 ± 43	471 ± 4	99
11XL15-1-49	8.05	0.1094 ± 0.0013	0.2547 ± 0.0019	3.8759 ± 0.0504	1791 ± 22	1463 ± 10	90
11XL15-1-50	2.07	0.0541 ± 0.0014	0.0414 ± 0.0005	0.3078 ± 0.0076	372 ± 55	261 ± 3	95
11XL15-1-51	7.94	0.1107 ± 0.0014	0.2303 ± 0.0020	3.5370 ± 0.0490	1811 ± 24	1336 ± 10	86

(continued)

Table B.1 (continued)

Sample	U/Th	$^{206}Pb^*/^{207}Pb^*$	$^{206}Pb^*/^{238}U$	$^{207}Pb^*/^{235}U$	$^{206}Pb^*/^{207}Pb^*-Age$ [Ma]	$^{238}U/^{206}Pb - Age$ [Ma]	Concordance [%]
11XL15-1-52	3.64	0.1092 ± 0.0015	0.3249 ± 0.0029	4.9124 ± 0.0689	1787 ± 25	1814 ± 14	99
11XL15-1-53	1.75	0.1150 ± 0.0046	0.0397 ± 0.0005	0.6668 ± 0.0335	1881 ± 72	251 ± 3	30
11XL15-1-54	1.78	0.0553 ± 0.0016	0.0445 ± 0.0006	0.3378 ± 0.0093	433 ± 63	281 ± 3	94
11XL15-1-55	2.52	0.0563 ± 0.0017	0.0406 ± 0.0005	0.3166 ± 0.0096	465 ± 67	256 ± 3	91
11XL15-1-56	2.69	0.0491 ± 0.0011	0.0431 ± 0.0004	0.2925 ± 0.0068	154 ± 54	272 ± 3	95
11XL15-1-57	2.43	0.0536 ± 0.0016	0.0655 ± 0.0007	0.4804 ± 0.0134	354 ± 67	409 ± 4	97
11XL15-1-58	2.23	0.0554 ± 0.0014	0.0781 ± 0.0009	0.5963 ± 0.0146	428 ± 54	485 ± 5	97
11XL15-1-59	2.94	0.0515 ± 0.0017	0.0428 ± 0.0004	0.3005 ± 0.0093	261 ± 81	270 ± 3	98
11XL15-1-60	1.91	0.0523 ± 0.0010	0.0479 ± 0.0005	0.3465 ± 0.0066	298 ± 43	301 ± 3	99
11XL15-1-61	2.50	0.0525 ± 0.0016	0.0423 ± 0.0005	0.3024 ± 0.0088	306 ± 69	267 ± 3	99
11XL15-1-62	2.76	0.0514 ± 0.0014	0.0441 ± 0.0005	0.3119 ± 0.0085	261 ± 63	278 ± 3	99
11XL15-1-63	3.41	0.0527 ± 0.0012	0.0436 ± 0.0004	0.3164 ± 0.0066	317 ± 50	275 ± 3	98
11XL15-1-64	1.24	0.0801 ± 0.0018	0.0798 ± 0.0009	0.8904 ± 0.0211	1267 ± 39	495 ± 5	73
11XL15-1-65	2.28	0.0642 ± 0.0011	0.0952 ± 0.0009	0.8449 ± 0.0142	748 ± 37	586 ± 5	94
11XL15-1-66	4.09	0.1154 ± 0.0033	0.0428 ± 0.0005	0.6860 ± 0.0209	1887 ± 53	270 ± 3	34
11XL15-1-67	3.51	0.0587 ± 0.0010	0.0440 ± 0.0004	0.3600 ± 0.0063	567 ± 35	278 ± 2	88
11XL15-1-68	4.37	0.1144 ± 0.0013	0.3465 ± 0.0028	5.5138 ± 0.0698	1872 ± 21	1918 ± 14	99
11XL15-1-69	2.22	0.0567 ± 0.0014	0.0711 ± 0.0007	0.5563 ± 0.0131	480 ± 83	443 ± 4	98
11XL15-1-70	1.67	0.0606 ± 0.0018	0.0817 ± 0.0010	0.6746 ± 0.0199	633 ± 67	506 ± 6	96
11XL15-1-71	1.70	0.0716 ± 0.0024	0.0412 ± 0.0005	0.4079 ± 0.0142	973 ± 70	260 ± 3	71
11XL15-1-72	1.69	0.0562 ± 0.0010	0.0428 ± 0.0003	0.3332 ± 0.0058	457 ± 39	270 ± 2	92
11XL15-1-73	3.27	0.0520 ± 0.0012	0.0425 ± 0.0004	0.3049 ± 0.0065	287 ± 52	268 ± 3	99
11XL15-1-74	1.78	0.0519 ± 0.0012	0.0425 ± 0.0004	0.3040 ± 0.0069	280 ± 49	269 ± 2	99

(continued)

Table B.1 (continued)

Sample	U/Th	$^{206}Pb^*/^{207}Pb^*$	$^{206}Pb^*/^{238}U$	$^{207}Pb^*/^{235}U$	$^{206}Pb^*/^{207}Pb^* - Age$ [Ma]	$^{238}U/^{206}Pb - Age$ [Ma]	Concordance [%]
11XL15-1-75	1.55	0.0537 ± 0.0011	0.0425 ± 0.0003	0.3162 ± 0.0065	367 ± 48	268 ± 2	96
11XL15-1-76	3.18	0.0606 ± 0.0008	0.0404 ± 0.0002	0.3412 ± 0.0043	633 ± 28	255 ± 1	84
11XL15-1-77	1.72	0.0581 ± 0.0013	0.0757 ± 0.0007	0.6072 ± 0.0123	600 ± 53	471 ± 4	97
11XL15-1-78	2.42	0.0594 ± 0.0014	0.0417 ± 0.0004	0.3430 ± 0.0076	583 ± 50	264 ± 2	87
11XL15-1-79	3.27	0.1154 ± 0.0016	0.3406 ± 0.0024	5.4795 ± 0.0723	1887 ± 24	1889 ± 12	99
11XL15-1-80	2.26	0.0594 ± 0.0017	0.0418 ± 0.0005	0.3474 ± 0.0105	589 ± 60	264 ± 3	86
11XL15-1-81	1.15	0.0609 ± 0.0021	0.0731 ± 0.0010	0.6167 ± 0.0209	635 ± 71	455 ± 6	92
11XL15-1-82	2.12	0.0570 ± 0.0018	0.0404 ± 0.0004	0.3229 ± 0.0105	494 ± 64	256 ± 3	89
11XL15-1-83	2.51	0.0581 ± 0.0009	0.0448 ± 0.0004	0.3626 ± 0.0054	600 ± 33	283 ± 2	89
11XL15-1-84	1.68	0.0571 ± 0.0012	0.0780 ± 0.0007	0.6201 ± 0.0128	498 ± 44	484 ± 4	98
11XL15-1-85	2.31	0.0581 ± 0.0013	0.0765 ± 0.0006	0.6163 ± 0.0133	532 ± 53	475 ± 4	97
11XL15-1-86	1.97	0.0689 ± 0.0014	0.0431 ± 0.0003	0.4133 ± 0.0082	896 ± 72	272 ± 2	74
11XL15-1-87	2.63	0.0721 ± 0.0011	0.0430 ± 0.0003	0.4304 ± 0.0063	988 ± 27	271 ± 2	70
11XL15-1-88	1.24	0.0554 ± 0.0011	0.0685 ± 0.0006	0.5263 ± 0.0104	428 ± 44	427 ± 3	99
11XL15-1-89	2.95	0.0536 ± 0.0011	0.0415 ± 0.0003	0.3079 ± 0.0063	354 ± 81	262 ± 2	96
11XL15-1-90	1.27	0.0539 ± 0.0014	0.0406 ± 0.0004	0.3025 ± 0.0078	365 ± 64	257 ± 2	95
11XL15-1-91	1.47	0.1170 ± 0.0016	0.3293 ± 0.0022	5.3686 ± 0.0767	1922 ± 25	1835 ± 11	97
11XL15-1-92	1.54	0.1130 ± 0.0015	0.3213 ± 0.0021	5.0552 ± 0.0691	1850 ± 24	1796 ± 10	98
11XL15-1-93	3.00	0.1126 ± 0.0015	0.3218 ± 0.0020	5.0405 ± 0.0660	1842 ± 23	1799 ± 10	98
11XL15-1-94	1.79	0.0819 ± 0.0020	0.0656 ± 0.0007	0.7442 ± 0.0183	1244 ± 53	410 ± 4	68
11XL15-1-95	2.69	0.0800 ± 0.0017	0.0670 ± 0.0006	0.7417 ± 0.0155	1198 ± 43	418 ± 4	70
11XL15-1-96	3.25	0.0540 ± 0.0011	0.0429 ± 0.0004	0.3204 ± 0.0064	369 ± 44	271 ± 2	95
11XL15-1-97	2.61	0.0538 ± 0.0012	0.0445 ± 0.0004	0.3313 ± 0.0072	361 ± 44	281 ± 2	96

(continued)

Table B.1 (continued)

Sample	U/Th	$^{206}Pb^*/^{207}Pb^*$	$^{206}Pb^*/^{238}U$	$^{207}Pb^*/^{235}U$	$^{206}Pb^*/^{207}Pb^*-Age$ [Ma]	$^{238}U/^{206}Pb-Age$ [Ma]	Concordance [%]
11XL15-1-98	1.72	0.0582 ± 0.0011	0.0766 ± 0.0006	0.6184 ± 0.0114	600 ± 39	476 ± 3	97
11XL15-1-99	2.56	0.0722 ± 0.0025	0.0605 ± 0.0008	0.5905 ± 0.0198	991 ± 70	379 ± 5	78
11XL16-1-01	1.34	0.0575 ± 0.0010	0.0712 ± 0.0005	0.5675 ± 0.0101	522 ± 39	444 ± 3	97
11XL16-1-02	2.96	0.0537 ± 0.0010	0.0745 ± 0.0005	0.5522 ± 0.0100	367 ± 38	464 ± 3	96
11XL16-1-03	9.07	0.1147 ± 0.0012	0.3628 ± 0.0018	5.7796 ± 0.0593	1876 ± 19	1996 ± 9	97
11XL16-1-04	3.01	0.1155 ± 0.0013	0.3630 ± 0.0021	5.8071 ± 0.0653	1887 ± 12	1996 ± 10	97
11XL16-1-05	1.26	0.1142 ± 0.0015	0.3627 ± 0.0025	5.7287 ± 0.0742	1933 ± 24	1995 ± 12	96
11XL16-1-06	1.34	0.0574 ± 0.0012	0.0697 ± 0.0005	0.5521 ± 0.0117	509 ± 46	434 ± 3	97
11XL16-1-07	1.84	0.0516 ± 0.0011	0.0700 ± 0.0006	0.4993 ± 0.0108	333 ± 52	436 ± 3	94
11XL16-1-08	1.61	0.0599 ± 0.0013	0.0774 ± 0.0006	0.6422 ± 0.0145	611 ± 50	480 ± 4	95
11XL16-1-09	2.07	0.0574 ± 0.0015	0.0750 ± 0.0008	0.5921 ± 0.0155	506 ± 55	466 ± 5	98
11XL16-1-10	1.60	0.0511 ± 0.0007	0.0437 ± 0.0003	0.3095 ± 0.0044	256 ± 33	276 ± 2	99
11XL16-1-11	0.79	0.0518 ± 0.0010	0.0474 ± 0.0003	0.3396 ± 0.0064	276 ± 44	299 ± 2	99
11XL16-1-12	1.70	0.1648 ± 0.0018	0.4719 ± 0.0025	10.7971 ± 0.1146	2506 ± 18	2492 ± 11	99
11XL16-1-13	1.55	0.0550 ± 0.0011	0.0691 ± 0.0005	0.5258 ± 0.0101	413 ± 43	431 ± 3	99
11XL16-1-14	1.37	0.0541 ± 0.0010	0.0691 ± 0.0005	0.5156 ± 0.0097	376 ± 43	431 ± 3	98
11XL16-1-15	1.02	0.0525 ± 0.0011	0.0635 ± 0.0005	0.4591 ± 0.0091	309 ± 53	397 ± 3	96
11XL16-1-16	1.46	0.0531 ± 0.0017	0.0442 ± 0.0004	0.3245 ± 0.0102	345 ± 74	279 ± 3	97
11XL16-1-17	1.42	0.0547 ± 0.0013	0.0676 ± 0.0006	0.5061 ± 0.0111	398 ± 52	422 ± 4	98
11XL16-1-18	1.82	0.0500 ± 0.0010	0.0432 ± 0.0003	0.2984 ± 0.0059	198 ± 46	272 ± 2	97
11XL16-1-19	1.64	0.0547 ± 0.0013	0.0789 ± 0.0007	0.5955 ± 0.0139	398 ± 56	490 ± 4	96
11XL16-1-20	1.63	0.0587 ± 0.0013	0.0797 ± 0.0007	0.6460 ± 0.0140	554 ± 53	494 ± 4	97
11XL16-1-21	0.90	0.0506 ± 0.0010	0.0473 ± 0.0004	0.3325 ± 0.0073	233 ± 48	298 ± 3	97

(continued)

Table B.1 (continued)

Sample	U/Th	$^{206}Pb^*/^{207}Pb^*$	$^{206}Pb^*/^{238}U$	$^{207}Pb^*/^{235}U$	$^{206}Pb^*/^{207}Pb^* - Age$ [Ma]	$^{238}U/^{206}Pb - Age$ [Ma]	Concordance [%]
11XL16-1-22	1.99	0.0571 ± 0.0010	0.0777 ± 0.0005	0.6139 ± 0.0102	494 ± 71	482 ± 3	99
11XL16-1-23	1.43	0.0580 ± 0.0013	0.0610 ± 0.0005	0.4879 ± 0.0112	532 ± 55	381 ± 3	94
11XL16-1-24	1.58	0.1653 ± 0.0020	0.4890 ± 0.0033	11.2102 ± 0.1365	2511 ± 20	2566 ± 14	98
11XL16-1-25	0.95	0.0529 ± 0.0010	0.0609 ± 0.0004	0.4457 ± 0.0083	324 ± 43	381 ± 2	98
11XL16-1-26	1.75	0.0529 ± 0.0016	0.0444 ± 0.0005	0.3224 ± 0.0095	324 ± 70	280 ± 3	98
11XL16-1-27	3.61	0.0574 ± 0.0018	0.0734 ± 0.0008	0.5737 ± 0.0173	506 ± 69	457 ± 5	99
11XL16-1-28	1.37	0.1652 ± 0.0027	0.4132 ± 0.0039	9.4599 ± 0.1612	2510 ± 28	2230 ± 18	93
11XL16-1-29	0.96	0.0541 ± 0.0014	0.0606 ± 0.0005	0.4490 ± 0.0108	376 ± 57	379 ± 3	99
11XL16-1-30	1.03	0.0538 ± 0.0009	0.0628 ± 0.0004	0.4676 ± 0.0079	361 ± 71	393 ± 3	99
11XL16-1-31	1.67	0.0505 ± 0.0010	0.0442 ± 0.0003	0.3076 ± 0.0058	217 ± 44	279 ± 2	97
11XL16-1-32	1.56	0.1129 ± 0.0015	0.3371 ± 0.0024	5.2730 ± 0.0736	1856 ± 24	1873 ± 12	99
11XL16-1-33	5.61	0.1143 ± 0.0016	0.3443 ± 0.0022	5.4585 ± 0.0760	1869 ± 19	1907 ± 10	99
11XL16-1-34	5.19	0.1106 ± 0.0014	0.3371 ± 0.0019	5.1797 ± 0.0660	1810 ± 22	1873 ± 9	98
11XL16-1-35	1.66	0.0507 ± 0.0010	0.0435 ± 0.0003	0.3046 ± 0.0060	233 ± 72	274 ± 2	98
11XL16-1-36	0.86	0.0527 ± 0.0011	0.0625 ± 0.0005	0.4536 ± 0.0096	317 ± 16	391 ± 3	97
11XL16-1-37	1.40	0.0559 ± 0.0011	0.0643 ± 0.0005	0.4987 ± 0.0105	456 ± 17	402 ± 3	97
11XL16-1-38	15.82	0.1132 ± 0.0015	0.3436 ± 0.0019	5.4005 ± 0.0714	1854 ± 24	1904 ± 9	99
11XL16-1-39	2.58	0.1014 ± 0.0013	0.3027 ± 0.0020	4.2645 ± 0.0563	1650 ± 23	1705 ± 10	98
11XL16-1-40	2.18	0.1720 ± 0.0019	0.5324 ± 0.0032	12.7147 ± 0.1517	2577 ± 19	2752 ± 14	96
11XL16-1-41	0.93	0.0554 ± 0.0012	0.0645 ± 0.0006	0.4907 ± 0.0104	432 ± 44	403 ± 4	99
11XL16-1-42	1.16	0.0588 ± 0.0017	0.0581 ± 0.0005	0.4683 ± 0.0127	567 ± 63	364 ± 3	93
11XL16-1-43	2.06	0.1719 ± 0.0020	0.5010 ± 0.0031	11.9588 ± 0.1488	2576 ± 14	2618 ± 13	99
11XL16-1-44	12.44	0.1672 ± 0.0021	0.4891 ± 0.0030	11.3532 ± 0.1435	2531 ± 20	2567 ± 13	99

(continued)

Table B.1 (continued)

Sample	U/Th	$^{206}Pb^*/^{207}Pb^*$	$^{206}Pb^*/^{238}U$	$^{207}Pb^*/^{235}U$	$^{206}Pb^*/^{207}Pb^*-Age$ [Ma]	$^{238}U/^{206}Pb-Age$ [Ma]	Concordance [%]
11XL16-1-45	3.28	0.0606 ± 0.0030	0.0757 ± 0.0013	0.6194 ± 0.0284	633 ± 106	470 ± 8	96
11XL16-1-46	1.63	0.0552 ± 0.0013	0.0730 ± 0.0007	0.5536 ± 0.0126	420 ± 54	454 ± 4	98
11XL16-1-47	1.45	0.1678 ± 0.0021	0.4994 ± 0.0029	11.6340 ± 0.1456	2536 ± 20	2611 ± 13	98
11XL16-1-48	4.65	0.1619 ± 0.0021	0.4105 ± 0.0025	9.2318 ± 0.1179	2476 ± 22	2217 ± 11	93
11XL16-1-49	1.55	0.1171 ± 0.0016	0.3385 ± 0.0028	5.4997 ± 0.0765	1922 ± 24	1879 ± 13	98
11XL16-1-50	2.05	0.1155 ± 0.0033	0.3527 ± 0.0028	5.6266 ± 0.1558	1887 ± 52	1948 ± 13	98
11XL16-1-52	1.14	0.0552 ± 0.0012	0.0697 ± 0.0007	0.4130 ± 0.0182	420 ± 48	435 ± 4	99
11XL16-1-53	1.93	0.0592 ± 0.0020	0.0742 ± 0.0009	0.5297 ± 0.0112	576 ± 77	462 ± 5	96
11XL16-1-54	2.33	0.0559 ± 0.0013	0.0821 ± 0.0007	0.6049 ± 0.0193	450 ± 54	509 ± 4	97
11XL16-1-55	1.91	0.0534 ± 0.0021	0.0844 ± 0.0011	0.6181 ± 0.0227	346 ± 87	522 ± 6	93
11XL16-1-56	2.17	0.0539 ± 0.0010	0.0797 ± 0.0006	0.5972 ± 0.0109	369 ± 43	494 ± 4	96
11XL16-1-57	3.01	0.0556 ± 0.0010	0.0762 ± 0.0005	0.5865 ± 0.0102	435 ± 41	473 ± 3	99
11XL16-1-58	2.48	0.0573 ± 0.0009	0.0775 ± 0.0005	0.6164 ± 0.0101	502 ± 37	481 ± 3	98
11XL16-1-59	1.54	0.0515 ± 0.0010	0.0743 ± 0.0005	0.5302 ± 0.0098	261 ± 43	462 ± 3	93
11XL16-1-60	2.40	0.0560 ± 0.0013	0.0754 ± 0.0006	0.5825 ± 0.0130	450 ± 52	469 ± 4	99
11XL16-1-61	1.40	0.1195 ± 0.0018	0.3260 ± 0.0025	5.4173 ± 0.0858	1950 ± 28	1819 ± 12	96
11XL16-1-62	5.59	0.1117 ± 0.0013	0.3302 ± 0.0020	5.1379 ± 0.0613	1828 ± 22	1840 ± 10	99
11XL16-1-63	1.79	0.0546 ± 0.0011	0.0731 ± 0.0006	0.5529 ± 0.0115	398 ± 46	455 ± 4	98
11XL16-1-64	1.31	0.0542 ± 0.0012	0.0705 ± 0.0006	0.5276 ± 0.0108	389 ± 48	439 ± 4	97
11XL16-1-65	1.64	0.0528 ± 0.0021	0.0460 ± 0.0006	0.3347 ± 0.0134	320 ± 88	290 ± 4	99
11XL16-1-66	1.31	0.1659 ± 0.0020	0.5032 ± 0.0039	11.6367 ± 0.1540	2517 ± 20	2628 ± 17	98
11XL16-1-67	1.68	0.0545 ± 0.0016	0.0481 ± 0.0005	0.3569 ± 0.0101	391 ± 67	303 ± 3	97
11XL16-1-68	1.26	0.0551 ± 0.0012	0.0607 ± 0.0005	0.4619 ± 0.0098	417 ± 50	380 ± 3	98

(continued)

Table B.1 (continued)

Sample	U/Th	$^{206}Pb^*/^{207}Pb^*$	$^{206}Pb^*/^{238}U$	$^{207}Pb^*/^{235}U$	$^{206}Pb^*/^{207}Pb^*-Age$ [Ma]	$^{238}U/^{206}Pb-Age$ [Ma]	Concordance [%]
11XL16-1-69	2.11	0.1116 ± 0.0015	0.3340 ± 0.0021	5.1813 ± 0.0669	1825 ± 19	1858 ± 10	99
11XL16-1-70	1.44	0.1130 ± 0.0019	0.3308 ± 0.0030	5.1856 ± 0.0879	1848 ± 31	1842 ± 15	99
11XL16-1-71	1.53	0.0522 ± 0.0014	0.0418 ± 0.0004	0.3007 ± 0.0076	295 ± 59	264 ± 2	98
11XL16-1-72	2.15	0.0522 ± 0.0012	0.0419 ± 0.0004	0.3026 ± 0.0067	295 ± 54	265 ± 2	98
11XL16-1-73	1.58	0.1621 ± 0.0025	0.4509 ± 0.0037	10.1723 ± 0.1540	2480 ± 25	2399 ± 16	97
11XL16-1-74	1.96	0.1632 ± 0.0024	0.4379 ± 0.0030	9.9310 ± 0.1388	2489 ± 24	2341 ± 13	96
11XL16-1-75	4.86	0.0685 ± 0.0011	0.1513 ± 0.0019	1.4431 ± 0.0285	885 ± 35	908 ± 11	99
11XL16-1-76	1.49	0.0563 ± 0.0013	0.0726 ± 0.0006	0.5652 ± 0.0124	465 ± 55	452 ± 4	99
11XL16-1-77	1.79	0.0583 ± 0.0013	0.0683 ± 0.0005	0.5485 ± 0.0120	539 ± 45	426 ± 3	95
11XL16-1-78	2.97	0.0614 ± 0.0025	0.0715 ± 0.0010	0.5919 ± 0.0224	654 ± 89	445 ± 6	94
11XL16-1-79	2.02	0.0642 ± 0.0018	0.0611 ± 0.0006	0.5409 ± 0.0133	750 ± 53	382 ± 3	86
11XL16-1-80	1.85	0.0564 ± 0.0013	0.0722 ± 0.0006	0.5627 ± 0.0132	478 ± 52	450 ± 4	99
11XL16-1-81	1.90	0.0557 ± 0.0012	0.0743 ± 0.0006	0.5731 ± 0.0120	439 ± 48	462 ± 3	99
11XL16-1-82	1.04	0.0587 ± 0.0009	0.0773 ± 0.0005	0.6297 ± 0.0091	554 ± 31	480 ± 3	96
11XL16-1-83	1.71	0.1130 ± 0.0014	0.3433 ± 0.0021	5.3860 ± 0.0666	1848 ± 23	1902 ± 10	98
11XL16-1-84	1.46	0.0544 ± 0.0008	0.0692 ± 0.0004	0.5229 ± 0.0082	387 ± 33	431 ± 2	99
11XL16-1-85	1.75	0.1157 ± 0.0013	0.3512 ± 0.0021	5.6508 ± 0.0670	1891 ± 19	1940 ± 10	99
11XL16-1-86	7.01	0.1096 ± 0.0013	0.2817 ± 0.0018	4.2916 ± 0.0541	1794 ± 22	1600 ± 9	94
11XL16-1-87	3.43	0.0832 ± 0.0029	0.0650 ± 0.0008	0.7426 ± 0.0241	1273 ± 67	406 ± 5	67
11XL16-1-88	2.39	0.0563 ± 0.0011	0.0732 ± 0.0006	0.5692 ± 0.0112	461 ± 44	456 ± 4	99
11XL16-1-89	2.69	0.0926 ± 0.0024	0.0687 ± 0.0008	0.8742 ± 0.0226	1481 ± 49	428 ± 5	60
11XL16-1-90	1.14	0.0868 ± 0.0036	0.0624 ± 0.0009	0.7396 ± 0.0290	1367 ± 81	390 ± 6	63
11XL17-2-01	5.48	0.1121 ± 0.0016	0.3259 ± 0.0021	5.0929 ± 0.0707	1833 ± 25	1819 ± 10	99

(continued)

Table B.1 (continued)

Sample	U/Th	$^{206}Pb^*/^{207}Pb^*$	$^{206}Pb^*/^{238}U$	$^{207}Pb^*/^{235}U$	$^{206}Pb^*/^{207}Pb^*-Age$ [Ma]	$^{238}U/^{206}Pb-Age$ [Ma]	Concordance [%]
11XL17-2-02	4.03	0.1123 ± 0.0015	0.3332 ± 0.0020	5.2121 ± 0.0668	1836 ± 24	1854 ± 10	99
11XL17-2-03	0.76	0.0657 ± 0.0025	0.0435 ± 0.0006	0.3960 ± 0.0158	798 ± 77	274 ± 4	79
11XL17-2-04	0.63	0.0540 ± 0.0020	0.0400 ± 0.0004	0.2983 ± 0.0104	372 ± 83	253 ± 3	95
11XL17-2-05	0.69	0.0599 ± 0.0028	0.0441 ± 0.0007	0.3505 ± 0.0158	611 ± 102	278 ± 4	90
11XL17-2-06	0.94	0.0524 ± 0.0012	0.0471 ± 0.0004	0.3425 ± 0.0079	302 ± 52	297 ± 2	99
11XL17-2-07	1.95	0.0578 ± 0.0019	0.0662 ± 0.0008	0.5227 ± 0.0164	520 ± 70	413 ± 5	96
11XL17-2-08	0.58	0.0531 ± 0.0011	0.0408 ± 0.0003	0.2998 ± 0.0059	332 ± 53	258 ± 2	96
11XL17-2-09	0.54	0.0564 ± 0.0022	0.0425 ± 0.0007	0.3260 ± 0.0124	478 ± 82	268 ± 4	93
11XL17-2-10	1.59	0.1628 ± 0.0019	0.4869 ± 0.0035	11.0257 ± 0.1291	2485 ± 21	2557 ± 15	98
11XL17-2-11	1.03	0.0509 ± 0.0012	0.0445 ± 0.0004	0.3130 ± 0.0073	239 ± 56	281 ± 3	98
11XL17-2-12	0.81	0.2575 ± 0.0122	0.0515 ± 0.0011	1.7354 ± 0.0639	3231 ± 75	324 ± 7	-4
11XL17-2-13	0.58	0.0530 ± 0.0019	0.0406 ± 0.0005	0.2954 ± 0.0098	328 ± 75	256 ± 3	97
11XL17-2-14	1.15	0.0615 ± 0.0026	0.0413 ± 0.0006	0.3463 ± 0.0138	657 ± 93	261 ± 4	85
11XL17-2-15	2.07	0.1081 ± 0.0012	0.3265 ± 0.0020	4.9108 ± 0.0552	1769 ± 21	1821 ± 10	99
11XL17-2-16	2.70	0.1131 ± 0.0012	0.3451 ± 0.0021	5.4370 ± 0.0611	1850 ± 20	1911 ± 10	98
11XL17-2-17	1.56	0.0554 ± 0.0016	0.0688 ± 0.0007	0.5244 ± 0.0144	428 ± 68	429 ± 4	99
11XL17-2-18	1.55	0.0597 ± 0.0018	0.0685 ± 0.0007	0.5601 ± 0.0162	594 ± 65	427 ± 4	94
11XL17-2-19	1.45	0.0589 ± 0.0017	0.0675 ± 0.0007	0.5438 ± 0.0154	561 ± 69	421 ± 4	95
11XL17-2-20	0.81	0.0533 ± 0.0011	0.0428 ± 0.0003	0.3156 ± 0.0065	339 ± 44	270 ± 2	96
11XL17-2-21	1.01	0.0521 ± 0.0013	0.0425 ± 0.0003	0.3054 ± 0.0071	300 ± 57	269 ± 2	99
11XL17-2-22	0.59	0.0559 ± 0.0021	0.0440 ± 0.0008	0.3347 ± 0.0118	450 ± 83	278 ± 5	94
11XL17-2-23	0.68	0.0545 ± 0.0016	0.0446 ± 0.0004	0.3336 ± 0.0093	391 ± 67	281 ± 3	96
11XL17-2-24	1.07	0.1636 ± 0.0023	0.5273 ± 0.0050	11.9419 ± 0.1745	2494 ± 23	2730 ± 21	95

(continued)

Table B.1 (continued)

Sample	U/Th	$^{206}Pb^*/^{207}Pb^*$	$^{206}Pb^*/^{238}U$	$^{207}Pb^*/^{235}U$	$^{206}Pb^*/^{207}Pb^* - Age$ [Ma]	$^{238}U/^{206}Pb - Age$ [Ma]	Concordance [%]
11XL17-2-25	3.45	0.1381 ± 0.0017	0.4031 ± 0.0027	7.7374 ± 0.0947	2203 ± 21	2183 ± 12	99
11XL17-2-26	1.27	0.1189 ± 0.0014	0.3495 ± 0.0022	5.7800 ± 0.0685	1939 ± 21	1932 ± 11	99
11XL17-2-27	1.32	0.1675 ± 0.0025	0.4723 ± 0.0041	10.9765 ± 0.1645	2533 ± 24	2494 ± 18	98
11XL17-2-28	0.86	0.0519 ± 0.0008	0.0423 ± 0.0003	0.3049 ± 0.0047	280 ± 31	267 ± 2	98
11XL17-2-29	0.44	0.1188 ± 0.0047	0.0450 ± 0.0010	0.7269 ± 0.0276	1939 ± 72	284 ± 6	35
11XL17-2-30	2.80	0.1598 ± 0.0017	0.3971 ± 0.0028	8.8470 ± 0.1032	2454 ± 18	2156 ± 13	92
11XL17-2-31	1.46	0.1084 ± 0.0019	0.3395 ± 0.0031	5.0894 ± 0.0850	1773 ± 31	1884 ± 15	97
11XL17-2-32	2.21	0.1434 ± 0.0014	0.3929 ± 0.0022	7.8630 ± 0.0810	2269 ± 17	2136 ± 10	96
11XL17-2-33	1.85	0.1476 ± 0.0016	0.2722 ± 0.0018	5.6027 ± 0.0604	2318 ± 18	1552 ± 9	78
11XL17-2-34	0.53	0.0551 ± 0.0017	0.0430 ± 0.0005	0.3224 ± 0.0095	417 ± 70	272 ± 3	95
11XL17-2-35	0.68	0.0541 ± 0.0014	0.0425 ± 0.0004	0.3180 ± 0.0077	376 ± 56	269 ± 2	95
11XL17-2-36	0.86	0.0494 ± 0.0012	0.0446 ± 0.0004	0.3060 ± 0.0074	169 ± 56	281 ± 3	96
11XL17-2-37	1.13	0.1079 ± 0.0019	0.3455 ± 0.0032	5.1886 ± 0.0900	1765 ± 32	1913 ± 15	96
11XL17-2-38	0.76	0.0529 ± 0.0013	0.0494 ± 0.0005	0.3640 ± 0.0093	328 ± 25	311 ± 3	98
11XL17-2-39	1.54	0.0550 ± 0.0017	0.0693 ± 0.0007	0.5211 ± 0.0154	409 ± 67	432 ± 4	98
11XL17-2-40	1.49	0.1612 ± 0.0019	0.4933 ± 0.0035	11.0786 ± 0.1320	2468 ± 20	2585 ± 15	97
11XL17-2-41	0.69	0.0519 ± 0.0020	0.0400 ± 0.0005	0.2889 ± 0.0114	280 ± 87	253 ± 3	98
11XL17-2-42	1.00	0.0515 ± 0.0011	0.0423 ± 0.0003	0.3008 ± 0.0061	261 ± 48	267 ± 2	99
11XL17-2-43	0.60	0.0555 ± 0.0018	0.0428 ± 0.0005	0.3239 ± 0.0099	435 ± 70	270 ± 3	94
11XL17-2-44	1.18	0.0522 ± 0.0013	0.0412 ± 0.0004	0.2961 ± 0.0074	295 ± 59	260 ± 2	98
11XL17-2-45	0.87	0.0507 ± 0.0011	0.0430 ± 0.0004	0.3014 ± 0.0062	233 ± 48	272 ± 2	98
11XL17-2-46	0.61	0.0625 ± 0.0028	0.0416 ± 0.0006	0.3561 ± 0.0178	694 ± 94	263 ± 4	83
11XL17-2-47	0.50	0.0574 ± 0.0012	0.0422 ± 0.0004	0.3357 ± 0.0072	506 ± 48	266 ± 2	90

(continued)

Table B.1 (continued)

Sample	U/Th	$^{206}Pb^*/^{207}Pb^*$	$^{206}Pb^*/^{238}U$	$^{207}Pb^*/^{235}U$	$^{206}Pb^*/^{207}Pb^* - Age$ [Ma]	$^{238}U/^{206}Pb - Age$ [Ma]	Concordance [%]
11XL17-2-48	1.13	0.0529 ± 0.0014	0.0424 ± 0.0004	0.3086 ± 0.0083	324 ± 61	268 ± 3	98
11XL17-2-49	0.72	0.1139 ± 0.0018	0.3298 ± 0.0026	5.2020 ± 0.0799	1862 ± 32	1837 ± 13	99
11XL17-2-50	0.92	0.0563 ± 0.0009	0.0702 ± 0.0005	0.5498 ± 0.0092	465 ± 37	437 ± 3	98
11XL17-2-51	1.23	0.0556 ± 0.0016	0.0654 ± 0.0007	0.4987 ± 0.0149	435 ± 67	409 ± 4	99
11XL17-2-52	0.91	0.0539 ± 0.0015	0.0449 ± 0.0005	0.3341 ± 0.0093	365 ± 63	283 ± 3	96
11XL17-2-53	0.63	0.0505 ± 0.0009	0.0389 ± 0.0003	0.2730 ± 0.0051	217 ± 43	246 ± 2	99
11XL17-2-54	2.15	0.0558 ± 0.0011	0.0778 ± 0.0007	0.6035 ± 0.0115	456 ± 10	483 ± 4	99
11XL17-2-55	0.82	0.0520 ± 0.0013	0.0413 ± 0.0004	0.2971 ± 0.0075	283 ± 55	261 ± 2	98
11XL17-2-56	0.62	0.0516 ± 0.0013	0.0419 ± 0.0004	0.2986 ± 0.0073	333 ± 59	264 ± 2	99
11XL17-2-57	2.05	0.1149 ± 0.0016	0.3396 ± 0.0027	5.4375 ± 0.0779	1880 ± 24	1885 ± 13	99
11XL17-2-58	0.93	0.0536 ± 0.0012	0.0504 ± 0.0004	0.3732 ± 0.0078	354 ± 50	317 ± 3	98
11XL17-2-59	1.41	0.0564 ± 0.0015	0.0500 ± 0.0004	0.3906 ± 0.0100	478 ± 57	315 ± 3	93
11XL17-2-60	1.15	0.0548 ± 0.0015	0.0610 ± 0.0005	0.4607 ± 0.0122	406 ± 61	382 ± 3	99
11XL17-2-61	0.40	0.0658 ± 0.0015	0.0431 ± 0.0004	0.3916 ± 0.0090	798 ± 53	272 ± 2	79
11XL17-2-62	0.92	0.0772 ± 0.0032	0.0435 ± 0.0006	0.4681 ± 0.0201	1126 ± 84	274 ± 3	65
11XL17-2-63	1.75	0.0565 ± 0.0014	0.0774 ± 0.0007	0.6071 ± 0.0153	472 ± 56	481 ± 4	99
11XL17-2-64	1.77	0.0590 ± 0.0012	0.0802 ± 0.0007	0.6580 ± 0.0134	569 ± 43	497 ± 4	96
11XL17-2-65	1.61	0.0552 ± 0.0014	0.0702 ± 0.0006	0.5357 ± 0.0130	420 ± 57	437 ± 4	99
11XL17-2-66	1.30	0.0591 ± 0.0015	0.0777 ± 0.0008	0.6323 ± 0.0156	572 ± 58	482 ± 5	96
11XL17-2-67	1.40	0.1154 ± 0.0019	0.3519 ± 0.0028	5.6319 ± 0.0900	1887 ± 29	1944 ± 13	98
11XL17-2-68	1.83	0.0562 ± 0.0010	0.0730 ± 0.0006	0.5708 ± 0.0108	457 ± 41	454 ± 4	99
11XL17-2-69	0.45	0.0787 ± 0.0013	0.0421 ± 0.0003	0.4602 ± 0.0075	1165 ± 32	266 ± 2	63
11XL17-2-70	0.65	0.0518 ± 0.0007	0.0406 ± 0.0003	0.2931 ± 0.0042	276 ± 31	257 ± 2	98

(continued)

Table B.1 (continued)

Sample	U/Th	$^{206}Pb^*/^{207}Pb^*$	$^{206}Pb^*/^{238}U$	$^{207}Pb^*/^{235}U$	$^{206}Pb^*/^{207}Pb^* - Age$ [Ma]	$^{238}U/^{206}Pb - Age$ [Ma]	Concordance [%]
11XL17-2-71	0.66	0.0651 ± 0.0015	0.0429 ± 0.0004	0.3865 ± 0.0087	789 ± 49	271 ± 2	79
11XL17-2-72	0.81	0.0524 ± 0.0015	0.0426 ± 0.0004	0.3073 ± 0.0085	302 ± 65	269 ± 3	98
11XL17-2-73	1.59	0.0603 ± 0.0013	0.0690 ± 0.0006	0.5741 ± 0.0123	613 ± 48	430 ± 4	93
11XL17-2-74	1.60	0.0542 ± 0.0012	0.0745 ± 0.0007	0.5601 ± 0.0130	389 ± 50	463 ± 4	97
11XL17-2-75	1.44	0.1676 ± 0.0022	0.5104 ± 0.0043	11.8753 ± 0.1598	2600 ± 17	2658 ± 18	97
11XL17-2-76	1.31	0.1136 ± 0.0015	0.3338 ± 0.0023	5.2735 ± 0.0702	1858 ± 24	1857 ± 11	99
11XL17-2-77	0.84	0.0573 ± 0.0019	0.0443 ± 0.0005	0.3456 ± 0.0106	502 ± 72	280 ± 3	92
11XL17-2-78	1.09	0.0513 ± 0.0010	0.0430 ± 0.0003	0.3059 ± 0.0060	257 ± 46	272 ± 2	99
11XL17-2-79	1.45	0.0546 ± 0.0013	0.0763 ± 0.0008	0.5770 ± 0.0138	394 ± 56	474 ± 5	97
11XL17-2-80	1.80	0.1613 ± 0.0024	0.4530 ± 0.0038	10.1509 ± 0.1543	2470 ± 19	2408 ± 17	98
11XL17-2-81	0.89	0.1620 ± 0.0027	0.4704 ± 0.0042	10.5192 ± 0.1659	2476 ± 29	2485 ± 19	99
11XL17-2-82	1.45	0.1666 ± 0.0020	0.4708 ± 0.0030	10.9184 ± 0.1311	2524 ± 20	2487 ± 13	98
11XL17-2-83	1.14	0.0522 ± 0.0011	0.0413 ± 0.0003	0.2993 ± 0.0063	295 ± 44	261 ± 2	98
11XL17-2-84	1.44	0.0555 ± 0.0015	0.0428 ± 0.0004	0.3284 ± 0.0086	435 ± 61	270 ± 3	93
11XL17-2-85	1.35	0.0578 ± 0.0015	0.0656 ± 0.0005	0.5232 ± 0.0127	524 ± 62	410 ± 3	95
11XL17-2-86	0.57	0.0515 ± 0.0016	0.0432 ± 0.0004	0.3059 ± 0.0085	265 ± 69	273 ± 3	99
11XL17-2-87	1.74	0.1197 ± 0.0022	0.3514 ± 0.0032	5.8068 ± 0.1042	1952 ± 33	1941 ± 15	99
11XL17-2-88	2.56	0.1147 ± 0.0015	0.3407 ± 0.0022	5.4389 ± 0.0699	1876 ± 24	1890 ± 11	99
11XL17-2-89	2.46	0.1174 ± 0.0024	0.3343 ± 0.0036	5.4340 ± 0.1139	1918 ± 37	1859 ± 18	98
11XL17-2-90	0.61	0.0556 ± 0.0013	0.0627 ± 0.0006	0.4840 ± 0.0115	435 ± 49	392 ± 3	97
11XL20-01	1.02	0.0534 ± 0.0021	0.0601 ± 0.0007	0.4415 ± 0.0172	343 ± 91	376 ± 4	98
11XL20-02	1.49	0.0599 ± 0.0013	0.0811 ± 0.0007	0.6712 ± 0.0146	611 ± 51	502 ± 4	96
11XL20-03	1.78	0.0560 ± 0.0010	0.0764 ± 0.0006	0.5899 ± 0.0103	454 ± 41	475 ± 3	99

(continued)

Table B.1 (continued)

Sample	U/Th	$^{206}Pb^*/^{207}Pb^*$	$^{206}Pb^*/^{238}U$	$^{207}Pb^*/^{235}U$	$^{206}Pb^*/^{207}Pb^* - Age$ [Ma]	$^{238}U/^{206}Pb - Age$ [Ma]	Concordance [%]
11XL20-04	2.02	0.0559 ± 0.0013	0.0699 ± 0.0005	0.5400 ± 0.0130	456 ± 52	436 ± 3	99
11XL20-05	1.50	0.1142 ± 0.0012	0.3359 ± 0.0018	5.3242 ± 0.0566	1933 ± 20	1867 ± 9	99
11XL20-06	4.82	0.1058 ± 0.0010	0.2942 ± 0.0019	4.3322 ± 0.0463	1729 ± 12	1663 ± 10	97
11XL20-07	8.44	0.1255 ± 0.0014	0.3681 ± 0.0021	6.4452 ± 0.0823	2037 ± 21	2021 ± 10	99
11XL20-08	0.71	0.0516 ± 0.0011	0.0536 ± 0.0005	0.3801 ± 0.0080	265 ± 53	336 ± 3	97
11XL20-09	1.27	0.1136 ± 0.0014	0.3402 ± 0.0020	5.3696 ± 0.0649	1857 ± 22	1888 ± 10	99
11XL20-10	1.93	0.0546 ± 0.0008	0.0727 ± 0.0004	0.5502 ± 0.0081	398 ± 35	452 ± 3	98
11XL20-11	4.29	0.0516 ± 0.0008	0.0441 ± 0.0003	0.3156 ± 0.0050	333 ± 35	278 ± 2	99
11XL20-12	1.37	0.0568 ± 0.0012	0.0732 ± 0.0006	0.5728 ± 0.0117	483 ± 48	456 ± 4	99
11XL20-13	0.50	0.0531 ± 0.0012	0.0447 ± 0.0004	0.3282 ± 0.0076	345 ± 54	282 ± 2	97
11XL20-14	7.07	0.1098 ± 0.0012	0.3273 ± 0.0020	4.9975 ± 0.0569	1796 ± 21	1825 ± 9	99
11XL20-15	1.61	0.0554 ± 0.0012	0.0757 ± 0.0007	0.5795 ± 0.0130	428 ± 50	470 ± 4	98
11XL20-16	2.51	0.0561 ± 0.0014	0.0743 ± 0.0007	0.5774 ± 0.0147	457 ± 62	462 ± 4	99
11XL20-17	1.99	0.0584 ± 0.0014	0.0779 ± 0.0007	0.6276 ± 0.0142	546 ± 50	483 ± 4	97
11XL20-18	1.27	0.0539 ± 0.0011	0.0534 ± 0.0004	0.3985 ± 0.0079	365 ± 48	336 ± 2	98
11XL20-19	1.28	0.0610 ± 0.0019	0.0561 ± 0.0006	0.4706 ± 0.0142	639 ± 65	352 ± 4	89
11XL20-20	1.13	0.1266 ± 0.0020	0.3967 ± 0.0032	6.9780 ± 0.1121	2052 ± 23	2154 ± 15	97
11XL20-21	3.10	0.0520 ± 0.0008	0.0502 ± 0.0003	0.3631 ± 0.0057	283 ± 32	316 ± 2	99
11XL20-22	1.26	0.0571 ± 0.0019	0.0684 ± 0.0008	0.5334 ± 0.0176	494 ± 74	426 ± 5	98
11XL20-23	0.99	0.0548 ± 0.0011	0.0666 ± 0.0005	0.5056 ± 0.0099	467 ± 44	415 ± 3	99
11XL20-24	2.17	0.0570 ± 0.0010	0.0824 ± 0.0006	0.6523 ± 0.0113	494 ± 39	510 ± 3	99
11XL20-25	2.00	0.1069 ± 0.0014	0.3098 ± 0.0019	4.6080 ± 0.0581	1747 ± 24	1740 ± 9	99
11XL20-26	4.28	0.1122 ± 0.0015	0.3345 ± 0.0027	5.2167 ± 0.0717	1835 ± 24	1860 ± 13	99

(continued)

Table B.1 (continued)

Sample	U/Th	$^{206}Pb^*/^{207}Pb^*$	$^{206}Pb^*/^{238}U$	$^{207}Pb^*/^{235}U$	$^{206}Pb^*/^{207}Pb^* - Age$ [Ma]	$^{238}U/^{206}Pb - Age$ [Ma]	Concordance [%]
11XL20-27	5.16	0.1737 ± 0.0023	0.5161 ± 0.0038	12.4925 ± 0.1722	2594 ± 23	2683 ± 16	98
11XL20-28	2.89	0.1133 ± 0.0015	0.3501 ± 0.0021	5.5141 ± 0.0706	1854 ± 24	1935 ± 10	98
11XL20-29	1.88	0.0574 ± 0.0013	0.0631 ± 0.0005	0.4997 ± 0.0113	506 ± 56	394 ± 3	95
11XL20-30	2.87	0.0555 ± 0.0015	0.0707 ± 0.0007	0.5458 ± 0.0156	432 ± 66	440 ± 4	99
11XL20-31	2.05	0.0670 ± 0.0023	0.0521 ± 0.0006	0.4777 ± 0.0156	839 ± 70	327 ± 3	80
11XL20-32	1.83	0.0551 ± 0.0007	0.0696 ± 0.0004	0.5328 ± 0.0069	417 ± 28	434 ± 2	99
11XL20-33	2.26	0.0551 ± 0.0009	0.0706 ± 0.0005	0.5387 ± 0.0091	413 ± 39	440 ± 3	99
11XL20-34	1.89	0.1166 ± 0.0014	0.3478 ± 0.0021	5.6356 ± 0.0685	1906 ± 21	1924 ± 10	99
11XL20-35	5.24	0.0518 ± 0.0012	0.0436 ± 0.0003	0.3107 ± 0.0069	276 ± 47	275 ± 2	99
11XL20-36	4.85	0.0511 ± 0.0012	0.0427 ± 0.0004	0.2998 ± 0.0070	256 ± 57	269 ± 2	98
11XL20-37	1.39	0.1590 ± 0.0023	0.4358 ± 0.0031	9.6159 ± 0.1348	2456 ± 24	2332 ± 14	97
11XL20-38	3.80	0.1640 ± 0.0021	0.3645 ± 0.0023	8.3071 ± 0.1032	2498 ± 21	2004 ± 11	87
11XL20-39	1.76	0.0568 ± 0.0011	0.0710 ± 0.0006	0.5556 ± 0.0106	487 ± 43	442 ± 4	98
11XL20-40	7.51	0.0526 ± 0.0012	0.0457 ± 0.0004	0.3325 ± 0.0073	322 ± 52	288 ± 2	98
11XL20-41	2.44	0.0552 ± 0.0009	0.0699 ± 0.0005	0.5372 ± 0.0087	420 ± 35	436 ± 3	99
11XL20-42	1.02	0.1639 ± 0.0023	0.4950 ± 0.0031	11.2889 ± 0.1484	2496 ± 24	2592 ± 13	98
11XL20-43	1.47	0.1635 ± 0.0021	0.4202 ± 0.0029	9.5602 ± 0.1156	2492 ± 20	2262 ± 13	94
11XL20-44	1.66	0.0565 ± 0.0010	0.0800 ± 0.0006	0.6277 ± 0.0106	478 ± 39	496 ± 4	99
11XL20-45	2.23	0.1101 ± 0.0015	0.3381 ± 0.0024	5.1959 ± 0.0688	1802 ± 25	1877 ± 12	98
11XL20-46	1.26	0.0578 ± 0.0012	0.0788 ± 0.0007	0.6365 ± 0.0136	524 ± 46	489 ± 4	97
11XL20-47	0.94	0.0954 ± 0.0013	0.2709 ± 0.0023	3.5933 ± 0.0490	1537 ± 27	1545 ± 12	99
11XL20-48	5.19	0.1165 ± 0.0013	0.3780 ± 0.0027	6.1507 ± 0.0747	1902 ± 20	2067 ± 13	96
11XL20-49	2.15	0.1126 ± 0.0013	0.3484 ± 0.0021	5.4737 ± 0.0626	1842 ± 22	1927 ± 10	98

(continued)

Table B.1 (continued)

Sample	U/Th	$^{206}Pb^*/^{207}Pb^*$	$^{206}Pb^*/^{238}U$	$^{207}Pb^*/^{235}U$	$^{206}Pb^*/^{207}Pb^*-Age$ [Ma]	$^{238}U/^{206}Pb-Age$ [Ma]	Concordance [%]
11XL20-50	1.62	0.0589 ± 0.0010	0.0718 ± 0.0005	0.5882 ± 0.0100	561 ± 37	447 ± 3	95
11XL20-51	1.28	0.1128 ± 0.0013	0.3465 ± 0.0023	5.4467 ± 0.0638	1856 ± 21	1918 ± 11	98
11XL20-52	1.51	0.1175 ± 0.0015	0.3571 ± 0.0024	5.8294 ± 0.0723	1918 ± 24	1969 ± 12	99
11XL20-53	2.03	0.0536 ± 0.0013	0.0423 ± 0.0003	0.3152 ± 0.0074	354 ± 54	267 ± 2	95
11XL20-54	2.04	0.0523 ± 0.0009	0.0470 ± 0.0003	0.3415 ± 0.0059	298 ± 44	296 ± 2	99
11XL20-55	2.35	0.0581 ± 0.0012	0.0734 ± 0.0007	0.5924 ± 0.0125	532 ± 44	457 ± 4	96
11XL20-56	0.74	0.0534 ± 0.0013	0.0482 ± 0.0004	0.3550 ± 0.0087	346 ± 90	303 ± 3	98
11XL20-57	1.99	0.1488 ± 0.0020	0.4550 ± 0.0031	9.4315 ± 0.1336	2332 ± 23	2417 ± 14	98
11XL20-58	2.10	0.1468 ± 0.0017	0.4232 ± 0.0026	8.6539 ± 0.1070	2310 ± 15	2275 ± 12	98
11XL20-59	1.02	0.0531 ± 0.0009	0.0463 ± 0.0003	0.3409 ± 0.0057	332 ± 34	292 ± 2	97
11XL20-60	0.63	0.1128 ± 0.0017	0.3496 ± 0.0029	5.4390 ± 0.0795	1856 ± 28	1933 ± 14	97
11XL20-61	1.03	0.1182 ± 0.0014	0.3193 ± 0.0021	5.2535 ± 0.0695	1929 ± 22	1786 ± 10	95
11XL20-62	2.12	0.0706 ± 0.0012	0.0595 ± 0.0004	0.5826 ± 0.0102	946 ± 36	372 ± 2	77
11XL20-63	2.07	0.0553 ± 0.0012	0.0756 ± 0.0006	0.5782 ± 0.0120	433 ± 42	470 ± 4	98
11XL20-64	0.70	0.1166 ± 0.0016	0.3388 ± 0.0023	5.4778 ± 0.0775	1906 ± 25	1881 ± 11	99
11XL20-65	1.52	0.0565 ± 0.0008	0.0774 ± 0.0005	0.6069 ± 0.0088	472 ± 33	481 ± 3	99
11XL20-66	1.78	0.0519 ± 0.0013	0.0470 ± 0.0005	0.3341 ± 0.0079	280 ± 56	296 ± 3	98
11XL20-67	2.14	0.0564 ± 0.0010	0.0815 ± 0.0007	0.6357 ± 0.0116	478 ± 38	505 ± 4	98
11XL20-68	1.88	0.1055 ± 0.0011	0.2944 ± 0.0021	4.3375 ± 0.0543	1724 ± 20	1663 ± 11	97
11XL20-69	0.81	0.0555 ± 0.0021	0.0466 ± 0.0008	0.3495 ± 0.0127	432 ± 88	293 ± 5	96
11XL20-70	1.14	0.1598 ± 0.0017	0.4683 ± 0.0034	10.4330 ± 0.1215	2453 ± 19	2476 ± 15	99
11XL20-71	1.82	0.0570 ± 0.0009	0.0802 ± 0.0007	0.6360 ± 0.0103	500 ± 35	497 ± 4	99
11XL20-72	1.21	0.0555 ± 0.0011	0.0743 ± 0.0007	0.5761 ± 0.0121	435 ± 43	462 ± 4	99

(continued)

Table B.1 (continued)

Sample	U/Th	$^{206}Pb^*/^{207}Pb^*$	$^{206}Pb^*/^{238}U$	$^{207}Pb^*/^{235}U$	$^{206}Pb^*/^{207}Pb^* - Age$ [Ma]	$^{238}U/^{206}Pb - Age$ [Ma]	Concordance [%]
11XL20-73	4.66	0.0778 ± 0.0012	0.1402 ± 0.0012	1.5240 ± 0.0238	1143 ± 25	846 ± 7	89
11XL20-74	2.26	0.0569 ± 0.0011	0.0639 ± 0.0005	0.5068 ± 0.0099	487 ± 43	399 ± 3	95
11XL20-75	1.77	0.0521 ± 0.0011	0.0449 ± 0.0004	0.3243 ± 0.0068	300 ± 50	283 ± 3	99
11XL20-76	1.34	0.1621 ± 0.0018	0.4564 ± 0.0028	10.3364 ± 0.1130	2477 ± 18	2424 ± 12	98
11XL20-77	1.54	0.0557 ± 0.0013	0.0703 ± 0.0006	0.5427 ± 0.0118	439 ± 56	438 ± 3	99
11XL20-78	1.78	0.0545 ± 0.0008	0.0714 ± 0.0005	0.5427 ± 0.0077	391 ± 33	445 ± 3	98
11XL20-79	3.01	0.0515 ± 0.0010	0.0428 ± 0.0003	0.3074 ± 0.0061	261 ± 46	270 ± 2	99
11XL20-80	1.58	0.0498 ± 0.0012	0.0443 ± 0.0004	0.3063 ± 0.0071	187 ± 54	280 ± 2	97
11XL20-81	5.40	0.1449 ± 0.0019	0.4128 ± 0.0028	8.3648 ± 0.1068	2287 ± 22	2228 ± 13	98
11XL20-82	1.75	0.0504 ± 0.0011	0.0399 ± 0.0004	0.2790 ± 0.0059	213 ± 52	252 ± 2	99
11XL20-83	1.41	0.0546 ± 0.0011	0.0698 ± 0.0006	0.5293 ± 0.0107	394 ± 46	435 ± 4	99
11XL20-84	3.05	0.0539 ± 0.0007	0.0658 ± 0.0004	0.4945 ± 0.0066	369 ± 27	411 ± 3	99
11XL20-85	2.93	0.1627 ± 0.0018	0.4655 ± 0.0029	10.5685 ± 0.1166	2484 ± 19	2464 ± 13	99
11XL20-86	1.40	0.1634 ± 0.0019	0.4907 ± 0.0033	11.1913 ± 0.1265	2491 ± 19	2574 ± 14	98
11XL20-87	2.04	0.0573 ± 0.0012	0.0624 ± 0.0005	0.4972 ± 0.0102	506 ± 46	390 ± 3	95
11XL20-88	2.60	0.0552 ± 0.0011	0.0695 ± 0.0005	0.5330 ± 0.0104	420 ± 46	433 ± 3	99
11XL20-89	3.97	0.0579 ± 0.0013	0.0638 ± 0.0005	0.5114 ± 0.0107	528 ± 48	399 ± 3	95
11XL20-90	1.86	0.0557 ± 0.0024	0.0391 ± 0.0005	0.2999 ± 0.0124	439 ± 94	247 ± 3	92
11XL20-91	1.17	0.0922 ± 0.0016	0.2595 ± 0.0020	3.3230 ± 0.0544	1472 ± 33	1487 ± 10	99
11XL20-92	5.41	0.1272 ± 0.0018	0.3578 ± 0.0027	6.3632 ± 0.0984	2061 ± 25	1972 ± 13	97
11XL20-93	1.70	0.0548 ± 0.0011	0.0669 ± 0.0006	0.5085 ± 0.0099	467 ± 44	418 ± 3	99
11XL20-94	2.07	0.0578 ± 0.0009	0.0798 ± 0.0005	0.6421 ± 0.0103	520 ± 40	495 ± 3	98
11XL20-95	2.73	0.1104 ± 0.0014	0.3381 ± 0.0018	5.1969 ± 0.0607	1806 ± 22	1878 ± 9	98

(continued)

Table B.1 (continued)

Sample	U/Th	$^{206}Pb^*/^{207}Pb^*$	$^{206}Pb^*/^{238}U$	$^{207}Pb^*/^{235}U$	$^{206}Pb^*/^{207}Pb^*-Age$ [Ma]	$^{238}U/^{206}Pb-Age$ [Ma]	Concordance [%]
11XL20-96	1.67	0.0551 ± 0.0008	0.0795 ± 0.0005	0.6094 ± 0.0087	417 ± 33	493 ± 3	97
11XL20-97	2.80	0.1081 ± 0.0014	0.3301 ± 0.0019	4.9767 ± 0.0599	1769 ± 24	1839 ± 9	98
11XL20-98	1.33	0.0518 ± 0.0011	0.0459 ± 0.0004	0.3284 ± 0.0062	276 ± 46	289 ± 3	99
11XL20-99	3.15	0.0903 ± 0.0015	0.1723 ± 0.0012	2.1687 ± 0.0346	1431 ± 32	1025 ± 7	86
11XL14-2-01	0.92	0.0531 ± 0.0010	0.0489 ± 0.0004	0.3603 ± 0.0063	332 ± 36	308 ± 2	98
11XL14-2-02	1.94	0.0530 ± 0.0008	0.0512 ± 0.0004	0.3774 ± 0.0059	332 ± 35	322 ± 2	98
11XL14-2-03	1.85	0.0518 ± 0.0010	0.0384 ± 0.0003	0.2750 ± 0.0051	276 ± 43	243 ± 2	98
11XL14-2-04	1.65	0.1196 ± 0.0012	0.3404 ± 0.0018	5.6681 ± 0.0591	1950 ± 19	1889 ± 9	98
11XL14-2-05	1.75	0.0531 ± 0.0012	0.0459 ± 0.0004	0.3351 ± 0.0070	332 ± 55	289 ± 2	98
11XL14-2-06	0.92	0.0656 ± 0.0017	0.0377 ± 0.0004	0.3373 ± 0.0083	794 ± 58	238 ± 2	78
11XL14-2-07	1.85	0.0576 ± 0.0022	0.0426 ± 0.0005	0.3305 ± 0.0118	517 ± 83	269 ± 3	92
11XL14-2-08	2.82	0.0523 ± 0.0011	0.0379 ± 0.0003	0.2737 ± 0.0053	298 ± 48	240 ± 2	97
11XL14-2-09	1.11	0.0561 ± 0.0017	0.0428 ± 0.0004	0.3292 ± 0.0097	457 ± 67	270 ± 3	93
11XL14-2-10	2.64	0.0560 ± 0.0007	0.0700 ± 0.0004	0.5442 ± 0.0072	450 ± 23	436 ± 3	98
11XL14-2-11	1.50	0.0640 ± 0.0021	0.0353 ± 0.0004	0.3054 ± 0.0092	743 ± 69	223 ± 3	80
11XL14-2-12	2.89	0.0560 ± 0.0015	0.0364 ± 0.0004	0.2807 ± 0.0073	454 ± 64	231 ± 2	91
11XL14-2-13	4.75	0.1791 ± 0.0021	0.4774 ± 0.0040	11.8754 ± 0.1471	2656 ± 19	2516 ± 18	96
11XL14-2-14	2.72	0.0527 ± 0.0012	0.0387 ± 0.0004	0.2821 ± 0.0064	317 ± 50	245 ± 2	97
11XL14-2-15	2.35	0.0527 ± 0.0014	0.0381 ± 0.0003	0.2755 ± 0.0068	317 ± 61	241 ± 2	97
11XL14-2-16	2.50	0.0506 ± 0.0011	0.0388 ± 0.0003	0.2711 ± 0.0059	220 ± 52	245 ± 2	99
11XL14-2-17	3.05	0.0693 ± 0.0025	0.0388 ± 0.0004	0.3740 ± 0.0138	907 ± 79	245 ± 3	72
11XL14-2-18	2.02	0.0527 ± 0.0010	0.0700 ± 0.0005	0.5121 ± 0.0099	322 ± 17	436 ± 3	96
11XL14-2-19	2.47	0.0514 ± 0.0012	0.0380 ± 0.0003	0.2708 ± 0.0062	257 ± 49	240 ± 2	98

(continued)

Table B.1 (continued)

Sample	U/Th	$^{206}Pb^*/^{207}Pb^*$	$^{206}Pb^*/^{238}U$	$^{207}Pb^*/^{235}U$	$^{206}Pb^*/^{207}Pb^* - Age$ [Ma]	$^{238}U/^{206}Pb - Age$ [Ma]	Concordance [%]
11XL14-2-20	1.00	0.0511 ± 0.0016	0.0384 ± 0.0004	0.2677 ± 0.0081	256 ± 74	243 ± 3	99
11XL14-2-21	0.98	0.0517 ± 0.0015	0.0456 ± 0.0005	0.3235 ± 0.0092	272 ± 64	287 ± 3	99
11XL14-2-22	5.47	0.0643 ± 0.0015	0.0533 ± 0.0006	0.4687 ± 0.0095	754 ± 249	335 ± 4	84
11XL14-2-23	2.05	0.0536 ± 0.0015	0.0390 ± 0.0003	0.2881 ± 0.0080	354 ± 63	247 ± 2	95
11XL14-2-24	1.71	0.0530 ± 0.0010	0.0393 ± 0.0003	0.2891 ± 0.0056	328 ± 43	249 ± 2	96
11XL14-2-25	1.24	0.0568 ± 0.0019	0.0343 ± 0.0004	0.2705 ± 0.0089	483 ± 72	218 ± 2	88
11XL14-2-26	2.13	0.0533 ± 0.0016	0.0365 ± 0.0004	0.2671 ± 0.0076	339 ± 67	231 ± 2	96
11XL14-2-27	0.73	0.0586 ± 0.0018	0.0413 ± 0.0004	0.3294 ± 0.0098	550 ± 67	261 ± 3	89
11XL14-2-28	1.52	0.0507 ± 0.0018	0.0383 ± 0.0005	0.2616 ± 0.0085	228 ± 80	242 ± 3	97
11XL14-2-29	4.94	0.0514 ± 0.0011	0.0405 ± 0.0003	0.2879 ± 0.0062	257 ± 50	256 ± 2	99
11XL14-2-30	1.57	0.0529 ± 0.0015	0.0384 ± 0.0005	0.2804 ± 0.0082	328 ± 67	243 ± 3	96
11XL14-2-31	0.73	0.0615 ± 0.0015	0.0297 ± 0.0002	0.2522 ± 0.0058	657 ± 52	189 ± 1	80
11XL14-2-32	0.61	0.0524 ± 0.0008	0.0392 ± 0.0002	0.2847 ± 0.0041	302 ± 6	248 ± 2	97
11XL14-2-33	1.90	0.0557 ± 0.0021	0.0345 ± 0.0004	0.2651 ± 0.0096	439 ± 85	219 ± 3	91
11XL14-2-34	1.88	0.0593 ± 0.0011	0.0724 ± 0.0005	0.5938 ± 0.0109	576 ± 8	450 ± 3	95
11XL14-2-35	4.81	0.0572 ± 0.0007	0.0683 ± 0.0004	0.5433 ± 0.0069	502 ± 28	426 ± 2	96
11XL14-2-36	1.75	0.0558 ± 0.0020	0.0414 ± 0.0005	0.3121 ± 0.0103	456 ± 80	262 ± 3	94
11XL14-2-37	2.95	0.0580 ± 0.0011	0.0749 ± 0.0006	0.6022 ± 0.0110	528 ± 41	465 ± 3	97
11XL14-2-38	1.56	0.0534 ± 0.0013	0.0456 ± 0.0004	0.3363 ± 0.0077	346 ± 52	288 ± 2	97
11XL14-2-39	2.66	0.0529 ± 0.0019	0.0345 ± 0.0003	0.2524 ± 0.0089	324 ± 112	218 ± 2	95
11XL14-2-40	1.31	0.0556 ± 0.0009	0.0763 ± 0.0006	0.5884 ± 0.0096	435 ± 37	474 ± 3	99
11XL14-2-41	1.91	0.1623 ± 0.0015	0.4582 ± 0.0025	10.3445 ± 0.1022	2480 ± 16	2432 ± 11	98
11XL14-2-42	1.31	0.0560 ± 0.0017	0.0530 ± 0.0006	0.4095 ± 0.0128	454 ± 69	333 ± 3	95

(continued)

Table B.1 (continued)

Sample	U/Th	$^{206}Pb^{*}/^{207}Pb^{*}$	$^{206}Pb^{*}/^{238}U$	$^{207}Pb^{*}/^{235}U$	$^{206}Pb^{*}/^{207}Pb^{*}-Age$ [Ma]	$^{238}U/^{206}Pb-Age$ [Ma]	Concordance [%]
11XL14-2-43	1.88	0.0519 ± 0.0007	0.0414 ± 0.0003	0.2983 ± 0.0043	283 ± 36	261 ± 2	98
11XL14-2-44	2.03	0.0560 ± 0.0011	0.0721 ± 0.0006	0.5574 ± 0.0110	450 ± 44	449 ± 3	99
11XL14-2-45	2.13	0.1105 ± 0.0014	0.3549 ± 0.0024	5.4489 ± 0.0699	1809 ± 24	1958 ± 12	96
11XL14-2-46	2.55	0.0529 ± 0.0011	0.0408 ± 0.0003	0.2983 ± 0.0059	324 ± 46	258 ± 2	97
11XL14-2-47	1.86	0.0877 ± 0.0010	0.2622 ± 0.0017	3.1902 ± 0.0401	1376 ± 23	1501 ± 9	96
11XL14-2-48	0.84	0.0524 ± 0.0013	0.0394 ± 0.0003	0.2844 ± 0.0067	306 ± 58	249 ± 2	98
11XL14-2-49	2.09	0.1559 ± 0.0019	0.4463 ± 0.0029	9.6521 ± 0.1323	2413 ± 21	2379 ± 13	99
11XL14-2-50	4.45	0.0534 ± 0.0018	0.0360 ± 0.0004	0.2631 ± 0.0085	346 ± 44	228 ± 2	96
11XL14-2-51	1.38	0.0524 ± 0.0020	0.0399 ± 0.0004	0.2872 ± 0.0107	302 ± 89	252 ± 3	98
11XL14-2-52	1.55	0.0537 ± 0.0013	0.0722 ± 0.0006	0.5330 ± 0.0138	367 ± 56	449 ± 4	96
11XL14-2-53	3.61	0.0532 ± 0.0010	0.0644 ± 0.0004	0.4746 ± 0.0096	345 ± 41	402 ± 2	97
11XL14-2-54	1.15	0.0539 ± 0.0010	0.0730 ± 0.0005	0.5447 ± 0.0119	365 ± 43	454 ± 3	97
11XL14-2-55	3.58	0.0536 ± 0.0019	0.0463 ± 0.0005	0.3388 ± 0.0121	354 ± 51	292 ± 3	98
11XL14-2-56	6.20	0.0553 ± 0.0014	0.0574 ± 0.0004	0.4392 ± 0.0115	433 ± 54	360 ± 3	97
11XL14-2-57	1.27	0.0506 ± 0.0013	0.0484 ± 0.0004	0.3398 ± 0.0092	220 ± 57	305 ± 3	97
11XL14-2-58	2.11	0.0531 ± 0.0012	0.0736 ± 0.0006	0.5369 ± 0.0126	332 ± 54	458 ± 4	95
11XL14-2-59	1.67	0.0499 ± 0.0010	0.0421 ± 0.0003	0.2919 ± 0.0062	191 ± 48	266 ± 2	97
11XL14-2-60	0.99	0.0534 ± 0.0015	0.0618 ± 0.0006	0.4514 ± 0.0123	343 ± 63	386 ± 4	97
11XL14-2-61	1.93	0.0557 ± 0.0014	0.0757 ± 0.0007	0.5817 ± 0.0139	439 ± 58	470 ± 4	99
11XL14-2-62	10.41	0.0698 ± 0.0010	0.1124 ± 0.0008	1.0941 ± 0.0169	924 ± 30	687 ± 5	91
11XL14-2-63	1.67	0.0559 ± 0.0020	0.0403 ± 0.0005	0.3087 ± 0.0097	450 ± 76	255 ± 3	93
11XL14-2-64	1.90	0.0535 ± 0.0011	0.0641 ± 0.0005	0.4768 ± 0.0092	350 ± 44	401 ± 3	98
11XL14-2-65	1.13	0.0525 ± 0.0013	0.0445 ± 0.0004	0.3230 ± 0.0075	306 ± 58	281 ± 3	98

(continued)

Table B.1 (continued)

Sample	U/Th	$^{206}Pb^*/^{207}Pb^*$	$^{206}Pb^*/^{238}U$	$^{207}Pb^*/^{235}U$	$^{206}Pb^*/^{207}Pb^* - Age$ [Ma]	$^{238}U/^{206}Pb - Age$ [Ma]	Concordance [%]
11XL14-2-66	3.23	0.0560 ± 0.0010	0.0351 ± 0.0002	0.2719 ± 0.0046	450 ± 44	222 ± 1	90
11XL14-2-67	1.10	0.0539 ± 0.0011	0.0465 ± 0.0003	0.3464 ± 0.0065	369 ± 43	293 ± 2	96
11XL14-2-68	1.43	0.0558 ± 0.0008	0.0676 ± 0.0004	0.5235 ± 0.0071	443 ± 30	422 ± 2	98
11XL14-2-69	1.15	0.0552 ± 0.0015	0.0435 ± 0.0004	0.3297 ± 0.0086	420 ± 56	275 ± 2	94
11XL14-2-70	7.34	0.0538 ± 0.0009	0.0429 ± 0.0003	0.3197 ± 0.0055	365 ± 71	271 ± 2	96
11XL14-2-71	1.80	0.0518 ± 0.0012	0.0416 ± 0.0003	0.2981 ± 0.0064	276 ± 47	263 ± 2	99
11XL14-2-72	3.90	0.1129 ± 0.0014	0.3231 ± 0.0018	5.0689 ± 0.0617	1847 ± 22	1805 ± 9	98
11XL14-2-73	3.76	0.0592 ± 0.0017	0.0391 ± 0.0004	0.3183 ± 0.0093	572 ± 63	247 ± 2	87
11XL14-2-74	3.10	0.0586 ± 0.0013	0.0380 ± 0.0003	0.3091 ± 0.0072	550 ± 48	241 ± 2	87
11XL14-2-75	3.56	0.0527 ± 0.0011	0.0386 ± 0.0004	0.2807 ± 0.0057	317 ± 14	244 ± 2	97
11XL14-2-76	1.73	0.0552 ± 0.0011	0.0375 ± 0.0003	0.2859 ± 0.0058	420 ± 46	237 ± 2	92
11XL14-2-77	1.65	0.0548 ± 0.0011	0.0395 ± 0.0003	0.2980 ± 0.0060	406 ± 42	250 ± 2	94
11XL14-2-78	0.83	0.1262 ± 0.0013	0.3574 ± 0.0018	6.2629 ± 0.0652	2056 ± 19	1970 ± 9	97
11XL14-2-79	1.09	0.0554 ± 0.0018	0.0424 ± 0.0004	0.3220 ± 0.0104	428 ± 72	268 ± 3	94
11XL14-2-80	1.03	0.0581 ± 0.0033	0.0487 ± 0.0020	0.3761 ± 0.0244	532 ± 94	307 ± 13	94
11XL14-2-81	1.42	0.0513 ± 0.0013	0.0389 ± 0.0004	0.2744 ± 0.0070	254 ± 59	246 ± 2	99
11XL14-2-82	3.04	0.0549 ± 0.0010	0.0408 ± 0.0003	0.3105 ± 0.0055	409 ± 44	258 ± 2	93
11XL14-2-83	1.68	0.0566 ± 0.0013	0.0460 ± 0.0004	0.3609 ± 0.0081	476 ± 50	290 ± 2	92
11XL14-2-84	2.15	0.0507 ± 0.0010	0.0434 ± 0.0003	0.3037 ± 0.0063	233 ± 48	274 ± 2	98
11XL14-2-85	1.47	0.0547 ± 0.0014	0.0428 ± 0.0004	0.3218 ± 0.0085	467 ± 59	270 ± 3	95
11XL14-2-86	1.15	0.0582 ± 0.0017	0.0458 ± 0.0004	0.3624 ± 0.0100	539 ± 63	289 ± 3	91
11XL14-2-87	1.54	0.0566 ± 0.0012	0.0374 ± 0.0003	0.2946 ± 0.0064	476 ± 46	237 ± 2	89
11XL14-2-88	1.78	0.0856 ± 0.0015	0.1318 ± 0.0013	1.5612 ± 0.0287	1329 ± 34	798 ± 7	82

(continued)

Table B.1 (continued)

Sample	U/Th	$^{206}Pb^*/^{207}Pb^*$	$^{206}Pb^*/^{238}U$	$^{207}Pb^*/^{235}U$	$^{206}Pb^*/^{207}Pb^* - Age$ [Ma]	$^{238}U/^{206}Pb - Age$ [Ma]	Concordance [%]
11XL14-2-89	1.63	0.0645 ± 0.0038	0.0379 ± 0.0007	0.3313 ± 0.0199	767 ± 126	240 ± 4	80
11XL14-2-90	1.20	0.0515 ± 0.0018	0.0387 ± 0.0004	0.2748 ± 0.0092	265 ± 77	245 ± 2	99
11XL24-1-01	2.21	0.0590 ± 0.0011	0.0797 ± 0.0006	0.6495 ± 0.0114	565 ± 41	494 ± 3	97
11XL24-1-02	1.16	0.0522 ± 0.0015	0.0375 ± 0.0004	0.2690 ± 0.0077	300 ± 67	237 ± 2	98
11XL24-1-03	0.97	0.0696 ± 0.0026	0.0374 ± 0.0005	0.3568 ± 0.0130	917 ± 77	237 ± 3	73
11XL24-1-04	1.28	0.0538 ± 0.0019	0.0391 ± 0.0004	0.2850 ± 0.0094	365 ± 78	247 ± 3	97
11XL24-1-05	1.10	0.0511 ± 0.0015	0.0391 ± 0.0004	0.2720 ± 0.0077	256 ± 73	247 ± 3	98
11XL24-1-06	1.03	0.0559 ± 0.0022	0.0369 ± 0.0004	0.2837 ± 0.0110	456 ± 82	234 ± 3	91
11XL24-1-07	1.14	0.0536 ± 0.0019	0.0393 ± 0.0004	0.2875 ± 0.0099	367 ± 81	249 ± 3	96
11XL24-1-08	1.24	0.0500 ± 0.0020	0.0388 ± 0.0005	0.2684 ± 0.0112	195 ± 93	246 ± 3	98
11XL24-1-09	1.28	0.0548 ± 0.0021	0.0394 ± 0.0005	0.2914 ± 0.0104	406 ± 85	249 ± 3	95
11XL24-1-10	0.89	0.0563 ± 0.0021	0.0366 ± 0.0005	0.2805 ± 0.0102	461 ± 83	232 ± 3	92
11XL24-1-11	1.03	0.0521 ± 0.0020	0.0389 ± 0.0004	0.2771 ± 0.0101	300 ± 82	246 ± 3	99
11XL24-1-12	1.15	0.0700 ± 0.0032	0.0351 ± 0.0005	0.3288 ± 0.0134	928 ± 94	222 ± 3	74
11XL24-1-13	1.10	0.0505 ± 0.0026	0.0366 ± 0.0005	0.2554 ± 0.0132	217 ± 122	232 ± 3	99
11XL24-1-14	1.29	0.0524 ± 0.0017	0.0387 ± 0.0004	0.2787 ± 0.0086	306 ± 72	245 ± 2	98
11XL24-1-15	1.17	0.0514 ± 0.0017	0.0380 ± 0.0004	0.2661 ± 0.0083	261 ± 78	240 ± 2	99
11XL24-1-16	1.22	0.1028 ± 0.0041	0.0379 ± 0.0005	0.5375 ± 0.0220	1676 ± 127	240 ± 3	41
11XL24-1-17	1.30	0.0542 ± 0.0019	0.0378 ± 0.0005	0.2772 ± 0.0092	376 ± 78	239 ± 3	96
11XL24-1-18	1.26	0.0570 ± 0.0027	0.0365 ± 0.0005	0.2859 ± 0.0137	500 ± 106	231 ± 3	90
11XL24-1-19	1.15	0.0588 ± 0.0023	0.0374 ± 0.0005	0.2985 ± 0.0114	561 ± 85	237 ± 3	88
11XL24-1-20	1.15	0.0554 ± 0.0026	0.0361 ± 0.0005	0.2742 ± 0.0125	428 ± 104	229 ± 3	92
11XL24-1-21	0.98	0.0571 ± 0.0026	0.0363 ± 0.0006	0.2782 ± 0.0111	494 ± 104	230 ± 3	91

(continued)

Table B.1 (continued)

Sample	U/Th	$^{206}Pb^*/^{207}Pb^*$	$^{206}Pb^*/^{238}U$	$^{207}Pb^*/^{235}U$	$^{206}Pb^*/^{207}Pb^*-Age$ [Ma]	$^{238}U/^{206}Pb-Age$ [Ma]	Concordance [%]
11XL24-1-22	1.23	0.0500 ± 0.0018	0.0386 ± 0.0004	0.2639 ± 0.0090	195 ± 83	244 ± 3	97
11XL24-1-23	1.17	0.0663 ± 0.0023	0.0371 ± 0.0004	0.3338 ± 0.0108	817 ± 72	235 ± 3	78
11XL24-1-24	1.13	0.0810 ± 0.0030	0.0378 ± 0.0005	0.4167 ± 0.0149	1220 ± 73	239 ± 3	61
11XL24-1-25	1.18	0.0539 ± 0.0021	0.0384 ± 0.0005	0.2845 ± 0.0112	365 ± 89	243 ± 3	95
11XL24-1-26	1.21	0.0502 ± 0.0020	0.0382 ± 0.0005	0.2573 ± 0.0095	206 ± 93	242 ± 3	96
11XL24-1-27	1.22	0.0544 ± 0.0019	0.0400 ± 0.0005	0.2947 ± 0.0094	387 ± 78	253 ± 3	96
11XL24-1-28	0.89	0.0574 ± 0.0012	0.0584 ± 0.0004	0.4622 ± 0.0093	506 ± 46	366 ± 3	94
11XL24-1-29	1.12	0.0545 ± 0.0024	0.0382 ± 0.0006	0.2813 ± 0.0119	391 ± 100	242 ± 3	95
11XL24-1-30	1.25	0.0529 ± 0.0022	0.0404 ± 0.0005	0.2891 ± 0.0121	324 ± 92	255 ± 3	98
11XL24-1-31	1.23	0.0638 ± 0.0020	0.0376 ± 0.0004	0.3262 ± 0.0097	744 ± 233	238 ± 2	81
11XL24-1-32	1.02	0.0546 ± 0.0016	0.0387 ± 0.0003	0.2899 ± 0.0083	398 ± 67	245 ± 2	94
11XL24-1-33	6.33	0.1649 ± 0.0014	0.4376 ± 0.0020	10.0130 ± 0.0883	2507 ± 14	2340 ± 9	95
11XL24-1-34	1.01	0.0703 ± 0.0032	0.0426 ± 0.0006	0.4048 ± 0.0170	1000 ± 94	269 ± 4	75
11XL24-1-35	1.34	0.0544 ± 0.0017	0.0400 ± 0.0004	0.2975 ± 0.0089	387 ± 70	253 ± 2	95
11XL24-1-36	1.18	0.0523 ± 0.0015	0.0397 ± 0.0003	0.2818 ± 0.0077	298 ± 67	251 ± 2	99
11XL24-1-37	1.19	0.0695 ± 0.0024	0.0370 ± 0.0004	0.3439 ± 0.0106	922 ± 71	234 ± 2	75
11XL24-1-38	1.19	0.0575 ± 0.0017	0.0406 ± 0.0004	0.3150 ± 0.0089	509 ± 65	257 ± 3	92
11XL24-1-39	0.95	0.0575 ± 0.0011	0.0598 ± 0.0004	0.4732 ± 0.0087	522 ± 38	374 ± 2	94
11XL24-1-40	1.15	0.0648 ± 0.0023	0.0411 ± 0.0004	0.3626 ± 0.0120	769 ± 74	260 ± 3	81
11XL24-1-41	1.14	0.0608 ± 0.0015	0.0385 ± 0.0003	0.3196 ± 0.0077	632 ± 56	243 ± 2	85
11XL24-1-42	1.22	0.0618 ± 0.0018	0.0382 ± 0.0003	0.3222 ± 0.0092	733 ± 58	242 ± 2	84
11XL24-1-43	1.04	0.0564 ± 0.0015	0.0403 ± 0.0004	0.3099 ± 0.0080	465 ± 59	255 ± 2	92
11XL24-1-44	1.13	0.0788 ± 0.0021	0.0391 ± 0.0003	0.4206 ± 0.0105	1169 ± 49	247 ± 2	63

(continued)

Table B.1 (continued)

Sample	U/Th	$^{206}Pb^*/^{207}Pb^*$	$^{206}Pb^*/^{238}U$	$^{207}Pb^*/^{235}U$	$^{206}Pb^*/^{207}Pb^* - Age$ [Ma]	$^{238}U/^{206}Pb - Age$ [Ma]	Concordance [%]
11XL24-1-45	1.06	0.0552 ± 0.0014	0.0386 ± 0.0003	0.2931 ± 0.0073	433 ± 56	244 ± 2	93
11XL24-1-46	1.11	0.0577 ± 0.0016	0.0377 ± 0.0004	0.2957 ± 0.0080	517 ± 66	238 ± 2	90
11XL24-1-47	4.03	0.1195 ± 0.0011	0.3491 ± 0.0018	5.7645 ± 0.0507	1948 ± 16	1930 ± 9	99
11XL24-1-48	1.34	0.0706 ± 0.0025	0.0384 ± 0.0004	0.3634 ± 0.0121	946 ± 72	243 ± 3	74
11XL24-1-49	1.06	0.0673 ± 0.0018	0.0384 ± 0.0004	0.3503 ± 0.0089	856 ± 57	243 ± 2	77
11XL24-1-50	1.18	0.0602 ± 0.0018	0.0361 ± 0.0004	0.2974 ± 0.0086	609 ± 65	229 ± 2	85
11XL24-1-51	1.06	0.0568 ± 0.0014	0.0397 ± 0.0004	0.3110 ± 0.0077	483 ± 54	251 ± 2	90
11XL24-1-52	1.53	0.0632 ± 0.0021	0.0384 ± 0.0004	0.3269 ± 0.0102	717 ± 72	243 ± 3	83
11XL24-1-53	1.02	0.0642 ± 0.0017	0.0391 ± 0.0004	0.3437 ± 0.0088	746 ± 250	247 ± 2	80
11XL24-1-54	1.21	0.0596 ± 0.0024	0.0377 ± 0.0004	0.3081 ± 0.0122	587 ± 87	239 ± 3	86
11XL24-1-55	1.19	0.0552 ± 0.0018	0.0394 ± 0.0004	0.2935 ± 0.0087	420 ± 77	249 ± 2	95
11XL24-1-56	1.29	0.1178 ± 0.0082	0.0418 ± 0.0007	0.6770 ± 0.0441	1924 ± 124	264 ± 4	33
11XL24-1-57	0.95	0.0626 ± 0.0021	0.0375 ± 0.0004	0.3224 ± 0.0107	694 ± 66	237 ± 3	82
11XL24-1-58	1.30	0.0538 ± 0.0011	0.0418 ± 0.0003	0.3094 ± 0.0062	361 ± 42	264 ± 2	96
11XL24-1-59	1.21	0.0553 ± 0.0020	0.0401 ± 0.0005	0.2991 ± 0.0103	433 ± 81	253 ± 3	95
11XL24-1-60	1.09	0.0516 ± 0.0015	0.0397 ± 0.0004	0.2809 ± 0.0081	333 ± 73	251 ± 2	99
11XL24-1-61	1.14	0.0730 ± 0.0022	0.0408 ± 0.0004	0.4038 ± 0.0115	1017 ± 61	258 ± 2	71
11XL24-1-62	0.94	0.0585 ± 0.0013	0.0388 ± 0.0003	0.3118 ± 0.0068	550 ± 48	245 ± 2	88
11XL24-1-63	0.94	0.0674 ± 0.0019	0.0400 ± 0.0004	0.3688 ± 0.0102	850 ± 58	253 ± 3	76
11XL24-1-64	1.08	0.0518 ± 0.0014	0.0413 ± 0.0004	0.2911 ± 0.0078	276 ± 68	261 ± 3	99
11XL24-1-65	0.94	0.0744 ± 0.0021	0.0403 ± 0.0003	0.4111 ± 0.0115	1054 ± 57	255 ± 2	68
11XL24-1-66	0.89	0.0534 ± 0.0012	0.0403 ± 0.0003	0.2951 ± 0.0065	346 ± 50	255 ± 2	96
11XL24-1-67	0.90	0.0577 ± 0.0017	0.0391 ± 0.0004	0.3096 ± 0.0088	520 ± 68	247 ± 2	89

(continued)

Table B.1 (continued)

Sample	U/Th	$^{206}Pb^*/^{207}Pb^*$	$^{206}Pb^*/^{238}U$	$^{207}Pb^*/^{235}U$	$^{206}Pb^*/^{207}Pb^*-Age$ [Ma]	$^{238}U/^{206}Pb-Age$ [Ma]	Concordance [%]
11XL24-1-68	1.08	0.0528 ± 0.0018	0.0388 ± 0.0004	0.2800 ± 0.0093	320 ± 80	245 ± 3	97
11XL24-1-69	1.23	0.0502 ± 0.0012	0.0417 ± 0.0004	0.2871 ± 0.0068	211 ± 56	263 ± 2	97
11XL24-1-70	1.20	0.0658 ± 0.0024	0.0381 ± 0.0004	0.3447 ± 0.0126	1200 ± 77	241 ± 3	77
11XL24-1-71	1.27	0.0531 ± 0.0022	0.0408 ± 0.0004	0.2950 ± 0.0117	332 ± 93	258 ± 3	98
11XL24-1-72	1.37	0.0549 ± 0.0010	0.0413 ± 0.0003	0.3132 ± 0.0054	409 ± 41	261 ± 2	94
11XL24-1-73	1.19	0.0680 ± 0.0025	0.0383 ± 0.0004	0.3536 ± 0.0121	878 ± 76	242 ± 3	76
11XL24-1-74	1.01	0.0606 ± 0.0025	0.0389 ± 0.0005	0.3200 ± 0.0120	633 ± 55	246 ± 3	86
11XL24-1-75	1.26	0.0526 ± 0.0017	0.0415 ± 0.0004	0.2950 ± 0.0086	322 ± 72	262 ± 2	99
11XL24-1-76	1.28	0.0720 ± 0.0016	0.0394 ± 0.0004	0.3875 ± 0.0080	987 ± 46	249 ± 2	71
11XL24-1-77	1.29	0.0541 ± 0.0016	0.0402 ± 0.0004	0.2969 ± 0.0084	376 ± 65	254 ± 3	96
11XL24-1-78	4.84	0.0566 ± 0.0006	0.0719 ± 0.0003	0.5631 ± 0.0055	476 ± 22	448 ± 2	98
11XL24-1-79	1.84	0.0595 ± 0.0006	0.0514 ± 0.0003	0.4217 ± 0.0044	583 ± 24	323 ± 2	89
11XL24-1-80	1.32	0.0565 ± 0.0021	0.0415 ± 0.0005	0.3174 ± 0.0123	478 ± 81	262 ± 3	93
11XL24-1-81	0.94	0.0673 ± 0.0019	0.0397 ± 0.0004	0.3628 ± 0.0100	856 ± 59	251 ± 2	77
11XL24-1-82	1.21	0.0520 ± 0.0017	0.0407 ± 0.0005	0.2857 ± 0.0090	283 ± 79	257 ± 3	99
11XL24-1-83	1.27	0.0527 ± 0.0015	0.0395 ± 0.0004	0.2832 ± 0.0078	322 ± 67	250 ± 2	98
11XL24-1-84	1.76	0.0550 ± 0.0008	0.0395 ± 0.0002	0.3002 ± 0.0044	413 ± 33	250 ± 1	93
11XL24-1-85	1.02	0.0516 ± 0.0011	0.0377 ± 0.0003	0.2673 ± 0.0053	333 ± 48	238 ± 2	99
11XL24-1-86	1.17	0.0829 ± 0.0022	0.0396 ± 0.0004	0.4451 ± 0.0115	1266 ± 52	251 ± 2	60
11XL24-1-87	1.09	0.0516 ± 0.0015	0.0394 ± 0.0004	0.2748 ± 0.0078	333 ± 73	249 ± 2	99
11XL24-1-88	1.19	0.0518 ± 0.0014	0.0394 ± 0.0003	0.2792 ± 0.0074	280 ± 63	249 ± 2	99
11XL24-1-89	1.13	0.0539 ± 0.0022	0.0370 ± 0.0006	0.2686 ± 0.0104	365 ± 62	234 ± 4	96
11XL24-1-90	1.09	0.0916 ± 0.0037	0.0377 ± 0.0005	0.4650 ± 0.0174	1461 ± 82	238 ± 3	52

(continued)

Table B.1 (continued)

Sample	U/Th	$^{206}Pb^*/^{207}Pb^*$	$^{206}Pb^*/^{238}U$	$^{207}Pb^*/^{235}U$	$^{206}Pb^*/^{207}Pb^* - Age$ [Ma]	$^{238}U/^{206}Pb - Age$ [Ma]	Concordance [%]
11XL24-1-91	1.24	0.0542 ± 0.0018	0.0392 ± 0.0004	0.2906 ± 0.0091	389 ± 72	248 ± 3	95
12XL18-3-1	2.02	0.0644 ± 0.0004	0.0590 ± 0.0013	0.5210 ± 0.0123	755 ± 12	369 ± 8	87
12XL18-3-2	1.41	0.0581 ± 0.0003	0.0610 ± 0.0013	0.4884 ± 0.0126	531 ± 11	382 ± 8	95
12XL18-3-3	1.33	0.1706 ± 0.0020	0.0572 ± 0.0012	1.3464 ± 0.0233	2563 ± 19	358 ± 7	41
12XL18-3-4	0.74	0.0896 ± 0.0006	0.0494 ± 0.0012	0.6101 ± 0.0127	1415 ± 13	311 ± 7	64
12XL18-3-5	1.72	0.0788 ± 0.0005	0.0518 ± 0.0012	0.5623 ± 0.0123	1165 ± 12	326 ± 7	72
12XL18-3-6	1.30	0.1238 ± 0.0020	0.0548 ± 0.0012	0.9348 ± 0.0195	2011 ± 28	344 ± 7	51
12XL18-3-7	2.05	0.0673 ± 0.0005	0.0572 ± 0.0012	0.5273 ± 0.0121	847 ± 14	359 ± 7	83
12XL18-3-8	1.30	0.0863 ± 0.0006	0.0608 ± 0.0013	0.7248 ± 0.0154	1345 ± 14	380 ± 8	69
12XL18-3-9	1.38	0.0779 ± 0.0010	0.0543 ± 0.0012	0.5857 ± 0.0153	1144 ± 26	341 ± 7	73
12XL18-3-10	1.45	0.0726 ± 0.0005	0.0599 ± 0.0012	0.6014 ± 0.0143	1003 ± 14	375 ± 8	78
12XL18-3-11	1.20	0.0641 ± 0.0003	0.0503 ± 0.0012	0.4442 ± 0.0120	744 ± 11	316 ± 7	85
12XL18-3-12	1.22	0.0637 ± 0.0004	0.0509 ± 0.0012	0.4469 ± 0.0121	732 ± 12	320 ± 7	85
12XL18-3-13	1.94	0.0575 ± 0.0002	0.0640 ± 0.0013	0.5072 ± 0.0129	510 ± 6	400 ± 8	96
12XL18-3-14	1.06	0.0642 ± 0.0004	0.0627 ± 0.0014	0.5604 ± 0.0156	748 ± 13	392 ± 8	87
12XL18-3-15	1.77	0.1046 ± 0.0018	0.0563 ± 0.0012	0.8255 ± 0.0232	1707 ± 31	353 ± 7	58
12XL18-3-16	1.08	0.0689 ± 0.0003	0.0620 ± 0.0013	0.5882 ± 0.0134	896 ± 10	388 ± 8	83
12XL18-3-17	1.27	0.2662 ± 0.0084	0.0812 ± 0.0017	3.0999 ± 0.1386	3283 ± 49	503 ± 10	35
12XL18-3-18	1.32	0.0768 ± 0.0012	0.0548 ± 0.0013	0.5825 ± 0.0179	1115 ± 30	344 ± 8	74
12XL18-3-19	1.42	0.1319 ± 0.0015	0.0582 ± 0.0014	1.0558 ± 0.0190	2122 ± 20	365 ± 8	50
12XL18-3-20	2.14	0.2466 ± 0.0024	0.0757 ± 0.0014	2.5912 ± 0.0481	3162 ± 15	471 ± 8	36
12XL18-3-21	1.53	0.0752 ± 0.0008	0.0573 ± 0.0013	0.5887 ± 0.0133	1073 ± 21	359 ± 8	76
12XL18-3-22	1.63	0.0958 ± 0.0015	0.0500 ± 0.0013	0.6626 ± 0.0187	1543 ± 29	315 ± 8	61

(continued)

Table B.1 (continued)

Sample	U/Th	$^{206}Pb^*/^{207}Pb^*$	$^{206}Pb^*/^{238}U$	$^{207}Pb^*/^{235}U$	$^{206}Pb^*/^{207}Pb^* - Age$ [Ma]	$^{238}U/^{206}Pb - Age$ [Ma]	Concordance [%]
12XL18-3-23	2.16	0.0603 ± 0.0004	0.0598 ± 0.0013	0.4959 ± 0.0139	613 ± 15	374 ± 8	91
12XL18-3-24	1.70	0.0784 ± 0.0007	0.0572 ± 0.0013	0.6145 ± 0.0136	1156 ± 18	359 ± 8	74
12XL18-3-25	1.38	0.0614 ± 0.0006	0.0576 ± 0.0013	0.4883 ± 0.0146	653 ± 22	361 ± 8	89
12XL18-3-26	1.34	0.0624 ± 0.0003	0.0552 ± 0.0013	0.4746 ± 0.0138	687 ± 10	346 ± 8	88
12XL18-3-27	1.79	0.0634 ± 0.0008	0.0505 ± 0.0013	0.4412 ± 0.0145	722 ± 25	317 ± 8	86
12XL18-3-28	2.08	0.0637 ± 0.0013	0.0642 ± 0.0013	0.5662 ± 0.0199	731 ± 43	401 ± 8	88
12XL18-3-29	1.51	0.0628 ± 0.0003	0.0578 ± 0.0014	0.4989 ± 0.0138	701 ± 10	362 ± 8	88
12XL18-3-30	1.40	0.0645 ± 0.0006	0.0653 ± 0.0013	0.5815 ± 0.0149	759 ± 21	408 ± 8	88
12XL18-3-31	1.86	0.1540 ± 0.0014	0.0623 ± 0.0015	1.3307 ± 0.0288	2390 ± 16	390 ± 9	45
12XL18-3-32	1.51	0.0712 ± 0.0013	0.0527 ± 0.0013	0.5175 ± 0.0172	963 ± 39	331 ± 8	78
12XL18-3-33	1.55	0.0868 ± 0.0008	0.0509 ± 0.0013	0.6112 ± 0.0160	1355 ± 19	320 ± 8	66
12XL18-3-34	1.15	0.1219 ± 0.0016	0.0496 ± 0.0014	0.8377 ± 0.0224	1984 ± 24	312 ± 9	51
12XL18-3-35	2.07	0.2331 ± 0.0088	0.0670 ± 0.0017	2.2158 ± 0.1330	3073 ± 60	418 ± 10	35
12XL18-3-36	1.94	0.0566 ± 0.0003	0.0556 ± 0.0013	0.4339 ± 0.0138	475 ± 10	349 ± 8	95
12XL18-3-37	1.57	0.0582 ± 0.0004	0.0572 ± 0.0014	0.4595 ± 0.0142	536 ± 14	359 ± 8	93
12XL18-3-38	1.65	0.0560 ± 0.0001	0.0600 ± 0.0014	0.4639 ± 0.0139	453 ± 6	376 ± 8	97
12XL18-3-39	1.52	0.0568 ± 0.0002	0.0578 ± 0.0015	0.4534 ± 0.0151	484 ± 9	362 ± 9	95
12XL18-3-40	2.97	0.0709 ± 0.0009	0.0585 ± 0.0014	0.5802 ± 0.0185	954 ± 25	367 ± 9	79
12XL18-3-41	1.87	0.0588 ± 0.0003	0.0564 ± 0.0014	0.4577 ± 0.0141	559 ± 10	354 ± 8	92
12XL18-3-42	1.91	0.0826 ± 0.0009	0.0501 ± 0.0013	0.5706 ± 0.0148	1260 ± 22	315 ± 8	69
12XL18-3-43	1.49	0.0612 ± 0.0003	0.0556 ± 0.0014	0.4689 ± 0.0137	645 ± 9	349 ± 8	89
12XL18-3-44	1.32	0.0741 ± 0.0006	0.0557 ± 0.0013	0.5708 ± 0.0153	1043 ± 16	350 ± 8	76
12XL18-3-45	1.56	0.0763 ± 0.0008	0.0538 ± 0.0013	0.5652 ± 0.0147	1103 ± 20	338 ± 8	74

(continued)

Table B.1 (continued)

Sample	U/Th	$^{206}Pb^*/^{207}Pb^*$	$^{206}Pb^*/^{238}U$	$^{207}Pb^*/^{235}U$	$^{206}Pb^*/^{207}Pb^* - Age$ [Ma]	$^{238}U/^{206}Pb - Age$ [Ma]	Concordance [%]
12XL18-3-46	1.55	0.0842 ± 0.0007	0.0544 ± 0.0014	0.6331 ± 0.0163	1296 ± 15	341 ± 9	69
12XL18-3-47	1.85	0.0572 ± 0.0004	0.0529 ± 0.0013	0.4173 ± 0.0145	499 ± 17	332 ± 8	94
12XL18-3-48	1.57	0.2125 ± 0.0038	0.0791 ± 0.0034	2.2965 ± 0.0837	2924 ± 29	491 ± 21	41
12XL18-3-49	2.11	0.3249 ± 0.0025	0.0799 ± 0.0015	3.5880 ± 0.0586	3593 ± 12	496 ± 9	32
12XL18-3-50	1.75	0.0690 ± 0.0007	0.0602 ± 0.0014	0.5699 ± 0.0154	896 ± 20	377 ± 9	82
12XL18-3-51	1.61	0.0559 ± 0.0001	0.0577 ± 0.0014	0.4446 ± 0.0148	448 ± 6	362 ± 9	97
12XL18-3-52	1.50	0.0567 ± 0.0002	0.0560 ± 0.0016	0.4376 ± 0.0161	478 ± 9	351 ± 10	95
12XL18-3-53	1.50	0.0567 ± 0.0002	0.0557 ± 0.0016	0.4355 ± 0.0162	477 ± 9	350 ± 10	95
12XL18-3-54	1.69	0.0557 ± 0.0002	0.0574 ± 0.0015	0.4403 ± 0.0153	441 ± 9	360 ± 9	97
12XL18-3-55	1.63	0.0572 ± 0.0003	0.0559 ± 0.0015	0.4398 ± 0.0153	500 ± 11	350 ± 9	95
12XL18-3-56	2.53	0.0631 ± 0.0006	0.0611 ± 0.0014	0.5307 ± 0.0157	710 ± 19	382 ± 9	88
12XL18-3-57	2.37	0.1294 ± 0.0019	0.0639 ± 0.0017	1.1417 ± 0.0302	2089 ± 26	399 ± 10	52
12XL18-3-58	1.66	0.0577 ± 0.0003	0.0589 ± 0.0015	0.4684 ± 0.0160	518 ± 10	369 ± 9	95
12XL18-3-59	2.20	0.0709 ± 0.0008	0.0580 ± 0.0016	0.5652 ± 0.0164	954 ± 22	363 ± 10	80
12XL18-3-60	1.04	0.0643 ± 0.0005	0.0556 ± 0.0016	0.4953 ± 0.0189	752 ± 17	349 ± 10	85
12XL18-3-61	1.45	0.0567 ± 0.0002	0.0581 ± 0.0016	0.4536 ± 0.0174	480 ± 9	364 ± 10	96
12XL18-3-62	1.64	0.0575 ± 0.0002	0.0572 ± 0.0017	0.4539 ± 0.0177	510 ± 7	359 ± 10	94
12XL18-3-63	1.75	0.0583 ± 0.0004	0.0587 ± 0.0017	0.4705 ± 0.0177	540 ± 14	368 ± 10	94
12XL18-3-64	1.14	0.0594 ± 0.0003	0.0581 ± 0.0017	0.4788 ± 0.0186	582 ± 13	364 ± 10	92
12XL18-3-65	1.52	0.0602 ± 0.0004	0.0491 ± 0.0016	0.4069 ± 0.0176	610 ± 16	309 ± 10	89
12XL18-3-66	1.64	0.0621 ± 0.0003	0.0575 ± 0.0016	0.4921 ± 0.0175	676 ± 9	361 ± 10	89
12XL18-3-67	1.74	0.0596 ± 0.0007	0.0486 ± 0.0016	0.3998 ± 0.0179	589 ± 25	306 ± 10	90
12XL18-3-68	0.72	0.0640 ± 0.0004	0.0512 ± 0.0016	0.4519 ± 0.0178	740 ± 13	322 ± 10	85

(continued)

Table B.1 (continued)

Sample	U/Th	$^{206}Pb^*/^{207}Pb^*$	$^{206}Pb^*/^{238}U$	$^{207}Pb^*/^{235}U$	$^{206}Pb^*/^{207}Pb^* - Age$ [Ma]	$^{238}U/^{206}Pb - Age$ [Ma]	Concordance [%]
12XL18-3-69	1.20	0.0630 ± 0.0008	0.0552 ± 0.0017	0.4748 ± 0.0180	708 ± 28	346 ± 10	88
12XL18-3-70	1.90	0.0567 ± 0.0003	0.0577 ± 0.0016	0.4522 ± 0.0179	481 ± 11	362 ± 10	96
12XL18-3-71	1.22	0.0822 ± 0.0011	0.0608 ± 0.0016	0.6872 ± 0.0191	1248 ± 27	380 ± 10	72
12XL18-3-72	1.53	0.0588 ± 0.0004	0.0541 ± 0.0016	0.4384 ± 0.0177	560 ± 15	339 ± 10	92
12XL18-3-73	1.17	0.0558 ± 0.0002	0.0602 ± 0.0017	0.4626 ± 0.0179	443 ± 8	377 ± 10	98
12XL18-3-74	1.93	0.0700 ± 0.0011	0.0579 ± 0.0017	0.5627 ± 0.0213	927 ± 34	363 ± 10	80
12XL18-3-75	2.22	0.0603 ± 0.0005	0.0610 ± 0.0016	0.5048 ± 0.0176	614 ± 19	382 ± 10	92
12XL18-3-76	1.81	0.1033 ± 0.0018	0.0688 ± 0.0017	0.9797 ± 0.0256	1684 ± 33	429 ± 10	62
12XL18-3-77	1.96	0.0556 ± 0.0002	0.0604 ± 0.0017	0.4629 ± 0.0178	436 ± 9	378 ± 10	98
12XL18-3-78	1.16	0.0846 ± 0.0005	0.0493 ± 0.0017	0.5704 ± 0.0179	1305 ± 10	310 ± 10	68
12XL18-3-79	2.35	0.0602 ± 0.0003	0.0565 ± 0.0017	0.4699 ± 0.0185	609 ± 12	355 ± 10	91
12XL18-3-80	2.05	0.0647 ± 0.0005	0.0553 ± 0.0017	0.4956 ± 0.0191	763 ± 17	347 ± 10	85
12XL18-3-81	1.94	0.0563 ± 0.0002	0.0610 ± 0.0017	0.4732 ± 0.0178	463 ± 10	382 ± 10	97
12XL18-3-82	1.79	0.0552 ± 0.0002	0.0589 ± 0.0017	0.4475 ± 0.0180	418 ± 7	369 ± 10	98
12XL18-3-83	1.31	0.0784 ± 0.0006	0.0563 ± 0.0017	0.6078 ± 0.0180	1157 ± 16	353 ± 10	73
12XL18-3-84	1.27	0.0826 ± 0.0017	0.0615 ± 0.0018	0.7097 ± 0.0343	1258 ± 39	385 ± 11	71
12XL18-3-85	2.04	0.2034 ± 0.0019	0.0761 ± 0.0021	2.1365 ± 0.0487	2853 ± 16	473 ± 13	41
12XL18-3-86	0.97	0.1126 ± 0.0010	0.0715 ± 0.0020	1.1004 ± 0.0225	1841 ± 16	445 ± 12	59
12XL18-3-87	1.44	0.0984 ± 0.0015	0.0638 ± 0.0017	0.8604 ± 0.0211	1593 ± 29	399 ± 10	63
12XL18-3-88	1.38	0.0561 ± 0.0002	0.0600 ± 0.0018	0.4639 ± 0.0186	455 ± 7	376 ± 11	97
12XL18-3-89	1.76	0.0823 ± 0.0013	0.0616 ± 0.0018	0.7175 ± 0.0261	1252 ± 32	385 ± 11	70
12XL18-3-90	1.28	0.0602 ± 0.0003	0.0559 ± 0.0018	0.4620 ± 0.0184	610 ± 10	350 ± 11	91
12XL16-1-1	1.67	0.0531 ± 0.0024	0.0540 ± 0.0008	0.3954 ± 0.0255	331 ± 102	339 ± 5	100

(continued)

Table B.1 (continued)

Sample	U/Th	$^{206}Pb^*/^{207}Pb^*$	$^{206}Pb^*/^{238}U$	$^{207}Pb^*/^{235}U$	$^{206}Pb^*/^{207}Pb^*-Age$ [Ma]	$^{238}U/^{206}Pb-Age$ [Ma]	Concordance [%]
12XL16-1-2	2.14	0.0525 ± 0.0018	0.0531 ± 0.0007	0.3844 ± 0.0188	305 ± 78	334 ± 4	101
12XL16-1-3	1.27	0.0510 ± 0.0014	0.0493 ± 0.0005	0.3467 ± 0.0138	240 ± 64	310 ± 3	103
12XL16-1-4	2.25	0.0548 ± 0.0018	0.0510 ± 0.0006	0.3857 ± 0.0177	405 ± 72	321 ± 4	97
12XL16-1-5	1.10	0.0532 ± 0.0016	0.0517 ± 0.0006	0.3795 ± 0.0160	338 ± 66	325 ± 3	99
12XL16-1-6	2.00	0.0525 ± 0.0017	0.0493 ± 0.0006	0.3571 ± 0.0165	307 ± 73	310 ± 4	100
12XL16-1-7	2.05	0.0532 ± 0.0021	0.0512 ± 0.0007	0.3755 ± 0.0219	336 ± 91	322 ± 4	99
12XL16-1-8	1.08	0.0519 ± 0.0016	0.0512 ± 0.0006	0.3665 ± 0.0168	280 ± 72	322 ± 4	101
12XL16-1-9	1.90	0.0582 ± 0.0019	0.0494 ± 0.0006	0.3970 ± 0.0186	538 ± 70	311 ± 4	92
12XL16-1-10	2.75	0.0577 ± 0.0027	0.0537 ± 0.0009	0.4274 ± 0.0292	517 ± 102	337 ± 6	93
12XL16-1-11	2.84	0.0553 ± 0.0027	0.0495 ± 0.0009	0.3773 ± 0.0277	422 ± 111	311 ± 5	96
12XL16-1-12	2.05	0.0528 ± 0.0031	0.0555 ± 0.0011	0.4038 ± 0.0344	318 ± 132	348 ± 7	101
12XL16-1-13	2.25	0.0550 ± 0.0032	0.0512 ± 0.0010	0.3884 ± 0.0326	410 ± 129	322 ± 6	97
12XL16-1-14	2.24	0.0511 ± 0.0021	0.0511 ± 0.0007	0.3596 ± 0.0212	243 ± 93	321 ± 4	103
12XL16-1-15	1.15	0.0633 ± 0.0019	0.0528 ± 0.0006	0.4607 ± 0.0197	718 ± 63	331 ± 4	86
12XL16-1-16	2.97	0.0559 ± 0.0023	0.0548 ± 0.0008	0.4223 ± 0.0248	447 ± 90	344 ± 5	96
12XL16-1-17	1.93	0.0543 ± 0.0022	0.0479 ± 0.0007	0.3587 ± 0.0211	381 ± 92	302 ± 4	97
12XL16-1-18	1.83	0.0524 ± 0.0034	0.0469 ± 0.0010	0.3392 ± 0.0317	302 ± 147	296 ± 6	100
12XL16-1-19	2.25	0.0529 ± 0.0018	0.0523 ± 0.0007	0.3814 ± 0.0189	325 ± 77	328 ± 4	100
12XL16-1-20	2.00	0.0542 ± 0.0018	0.0510 ± 0.0006	0.3817 ± 0.0185	379 ± 75	321 ± 4	98
12XL16-1-21	1.35	0.0584 ± 0.0028	0.0510 ± 0.0009	0.4105 ± 0.0294	543 ± 105	321 ± 5	92
12XL16-1-22	1.12	0.0533 ± 0.0015	0.0500 ± 0.0006	0.3678 ± 0.0157	342 ± 65	314 ± 4	99
12XL16-1-23	1.16	0.0528 ± 0.0018	0.0483 ± 0.0006	0.3521 ± 0.0178	318 ± 77	304 ± 4	99
12XL16-1-24	2.50	0.0568 ± 0.0019	0.0504 ± 0.0007	0.3950 ± 0.0203	483 ± 75	317 ± 4	94

(continued)

Table B.1 (continued)

Sample	U/Th	$^{206}Pb^*/^{207}Pb^*$	$^{206}Pb^*/^{238}U$	$^{207}Pb^*/^{235}U$	$^{206}Pb^*/^{207}Pb^* - Age$ [Ma]	$^{238}U/^{206}Pb - Age$ [Ma]	Concordance [%]
12XL16-1-25	1.78	0.0554 ± 0.0016	0.0500 ± 0.0006	0.3821 ± 0.0168	427 ± 65	315 ± 4	96
12XL16-1-26	1.72	0.0541 ± 0.0020	0.0481 ± 0.0007	0.3595 ± 0.0198	375 ± 82	303 ± 4	97
12XL16-1-27	1.88	0.0527 ± 0.0018	0.0485 ± 0.0006	0.3527 ± 0.0179	314 ± 77	305 ± 4	100
12XL16-1-28	1.61	0.0537 ± 0.0017	0.0504 ± 0.0006	0.3731 ± 0.0175	356 ± 71	317 ± 4	98
12XL16-1-29	2.54	0.0549 ± 0.0019	0.0495 ± 0.0007	0.3748 ± 0.0195	408 ± 79	311 ± 4	96
12XL16-1-30	0.73	0.0639 ± 0.0018	0.0467 ± 0.0005	0.4119 ± 0.0168	738 ± 59	294 ± 3	84
12XL16-1-31	2.30	0.0519 ± 0.0017	0.0510 ± 0.0006	0.3652 ± 0.0172	281 ± 73	321 ± 4	101
12XL16-1-32	1.76	0.0634 ± 0.0020	0.0508 ± 0.0006	0.4444 ± 0.0202	722 ± 66	319 ± 4	86
12XL16-1-33	1.53	0.0546 ± 0.0017	0.0507 ± 0.0006	0.3814 ± 0.0173	393 ± 69	319 ± 4	97
12XL16-1-34	3.41	0.0412 ± 0.0511	0.0532 ± 0.0053	0.3025 ± 0.5719	NaN ± 0	334 ± 32	125
12XL16-1-35	1.75	0.0446 ± 0.0042	0.0503 ± 0.0007	0.3097 ± 0.0448	NaN ± 0	316 ± 4	115
12XL16-1-36	2.25	0.0620 ± 0.0021	0.0475 ± 0.0007	0.4061 ± 0.0210	675 ± 74	299 ± 4	86
12XL16-1-37	1.19	0.0559 ± 0.0016	0.0506 ± 0.0006	0.3897 ± 0.0171	447 ± 65	318 ± 4	95
12XL16-1-38	0.88	0.0544 ± 0.0014	0.0510 ± 0.0005	0.3828 ± 0.0150	386 ± 59	321 ± 3	98
12XL16-1-39	1.68	0.0542 ± 0.0020	0.0513 ± 0.0007	0.3841 ± 0.0211	380 ± 82	323 ± 4	98
12XL16-1-40	1.60	0.0575 ± 0.0027	0.0541 ± 0.0009	0.4287 ± 0.0299	509 ± 102	340 ± 6	94
12XL16-1-41	2.00	0.0558 ± 0.0016	0.0496 ± 0.0006	0.3821 ± 0.0166	445 ± 64	312 ± 4	95
12XL16-1-42	3.54	0.0490 ± 0.0018	0.0498 ± 0.0007	0.3372 ± 0.0183	148 ± 84	314 ± 4	106
12XL16-1-43	2.10	0.0522 ± 0.0017	0.0503 ± 0.0006	0.3619 ± 0.0180	292 ± 75	316 ± 4	101
12XL16-1-44	1.69	0.0544 ± 0.0025	0.0540 ± 0.0009	0.4053 ± 0.0281	386 ± 102	339 ± 6	98
12XL16-1-45	1.06	0.0523 ± 0.0016	0.0481 ± 0.0006	0.3467 ± 0.0165	295 ± 71	303 ± 4	100
12XL16-1-46	2.11	0.0518 ± 0.0016	0.0499 ± 0.0006	0.3567 ± 0.0164	277 ± 69	314 ± 4	101
12XL16-1-47	1.45	0.0644 ± 0.0019	0.0468 ± 0.0006	0.4162 ± 0.0185	755 ± 62	295 ± 4	83

(continued)

Table B.1 (continued)

Sample	U/Th	$^{206}Pb^*/^{207}Pb^*$	$^{206}Pb^*/^{238}U$	$^{207}Pb^*/^{235}U$	$^{206}Pb^*/^{207}Pb^* - Age$ [Ma]	$^{238}U/^{206}Pb - Age$ [Ma]	Concordance [%]
12XL16-1-48	1.15	0.0549 ± 0.0016	0.0523 ± 0.0006	0.3961 ± 0.0178	408 ± 67	328 ± 4	97
12XL16-1-49	1.62	0.0537 ± 0.0019	0.0519 ± 0.0007	0.3846 ± 0.0199	358 ± 78	326 ± 4	99
12XL16-1-50	1.93	0.0512 ± 0.0020	0.0497 ± 0.0007	0.3513 ± 0.0205	250 ± 90	313 ± 4	102
12XL16-1-51	1.71	0.0512 ± 0.0018	0.0533 ± 0.0007	0.3763 ± 0.0199	250 ± 82	335 ± 4	103
12XL16-1-52	1.18	0.0534 ± 0.0016	0.0490 ± 0.0006	0.3611 ± 0.0160	344 ± 68	309 ± 4	99
12XL16-1-53	1.68	0.0576 ± 0.0018	0.0509 ± 0.0006	0.4047 ± 0.0183	514 ± 67	320 ± 4	93
12XL16-1-54	1.22	0.0534 ± 0.0018	0.0553 ± 0.0007	0.4072 ± 0.0203	343 ± 75	347 ± 4	100
12XL16-1-55	1.64	0.0582 ± 0.0026	0.0523 ± 0.0009	0.4204 ± 0.0285	537 ± 99	329 ± 5	92
12XL16-1-56	1.66	0.0574 ± 0.0040	0.0529 ± 0.0014	0.4186 ± 0.0439	505 ± 154	332 ± 8	94
12XL16-1-57	1.70	0.0551 ± 0.0018	0.0523 ± 0.0007	0.3970 ± 0.0196	414 ± 73	328 ± 4	97
12XL16-1-58	1.51	0.0535 ± 0.0017	0.0484 ± 0.0006	0.3574 ± 0.0169	351 ± 71	305 ± 4	98
12XL16-1-59	2.32	0.0543 ± 0.0018	0.0507 ± 0.0007	0.3792 ± 0.0195	381 ± 77	319 ± 4	98
12XL16-1-60	2.60	0.0535 ± 0.0023	0.0484 ± 0.0008	0.3574 ± 0.0236	351 ± 99	305 ± 5	98
12XL16-1-61	2.63	0.0539 ± 0.0015	0.0499 ± 0.0006	0.3711 ± 0.0158	366 ± 64	314 ± 4	98
12XL16-1-62	2.58	0.0529 ± 0.0026	0.0532 ± 0.0010	0.3879 ± 0.0286	324 ± 111	334 ± 6	100
12XL16-1-63	3.14	0.0527 ± 0.0022	0.0540 ± 0.0008	0.3929 ± 0.0243	316 ± 94	339 ± 5	101
12XL16-1-64	2.04	0.0540 ± 0.0020	0.0501 ± 0.0007	0.3730 ± 0.0209	370 ± 85	315 ± 4	98
12XL16-1-65	1.60	0.0757 ± 0.0022	0.0501 ± 0.0006	0.5228 ± 0.0230	1086 ± 59	315 ± 4	74
12XL16-1-66	1.70	0.0467 ± 0.0026	0.0520 ± 0.0009	0.3349 ± 0.0276	35 ± 132	327 ± 6	111
12XL16-1-67	2.00	0.0545 ± 0.0033	0.0501 ± 0.0011	0.3761 ± 0.0342	389 ± 136	315 ± 7	97
12XL16-1-68	1.62	−0.0325 ± −0.0178	0.0467 ± 0.0018	−0.2090 ± −0.1765	NaN ± 0	294 ± 11	−124
12XL16-1-69	1.12	0.0700 ± 0.0030	0.0524 ± 0.0009	0.5066 ± 0.0321	929 ± 87	330 ± 6	79
12XL16-1-70	1.24	0.0508 ± 0.0018	0.0530 ± 0.0007	0.3715 ± 0.0195	233 ± 80	333 ± 4	104

(continued)

Table B.1 (continued)

Sample	U/Th	$^{206}Pb^*/^{207}Pb^*$	$^{206}Pb^*/^{238}U$	$^{207}Pb^*/^{235}U$	$^{206}Pb^*/^{207}Pb^*-Age$ [Ma]	$^{238}U/^{206}Pb - Age$ [Ma]	Concordance [%]
12XL16-1-71	0.80	0.0529 ± 0.0048	0.0476 ± 0.0007	0.3472 ± 0.0480	322 ± 204	300 ± 4	99
12XL16-1-72	0.81	0.0849 ± 0.0024	0.0512 ± 0.0006	0.5999 ± 0.0251	1312 ± 54	322 ± 4	67
12XL16-1-73	1.30	0.0593 ± 0.0029	0.0543 ± 0.0010	0.4441 ± 0.0327	578 ± 107	341 ± 6	91
12XL16-1-74	2.94	0.0501 ± 0.0033	0.0487 ± 0.0010	0.3366 ± 0.0330	199 ± 152	307 ± 6	104
12XL16-1-75	1.76	0.0701 ± 0.0038	0.0515 ± 0.0011	0.4985 ± 0.0401	932 ± 112	324 ± 7	79
12XL16-1-76	1.24	0.0523 ± 0.0023	0.0520 ± 0.0008	0.3751 ± 0.0246	300 ± 100	327 ± 5	101
12XL16-1-77	3.59	0.0505 ± 0.0020	0.0506 ± 0.0007	0.3525 ± 0.0208	219 ± 92	318 ± 4	104
12XL16-1-78	2.23	0.0532 ± 0.0020	0.0500 ± 0.0007	0.3668 ± 0.0210	336 ± 87	315 ± 4	99
12XL16-1-79	1.33	0.0530 ± 0.0015	0.0515 ± 0.0006	0.3760 ± 0.0160	326 ± 65	323 ± 4	100
12XL16-1-80	1.50	0.0629 ± 0.0027	0.0535 ± 0.0009	0.4642 ± 0.0295	703 ± 91	336 ± 5	87
12XL16-1-81	1.86	0.0601 ± 0.0019	0.0480 ± 0.0006	0.3980 ± 0.0186	607 ± 68	302 ± 4	89
12XL16-1-82	2.05	0.0597 ± 0.0034	0.0448 ± 0.0010	0.3683 ± 0.0315	591 ± 124	282 ± 6	89
12XL16-1-83	1.34	0.0580 ± 0.0017	0.0500 ± 0.0006	0.3999 ± 0.0178	528 ± 65	315 ± 4	92
12XL16-1-84	1.77	0.0523 ± 0.0017	0.0493 ± 0.0006	0.3555 ± 0.0179	298 ± 76	310 ± 4	100
12XL16-1-85	2.30	0.0549 ± 0.0018	0.0477 ± 0.0006	0.3613 ± 0.0175	409 ± 72	300 ± 4	96
12XL16-1-86	2.05	0.0575 ± 0.0020	0.0509 ± 0.0007	0.4041 ± 0.0216	511 ± 78	320 ± 4	93
12XL16-1-87	2.04	0.0622 ± 0.0021	0.0482 ± 0.0007	0.4129 ± 0.0211	679 ± 72	303 ± 4	86
12XL16-1-88	1.41	0.0527 ± 0.0024	0.0491 ± 0.0008	0.3566 ± 0.0246	314 ± 104	309 ± 5	100
12XL16-1-89	1.23	0.0487 ± 0.0015	0.0495 ± 0.0006	0.3325 ± 0.0158	132 ± 74	312 ± 4	107
12XL16-1-90	2.63	0.0617 ± 0.0054	0.0469 ± 0.0015	0.3994 ± 0.0530	664 ± 189	296 ± 9	87
12XL16-1-91	1.73	0.0487 ± 0.0020	0.0486 ± 0.0007	0.3265 ± 0.0207	134 ± 98	306 ± 5	107
12XL16-1-92	2.06	0.0544 ± 0.0019	0.0481 ± 0.0007	0.3612 ± 0.0193	386 ± 80	303 ± 4	97
12XL16-1-93	1.39	0.0495 ± 0.0032	0.0488 ± 0.0010	0.3329 ± 0.0321	171 ± 149	307 ± 6	105

(continued)

Table B.1 (continued)

Sample	U/Th	$^{206}Pb^*/^{207}Pb^*$	$^{206}Pb^*/^{238}U$	$^{207}Pb^*/^{235}U$	$^{206}Pb^*/^{207}Pb^*-Age$ [Ma]	$^{238}U/^{206}Pb-Age$ [Ma]	Concordance [%]
12XL16-1-94	1.34	0.0561 ± 0.0019	0.0483 ± 0.0006	0.3737 ± 0.0190	456 ± 75	304 ± 4	94
12XL16-1-95	2.26	0.0498 ± 0.0030	0.0499 ± 0.0010	0.3425 ± 0.0311	185 ± 140	314 ± 6	105
12XL16-1-96	1.24	0.0555 ± 0.0018	0.0494 ± 0.0006	0.3773 ± 0.0189	430 ± 74	311 ± 4	96
12XL16-1-97	2.45	0.0517 ± 0.0018	0.0484 ± 0.0007	0.3449 ± 0.0185	271 ± 81	305 ± 4	101
12XL16-1-98	2.77	0.0499 ± 0.0019	0.0476 ± 0.0007	0.3274 ± 0.0187	188 ± 87	300 ± 4	104
12XL16-1-99	0.59	0.0496 ± 0.0147	0.0331 ± 0.0013	0.2262 ± 0.1052	176 ± 692	210 ± 8	101
12XL16-1-100	1.53	0.0456 ± 0.0018	0.0497 ± 0.0007	0.3125 ± 0.0189	NaN ± 0	313 ± 4	113
12XL16-1-101	1.85	0.0449 ± 0.0019	0.0474 ± 0.0007	0.2934 ± 0.0193	NaN ± 0	299 ± 4	114
12XL16-1-102	1.36	0.0468 ± 0.0018	0.0488 ± 0.0007	0.3147 ± 0.0188	40 ± 94	307 ± 4	111
12XL16-1-103	2.94	0.0582 ± 0.0041	0.0469 ± 0.0012	0.3764 ± 0.0398	537 ± 153	296 ± 7	91
12XL16-1-104	2.46	0.0508 ± 0.0018	0.0479 ± 0.0006	0.3355 ± 0.0179	231 ± 82	302 ± 4	103
12XL16-1-105	1.61	0.0548 ± 0.0018	0.0521 ± 0.0007	0.3937 ± 0.0189	403 ± 72	328 ± 4	97
12XL16-1-106	1.64	0.0512 ± 0.0028	0.0500 ± 0.0009	0.3532 ± 0.0284	249 ± 124	315 ± 5	102
12XL16-1-107	2.29	0.0512 ± 0.0016	0.0502 ± 0.0006	0.3545 ± 0.0164	250 ± 72	316 ± 4	102
12XL16-1-108	1.29	0.0611 ± 0.0028	0.0490 ± 0.0008	0.4123 ± 0.0283	641 ± 100	308 ± 5	88
12XL16-1-109	2.56	0.0550 ± 0.0020	0.0520 ± 0.0007	0.3939 ± 0.0214	410 ± 82	327 ± 4	97
12XL16-1-110	2.40	0.0706 ± 0.0027	0.0498 ± 0.0008	0.4848 ± 0.0270	946 ± 78	313 ± 5	78
11XL42-1-1	1.94	0.0535 ± 0.0003	0.0524 ± 0.0004	0.3866 ± 0.0041	346 ± 8	329 ± 3	99
11XL42-1-2	1.24	0.0636 ± 0.0007	0.0535 ± 0.0004	0.4693 ± 0.0061	728 ± 25	336 ± 3	85
11XL42-1-3	2.57	0.0598 ± 0.0006	0.0569 ± 0.0005	0.4689 ± 0.0059	594 ± 24	357 ± 3	91
11XL42-1-4	2.46	0.0536 ± 0.0005	0.0591 ± 0.0005	0.4366 ± 0.0055	354 ± 22	370 ± 3	99
11XL42-1-5	1.83	0.0546 ± 0.0004	0.0515 ± 0.0004	0.3879 ± 0.0036	394 ± 10	324 ± 2	97
11XL42-1-6	1.91	0.0549 ± 0.0002	0.0528 ± 0.0004	0.3998 ± 0.0032	406 ± 7	332 ± 2	97

(continued)

Table B.1 (continued)

Sample	U/Th	$^{206}Pb^*/^{207}Pb^*$	$^{206}Pb^*/^{238}U$	$^{207}Pb^*/^{235}U$	$^{206}Pb^*/^{207}Pb^* - Age$ [Ma]	$^{238}U/^{206}Pb - Age$ [Ma]	Concordance [%]
11XL42-1-7	1.57	0.0551 ± 0.0002	0.0523 ± 0.0003	0.3966 ± 0.0029	413 ± 14	328 ± 2	96
11XL42-1-8	1.19	0.0664 ± 0.0007	0.0551 ± 0.0003	0.5058 ± 0.0062	820 ± 21	346 ± 2	81
11XL42-1-9	1.22	0.0575 ± 0.0007	0.0539 ± 0.0004	0.4269 ± 0.0046	522 ± 26	339 ± 2	93
11XL42-1-10	1.50	0.0567 ± 0.0003	0.0594 ± 0.0005	0.4636 ± 0.0037	480 ± 14	372 ± 3	96
11XL42-1-11	2.21	0.0563 ± 0.0004	0.0529 ± 0.0005	0.4104 ± 0.0043	465 ± 15	332 ± 3	95
11XL42-1-12	2.36	0.0561 ± 0.0002	0.0803 ± 0.0004	0.6207 ± 0.0035	454 ± 3	498 ± 2	98
11XL42-1-13	1.67	0.0541 ± 0.0002	0.0570 ± 0.0005	0.4259 ± 0.0042	376 ± 9	358 ± 3	99
11XL42-1-14	1.44	0.0535 ± 0.0002	0.0561 ± 0.0004	0.4140 ± 0.0033	350 ± 12	352 ± 2	99
11XL42-1-15	0.78	0.0584 ± 0.0002	0.0517 ± 0.0002	0.4170 ± 0.0023	546 ± 7	325 ± 1	91
11XL42-1-16	1.78	0.0599 ± 0.0003	0.0511 ± 0.0003	0.4226 ± 0.0030	598 ± 9	321 ± 2	89
11XL42-1-17	1.25	0.0533 ± 0.0003	0.0433 ± 0.0004	0.3184 ± 0.0031	343 ± 13	273 ± 2	97
11XL42-1-18	1.41	0.0545 ± 0.0003	0.0532 ± 0.0004	0.3999 ± 0.0039	391 ± 39	334 ± 3	97
11XL42-1-19	1.95	0.0534 ± 0.0002	0.0562 ± 0.0004	0.4135 ± 0.0035	346 ± 5	352 ± 3	99
11XL42-1-20	1.46	0.0544 ± 0.0003	0.0531 ± 0.0004	0.3995 ± 0.0039	387 ± 11	334 ± 2	97
11XL42-1-21	1.82	0.0559 ± 0.0003	0.0546 ± 0.0006	0.4219 ± 0.0058	456 ± 15	343 ± 3	95
11XL42-1-22	1.92	0.0560 ± 0.0004	0.0506 ± 0.0003	0.3912 ± 0.0042	450 ± 21	318 ± 2	94
11XL42-1-23	1.33	0.0531 ± 0.0002	0.0499 ± 0.0003	0.3655 ± 0.0024	332 ± 6	314 ± 2	99
11XL42-1-24	2.07	0.0532 ± 0.0002	0.0545 ± 0.0003	0.3996 ± 0.0026	345 ± 9	342 ± 2	99
11XL42-1-25	2.01	0.0533 ± 0.0002	0.0525 ± 0.0003	0.3858 ± 0.0032	339 ± 11	330 ± 2	99
11XL42-1-26	2.17	0.0528 ± 0.0003	0.0526 ± 0.0005	0.3830 ± 0.0042	320 ± 11	331 ± 3	99
11XL42-1-27	2.00	0.0533 ± 0.0004	0.0573 ± 0.0004	0.4206 ± 0.0032	343 ± 21	359 ± 2	99
11XL42-1-28	1.47	0.0536 ± 0.0002	0.0539 ± 0.0004	0.3982 ± 0.0032	354 ± 11	338 ± 2	99
11XL42-1-29	1.81	0.0531 ± 0.0003	0.0510 ± 0.0005	0.3733 ± 0.0039	332 ± 11	321 ± 3	99

(continued)

Table B.1 (continued)

Sample	U/Th	$^{206}Pb^*/^{207}Pb^*$	$^{206}Pb^*/^{238}U$	$^{207}Pb^*/^{235}U$	$^{206}Pb^*/^{207}Pb^* - Age$ [Ma]	$^{238}U/^{206}Pb - Age$ [Ma]	Concordance [%]
11XL42-1-30	1.57	0.0551 ± 0.0002	0.0540 ± 0.0004	0.4100 ± 0.0033	417 ± 14	339 ± 2	97
11XL42-1-31	2.14	0.0557 ± 0.0003	0.0536 ± 0.0002	0.4117 ± 0.0024	443 ± 13	337 ± 1	96
11XL42-1-32	1.97	0.0544 ± 0.0004	0.0590 ± 0.0003	0.4425 ± 0.0036	387 ± 47	370 ± 2	99
11XL42-1-33	4.48	0.0579 ± 0.0005	0.0506 ± 0.0003	0.4036 ± 0.0039	524 ± 20	318 ± 2	92
11XL42-1-34	1.55	0.0536 ± 0.0003	0.0486 ± 0.0004	0.3587 ± 0.0029	354 ± 11	306 ± 2	98
11XL42-1-35	1.52	0.0548 ± 0.0003	0.0480 ± 0.0005	0.3630 ± 0.0044	467 ± 11	302 ± 3	96
11XL42-1-36	1.93	0.0601 ± 0.0008	0.0569 ± 0.0004	0.4738 ± 0.0096	606 ± 30	357 ± 3	90
11XL42-1-37	2.07	0.0555 ± 0.0003	0.0523 ± 0.0002	0.4003 ± 0.0023	435 ± 18	329 ± 1	96
11XL42-1-38	1.51	0.0541 ± 0.0002	0.0469 ± 0.0003	0.3501 ± 0.0034	376 ± 9	295 ± 2	96
11XL42-1-39	0.98	0.1120 ± 0.0002	0.2928 ± 0.0026	4.5232 ± 0.0416	1832 ± 4	1656 ± 13	95
11XL42-1-40	1.05	0.0552 ± 0.0003	0.0534 ± 0.0003	0.4061 ± 0.0029	420 ± 11	335 ± 2	96
11XL42-1-41	1.92	0.0535 ± 0.0002	0.0506 ± 0.0002	0.3736 ± 0.0021	350 ± 12	318 ± 2	98
11XL42-1-42	1.58	0.0549 ± 0.0003	0.0484 ± 0.0004	0.3672 ± 0.0044	409 ± 13	305 ± 2	95
11XL42-1-43	1.33	0.0573 ± 0.0006	0.0442 ± 0.0003	0.3485 ± 0.0039	502 ± 24	279 ± 2	91
11XL42-1-44	0.89	0.0532 ± 0.0002	0.0484 ± 0.0003	0.3550 ± 0.0028	345 ± 9	305 ± 2	98
11XL42-1-45	1.38	0.0534 ± 0.0004	0.0496 ± 0.0003	0.3651 ± 0.0029	346 ± 15	312 ± 2	98
11XL42-1-46	2.91	0.0560 ± 0.0005	0.0562 ± 0.0005	0.4324 ± 0.0040	450 ± 23	352 ± 3	96
11XL42-1-47	1.62	0.0561 ± 0.0003	0.0497 ± 0.0004	0.3840 ± 0.0028	457 ± 11	313 ± 3	94
11XL42-1-48	1.79	0.0533 ± 0.0003	0.0489 ± 0.0004	0.3596 ± 0.0039	343 ± 19	308 ± 3	98
11XL42-1-49	1.79	0.0542 ± 0.0002	0.0564 ± 0.0003	0.4223 ± 0.0030	389 ± 9	354 ± 2	98
11XL42-1-50	1.50	0.0575 ± 0.0005	0.0474 ± 0.0003	0.3761 ± 0.0044	509 ± 16	298 ± 2	91
11XL42-1-51	1.40	0.0552 ± 0.0002	0.0525 ± 0.0003	0.4000 ± 0.0023	420 ± 6	330 ± 2	96
11XL42-1-52	1.73	0.0540 ± 0.0003	0.0472 ± 0.0003	0.3516 ± 0.0032	372 ± 11	297 ± 2	97

(continued)

Table B.1 (continued)

Sample	U/Th	$^{206}Pb^*/^{207}Pb^*$	$^{206}Pb^*/^{238}U$	$^{207}Pb^*/^{235}U$	$^{206}Pb^*/^{207}Pb^*-Age$ [Ma]	$^{238}U/^{206}Pb-Age$ [Ma]	Concordance [%]
11XL42-1-53	1.97	0.0529 ± 0.0002	0.0546 ± 0.0002	0.3978 ± 0.0023	324 ± 5	342 ± 1	99
11XL42-1-54	1.61	0.0589 ± 0.0003	0.0460 ± 0.0004	0.3743 ± 0.0047	565 ± 10	290 ± 3	89
11XL42-1-55	1.76	0.0539 ± 0.0002	0.0538 ± 0.0003	0.4003 ± 0.0025	369 ± 7	338 ± 2	98
11XL42-1-56	1.45	0.0538 ± 0.0002	0.0557 ± 0.0003	0.4134 ± 0.0031	361 ± 9	350 ± 2	99
11XL42-1-57	2.00	0.0537 ± 0.0002	0.0535 ± 0.0005	0.3964 ± 0.0040	367 ± 11	336 ± 3	99
11XL42-1-58	1.61	0.0580 ± 0.0003	0.0500 ± 0.0003	0.4003 ± 0.0034	532 ± 11	314 ± 2	91
11XL42-1-59	1.18	0.0535 ± 0.0003	0.0532 ± 0.0005	0.3923 ± 0.0045	350 ± 8	334 ± 3	99
11XL42-1-60	1.98	0.0588 ± 0.0006	0.0424 ± 0.0003	0.3440 ± 0.0041	561 ± 25	268 ± 2	88
11XL42-1-61	1.42	0.0563 ± 0.0002	0.0522 ± 0.0003	0.4059 ± 0.0031	465 ± 9	328 ± 2	94
11XL42-1-62	2.73	0.0574 ± 0.0005	0.0462 ± 0.0004	0.3660 ± 0.0045	509 ± 14	291 ± 2	91
11XL42-1-63	2.05	0.0536 ± 0.0003	0.0519 ± 0.0004	0.3833 ± 0.0035	354 ± 11	326 ± 2	98
11XL42-1-64	1.16	0.0532 ± 0.0002	0.0545 ± 0.0005	0.4004 ± 0.0043	339 ± 11	342 ± 3	99
11XL42-1-65	1.74	0.0555 ± 0.0002	0.0525 ± 0.0004	0.4022 ± 0.0037	435 ± 5	330 ± 3	96
11XL42-1-66	1.44	0.0543 ± 0.0002	0.0524 ± 0.0004	0.3924 ± 0.0030	389 ± 6	329 ± 2	97
11XL42-1-67	2.21	0.0536 ± 0.0002	0.0522 ± 0.0004	0.3860 ± 0.0029	367 ± 9	328 ± 2	98
11XL42-1-68	1.65	0.0533 ± 0.0002	0.0553 ± 0.0005	0.4067 ± 0.0042	343 ± 5	347 ± 3	99
11XL42-1-69	1.15	0.0576 ± 0.0005	0.0503 ± 0.0003	0.4011 ± 0.0046	517 ± 51	316 ± 2	92
11XL42-1-70	1.38	0.0575 ± 0.0004	0.0484 ± 0.0005	0.3839 ± 0.0045	522 ± 15	305 ± 3	92
11XL42-1-71	2.13	0.0542 ± 0.0002	0.0543 ± 0.0004	0.4057 ± 0.0033	389 ± 9	341 ± 3	98
11XL42-1-72	1.19	0.0539 ± 0.0002	0.0528 ± 0.0003	0.3925 ± 0.0028	369 ± 5	332 ± 2	98
11XL42-1-73	2.02	0.0534 ± 0.0002	0.0540 ± 0.0005	0.3984 ± 0.0037	346 ± 14	339 ± 3	99
11XL42-1-74	1.54	0.0527 ± 0.0002	0.0527 ± 0.0004	0.3831 ± 0.0031	317 ± 9	331 ± 2	99
11XL42-1-75	0.99	0.0578 ± 0.0004	0.0480 ± 0.0003	0.3818 ± 0.0024	520 ± 17	302 ± 2	91

(continued)

Table B.1 (continued)

Sample	U/Th	$^{206}Pb^*/^{207}Pb^*$	$^{206}Pb^*/^{238}U$	$^{207}Pb^*/^{235}U$	$^{206}Pb^*/^{207}Pb^*-Age$ [Ma]	$^{238}U/^{206}Pb-Age$ [Ma]	Concordance [%]
11XL42-1-76	1.53	0.0541 ± 0.0004	0.0584 ± 0.0004	0.4355 ± 0.0034	376 ± 15	366 ± 2	99
11XL42-1-77	1.30	0.0530 ± 0.0002	0.0515 ± 0.0005	0.3765 ± 0.0041	328 ± 9	324 ± 3	99
11XL42-1-78	1.02	0.0528 ± 0.0002	0.0541 ± 0.0004	0.3943 ± 0.0033	320 ± 3	340 ± 3	99
11XL42-1-79	1.53	0.0537 ± 0.0002	0.0512 ± 0.0003	0.3782 ± 0.0021	367 ± 11	322 ± 2	98
11XL42-1-80	1.41	0.0535 ± 0.0003	0.0551 ± 0.0004	0.4068 ± 0.0033	350 ± 11	346 ± 2	99
11XL42-1-81	1.07	0.0588 ± 0.0006	0.0483 ± 0.0002	0.3920 ± 0.0045	561 ± 25	304 ± 1	90
11XL42-1-82	0.94	0.0551 ± 0.0003	0.0543 ± 0.0004	0.4125 ± 0.0033	417 ± 13	341 ± 2	97
11XL42-1-83	0.76	0.0535 ± 0.0002	0.0547 ± 0.0004	0.4039 ± 0.0033	350 ± 12	344 ± 2	99
11XL42-1-84	1.16	0.0535 ± 0.0002	0.0562 ± 0.0004	0.4146 ± 0.0038	350 ± 14	352 ± 3	99
11XL42-1-85	0.70	0.0551 ± 0.0004	0.0575 ± 0.0003	0.4365 ± 0.0029	417 ± −18	361 ± 2	98
11XL42-1-86	0.41	0.0531 ± 0.0002	0.0493 ± 0.0002	0.3615 ± 0.0019	345 ± 7	310 ± 1	99
11XL42-1-87	0.52	0.0553 ± 0.0005	0.0505 ± 0.0004	0.3853 ± 0.0045	433 ± 19	318 ± 3	95
11XL42-1-88	0.16	0.0546 ± 0.0004	0.0462 ± 0.0003	0.3483 ± 0.0035	394 ± 12	291 ± 2	95
11XL42-1-89	0.73	0.0535 ± 0.0006	0.0511 ± 0.0005	0.3776 ± 0.0057	350 ± 26	321 ± 3	98
11XL42-1-90	0.11	0.0567 ± 0.0004	0.0542 ± 0.0003	0.4224 ± 0.0027	480 ± 17	340 ± 2	94
12XL19-1-1	1.92	0.0546 ± 0.0020	0.0494 ± 0.0008	0.3722 ± 0.0219	395 ± 84	311 ± 5	97
12XL19-1-2	1.45	0.0504 ± 0.0029	0.0513 ± 0.0011	0.3571 ± 0.0319	214 ± 131	323 ± 7	104
12XL19-1-3	1.32	0.0538 ± 0.0025	0.0482 ± 0.0009	0.3577 ± 0.0258	361 ± 104	304 ± 5	98
12XL19-1-4	1.63	0.0527 ± 0.0019	0.0493 ± 0.0007	0.3584 ± 0.0203	316 ± 83	310 ± 4	100
12XL19-1-5	2.04	0.0420 ± 0.0036	0.0488 ± 0.0014	0.2831 ± 0.0383	NaN ± 0	307 ± 9	121
12XL19-1-6	1.98	0.0477 ± 0.0035	0.0493 ± 0.0012	0.3246 ± 0.0371	86 ± 174	310 ± 8	109
12XL19-1-7	1.59	0.0555 ± 0.0020	0.0513 ± 0.0008	0.3925 ± 0.0220	431 ± 80	322 ± 5	96
12XL19-1-8	1.81	0.0506 ± 0.0029	0.0527 ± 0.0011	0.3680 ± 0.0332	223 ± 134	331 ± 7	104

(continued)

Table B.1 (continued)

Sample	U/Th	$^{206}Pb^*/^{207}Pb^*$	$^{206}Pb^*/^{238}U$	$^{207}Pb^*/^{235}U$	$^{206}Pb^*/^{207}Pb^* - Age$ [Ma]	$^{238}U/^{206}Pb - Age$ [Ma]	Concordance [%]
12XL19-1-9	1.71	0.0562 ± 0.0043	0.0480 ± 0.0007	0.3726 ± 0.0456	460 ± 171	303 ± 4	94
12XL19-1-10	1.47	0.0536 ± 0.0018	0.0504 ± 0.0007	0.3722 ± 0.0199	352 ± 77	317 ± 4	99
12XL19-1-11	1.06	0.0624 ± 0.0024	0.0484 ± 0.0008	0.4168 ± 0.0247	688 ± 81	305 ± 5	86
12XL19-1-12	2.25	0.0530 ± 0.0018	0.0500 ± 0.0007	0.3653 ± 0.0192	329 ± 76	314 ± 4	99
12XL19-1-13	1.91	0.0494 ± 0.0051	0.0466 ± 0.0017	0.3179 ± 0.0513	167 ± 239	294 ± 10	105
12XL19-1-14	1.00	0.0602 ± 0.0026	0.0484 ± 0.0009	0.4016 ± 0.0277	611 ± 95	304 ± 5	89
12XL19-1-15	2.17	0.0548 ± 0.0020	0.0505 ± 0.0008	0.3815 ± 0.0222	401 ± 83	318 ± 5	97
12XL19-1-16	1.86	0.0517 ± 0.0021	0.0490 ± 0.0008	0.3496 ± 0.0231	272 ± 95	308 ± 5	101
12XL19-1-17	1.83	0.0560 ± 0.0030	0.0526 ± 0.0012	0.4066 ± 0.0349	451 ± 119	331 ± 7	95
12XL19-1-18	1.83	0.0566 ± 0.0025	0.0498 ± 0.0010	0.3892 ± 0.0281	476 ± 98	313 ± 6	94
12XL19-1-19	0.98	0.0539 ± 0.0019	0.0481 ± 0.0008	0.3578 ± 0.0205	366 ± 78	303 ± 5	97
12XL19-1-20	1.19	0.0586 ± 0.0028	0.0473 ± 0.0010	0.3827 ± 0.0300	551 ± 103	298 ± 6	91
12XL19-1-21	1.51	0.0602 ± 0.0042	0.0469 ± 0.0014	0.3899 ± 0.0452	611 ± 150	296 ± 9	88
12XL19-1-22	1.42	0.0686 ± 0.0032	0.0501 ± 0.0011	0.4748 ± 0.0367	887 ± 96	315 ± 7	80
12XL19-1-23	1.67	0.0600 ± 0.0029	0.0491 ± 0.0011	0.4066 ± 0.0327	602 ± 105	309 ± 7	89
12XL19-1-24	1.98	0.0512 ± 0.0022	0.0498 ± 0.0009	0.3523 ± 0.0246	250 ± 97	314 ± 6	102
12XL19-1-25	1.54	0.0558 ± 0.0036	0.0466 ± 0.0012	0.3586 ± 0.0381	444 ± 145	293 ± 8	94
12XL19-1-26	1.87	0.0538 ± 0.0031	0.0464 ± 0.0010	0.3445 ± 0.0320	362 ± 128	293 ± 6	97
12XL19-1-27	1.64	0.0527 ± 0.0020	0.0493 ± 0.0008	0.3582 ± 0.0220	314 ± 86	310 ± 5	100
12XL19-1-28	1.09	0.0538 ± 0.0024	0.0480 ± 0.0009	0.3561 ± 0.0257	361 ± 100	302 ± 5	98
12XL19-1-29	1.51	0.0649 ± 0.0029	0.0496 ± 0.0010	0.4437 ± 0.0328	771 ± 96	312 ± 6	84
12XL19-1-30	1.53	0.0765 ± 0.0056	0.0530 ± 0.0018	0.5591 ± 0.0662	1108 ± 146	333 ± 11	74
12XL19-1-31	0.94	0.0368 ± 0.0072	0.0343 ± 0.0008	0.1742 ± 0.0566	NaN ± 0	218 ± 5	134

(continued)

Table B.1 (continued)

Sample	U/Th	$^{206}Pb^*/^{207}Pb^*$	$^{206}Pb^*/^{238}U$	$^{207}Pb^*/^{235}U$	$^{206}Pb^*/^{207}Pb^* - Age$ [Ma]	$^{238}U/^{206}Pb - Age$ [Ma]	Concordance [%]
12XL19-1-32	1.32	0.0672 ± 0.0027	0.0469 ± 0.0009	0.4346 ± 0.0284	844 ± 84	295 ± 5	81
12XL19-1-33	1.21	0.0574 ± 0.0020	0.0503 ± 0.0008	0.3978 ± 0.0223	505 ± 76	316 ± 5	93
12XL19-1-34	1.64	0.0561 ± 0.0035	0.0474 ± 0.0012	0.3670 ± 0.0374	456 ± 140	299 ± 7	94
12XL19-1-35	1.04	0.0534 ± 0.0023	0.0529 ± 0.0009	0.3899 ± 0.0265	346 ± 96	332 ± 6	99
12XL19-1-36	1.48	0.0479 ± 0.0025	0.0514 ± 0.0010	0.3392 ± 0.0281	92 ± 122	323 ± 6	109
12XL19-1-37	1.70	0.0549 ± 0.0032	0.0474 ± 0.0011	0.3587 ± 0.0332	406 ± 130	299 ± 7	96
12XL19-1-38	1.62	0.0548 ± 0.0029	0.0485 ± 0.0010	0.3660 ± 0.0314	401 ± 120	305 ± 6	96
12XL19-1-39	1.10	0.0545 ± 0.0017	0.0489 ± 0.0007	0.3677 ± 0.0184	392 ± 70	308 ± 4	97
12XL19-1-40	1.35	0.0549 ± 0.0020	0.0486 ± 0.0008	0.3686 ± 0.0211	409 ± 80	306 ± 5	96
12XL19-1-41	1.85	0.0552 ± 0.0018	0.0519 ± 0.0007	0.3946 ± 0.0202	419 ± 71	326 ± 5	97
12XL19-1-42	1.35	0.0616 ± 0.0021	0.0492 ± 0.0007	0.4183 ± 0.0226	660 ± 72	310 ± 5	87
12XL19-1-43	1.57	0.0531 ± 0.0048	0.0531 ± 0.0018	0.3885 ± 0.0578	331 ± 207	334 ± 11	100
12XL19-1-44	2.43	0.0563 ± 0.0021	0.0496 ± 0.0008	0.3852 ± 0.0236	462 ± 83	312 ± 5	94
12XL19-1-45	1.18	0.0568 ± 0.0017	0.0507 ± 0.0007	0.3968 ± 0.0189	482 ± 64	319 ± 4	94
12XL19-1-46	1.34	0.0608 ± 0.0029	0.0477 ± 0.0010	0.4001 ± 0.0309	631 ± 102	301 ± 6	88
12XL19-1-47	1.64	0.0555 ± 0.0025	0.0487 ± 0.0009	0.3724 ± 0.0276	430 ± 101	306 ± 6	95
12XL19-1-48	1.18	0.0732 ± 0.0041	0.0500 ± 0.0012	0.5046 ± 0.0457	1018 ± 114	315 ± 8	76
12XL19-1-49	2.20	0.0558 ± 0.0039	0.0449 ± 0.0012	0.3452 ± 0.0391	444 ± 157	283 ± 8	94
12XL19-1-50	0.57	0.0574 ± 0.0018	0.0473 ± 0.0007	0.3746 ± 0.0192	506 ± 71	298 ± 4	92
12XL19-1-51	1.41	0.0328 ± 0.0070	0.0456 ± 0.0009	0.2059 ± 0.0720	NaN ± 0	287 ± 6	151
12XL19-1-52	1.91	0.0534 ± 0.0022	0.0504 ± 0.0009	0.3715 ± 0.0248	345 ± 94	317 ± 5	99
12XL19-1-53	0.93	0.0594 ± 0.0019	0.0486 ± 0.0007	0.3980 ± 0.0209	581 ± 71	306 ± 4	90
12XL19-1-54	1.50	0.0591 ± 0.0020	0.0482 ± 0.0007	0.3922 ± 0.0219	568 ± 75	303 ± 4	90

(continued)

Table B.1 (continued)

Sample	U/Th	$^{206}Pb^*/^{207}Pb^*$	$^{206}Pb^*/^{238}U$	$^{207}Pb^*/^{235}U$	$^{206}Pb^*/^{207}Pb^* - Age$ [Ma]	$^{238}U/^{206}Pb - Age$ [Ma]	Concordance [%]
12XL19-1-55	1.73	0.0404 ± 0.0080	0.0371 ± 0.0009	0.2065 ± 0.0676	NaN ± 0	235 ± 5	123
12XL19-1-56	1.98	0.0583 ± 0.0034	0.0493 ± 0.0012	0.3967 ± 0.0376	541 ± 128	310 ± 7	91
12XL19-1-57	1.48	0.0530 ± 0.0019	0.0483 ± 0.0007	0.3527 ± 0.0201	328 ± 80	304 ± 5	99
12XL19-1-58	1.47	0.0534 ± 0.0034	0.0505 ± 0.0012	0.3719 ± 0.0381	344 ± 143	318 ± 8	99
12XL19-1-59	1.67	0.0651 ± 0.0037	0.0468 ± 0.0011	0.4197 ± 0.0380	776 ± 119	295 ± 7	83
12XL19-1-60	1.95	0.0522 ± 0.0020	0.0487 ± 0.0008	0.3506 ± 0.0222	295 ± 89	306 ± 5	100
12XL19-1-61	1.27	0.0593 ± 0.0021	0.0538 ± 0.0008	0.4403 ± 0.0245	579 ± 76	338 ± 5	91
12XL19-1-62	1.62	0.0609 ± 0.0031	0.0500 ± 0.0010	0.4196 ± 0.0338	634 ± 109	314 ± 6	88
12XL19-1-63	1.86	0.0536 ± 0.0020	0.0523 ± 0.0008	0.3865 ± 0.0225	353 ± 83	328 ± 5	99
12XL19-1-64	1.25	0.0783 ± 0.0048	0.0448 ± 0.0012	0.4840 ± 0.0471	1154 ± 122	283 ± 8	70
12XL19-1-65	1.74	0.0490 ± 0.0046	0.0505 ± 0.0016	0.3411 ± 0.0509	148 ± 219	317 ± 10	106
12XL19-1-66	1.70	0.0549 ± 0.0022	0.0487 ± 0.0008	0.3685 ± 0.0232	407 ± 89	306 ± 5	96
12XL19-1-67	1.65	0.0781 ± 0.0037	0.0489 ± 0.0010	0.5266 ± 0.0398	1148 ± 95	308 ± 6	72
12XL19-1-68	1.86	0.0544 ± 0.0019	0.0497 ± 0.0007	0.3732 ± 0.0204	388 ± 77	313 ± 4	97
12XL19-1-69	1.81	0.0522 ± 0.0028	0.0477 ± 0.0010	0.3437 ± 0.0297	294 ± 123	301 ± 6	100
12XL19-1-70	2.14	0.0519 ± 0.0018	0.0505 ± 0.0007	0.3615 ± 0.0202	279 ± 80	318 ± 5	101
12XL19-1-71	1.57	0.0521 ± 0.0020	0.0536 ± 0.0008	0.3848 ± 0.0235	288 ± 88	336 ± 5	102
12XL19-1-72	1.26	0.0913 ± 0.0043	0.0520 ± 0.0012	0.6551 ± 0.0483	1452 ± 90	327 ± 7	64
12XL19-1-73	0.99	0.0591 ± 0.0021	0.0527 ± 0.0008	0.4293 ± 0.0244	569 ± 79	331 ± 5	91
12XL19-1-74	1.56	0.0655 ± 0.0025	0.0457 ± 0.0007	0.4125 ± 0.0244	788 ± 80	288 ± 5	82
12XL19-1-75	0.96	0.0855 ± 0.0033	0.0483 ± 0.0008	0.5695 ± 0.0335	1327 ± 74	304 ± 5	66
12XL19-1-76	1.35	0.0548 ± 0.0022	0.0517 ± 0.0009	0.3906 ± 0.0246	403 ± 91	325 ± 5	97
12XL19-1-77	1.71	0.0555 ± 0.0020	0.0525 ± 0.0008	0.4019 ± 0.0223	430 ± 80	330 ± 5	96

(continued)

Table B.1 (continued)

Sample	U/Th	$^{206}Pb^*/^{207}Pb^*$	$^{206}Pb^*/^{238}U$	$^{207}Pb^*/^{235}U$	$^{206}Pb^*/^{207}Pb^*-Age$ [Ma]	$^{238}U/^{206}Pb-Age$ [Ma]	Concordance [%]
12XL19-1-78	1.08	0.0605 ± 0.0028	0.0492 ± 0.0009	0.4107 ± 0.0295	621 ± 99	310 ± 6	89
12XL19-1-79	2.02	0.0523 ± 0.0034	0.0531 ± 0.0013	0.3831 ± 0.0395	297 ± 149	334 ± 8	101
12XL19-1-80	0.97	0.0601 ± 0.0026	0.0534 ± 0.0010	0.4424 ± 0.0301	605 ± 93	335 ± 6	90
12XL19-1-81	1.81	0.0597 ± 0.0027	0.0480 ± 0.0009	0.3960 ± 0.0283	593 ± 97	302 ± 6	89
12XL19-1-82	1.47	0.0504 ± 0.0033	0.0520 ± 0.0013	0.3617 ± 0.0375	213 ± 151	327 ± 8	104
12XL19-1-83	1.15	0.0505 ± 0.0018	0.0517 ± 0.0008	0.3600 ± 0.0201	215 ± 82	325 ± 5	104
12XL19-1-84	1.41	0.0517 ± 0.0019	0.0504 ± 0.0007	0.3592 ± 0.0202	269 ± 82	317 ± 5	102
12XL19-1-85	1.71	0.0516 ± 0.0019	0.0481 ± 0.0007	0.3421 ± 0.0200	266 ± 86	303 ± 4	101
12XL19-1-86	1.16	0.0506 ± 0.0020	0.0528 ± 0.0008	0.3681 ± 0.0225	221 ± 90	331 ± 5	104
12XL19-1-87	5.07	0.0510 ± 0.0019	0.0481 ± 0.0007	0.3383 ± 0.0194	238 ± 85	303 ± 4	102
12XL19-1-88	1.08	0.0513 ± 0.0019	0.0531 ± 0.0008	0.3758 ± 0.0214	255 ± 84	333 ± 5	103
12XL19-1-89	1.91	0.0560 ± 0.0038	0.0494 ± 0.0013	0.3815 ± 0.0404	453 ± 150	311 ± 8	95
12XL19-1-90	1.18	0.0534 ± 0.0025	0.0487 ± 0.0009	0.3585 ± 0.0267	343 ± 108	307 ± 6	99
12XL19-1-91	1.37	0.0541 ± 0.0028	0.0510 ± 0.0010	0.3806 ± 0.0311	375 ± 116	321 ± 6	98
12XL19-1-92	1.13	0.0959 ± 0.0034	0.0535 ± 0.0009	0.7081 ± 0.0397	1545 ± 67	336 ± 6	62
12XL19-1-93	1.15	0.0610 ± 0.0023	0.0508 ± 0.0008	0.4270 ± 0.0261	637 ± 82	319 ± 5	88
12XL19-1-94	1.47	0.0508 ± 0.0017	0.0491 ± 0.0007	0.3441 ± 0.0180	233 ± 75	309 ± 4	103
12XL19-1-95	1.27	0.0541 ± 0.0019	0.0491 ± 0.0007	0.3668 ± 0.0206	375 ± 78	309 ± 5	97
12XL19-1-96	2.36	0.0249 ± 0.0060	0.0441 ± 0.0018	0.1513 ± 0.0607	NaN $\pm$ 0	278 ± 11	194
12XL19-1-97	1.64	0.0632 ± 0.0029	0.0478 ± 0.0009	0.4168 ± 0.0311	714 ± 97	301 ± 6	85
12XL19-1-98	2.36	0.0585 ± 0.0033	0.0535 ± 0.0012	0.4317 ± 0.0400	549 ± 123	336 ± 8	92
12XL19-1-99	1.08	0.0823 ± 0.0038	0.0532 ± 0.0012	0.6035 ± 0.0448	1251 ± 89	334 ± 7	70
12XL19-1-100	2.04	0.0704 ± 0.0031	0.0482 ± 0.0010	0.4686 ± 0.0338	940 ± 90	304 ± 6	78

(continued)

Table B.1 (continued)

Sample	U/Th	$^{206}Pb^*/^{207}Pb^*$	$^{206}Pb^*/^{238}U$	$^{207}Pb^*/^{235}U$	$^{206}Pb^*/^{207}Pb^* - Age$ [Ma]	$^{238}U/^{206}Pb - Age$ [Ma]	Concordance [%]
12XL19-1-101	2.24	0.0578 ± 0.0022	0.0485 ± 0.0008	0.3864 ± 0.0238	520 ± 82	305 ± 5	92
12XL19-1-102	1.91	0.0517 ± 0.0023	0.0488 ± 0.0009	0.3486 ± 0.0252	273 ± 101	307 ± 5	101
12XL19-1-103	1.38	0.0533 ± 0.0020	0.0496 ± 0.0008	0.3649 ± 0.0221	342 ± 84	312 ± 5	99
12XL19-1-104	1.97	0.0567 ± 0.0025	0.0501 ± 0.0009	0.3919 ± 0.0276	479 ± 96	315 ± 6	94
12XL19-1-105	1.64	0.0561 ± 0.0023	0.0515 ± 0.0009	0.3985 ± 0.0268	454 ± 92	324 ± 5	95
12XL19-1-106	1.21	0.0502 ± 0.0024	0.0457 ± 0.0008	0.3165 ± 0.0240	204 ± 109	288 ± 5	103
12XL19-1-107	1.67	0.0582 ± 0.0027	0.0521 ± 0.0010	0.4183 ± 0.0314	537 ± 101	327 ± 6	92
12XL19-1-108	2.18	0.0527 ± 0.0026	0.0489 ± 0.0010	0.3554 ± 0.0286	317 ± 113	308 ± 6	100
12XL19-1-109	1.25	0.0516 ± 0.0023	0.0467 ± 0.0009	0.3327 ± 0.0242	268 ± 103	294 ± 5	101
12XL19-1-110	1.41	0.0648 ± 0.0024	0.0468 ± 0.0008	0.4180 ± 0.0256	767 ± 80	295 ± 5	83
12XL19-1-111	1.75	0.0580 ± 0.0031	0.0493 ± 0.0010	0.3941 ± 0.0343	529 ± 117	310 ± 6	92
12XL19-1-112	1.94	0.0552 ± 0.0020	0.0516 ± 0.0008	0.3930 ± 0.0231	421 ± 81	324 ± 5	96
12XL19-1-113	1.14	0.0598 ± 0.0033	0.0497 ± 0.0011	0.4103 ± 0.0372	596 ± 121	313 ± 7	90
12XL19-1-114	1.66	0.0511 ± 0.0016	0.0490 ± 0.0007	0.3452 ± 0.0181	245 ± 74	308 ± 4	102
12XL19-1-115	1.51	0.0550 ± 0.0025	0.0470 ± 0.0009	0.3570 ± 0.0266	412 ± 103	296 ± 6	96
12XL19-1-116	1.72	0.0757 ± 0.0027	0.0495 ± 0.0008	0.5170 ± 0.0294	1086 ± 71	312 ± 5	74
12XL19-1-117	1.72	0.0651 ± 0.0033	0.0504 ± 0.0011	0.4524 ± 0.0373	776 ± 108	317 ± 7	84
12XL19-1-118	1.05	0.1058 ± 0.0037	0.0530 ± 0.0009	0.7733 ± 0.0426	1727 ± 64	333 ± 6	57
12XL19-1-119	1.66	0.0550 ± 0.0017	0.0500 ± 0.0007	0.3796 ± 0.0188	413 ± 70	315 ± 4	96
12XL19-1-120	1.96	0.0517 ± 0.0020	0.0508 ± 0.0008	0.3622 ± 0.0220	273 ± 87	319 ± 5	102
11XL45-1-1	3.53	0.0755 ± 0.0003	0.1430 ± 0.0010	1.4870 ± 0.0100	1083 ± 13	861 ± 6	92
11XL45-1-2	1.84	0.0742 ± 0.0003	0.1488 ± 0.0012	1.5191 ± 0.0102	1047 ± 7	894 ± 6	95
11XL45-1-3	1.63	0.0586 ± 0.0002	0.0701 ± 0.0005	0.5660 ± 0.0040	554 ± 7	436 ± 3	95

(continued)

Table B.1 (continued)

Sample	U/Th	$^{206}Pb^*/^{207}Pb^*$	$^{206}Pb^*/^{238}U$	$^{207}Pb^*/^{235}U$	$^{206}Pb^*/^{207}Pb^* - Age$ [Ma]	$^{238}U/^{206}Pb - Age$ [Ma]	Concordance [%]
11XL45-1-4	7.10	0.0719 ± 0.0002	0.1314 ± 0.0008	1.3016 ± 0.0082	983 ± 5	796 ± 5	93
11XL45-1-5	0.74	0.0858 ± 0.0004	0.1723 ± 0.0022	2.0375 ± 0.0272	1400 ± 9	1025 ± 12	90
11XL45-1-6	0.52	0.0587 ± 0.0003	0.0585 ± 0.0004	0.4730 ± 0.0040	567 ± 9	366 ± 3	92
11XL45-1-7	2.68	0.0590 ± 0.0002	0.0691 ± 0.0005	0.5619 ± 0.0045	569 ± 7	431 ± 3	94
11XL45-1-8	3.12	0.0713 ± 0.0002	0.1445 ± 0.0012	1.4214 ± 0.0120	966 ± 6	870 ± 7	96
11XL45-1-9	2.10	0.0614 ± 0.0002	0.0672 ± 0.0005	0.5685 ± 0.0044	654 ± 1	419 ± 3	91
11XL45-1-10	3.44	0.1139 ± 0.0004	0.2983 ± 0.0024	4.6889 ± 0.0487	1863 ± 6	1683 ± 12	95
11XL45-1-11	3.27	0.2430 ± 0.0010	0.3805 ± 0.0030	12.7539 ± 0.1254	3140 ± 1	2078 ± 14	75
11XL45-1-12	1.86	0.0701 ± 0.0004	0.1304 ± 0.0015	1.2547 ± 0.0134	931 ± 11	790 ± 9	95
11XL45-1-13	0.98	0.0846 ± 0.0002	0.2270 ± 0.0023	2.6493 ± 0.0281	1309 ± 10	1319 ± 12	99
11XL45-1-14	2.81	0.0558 ± 0.0002	0.0706 ± 0.0008	0.5432 ± 0.0065	443 ± 6	440 ± 5	99
11XL45-1-15	4.56	0.0811 ± 0.0007	0.1354 ± 0.0015	1.5190 ± 0.0243	1224 ± 17	818 ± 9	86
11XL45-1-16	2.72	0.0885 ± 0.0004	0.2012 ± 0.0020	2.4565 ± 0.0293	1392 ± 13	1182 ± 11	93
11XL45-1-17	1.66	0.0710 ± 0.0002	0.0652 ± 0.0006	0.6383 ± 0.0061	967 ± 7	407 ± 4	79
11XL45-1-18	1.67	0.0567 ± 0.0001	0.0664 ± 0.0006	0.5195 ± 0.0048	480 ± 6	415 ± 3	97
11XL45-1-19	1.43	0.1589 ± 0.0003	0.4298 ± 0.0037	9.4119 ± 0.0831	2444 ± 2	2305 ± 17	96
11XL45-1-20	1.36	0.0906 ± 0.0002	0.2480 ± 0.0016	3.0972 ± 0.0227	1439 ± 5	1428 ± 8	99
11XL45-1-21	2.34	0.0559 ± 0.0002	0.0679 ± 0.0006	0.5228 ± 0.0048	450 ± 7	423 ± 4	99
11XL45-1-22	1.77	0.0911 ± 0.0002	0.2160 ± 0.0017	2.7127 ± 0.0218	1450 ± −1	1261 ± 9	94
11XL45-1-23	2.90	0.1017 ± 0.0002	0.2189 ± 0.0013	3.0717 ± 0.0217	1657 ± 5	1276 ± 7	88
11XL45-1-24	1.30	0.0554 ± 0.0003	0.0663 ± 0.0005	0.5055 ± 0.0045	428 ± 11	414 ± 3	99
11XL45-1-25	1.10	0.0563 ± 0.0002	0.0679 ± 0.0004	0.5276 ± 0.0036	465 ± 7	424 ± 3	98
11XL45-1-26	1.58	0.0701 ± 0.0002	0.1557 ± 0.0011	1.5054 ± 0.0118	931 ± 4	933 ± 6	99

(continued)

Table B.1 (continued)

Sample	U/Th	$^{206}Pb^*/^{207}Pb^*$	$^{206}Pb^*/^{238}U$	$^{207}Pb^*/^{235}U$	$^{206}Pb^*/^{207}Pb^* - Age$ [Ma]	$^{238}U/^{206}Pb - Age$ [Ma]	Concordance [%]
11XL45-1-27	1.02	0.0774 ± 0.0001	0.1908 ± 0.0015	2.0356 ± 0.0161	1131 ± 8	1126 ± 8	99
11XL45-1-28	1.82	0.0712 ± 0.0001	0.1631 ± 0.0011	1.5998 ± 0.0116	962 ± 0	974 ± 6	99
11XL45-1-29	1.68	0.0601 ± 0.0002	0.0686 ± 0.0004	0.5688 ± 0.0037	606 ± 9	428 ± 2	93
11XL45-1-30	1.18	0.0629 ± 0.0003	0.1019 ± 0.0006	0.8834 ± 0.0057	706 ± 13	625 ± 3	97
11XL45-1-31	1.78	0.0976 ± 0.0009	0.1222 ± 0.0007	1.6389 ± 0.0107	1589 ± 17	743 ± 4	71
11XL45-1-32	1.48	0.0565 ± 0.0002	0.0689 ± 0.0004	0.5362 ± 0.0033	472 ± 6	429 ± 2	98
11XL45-1-33	1.39	0.1802 ± 0.0003	0.4838 ± 0.0043	12.0249 ± 0.1113	2654 ± 3	2544 ± 19	97
11XL45-1-34	5.40	0.0692 ± 0.0001	0.1390 ± 0.0010	1.3274 ± 0.0092	906 ± 4	839 ± 5	97
11XL45-1-35	2.58	0.0894 ± 0.0003	0.1477 ± 0.0009	1.8226 ± 0.0155	1413 ± 7	888 ± 5	82
11XL45-1-36	1.40	0.0863 ± 0.0004	0.0593 ± 0.0004	0.7050 ± 0.0046	1344 ± −23	372 ± 2	62
11XL45-1-37	4.81	0.0855 ± 0.0005	0.1418 ± 0.0006	1.6709 ± 0.0103	1328 ± 11	855 ± 4	84
11XL45-1-38	2.24	0.0697 ± 0.0001	0.1529 ± 0.0009	1.4699 ± 0.0087	920 ± 4	917 ± 5	99
11XL45-1-39	1.44	0.0559 ± 0.0002	0.0741 ± 0.0003	0.5714 ± 0.0027	450 ± 7	461 ± 2	99
11XL45-1-40	1.81	0.0597 ± 0.0002	0.0694 ± 0.0003	0.5721 ± 0.0036	594 ± 12	433 ± 2	93
11XL45-1-41	0.56	0.0914 ± 0.0008	0.0844 ± 0.0011	1.0709 ± 0.0216	1454 ± 18	522 ± 7	65
11XL45-1-42	1.22	0.0580 ± 0.0002	0.0731 ± 0.0004	0.5841 ± 0.0034	528 ± 40	455 ± 2	97
11XL45-1-43	1.11	0.1419 ± 0.0009	0.0481 ± 0.0005	0.9397 ± 0.0081	2250 ± 11	303 ± 3	24
11XL45-1-44	9.60	0.0698 ± 0.0002	0.1376 ± 0.0010	1.3257 ± 0.0098	924 ± 6	831 ± 5	96
11XL45-1-45	3.99	0.0700 ± 0.0002	0.1351 ± 0.0012	1.3040 ± 0.0116	928 ± 40	817 ± 7	96
11XL45-1-46	0.71	0.1600 ± 0.0004	0.4404 ± 0.0026	9.7175 ± 0.0553	2457 ± 4	2353 ± 11	97
11XL45-1-47	2.28	0.1647 ± 0.0004	0.3295 ± 0.0016	7.4863 ± 0.0412	2506 ± 4	1836 ± 8	83
11XL45-1-48	2.22	0.1542 ± 0.0004	0.2811 ± 0.0022	5.9758 ± 0.0450	2392 ± 5	1597 ± 11	78
11XL45-1-49	1.94	0.0617 ± 0.0003	0.0651 ± 0.0002	0.5544 ± 0.0040	663 ± 13	407 ± 1	90

(continued)

Table B.1 (continued)

Sample	U/Th	$^{206}Pb^*/^{207}Pb^*$	$^{206}Pb^*/^{238}U$	$^{207}Pb^*/^{235}U$	$^{206}Pb^*/^{207}Pb^* - Age$ [Ma]	$^{238}U/^{206}Pb - Age$ [Ma]	Concordance [%]
11XL45-1-50	2.05	0.0596 ± 0.0002	0.0643 ± 0.0003	0.5286 ± 0.0025	591 ± 7	402 ± 2	92
11XL45-1-51	5.79	0.1080 ± 0.0002	0.2727 ± 0.0017	4.0602 ± 0.0251	1766 ± 3	1554 ± 9	94
11XL45-1-52	10.01	0.0573 ± 0.0002	0.0732 ± 0.0005	0.5784 ± 0.0043	506 ± 12	455 ± 3	98
11XL45-1-53	2.02	0.0734 ± 0.0002	0.1472 ± 0.0009	1.4868 ± 0.0074	1033 ± 7	885 ± 5	95
11XL45-1-54	1.30	0.1042 ± 0.0003	0.2191 ± 0.0024	3.1582 ± 0.0398	1702 ± 5	1277 ± 13	87
11XL45-1-55	2.83	0.0614 ± 0.0002	0.0980 ± 0.0009	0.8317 ± 0.0091	654 ± 3	602 ± 5	98
11XL45-1-56	3.88	0.0726 ± 0.0003	0.1353 ± 0.0008	1.3522 ± 0.0078	1011 ± 9	818 ± 5	93
11XL45-1-57	0.73	0.0803 ± 0.0002	0.2009 ± 0.0016	2.2254 ± 0.0182	1206 ± −29	1180 ± 8	99
11XL45-1-58	1.79	0.0732 ± 0.0003	0.1471 ± 0.0008	1.4848 ± 0.0100	1020 ± 9	885 ± 5	95
11XL45-1-59	1.99	0.0714 ± 0.0003	0.1174 ± 0.0011	1.1532 ± 0.0102	969 ± 14	716 ± 6	91
11XL45-1-60	3.23	0.0566 ± 0.0002	0.0620 ± 0.0005	0.4836 ± 0.0043	476 ± 3	388 ± 3	96
11XL45-1-61	1.65	0.0561 ± 0.0002	0.0619 ± 0.0004	0.4790 ± 0.0034	454 ± 6	387 ± 2	97
11XL45-1-62	1.17	0.1807 ± 0.0004	0.3982 ± 0.0040	9.9237 ± 0.1050	2661 ± 5	2161 ± 18	88
11XL45-1-63	1.34	0.0565 ± 0.0002	0.0650 ± 0.0006	0.5060 ± 0.0048	472 ± 6	406 ± 4	97
11XL45-1-64	1.09	0.0567 ± 0.0003	0.0744 ± 0.0017	0.5813 ± 0.0135	480 ± 11	462 ± 10	99
11XL45-1-65	1.30	0.0804 ± 0.0011	0.0849 ± 0.0009	0.9333 ± 0.0095	1209 ± 27	525 ± 5	75
11XL45-1-66	2.14	0.1011 ± 0.0002	0.1870 ± 0.0017	2.6099 ± 0.0251	1644 ± 4	1105 ± 9	83
11XL45-1-67	1.63	0.0770 ± 0.0004	0.1505 ± 0.0011	1.5952 ± 0.0100	1121 ± 5	904 ± 6	93
11XL45-1-68	1.42	0.0750 ± 0.0002	0.1366 ± 0.0012	1.4134 ± 0.0134	1133 ± 7	825 ± 7	91
11XL45-1-69	1.14	0.0683 ± 0.0005	0.0576 ± 0.0006	0.5413 ± 0.0043	880 ± 15	361 ± 4	80
11XL45-1-70	1.42	0.2592 ± 0.0005	0.6666 ± 0.0065	23.8505 ± 0.2430	3242 ± 3	3293 ± 25	99
11XL45-1-71	2.85	0.0807 ± 0.0002	0.1900 ± 0.0016	2.1148 ± 0.0180	1215 ± 4	1121 ± 9	97
11XL45-1-72	0.84	0.0579 ± 0.0002	0.0661 ± 0.0005	0.5281 ± 0.0042	528 ± 42	413 ± 3	95

(continued)

Table B.1 (continued)

Sample	U/Th	$^{206}Pb^*/^{207}Pb^*$	$^{206}Pb^*/^{238}U$	$^{207}Pb^*/^{235}U$	$^{206}Pb^*/^{207}Pb^* - Age$ [Ma]	$^{238}U/^{206}Pb - Age$ [Ma]	Concordance [%]
11XL45-1-73	0.73	0.0999 ± 0.0002	0.2281 ± 0.0027	3.1428 ± 0.0366	1622 ± 5	1325 ± 14	91
11XL45-1-74	0.69	0.0558 ± 0.0002	0.0701 ± 0.0007	0.5392 ± 0.0053	443 ± 6	437 ± 4	99
11XL45-1-75	1.23	0.0707 ± 0.0002	0.1337 ± 0.0013	1.3046 ± 0.0129	950 ± 6	809 ± 7	95
11XL45-1-76	1.29	0.0625 ± 0.0002	0.0742 ± 0.0006	0.6400 ± 0.0051	692 ± 8	461 ± 4	91
11XL45-1-77	0.86	0.1647 ± 0.0004	0.4322 ± 0.0171	9.8302 ± 0.3884	2506 ± 3	2316 ± 77	95
11XL45-1-78	2.03	0.0573 ± 0.0003	0.0686 ± 0.0006	0.5433 ± 0.0058	506 ± 14	428 ± 4	97
11XL45-1-79	2.66	0.0702 ± 0.0002	0.1407 ± 0.0012	1.3611 ± 0.0113	933 ± 6	848 ± 7	97
11XL45-1-80	2.52	0.0718 ± 0.0002	0.1428 ± 0.0014	1.4120 ± 0.0134	989 ± 5	861 ± 8	96
11XL45-1-81	0.98	0.0565 ± 0.0001	0.0652 ± 0.0005	0.5081 ± 0.0042	472 ± 6	407 ± 3	97
11XL45-1-82	1.77	0.0766 ± 0.0001	0.1670 ± 0.0011	1.7643 ± 0.0114	1122 ± 4	995 ± 6	96
11XL45-1-83	4.02	0.0837 ± 0.0005	0.0883 ± 0.0005	1.0189 ± 0.0079	1287 ± 11	545 ± 3	73
11XL45-1-84	1.03	0.0563 ± 0.0001	0.0666 ± 0.0006	0.5165 ± 0.0043	465 ± 10	416 ± 3	98
11XL45-1-85	1.80	0.1093 ± 0.0003	0.3011 ± 0.0025	4.5395 ± 0.0401	1788 ± 4	1697 ± 12	97
11XL45-1-86	1.58	0.0771 ± 0.0004	0.1610 ± 0.0015	1.7166 ± 0.0237	1124 ± 11	962 ± 8	94
11XL45-1-87	4.55	0.0770 ± 0.0002	0.1779 ± 0.0010	1.8873 ± 0.0113	1120 ± 4	1056 ± 6	98
11XL45-1-88	1.64	0.0685 ± 0.0002	0.1278 ± 0.0008	1.2060 ± 0.0082	883 ± 12	775 ± 5	96
11XL45-1-89	2.03	0.0708 ± 0.0002	0.1550 ± 0.0012	1.5137 ± 0.0126	954 ± 9	929 ± 7	99
11XL45-1-90	5.40	0.0707 ± 0.0003	0.1344 ± 0.0013	1.3116 ± 0.0142	950 ± 12	813 ± 7	95
12XL21-1-1	1.71	0.0575 ± 0.0003	0.0472 ± 0.0017	0.3758 ± 0.0186	510 ± 11	297 ± 11	92
12XL21-1-2	2.59	0.0572 ± 0.0003	0.0415 ± 0.0017	0.3260 ± 0.0181	498 ± 12	262 ± 11	91
12XL21-1-3	2.15	0.1885 ± 0.0023	0.0550 ± 0.0024	1.3934 ± 0.0374	2728 ± 20	345 ± 15	39
12XL21-1-4	3.13	0.0541 ± 0.0002	0.0484 ± 0.0017	0.3609 ± 0.0180	375 ± 7	305 ± 10	97
12XL21-1-5	2.19	0.2277 ± 0.0023	0.0539 ± 0.0018	1.6991 ± 0.0474	3036 ± 16	339 ± 11	34

(continued)

Table B.1 (continued)

Sample	U/Th	$^{206}Pb^*/^{207}Pb^*$	$^{206}Pb^*/^{238}U$	$^{207}Pb^*/^{235}U$	$^{206}Pb^*/^{207}Pb^*-Age$ [Ma]	$^{238}U/^{206}Pb-Age$ [Ma]	Concordance [%]
12XL21-1-6	2.13	0.1311 ± 0.0022	0.0510 ± 0.0020	0.9362 ± 0.0405	2112 ± 30	321 ± 12	48
12XL21-1-7	2.49	0.0644 ± 0.0008	0.0426 ± 0.0017	0.3771 ± 0.0182	755 ± 26	269 ± 10	83
12XL21-1-8	1.66	0.0559 ± 0.0003	0.0457 ± 0.0018	0.3527 ± 0.0185	447 ± 11	288 ± 11	94
12XL21-1-9	2.98	0.0907 ± 0.0023	0.0488 ± 0.0017	0.6213 ± 0.0278	1440 ± 49	307 ± 10	63
12XL21-1-10	1.73	0.0560 ± 0.0003	0.0468 ± 0.0018	0.3620 ± 0.0186	453 ± 11	295 ± 11	94
12XL21-1-11	2.19	0.0542 ± 0.0002	0.0518 ± 0.0017	0.3866 ± 0.0179	378 ± 9	326 ± 10	98
12XL21-1-12	2.20	0.1191 ± 0.0015	0.0434 ± 0.0018	0.7180 ± 0.0248	1941 ± 23	274 ± 11	50
12XL21-1-13	2.14	0.0664 ± 0.0008	0.0425 ± 0.0016	0.3891 ± 0.0182	819 ± 24	268 ± 10	80
12XL21-1-14	1.87	0.1099 ± 0.0010	0.0421 ± 0.0016	0.6435 ± 0.0205	1796 ± 16	266 ± 10	53
12XL21-1-15	2.62	0.0560 ± 0.0005	0.0476 ± 0.0017	0.3683 ± 0.0181	450 ± 18	300 ± 10	94
12XL21-1-16	1.95	0.0897 ± 0.0015	0.0380 ± 0.0016	0.4729 ± 0.0207	1417 ± 32	241 ± 10	61
12XL21-1-17	2.57	0.0586 ± 0.0006	0.0437 ± 0.0016	0.3518 ± 0.0179	550 ± 21	276 ± 10	90
12XL21-1-18	2.46	0.0701 ± 0.0013	0.0429 ± 0.0016	0.4112 ± 0.0187	931 ± 39	271 ± 10	77
12XL21-1-19	2.53	0.0561 ± 0.0002	0.0449 ± 0.0016	0.3466 ± 0.0173	455 ± 8	283 ± 10	94
12XL21-1-20	2.38	0.0611 ± 0.0005	0.0410 ± 0.0016	0.3444 ± 0.0171	641 ± 18	259 ± 10	86
12XL21-1-21	2.49	0.0592 ± 0.0005	0.0471 ± 0.0016	0.3813 ± 0.0172	572 ± 17	297 ± 10	90
12XL21-1-22	2.25	0.0549 ± 0.0002	0.0516 ± 0.0016	0.3906 ± 0.0172	408 ± 9	324 ± 10	97
12XL21-1-23	1.97	0.0560 ± 0.0003	0.0494 ± 0.0016	0.3808 ± 0.0171	453 ± 10	311 ± 10	95
12XL21-1-24	2.51	0.0549 ± 0.0002	0.0473 ± 0.0016	0.3572 ± 0.0173	406 ± 7	298 ± 10	96
12XL21-1-25	2.49	0.0878 ± 0.0011	0.0447 ± 0.0015	0.5406 ± 0.0180	1377 ± 23	282 ± 9	64
12XL21-1-26	1.40	0.0577 ± 0.0002	0.0454 ± 0.0016	0.3608 ± 0.0174	516 ± 8	286 ± 10	91
12XL21-1-27	2.02	0.0579 ± 0.0003	0.0445 ± 0.0015	0.3561 ± 0.0172	525 ± 10	281 ± 10	91
12XL21-1-28	2.17	0.0535 ± 0.0001	0.0542 ± 0.0017	0.3992 ± 0.0180	347 ± 6	340 ± 11	100

(continued)

Table B.1 (continued)

Sample	U/Th	$^{206}Pb^*/^{207}Pb^*$	$^{206}Pb^*/^{238}U$	$^{207}Pb^*/^{235}U$	$^{206}Pb^*/^{207}Pb^* - Age$ [Ma]	$^{238}U/^{206}Pb - Age$ [Ma]	Concordance [%]
12XL21-1-29	2.27	0.0545 ± 0.0005	0.0425 ± 0.0016	0.3193 ± 0.0173	391 ± 19	268 ± 10	95
12XL21-1-30	2.23	0.0537 ± 0.0002	0.0486 ± 0.0016	0.3598 ± 0.0170	357 ± 8	306 ± 10	98
12XL21-1-31	1.78	0.0536 ± 0.0002	0.0467 ± 0.0017	0.3450 ± 0.0174	355 ± 7	294 ± 10	98
12XL21-1-32	2.14	0.0556 ± 0.0002	0.0468 ± 0.0016	0.3581 ± 0.0173	434 ± 10	295 ± 10	95
12XL21-1-33	2.94	0.0549 ± 0.0002	0.0482 ± 0.0017	0.3635 ± 0.0175	408 ± 10	303 ± 10	96
12XL21-1-34	1.49	0.0895 ± 0.0019	0.0413 ± 0.0017	0.5093 ± 0.0216	1414 ± 41	261 ± 10	62
12XL21-1-35	2.59	0.0539 ± 0.0002	0.0497 ± 0.0017	0.3690 ± 0.0176	366 ± 7	312 ± 10	98
12XL21-1-36	1.40	0.0611 ± 0.0005	0.0411 ± 0.0017	0.3451 ± 0.0174	641 ± 17	259 ± 10	86
12XL21-1-37	2.02	0.0621 ± 0.0008	0.0458 ± 0.0017	0.3954 ± 0.0190	677 ± 27	288 ± 10	85
12XL21-1-38	2.36	0.0548 ± 0.0002	0.0496 ± 0.0017	0.3745 ± 0.0177	404 ± 9	312 ± 10	97
12XL21-1-39	2.38	0.0582 ± 0.0004	0.0413 ± 0.0017	0.3301 ± 0.0173	537 ± 14	261 ± 10	90
12XL21-1-40	2.15	0.0601 ± 0.0008	0.0454 ± 0.0017	0.3717 ± 0.0175	605 ± 28	286 ± 10	89
12XL21-1-41	1.78	0.0749 ± 0.0005	0.0464 ± 0.0017	0.4802 ± 0.0190	1065 ± 15	292 ± 11	73
12XL21-1-42	1.61	0.1037 ± 0.0011	0.0352 ± 0.0016	0.5036 ± 0.0189	1691 ± 19	223 ± 10	54
12XL21-1-43	2.64	0.0586 ± 0.0004	0.0527 ± 0.0016	0.4252 ± 0.0172	552 ± 13	331 ± 10	92
12XL21-1-44	2.44	0.0542 ± 0.0002	0.0494 ± 0.0016	0.3693 ± 0.0172	379 ± 8	311 ± 10	97
12XL21-1-46	2.01	0.0566 ± 0.0003	0.0511 ± 0.0017	0.3988 ± 0.0189	474 ± 10	321 ± 11	94
12XL21-1-47	2.17	0.0582 ± 0.0004	0.0479 ± 0.0018	0.3839 ± 0.0189	537 ± 14	302 ± 11	91
12XL21-1-48	2.43	0.0651 ± 0.0010	0.0392 ± 0.0018	0.3494 ± 0.0190	776 ± 31	248 ± 11	81
12XL21-1-49	2.39	0.0534 ± 0.0001	0.0481 ± 0.0018	0.3535 ± 0.0188	345 ± 6	303 ± 11	99
12XL21-1-50	2.26	0.0748 ± 0.0005	0.0436 ± 0.0018	0.4510 ± 0.0201	1062 ± 13	275 ± 11	73
12XL21-1-51	2.16	0.0563 ± 0.0005	0.0500 ± 0.0018	0.3894 ± 0.0197	461 ± 18	315 ± 11	94
12XL21-1-52	1.71	0.0741 ± 0.0006	0.0459 ± 0.0018	0.4692 ± 0.0195	1042 ± 15	289 ± 11	74

(continued)

Table B.1 (continued)

Sample	U/Th	$^{206}Pb^*/^{207}Pb^*$	$^{206}Pb^*/^{238}U$	$^{207}Pb^*/^{235}U$	$^{206}Pb^*/^{207}Pb^*-Age$ [Ma]	$^{238}U/^{206}Pb-Age$ [Ma]	Concordance [%]
12XL21-1-53	2.23	0.0550 ± 0.0002	0.0433 ± 0.0018	0.3279 ± 0.0184	410 ± 8	273 ± 11	95
12XL21-1-54	2.78	0.0560 ± 0.0003	0.0485 ± 0.0017	0.3742 ± 0.0181	450 ± 10	305 ± 10	95
12XL21-1-55	1.89	0.0536 ± 0.0002	0.0481 ± 0.0017	0.3552 ± 0.0182	355 ± 7	303 ± 11	98
12XL21-1-56	2.17	0.0618 ± 0.0003	0.0380 ± 0.0017	0.3240 ± 0.0181	667 ± 12	240 ± 10	84
12XL21-1-57	1.85	0.0542 ± 0.0002	0.0443 ± 0.0017	0.3305 ± 0.0181	377 ± 7	279 ± 11	96
12XL21-1-58	2.26	0.0550 ± 0.0002	0.0521 ± 0.0017	0.3955 ± 0.0179	413 ± 7	328 ± 10	97
12XL21-1-59	1.53	0.0553 ± 0.0002	0.0481 ± 0.0017	0.3663 ± 0.0176	421 ± 7	303 ± 10	96
12XL21-1-60	2.48	0.0536 ± 0.0002	0.0488 ± 0.0017	0.3599 ± 0.0177	353 ± 7	307 ± 10	98
12XL21-1-61	2.54	0.0547 ± 0.0002	0.0465 ± 0.0017	0.3499 ± 0.0178	399 ± 9	293 ± 10	96
12XL21-1-62	2.30	0.0619 ± 0.0006	0.0376 ± 0.0016	0.3199 ± 0.0177	668 ± 20	238 ± 10	84
12XL21-1-63	1.83	0.0550 ± 0.0002	0.0487 ± 0.0017	0.3694 ± 0.0177	410 ± 7	307 ± 10	96
12XL21-1-64	2.31	0.0570 ± 0.0002	0.0447 ± 0.0017	0.3510 ± 0.0177	490 ± 8	282 ± 10	92
12XL21-1-65	2.66	0.0559 ± 0.0002	0.0492 ± 0.0017	0.3798 ± 0.0180	446 ± 7	310 ± 10	95
12XL21-1-66	2.24	0.1149 ± 0.0015	0.0385 ± 0.0016	0.6104 ± 0.0202	1877 ± 23	243 ± 10	50
12XL21-1-67	1.96	0.1481 ± 0.0025	0.0495 ± 0.0021	1.0012 ± 0.0316	2323 ± 29	311 ± 13	44
12XL21-1-68	1.67	0.0536 ± 0.0002	0.0541 ± 0.0016	0.3999 ± 0.0175	354 ± 7	339 ± 10	99
12XL21-1-69	1.58	0.0550 ± 0.0002	0.0492 ± 0.0018	0.3723 ± 0.0183	410 ± 9	310 ± 11	96
12XL21-1-70	2.43	0.0586 ± 0.0004	0.0546 ± 0.0016	0.4407 ± 0.0176	550 ± 16	343 ± 10	92
12XL21-1-71	3.20	0.0578 ± 0.0006	0.0536 ± 0.0017	0.4274 ± 0.0184	522 ± 22	336 ± 10	93
12XL21-1-72	1.89	0.0632 ± 0.0007	0.0387 ± 0.0017	0.3373 ± 0.0178	715 ± 22	245 ± 10	83
12XL21-1-73	2.95	0.0538 ± 0.0003	0.0571 ± 0.0016	0.4240 ± 0.0176	361 ± 11	358 ± 10	100
12XL21-1-74	2.52	0.0589 ± 0.0007	0.0354 ± 0.0017	0.2879 ± 0.0178	563 ± 25	225 ± 10	87
12XL21-1-75	2.03	0.0538 ± 0.0002	0.0504 ± 0.0017	0.3732 ± 0.0176	360 ± 8	317 ± 10	98

(continued)

Table B.1 (continued)

Sample	U/Th	$^{206}Pb^*/^{207}Pb^*$	$^{206}Pb^*/^{238}U$	$^{207}Pb^*/^{235}U$	$^{206}Pb^*/^{207}Pb^*-Age$ [Ma]	$^{238}U/^{206}Pb-Age$ [Ma]	Concordance [%]
12XL21-1-76	2.04	0.0566 ± 0.0004	0.0444 ± 0.0017	0.3452 ± 0.0168	475 ± 14	280 ± 10	93
12XL21-1-77	2.40	0.0958 ± 0.0018	0.0413 ± 0.0016	0.5509 ± 0.0223	1543 ± 35	261 ± 10	59
12XL21-1-78	1.98	0.2599 ± 0.0029	0.0698 ± 0.0019	2.5022 ± 0.0520	3245 ± 17	435 ± 11	34
12XL21-1-79	1.91	0.0610 ± 0.0007	0.0414 ± 0.0016	0.3486 ± 0.0174	638 ± 26	261 ± 10	86
12XL21-1-80	1.96	0.0623 ± 0.0004	0.0408 ± 0.0016	0.3500 ± 0.0169	682 ± 14	258 ± 10	85
12XL21-1-81	2.14	0.0636 ± 0.0003	0.0414 ± 0.0016	0.3638 ± 0.0172	727 ± 10	262 ± 10	83
12XL21-1-82	2.27	0.0539 ± 0.0002	0.0485 ± 0.0016	0.3599 ± 0.0170	366 ± 7	305 ± 10	98
12XL21-1-83	2.41	0.0547 ± 0.0002	0.0464 ± 0.0017	0.3499 ± 0.0173	400 ± 8	292 ± 10	96
12XL21-1-84	2.26	0.0650 ± 0.0003	0.0535 ± 0.0016	0.4799 ± 0.0173	774 ± 10	336 ± 10	84
12XL21-1-85	2.16	0.0534 ± 0.0002	0.0471 ± 0.0016	0.3463 ± 0.0171	343 ± 7	297 ± 10	98
12XL21-1-86	1.38	0.0710 ± 0.0007	0.0412 ± 0.0017	0.4016 ± 0.0176	957 ± 20	260 ± 10	76
12XL21-1-87	2.78	0.0542 ± 0.0002	0.0495 ± 0.0017	0.3694 ± 0.0175	380 ± 7	311 ± 10	98
12XL21-1-88	1.55	0.0632 ± 0.0007	0.0421 ± 0.0017	0.3668 ± 0.0181	712 ± 25	266 ± 10	84
12XL21-1-89	2.70	0.0534 ± 0.0002	0.0518 ± 0.0017	0.3813 ± 0.0178	344 ± 8	326 ± 10	99
12XL21-1-90	2.64	0.0567 ± 0.0003	0.0486 ± 0.0017	0.3813 ± 0.0179	478 ± 13	306 ± 10	93
11XL41-2-1	1.26	0.0542 ± 0.0004	0.0520 ± 0.0004	0.3889 ± 0.0044	389 ± 17	327 ± 2	97
11XL41-2-2	1.45	0.0547 ± 0.0004	0.0545 ± 0.0004	0.4113 ± 0.0043	467 ± 17	342 ± 3	97
11XL41-2-3	1.22	0.0761 ± 0.0008	0.0561 ± 0.0003	0.5884 ± 0.0071	1098 ± 22	352 ± 2	71
11XL41-2-4	0.88	0.0568 ± 0.0003	0.0506 ± 0.0003	0.3964 ± 0.0029	483 ± 9	318 ± 2	93
11XL41-2-5	2.26	0.0572 ± 0.0002	0.0713 ± 0.0004	0.5624 ± 0.0038	498 ± 6	444 ± 3	97
11XL41-2-6	3.23	0.0571 ± 0.0002	0.0729 ± 0.0005	0.5732 ± 0.0042	494 ± 7	453 ± 3	98
11XL41-2-7	10.77	0.0577 ± 0.0002	0.0682 ± 0.0004	0.5429 ± 0.0037	517 ± 7	426 ± 3	96
11XL41-2-8	1.71	0.0574 ± 0.0004	0.0524 ± 0.0003	0.4152 ± 0.0035	509 ± 13	329 ± 2	93

(continued)

Table B.1 (continued)

Sample	U/Th	$^{206}Pb^*/^{207}Pb^*$	$^{206}Pb^*/^{238}U$	$^{207}Pb^*/^{235}U$	$^{206}Pb^*/^{207}Pb^*-Age$ [Ma]	$^{238}U/^{206}Pb-Age$ [Ma]	Concordance [%]
11XL41-2-9	2.75	0.0603 ± 0.0003	0.0688 ± 0.0005	0.5729 ± 0.0055	613 ± 11	429 ± 3	92
11XL41-2-10	1.66	0.0618 ± 0.0002	0.0909 ± 0.0008	0.7753 ± 0.0073	733 ± 6	561 ± 5	96
11XL41-2-11	3.85	0.1277 ± 0.0003	0.3063 ± 0.0015	5.3918 ± 0.0268	2066 ± 5	1722 ± 7	91
11XL41-2-12	1.82	0.1628 ± 0.0003	0.4992 ± 0.0033	11.2099 ± 0.0767	2485 ± 3	2610 ± 14	97
11XL41-2-13	2.26	0.0568 ± 0.0002	0.0570 ± 0.0002	0.4462 ± 0.0026	483 ± 9	357 ± 1	95
11XL41-2-14	2.25	0.1856 ± 0.0004	0.5452 ± 0.0048	13.9554 ± 0.1254	2703 ± 3	2805 ± 20	97
11XL41-2-15	1.66	0.0845 ± 0.0011	0.0685 ± 0.0006	0.8024 ± 0.0146	1306 ± 26	427 ± 4	66
11XL41-2-16	2.04	0.0756 ± 0.0005	0.1556 ± 0.0011	1.6181 ± 0.0123	1085 ± 15	932 ± 6	95
11XL41-2-17	2.31	0.0604 ± 0.0003	0.0720 ± 0.0006	0.6000 ± 0.0055	620 ± 9	448 ± 4	93
11XL41-2-18	4.72	0.0709 ± 0.0002	0.1450 ± 0.0014	1.4170 ± 0.0133	954 ± 6	873 ± 8	97
11XL41-2-19	0.85	0.1632 ± 0.0003	0.3999 ± 0.0020	9.0028 ± 0.0493	2500 ± 4	2169 ± 9	92
11XL41-2-20	1.33	0.0582 ± 0.0004	0.0566 ± 0.0005	0.4566 ± 0.0061	539 ± 15	355 ± 3	92
11XL41-2-21	2.18	0.0543 ± 0.0002	0.0539 ± 0.0004	0.4039 ± 0.0036	383 ± 9	338 ± 2	98
11XL41-2-22	1.46	0.0552 ± 0.0003	0.0521 ± 0.0003	0.3962 ± 0.0029	420 ± 13	327 ± 2	96
11XL41-2-23	0.00	0.0562 ± 0.0001	0.0682 ± 0.0006	0.5291 ± 0.0049	461 ± 10	425 ± 4	98
11XL41-2-24	1.17	0.0539 ± 0.0002	0.0533 ± 0.0004	0.3965 ± 0.0031	369 ± 5	335 ± 2	98
11XL41-2-25	0.79	0.0540 ± 0.0002	0.0504 ± 0.0004	0.3756 ± 0.0034	372 ± 12	317 ± 2	97
11XL41-2-26	1.31	0.0544 ± 0.0003	0.0535 ± 0.0005	0.4016 ± 0.0045	387 ± 11	336 ± 3	97
11XL41-2-27	1.84	0.0571 ± 0.0002	0.0736 ± 0.0006	0.5802 ± 0.0056	494 ± 9	458 ± 4	98
11XL41-2-28	1.54	0.0554 ± 0.0002	0.0657 ± 0.0005	0.5017 ± 0.0042	428 ± 7	410 ± 3	99
11XL41-2-29	1.19	0.1030 ± 0.0006	0.0643 ± 0.0008	0.9132 ± 0.0119	1680 ± 5	402 ± 5	51
11XL41-2-30	0.85	0.0920 ± 0.0003	0.2477 ± 0.0017	3.1431 ± 0.0228	1533 ± 6	1427 ± 9	98
11XL41-2-31	2.30	0.0550 ± 0.0003	0.0542 ± 0.0004	0.4109 ± 0.0039	413 ± −17	340 ± 3	97

(continued)

Table B.1 (continued)

Sample	U/Th	$^{206}Pb^*/^{207}Pb^*$	$^{206}Pb^*/^{238}U$	$^{207}Pb^*/^{235}U$	$^{206}Pb^*/^{207}Pb^* - Age$ [Ma]	$^{238}U/^{206}Pb - Age$ [Ma]	Concordance [%]
11XL41-2-32	1.55	0.0538 ± 0.0004	0.0520 ± 0.0003	0.3857 ± 0.0035	361 ± 21	327 ± 2	98
11XL41-2-33	1.67	0.1093 ± 0.0027	0.0637 ± 0.0005	0.9421 ± 0.0201	1788 ± 45	398 ± 3	48
11XL41-2-34	2.52	0.0568 ± 0.0005	0.0551 ± 0.0003	0.4305 ± 0.0032	483 ± 17	346 ± 2	94
11XL41-2-35	1.74	0.0560 ± 0.0001	0.0677 ± 0.0004	0.5226 ± 0.0032	450 ± 1	422 ± 2	98
11XL41-2-36	3.19	0.0725 ± 0.0002	0.1463 ± 0.0013	1.4626 ± 0.0126	1011 ± 6	880 ± 7	96
11XL41-2-37	1.74	0.0988 ± 0.0007	0.0650 ± 0.0005	0.8803 ± 0.0056	2000 ± 14	406 ± 3	55
11XL41-2-38	1.48	0.0944 ± 0.0002	0.2184 ± 0.0016	2.8427 ± 0.0222	1517 ± −1	1273 ± 8	92
11XL41-2-39	1.83	0.0550 ± 0.0003	0.0547 ± 0.0003	0.4145 ± 0.0028	409 ± 11	343 ± 2	97
11XL41-2-40	2.07	0.0557 ± 0.0002	0.0701 ± 0.0004	0.5386 ± 0.0036	439 ± 10	437 ± 3	99
11XL41-2-41	2.83	0.0539 ± 0.0002	0.0571 ± 0.0003	0.4238 ± 0.0024	369 ± 5	358 ± 2	99
11XL41-2-42	1.67	0.0541 ± 0.0003	0.0542 ± 0.0003	0.4035 ± 0.0029	372 ± 11	340 ± 2	98
11XL41-2-43	1.19	0.0537 ± 0.0003	0.0512 ± 0.0003	0.3790 ± 0.0030	367 ± 11	322 ± 2	98
11XL41-2-44	1.52	0.0532 ± 0.0003	0.0513 ± 0.0003	0.3758 ± 0.0034	345 ± 15	322 ± 2	99
11XL41-2-45	1.24	0.0529 ± 0.0003	0.0522 ± 0.0004	0.3809 ± 0.0034	328 ± 8	328 ± 2	99
11XL41-2-46	2.75	0.0819 ± 0.0007	0.1560 ± 0.0011	1.7540 ± 0.0113	1244 ± 16	934 ± 6	90
11XL41-2-47	1.22	0.0532 ± 0.0003	0.0486 ± 0.0003	0.3570 ± 0.0029	339 ± 13	306 ± 2	98
11XL41-2-48	1.67	0.0533 ± 0.0003	0.0505 ± 0.0004	0.3718 ± 0.0036	343 ± 19	318 ± 2	99
11XL41-2-49	2.20	0.0563 ± 0.0002	0.0498 ± 0.0004	0.3865 ± 0.0034	465 ± 7	313 ± 3	94
11XL41-2-50	1.73	0.0589 ± 0.0003	0.0653 ± 0.0005	0.5313 ± 0.0053	565 ± 13	408 ± 3	94
11XL41-2-51	2.40	0.0552 ± 0.0004	0.0461 ± 0.0003	0.3508 ± 0.0033	420 ± 15	290 ± 2	94
11XL41-2-52	1.19	0.0553 ± 0.0003	0.0520 ± 0.0004	0.3962 ± 0.0036	433 ± 13	327 ± 3	96
11XL41-2-53	0.81	0.0784 ± 0.0002	0.1771 ± 0.0013	1.9158 ± 0.0142	1167 ± 6	1051 ± 7	96
11XL41-2-54	7.83	0.0724 ± 0.0002	0.1402 ± 0.0016	1.4023 ± 0.0176	998 ± 7	846 ± 9	94

(continued)

Table B.1 (continued)

Sample	U/Th	$^{206}Pb^*/^{207}Pb^*$	$^{206}Pb^*/^{238}U$	$^{207}Pb^*/^{235}U$	$^{206}Pb^*/^{207}Pb^* - Age$ [Ma]	$^{238}U/^{206}Pb - Age$ [Ma]	Concordance [%]
11XL41-2-55	23.94	0.0718 ± 0.0001	0.1570 ± 0.0016	1.5553 ± 0.0155	989 ± 4	940 ± 9	98
11XL41-2-56	1.59	0.1153 ± 0.0003	0.3228 ± 0.0034	5.1342 ± 0.0543	1884 ± 10	1803 ± 17	97
11XL41-2-57	1.41	0.2189 ± 0.0014	0.4993 ± 0.0059	15.0654 ± 0.1572	2973 ± 10	2611 ± 25	92
11XL41-2-58	1.17	0.1667 ± 0.0004	0.3942 ± 0.0046	9.0677 ± 0.1030	2525 ± 4	2142 ± 21	90
11XL41-2-59	80.01	0.0559 ± 0.0001	0.0674 ± 0.0008	0.5199 ± 0.0062	450 ± 6	420 ± 5	98
11XL41-2-60	2.22	0.0566 ± 0.0002	0.0734 ± 0.0009	0.5734 ± 0.0070	476 ± 3	457 ± 5	99
11XL41-2-61	2.03	0.1655 ± 0.0003	0.3230 ± 0.0035	7.3749 ± 0.0780	2512 ± 4	1804 ± 17	82
11XL41-2-62	1.90	0.0703 ± 0.0002	0.1513 ± 0.0016	1.4680 ± 0.0152	939 ± −29	908 ± 9	98
11XL41-2-63	2.50	0.1046 ± 0.0002	0.1890 ± 0.0020	2.7267 ± 0.0281	1706 ± 4	1116 ± 11	82
11XL41-2-64	1.56	0.0573 ± 0.0001	0.0701 ± 0.0007	0.5548 ± 0.0053	506 ± 6	437 ± 4	97
11XL41-2-65	1.55	0.0578 ± 0.0004	0.0503 ± 0.0004	0.4002 ± 0.0041	520 ± 47	316 ± 3	92
11XL41-2-66	24.81	0.0558 ± 0.0002	0.0675 ± 0.0006	0.5196 ± 0.0051	443 ± 9	421 ± 4	99
11XL41-2-67	1.64	0.0534 ± 0.0003	0.0524 ± 0.0005	0.3852 ± 0.0039	343 ± 18	329 ± 3	99
11XL41-2-68	2.12	0.0578 ± 0.0002	0.0712 ± 0.0006	0.5686 ± 0.0055	520 ± 5	443 ± 3	96
11XL41-2-69	1.59	0.0535 ± 0.0002	0.0541 ± 0.0004	0.3993 ± 0.0033	350 ± 14	340 ± 2	99
11XL41-2-70	1.88	0.0542 ± 0.0002	0.0512 ± 0.0003	0.3829 ± 0.0027	389 ± 9	322 ± 2	97
11XL41-2-71	1.61	0.0533 ± 0.0003	0.0523 ± 0.0004	0.3851 ± 0.0033	343 ± 11	329 ± 2	99
11XL41-2-72	9.84	0.1393 ± 0.0006	0.3708 ± 0.0021	7.1301 ± 0.0571	2220 ± 7	2033 ± 10	95
11XL41-2-73	1.63	0.0538 ± 0.0002	0.0534 ± 0.0004	0.3965 ± 0.0035	365 ± 11	335 ± 2	98
11XL41-2-74	2.25	0.0541 ± 0.0002	0.0530 ± 0.0003	0.3952 ± 0.0021	376 ± 7	333 ± 2	98
11XL41-2-75	1.42	0.0625 ± 0.0004	0.0527 ± 0.0003	0.4546 ± 0.0041	700 ± 15	331 ± 2	86
11XL41-2-76	1.85	0.0557 ± 0.0003	0.0498 ± 0.0004	0.3831 ± 0.0043	439 ± 8	314 ± 2	95
11XL41-2-77	1.00	0.0559 ± 0.0004	0.0571 ± 0.0003	0.4407 ± 0.0037	450 ± 13	358 ± 2	96

(continued)

Table B.1 (continued)

Sample	U/Th	$^{206}Pb^*/^{207}Pb^*$	$^{206}Pb^*/^{238}U$	$^{207}Pb^*/^{235}U$	$^{206}Pb^*/^{207}Pb^* - Age$ [Ma]	$^{238}U/^{206}Pb - Age$ [Ma]	Concordance [%]
11XL41-2-78	1.05	0.1551 ± 0.0003	0.3693 ± 0.0026	7.8984 ± 0.0533	2403 ± 3	2026 ± 12	90
11XL41-2-79	1.77	0.0560 ± 0.0002	0.0710 ± 0.0004	0.5483 ± 0.0032	454 ± 1	442 ± 2	99
11XL41-2-80	1.80	0.0560 ± 0.0002	0.0693 ± 0.0004	0.5351 ± 0.0034	454 ± 3	432 ± 3	99
11XL41-2-81	1.76	0.0534 ± 0.0001	0.0538 ± 0.0003	0.3963 ± 0.0027	346 ± 6	338 ± 2	99
11XL41-2-82	0.99	0.0870 ± 0.0002	0.2102 ± 0.0018	2.5206 ± 0.0204	1361 ± 5	1230 ± 10	96
11XL41-2-83	1.16	0.0796 ± 0.0002	0.1989 ± 0.0012	2.1832 ± 0.0143	1187 ± 4	1169 ± 7	99
11XL41-2-84	0.95	0.0539 ± 0.0002	0.0566 ± 0.0003	0.4209 ± 0.0028	369 ± 7	355 ± 2	99
11XL41-2-85	1.19	0.0562 ± 0.0002	0.0691 ± 0.0004	0.5359 ± 0.0036	461 ± 12	431 ± 2	98
11XL41-2-86	0.80	0.0531 ± 0.0002	0.0501 ± 0.0003	0.3667 ± 0.0025	345 ± 9	315 ± 2	99
11XL41-2-87	4.37	0.0564 ± 0.0002	0.0700 ± 0.0005	0.5447 ± 0.0047	478 ± 7	436 ± 3	98
11XL41-2-88	0.46	0.0532 ± 0.0002	0.0535 ± 0.0004	0.3925 ± 0.0034	345 ± 7	336 ± 3	99
11XL41-2-89	1.03	0.0562 ± 0.0003	0.0517 ± 0.0003	0.3989 ± 0.0022	457 ± 11	325 ± 2	95
11XL41-2-90	0.67	0.0565 ± 0.0003	0.0705 ± 0.0006	0.5497 ± 0.0057	472 ± 11	439 ± 4	98
11XL37-1-1	1.18	0.0593 ± 0.0003	0.0726 ± 0.0005	0.5913 ± 0.0030	589 ± 11	452 ± 3	95
11XL37-1-2	0.89	0.0553 ± 0.0002	0.0568 ± 0.0004	0.4339 ± 0.0034	433 ± 9	356 ± 2	97
11XL37-1-3	10.32	0.0566 ± 0.0001	0.0654 ± 0.0004	0.5112 ± 0.0030	476 ± 6	409 ± 2	97
11XL37-1-4	1.32	0.0579 ± 0.0002	0.0620 ± 0.0005	0.4945 ± 0.0037	528 ± 40	388 ± 3	94
11XL37-1-5	3.50	0.0594 ± 0.0003	0.0612 ± 0.0004	0.5013 ± 0.0045	589 ± 13	383 ± 2	92
11XL37-1-6	1.59	0.0613 ± 0.0003	0.0668 ± 0.0003	0.5645 ± 0.0028	650 ± 9	417 ± 2	91
11XL37-1-7	3.25	0.0936 ± 0.0002	0.2456 ± 0.0009	3.1696 ± 0.0132	1500 ± 5	1416 ± 5	97
11XL37-1-8	3.55	0.0756 ± 0.0006	0.1067 ± 0.0028	1.1424 ± 0.0367	1085 ± 16	654 ± 16	83
11XL37-1-9	2.74	0.0749 ± 0.0002	0.1660 ± 0.0010	1.7144 ± 0.0107	1065 ± 36	990 ± 5	97
11XL37-1-10	5.01	0.0783 ± 0.0007	0.0864 ± 0.0004	0.9319 ± 0.0070	1155 ± 17	534 ± 2	77

(continued)

Table B.1 (continued)

Sample	U/Th	$^{206}Pb^*/^{207}Pb^*$	$^{206}Pb^*/^{238}U$	$^{207}Pb^*/^{235}U$	$^{206}Pb^*/^{207}Pb^* - Age$ [Ma]	$^{238}U/^{206}Pb - Age$ [Ma]	Concordance [%]
11XL37-1-11	1.96	0.0757 ± 0.0002	0.1329 ± 0.0009	1.3879 ± 0.0096	1089 ± 6	804 ± 5	90
11XL37-1-12	1.99	0.0576 ± 0.0003	0.0743 ± 0.0005	0.5915 ± 0.0060	522 ± 13	462 ± 3	97
11XL37-1-13	4.02	0.0977 ± 0.0003	0.2504 ± 0.0017	3.3751 ± 0.0233	1581 ± 6	1440 ± 9	96
11XL37-1-14	1.75	0.0634 ± 0.0006	0.0593 ± 0.0005	0.5199 ± 0.0082	724 ± 20	371 ± 3	86
11XL37-1-15	2.31	0.0875 ± 0.0007	0.1345 ± 0.0008	1.6248 ± 0.0176	1372 ± 16	814 ± 4	81
11XL37-1-16	89.00	0.0602 ± 0.0002	0.0991 ± 0.0008	0.8235 ± 0.0070	613 ± 6	609 ± 5	99
11XL37-1-17	5.52	0.0591 ± 0.0004	0.0685 ± 0.0004	0.5584 ± 0.0050	572 ± 8	427 ± 2	94
11XL37-1-18	2.16	0.0594 ± 0.0003	0.0715 ± 0.0003	0.5864 ± 0.0043	583 ± 13	445 ± 2	94
11XL37-1-19	2.31	0.0594 ± 0.0003	0.0627 ± 0.0004	0.5132 ± 0.0034	583 ± 9	392 ± 2	92
11XL37-1-20	4.18	0.0750 ± 0.0002	0.1607 ± 0.0009	1.6619 ± 0.0095	1133 ± 6	961 ± 5	96
11XL37-1-21	1.37	0.0558 ± 0.0002	0.0631 ± 0.0003	0.4855 ± 0.0028	443 ± 7	394 ± 2	98
11XL37-1-22	7.96	0.0610 ± 0.0003	0.0680 ± 0.0007	0.5737 ± 0.0076	639 ± 14	424 ± 4	91
11XL37-1-23	0.84	0.0586 ± 0.0003	0.0625 ± 0.0004	0.5050 ± 0.0029	554 ± 11	391 ± 2	93
11XL37-1-24	1.45	0.0565 ± 0.0004	0.0520 ± 0.0003	0.4051 ± 0.0032	478 ± 17	327 ± 2	94
11XL37-1-25	0.76	0.0549 ± 0.0003	0.0568 ± 0.0003	0.4303 ± 0.0033	409 ± 11	356 ± 2	97
11XL37-1-26	1.74	0.0552 ± 0.0003	0.0651 ± 0.0008	0.4958 ± 0.0067	420 ± 15	406 ± 5	99
11XL37-1-27	3.51	0.0720 ± 0.0003	0.1392 ± 0.0006	1.3816 ± 0.0067	987 ± 3	840 ± 3	95
11XL37-1-28	3.63	0.0703 ± 0.0003	0.1310 ± 0.0012	1.2714 ± 0.0138	939 ± 9	794 ± 7	95
11XL37-1-29	2.04	0.0920 ± 0.0004	0.1224 ± 0.0010	1.5541 ± 0.0164	1533 ± 8	744 ± 6	75
11XL37-1-30	1.53	0.0833 ± 0.0003	0.2090 ± 0.0018	2.4036 ± 0.0243	1276 ± 3	1223 ± 9	98
11XL37-1-31	4.04	0.1989 ± 0.0007	0.1422 ± 0.0010	3.9070 ± 0.0366	2818 ± 11	857 ± 6	38
11XL37-1-32	0.93	0.0556 ± 0.0002	0.0596 ± 0.0003	0.4573 ± 0.0032	439 ± 6	373 ± 2	97
11XL37-1-33	1.48	0.0649 ± 0.0005	0.0616 ± 0.0007	0.5492 ± 0.0054	772 ± 19	386 ± 4	85

(continued)

Table B.1 (continued)

Sample	U/Th	$^{206}Pb^*/^{207}Pb^*$	$^{206}Pb^*/^{238}U$	$^{207}Pb^*/^{235}U$	$^{206}Pb^*/^{207}Pb^* - Age$ [Ma]	$^{238}U/^{206}Pb - Age$ [Ma]	Concordance [%]
11XL37-1-34	0.79	0.0552 ± 0.0002	0.0644 ± 0.0002	0.4908 ± 0.0020	433 ± 6	402 ± 1	99
11XL37-1-35	2.33	0.0826 ± 0.0003	0.1414 ± 0.0016	1.6133 ± 0.0212	1261 ± 12	853 ± 9	86
11XL37-1-36	2.11	0.0569 ± 0.0004	0.0658 ± 0.0005	0.5150 ± 0.0040	487 ± 13	411 ± 3	97
11XL37-1-37	1.70	0.0558 ± 0.0002	0.0627 ± 0.0003	0.4825 ± 0.0027	443 ± 9	392 ± 2	98
11XL37-1-38	1.52	0.0894 ± 0.0002	0.2362 ± 0.0014	2.9124 ± 0.0178	1413 ± 4	1367 ± 7	98
11XL37-1-39	17.30	0.1566 ± 0.0002	0.4284 ± 0.0030	9.2544 ± 0.0677	2420 ± 3	2299 ± 14	97
11XL37-1-40	2.01	0.0584 ± 0.0003	0.0692 ± 0.0005	0.5585 ± 0.0062	543 ± 18	431 ± 3	95
11XL37-1-41	4.61	0.0614 ± 0.0004	0.0680 ± 0.0004	0.5790 ± 0.0067	654 ± 47	424 ± 3	91
11XL37-1-42	4.55	0.0543 ± 0.0002	0.0585 ± 0.0004	0.4383 ± 0.0036	383 ± 9	366 ± 2	99
11XL37-1-43	2.11	0.1034 ± 0.0003	0.1949 ± 0.0010	2.7793 ± 0.0157	1687 ± 5	1148 ± 5	83
11XL37-1-44	2.28	0.0895 ± 0.0002	0.2407 ± 0.0024	2.9707 ± 0.0298	1417 ± 5	1390 ± 12	99
11XL37-1-45	2.80	0.0624 ± 0.0004	0.0613 ± 0.0005	0.5271 ± 0.0051	687 ± 13	383 ± 3	88
11XL37-1-46	1.19	0.1018 ± 0.0004	0.2550 ± 0.0036	3.5815 ± 0.0532	1658 ± 8	1464 ± 19	94
11XL37-1-47	1.54	0.0672 ± 0.0003	0.1207 ± 0.0008	1.1188 ± 0.0101	843 ± 7	735 ± 5	96
11XL37-1-48	2.07	0.0553 ± 0.0003	0.0595 ± 0.0005	0.4546 ± 0.0048	433 ± 11	373 ± 3	97
11XL37-1-49	3.54	0.0565 ± 0.0002	0.0641 ± 0.0004	0.4989 ± 0.0030	472 ± 7	400 ± 2	97
11XL37-1-50	1.63	0.0561 ± 0.0002	0.0585 ± 0.0006	0.4533 ± 0.0052	457 ± 7	367 ± 4	96
11XL37-1-51	1.55	0.0571 ± 0.0002	0.0743 ± 0.0006	0.5845 ± 0.0050	494 ± 7	462 ± 4	98
11XL37-1-52	1.14	0.1054 ± 0.0003	0.2588 ± 0.0019	3.7594 ± 0.0284	1721 ± 4	1484 ± 10	93
11XL37-1-53	2.05	0.0565 ± 0.0002	0.0689 ± 0.0005	0.5369 ± 0.0046	472 ± 7	430 ± 3	98
11XL37-1-54	1.98	0.0559 ± 0.0003	0.0572 ± 0.0005	0.4405 ± 0.0048	456 ± 13	358 ± 3	96
11XL37-1-55	2.28	0.0557 ± 0.0002	0.0643 ± 0.0006	0.4937 ± 0.0044	439 ± 12	402 ± 3	98
11XL37-1-56	1.95	0.1127 ± 0.0002	0.3136 ± 0.0031	4.8746 ± 0.0494	1844 ± 3	1758 ± 15	97

(continued)

Table B.1 (continued)

Sample	U/Th	$^{206}Pb^*/^{207}Pb^*$	$^{206}Pb^*/^{238}U$	$^{207}Pb^*/^{235}U$	$^{206}Pb^*/^{207}Pb^* - Age$ [Ma]	$^{238}U/^{206}Pb - Age$ [Ma]	Concordance [%]
11XL37-1-57	1.42	0.0552 ± 0.0002	0.0600 ± 0.0006	0.4569 ± 0.0043	420 ± 9	376 ± 3	98
11XL37-1-58	5.53	0.0947 ± 0.0002	0.2024 ± 0.0024	2.6441 ± 0.0314	1524 ± 5	1188 ± 13	90
11XL37-1-59	1.61	0.0567 ± 0.0002	0.0713 ± 0.0009	0.5569 ± 0.0069	480 ± 7	444 ± 5	98
11XL37-1-60	4.57	0.0627 ± 0.0003	0.0614 ± 0.0008	0.5289 ± 0.0060	698 ± 10	384 ± 5	88
11XL37-1-61	1.70	0.0554 ± 0.0003	0.0561 ± 0.0006	0.4282 ± 0.0054	428 ± 11	352 ± 4	97
11XL37-1-62	2.76	0.0587 ± 0.0002	0.0670 ± 0.0006	0.5437 ± 0.0059	567 ± 9	418 ± 4	94
11XL37-1-63	1.54	0.0573 ± 0.0002	0.0702 ± 0.0007	0.5553 ± 0.0056	502 ± 6	438 ± 4	97
11XL37-1-64	1.93	0.0993 ± 0.0005	0.1818 ± 0.0029	2.4958 ± 0.0449	1611 ± −190	1077 ± 16	83
11XL37-1-65	1.41	0.0595 ± 0.0004	0.0571 ± 0.0005	0.4685 ± 0.0057	583 ± 13	358 ± 3	91
11XL37-1-66	3.83	0.0584 ± 0.0004	0.0577 ± 0.0004	0.4648 ± 0.0043	546 ± 15	362 ± 2	93
11XL37-1-67	2.57	0.0555 ± 0.0002	0.0626 ± 0.0005	0.4789 ± 0.0041	432 ± 3	392 ± 3	98
11XL37-1-68	1.76	0.0549 ± 0.0002	0.0581 ± 0.0004	0.4399 ± 0.0037	406 ± 7	364 ± 3	98
11XL37-1-69	1.91	0.0561 ± 0.0001	0.0704 ± 0.0006	0.5448 ± 0.0044	457 ± 4	438 ± 3	99
11XL37-1-70	1.64	0.0561 ± 0.0002	0.0626 ± 0.0006	0.4838 ± 0.0043	457 ± 7	391 ± 4	97
11XL37-1-71	2.63	0.0708 ± 0.0002	0.1454 ± 0.0023	1.4271 ± 0.0254	952 ± 6	875 ± 13	97
11XL37-1-72	2.03	0.0707 ± 0.0002	0.1519 ± 0.0010	1.4816 ± 0.0107	950 ± 6	912 ± 6	98
11XL37-1-73	1.18	0.1023 ± 0.0002	0.2721 ± 0.0026	3.8411 ± 0.0385	1678 ± 5	1551 ± 13	96
11XL37-1-74	2.74	0.0963 ± 0.0007	0.2109 ± 0.0016	2.7981 ± 0.0255	1554 ± 14	1234 ± 8	90
11XL37-1-75	5.12	0.0619 ± 0.0005	0.0612 ± 0.0003	0.5227 ± 0.0043	672 ± 17	383 ± 2	89
11XL37-1-76	1.68	0.0566 ± 0.0002	0.0698 ± 0.0004	0.5445 ± 0.0029	476 ± 3	435 ± 2	98
11XL37-1-77	2.23	0.0568 ± 0.0002	0.0673 ± 0.0004	0.5277 ± 0.0036	487 ± 9	420 ± 3	97
11XL37-1-78	1.21	0.1529 ± 0.0019	0.2896 ± 0.0045	6.2062 ± 0.1732	2389 ± 17	1640 ± 22	79
11XL37-1-79	1.22	0.0578 ± 0.0002	0.0800 ± 0.0006	0.6374 ± 0.0044	524 ± 7	496 ± 3	99

(continued)

Table B.1 (continued)

Sample	U/Th	$^{206}Pb^*/^{207}Pb^*$	$^{206}Pb^*/^{238}U$	$^{207}Pb^*/^{235}U$	$^{206}Pb^*/^{207}Pb^* - Age$ [Ma]	$^{238}U/^{206}Pb - Age$ [Ma]	Concordance [%]
11XL37-1-80	2.62	0.0733 ± 0.0002	0.1507 ± 0.0015	1.5240 ± 0.0153	1033 ± 6	905 ± 8	96
11XL37-1-81	3.95	0.0554 ± 0.0001	0.0620 ± 0.0004	0.4730 ± 0.0030	428 ± 1	388 ± 3	98
11XL37-1-82	0.95	0.0558 ± 0.0001	0.0700 ± 0.0004	0.5386 ± 0.0035	443 ± 8	436 ± 3	99
11XL37-1-83	3.83	0.0583 ± 0.0007	0.0609 ± 0.0003	0.4891 ± 0.0065	539 ± 21	381 ± 2	94
11XL37-1-84	2.59	0.0584 ± 0.0003	0.0570 ± 0.0003	0.4591 ± 0.0037	543 ± −23	357 ± 2	92
11XL37-1-85	3.67	0.0560 ± 0.0002	0.0626 ± 0.0005	0.4835 ± 0.0044	450 ± 7	392 ± 3	97
11XL37-1-86	1.72	0.0601 ± 0.0003	0.0691 ± 0.0004	0.5710 ± 0.0026	606 ± 9	430 ± 2	93
11XL37-1-87	1.79	0.0750 ± 0.0001	0.1739 ± 0.0012	1.7971 ± 0.0128	1133 ± 4	1033 ± 7	98
11XL37-1-88	3.51	0.0552 ± 0.0003	0.0566 ± 0.0004	0.4314 ± 0.0047	420 ± 11	355 ± 3	97
11XL37-1-89	0.70	0.0837 ± 0.0004	0.1757 ± 0.0011	2.0246 ± 0.0101	1287 ± 8	1043 ± 6	92
11XL37-1-90	2.43	0.0561 ± 0.0002	0.0698 ± 0.0006	0.5397 ± 0.0049	454 ± 6	435 ± 4	99
12XL24-1-1	1.30	0.1574 ± 0.0001	0.4374 ± 0.0055	9.4865 ± 0.1152	2427 ± 2	2339 ± 25	98
12XL24-1-2	1.73	0.0546 ± 0.0001	0.0679 ± 0.0018	0.5100 ± 0.0179	393 ± 6	424 ± 11	101
12XL24-1-3	1.97	0.0637 ± 0.0002	0.0630 ± 0.0018	0.5524 ± 0.0182	731 ± 6	394 ± 11	88
12XL24-1-4	18.89	0.0715 ± 0.0005	0.1062 ± 0.0017	1.0470 ± 0.0189	971 ± 14	651 ± 10	89
12XL24-1-5	2.30	0.0684 ± 0.0001	0.1504 ± 0.0017	1.4185 ± 0.0176	879 ± 4	903 ± 9	101
12XL24-1-6	1.57	0.1536 ± 0.0002	0.2758 ± 0.0027	5.8444 ± 0.0522	2386 ± 2	1570 ± 14	80
12XL24-1-7	2.03	0.0583 ± 0.0005	0.0664 ± 0.0017	0.5320 ± 0.0182	540 ± 18	415 ± 10	96
12XL24-1-8	1.45	0.0676 ± 0.0006	0.0522 ± 0.0017	0.4846 ± 0.0174	854 ± 20	328 ± 10	82
12XL24-1-9	2.65	0.0597 ± 0.0002	0.0594 ± 0.0018	0.4889 ± 0.0184	592 ± 7	372 ± 11	92
12XL24-1-10	3.05	0.0578 ± 0.0002	0.0564 ± 0.0017	0.4489 ± 0.0175	522 ± 9	354 ± 10	94
12XL24-1-11	2.85	0.0602 ± 0.0003	0.0607 ± 0.0018	0.5001 ± 0.0178	609 ± 11	380 ± 11	92
12XL24-1-12	2.36	0.0689 ± 0.0001	0.1330 ± 0.0024	1.2635 ± 0.0238	896 ± 4	805 ± 14	97

(continued)

Table B.1 (continued)

Sample	U/Th	$^{206}Pb^*/^{207}Pb^*$	$^{206}Pb^*/^{238}U$	$^{207}Pb^*/^{235}U$	$^{206}Pb^*/^{207}Pb^* - Age$ [Ma]	$^{238}U/^{206}Pb - Age$ [Ma]	Concordance [%]
12XL24-1-13	1.35	0.0643 ± 0.0004	0.0623 ± 0.0020	0.5484 ± 0.0194	749 ± 12	389 ± 12	88
12XL24-1-14	1.73	0.0675 ± 0.0005	0.0637 ± 0.0018	0.5925 ± 0.0189	852 ± 16	398 ± 11	84
12XL24-1-15	2.32	0.0574 ± 0.0003	0.0600 ± 0.0018	0.4729 ± 0.0179	508 ± 10	376 ± 11	96
12XL24-1-16	1.76	0.0570 ± 0.0002	0.0563 ± 0.0017	0.4423 ± 0.0175	491 ± 6	353 ± 10	95
12XL24-1-17	2.22	0.0965 ± 0.0002	0.1702 ± 0.0028	2.2629 ± 0.0337	1557 ± 4	1013 ± 15	84
12XL24-1-18	2.76	0.0571 ± 0.0001	0.0639 ± 0.0018	0.5031 ± 0.0183	494 ± 5	399 ± 11	97
12XL24-1-19	1.95	0.0703 ± 0.0003	0.1691 ± 0.0022	1.6405 ± 0.0235	937 ± 8	1007 ± 12	102
12XL24-1-20	2.16	0.0597 ± 0.0003	0.0649 ± 0.0017	0.5340 ± 0.0177	591 ± 11	405 ± 10	93
12XL24-1-21	1.46	0.1974 ± 0.0005	0.4152 ± 0.0029	11.2989 ± 0.0593	2804 ± 4	2239 ± 13	88
12XL24-1-22	3.40	0.1058 ± 0.0002	0.1935 ± 0.0022	2.8239 ± 0.0279	1727 ± 3	1140 ± 12	84
12XL24-1-23	2.48	0.0600 ± 0.0001	0.0544 ± 0.0016	0.4497 ± 0.0170	602 ± 5	341 ± 10	91
12XL24-1-24	1.21	0.0642 ± 0.0005	0.0686 ± 0.0017	0.6039 ± 0.0172	747 ± 15	428 ± 10	89
12XL24-1-25	4.37	0.0705 ± 0.0005	0.1565 ± 0.0020	1.5227 ± 0.0233	943 ± 14	937 ± 11	100
12XL24-1-26	2.43	0.0585 ± 0.0002	0.0635 ± 0.0017	0.5117 ± 0.0173	547 ± 6	397 ± 10	95
12XL24-1-27	1.49	0.0720 ± 0.0005	0.0604 ± 0.0019	0.5934 ± 0.0186	986 ± 14	378 ± 12	80
12XL24-1-28	2.03	0.0663 ± 0.0001	0.1137 ± 0.0022	1.0387 ± 0.0216	814 ± 4	694 ± 13	96
12XL24-1-29	2.91	0.0760 ± 0.0004	0.1460 ± 0.0022	1.5245 ± 0.0207	1093 ± 9	878 ± 12	93
12XL24-1-30	1.80	0.0724 ± 0.0011	0.0632 ± 0.0016	0.6267 ± 0.0181	995 ± 30	395 ± 10	80
12XL24-1-31	2.29	0.0755 ± 0.0003	0.1174 ± 0.0023	1.2203 ± 0.0219	1081 ± 7	716 ± 13	88
12XL24-1-32	2.28	0.0845 ± 0.0003	0.2016 ± 0.0036	2.3385 ± 0.0371	1303 ± 6	1184 ± 19	97
12XL24-1-33	0.75	0.1226 ± 0.0004	0.0391 ± 0.0017	0.6606 ± 0.0173	1994 ± 6	247 ± 10	48
12XL24-1-34	1.35	0.0711 ± 0.0001	0.1328 ± 0.0024	1.3001 ± 0.0234	958 ± 4	804 ± 14	95
12XL24-1-35	1.08	0.0839 ± 0.0003	0.0560 ± 0.0017	0.6467 ± 0.0178	1289 ± 7	351 ± 11	69

(continued)

Table B.1 (continued)

Sample	U/Th	$^{206}Pb^*/^{207}Pb^*$	$^{206}Pb^*/^{238}U$	$^{207}Pb^*/^{235}U$	$^{206}Pb^*/^{207}Pb^* - Age$ [Ma]	$^{238}U/^{206}Pb - Age$ [Ma]	Concordance [%]
12XL24-1-36	0.85	0.0665 ± 0.0003	0.0538 ± 0.0017	0.4936 ± 0.0175	821 ± 8	338 ± 10	83
12XL24-1-37	2.38	0.0756 ± 0.0002	0.1231 ± 0.0022	1.2811 ± 0.0214	1084 ± 6	748 ± 12	89
12XL24-1-38	2.85	0.0578 ± 0.0001	0.0623 ± 0.0018	0.4957 ± 0.0177	520 ± 6	389 ± 11	95
12XL24-1-39	1.84	0.0732 ± 0.0002	0.1298 ± 0.0021	1.3088 ± 0.0211	1018 ± 5	787 ± 12	93
12XL24-1-40	2.78	0.0638 ± 0.0004	0.0618 ± 0.0018	0.5429 ± 0.0185	735 ± 12	386 ± 11	88
12XL24-1-41	2.53	0.0581 ± 0.0002	0.0624 ± 0.0018	0.5013 ± 0.0189	531 ± 7	390 ± 11	95
12XL24-1-42	1.34	0.2998 ± 0.0004	0.4464 ± 0.0043	18.4481 ± 0.1474	3468 ± 2	2379 ± 19	79
12XL24-1-43	2.20	0.0634 ± 0.0002	0.0517 ± 0.0017	0.4521 ± 0.0176	721 ± 5	325 ± 11	86
12XL24-1-44	2.12	0.0607 ± 0.0004	0.0621 ± 0.0018	0.5187 ± 0.0181	627 ± 14	388 ± 11	91
12XL24-1-45	2.12	0.0607 ± 0.0004	0.0620 ± 0.0018	0.5186 ± 0.0181	628 ± 14	388 ± 11	91
12XL24-1-46	2.45	0.0580 ± 0.0002	0.0589 ± 0.0016	0.4710 ± 0.0167	530 ± 7	369 ± 10	94
12XL24-1-47	1.19	0.0814 ± 0.0006	0.1232 ± 0.0017	1.3789 ± 0.0176	1229 ± 14	749 ± 10	85
12XL24-1-48	1.62	0.1008 ± 0.0001	0.2253 ± 0.0029	3.1338 ± 0.0373	1639 ± 2	1310 ± 15	91
12XL24-1-49	2.29	0.0592 ± 0.0003	0.0639 ± 0.0017	0.5192 ± 0.0166	575 ± 12	399 ± 10	94
12XL24-1-50	1.91	0.0768 ± 0.0001	0.1106 ± 0.0019	1.1710 ± 0.0202	1115 ± 4	676 ± 11	86
12XL24-1-51	1.51	0.2646 ± 0.0003	0.7685 ± 0.0050	28.0261 ± 0.1542	3273 ± 2	3675 ± 18	107
12XL24-1-52	1.94	0.0620 ± 0.0003	0.0722 ± 0.0016	0.6170 ± 0.0165	675 ± 10	449 ± 10	92
12XL24-1-53	2.85	0.0727 ± 0.0001	0.1415 ± 0.0019	1.4192 ± 0.0197	1005 ± 3	853 ± 11	95
12XL24-1-54	1.66	0.0834 ± 0.0002	0.1202 ± 0.0018	1.3842 ± 0.0203	1278 ± 5	732 ± 10	83
12XL24-1-55	1.93	0.0560 ± 0.0002	0.0611 ± 0.0017	0.4712 ± 0.0167	453 ± 6	382 ± 10	97
12XL24-1-56	1.43	0.0595 ± 0.0003	0.0602 ± 0.0016	0.4918 ± 0.0165	583 ± 10	377 ± 10	93
12XL24-1-57	1.21	0.1602 ± 0.0002	0.3601 ± 0.0071	7.9668 ± 0.1578	2457 ± 2	1983 ± 34	89
12XL24-1-58	1.87	0.0618 ± 0.0002	0.0620 ± 0.0017	0.5278 ± 0.0172	667 ± 6	388 ± 10	90

(continued)

Table B.1 (continued)

Sample	U/Th	$^{206}Pb^*/^{207}Pb^*$	$^{206}Pb^*/^{238}U$	$^{207}Pb^*/^{235}U$	$^{206}Pb^*/^{207}Pb^* - Age$ [Ma]	$^{238}U/^{206}Pb - Age$ [Ma]	Concordance [%]
12XL24-1-59	2.24	0.0658 ± 0.0005	0.0721 ± 0.0016	0.6496 ± 0.0166	798 ± 14	449 ± 10	88
12XL24-1-60	4.30	0.0666 ± 0.0005	0.0648 ± 0.0017	0.6007 ± 0.0193	824 ± 14	405 ± 10	85
12XL24-1-61	1.91	0.0584 ± 0.0002	0.0528 ± 0.0016	0.4251 ± 0.0168	545 ± 7	332 ± 10	92
12XL24-1-62	3.25	0.0725 ± 0.0001	0.1455 ± 0.0021	1.4539 ± 0.0213	1000 ± 4	875 ± 12	96
12XL24-1-63	2.42	0.0584 ± 0.0002	0.0657 ± 0.0017	0.5299 ± 0.0175	544 ± 7	410 ± 10	95
12XL24-1-64	1.87	0.1054 ± 0.0002	0.2339 ± 0.0022	3.4009 ± 0.0286	1721 ± 3	1355 ± 12	90
12XL24-1-65	1.74	0.0827 ± 0.0002	0.1541 ± 0.0024	1.7551 ± 0.0252	1260 ± 4	924 ± 14	90
12XL24-1-66	11.14	0.0696 ± 0.0002	0.1301 ± 0.0018	1.2484 ± 0.0187	916 ± 7	788 ± 10	96
12XL24-1-67	0.79	0.0592 ± 0.0002	0.0675 ± 0.0017	0.5490 ± 0.0171	572 ± 7	421 ± 10	95
12XL24-1-68	1.28	0.0609 ± 0.0003	0.0567 ± 0.0016	0.4773 ± 0.0168	634 ± 11	356 ± 10	90
12XL24-1-69	2.75	0.0567 ± 0.0001	0.0625 ± 0.0016	0.4879 ± 0.0165	477 ± 6	391 ± 10	97
12XL24-1-70	1.62	0.0570 ± 0.0002	0.0587 ± 0.0016	0.4612 ± 0.0164	490 ± 8	368 ± 10	96
12XL24-1-71	2.21	0.0732 ± 0.0008	0.0514 ± 0.0016	0.5200 ± 0.0187	1018 ± 21	323 ± 10	76
12XL24-1-72	2.15	0.0581 ± 0.0004	0.0596 ± 0.0015	0.4774 ± 0.0163	531 ± 16	373 ± 9	94
12XL24-1-73	2.64	0.1308 ± 0.0002	0.3855 ± 0.0026	6.9515 ± 0.0407	2107 ± 3	2102 ± 12	100
12XL24-1-74	6.24	0.1031 ± 0.0006	0.2008 ± 0.0025	2.8768 ± 0.0463	1680 ± 11	1179 ± 14	86
12XL24-1-75	1.34	0.0696 ± 0.0004	0.0556 ± 0.0017	0.5295 ± 0.0163	915 ± 13	349 ± 10	81
12XL24-1-76	0.64	0.1637 ± 0.0008	0.3088 ± 0.0036	6.9789 ± 0.0943	2494 ± 8	1735 ± 18	82
12XL24-1-77	0.91	0.0790 ± 0.0012	0.0545 ± 0.0018	0.5813 ± 0.0173	1172 ± 30	342 ± 11	73
12XL24-1-78	4.83	0.0863 ± 0.0002	0.2310 ± 0.0030	2.7483 ± 0.0332	1344 ± 4	1340 ± 15	100
12XL24-1-79	1.18	0.0761 ± 0.0008	0.1338 ± 0.0018	1.4012 ± 0.0221	1097 ± 20	809 ± 10	91
12XL24-1-80	1.41	0.0794 ± 0.0007	0.0479 ± 0.0017	0.5243 ± 0.0187	1182 ± 17	301 ± 11	70
12XL24-1-81	1.31	0.1608 ± 0.0002	0.3448 ± 0.0052	7.6408 ± 0.1058	2463 ± 2	1910 ± 25	87

(continued)

Table B.1 (continued)

Sample	U/Th	$^{206}Pb^*/^{207}Pb^*$	$^{206}Pb^*/^{238}U$	$^{207}Pb^*/^{235}U$	$^{206}Pb^*/^{207}Pb^* - Age$ [Ma]	$^{238}U/^{206}Pb - Age$ [Ma]	Concordance [%]
12XL24-1-82	1.95	0.0696 ± 0.0002	0.1471 ± 0.0024	1.4087 ± 0.0229	914 ± 5	885 ± 14	99
12XL24-1-83	2.34	0.1021 ± 0.0002	0.2340 ± 0.0019	3.2955 ± 0.0211	1663 ± 3	1355 ± 10	92
12XL24-1-84	1.56	0.0753 ± 0.0003	0.0737 ± 0.0016	0.7640 ± 0.0160	1076 ± 8	458 ± 10	80
12XL24-1-85	1.20	0.0826 ± 0.0004	0.0468 ± 0.0015	0.5332 ± 0.0161	1260 ± 11	295 ± 9	68
12XL24-1-86	2.44	0.0578 ± 0.0002	0.0589 ± 0.0016	0.4695 ± 0.0159	522 ± 6	369 ± 10	94
12XL24-1-87	2.57	0.0611 ± 0.0003	0.0617 ± 0.0015	0.5180 ± 0.0152	643 ± 11	386 ± 9	91
12XL24-1-88	3.85	0.0560 ± 0.0002	0.0612 ± 0.0016	0.4721 ± 0.0156	450 ± 6	383 ± 10	98
12XL24-1-89	17.10	0.0571 ± 0.0001	0.0791 ± 0.0017	0.6232 ± 0.0161	496 ± 5	491 ± 10	100
12XL24-1-90	1.61	0.0563 ± 0.0001	0.0718 ± 0.0016	0.5567 ± 0.0157	462 ± 5	447 ± 10	99
11XL29-1-1	1.32	0.0530 ± 0.0004	0.0366 ± 0.0002	0.2680 ± 0.0031	332 ± 14	232 ± 2	95
11XL29-1-3	1.02	0.0582 ± 0.0003	0.0654 ± 0.0004	0.5254 ± 0.0048	600 ± 11	408 ± 2	95
11XL29-1-3	0.39	0.0644 ± 0.0005	0.0780 ± 0.0006	0.6909 ± 0.0065	754 ± 17	484 ± 4	90
11XL29-1-4	0.79	0.0559 ± 0.0004	0.0541 ± 0.0003	0.4172 ± 0.0038	456 ± 15	340 ± 2	95
11XL29-1-5	0.85	0.0556 ± 0.0003	0.0492 ± 0.0002	0.3771 ± 0.0024	435 ± 11	310 ± 1	95
11XL29-1-6	0.82	0.0944 ± 0.0010	0.0604 ± 0.0005	0.7864 ± 0.0114	1517 ± 21	378 ± 3	56
11XL29-1-7	0.91	0.0555 ± 0.0004	0.0497 ± 0.0004	0.3805 ± 0.0040	432 ± 17	313 ± 2	95
11XL29-1-8	1.23	0.0547 ± 0.0003	0.0483 ± 0.0003	0.3644 ± 0.0035	398 ± 11	304 ± 2	96
11XL29-1-9	1.34	0.0532 ± 0.0002	0.0510 ± 0.0004	0.3746 ± 0.0031	345 ± 9	321 ± 2	99
11XL29-1-10	0.49	0.0559 ± 0.0003	0.0583 ± 0.0005	0.4493 ± 0.0045	456 ± 13	365 ± 3	96
11XL29-1-11	1.31	0.0531 ± 0.0004	0.0572 ± 0.0004	0.4190 ± 0.0041	345 ± 19	359 ± 2	99
11XL29-1-12	1.25	0.1596 ± 0.0004	0.4439 ± 0.0024	9.7688 ± 0.0559	2452 ± 5	2368 ± 11	98
11XL29-1-13	1.84	0.0563 ± 0.0003	0.0532 ± 0.0004	0.4131 ± 0.0041	465 ± 13	334 ± 2	95
11XL29-1-14	1.41	0.0557 ± 0.0003	0.0527 ± 0.0004	0.4057 ± 0.0039	443 ± 11	331 ± 2	95

(continued)

Table B.1 (continued)

Sample	U/Th	$^{206}Pb^*/^{207}Pb^*$	$^{206}Pb^*/^{238}U$	$^{207}Pb^*/^{235}U$	$^{206}Pb^*/^{207}Pb^* - Age$ [Ma]	$^{238}U/^{206}Pb - Age$ [Ma]	Concordance [%]
11XL29-1-15	0.94	0.0565 ± 0.0002	0.0617 ± 0.0005	0.4804 ± 0.0041	472 ± 7	386 ± 3	96
11XL29-1-16	1.65	0.0550 ± 0.0009	0.0543 ± 0.0007	0.4118 ± 0.0084	413 ± 40	341 ± 4	97
11XL29-1-17	1.14	0.0543 ± 0.0004	0.0533 ± 0.0003	0.3987 ± 0.0034	383 ± 13	335 ± 2	98
11XL29-1-18	1.08	0.0537 ± 0.0003	0.0517 ± 0.0004	0.3829 ± 0.0038	367 ± 13	325 ± 2	98
11XL29-1-19	0.92	0.0667 ± 0.0003	0.1331 ± 0.0009	1.2246 ± 0.0100	828 ± 9	806 ± 5	99
11XL29-1-20	1.60	0.0603 ± 0.0005	0.0550 ± 0.0003	0.4568 ± 0.0042	613 ± 19	345 ± 2	89
11XL29-1-21	1.46	0.1741 ± 0.0004	0.5258 ± 0.0053	12.6298 ± 0.1354	2597 ± 4	2724 ± 23	97
11XL29-1-22	2.17	0.0572 ± 0.0002	0.0841 ± 0.0005	0.6638 ± 0.0044	502 ± 6	521 ± 3	99
11XL29-1-23	0.62	0.1103 ± 0.0007	0.2574 ± 0.0022	3.8873 ± 0.0186	1806 ± 11	1477 ± 11	91
11XL29-1-24	1.43	0.0612 ± 0.0007	0.0427 ± 0.0002	0.3605 ± 0.0037	656 ± 50	270 ± 1	85
11XL29-1-25	1.78	0.0570 ± 0.0005	0.0573 ± 0.0004	0.4496 ± 0.0045	500 ± 22	359 ± 2	95
11XL29-1-26	0.94	0.0582 ± 0.0004	0.0799 ± 0.0004	0.6410 ± 0.0046	539 ± 15	495 ± 2	98
11XL29-1-27	0.69	0.0583 ± 0.0002	0.0716 ± 0.0005	0.5749 ± 0.0040	539 ± 9	446 ± 3	96
11XL29-1-28	1.29	0.0538 ± 0.0003	0.0538 ± 0.0004	0.3992 ± 0.0036	365 ± 13	338 ± 2	99
11XL29-1-29	1.06	0.1476 ± 0.0008	0.3216 ± 0.0029	6.5734 ± 0.0878	2320 ± 9	1798 ± 14	86
11XL29-1-30	2.09	0.0660 ± 0.0011	0.0489 ± 0.0004	0.4459 ± 0.0090	806 ± 33	308 ± 2	80
11XL29-1-31	1.62	0.0592 ± 0.0005	0.0497 ± 0.0003	0.4063 ± 0.0040	576 ± 14	313 ± 2	89
11XL29-1-32	1.19	0.0572 ± 0.0003	0.0749 ± 0.0005	0.5914 ± 0.0052	498 ± 11	466 ± 3	98
11XL29-1-33	0.82	0.0556 ± 0.0002	0.0635 ± 0.0003	0.4861 ± 0.0027	435 ± 7	397 ± 2	98
11XL29-1-34	1.52	0.0588 ± 0.0003	0.0781 ± 0.0003	0.6339 ± 0.0041	561 ± 11	485 ± 2	97
11XL29-1-35	2.35	0.0575 ± 0.0002	0.0684 ± 0.0003	0.5420 ± 0.0029	509 ± 6	426 ± 2	96
11XL29-1-36	1.19	0.0530 ± 0.0003	0.0561 ± 0.0004	0.4101 ± 0.0037	328 ± 10	352 ± 2	99
11XL29-1-37	1.67	0.0629 ± 0.0005	0.0543 ± 0.0004	0.4736 ± 0.0066	706 ± 19	341 ± 3	85

(continued)

Table B.1 (continued)

Sample	U/Th	$^{206}Pb^*/^{207}Pb^*$	$^{206}Pb^*/^{238}U$	$^{207}Pb^*/^{235}U$	$^{206}Pb^*/^{207}Pb^* - Age$ [Ma]	$^{238}U/^{206}Pb - Age$ [Ma]	Concordance [%]
11XL29-1-38	1.14	0.0550 ± 0.0002	0.0620 ± 0.0003	0.4701 ± 0.0025	413 ± 14	388 ± 2	99
11XL29-1-39	1.83	0.0558 ± 0.0003	0.0518 ± 0.0002	0.3984 ± 0.0026	456 ± 11	325 ± 1	95
11XL29-1-40	2.01	0.0533 ± 0.0003	0.0522 ± 0.0002	0.3840 ± 0.0024	343 ± 11	328 ± 1	99
11XL29-1-41	1.53	0.0537 ± 0.0002	0.0535 ± 0.0003	0.3961 ± 0.0028	367 ± 9	336 ± 2	99
11XL29-1-42	1.75	0.0530 ± 0.0004	0.0526 ± 0.0003	0.3843 ± 0.0034	328 ± 12	331 ± 2	99
11XL29-1-43	2.23	0.0539 ± 0.0004	0.0573 ± 0.0003	0.4262 ± 0.0037	365 ± 19	359 ± 2	99
11XL29-1-44	1.47	0.0736 ± 0.0002	0.1776 ± 0.0011	1.8033 ± 0.0126	1031 ± 1	1054 ± 6	99
11XL29-1-45	1.75	0.0536 ± 0.0003	0.0510 ± 0.0003	0.3766 ± 0.0034	354 ± 13	321 ± 2	98
11XL29-1-46	6.17	0.0650 ± 0.0002	0.1524 ± 0.0012	1.3675 ± 0.0119	776 ± 7	914 ± 6	95
11XL29-1-47	1.91	0.0548 ± 0.0005	0.0650 ± 0.0006	0.4916 ± 0.0068	467 ± 19	406 ± 4	99
11XL29-1-48	1.25	0.0907 ± 0.0008	0.0404 ± 0.0002	0.5054 ± 0.0054	1440 ± 12	255 ± 1	52
11XL29-1-49	0.85	0.0555 ± 0.0003	0.0578 ± 0.0004	0.4415 ± 0.0032	432 ± 11	362 ± 2	97
11XL29-1-50	1.32	0.0558 ± 0.0002	0.0612 ± 0.0003	0.4715 ± 0.0029	456 ± 9	383 ± 2	97
11XL29-1-51	1.59	0.0995 ± 0.0003	0.2045 ± 0.0010	2.8080 ± 0.0156	1617 ± 6	1200 ± 5	87
11XL29-1-52	1.28	0.0550 ± 0.0003	0.0631 ± 0.0003	0.4785 ± 0.0040	409 ± 18	394 ± 2	99
11XL29-1-53	3.77	0.0671 ± 0.0002	0.1389 ± 0.0007	1.2848 ± 0.0076	839 ± 10	838 ± 4	99
11XL29-1-54	1.67	0.0563 ± 0.0002	0.0683 ± 0.0004	0.5297 ± 0.0038	465 ± 7	426 ± 3	98
11XL29-1-55	1.31	0.1346 ± 0.0003	0.4332 ± 0.0029	8.0440 ± 0.0583	2158 ± 4	2320 ± 13	96
11XL29-1-56	1.09	0.1547 ± 0.0005	0.4409 ± 0.0039	9.4254 ± 0.0972	2399 ± 6	2355 ± 18	98
11XL29-1-57	1.92	0.0583 ± 0.0002	0.0845 ± 0.0005	0.6796 ± 0.0044	543 ± −25	523 ± 3	99
11XL29-1-58	2.11	0.0504 ± 0.0003	0.0405 ± 0.0003	0.2813 ± 0.0025	213 ± 18	256 ± 2	98
11XL29-1-59	1.35	0.0548 ± 0.0004	0.0588 ± 0.0003	0.4450 ± 0.0041	406 ± 23	369 ± 2	98
11XL29-1-60	2.04	0.0537 ± 0.0003	0.0477 ± 0.0004	0.3536 ± 0.0035	361 ± 15	300 ± 2	97

(continued)

Table B.1 (continued)

Sample	U/Th	$^{206}Pb^*/^{207}Pb^*$	$^{206}Pb^*/^{238}U$	$^{207}Pb^*/^{235}U$	$^{206}Pb^*/^{207}Pb^* - Age$ [Ma]	$^{238}U/^{206}Pb - Age$ [Ma]	Concordance [%]
12XL14-1-1	2.63	0.0623 ± 0.0031	0.0671 ± 0.0011	0.5763 ± 0.0381	683 ± 106	419 ± 7	91
12XL14-1-2	1.17	0.0705 ± 0.0019	0.1586 ± 0.0016	1.5434 ± 0.0556	943 ± 55	949 ± 9	100
12XL14-1-3	6.16	0.0743 ± 0.0021	0.1570 ± 0.0017	1.6095 ± 0.0598	1049 ± 56	940 ± 9	97
12XL14-1-4	1.07	0.0588 ± 0.0022	0.0654 ± 0.0009	0.5302 ± 0.0271	558 ± 83	408 ± 5	95
12XL14-1-5	2.48	0.0585 ± 0.0023	0.0835 ± 0.0011	0.6739 ± 0.0355	549 ± 85	517 ± 7	99
12XL14-1-6	1.60	0.0625 ± 0.0026	0.0665 ± 0.0010	0.5735 ± 0.0320	691 ± 87	415 ± 6	90
12XL14-1-7	1.51	0.0567 ± 0.0023	0.0650 ± 0.0009	0.5076 ± 0.0285	477 ± 90	406 ± 6	97
12XL14-1-8	1.82	0.0666 ± 0.0019	0.1264 ± 0.0014	1.1600 ± 0.0458	825 ± 59	767 ± 8	98
12XL14-1-9	3.87	0.0625 ± 0.0027	0.0722 ± 0.0011	0.6212 ± 0.0381	689 ± 94	449 ± 7	92
12XL14-1-10	2.61	0.0565 ± 0.0025	0.0674 ± 0.0011	0.5249 ± 0.0332	471 ± 99	421 ± 7	98
12XL14-1-12	1.88	0.0566 ± 0.0023	0.0642 ± 0.0009	0.5009 ± 0.0282	475 ± 89	401 ± 6	97
12XL14-1-13	0.69	0.0577 ± 0.0019	0.0805 ± 0.0010	0.6407 ± 0.0302	517 ± 74	499 ± 6	99
12XL14-1-14	1.66	0.0550 ± 0.0022	0.0696 ± 0.0010	0.5275 ± 0.0287	409 ± 88	434 ± 6	101
12XL14-1-15	1.33	0.1517 ± 0.0041	0.4427 ± 0.0049	9.2595 ± 0.3425	2364 ± 46	2363 ± 22	100
12XL14-1-15	2.13	0.0810 ± 0.0024	0.1103 ± 0.0012	1.2331 ± 0.0506	1221 ± 59	675 ± 7	83
12XL14-1-16	2.53	0.0581 ± 0.0017	0.0849 ± 0.0009	0.6811 ± 0.0271	534 ± 64	525 ± 5	100
12XL14-1-17	1.60	0.0554 ± 0.0035	0.0653 ± 0.0014	0.4996 ± 0.0435	429 ± 142	408 ± 8	99
12XL14-1-18	1.34	0.0613 ± 0.0023	0.0798 ± 0.0011	0.6753 ± 0.0348	649 ± 80	495 ± 7	94
12XL14-1-19	1.25	0.0584 ± 0.0017	0.0813 ± 0.0009	0.6552 ± 0.0263	543 ± 63	504 ± 5	99
12XL14-1-20	0.78	0.0643 ± 0.0033	0.0605 ± 0.0008	0.5364 ± 0.0386	749 ± 107	379 ± 5	87
12XL14-1-21	1.81	0.0524 ± 0.0019	0.0680 ± 0.0009	0.4917 ± 0.0253	300 ± 84	424 ± 5	104
12XL14-1-22	3.26	0.0639 ± 0.0037	0.0701 ± 0.0014	0.6188 ± 0.0494	738 ± 121	436 ± 8	89
12XL14-1-23	1.03	0.0496 ± 0.0025	0.0690 ± 0.0011	0.4728 ± 0.0331	175 ± 117	430 ± 7	109

(continued)

Table B.1 (continued)

Sample	U/Th	$^{206}Pb^*/^{207}Pb^*$	$^{206}Pb^*/^{238}U$	$^{207}Pb^*/^{235}U$	$^{206}Pb^*/^{207}Pb^* - Age$ [Ma]	$^{238}U/^{206}Pb - Age$ [Ma]	Concordance [%]
12XL14-1-24	2.27	0.0470 ± 0.0021	0.0641 ± 0.0009	0.4163 ± 0.0261	48 ± 108	401 ± 6	113
12XL14-1-25	2.94	0.0430 ± 0.0033	0.0724 ± 0.0010	0.4295 ± 0.0462	NaN ± 0	451 ± 6	124
12XL14-1-26	2.13	0.0514 ± 0.0028	0.0685 ± 0.0012	0.4854 ± 0.0368	256 ± 127	427 ± 7	106
12XL14-1-27	2.04	0.0506 ± 0.0032	0.0646 ± 0.0012	0.4510 ± 0.0388	222 ± 145	404 ± 7	107
12XL14-1-28	2.01	0.0576 ± 0.0021	0.1229 ± 0.0016	0.9763 ± 0.0480	515 ± 79	747 ± 9	108
12XL14-1-28	1.52	0.0744 ± 0.0047	0.0677 ± 0.0015	0.6950 ± 0.0596	1052 ± 126	423 ± 9	79
12XL14-1-29	6.65	0.1103 ± 0.0030	0.3106 ± 0.0034	4.7220 ± 0.1767	1803 ± 50	1744 ± 17	98
12XL14-1-31	2.93	0.0637 ± 0.0029	0.0713 ± 0.0012	0.6267 ± 0.0388	732 ± 95	444 ± 7	90
12XL14-1-32	2.24	0.0623 ± 0.0037	0.0640 ± 0.0013	0.5496 ± 0.0455	684 ± 128	400 ± 8	90
12XL14-1-33	2.93	0.0639 ± 0.0036	0.0688 ± 0.0014	0.6063 ± 0.0473	738 ± 119	429 ± 8	89
12XL14-1-34	3.43	0.0571 ± 0.0023	0.0754 ± 0.0011	0.5937 ± 0.0338	494 ± 90	469 ± 7	99
12XL14-1-35	1.83	0.0587 ± 0.0018	0.0864 ± 0.0010	0.6991 ± 0.0294	555 ± 66	534 ± 6	99
12XL14-1-36	0.90	0.0664 ± 0.0021	0.1262 ± 0.0016	1.1559 ± 0.0515	819 ± 67	766 ± 9	98
12XL14-1-37	2.37	0.0680 ± 0.0041	0.0691 ± 0.0014	0.6489 ± 0.0539	869 ± 124	431 ± 9	85
12XL14-1-38	1.56	0.0557 ± 0.0023	0.0681 ± 0.0010	0.5229 ± 0.0301	440 ± 92	424 ± 6	99
12XL14-1-39	1.63	0.0560 ± 0.0026	0.0668 ± 0.0010	0.5163 ± 0.0328	451 ± 102	417 ± 6	99
12XL14-1-40	1.41	0.0545 ± 0.0035	0.0671 ± 0.0014	0.5043 ± 0.0450	391 ± 144	418 ± 8	101
12XL14-1-41	1.57	0.0544 ± 0.0018	0.0822 ± 0.0010	0.6166 ± 0.0278	387 ± 73	509 ± 6	104
12XL14-1-42	1.49	0.0846 ± 0.0029	0.2433 ± 0.0035	2.8394 ± 0.1359	1305 ± 67	1404 ± 18	103
12XL14-1-43	4.10	0.0556 ± 0.0017	0.0775 ± 0.0009	0.5941 ± 0.0252	434 ± 68	481 ± 5	102
12XL14-1-44	1.65	0.0563 ± 0.0022	0.0670 ± 0.0009	0.5210 ± 0.0279	465 ± 85	418 ± 6	98
12XL14-1-45	5.04	0.0567 ± 0.0017	0.0795 ± 0.0009	0.6213 ± 0.0257	477 ± 65	493 ± 5	101
12XL14-1-46	1.11	0.0564 ± 0.0022	0.0741 ± 0.0011	0.5766 ± 0.0316	468 ± 86	461 ± 6	100

(continued)

Table B.1 (continued)

Sample	U/Th	$^{206}Pb^*/^{207}Pb^*$	$^{206}Pb^*/^{238}U$	$^{207}Pb^*/^{235}U$	$^{206}Pb^*/^{207}Pb^* - Age$ [Ma]	$^{238}U/^{206}Pb - Age$ [Ma]	Concordance [%]
12XL14-1-47	2.11	0.0598 ± 0.0018	0.0877 ± 0.0010	0.7238 ± 0.0310	596 ± 65	542 ± 6	98
12XL14-1-48	1.40	0.0574 ± 0.0027	0.0721 ± 0.0012	0.5706 ± 0.0381	506 ± 103	449 ± 7	98
12XL14-1-49	1.41	0.0788 ± 0.0035	0.0677 ± 0.0012	0.7359 ± 0.0471	1167 ± 89	422 ± 7	75
12XL14-1-50	0.89	0.0931 ± 0.0028	0.1325 ± 0.0016	1.7005 ± 0.0743	1488 ± 57	802 ± 9	80
12XL14-1-51	1.94	0.0553 ± 0.0022	0.0822 ± 0.0012	0.6267 ± 0.0368	422 ± 90	509 ± 7	103
12XL14-1-52	2.19	0.0572 ± 0.0019	0.0739 ± 0.0010	0.5831 ± 0.0282	499 ± 74	459 ± 6	99
12XL14-1-53	2.55	0.0621 ± 0.0036	0.0851 ± 0.0017	0.7288 ± 0.0608	676 ± 124	527 ± 10	95
12XL14-1-54	3.54	0.0624 ± 0.0017	0.1261 ± 0.0014	1.0854 ± 0.0434	687 ± 60	766 ± 8	103
12XL14-1-55	1.20	0.0573 ± 0.0022	0.0858 ± 0.0012	0.6777 ± 0.0368	501 ± 84	531 ± 7	101
12XL14-1-56	1.29	0.0575 ± 0.0026	0.0670 ± 0.0011	0.5312 ± 0.0343	509 ± 100	418 ± 7	97
12XL14-1-57	1.71	0.0490 ± 0.0019	0.0638 ± 0.0009	0.4311 ± 0.0238	145 ± 91	399 ± 5	110
12XL14-1-58	5.30	0.0558 ± 0.0030	0.0861 ± 0.0017	0.6623 ± 0.0516	444 ± 121	532 ± 10	103
12XL14-1-59	2.66	0.0679 ± 0.0022	0.1579 ± 0.0018	1.4773 ± 0.0675	863 ± 66	945 ± 10	103
12XL14-1-60	2.36	0.0553 ± 0.0294	0.0692 ± 0.0038	0.5278 ± 0.4131	424 ± 1185	431 ± 23	100
12XL14-1-61	2.19	0.0591 ± 0.0019	0.0859 ± 0.0011	0.6996 ± 0.0318	570 ± 69	531 ± 6	99
12XL14-1-62	0.80	0.0669 ± 0.0023	0.1052 ± 0.0015	0.9697 ± 0.0479	832 ± 72	645 ± 8	94
12XL14-1-63	1.73	0.0566 ± 0.0033	0.0773 ± 0.0016	0.6028 ± 0.0509	475 ± 130	480 ± 10	100
12XL14-1-64	1.93	0.0643 ± 0.0029	0.0639 ± 0.0011	0.5668 ± 0.0371	751 ± 97	399 ± 7	88
12XL14-1-65	1.97	0.0590 ± 0.0020	0.0814 ± 0.0011	0.6620 ± 0.0319	566 ± 74	504 ± 6	98
12XL14-1-66	1.26	0.0602 ± 0.0022	0.0842 ± 0.0012	0.6994 ± 0.0356	611 ± 77	521 ± 7	97
12XL14-1-67	1.54	0.0566 ± 0.0023	0.0666 ± 0.0010	0.5195 ± 0.0299	473 ± 89	416 ± 6	98
12XL14-1-68	2.43	0.0565 ± 0.0018	0.0890 ± 0.0011	0.6937 ± 0.0313	471 ± 70	550 ± 7	103
12XL14-1-69	1.69	0.0599 ± 0.0025	0.0776 ± 0.0012	0.6410 ± 0.0382	599 ± 90	482 ± 7	96

(continued)

Table B.1 (continued)

Sample	U/Th	$^{206}Pb^*/^{207}Pb^*$	$^{206}Pb^*/^{238}U$	$^{207}Pb^*/^{235}U$	$^{206}Pb^*/^{207}Pb^* - Age$ [Ma]	$^{238}U/^{206}Pb - Age$ [Ma]	Concordance [%]
12XL14-1-70	4.14	0.1478 ± 0.0044	0.3716 ± 0.0052	7.5750 ± 0.3213	2320 ± 51	2037 ± 24	93
12XL14-1-71	0.79	0.0615 ± 0.0023	0.1270 ± 0.0019	1.0769 ± 0.0578	656 ± 80	770 ± 11	104
12XL14-1-72	2.32	0.0633 ± 0.0020	0.0677 ± 0.0008	0.5914 ± 0.0261	717 ± 66	423 ± 5	90
12XL14-1-73	2.61	0.0545 ± 0.0031	0.0746 ± 0.0015	0.5606 ± 0.0453	390 ± 127	464 ± 9	103
12XL14-1-74	1.40	0.0585 ± 0.0025	0.0768 ± 0.0012	0.6188 ± 0.0376	546 ± 93	477 ± 7	97
12XL14-1-75	1.79	0.0563 ± 0.0017	0.0826 ± 0.0010	0.6413 ± 0.0274	464 ± 66	511 ± 6	102
12XL14-1-76	3.19	0.0514 ± 0.0044	0.0661 ± 0.0018	0.4690 ± 0.0583	259 ± 199	413 ± 11	106
12XL14-1-77	2.08	0.0546 ± 0.0024	0.0669 ± 0.0011	0.5038 ± 0.0322	396 ± 100	417 ± 6	101
12XL14-1-78	2.36	0.1111 ± 0.0036	0.3162 ± 0.0048	4.8484 ± 0.2260	1817 ± 59	1771 ± 23	99
12XL14-1-79	2.84	0.0574 ± 0.0018	0.0823 ± 0.0010	0.6515 ± 0.0300	504 ± 70	510 ± 6	100
12XL14-1-80	2.53	0.0618 ± 0.0024	0.0808 ± 0.0012	0.6892 ± 0.0389	668 ± 83	501 ± 7	94
12XL14-1-81	1.61	0.0791 ± 0.0036	0.1508 ± 0.0029	1.6453 ± 0.1082	1174 ± 89	905 ± 16	92
12XL14-1-82	1.65	0.0566 ± 0.0020	0.0665 ± 0.0009	0.5195 ± 0.0274	477 ± 80	415 ± 6	98
12XL14-1-83	2.97	0.0685 ± 0.0020	0.1556 ± 0.0019	1.4701 ± 0.0638	883 ± 62	932 ± 11	102
12XL14-1-84	3.14	0.0588 ± 0.0024	0.0623 ± 0.0010	0.5052 ± 0.0299	557 ± 89	390 ± 6	94
12XL14-1-85	1.60	0.0574 ± 0.0021	0.0757 ± 0.0011	0.5999 ± 0.0312	507 ± 79	471 ± 6	99
12XL14-1-86	2.48	0.0568 ± 0.0019	0.0787 ± 0.0010	0.6169 ± 0.0294	484 ± 72	488 ± 6	100
12XL14-1-87	1.41	0.0653 ± 0.0020	0.1163 ± 0.0015	1.0467 ± 0.0476	782 ± 66	709 ± 9	98
12XL14-1-88	1.33	0.0793 ± 0.0025	0.1764 ± 0.0024	1.9286 ± 0.0887	1179 ± 63	1047 ± 13	96
12XL14-1-89	6.24	0.1095 ± 0.0028	0.1377 ± 0.0015	2.0789 ± 0.0764	1790 ± 46	832 ± 8	73
12XL14-1-90	1.48	0.0644 ± 0.0018	0.0722 ± 0.0008	0.6408 ± 0.0260	752 ± 59	449 ± 5	89
12XL14-1-91	3.89	0.0820 ± 0.0023	0.1355 ± 0.0016	1.5321 ± 0.0619	1245 ± 55	819 ± 9	87
12XL14-1-92	2.73	0.0561 ± 0.0022	0.0727 ± 0.0011	0.5622 ± 0.0315	456 ± 87	452 ± 6	100

(continued)

Table B.1 (continued)

Sample	U/Th	$^{206}Pb^*/^{207}Pb^*$	$^{206}Pb^*/^{238}U$	$^{207}Pb^*/^{235}U$	$^{206}Pb^*/^{207}Pb^*-Age$ [Ma]	$^{238}U/^{206}Pb-Age$ [Ma]	Concordance [%]
12XL14-1-93	1.89	0.0611 ± 0.0038	0.0718 ± 0.0016	0.6054 ± 0.0532	643 ± 134	447 ± 10	93
12XL14-1-94	1.25	0.0614 ± 0.0021	0.0855 ± 0.0012	0.7236 ± 0.0356	652 ± 75	529 ± 7	96
12XL14-1-95	1.90	0.0728 ± 0.0021	0.1509 ± 0.0018	1.5154 ± 0.0611	1008 ± 59	906 ± 10	97
12XL14-1-96	7.29	0.0753 ± 0.0022	0.1631 ± 0.0019	1.6943 ± 0.0686	1076 ± 58	974 ± 11	97
12XL14-1-97	1.50	0.0613 ± 0.0022	0.0925 ± 0.0013	0.7816 ± 0.0393	648 ± 77	570 ± 8	97
12XL14-1-98	1.98	0.0644 ± 0.0048	0.0668 ± 0.0017	0.5922 ± 0.0623	752 ± 158	417 ± 11	88
12XL14-1-99	1.43	0.0569 ± 0.0021	0.0619 ± 0.0009	0.4850 ± 0.0258	486 ± 83	387 ± 5	96
12XL14-1-100	1.12	0.0598 ± 0.0018	0.0730 ± 0.0009	0.6021 ± 0.0254	596 ± 64	454 ± 5	95
12XL14-1-101	1.58	0.1608 ± 0.0042	0.4155 ± 0.0047	9.2151 ± 0.3441	2464 ± 44	2240 ± 22	95
12XL14-1-102	1.66	0.0574 ± 0.0024	0.0661 ± 0.0010	0.5234 ± 0.0318	506 ± 94	413 ± 6	97
12XL14-1-103	1.56	0.0598 ± 0.0023	0.0819 ± 0.0012	0.6751 ± 0.0373	596 ± 84	507 ± 7	97
12XL14-1-104	3.30	0.0552 ± 0.0017	0.0852 ± 0.0010	0.6486 ± 0.0283	420 ± 68	527 ± 6	104
12XL14-1-105	2.07	0.0533 ± 0.0034	0.0706 ± 0.0015	0.5186 ± 0.0468	340 ± 143	440 ± 9	104
12XL14-1-106	1.67	0.0546 ± 0.0026	0.0650 ± 0.0011	0.4892 ± 0.0336	395 ± 108	406 ± 7	100
12XL14-1-107	1.45	0.0562 ± 0.0026	0.0855 ± 0.0014	0.6621 ± 0.0434	459 ± 102	529 ± 8	102
12XL14-1-108	1.91	0.0559 ± 0.0019	0.0723 ± 0.0009	0.5572 ± 0.0269	447 ± 75	450 ± 6	100
12XL14-1-109	1.46	0.0914 ± 0.0048	0.0710 ± 0.0016	0.8956 ± 0.0670	1455 ± 101	442 ± 9	68
12XL14-1-110	2.86	0.0709 ± 0.0021	0.0998 ± 0.0012	0.9752 ± 0.0409	953 ± 60	613 ± 7	89
12XL14-1-111	2.51	0.0660 ± 0.0036	0.0706 ± 0.0015	0.6420 ± 0.0507	805 ± 116	440 ± 9	87
12XL14-1-112	2.56	0.0595 ± 0.0029	0.0647 ± 0.0011	0.5308 ± 0.0370	583 ± 105	404 ± 7	94
12XL14-1-113	1.50	0.0614 ± 0.0028	0.0989 ± 0.0017	0.8366 ± 0.0548	651 ± 98	608 ± 10	98
12XL14-1-114	1.95	0.0583 ± 0.0018	0.0842 ± 0.0010	0.6769 ± 0.0295	539 ± 66	521 ± 6	99
12XL14-1-115	1.99	0.0530 ± 0.0031	0.0705 ± 0.0014	0.5147 ± 0.0433	326 ± 132	439 ± 8	104

(continued)

Table B.1 (continued)

Sample	U/Th	$^{206}Pb^{*}/^{207}Pb^{*}$	$^{206}Pb^{*}/^{238}U$	$^{207}Pb^{*}/^{235}U$	$^{206}Pb^{*}/^{207}Pb^{*}-Age$ [Ma]	$^{238}U/^{206}Pb - Age$ [Ma]	Concordance [%]
12XL14-1-116	5.34	0.0688 ± 0.0024	0.1372 ± 0.0019	1.3014 ± 0.0653	892 ± 72	829 ± 11	98
12XL14-1-117	1.71	0.0548 ± 0.0020	0.0671 ± 0.0009	0.5071 ± 0.0269	402 ± 82	419 ± 6	101
12XL14-1-118	2.87	0.0572 ± 0.0023	0.0657 ± 0.0010	0.5183 ± 0.0301	498 ± 89	410 ± 6	97
12XL14-1-119	0.99	0.0599 ± 0.0019	0.0733 ± 0.0009	0.6058 ± 0.0272	600 ± 68	456 ± 5	95
12XL14-1-120	1.36	0.0579 ± 0.0021	0.0824 ± 0.0012	0.6570 ± 0.0348	523 ± 81	510 ± 7	99
12XL15-1-1	1.60	0.0593 ± 0.0034	0.0698 ± 0.0017	0.5707 ± 0.0538	577 ± 126	435 ± 11	95
12XL15-1-2	1.59	0.0615 ± 0.0027	0.0655 ± 0.0013	0.5556 ± 0.0398	655 ± 94	409 ± 8	91
12XL15-1-3	1.32	0.0591 ± 0.0034	0.0652 ± 0.0016	0.5315 ± 0.0502	571 ± 126	407 ± 10	94
12XL15-1-4	2.87	0.0557 ± 0.0017	0.0851 ± 0.0012	0.6536 ± 0.0317	439 ± 66	527 ± 7	103
12XL15-1-5	1.71	0.1063 ± 0.0029	0.3023 ± 0.0044	4.4325 ± 0.1990	1736 ± 51	1703 ± 22	99
12XL15-1-6	1.67	0.0756 ± 0.0035	0.0633 ± 0.0014	0.6601 ± 0.0490	1084 ± 92	396 ± 8	77
12XL15-1-7	0.94	0.0570 ± 0.0031	0.0651 ± 0.0015	0.5116 ± 0.0449	490 ± 119	407 ± 9	97
12XL15-1-8	1.25	0.0651 ± 0.0021	0.1447 ± 0.0023	1.2987 ± 0.0690	776 ± 69	871 ± 13	103
12XL15-1-9	1.24	0.0624 ± 0.0025	0.0617 ± 0.0011	0.5310 ± 0.0348	688 ± 86	386 ± 7	89
12XL15-1-10	2.57	0.0561 ± 0.0027	0.0646 ± 0.0013	0.5001 ± 0.0385	457 ± 105	403 ± 8	98
12XL15-1-11	2.35	0.0570 ± 0.0025	0.0635 ± 0.0012	0.4994 ± 0.0353	491 ± 96	397 ± 7	97
12XL15-1-12	1.59	0.0612 ± 0.0037	0.0616 ± 0.0016	0.5203 ± 0.0515	646 ± 131	385 ± 10	91
12XL15-1-13	0.90	0.0569 ± 0.0025	0.0639 ± 0.0012	0.5009 ± 0.0358	486 ± 97	399 ± 7	97
12XL15-1-14	2.02	0.0509 ± 0.0031	0.0670 ± 0.0016	0.4700 ± 0.0462	235 ± 139	418 ± 10	107
12XL15-1-15	2.99	0.0626 ± 0.0030	0.0609 ± 0.0013	0.5259 ± 0.0408	695 ± 101	381 ± 8	89
12XL15-1-16	1.52	0.0565 ± 0.0039	0.0645 ± 0.0019	0.5027 ± 0.0568	471 ± 153	403 ± 11	97
12XL15-1-17	2.31	0.0615 ± 0.0034	0.0790 ± 0.0020	0.6707 ± 0.0608	657 ± 120	490 ± 12	94
12XL15-1-18	1.01	0.0525 ± 0.0028	0.0658 ± 0.0015	0.4768 ± 0.0414	307 ± 122	411 ± 9	104

(continued)

Table B.1 (continued)

Sample	U/Th	$^{206}Pb^*/^{207}Pb^*$	$^{206}Pb^*/^{238}U$	$^{207}Pb^*/^{235}U$	$^{206}Pb^*/^{207}Pb^* - Age$ [Ma]	$^{238}U/^{206}Pb - Age$ [Ma]	Concordance [%]
12XL15-1-19	1.66	0.0570 ± 0.0027	0.0639 ± 0.0013	0.5029 ± 0.0394	491 ± 106	400 ± 8	97
12XL15-1-20	3.00	0.0510 ± 0.0028	0.0753 ± 0.0016	0.5293 ± 0.0479	238 ± 128	468 ± 10	109
12XL15-1-21	2.03	0.0624 ± 0.0025	0.0939 ± 0.0017	0.8077 ± 0.0528	687 ± 87	578 ± 10	96
12XL15-1-22	2.25	0.0867 ± 0.0030	0.1973 ± 0.0035	2.3588 ± 0.1323	1353 ± 68	1161 ± 19	94
12XL15-1-23	1.21	0.0640 ± 0.0036	0.0614 ± 0.0015	0.5420 ± 0.0487	739 ± 119	384 ± 9	87
12XL15-1-24	1.18	0.0670 ± 0.0051	0.0614 ± 0.0020	0.5676 ± 0.0691	837 ± 159	384 ± 12	84
12XL15-1-25	2.64	0.0569 ± 0.0017	0.0845 ± 0.0012	0.6630 ± 0.0312	485 ± 65	523 ± 7	101
12XL15-1-26	1.28	0.0515 ± 0.0025	0.0648 ± 0.0013	0.4602 ± 0.0363	262 ± 113	405 ± 8	105
12XL15-1-27	1.62	0.0657 ± 0.0025	0.0624 ± 0.0011	0.5658 ± 0.0345	796 ± 80	390 ± 7	86
12XL15-1-28	1.48	0.0595 ± 0.0026	0.0614 ± 0.0012	0.5036 ± 0.0350	584 ± 94	384 ± 7	93
12XL15-1-29	0.82	0.0660 ± 0.0047	0.0583 ± 0.0018	0.5311 ± 0.0609	806 ± 149	365 ± 11	84
12XL15-1-30	1.89	0.0627 ± 0.0018	0.0695 ± 0.0010	0.6016 ± 0.0283	698 ± 62	433 ± 6	91
12XL15-1-31	1.71	0.0744 ± 0.0032	0.0594 ± 0.0012	0.6088 ± 0.0429	1052 ± 87	372 ± 8	77
12XL15-1-32	1.03	0.0631 ± 0.0026	0.0613 ± 0.0011	0.5325 ± 0.0360	710 ± 88	383 ± 7	88
12XL15-1-33	1.26	0.0651 ± 0.0029	0.0599 ± 0.0012	0.5372 ± 0.0392	777 ± 93	375 ± 7	86
12XL15-1-34	1.35	0.0526 ± 0.0021	0.0632 ± 0.0011	0.4583 ± 0.0303	312 ± 91	395 ± 7	103
12XL15-1-35	1.54	0.0584 ± 0.0023	0.0631 ± 0.0011	0.5083 ± 0.0332	544 ± 86	395 ± 7	95
12XL15-1-36	1.82	0.0548 ± 0.0027	0.0632 ± 0.0013	0.4776 ± 0.0391	404 ± 111	395 ± 8	100
12XL15-1-37	2.10	0.0545 ± 0.0026	0.0621 ± 0.0012	0.4662 ± 0.0360	390 ± 106	388 ± 7	100
12XL15-1-38	1.99	0.0545 ± 0.0029	0.0646 ± 0.0014	0.4850 ± 0.0423	390 ± 121	404 ± 9	100
12XL15-1-39	1.36	0.0535 ± 0.0023	0.0629 ± 0.0011	0.4637 ± 0.0318	350 ± 97	393 ± 7	102
12XL15-1-40	1.73	0.0544 ± 0.0025	0.0652 ± 0.0012	0.4887 ± 0.0358	385 ± 103	407 ± 7	101
12XL15-1-41	1.75	0.0566 ± 0.0032	0.0652 ± 0.0015	0.5087 ± 0.0458	473 ± 126	407 ± 9	98

(continued)

Table B.1 (continued)

Sample	U/Th	$^{206}Pb^*/^{207}Pb^*$	$^{206}Pb^*/^{238}U$	$^{207}Pb^*/^{235}U$	$^{206}Pb^*/^{207}Pb^* - Age$ [Ma]	$^{238}U/^{206}Pb - Age$ [Ma]	Concordance [%]
12XL15-1-42	1.67	0.0540 ± 0.0025	0.0662 ± 0.0012	0.4929 ± 0.0359	368 ± 103	413 ± 7	102
12XL15-1-43	3.29	0.0571 ± 0.0018	0.0841 ± 0.0012	0.6626 ± 0.0340	495 ± 70	521 ± 7	101
12XL15-1-44	2.84	0.0600 ± 0.0038	0.0656 ± 0.0018	0.5424 ± 0.0563	602 ± 139	409 ± 11	93
12XL15-1-45	1.52	0.0424 ± 0.0028	0.0626 ± 0.0014	0.3663 ± 0.0399	NaN ± 0	391 ± 8	123
12XL15-1-46	3.37	0.0639 ± 0.0028	0.0664 ± 0.0013	0.5847 ± 0.0425	736 ± 94	414 ± 8	89
12XL15-1-47	2.05	0.0603 ± 0.0022	0.0781 ± 0.0013	0.6493 ± 0.0389	613 ± 80	485 ± 8	95
12XL15-1-48	1.28	0.0562 ± 0.0026	0.0639 ± 0.0012	0.4950 ± 0.0368	459 ± 102	399 ± 7	98
12XL15-1-49	1.23	0.0538 ± 0.0019	0.0725 ± 0.0011	0.5385 ± 0.0308	362 ± 80	451 ± 7	103
12XL15-1-50	2.05	0.0547 ± 0.0018	0.0671 ± 0.0010	0.5062 ± 0.0268	398 ± 74	419 ± 6	101
12XL15-1-51	1.63	0.0531 ± 0.0028	0.0684 ± 0.0015	0.5013 ± 0.0427	334 ± 120	426 ± 9	103
12XL15-1-52	1.63	0.0671 ± 0.0028	0.1437 ± 0.0029	1.3287 ± 0.0901	838 ± 87	865 ± 16	101
12XL15-1-53	0.92	0.0528 ± 0.0035	0.0605 ± 0.0017	0.4408 ± 0.0473	319 ± 150	379 ± 10	102
12XL15-1-54	1.73	0.0555 ± 0.0028	0.0665 ± 0.0016	0.5085 ± 0.0419	431 ± 112	415 ± 9	99
12XL15-1-55	1.51	0.0636 ± 0.0043	0.0646 ± 0.0020	0.5670 ± 0.0634	729 ± 145	404 ± 12	88
12XL15-1-56	2.73	0.0577 ± 0.0029	0.0616 ± 0.0015	0.4907 ± 0.0408	519 ± 111	385 ± 9	95
12XL15-1-57	1.77	0.0560 ± 0.0026	0.0693 ± 0.0015	0.5355 ± 0.0401	453 ± 102	432 ± 9	99
12XL15-1-58	1.59	0.0525 ± 0.0032	0.0648 ± 0.0016	0.4694 ± 0.0461	307 ± 137	405 ± 10	104
12XL15-1-59	1.24	0.0545 ± 0.0030	0.0641 ± 0.0015	0.4820 ± 0.0425	392 ± 122	401 ± 9	100
12XL15-1-60	2.17	0.0572 ± 0.0024	0.0668 ± 0.0012	0.5271 ± 0.0350	500 ± 91	417 ± 7	97
12XL15-1-61	2.10	0.0533 ± 0.0026	0.0676 ± 0.0013	0.4964 ± 0.0382	338 ± 109	422 ± 8	103
12XL15-1-62	2.87	0.0504 ± 0.0036	0.0711 ± 0.0018	0.4939 ± 0.0562	211 ± 164	443 ± 11	109
12XL15-1-63	3.03	0.0491 ± 0.0019	0.0663 ± 0.0011	0.4490 ± 0.0286	154 ± 93	414 ± 7	110
12XL15-1-64	1.05	0.0524 ± 0.0025	0.0626 ± 0.0012	0.4524 ± 0.0347	301 ± 108	392 ± 7	103

(continued)

Table B.1 (continued)

Sample	U/Th	$^{206}Pb^*/^{207}Pb^*$	$^{206}Pb^*/^{238}U$	$^{207}Pb^*/^{235}U$	$^{206}Pb^*/^{207}Pb^*-Age$ [Ma]	$^{238}U/^{206}Pb-Age$ [Ma]	Concordance [%]
12XL15-1-65	2.19	0.0565 ± 0.0039	0.0615 ± 0.0017	0.4797 ± 0.0529	472 ± 151	385 ± 10	97
12XL15-1-66	2.56	0.0507 ± 0.0022	0.0682 ± 0.0012	0.4767 ± 0.0329	225 ± 99	426 ± 7	108
12XL15-1-67	2.36	0.0577 ± 0.0043	0.0584 ± 0.0017	0.4646 ± 0.0554	518 ± 163	366 ± 11	94
12XL15-1-68	1.20	0.0537 ± 0.0024	0.0635 ± 0.0012	0.4706 ± 0.0341	359 ± 102	397 ± 7	101
12XL15-1-69	2.02	0.0612 ± 0.0035	0.0671 ± 0.0016	0.5661 ± 0.0514	646 ± 122	419 ± 10	92
12XL15-1-70	0.84	0.0790 ± 0.0043	0.0627 ± 0.0015	0.6830 ± 0.0580	1172 ± 107	392 ± 9	74
12XL15-1-71	1.03	0.0624 ± 0.0033	0.0621 ± 0.0014	0.5342 ± 0.0447	685 ± 112	388 ± 9	89
12XL15-1-72	2.56	0.0643 ± 0.0030	0.0827 ± 0.0017	0.7332 ± 0.0543	750 ± 98	512 ± 10	92
12XL15-1-73	1.88	0.0542 ± 0.0021	0.0641 ± 0.0011	0.4791 ± 0.0295	379 ± 86	400 ± 7	101
12XL15-1-74	2.64	0.0554 ± 0.0028	0.0664 ± 0.0014	0.5077 ± 0.0418	429 ± 113	414 ± 8	99
12XL15-1-75	1.99	0.0607 ± 0.0025	0.0651 ± 0.0012	0.5446 ± 0.0364	627 ± 89	406 ± 7	92
12XL15-1-76	1.91	0.0597 ± 0.0021	0.0760 ± 0.0012	0.6253 ± 0.0355	591 ± 76	472 ± 7	96
12XL15-1-77	0.97	0.0551 ± 0.0021	0.0664 ± 0.0011	0.5048 ± 0.0306	414 ± 84	415 ± 7	100
12XL15-1-78	1.25	0.0556 ± 0.0023	0.0653 ± 0.0012	0.5013 ± 0.0336	436 ± 93	408 ± 7	99
12XL15-1-79	3.01	0.0880 ± 0.0028	0.1842 ± 0.0029	2.2369 ± 0.1127	1383 ± 61	1090 ± 16	91
12XL15-1-80	2.48	0.0629 ± 0.0031	0.0723 ± 0.0016	0.6282 ± 0.0487	706 ± 104	450 ± 9	91
12XL15-1-81	1.68	0.1764 ± 0.0055	0.4344 ± 0.0076	10.5589 ± 0.5198	2618 ± 52	2326 ± 34	94
12XL15-1-82	2.90	0.0547 ± 0.0017	0.0808 ± 0.0012	0.6095 ± 0.0301	401 ± 69	501 ± 7	104
12XL15-1-83	1.04	0.0558 ± 0.0023	0.0647 ± 0.0011	0.4969 ± 0.0324	442 ± 90	404 ± 7	99
12XL15-1-84	2.21	0.0610 ± 0.0047	0.0687 ± 0.0022	0.5771 ± 0.0722	638 ± 167	428 ± 13	93
12XL15-1-85	2.34	0.0521 ± 0.0025	0.0595 ± 0.0012	0.4270 ± 0.0335	288 ± 110	372 ± 7	103
12XL15-1-86	2.26	0.0568 ± 0.0018	0.0577 ± 0.0008	0.4518 ± 0.0237	483 ± 72	361 ± 5	95
12XL15-1-87	1.94	0.0600 ± 0.0042	0.0624 ± 0.0017	0.5160 ± 0.0584	602 ± 152	390 ± 11	92

(continued)

Table B.1 (continued)

Sample	U/Th	$^{206}Pb^*/^{207}Pb^*$	$^{206}Pb^*/^{238}U$	$^{207}Pb^*/^{235}U$	$^{206}Pb^*/^{207}Pb^* - Age$ [Ma]	$^{238}U/^{206}Pb - Age$ [Ma]	Concordance [%]
12XL15-1-88	1.89	0.0484 ± 0.0028	0.0689 ± 0.0015	0.4602 ± 0.0423	119 ± 135	429 ± 9	112
12XL15-1-89	2.36	0.0537 ± 0.0020	0.0822 ± 0.0013	0.6090 ± 0.0354	357 ± 82	509 ± 7	105
12XL15-1-90	1.20	0.0541 ± 0.0022	0.0656 ± 0.0011	0.4891 ± 0.0316	373 ± 92	409 ± 7	101
12XL15-1-91	1.74	0.0542 ± 0.0028	0.0659 ± 0.0013	0.4931 ± 0.0406	378 ± 117	412 ± 8	101
12XL15-1-92	1.74	0.1074 ± 0.0032	0.3418 ± 0.0051	5.0672 ± 0.2400	1755 ± 55	1895 ± 24	104
12XL15-1-93	0.66	0.0531 ± 0.0024	0.0347 ± 0.0006	0.2543 ± 0.0182	333 ± 102	220 ± 4	96
12XL15-1-94	1.84	0.0560 ± 0.0024	0.0657 ± 0.0012	0.5078 ± 0.0342	451 ± 93	410 ± 7	98
12XL15-1-95	1.84	0.0508 ± 0.0046	0.0628 ± 0.0022	0.4396 ± 0.0650	229 ± 211	392 ± 13	106
12XL15-1-96	1.98	0.0678 ± 0.0022	0.1237 ± 0.0019	1.1565 ± 0.0603	861 ± 67	752 ± 11	96
12XL15-1-97	1.32	0.0543 ± 0.0023	0.0635 ± 0.0011	0.4757 ± 0.0326	383 ± 95	397 ± 7	100
12XL15-1-98	1.70	0.0541 ± 0.0024	0.0638 ± 0.0012	0.4764 ± 0.0345	376 ± 101	399 ± 7	101
12XL15-1-99	1.48	0.0626 ± 0.0032	0.0575 ± 0.0013	0.4960 ± 0.0411	693 ± 110	360 ± 8	88
12XL15-1-100	1.51	0.0545 ± 0.0025	0.0626 ± 0.0012	0.4708 ± 0.0352	391 ± 104	392 ± 7	100
12XL15-1-101	1.58	0.0931 ± 0.0051	0.0600 ± 0.0017	0.7705 ± 0.0682	1488 ± 103	375 ± 10	65
12XL15-1-102	0.88	0.0594 ± 0.0028	0.0616 ± 0.0013	0.5055 ± 0.0399	582 ± 104	385 ± 8	93
12XL15-1-103	0.17	0.5437 ± 0.0283	0.1373 ± 0.0068	10.3078 ± 0.8285	4364 ± 76	830 ± 38	34
12XL15-1-104	2.15	0.0635 ± 0.0035	0.0569 ± 0.0015	0.4989 ± 0.0460	724 ± 116	357 ± 9	87
12XL15-1-105	1.33	0.0601 ± 0.0030	0.0605 ± 0.0015	0.5023 ± 0.0424	607 ± 107	379 ± 9	92
12XL15-1-106	2.22	0.0571 ± 0.0029	0.0643 ± 0.0016	0.5064 ± 0.0443	496 ± 113	402 ± 10	97
12XL15-1-107	1.17	0.0546 ± 0.0029	0.0594 ± 0.0015	0.4473 ± 0.0397	396 ± 117	372 ± 9	99
12XL15-1-108	4.35	0.0607 ± 0.0026	0.0786 ± 0.0017	0.6579 ± 0.0471	626 ± 91	488 ± 10	95
12XL15-1-109	1.29	0.0563 ± 0.0023	0.0646 ± 0.0013	0.5017 ± 0.0339	465 ± 89	403 ± 8	98
12XL15-1-110	1.43	0.0592 ± 0.0033	0.0647 ± 0.0016	0.5281 ± 0.0495	572 ± 123	404 ± 10	94

(continued)

Table B.1 (continued)

Sample	U/Th	$^{206}Pb^*/^{207}Pb^*$	$^{206}Pb^*/^{238}U$	$^{207}Pb^*/^{235}U$	$^{206}Pb^*/^{207}Pb^* - Age$ [Ma]	$^{238}U/^{206}Pb - Age$ [Ma]	Concordance [%]
12XL15-1-111	1.48	0.0649 ± 0.0035	0.0615 ± 0.0015	0.5504 ± 0.0473	770 ± 112	385 ± 9	86
12XL15-1-112	1.19	0.0670 ± 0.0039	0.0831 ± 0.0022	0.7689 ± 0.0722	838 ± 123	515 ± 13	89
12XL15-1-113	1.27	0.0554 ± 0.0022	0.0680 ± 0.0012	0.5201 ± 0.0328	429 ± 89	424 ± 7	100
12XL15-1-114	2.52	0.0598 ± 0.0031	0.0690 ± 0.0016	0.5700 ± 0.0465	597 ± 113	430 ± 9	94
12XL15-1-115	1.61	0.0697 ± 0.0035	0.0679 ± 0.0015	0.6525 ± 0.0507	917 ± 103	424 ± 9	83
12XL15-1-116	34.32	0.1241 ± 0.0046	0.4009 ± 0.0080	6.8566 ± 0.3929	2015 ± 65	2173 ± 37	104
12XL15-1-117	0.71	0.0486 ± 0.0038	0.0676 ± 0.0020	0.4529 ± 0.0558	127 ± 184	422 ± 12	111
12XL15-1-118	2.09	0.0584 ± 0.0022	0.0803 ± 0.0014	0.6460 ± 0.0383	542 ± 82	498 ± 8	98
12XL15-1-119	2.35	0.0530 ± 0.0028	0.0644 ± 0.0014	0.4704 ± 0.0395	328 ± 120	402 ± 8	103
12XL15-1-120	2.54	0.0552 ± 0.0017	0.0820 ± 0.0012	0.6243 ± 0.0312	419 ± 70	508 ± 7	103
12XL17-1-1	2.06	0.0848 ± 0.0020	0.1837 ± 0.0020	2.1489 ± 0.0781	1311 ± 47	1087 ± 11	93
12XL17-1-2	2.18	0.0645 ± 0.0015	0.1172 ± 0.0012	1.0423 ± 0.0371	757 ± 50	715 ± 7	99
12XL17-1-3	3.01	0.0608 ± 0.0015	0.1133 ± 0.0011	0.9490 ± 0.0343	630 ± 52	692 ± 7	102
12XL17-1-4	1.70	0.0539 ± 0.0019	0.0812 ± 0.0011	0.6042 ± 0.0321	368 ± 79	503 ± 6	105
12XL17-1-5	1.57	0.0738 ± 0.0060	0.0915 ± 0.0028	0.9302 ± 0.1130	1034 ± 163	564 ± 17	84
12XL17-1-6	0.90	0.0957 ± 0.0023	0.3297 ± 0.0036	4.3500 ± 0.1616	1540 ± 46	1837 ± 17	108
12XL17-1-7	5.02	0.0626 ± 0.0015	0.1630 ± 0.0016	1.4077 ± 0.0515	693 ± 51	974 ± 9	109
12XL17-1-8	2.59	0.0733 ± 0.0017	0.2009 ± 0.0019	2.0309 ± 0.0701	1021 ± 46	1180 ± 10	105
12XL17-1-9	2.33	0.0795 ± 0.0021	0.2196 ± 0.0025	2.4069 ± 0.0949	1182 ± 51	1280 ± 13	103
12XL17-1-10	2.00	0.0570 ± 0.0015	0.0942 ± 0.0010	0.7409 ± 0.0292	491 ± 57	580 ± 6	103
12XL17-1-11	2.05	0.1093 ± 0.0024	0.3229 ± 0.0033	4.8681 ± 0.1638	1787 ± 40	1804 ± 16	100
12XL17-1-12	5.51	0.0744 ± 0.0017	0.1493 ± 0.0015	1.5320 ± 0.0543	1052 ± 47	897 ± 9	95
12XL17-1-13	2.49	0.0574 ± 0.0014	0.0844 ± 0.0009	0.6677 ± 0.0244	506 ± 52	522 ± 5	101

(continued)

Table B.1 (continued)

Sample	U/Th	$^{206}Pb^*/^{207}Pb^*$	$^{206}Pb^*/^{238}U$	$^{207}Pb^*/^{235}U$	$^{206}Pb^*/^{207}Pb^* - Age$ [Ma]	$^{238}U/^{206}Pb - Age$ [Ma]	Concordance [%]
12XL17-1-14	2.83	0.0879 ± 0.0020	0.2416 ± 0.0025	2.9288 ± 0.1019	1379 ± 44	1395 ± 13	100
12XL17-1-15	1.36	0.0569 ± 0.0014	0.0869 ± 0.0009	0.6818 ± 0.0262	486 ± 55	537 ± 5	102
12XL17-1-16	3.29	0.0944 ± 0.0020	0.2688 ± 0.0026	3.4998 ± 0.1135	1515 ± 40	1535 ± 13	101
12XL17-1-17	1.54	0.0630 ± 0.0024	0.0745 ± 0.0011	0.6466 ± 0.0373	706 ± 80	463 ± 7	91
12XL17-1-18	0.90	0.1603 ± 0.0036	0.4696 ± 0.0052	10.3779 ± 0.3593	2458 ± 38	2482 ± 23	101
12XL17-1-19	9.44	0.0574 ± 0.0017	0.1164 ± 0.0011	0.9217 ± 0.0410	507 ± 63	710 ± 7	107
12XL17-1-20	5.60	0.0647 ± 0.0015	0.1604 ± 0.0016	1.4312 ± 0.0514	764 ± 49	959 ± 9	106
12XL17-1-21	26.50	0.0834 ± 0.0021	0.1617 ± 0.0018	1.8591 ± 0.0725	1277 ± 50	966 ± 10	91
12XL17-1-22	2.82	0.0915 ± 0.0023	0.2962 ± 0.0034	3.7383 ± 0.1434	1457 ± 48	1673 ± 17	106
12XL17-1-23	5.83	0.0645 ± 0.0014	0.1187 ± 0.0011	1.0551 ± 0.0354	756 ± 46	723 ± 6	99
12XL17-1-24	8.33	0.0682 ± 0.0015	0.1550 ± 0.0015	1.4565 ± 0.0479	872 ± 45	929 ± 8	102
12XL17-1-25	2.49	0.0685 ± 0.0035	0.1748 ± 0.0022	1.6504 ± 0.1285	882 ± 104	1039 ± 12	105
12XL17-1-26	1.88	0.0728 ± 0.0019	0.1642 ± 0.0016	1.6486 ± 0.0654	1007 ± 53	980 ± 9	99
12XL17-1-27	1.48	0.0484 ± 0.0069	0.0930 ± 0.0016	0.6208 ± 0.1355	117 ± 336	573 ± 9	117
12XL17-1-28	2.18	0.0540 ± 0.0013	0.0832 ± 0.0008	0.6201 ± 0.0226	371 ± 55	515 ± 5	105
12XL17-1-29	8.86	0.0602 ± 0.0016	0.1248 ± 0.0012	1.0366 ± 0.0418	609 ± 59	758 ± 7	105
12XL17-1-30	1.50	0.0541 ± 0.0033	0.1001 ± 0.0012	0.7461 ± 0.0674	372 ± 136	615 ± 7	109
12XL17-1-31	1.40	0.0701 ± 0.0034	0.1631 ± 0.0022	1.5772 ± 0.1154	929 ± 100	974 ± 12	101
12XL17-1-32	1.48	0.0885 ± 0.0052	0.2469 ± 0.0034	3.0168 ± 0.2696	1393 ± 113	1423 ± 18	101
12XL17-1-33	4.38	0.0741 ± 0.0061	0.1814 ± 0.0029	1.8566 ± 0.2345	1044 ± 167	1075 ± 16	101
12XL17-1-34	0.87	0.0749 ± 0.0064	0.1793 ± 0.0033	1.8537 ± 0.2423	1065 ± 171	1063 ± 18	100
12XL17-1-35	4.52	0.0699 ± 0.0068	0.1627 ± 0.0028	1.5697 ± 0.2350	925 ± 199	972 ± 15	101
12XL17-1-36	3.47	0.0711 ± 0.0075	0.1623 ± 0.0031	1.5905 ± 0.2582	959 ± 215	969 ± 17	100

(continued)

Table B.1 (continued)

Sample	U/Th	$^{206}Pb^*/^{207}Pb^*$	$^{206}Pb^*/^{238}U$	$^{207}Pb^*/^{235}U$	$^{206}Pb^*/^{207}Pb^* - Age$ [Ma]	$^{238}U/^{206}Pb - Age$ [Ma]	Concordance [%]
12XL17-1-37	6.55	0.0688 ± 0.0057	0.1630 ± 0.0025	1.5460 ± 0.1993	891 ± 172	974 ± 14	103
12XL17-1-38	6.24	0.0731 ± 0.0053	0.1654 ± 0.0024	1.6683 ± 0.1854	1017 ± 146	987 ± 13	99
12XL17-1-39	2.01	0.1013 ± 0.0067	0.3127 ± 0.0049	4.3673 ± 0.4486	1647 ± 123	1754 ± 24	103
12XL17-1-40	2.30	0.0655 ± 0.0037	0.1021 ± 0.0018	0.9223 ± 0.0804	790 ± 119	627 ± 11	94
12XL17-1-41	5.22	0.0566 ± 0.0017	0.0754 ± 0.0008	0.5887 ± 0.0284	475 ± 68	469 ± 5	100
12XL17-1-42	4.72	0.0700 ± 0.0016	0.1627 ± 0.0017	1.5706 ± 0.0568	927 ± 48	972 ± 9	101
12XL17-1-43	1.31	0.0548 ± 0.0013	0.0818 ± 0.0009	0.6176 ± 0.0237	402 ± 55	507 ± 5	104
12XL17-1-44	0.85	0.0835 ± 0.0041	0.2010 ± 0.0047	2.3158 ± 0.1762	1281 ± 95	1181 ± 25	97
12XL17-1-45	2.56	0.1184 ± 0.0028	0.3511 ± 0.0040	5.7325 ± 0.2101	1931 ± 42	1940 ± 19	100
12XL17-1-46	3.17	0.0539 ± 0.0017	0.0763 ± 0.0008	0.5677 ± 0.0288	367 ± 72	474 ± 5	104
12XL17-1-47	0.67	0.1189 ± 0.0032	0.3402 ± 0.0047	5.5778 ± 0.2298	1939 ± 48	1888 ± 22	99
12XL17-1-48	1.46	0.0589 ± 0.0016	0.0933 ± 0.0011	0.7584 ± 0.0312	564 ± 59	575 ± 6	100
12XL17-1-49	0.83	0.0529 ± 0.0018	0.0816 ± 0.0011	0.5957 ± 0.0312	324 ± 78	506 ± 6	107
12XL17-1-50	2.45	0.0918 ± 0.0021	0.2691 ± 0.0027	3.4078 ± 0.1139	1463 ± 42	1536 ± 14	102
12XL17-1-51	5.01	0.0725 ± 0.0017	0.1757 ± 0.0017	1.7579 ± 0.0597	1000 ± 46	1044 ± 10	101
12XL17-1-52	3.79	0.0755 ± 0.0019	0.2258 ± 0.0023	2.3511 ± 0.0913	1081 ± 52	1312 ± 12	107
12XL17-1-53	8.21	0.0707 ± 0.0016	0.1613 ± 0.0016	1.5732 ± 0.0546	948 ± 47	964 ± 9	100
12XL17-1-54	1.53	0.0731 ± 0.0020	0.1803 ± 0.0022	1.8171 ± 0.0741	1015 ± 54	1069 ± 12	102
12XL17-1-55	2.33	0.0855 ± 0.0048	0.2587 ± 0.0039	3.0509 ± 0.2680	1327 ± 109	1483 ± 20	104
12XL17-1-56	1.18	0.0537 ± 0.0019	0.0719 ± 0.0008	0.5328 ± 0.0299	359 ± 80	448 ± 5	103
12XL17-1-57	3.14	0.0744 ± 0.0017	0.1818 ± 0.0019	1.8659 ± 0.0678	1052 ± 47	1077 ± 11	101
12XL17-1-58	1.08	0.0692 ± 0.0018	0.1515 ± 0.0018	1.4452 ± 0.0584	903 ± 54	909 ± 10	100
12XL17-1-59	2.27	0.0582 ± 0.0018	0.0953 ± 0.0012	0.7648 ± 0.0372	536 ± 69	587 ± 7	102

(continued)

Table B.1 (continued)

Sample	U/Th	$^{206}Pb^*/^{207}Pb^*$	$^{206}Pb^*/^{238}U$	$^{207}Pb^*/^{235}U$	$^{206}Pb^*/^{207}Pb^*-Age$ [Ma]	$^{238}U/^{206}Pb-Age$ [Ma]	Concordance [%]
12XL17-1-60	7.00	0.0685 ± 0.0019	0.1650 ± 0.0020	1.5578 ± 0.0661	882 ± 57	984 ± 11	103
12XL17-1-61	6.69	0.0691 ± 0.0016	0.1595 ± 0.0016	1.5197 ± 0.0526	901 ± 47	954 ± 9	102
12XL17-1-62	2.65	0.0758 ± 0.0017	0.1964 ± 0.0020	2.0515 ± 0.0701	1088 ± 45	1156 ± 11	102
12XL17-1-63	13.79	0.0546 ± 0.0015	0.0821 ± 0.0008	0.6180 ± 0.0258	394 ± 61	509 ± 5	104
12XL17-1-64	2.51	0.0834 ± 0.0024	0.2254 ± 0.0030	2.5925 ± 0.1116	1278 ± 56	1311 ± 16	101
12XL17-1-65	2.11	0.0576 ± 0.0013	0.0842 ± 0.0008	0.6691 ± 0.0220	514 ± 48	521 ± 5	100
12XL17-1-66	6.39	0.0688 ± 0.0015	0.1663 ± 0.0016	1.5779 ± 0.0526	892 ± 46	992 ± 9	103
12XL17-1-67	0.81	0.0609 ± 0.0014	0.0916 ± 0.0009	0.7685 ± 0.0257	633 ± 48	565 ± 5	98
12XL17-1-68	1.79	0.0628 ± 0.0015	0.1239 ± 0.0012	1.0737 ± 0.0378	701 ± 50	753 ± 7	102
12XL17-1-69	1.63	0.0724 ± 0.0017	0.1674 ± 0.0017	1.6718 ± 0.0590	997 ± 48	998 ± 10	100
12XL17-1-70	8.95	0.0690 ± 0.0015	0.1616 ± 0.0016	1.5382 ± 0.0508	898 ± 46	966 ± 9	102
12XL17-1-71	3.02	0.0911 ± 0.0023	0.2436 ± 0.0028	3.0597 ± 0.1170	1449 ± 49	1405 ± 15	99
12XL17-1-72	1.95	0.0619 ± 0.0027	0.0843 ± 0.0014	0.7189 ± 0.0467	670 ± 92	522 ± 8	95
12XL17-1-73	2.72	0.0602 ± 0.0014	0.1222 ± 0.0012	1.0146 ± 0.0353	611 ± 50	743 ± 7	105
12XL17-1-74	0.84	0.0969 ± 0.0024	0.2799 ± 0.0031	3.7369 ± 0.1399	1564 ± 46	1591 ± 15	101
12XL17-1-75	2.58	0.0819 ± 0.0022	0.2403 ± 0.0029	2.7125 ± 0.1127	1241 ± 54	1388 ± 15	104
12XL17-1-76	6.59	0.0512 ± 0.0012	0.0837 ± 0.0008	0.5904 ± 0.0219	247 ± 56	518 ± 5	110
12XL17-1-77	1.56	0.1006 ± 0.0025	0.3291 ± 0.0036	4.5674 ± 0.1717	1635 ± 46	1834 ± 17	105
12XL17-1-78	4.98	0.0571 ± 0.0014	0.1215 ± 0.0012	0.9566 ± 0.0357	493 ± 54	739 ± 7	108
12XL17-1-79	3.20	0.0764 ± 0.0019	0.2265 ± 0.0024	2.3861 ± 0.0911	1104 ± 50	1316 ± 13	106
12XL17-1-80	5.40	0.0931 ± 0.0027	0.2884 ± 0.0037	3.7052 ± 0.1612	1490 ± 54	1634 ± 19	104
12XL17-1-81	3.00	0.0505 ± 0.0013	0.0836 ± 0.0009	0.5828 ± 0.0223	218 ± 58	518 ± 5	111
12XL17-1-82	1.86	0.0567 ± 0.0025	0.0970 ± 0.0011	0.7581 ± 0.0511	477 ± 96	597 ± 6	104

(continued)

Table B.1 (continued)

Sample	U/Th	$^{206}Pb^*/^{207}Pb^*$	$^{206}Pb^*/^{238}U$	$^{207}Pb^*/^{235}U$	$^{206}Pb^*/^{207}Pb^* - Age$ [Ma]	$^{238}U/^{206}Pb - Age$ [Ma]	Concordance [%]
12XL17-1-83	1.33	0.0397 ± 0.0085	0.0725 ± 0.0016	0.3971 ± 0.1336	NaN ± 0	451 ± 10	133
12XL17-1-84	2.68	0.0633 ± 0.0017	0.1564 ± 0.0016	1.3659 ± 0.0573	718 ± 58	937 ± 9	107
12XL17-1-85	3.64	0.0651 ± 0.0018	0.1578 ± 0.0016	1.4178 ± 0.0621	778 ± 59	945 ± 9	105
12XL17-1-86	1.75	0.0550 ± 0.0027	0.0753 ± 0.0009	0.5712 ± 0.0443	411 ± 111	468 ± 5	102
12XL17-1-87	2.07	0.0673 ± 0.0016	0.1473 ± 0.0015	1.3669 ± 0.0484	845 ± 48	886 ± 8	101
12XL17-1-88	16.19	0.0705 ± 0.0016	0.1548 ± 0.0015	1.5053 ± 0.0530	943 ± 47	928 ± 8	99
12XL17-1-89	4.46	0.0613 ± 0.0016	0.1220 ± 0.0012	1.0312 ± 0.0422	648 ± 57	742 ± 7	103
12XL17-1-90	2.44	0.0817 ± 0.0020	0.2078 ± 0.0023	2.3398 ± 0.0871	1236 ± 48	1217 ± 12	99
12XL17-1-91	4.62	0.0706 ± 0.0016	0.1607 ± 0.0016	1.5640 ± 0.0547	944 ± 47	961 ± 9	100
12XL17-1-92	9.04	0.0662 ± 0.0018	0.1122 ± 0.0013	1.0240 ± 0.0412	810 ± 55	686 ± 7	96
12XL17-1-93	0.94	0.1113 ± 0.0029	0.3369 ± 0.0042	5.1695 ± 0.2022	1820 ± 47	1872 ± 20	101
12XL17-1-94	0.73	0.1072 ± 0.0027	0.3507 ± 0.0043	5.1853 ± 0.2001	1752 ± 46	1938 ± 20	105
12XL17-1-95	1.95	0.0871 ± 0.0024	0.2252 ± 0.0028	2.7041 ± 0.1114	1361 ± 52	1310 ± 15	98
12XL17-1-96	2.08	0.0603 ± 0.0014	0.1162 ± 0.0011	0.9665 ± 0.0349	614 ± 51	709 ± 6	103
12XL17-1-97	2.09	0.0598 ± 0.0017	0.0830 ± 0.0010	0.6849 ± 0.0299	596 ± 62	514 ± 6	97
12XL17-1-98	2.88	0.0566 ± 0.0016	0.0826 ± 0.0010	0.6446 ± 0.0276	474 ± 62	512 ± 6	101
12XL17-1-99	2.60	0.0793 ± 0.0020	0.1186 ± 0.0013	1.2973 ± 0.0488	1180 ± 49	722 ± 7	86
12XL17-1-100	1.89	0.0575 ± 0.0019	0.0819 ± 0.0011	0.6493 ± 0.0325	509 ± 72	507 ± 6	100
12XL17-1-101	5.68	0.0684 ± 0.0018	0.1776 ± 0.0020	1.6763 ± 0.0653	880 ± 53	1054 ± 11	105
12XL17-1-102	1.62	0.0528 ± 0.0017	0.0925 ± 0.0010	0.6735 ± 0.0331	320 ± 73	570 ± 6	109
12XL17-1-103	2.46	0.0855 ± 0.0027	0.2439 ± 0.0027	2.8753 ± 0.1381	1325 ± 61	1407 ± 14	102
12XL17-1-104	21.24	0.0698 ± 0.0017	0.1615 ± 0.0017	1.5559 ± 0.0558	922 ± 49	965 ± 9	101
12XL17-1-105	2.67	0.0667 ± 0.0017	0.1618 ± 0.0018	1.4899 ± 0.0576	829 ± 54	967 ± 10	104

(continued)

Table B.1 (continued)

Sample	U/Th	$^{206}Pb^*/^{207}Pb^*$	$^{206}Pb^*/^{238}U$	$^{207}Pb^*/^{235}U$	$^{206}Pb^*/^{207}Pb^*-Age$ [Ma]	$^{238}U/^{206}Pb-Age$ [Ma]	Concordance [%]
12XL17-1-106	2.18	0.1025 ± 0.0025	0.3050 ± 0.0033	4.3128 ± 0.1535	1669 ± 44	1716 ± 16	101
12XL17-1-107	1.44	0.1114 ± 0.0027	0.3551 ± 0.0040	5.4600 ± 0.1979	1822 ± 44	1959 ± 19	103
12XL17-1-108	2.98	0.1071 ± 0.0024	0.3069 ± 0.0031	4.5362 ± 0.1510	1749 ± 41	1726 ± 15	99
12XL17-1-109	4.17	0.0576 ± 0.0016	0.0875 ± 0.0009	0.6960 ± 0.0287	514 ± 59	541 ± 5	101
12XL17-1-110	2.83	0.0951 ± 0.0023	0.2608 ± 0.0030	3.4214 ± 0.1265	1529 ± 46	1494 ± 15	99

Appendix C
Zircon Hf Data

The data tables on the following pages comprise the results of all single zircon grain Hf isotope analyses after data reduction. All analyses were performed during the four-year Ph.D. study period at the Department of Earth Sciences of The University of Hong Kong. Uncertainties are given at a 1σ level. Table columns correspond to laser-ablation spots, $^{176}Hf/^{177}Hf$ ratios and their uncertainties, $^{176}Lu/^{177}Hf$ ratios and their uncertainties, $^{176}Yb/^{177}Hf$ ratios and their uncertainties, zircon age and ϵHf(t) values. For detailed methodological procedures please refer to Sect. 3.3 of this dissertation (Table C.1).

Table C.1 Zircon Hf data

Sample	$^{176}Hf/^{177}Hf$	$^{176}Lu/^{177}Hf$	$^{176}Yb/^{177}Hf$	Age [Ma]	ϵ_{Hf}
11XL42-1-1	0.28284 ± 0.00003	0.00166 ± 0.00004	0.001517 ± 0.000027	329 ± 7	9.3 ± 0.50
11XL42-1-4	0.28286 ± 0.00003	0.0011 ± 0.00003	0.001007 ± 0.00002	370 ± 7	10.9 ± 0.50
11XL42-1-12	0.28243 ± 0.00003	0.00103 ± 0.00003	0.000945 ± 0.00002	498 ± 5	−1.6 ± 0.50
11XL42-1-13	0.28277 ± 0.00004	0.00193 ± 0.00003	0.001769 ± 0.000014	358 ± 6	7.3 ± 0.60
11XL42-1-14	0.28274 ± 0.00005	0.0016 ± 0.00003	0.001467 ± 0.000014	352 ± 5	6.2 ± 0.70
11XL42-1-19	0.28271 ± 0.00005	0.00167 ± 0.00003	0.001535 ± 0.000012	352 ± 6	5.2 ± 0.70
11XL42-1-23	0.28272 ± 0.00004	0.00188 ± 0.00005	0.001733 ± 0.000048	314 ± 4	4.7 ± 0.60
11XL42-1-24	0.28293 ± 0.00004	0.00147 ± 0.00003	0.001356 ± 0.000025	342 ± 4	12.6 ± 0.60
11XL42-1-25	0.28289 ± 0.00004	0.00113 ± 0.00003	0.00104 ± 0.000013	330 ± 5	11.2 ± 0.60
11XL42-1-26	0.28292 ± 0.00004	0.00136 ± 0.00003	0.001258 ± 0.000019	331 ± 7	12.4 ± 0.60
11XL42-1-27	0.28271 ± 0.00007	0.0021 ± 0.00006	0.001947 ± 0.00006	359 ± 5	5.3 ± 1.00
11XL42-1-28	0.28275 ± 0.00004	0.00121 ± 0.00004	0.001123 ± 0.000027	338 ± 5	6.4 ± 0.60
11XL42-1-29	0.28263 ± 0.00006	0.0017 ± 0.00003	0.001582 ± 0.000013	321 ± 6	1.5 ± 0.90
11XL42-1-32	0.28266 ± 0.00004	0.00214 ± 0.00003	0.001992 ± 0.000024	370 ± 4	3.8 ± 0.60
11XL42-1-34	0.28277 ± 0.00003	0.00177 ± 0.00007	0.001649 ± 0.000062	306 ± 5	6.3 ± 0.50
11XL42-1-41	0.28274 ± 0.00004	0.00164 ± 0.00003	0.001533 ± 0.000011	318 ± 4	5.6 ± 0.70
11XL42-1-44	0.28278 ± 0.00003	0.00134 ± 0.00003	0.001257 ± 0.000012	305 ± 5	6.8 ± 0.50
11XL42-1-45	0.28279 ± 0.00003	0.00168 ± 0.00005	0.001572 ± 0.000047	312 ± 4	7.1 ± 0.50

(continued)

P. R. Eizenhöfer, *Subduction and Closure of the Palaeo-Asian Ocean along the Solonker Suture Zone: Constraints from an Integrated Sedimentary Provenance Analysis*, Springer Theses, https://doi.org/10.1007/978-981-32-9200-0

Table C.1 (continued)

Sample	$^{176}Hf/^{177}Hf$	$^{176}Lu/^{177}Hf$	$^{176}Yb/^{177}Hf$	Age [Ma]	ϵ_{Hf}
11XL42-1-48	0.28289 ± 0.00007	0.00145 ± 0.00003	0.001362 ± 0.000017	308 ± 6	10.5 ± 1.00
11XL42-1-49	0.28271 ± 0.00004	0.00128 ± 0.00003	0.001197 ± 0.000019	354 ± 4	5.3 ± 0.60
11XL42-1-53	0.28278 ± 0.00004	0.00208 ± 0.00006	0.001957 ± 0.000061	342 ± 3	7.4 ± 0.60
11XL42-1-56	0.28278 ± 0.00003	0.00173 ± 0.00004	0.001619 ± 0.000029	350 ± 4	7.4 ± 0.50
11XL42-1-57	0.28278 ± 0.00003	0.002 ± 0.00006	0.001869 ± 0.000062	336 ± 6	7.1 ± 0.40
11XL42-1-59	0.28273 ± 0.00004	0.00233 ± 0.00003	0.002169 ± 0.000021	334 ± 7	5.3 ± 0.60
11XL42-1-64	0.28267 ± 0.00004	0.00209 ± 0.00007	0.001944 ± 0.000067	342 ± 7	3.4 ± 0.60
11XL42-1-68	0.28277 ± 0.00004	0.00123 ± 0.00002	0.00114 ± 0.00001	347 ± 7	7.4 ± 0.60
11XL42-1-73	0.28281 ± 0.00004	0.00135 ± 0.00003	0.001248 ± 0.000023	339 ± 6	8.5 ± 0.60
11XL42-1-74	0.28281 ± 0.00003	0.00168 ± 0.00002	0.00155 ± 0.00001	331 ± 5	8.1 ± 0.40
11XL42-1-76	0.28285 ± 0.00005	0.00156 ± 0.00004	0.001429 ± 0.000039	366 ± 5	10.3 ± 0.70
11XL42-1-77	0.28258 ± 0.00006	0.00255 ± 0.00003	0.002338 ± 0.000016	324 ± 7	0 ± 0.90
11XL45-1-8	0.28216 ± 0.00004	0.0004 ± 0.00003	0.000356 ± 0.000015	870 ± 14	−2.8 ± 0.60
11XL45-1-13	0.28201 ± 0.00003	0.00111 ± 0.00003	0.00101 ± 0.000025	1306 ± 24	1 ± 0.50
11XL45-1-18	0.2822 ± 0.00003	0.00086 ± 0.00002	0.000787 ± 0.000007	415 ± 7	−11.4 ± 0.50
11XL45-1-19	0.28135 ± 0.00003	0.00073 ± 0.00003	0.00068 ± 0.000017	2444 ± 34	3.2 ± 0.40
11XL45-1-20	0.28211 ± 0.00004	0.00146 ± 0.00003	0.001371 ± 0.000021	1439 ± 17	7.2 ± 0.50
11XL45-1-21	0.28211 ± 0.00003	0.001 ± 0.00003	0.000949 ± 0.000026	423 ± 8	−14.3 ± 0.50
11XL45-1-25	0.28227 ± 0.00011	0.00052 ± 0.00002	0.000495 ± 0.000007	424 ± 6	−8.5 ± 1.60
11XL45-1-32	0.28216 ± 0.00006	0.00073 ± 0.00003	0.000709 ± 0.000014	429 ± 5	−12.6 ± 0.80
11XL45-1-33	0.28123 ± 0.00005	0.00115 ± 0.00008	0.001125 ± 0.000079	2654 ± 38	2.9 ± 0.70
11XL45-1-34	0.28202 ± 0.00006	0.00196 ± 0.00004	0.001937 ± 0.000031	839 ± 11	−9 ± 0.90
11XL45-1-38	0.28215 ± 0.00004	0.00139 ± 0.00002	0.001404 ± 0.000007	917 ± 10	−2.4 ± 0.60
11XL45-1-39	0.28226 ± 0.00004	0.00083 ± 0.00003	0.000835 ± 0.000017	461 ± 4	−8.2 ± 0.60
11XL45-1-42	0.28243 ± 0.00006	0.00077 ± 0.00003	0.000765 ± 0.000021	455 ± 5	−2.4 ± 0.90
11XL45-1-44	0.28214 ± 0.00004	0.00032 ± 0.00003	0.000316 ± 0.000025	831 ± 11	−4.1 ± 0.60
11XL45-1-45	0.28166 ± 0.00012	0.00128 ± 0.00003	0.001261 ± 0.000015	817 ± 14	−21.9 ± 1.70
11XL45-1-46	0.28027 ± 0.00004	0.0003 ± 0.00002	0.000297 ± 0.000004	407 ± 7	−79.7 ± 0.50
11XL45-1-52	0.28246 ± 0.00003	0.00003 ± 0.00002	0.000031 ± 0.000002	455 ± 7	−0.9 ± 0.50
11XL45-1-55	0.28213 ± 0.00005	0.0009 ± 0.00003	0.00086 ± 0.000017	602 ± 11	−9.8 ± 0.80
11XL45-1-58	0.28189 ± 0.00004	0.00054 ± 0.00002	0.000515 ± 0.000002	885 ± 10	−11.9 ± 0.60
11XL45-1-60	0.28261 ± 0.00004	0.00117 ± 0.00003	0.001101 ± 0.00002	388 ± 7	2.4 ± 0.60
11XL45-1-61	0.28233 ± 0.00005	0.00217 ± 0.00004	0.002024 ± 0.000029	387 ± 5	−7.6 ± 0.80
11XL45-1-63	0.28236 ± 0.00004	0.00093 ± 0.00004	0.000871 ± 0.000023	406 ± 8	−5.7 ± 0.50
11XL45-1-68	0.28273 ± 0.00003	0.00057 ± 0.00004	0.000544 ± 0.000021	825 ± 14	16.4 ± 0.50
11XL45-1-70	0.28071 ± 0.00004	0.00078 ± 0.00003	0.000745 ± 0.000014	3242 ± 51	−1.3 ± 0.60
11XL45-1-72	0.28201 ± 0.00004	0.00031 ± 0.00003	0.000295 ± 0.000014	413 ± 7	−18 ± 0.50
11XL45-1-75	0.28234 ± 0.00003	0.0008 ± 0.00003	0.000782 ± 0.000011	809 ± 15	2.1 ± 0.50
11XL45-1-76	0.28245 ± 0.00022	0.00067 ± 0.00003	0.000658 ± 0.000017	461 ± 8	−1.6 ± 3.10
11XL45-1-78	0.28231 ± 0.00003	0.00102 ± 0.00003	0.001007 ± 0.000023	428 ± 8	−7.1 ± 0.50
11XL45-1-79	0.28209 ± 0.00005	0.00051 ± 0.00003	0.000513 ± 0.000021	848 ± 14	−5.7 ± 0.80
11XL45-1-81	0.28232 ± 0.00003	0.00064 ± 0.00003	0.000641 ± 0.000012	407 ± 7	−7.2 ± 0.40
11XL41-2-6	0.28224 ± 0.00005	0.00059 ± 0.00004	0.000598 ± 0.000033	453 ± 7	−8.9 ± 0.70
11XL41-2-21	0.28258 ± 0.00009	0.00122 ± 0.00003	0.001231 ± 0.000023	338 ± 5	0.4 ± 1.20
11XL41-2-23	0.28245 ± 0.00003	0.00029 ± 0.00003	0.000289 ± 0.000007	425 ± 8	−2.2 ± 0.50
11XL41-2-24	0.28276 ± 0.00003	0.00096 ± 0.00003	0.000954 ± 0.000024	335 ± 5	6.8 ± 0.50

(continued)

Table C.1 (continued)

Sample	$^{176}Hf/^{177}Hf$	$^{176}Lu/^{177}Hf$	$^{176}Yb/^{177}Hf$	Age [Ma]	ϵ_{Hf}
11XL41-2-28	0.28255 ± 0.00004	0.00067 ± 0.00003	0.000657 ± 0.000017	410 ± 7	1 ± 0.50
11XL41-2-27	0.28229 ± 0.00004	0.00073 ± 0.00003	0.000715 ± 0.000008	458 ± 8	−7.3 ± 0.60
11XL41-2-30	0.2818 ± 0.00003	0.0005 ± 0.00003	0.000485 ± 0.000008	1533 ± 18	−0.9 ± 0.50
11XL41-2-32	0.28273 ± 0.00004	0.00068 ± 0.00003	0.000654 ± 0.000006	327 ± 5	5.7 ± 0.70
11XL41-2-35	0.28265 ± 0.00006	0.00072 ± 0.00004	0.000683 ± 0.000019	422 ± 5	4.8 ± 0.80
11XL41-2-40	0.28224 ± 0.00004	0.00071 ± 0.00003	0.000665 ± 0.000007	437 ± 6	−9.4 ± 0.60
11XL41-2-41	0.28286 ± 0.00003	0.00121 ± 0.00004	0.001115 ± 0.000025	358 ± 4	10.5 ± 0.50
11XL41-2-42	0.28281 ± 0.00003	0.00062 ± 0.00003	0.000572 ± 0.000002	340 ± 4	8.8 ± 0.50
11XL41-2-43	0.28248 ± 0.00006	0.00096 ± 0.00003	0.000878 ± 0.000009	322 ± 4	−3.5 ± 0.90
11XL41-2-44	0.28266 ± 0.00004	0.00104 ± 0.00003	0.000958 ± 0.000015	322 ± 5	3.1 ± 0.60
11XL41-2-45	0.28274 ± 0.00004	0.00068 ± 0.00003	0.000627 ± 0.000007	328 ± 5	6 ± 0.60
11XL41-2-47	0.28271 ± 0.00004	0.00088 ± 0.00003	0.00081 ± 0.00001	306 ± 4	4.5 ± 0.60
11XL41-2-48	0.28269 ± 0.00003	0.00072 ± 0.00003	0.000658 ± 0.00001	318 ± 5	4 ± 0.50
11XL41-2-55	0.28192 ± 0.00003	0.00017 ± 0.00003	0.000155 ± 0.000001	846 ± 18	−11.6 ± 0.50
11XL41-2-59	0.28229 ± 0.00003	0.00005 ± 0.00003	0.000048 ± 0.000001	1884 ± 11	25.1 ± 0.50
11XL41-2-60	0.28236 ± 0.00004	0.00082 ± 0.00003	0.000748 ± 0.000005	437 ± 11	−5.3 ± 0.70
11XL41-2-62	0.28221 ± 0.00003	0.00124 ± 0.00007	0.001147 ± 0.000067	316 ± 19	−13.4 ± 0.50
11XL41-2-66	0.28251 ± 0.00003	0.00049 ± 0.00002	0.000465 ± 0.000004	421 ± 8	0 ± 0.50
11XL41-2-67	0.28271 ± 0.00003	0.00069 ± 0.00002	0.000661 ± 0.000006	329 ± 6	4.8 ± 0.50
11XL41-2-69	0.28228 ± 0.00015	0.00099 ± 0.00002	0.000964 ± 0.000011	340 ± 5	−10.3 ± 2.10
11XL41-2-71	0.28274 ± 0.00003	0.00054 ± 0.00002	0.000536 ± 0.000003	329 ± 5	6 ± 0.40
11XL41-2-73	0.28276 ± 0.00004	0.00097 ± 0.00003	0.000974 ± 0.000019	335 ± 5	6.6 ± 0.60
11XL41-2-74	0.2828 ± 0.00002	0.00135 ± 0.00006	0.001373 ± 0.000058	358 ± 4	8.5 ± 0.40
11XL41-2-79	0.28226 ± 0.00002	0.00089 ± 0.00002	0.000916 ± 0.000006	442 ± 5	−8.8 ± 0.4
11XL41-2-80	0.28232 ± 0.00003	0.00139 ± 0.00005	0.001447 ± 0.000047	432 ± 6	−6.7 ± 0.5
11XL41-2-81	0.28285 ± 0.00003	0.0014 ± 0.00003	0.001482 ± 0.000026	338 ± 4	9.9 ± 0.5
11XL37-1-2	0.28084 ± 0.00104	0.00221 ± 0.00015	0.002388 ± 0.000149	356 ± 5	−61 ± 14.5
11XL37-1-3	0.28239 ± 0.00004	0.00102 ± 0.00005	0.001087 ± 0.000044	409 ± 5	−4.7 ± 0.6
11XL37-1-7	0.28218 ± 0.00004	0.00098 ± 0.00003	0.001026 ± 0.000018	1500 ± 10	11.4 ± 0.7
11XL37-1-9	0.28231 ± 0.00002	0.00057 ± 0.00002	0.000595 ± 0.000004	990 ± 11	5.3 ± 0.4
11XL37-1-12	0.28226 ± 0.00004	0.00118 ± 0.00004	0.001204 ± 0.000036	462 ± 7	−8.3 ± 0.6
11XL37-1-21	0.28256 ± 0.00003	0.00081 ± 0.00003	0.000813 ± 0.000019	394 ± 4	0.8 ± 0.5
11XL37-1-25	0.28239 ± 0.00012	0.00079 ± 0.00002	0.000781 ± 0.000013	356 ± 5	−5.9 ± 1.7
11XL37-1-30	0.2822 ± 0.00003	0.00163 ± 0.00003	0.001581 ± 0.000023	1276 ± 19	6.7 ± 0.4
11XL37-1-32	0.28264 ± 0.00004	0.00171 ± 0.00007	0.001634 ± 0.000063	373 ± 5	3.1 ± 0.6
11XL37-1-34	0.28239 ± 0.00006	0.00328 ± 0.00004	0.003076 ± 0.000038	402 ± 3	−5.6 ± 1
11XL37-1-36	0.28238 ± 0.00004	0.00131 ± 0.00003	0.001171 ± 0.000019	411 ± 6	−5.2 ± 0.6
11XL37-1-37	0.28255 ± 0.00006	0.00189 ± 0.00003	0.001689 ± 0.000024	392 ± 4	0.1 ± 0.9
11XL37-1-38	0.28202 ± 0.00004	0.00098 ± 0.00002	0.000876 ± 0.000004	1413 ± 15	3.8 ± 0.5
11XL37-1-39	0.28123 ± 0.00003	0.00199 ± 0.00003	0.001791 ± 0.00001	2420 ± 28	−3.7 ± 0.5
11XL37-1-42	0.28268 ± 0.00025	0.00131 ± 0.00005	0.001186 ± 0.000041	366 ± 5	4.5 ± 3.6
11XL37-1-44	0.28208 ± 0.00004	0.00058 ± 0.00003	0.000526 ± 0.000007	1417 ± 25	6.4 ± 0.6
11XL37-1-48	0.28229 ± 0.00005	0.00036 ± 0.00004	0.000328 ± 0.000035	373 ± 7	−8.8 ± 0.7
11XL37-1-50	0.28244 ± 0.00004	0.00098 ± 0.00003	0.000889 ± 0.000013	367 ± 8	−4.1 ± 0.5
11XL37-1-51	0.28232 ± 0.00005	0.00116 ± 0.00006	0.001061 ± 0.000049	462 ± 8	−6.3 ± 0.7
11XL37-1-55	0.28254 ± 0.00004	0.00045 ± 0.00003	0.000412 ± 0.000002	402 ± 7	0.5 ± 0.6

(continued)

Table C.1 (continued)

Sample	$^{176}Hf/^{177}Hf$	$^{176}Lu/^{177}Hf$	$^{176}Yb/^{177}Hf$	Age [Ma]	ϵ_{Hf}
11XL37-1-56	0.28177 ± 0.00004	0.00143 ± 0.00011	0.001318 ± 0.000111	1844 ± 31	4.1 ± 0.6
11XL37-1-57	0.28235 ± 0.00007	0.00177 ± 0.00021	0.001632 ± 0.00021	376 ± 7	−7.3 ± 1
11XL37-1-59	0.28222 ± 0.00004	0.00102 ± 0.00002	0.000945 ± 0.000012	444 ± 11	−10.1 ± 0.6
11XL37-1-61	0.28228 ± 0.00009	0.00093 ± 0.00004	0.000862 ± 0.00004	352 ± 8	−10 ± 1.3
11XL37-1-63	0.28226 ± 0.00006	0.00106 ± 0.00005	0.000986 ± 0.000042	438 ± 8	−8.7 ± 0.8
11XL37-1-67	0.28238 ± 0.00003	0.0017 ± 0.00007	0.001577 ± 0.000066	392 ± 7	−5.6 ± 0.5
11XL37-1-68	0.28249 ± 0.00003	0.00066 ± 0.00002	0.000611 ± 0.000004	364 ± 6	−2.1 ± 0.5
11XL37-1-69	0.2826 ± 0.00004	0.00249 ± 0.00012	0.002307 ± 0.000114	439 ± 7	2.7 ± 0.6
11XL37-1-72	0.28224 ± 0.00003	0.00138 ± 0.00002	0.001284 ± 0.000007	912 ± 12	0.4 ± 0.4
11XL37-1-76	0.28224 ± 0.00003	0.0008 ± 0.00003	0.000746 ± 0.000012	435 ± 5	−9.6 ± 0.5
11XL29-1-9	0.28283 ± 0.00004	0.00131 ± 0.00006	0.001347 ± 0.000049	321 ± 5	8.8 ± 0.6
11XL29-1-11	0.28297 ± 0.00005	0.00094 ± 0.00005	0.000968 ± 0.000036	359 ± 5	14.8 ± 0.7
11XL29-1-16	0.28303 ± 0.00005	0.00189 ± 0.00007	0.001938 ± 0.000067	341 ± 8	16.1 ± 0.7
11XL29-1-18	0.28273 ± 0.00006	0.00094 ± 0.00004	0.000969 ± 0.000028	325 ± 5	5.4 ± 0.9
11XL29-1-19	0.28254 ± 0.00004	0.00075 ± 0.00003	0.000771 ± 0.00001	806 ± 10	9.1 ± 0.6
11XL29-1-22	0.28234 ± 0.00004	0.00061 ± 0.00004	0.00063 ± 0.000029	521 ± 7	−3.9 ± 0.6
11XL29-1-26	0.28259 ± 0.00004	0.00174 ± 0.00004	0.001787 ± 0.000022	495 ± 5	3.8 ± 0.6
11XL29-1-28	0.28295 ± 0.00005	0.00236 ± 0.00009	0.002425 ± 0.000086	338 ± 5	13.4 ± 0.7
11XL29-1-32	0.28238 ± 0.00004	0.00096 ± 0.00004	0.00098 ± 0.000016	466 ± 7	−3.8 ± 0.6
11XL29-1-33	0.28178 ± 0.00031	0.00181 ± 0.00011	0.001853 ± 0.000101	397 ± 4	−27 ± 4.4
11XL29-1-36	0.28232 ± 0.00005	0.00138 ± 0.00004	0.00141 ± 0.000015	352 ± 5	−8.6 ± 0.8
11XL29-1-39	0.28256 ± 0.00005	0.00248 ± 0.00014	0.002543 ± 0.000137	325 ± 3	−0.8 ± 0.8
11XL29-1-40	0.28288 ± 0.00004	0.00122 ± 0.00006	0.001251 ± 0.000053	328 ± 3	10.6 ± 0.6
11XL29-1-41	0.28279 ± 0.00004	0.00139 ± 0.00004	0.001425 ± 0.000024	336 ± 4	7.7 ± 0.6
11XL29-1-42	0.28281 ± 0.00004	0.00091 ± 0.00004	0.000935 ± 0.000003	331 ± 5	8.3 ± 0.7
11XL29-1-43	0.2827 ± 0.00008	0.00144 ± 0.00004	0.001474 ± 0.000014	359 ± 4	4.9 ± 1.2
11XL29-1-44	0.28202 ± 0.00005	0.00072 ± 0.00004	0.000737 ± 0.000008	1031 ± 12	−4.2 ± 0.7
11XL29-1-45	0.28282 ± 0.00004	0.00114 ± 0.00004	0.001163 ± 0.000019	321 ± 5	8.4 ± 0.6
11XL29-1-47	0.28278 ± 0.00005	0.00133 ± 0.00005	0.001362 ± 0.000034	406 ± 8	8.8 ± 0.7
11XL29-1-52	0.28288 ± 0.00008	0.00316 ± 0.00006	0.003223 ± 0.000055	394 ± 4	11.5 ± 1.2
11XL51-1-5	0.28227 ± 0.00005	0.00051 ± 0.00002	0.000559 ± 0.000006	439 ± 3	−8.2 ± 0.8
11XL51-1-7	0.28251 ± 0.00003	0.00053 ± 0.00003	0.000582 ± 0.000015	436 ± 3	0.1 ± 0.4
11XL51-1-13	0.28256 ± 0.00005	0.00039 ± 0.00002	0.000424 ± 0.00001	431 ± 3	1.9 ± 0.7
11XL51-1-16	0.28255 ± 0.00003	0.00053 ± 0.00002	0.000578 ± 0.000008	454 ± 4	1.9 ± 0.4
11XL51-1-18	0.28227 ± 0.00003	0.00077 ± 0.00002	0.000825 ± 0.00001	455 ± 3	−7.9 ± 0.5
11XL51-1-20	0.28259 ± 0.00004	0.00045 ± 0.00002	0.000485 ± 0.000006	461 ± 3	3.7 ± 0.5
11XL51-1-23	0.28261 ± 0.00003	0.00054 ± 0.00002	0.000571 ± 0.000007	447 ± 4	4 ± 0.4
11XL51-1-25	0.28255 ± 0.00005	0.00159 ± 0.00003	0.001683 ± 0.000014	280 ± 3	−1.9 ± 0.7
11XL51-1-28	0.2825 ± 0.00003	0.00135 ± 0.00004	0.001415 ± 0.000033	300 ± 2	−3.2 ± 0.5
11XL51-1-29	0.2826 ± 0.00003	0.00036 ± 0.00002	0.000374 ± 0.000008	463 ± 5	3.9 ± 0.5
11XL51-1-30	0.28268 ± 0.00003	0.00114 ± 0.00003	0.001159 ± 0.000021	297 ± 2	2.9 ± 0.5
11XL51-1-31	0.28261 ± 0.00004	0.00098 ± 0.00003	0.000984 ± 0.000019	450 ± 3	4 ± 0.6
11XL51-1-33	0.28253 ± 0.00003	0.00092 ± 0.00002	0.000919 ± 0.000005	286 ± 3	−2.6 ± 0.5
11XL51-1-34	0.28261 ± 0.00004	0.00226 ± 0.00005	0.002245 ± 0.000046	269 ± 2	−0.4 ± 0.6
11XL51-1-35	0.28263 ± 0.00003	0.00081 ± 0.00002	0.000794 ± 0.000005	309 ± 3	1.5 ± 0.5
11XL51-1-36	0.28252 ± 0.00003	0.00101 ± 0.00003	0.000982 ± 0.000017	269 ± 2	−3.3 ± 0.5

(continued)

Table C.1 (continued)

Sample	^{176}Hf/^{177}Hf	^{176}Lu/^{177}Hf	^{176}Yb/^{177}Hf	Age [Ma]	ϵ_{Hf}
11XL51-1-38	0.28165 ± 0.00003	0.00026 ± 0.00002	0.000248 ± 0.000002	1833 ± 17	1 ± 0.5
11XL51-1-40	0.28253 ± 0.00003	0.00088 ± 0.00002	0.000845 ± 0.000006	278 ± 2	−2.6 ± 0.5
11XL51-1-46	0.28263 ± 0.00004	0.00069 ± 0.00002	0.000657 ± 0.000001	461 ± 4	5 ± 0.6
11XL51-1-48	0.28279 ± 0.00003	0.00112 ± 0.00003	0.001059 ± 0.000021	449 ± 4	10.1 ± 0.5
11XL51-1-50	0.28261 ± 0.00002	0.00067 ± 0.00002	0.000613 ± 0.000016	427 ± 4	3.6 ± 0.4
11XL51-1-66	0.28256 ± 0.00003	0.00059 ± 0.00002	0.000546 ± 0.000002	477 ± 3	2.9 ± 0.4
11XL51-1-71	0.28264 ± 0.00002	0.00133 ± 0.00005	0.00122 ± 0.000042	274 ± 2	1 ± 0.4
11XL51-1-72	0.28268 ± 0.00003	0.0009 ± 0.00003	0.000827 ± 0.000028	424 ± 3	5.7 ± 0.4
11XL51-1-73	0.28274 ± 0.00003	0.00154 ± 0.00002	0.00141 ± 0.000012	452 ± 5	8.4 ± 0.5
11XL51-1-75	0.28254 ± 0.00003	0.00199 ± 0.00007	0.001824 ± 0.000072	285 ± 2	−2.2 ± 0.4
11XL51-1-78	0.28259 ± 0.00004	0.00118 ± 0.00004	0.001082 ± 0.00003	438 ± 5	3 ± 0.5
11XL51-1-79	0.28261 ± 0.00003	0.00061 ± 0.00002	0.000559 ± 0.000006	454 ± 5	4 ± 0.5
11XL51-1-85	0.28258 ± 0.00003	0.00127 ± 0.00004	0.001165 ± 0.000038	450 ± 4	2.9 ± 0.5
11XL27-1	0.27816 ± 0.00175	0.00106 ± 0.00003	0.001068 ± 0.000013	278 ± 2	−157.3 ± 24.5
11XL27-2	0.28266 ± 0.00004	0.0007 ± 0.00004	0.000711 ± 0.000021	279 ± 2	2.1 ± 0.6
11XL27-4	0.28236 ± 0.00007	0.00133 ± 0.00003	0.001344 ± 0.000018	308 ± 3	−8.2 ± 1
11XL27-6	0.28216 ± 0.00004	0.00064 ± 0.00003	0.000646 ± 0.000005	402 ± 3	−12.9 ± 0.6
11XL27-7	0.28253 ± 0.00004	0.00068 ± 0.00003	0.000692 ± 0.000015	308 ± 4	−2 ± 0.7
11XL27-10	0.28229 ± 0.00014	0.00102 ± 0.00003	0.00104 ± 0.000015	259 ± 2	−11.5 ± 2
11XL27-14	0.28209 ± 0.0001	0.00059 ± 0.00004	0.000607 ± 0.000025	423 ± 3	−15 ± 1.4
11XL27-15	0.28222 ± 0.00029	0.00111 ± 0.00005	0.001132 ± 0.000039	277 ± 2	−13.7 ± 4
11XL27-17	0.28259 ± 0.00005	0.00095 ± 0.00008	0.000974 ± 0.000079	282 ± 3	−0.5 ± 0.7
11XL27-25	0.28267 ± 0.00004	0.0009 ± 0.00003	0.000931 ± 0.000013	272 ± 2	2.3 ± 0.5
11XL27-28	0.28229 ± 0.00012	0.00063 ± 0.00003	0.000649 ± 0.000011	287 ± 3	−10.8 ± 1.8
11XL27-31	0.28205 ± 0.00012	0.00065 ± 0.00003	0.000673 ± 0.000005	453 ± 3	−15.7 ± 1.7
11XL27-35	0.28206 ± 0.00018	0.00062 ± 0.00003	0.000642 ± 0.000018	437 ± 3	−15.9 ± 2.5
11XL27-42	0.28143 ± 0.00007	0.00093 ± 0.00004	0.000961 ± 0.000019	1702 ± 26	−10.8 ± 1.1
11XL27-44	0.28258 ± 0.00004	0.00122 ± 0.00006	0.001254 ± 0.000055	258 ± 2	−1.4 ± 0.6
11XL27-45	0.2822 ± 0.00028	0.00101 ± 0.00004	0.001034 ± 0.000029	274 ± 2	−14.3 ± 4
11XL27-47	0.28257 ± 0.00004	0.00051 ± 0.00003	0.000519 ± 0.000012	421 ± 4	2 ± 0.6
11XL27-48	0.28196 ± 0.00005	0.00078 ± 0.00003	0.000794 ± 0.000014	1198 ± 24	−2.9 ± 0.8
11XL27-50	0.28248 ± 0.0001	0.00152 ± 0.00005	0.001555 ± 0.000042	269 ± 2	−4.6 ± 1.5
11XL27-51	0.28243 ± 0.00022	0.00067 ± 0.00003	0.000679 ± 0.000017	438 ± 3	−2.8 ± 3
11XL27-52	0.28233 ± 0.00003	0.00064 ± 0.00003	0.000648 ± 0.000005	437 ± 3	−6.1 ± 0.5
11XL27-61	0.28233 ± 0.00007	0.00074 ± 0.00003	0.000758 ± 0.000018	985 ± 8	5.7 ± 1
11XL27-63	0.28255 ± 0.00003	0.00071 ± 0.00003	0.000722 ± 0.000014	286 ± 3	−1.8 ± 0.4
11XL27-64	0.28196 ± 0.00007	0.00085 ± 0.00004	0.000863 ± 0.000032	420 ± 4	−19.8 ± 1
11XL27-66	0.28197 ± 0.00003	0.00052 ± 0.00003	0.000529 ± 0.000007	489 ± 4	−17.7 ± 0.5
11XL27-69	0.28243 ± 0.00004	0.00084 ± 0.00005	0.000862 ± 0.000045	430 ± 4	−3 ± 0.6
11XL27-70	0.28269 ± 0.00004	0.00087 ± 0.00003	0.000892 ± 0.000013	290 ± 3	3.4 ± 0.5
11XL27-76	0.28247 ± 0.00004	0.00054 ± 0.00002	0.00055 ± 0.000006	409 ± 3	−1.9 ± 0.6
11XL27-79	0.28233 ± 0.00007	0.00124 ± 0.00004	0.001272 ± 0.000036	275 ± 3	−9.8 ± 1
11XL26-3	0.28237 ± 0.00004	0.00091 ± 0.00004	0.000934 ± 0.00003	433 ± 3	−5 ± 0.7
11XL26-4	0.28251 ± 0.00007	0.00043 ± 0.00003	0.000437 ± 0.000022	418 ± 4	−0.1 ± 1.1
11XL26-6	0.28251 ± 0.00007	0.00121 ± 0.00005	0.001234 ± 0.00004	267 ± 2	−3.5 ± 1
11XL26-7	0.28243 ± 0.00004	0.00076 ± 0.00003	0.00078 ± 0.000016	418 ± 3	−3.2 ± 0.7
11XL26-8	0.2821 ± 0.00007	0.0012 ± 0.00003	0.001222 ± 0.000012	260 ± 2	−18.2 ± 1

(continued)

Table C.1 (continued)

Sample	$^{176}Hf/^{177}Hf$	$^{176}Lu/^{177}Hf$	$^{176}Yb/^{177}Hf$	Age [Ma]	ϵ_{Hf}
11XL26-10	0.28183 ± 0.00032	0.00198 ± 0.00025	0.002021 ± 0.000248	316 ± 4	−26.7 ± 4.6
11XL26-13	0.28237 ± 0.00009	0.0005 ± 0.00004	0.000514 ± 0.00003	432 ± 4	−4.8 ± 1.3
11XL26-14	0.28247 ± 0.00008	0.00084 ± 0.00004	0.000859 ± 0.000033	274 ± 2	−4.7 ± 1.2
11XL26-16	0.28258 ± 0.00003	0.00112 ± 0.00004	0.00114 ± 0.000032	276 ± 2	−0.8 ± 0.5
11XL26-18	0.28243 ± 0.00004	0.00051 ± 0.00002	0.000518 ± 0.000005	412 ± 3	−3.2 ± 0.6
11XL26-19	0.28259 ± 0.00004	0.00076 ± 0.00004	0.000775 ± 0.000026	426 ± 5	2.6 ± 0.6
11XL26-25	0.28231 ± 0.00033	0.00112 ± 0.00004	0.001139 ± 0.000031	269 ± 5	−10.8 ± 4.6
11XL26-28	0.28273 ± 0.00004	0.00152 ± 0.00003	0.001541 ± 0.000025	254 ± 2	4 ± 0.6
11XL26-31	0.2827 ± 0.00005	0.0022 ± 0.00004	0.002237 ± 0.000037	367 ± 2	4.9 ± 0.7
11XL26-33	0.28242 ± 0.00007	0.00094 ± 0.00004	0.00095 ± 0.000029	271 ± 2	−6.6 ± 1.1
11XL26-42	0.28262 ± 0.00005	0.00096 ± 0.00004	0.000978 ± 0.00003	268 ± 2	0.5 ± 0.8
11XL26-45	0.28236 ± 0.0001	0.0007 ± 0.00002	0.000713 ± 0.000004	439 ± 3	−5.1 ± 1.4
11XL26-46	0.28273 ± 0.00005	0.00144 ± 0.00003	0.001466 ± 0.000027	234 ± 2	3.3 ± 0.7
11XL26-47	0.28274 ± 0.00006	0.00163 ± 0.00003	0.001657 ± 0.000024	264 ± 2	4.3 ± 0.9
11XL26-48	0.28253 ± 0.00005	0.00142 ± 0.00003	0.001437 ± 0.000022	255 ± 2	−3.3 ± 0.8
11XL26-49	0.28234 ± 0.00003	0.00091 ± 0.00003	0.000918 ± 0.000023	424 ± 3	−6.1 ± 0.5
11XL26-51	0.28228 ± 0.00008	0.0013 ± 0.00002	0.001324 ± 0.000015	243 ± 2	−12.3 ± 1.2
11XL26-52	0.28248 ± 0.00004	0.00158 ± 0.0001	0.001602 ± 0.000097	252 ± 2	−5.1 ± 0.6
11XL26-53	0.28151 ± 0.00005	0.00047 ± 0.00003	0.000481 ± 0.000014	1698 ± 22	−7.5 ± 0.7
11XL26-56	0.28118 ± 0.00064	0.00181 ± 0.00003	0.001835 ± 0.000018	258 ± 2	−51 ± 9
11XL26-60	0.28241 ± 0.00009	0.00097 ± 0.00003	0.000987 ± 0.000017	271 ± 2	−6.9 ± 1.3
11XL26-65	0.28258 ± 0.00004	0.00165 ± 0.00008	0.001672 ± 0.000075	311 ± 3	−0.4 ± 0.7
11XL26-67	0.28238 ± 0.00004	0.00105 ± 0.00005	0.001061 ± 0.000046	270 ± 4	−8.2 ± 0.6
11XL26-70	0.28209 ± 0.00006	0.00136 ± 0.00004	0.001379 ± 0.000028	1400 ± 33	5.8 ± 0.8
11XL26-80	0.28245 ± 0.00005	0.00126 ± 0.00003	0.001278 ± 0.000021	261 ± 2	−5.9 ± 0.8
11XL13-2	0.28258 ± 0.00004	0.00063 ± 0.00003	0.00064 ± 0.000011	447 ± 3	2.7 ± 0.6
11XL13-3	0.28247 ± 0.00004	0.00139 ± 0.00004	0.001414 ± 0.000031	298 ± 2	−4.5 ± 0.5
11XL13-6	0.28243 ± 0.00004	0.00204 ± 0.00005	0.002063 ± 0.000043	271 ± 2	−6.5 ± 0.6
11XL13-8	0.28151 ± 0.00003	0.0006 ± 0.00004	0.000608 ± 0.000022	1836 ± 22	−4.5 ± 0.5
11XL13-9	0.28153 ± 0.00004	0.00057 ± 0.00003	0.000573 ± 0.000005	1914 ± 30	−2 ± 0.6
11XL13-12	0.28113 ± 0.00004	0.00053 ± 0.00003	0.000527 ± 0.000014	2551 ± 22	−1.6 ± 0.6
11XL13-13	0.28123 ± 0.00004	0.00135 ± 0.00003	0.001345 ± 0.000018	2543 ± 20	0.2 ± 0.5
11XL13-15	0.28201 ± 0.00003	0.00105 ± 0.00005	0.001043 ± 0.000041	372 ± 3	−19.2 ± 0.5
11XL13-17	0.28128 ± 0.00004	0.00106 ± 0.00006	0.001045 ± 0.000051	2534 ± 20	2.3 ± 0.6
11XL13-18	0.28115 ± 0.00004	0.00087 ± 0.00004	0.000854 ± 0.000032	2509 ± 19	−2.4 ± 0.6
11XL13-19	0.28138 ± 0.00004	0.00042 ± 0.00003	0.000409 ± 0.000006	1843 ± 25	−8.8 ± 0.6
11XL13-20	0.28152 ± 0.00008	0.00087 ± 0.00003	0.000845 ± 0.000004	2565 ± 20	11.9 ± 1.2
11XL13-21	0.28257 ± 0.00003	0.0004 ± 0.00003	0.000385 ± 0.000005	430 ± 5	2.1 ± 0.5
11XL13-22	0.28119 ± 0.00003	0.00056 ± 0.00003	0.000537 ± 0.000016	2506 ± 18	−0.6 ± 0.5
11XL13-23	0.28246 ± 0.00003	0.00072 ± 0.00004	0.000694 ± 0.000029	1843 ± 23	29.3 ± 0.4
11XL13-24	0.28153 ± 0.00003	0.00032 ± 0.00002	0.000312 ± 0.000001	1773 ± 26	−4.7 ± 0.4
11XL13-25	0.28265 ± 0.00003	0.00133 ± 0.00003	0.001272 ± 0.000023	478 ± 4	5.9 ± 0.5
11XL13-27	0.28142 ± 0.00017	0.00085 ± 0.00003	0.000808 ± 0.000016	340 ± 4	−40.5 ± 2.4
11XL13-28	0.28155 ± 0.00003	0.00041 ± 0.00003	0.000391 ± 0.000016	1781 ± 19	−4.2 ± 0.5
11XL13-29	0.28157 ± 0.00003	0.00021 ± 0.00002	0.0002 ± 0.000006	1792 ± 26	−2.7 ± 0.5
11XL13-31	0.28115 ± 0.00003	0.00029 ± 0.00002	0.000272 ± 0.000006	2487 ± 22	−2.2 ± 0.4
11XL13-37	0.282 ± 0.00003	0.00104 ± 0.00002	0.000972 ± 0.000009	404 ± 4	−18.6 ± 0.4

(continued)

Table C.1 (continued)

Sample	$^{176}Hf/^{177}Hf$	$^{176}Lu/^{177}Hf$	$^{176}Yb/^{177}Hf$	Age [Ma]	ϵ_{Hf}
11XL13-47	0.28131 ± 0.00056	0.00167 ± 0.00003	0.00156 ± 0.000025	469 ± 3	−41.8 ± 7.9
11XL13-48	0.28117 ± 0.00006	0.00058 ± 0.00002	0.000541 ± 0.000018	2606 ± 18	1 ± 0.8
11XL13-50	0.28204 ± 0.00002	0.00074 ± 0.00002	0.000696 ± 0.000013	410 ± 5	−17.2 ± 0.4
11XL13-52	0.28255 ± 0.00005	0.00114 ± 0.00006	0.001062 ± 0.000054	432 ± 4	1.3 ± 0.8
11XL13-53	0.28128 ± 0.00003	0.00044 ± 0.00002	0.000408 ± 0.000004	2520 ± 21	3.1 ± 0.5
11XL13-56	0.28253 ± 0.00004	0.00151 ± 0.00002	0.001407 ± 0.000012	314 ± 3	−2.1 ± 0.6
11XL13-59	0.2826 ± 0.00003	0.00083 ± 0.00003	0.000775 ± 0.000021	447 ± 4	3.7 ± 0.5
11XL13-60	0.28127 ± 0.00003	0.00039 ± 0.00002	0.000363 ± 0.000002	2461 ± 18	1.3 ± 0.4
11XL20-3	0.28249 ± 0.00003	0.00072 ± 0.00002	0.00073 ± 0.000009	475 ± 3	0.3 ± 0.5
11XL20-4	0.2827 ± 0.00003	0.00081 ± 0.00002	0.000829 ± 0.000008	436 ± 3	6.9 ± 0.5
11XL20-5	0.28148 ± 0.00006	0.00058 ± 0.00002	0.000586 ± 0.000009	1933 ± 20	−3.2 ± 0.8
11XL20-7	0.2808 ± 0.00013	0.00044 ± 0.00003	0.000444 ± 0.000024	2037 ± 21	−25.1 ± 1.9
11XL20-9	0.28152 ± 0.00005	0.00054 ± 0.00004	0.000548 ± 0.00003	1857 ± 22	−3.6 ± 0.7
11XL20-11	0.28225 ± 0.00006	0.0008 ± 0.00004	0.000817 ± 0.000031	278 ± 2	−12.5 ± 0.9
11XL20-12	0.28239 ± 0.00004	0.00087 ± 0.00003	0.000883 ± 0.000009	456 ± 4	−3.8 ± 0.6
11XL20-14	0.28162 ± 0.00003	0.00048 ± 0.00003	0.000488 ± 0.000011	1796 ± 21	−1.4 ± 0.5
11XL20-16	0.28237 ± 0.00003	0.00076 ± 0.00002	0.00077 ± 0.000006	462 ± 4	−4.1 ± 0.5
11XL20-21	0.2821 ± 0.00004	0.00102 ± 0.00003	0.001031 ± 0.000017	316 ± 2	−17 ± 0.5
11XL20-23	0.28195 ± 0.00004	0.00074 ± 0.00004	0.00075 ± 0.000025	415 ± 3	−20.1 ± 0.6
11XL20-24	0.28179 ± 0.00009	0.00059 ± 0.00004	0.000594 ± 0.000023	510 ± 3	−23.6 ± 1.2
11XL20-25	0.28173 ± 0.00004	0.00085 ± 0.00004	0.000865 ± 0.000031	1747 ± 24	0.9 ± 0.7
11XL20-26	0.28126 ± 0.0001	0.00004 ± 0.00003	0.000045 ± 0.000004	1835 ± 24	−12.6 ± 1.4
11XL20-30	0.28164 ± 0.00022	0.00104 ± 0.00008	0.001058 ± 0.000075	440 ± 4	−30.6 ± 3.1
11XL20-32	0.28228 ± 0.00003	0.00121 ± 0.00004	0.001225 ± 0.00003	434 ± 2	−8.3 ± 0.5
11XL20-33	0.28229 ± 0.00005	0.00048 ± 0.00003	0.000489 ± 0.000004	440 ± 4	−7.6 ± 0.7
11XL20-34	0.28159 ± 0.00004	0.0005 ± 0.00003	0.000502 ± 0.000007	1906 ± 21	0.1 ± 0.5
11XL20-35	0.28237 ± 0.00003	0.00069 ± 0.00003	0.000697 ± 0.000015	275 ± 2	−8.2 ± 0.4
11XL20-41	0.28266 ± 0.00004	0.00059 ± 0.00003	0.000599 ± 0.000014	436 ± 3	5.6 ± 0.7
11XL20-44	0.28199 ± 0.00004	0.00097 ± 0.00003	0.000986 ± 0.000024	496 ± 4	−17 ± 0.6
11XL20-47	0.28193 ± 0.00003	0.00087 ± 0.00003	0.000882 ± 0.00002	1537 ± 27	3.4 ± 0.5
11XL20-52	0.2816 ± 0.00004	0.00075 ± 0.00003	0.000762 ± 0.000015	1918 ± 24	0.4 ± 0.5
11XL20-54	0.28218 ± 0.00003	0.00101 ± 0.00004	0.001019 ± 0.000027	296 ± 2	−14.6 ± 0.5
11XL20-64	0.28149 ± 0.00003	0.00041 ± 0.00002	0.000419 ± 0.000002	1906 ± 25	−3.2 ± 0.5
11XL20-65	0.28275 ± 0.00003	0.00128 ± 0.00004	0.001291 ± 0.000034	481 ± 3	9.3 ± 0.5
11XL20-70	0.28126 ± 0.00004	0.00068 ± 0.00003	0.000689 ± 0.000006	2453 ± 19	0.2 ± 0.6
11XL20-71	0.28188 ± 0.00007	0.00091 ± 0.00005	0.00092 ± 0.000039	497 ± 4	−20.9 ± 1
11XL20-72	0.28241 ± 0.00005	0.00077 ± 0.00005	0.000775 ± 0.000046	462 ± 4	−2.9 ± 0.8
11XL20-75	0.28117 ± 0.00025	0.00075 ± 0.00003	0.000751 ± 0.000017	283 ± 3	−50.8 ± 3.5
11XL25-5	0.28205 ± 0.00008	0.00108 ± 0.00002	0.001008 ± 0.00001	339 ± 2	−18.5 ± 1.1
11XL25-6	0.28276 ± 0.00004	0.00123 ± 0.00005	0.001147 ± 0.00004	433 ± 3	8.7 ± 0.6
11XL25-15	0.2812 ± 0.00003	0.00034 ± 0.00002	0.000319 ± 0.000003	2503 ± 18	−0.1 ± 0.5
11XL25-16	0.28252 ± 0.00004	0.00061 ± 0.00002	0.000569 ± 0.000002	475 ± 3	1.4 ± 0.6
11XL25-18	0.28258 ± 0.00003	0.00055 ± 0.00002	0.000508 ± 0.000006	449 ± 4	3 ± 0.5
11XL25-32	0.28195 ± 0.00004	0.00093 ± 0.00003	0.000858 ± 0.000026	385 ± 3	−20.9 ± 0.6
11XL25-33	0.28143 ± 0.00004	0.00033 ± 0.00002	0.000307 ± 0.000008	1800 ± 25	−7.9 ± 0.6
11XL25-36	0.28132 ± 0.00004	0.00112 ± 0.00003	0.001038 ± 0.000015	2539 ± 23	3.6 ± 0.5

(continued)

Table C.1 (continued)

Sample	$^{176}Hf/^{177}Hf$	$^{176}Lu/^{177}Hf$	$^{176}Yb/^{177}Hf$	Age [Ma]	ϵ_{Hf}
11XL25-37	0.28127 ± 0.00004	0.00069 ± 0.00002	0.000639 ± 0.000002	2439 ± 23	0.4 ± 0.6
11XL25-41	0.28125 ± 0.00004	0.00065 ± 0.00003	0.000602 ± 0.000009	2494 ± 24	1 ± 0.5
11XL25-43	0.28108 ± 0.00004	0.00057 ± 0.00002	0.000525 ± 0.000003	456 ± 4	−49.9 ± 0.5
11XL25-44	0.28278 ± 0.00003	0.00047 ± 0.00003	0.000435 ± 0.000012	2702 ± 22	60.4 ± 0.5
11XL25-45	0.28126 ± 0.00003	0.00058 ± 0.00002	0.000543 ± 0.000006	288 ± 4	−47.4 ± 0.5
11XL25-49	0.28213 ± 0.00017	0.00052 ± 0.00002	0.00049 ± 0.000008	269 ± 3	−17 ± 2.4
11XL25-55	0.28149 ± 0.00003	0.00112 ± 0.00003	0.001063 ± 0.000014	2009 ± 25	−2 ± 0.4
11XL25-56	0.28271 ± 0.00002	0.00066 ± 0.00002	0.000627 ± 0.000012	450 ± 4	7.4 ± 0.4
11XL25-57	0.28128 ± 0.00004	0.00051 ± 0.00002	0.000486 ± 0.00001	2568 ± 26	4.2 ± 0.6
11XL25-59	0.28145 ± 0.00007	0.00079 ± 0.00006	0.000759 ± 0.000054	2047 ± 19	−2.1 ± 1
11XL25-60	0.28229 ± 0.00004	0.00093 ± 0.00002	0.000902 ± 0.000009	288 ± 2	−10.8 ± 0.6
11XL25-63	0.28267 ± 0.00004	0.00106 ± 0.00003	0.001036 ± 0.000021	446 ± 5	5.9 ± 0.6
11XL25-65	0.2816 ± 0.00004	0.00075 ± 0.00004	0.000737 ± 0.000014	1788 ± 27	−2.4 ± 0.6
11XL25-67	0.28121 ± 0.00004	0.00084 ± 0.00003	0.000829 ± 0.000004	2521 ± 19	−0.2 ± 0.6
11XL25-70	0.28115 ± 0.00004	0.00047 ± 0.00003	0.000456 ± 0.000004	2331 ± 21	−5.9 ± 0.6
11XL25-71	0.28198 ± 0.00004	0.00052 ± 0.00003	0.000509 ± 0.000007	381 ± 4	−19.6 ± 0.6
11XL25-72	0.28152 ± 0.00004	0.00069 ± 0.00003	0.000671 ± 0.000003	1746 ± 33	−6 ± 0.6
11XL25-73	0.28255 ± 0.00004	0.00031 ± 0.00003	0.000297 ± 0.000003	455 ± 3	2.2 ± 0.6
11XL25-74	0.28157 ± 0.00004	0.00032 ± 0.00003	0.000312 ± 0.000002	1826 ± 27	−2.2 ± 0.6
11XL25-78	0.28191 ± 0.00004	0.00071 ± 0.00003	0.000679 ± 0.000008	378 ± 4	−22.5 ± 0.7
11XL25-82	0.2823 ± 0.00004	0.00095 ± 0.00004	0.000906 ± 0.000033	428 ± 3	−7.5 ± 0.7
11XL25-83	0.28206 ± 0.00003	0.00108 ± 0.00003	0.001025 ± 0.000015	404 ± 3	−16.8 ± 0.5
11XL7-1-2	0.28215 ± 0.00004	0.00145 ± 0.00003	0.001352 ± 0.000002	476 ± 4	−12.1 ± 0.6
11XL7-1-5	0.28151 ± 0.00003	0.0005 ± 0.00003	0.000467 ± 0.000015	474 ± 3	−34.4 ± 0.5
11XL7-1-8	0.28225 ± 0.00004	0.00153 ± 0.00003	0.001429 ± 0.000018	490 ± 4	−8.2 ± 0.6
11XL7-1-12	0.28262 ± 0.00003	0.00082 ± 0.00003	0.000762 ± 0.000006	1839 ± 21	34.8 ± 0.5
11XL7-1-12	0.28262 ± 0.00003	0.00082 ± 0.00003	0.000762 ± 0.000006	1839 ± 21	34.8 ± 0.5
11XL7-1-13	0.28244 ± 0.00003	0.00043 ± 0.00002	0.000397 ± 0.000002	488 ± 3	−1.1 ± 0.5
11XL7-1-15	0.28159 ± 0.00003	0.00041 ± 0.00002	0.000381 ± 0.000005	1847 ± 19	−1.2 ± 0.5
11XL7-1-18	0.28265 ± 0.00003	0.00071 ± 0.00003	0.000659 ± 0.000016	466 ± 4	5.7 ± 0.5
11XL7-1-19	0.2826 ± 0.00003	0.00145 ± 0.00002	0.001353 ± 0.000011	426 ± 4	3 ± 0.4
11XL7-1-20	0.28233 ± 0.00004	0.0014 ± 0.00004	0.001302 ± 0.000035	481 ± 4	−5.6 ± 0.5
11XL7-1-22	0.28022 ± 0.00033	0.00125 ± 0.00003	0.001172 ± 0.000012	2327 ± 19	−40.1 ± 4.6
11XL7-1-23	0.2815 ± 0.00004	0.00004 ± 0.00003	0.000035 ± 0.000001	1828 ± 22	−4.2 ± 0.5
11XL7-1-27	0.28159 ± 0.00003	0.00017 ± 0.00003	0.000163 ± 0.000009	1962 ± 22	1.7 ± 0.5
11XL7-1-31	0.28251 ± 0.00008	0.00066 ± 0.00003	0.00063 ± 0.000005	451 ± 4	0.6 ± 1.1
11XL7-1-34	0.28212 ± 0.00003	0.00089 ± 0.00003	0.000849 ± 0.000022	459 ± 3	−13.3 ± 0.5
11XL7-1-37	0.28198 ± 0.00004	0.00104 ± 0.00003	0.001001 ± 0.000004	357 ± 3	−20.5 ± 0.6
11XL7-1-38	0.2825 ± 0.00006	0.00098 ± 0.00004	0.000942 ± 0.000027	414 ± 4	−0.7 ± 0.9
11XL7-1-39	0.28223 ± 0.00079	0.00095 ± 0.00005	0.000926 ± 0.000043	487 ± 4	−8.9 ± 11
11XL7-1-40	0.28252 ± 0.00004	0.0006 ± 0.00003	0.000586 ± 0.000017	399 ± 4	−0.2 ± 0.6
11XL7-1-46	0.28256 ± 0.00004	0.00078 ± 0.00003	0.000763 ± 0.000015	435 ± 3	1.9 ± 0.6
11XL7-1-48	0.28234 ± 0.00003	0.00072 ± 0.00003	0.000716 ± 0.000019	469 ± 4	−5.1 ± 0.5
11XL7-1-50	0.28209 ± 0.00008	0.00112 ± 0.00002	0.001119 ± 0.000012	501 ± 4	−13.6 ± 1.2
11XL7-1-52	0.28258 ± 0.00003	0.00063 ± 0.00002	0.000632 ± 0.000002	455 ± 4	3.1 ± 0.5
11XL7-1-56	0.28204 ± 0.00003	0.00078 ± 0.00003	0.00078 ± 0.000015	501 ± 4	−15 ± 0.4

(continued)

Table C.1 (continued)

Sample	$^{176}Hf/^{177}Hf$	$^{176}Lu/^{177}Hf$	$^{176}Yb/^{177}Hf$	Age [Ma]	ϵ_{Hf}
11XL7-1-57	0.282 ± 0.00003	0.00109 ± 0.00002	0.001099 ± 0.00001	504 ± 5	−16.4 ± 0.5
11XL7-1-58	0.2822 ± 0.00003	0.00109 ± 0.00003	0.001098 ± 0.000021	493 ± 4	−9.7 ± 0.5
11XL7-1-62	0.2824 ± 0.00003	0.00091 ± 0.00002	0.000918 ± 0.00001	473 ± 4	−3 ± 0.5
11XL7-1-67	0.2818 ± 0.0004	0.00067 ± 0.00003	0.000677 ± 0.000024	425 ± 3	−25.2 ± 5.6
11XL7-1-68	0.28254 ± 0.00005	0.00083 ± 0.00004	0.000844 ± 0.000034	416 ± 4	0.6 ± 0.8
11XL7-1-75	0.28154 ± 0.00003	0.00069 ± 0.00003	0.000696 ± 0.000019	1821 ± 22	−3.7 ± 0.4
11XL17-2-6	0.28271 ± 0.00003	0.00144 ± 0.00003	0.001333 ± 0.000016	297 ± 2	4.1 ± 0.5
11XL17-2-10	0.28134 ± 0.00003	0.00089 ± 0.00002	0.000825 ± 0.000005	2485 ± 21	3.7 ± 0.5
11XL17-2-11	0.28261 ± 0.00006	0.00128 ± 0.00003	0.001176 ± 0.000014	281 ± 3	0.3 ± 0.9
11XL17-2-15	0.28169 ± 0.00003	0.00128 ± 0.00003	0.001177 ± 0.000022	1769 ± 21	−0.4 ± 0.5
11XL17-2-16	0.28155 ± 0.00003	0.00094 ± 0.00006	0.000868 ± 0.000055	1850 ± 20	−3.1 ± 0.5
11XL17-2-17	0.28263 ± 0.00003	0.00122 ± 0.00004	0.001124 ± 0.000037	429 ± 4	4.2 ± 0.5
11XL17-2-20	0.2827 ± 0.00003	0.00118 ± 0.00003	0.001088 ± 0.000028	270 ± 2	3.3 ± 0.4
11XL17-2-25	0.28123 ± 0.00003	0.00032 ± 0.00002	0.00029 ± 0.000002	2203 ± 21	−5.8 ± 0.5
11XL17-2-26	0.28164 ± 0.00003	0.00094 ± 0.00003	0.000867 ± 0.000022	1939 ± 21	2.1 ± 0.5
11XL17-2-27	0.28319 ± 0.00051	0.00069 ± 0.00002	0.000638 ± 0.000009	2533 ± 24	70.8 ± 7.2
11XL17-2-28	0.28175 ± 0.00109	0.00199 ± 0.00004	0.001822 ± 0.000032	267 ± 2	−30.6 ± 15.3
11XL17-2-38	0.28215 ± 0.00003	0.00114 ± 0.00002	0.001045 ± 0.000016	311 ± 3	−15.4 ± 0.4
11XL17-2-39	0.28203 ± 0.00002	0.00077 ± 0.00002	0.000701 ± 0.000003	432 ± 4	−16.8 ± 0.4
11XL17-2-42	0.28271 ± 0.00003	0.00126 ± 0.00002	0.001156 ± 0.000002	253 ± 3	3.2 ± 0.4
11XL17-2-44	0.28269 ± 0.00003	0.00142 ± 0.00002	0.0013 ± 0.000015	260 ± 2	2.5 ± 0.4
11XL17-2-45	0.28272 ± 0.00003	0.0012 ± 0.00002	0.001096 ± 0.000004	272 ± 2	3.8 ± 0.4
11XL17-2-48	0.28272 ± 0.00003	0.00105 ± 0.00002	0.000954 ± 0.000014	268 ± 3	4 ± 0.5
11XL17-2-49	0.28162 ± 0.00003	0.00057 ± 0.00002	0.000516 ± 0.000003	1862 ± 32	0 ± 0.5
11XL17-2-50	0.28258 ± 0.00003	0.00117 ± 0.00005	0.001065 ± 0.00004	437 ± 3	2.6 ± 0.4
11XL17-2-51	0.28208 ± 0.00003	0.00091 ± 0.00002	0.00083 ± 0.000007	409 ± 4	−15.8 ± 0.5
11XL17-2-53	0.28264 ± 0.00004	0.00232 ± 0.00004	0.002097 ± 0.000023	246 ± 2	0.5 ± 0.5
11XL17-2-54	0.28237 ± 0.00003	0.00134 ± 0.00003	0.001211 ± 0.000011	483 ± 4	−4.1 ± 0.5
11XL17-2-55	0.28266 ± 0.00003	0.00106 ± 0.00003	0.000955 ± 0.000013	261 ± 2	1.6 ± 0.4
11XL17-2-56	0.2827 ± 0.00003	0.0017 ± 0.00003	0.001527 ± 0.000016	264 ± 2	2.8 ± 0.5
11XL17-2-57	0.28164 ± 0.00003	0.00106 ± 0.00002	0.000954 ± 0.000006	1880 ± 24	0.4 ± 0.5
11XL17-2-60	0.282 ± 0.00003	0.0008 ± 0.00003	0.000721 ± 0.000015	382 ± 3	−19.3 ± 0.5
11XL17-2-63	0.28257 ± 0.00003	0.00062 ± 0.00002	0.000553 ± 0.000006	481 ± 4	3.3 ± 0.5
11XL17-2-65	0.28261 ± 0.00003	0.00057 ± 0.00002	0.000507 ± 0.000001	437 ± 4	3.6 ± 0.5
11XL17-2-68	0.28238 ± 0.00003	0.00111 ± 0.00004	0.000988 ± 0.000029	454 ± 4	−4.3 ± 0.4
11XL17-2-76	0.28159 ± 0.00004	0.00052 ± 0.00002	0.000467 ± 0.000006	1858 ± 24	−1.1 ± 0.6
11XL15-1-3	0.28262 ± 0.00026	0.00124 ± 0.0001	0.001135 ± 0.000032	286 ± 3	0.7 ± 3.6
11XL15-1-5	0.28242 ± 0.00023	0.00126 ± 0.0001	0.001157 ± 0.000023	504 ± 7	−1.7 ± 3.3
11XL15-1-8	0.28275 ± 0.00021	0.00059 ± 0.0001	0.000545 ± 0.000011	274 ± 5	5 ± 3
11XL15-1-9	0.28229 ± 0.00021	0.00092 ± 0.0001	0.000857 ± 0.000023	275 ± 3	−11.3 ± 3
11XL15-1-10	0.28152 ± 0.00023	0.00096 ± 0.0001	0.000898 ± 0.000031	2447 ± 27	9.1 ± 3.2
11XL15-1-11	0.28244 ± 0.00019	0.00105 ± 0.0001	0.000979 ± 0.000019	281 ± 3	−5.7 ± 2.7
11XL15-1-12	0.28218 ± 0.00026	0.00171 ± 0.00012	0.001605 ± 0.000076	292 ± 4	−14.9 ± 3.7
11XL15-1-13	0.28243 ± 0.00016	0.00111 ± 0.0001	0.001047 ± 0.000013	272 ± 2	−6.5 ± 2.3
11XL15-1-15	0.28233 ± 0.00025	0.00106 ± 0.0001	0.001001 ± 0.00002	284 ± 3	−9.7 ± 3.5
11XL15-1-18	0.28199 ± 0.00018	0.00059 ± 0.0001	0.000566 ± 0.000003	562 ± 5	−15.4 ± 2.5
11XL15-1-25	0.282 ± 0.00015	0.00025 ± 0.0001	0.000241 ± 0	416 ± 4	−18.2 ± 2.1

(continued)

Table C.1 (continued)

Sample	$^{176}Hf/^{177}Hf$	$^{176}Lu/^{177}Hf$	$^{176}Yb/^{177}Hf$	Age [Ma]	ϵ_{Hf}
11XL15-1-25	0.28242 ± 0.00011	0.00083 ± 0.00002	0.00082 ± 0.000008	416 ± 4	−3.6 ± 1.6
11XL15-1-29	0.28177 ± 0.00004	0.00111 ± 0.00003	0.001094 ± 0.000011	1298 ± 28	−7.6 ± 0.6
11XL15-1-32	0.28254 ± 0.00004	0.00073 ± 0.00002	0.000719 ± 0.000005	278 ± 2	−2.2 ± 0.5
11XL15-1-33	0.2786 ± 0.00104	0.00174 ± 0.00012	0.001734 ± 0.000119	473 ± 3	−137.8 ± 14.6
11XL15-1-39	0.2816 ± 0.00003	0.0004 ± 0.00003	0.000401 ± 0.000012	1811 ± 26	−1.5 ± 0.5
11XL15-1-42	0.2826 ± 0.00004	0.00112 ± 0.00004	0.001124 ± 0.000031	266 ± 3	−0.4 ± 0.7
11XL15-1-44	0.28236 ± 0.00003	0.00123 ± 0.00002	0.00123 ± 0.000011	298 ± 4	−8.2 ± 0.5
11XL15-1-48	0.28237 ± 0.00003	0.00079 ± 0.00002	0.000796 ± 0.000008	471 ± 4	−4.1 ± 0.5
11XL15-1-52	0.28157 ± 0.00004	0.00017 ± 0.00002	0.000171 ± 0.000001	1787 ± 25	−2.9 ± 0.5
11XL15-1-57	0.28269 ± 0.00003	0.00062 ± 0.00004	0.00063 ± 0.00003	409 ± 4	6 ± 0.5
11XL15-1-58	0.28233 ± 0.00004	0.00071 ± 0.00003	0.000724 ± 0.000017	485 ± 5	−5.3 ± 0.5
11XL15-1-59	0.28241 ± 0.00003	0.00089 ± 0.00003	0.000892 ± 0.000003	270 ± 3	−7 ± 0.5
11XL15-1-60	0.28233 ± 0.00007	0.00163 ± 0.00003	0.001618 ± 0.000016	301 ± 3	−9.2 ± 1.1
11XL15-1-61	0.28239 ± 0.00004	0.00134 ± 0.00004	0.001319 ± 0.000025	267 ± 3	−7.8 ± 0.6
11XL15-1-62	0.28243 ± 0.00003	0.00078 ± 0.00003	0.000759 ± 0.000007	278 ± 3	−6.2 ± 0.5
11XL15-1-68	0.2816 ± 0.00004	0.0007 ± 0.00008	0.000682 ± 0.000075	275 ± 3	−35.5 ± 0.6
11XL15-1-69	0.28133 ± 0.00036	0.00066 ± 0.00004	0.000635 ± 0.000034	443 ± 4	−41.3 ± 5
11XL15-1-73	0.2824 ± 0.00004	0.00082 ± 0.00003	0.000782 ± 0.000001	268 ± 3	−7.3 ± 0.6
11XL15-1-77	0.27866 ± 0.00163	0.00105 ± 0.00005	0.000988 ± 0.000046	471 ± 4	−135.4 ± 22.8
11XL15-1-79	0.28164 ± 0.00004	0.00062 ± 0.00003	0.000582 ± 0.000012	1887 ± 24	1.3 ± 0.5
11XL16-1-1	0.28261 ± 0.00005	0.00117 ± 0.00003	0.001185 ± 0.000013	444 ± 3	3.6 ± 0.7
11XL16-1-10	0.28212 ± 0.00004	0.00162 ± 0.00008	0.00164 ± 0.00008	276 ± 2	−17.4 ± 0.6
11XL16-1-11	0.28208 ± 0.00003	0.00162 ± 0.00003	0.001651 ± 0.000011	299 ± 2	−18.4 ± 0.5
11XL16-1-12	0.28121 ± 0.00003	0.00083 ± 0.00002	0.000846 ± 0.000007	2506 ± 18	−0.5 ± 0.5
11XL16-1-13	0.28244 ± 0.00003	0.00071 ± 0.00002	0.000729 ± 0.000005	431 ± 3	−2.3 ± 0.5
11XL16-1-14	0.28262 ± 0.00003	0.00078 ± 0.00003	0.0008 ± 0.00001	431 ± 3	3.9 ± 0.5
11XL16-1-17	0.28194 ± 0.00003	0.00095 ± 0.00003	0.000974 ± 0.000014	422 ± 4	−20.3 ± 0.5
11XL16-1-22	0.28237 ± 0.00003	0.00101 ± 0.00003	0.001044 ± 0.000023	482 ± 3	−3.8 ± 0.5
11XL16-1-24	0.28084 ± 0.00011	0.00032 ± 0.00002	0.000327 ± 0.000008	2511 ± 20	−12.4 ± 1.5
11XL16-1-25	0.28185 ± 0.00005	0.00184 ± 0.00007	0.001899 ± 0.000062	381 ± 2	−24.8 ± 0.8
11XL16-1-26	0.28246 ± 0.00004	0.00171 ± 0.00009	0.00178 ± 0.000088	280 ± 3	−5.3 ± 0.6
11XL16-1-27	0.28264 ± 0.00003	0.00085 ± 0.00003	0.000888 ± 0.000014	457 ± 5	5.2 ± 0.5
11XL16-1-30	0.28175 ± 0.00019	0.00152 ± 0.00008	0.001588 ± 0.00007	393 ± 3	−27.9 ± 2.7
11XL16-1-32	0.28159 ± 0.00004	0.00057 ± 0.00003	0.000596 ± 0.000005	1856 ± 24	−1 ± 0.6
11XL16-1-33	0.28161 ± 0.00004	0.00053 ± 0.00004	0.000552 ± 0.000029	1869 ± 19	−0.1 ± 0.6
11XL16-1-35	0.2821 ± 0.00014	0.00096 ± 0.00005	0.000997 ± 0.000039	274 ± 2	−17.8 ± 2
11XL16-1-38	0.28147 ± 0.00007	0.0001 ± 0.00003	0.000104 ± 0.000014	1854 ± 24	−4.7 ± 1
11XL16-1-39	0.28164 ± 0.00004	0.00035 ± 0.00003	0.00037 ± 0.000003	1650 ± 23	−3.7 ± 0.6
11XL16-1-41	0.28166 ± 0.0001	0.0009 ± 0.00004	0.000939 ± 0.000025	403 ± 4	−30.7 ± 1.4
11XL16-1-43	0.28111 ± 0.00005	0.00027 ± 0.00003	0.000283 ± 0.000002	2576 ± 14	−1.3 ± 0.7
11XL16-1-46	0.28253 ± 0.00003	0.00066 ± 0.00002	0.000688 ± 0.000009	454 ± 4	1.4 ± 0.4
11XL16-1-47	0.28125 ± 0.00003	0.00049 ± 0.00002	0.00051 ± 0.000016	2536 ± 20	2.2 ± 0.5
11XL16-1-49	0.28163 ± 0.00003	0.00093 ± 0.00003	0.000969 ± 0.000028	1922 ± 24	1.2 ± 0.5
11XL16-1-52	0.28231 ± 0.00006	0.00176 ± 0.00003	0.001823 ± 0.000026	435 ± 4	−7.4 ± 0.8
11XL16-1-57	0.28259 ± 0.00003	0.00051 ± 0.00002	0.000524 ± 0.000006	473 ± 3	3.9 ± 0.5
11XL16-1-60	0.28253 ± 0.00004	0.00036 ± 0.00002	0.000374 ± 0.000002	469 ± 4	1.7 ± 0.5

(continued)

Table C.1 (continued)

Sample	$^{176}Hf/^{177}Hf$	$^{176}Lu/^{177}Hf$	$^{176}Yb/^{177}Hf$	Age [Ma]	ϵ_{Hf}
11XL16-1-62	0.28153 ± 0.00003	0.00046 ± 0.00002	0.000477 ± 0.000003	1828 ± 22	−3.7 ± 0.5
11XL16-1-63	0.28266 ± 0.00004	0.00099 ± 0.00003	0.001014 ± 0.000023	455 ± 4	5.8 ± 0.5
11XL16-1-65	0.28282 ± 0.00003	0.00081 ± 0.00003	0.000831 ± 0.000023	290 ± 4	8.1 ± 0.5
11XL16-1-69	0.28156 ± 0.00003	0.00026 ± 0.00004	0.000265 ± 0.000038	1825 ± 19	−2.5 ± 0.5
11XL54-1-2	0.28208 ± 0.00008	0.00128 ± 0.00003	0.001306 ± 0.000015	275 ± 2	−18.8 ± 1.2
11XL54-1-8	0.28266 ± 0.00003	0.00127 ± 0.00003	0.0013 ± 0.000017	267 ± 2	1.7 ± 0.5
11XL54-1-13	0.28258 ± 0.00005	0.00083 ± 0.00006	0.000851 ± 0.000054	283 ± 4	−0.8 ± 0.7
11XL54-1-14	0.28181 ± 0.0002	0.00157 ± 0.00003	0.001609 ± 0.000019	272 ± 2	−28.4 ± 2.8
11XL54-1-15	0.28226 ± 0.00004	0.00096 ± 0.00003	0.000982 ± 0.000019	269 ± 2	−12.5 ± 0.7
11XL54-1-16	0.28223 ± 0.00011	0.00163 ± 0.00004	0.001676 ± 0.000034	270 ± 2	−13.5 ± 1.6
11XL54-1-18	0.28225 ± 0.00005	0.00118 ± 0.00003	0.001211 ± 0.00002	281 ± 3	−12.6 ± 0.8
11XL54-1-21	0.28152 ± 0.00023	0.0011 ± 0.00003	0.001132 ± 0.00002	261 ± 2	−38.8 ± 3.3
11XL54-1-22	0.2825 ± 0.00004	0.00107 ± 0.00003	0.0011 ± 0.000018	258 ± 2	−4.1 ± 0.7
11XL54-1-24	0.28245 ± 0.00005	0.00083 ± 0.00003	0.000853 ± 0.00001	277 ± 3	−5.4 ± 0.8
11XL54-1-26	0.28222 ± 0.00005	0.00117 ± 0.00003	0.001214 ± 0.000021	263 ± 2	−14.1 ± 0.8
11XL54-1-27	0.28229 ± 0.00003	0.00104 ± 0.00005	0.001078 ± 0.000045	256 ± 2	−11.7 ± 0.5
11XL54-1-29	0.2823 ± 0.00003	0.00092 ± 0.00004	0.000948 ± 0.000029	272 ± 3	−11 ± 0.5
11XL54-1-30	0.28233 ± 0.00004	0.00103 ± 0.00002	0.001062 ± 0.000009	257 ± 2	−10 ± 0.5
11XL54-1-31	0.28252 ± 0.00004	0.00109 ± 0.00007	0.001127 ± 0.000061	267 ± 2	−3.1 ± 0.6
11XL54-1-34	0.2823 ± 0.00003	0.0011 ± 0.00003	0.001134 ± 0.000017	269 ± 2	−11.1 ± 0.5
11XL54-1-37	0.28206 ± 0.00016	0.00108 ± 0.00006	0.00111 ± 0.000058	277 ± 2	−19.3 ± 2.3
11XL54-1-38	0.28234 ± 0.00003	0.00128 ± 0.00004	0.001319 ± 0.000033	270 ± 2	−9.5 ± 0.4
11XL54-1-41	0.28172 ± 0.00018	0.00118 ± 0.00004	0.00121 ± 0.000032	281 ± 2	−31.4 ± 2.5
11XL54-1-44	0.28208 ± 0.00006	0.00174 ± 0.00004	0.001789 ± 0.000036	262 ± 2	−18.9 ± 0.8
11XL54-1-45	0.28224 ± 0.00005	0.0013 ± 0.00004	0.001328 ± 0.000032	266 ± 3	−13.1 ± 0.8
11XL54-1-48	0.28255 ± 0.00004	0.00098 ± 0.00004	0.001004 ± 0.00002	285 ± 3	−1.9 ± 0.6
11XL54-1-53	0.28227 ± 0.00004	0.00068 ± 0.00005	0.000697 ± 0.000046	271 ± 2	−11.9 ± 0.6
11XL54-1-54	0.28267 ± 0.00004	0.00097 ± 0.00003	0.000994 ± 0.000015	257 ± 3	2 ± 0.5
11XL54-1-55	0.28234 ± 0.00003	0.00101 ± 0.00003	0.001032 ± 0.000019	276 ± 2	−9.2 ± 0.5
11XL54-1-58	0.28238 ± 0.00004	0.00148 ± 0.00007	0.001509 ± 0.00006	276 ± 3	−8.1 ± 0.6
11XL54-1-63	0.28226 ± 0.00004	0.00098 ± 0.00003	0.000996 ± 0.00002	1431 ± 26	12.6 ± 0.6
11XL54-1-66	0.28259 ± 0.00004	0.00135 ± 0.00004	0.001376 ± 0.000027	279 ± 2	−0.5 ± 0.6
11XL54-1-67	0.28234 ± 0.00003	0.00098 ± 0.00003	0.000996 ± 0.000022	281 ± 2	−9.4 ± 0.5
11XL54-1-68	0.28204 ± 0.00018	0.00115 ± 0.00004	0.001171 ± 0.000032	276 ± 4	−19.9 ± 2.5
11XL23-1	0.28123 ± 0.00004	0.00067 ± 0.00003	0.000681 ± 0.000012	2603 ± 23	2.9 ± 0.5
11XL23-6	0.28256 ± 0.00003	0.00063 ± 0.00004	0.000636 ± 0.000026	282 ± 3	−1.5 ± 0.5
11XL23-7	0.28244 ± 0.00008	0.00046 ± 0.00003	0.00047 ± 0.000002	442 ± 5	−2.1 ± 1.1
11XL23-9	0.28252 ± 0.00003	0.00079 ± 0.00006	0.000803 ± 0.000049	254 ± 3	−3.3 ± 0.5
11XL23-12	0.28206 ± 0.00004	0.00084 ± 0.00003	0.000849 ± 0.000019	501 ± 3	−14.5 ± 0.6
11XL23-15	0.2824 ± 0.00005	0.00192 ± 0.00003	0.001942 ± 0.000017	266 ± 2	−7.6 ± 0.7
11XL23-18	0.28209 ± 0.00004	0.00099 ± 0.00003	0.001007 ± 0.000005	259 ± 2	−18.6 ± 0.6
11XL23-20	0.28198 ± 0.00003	0.00069 ± 0.00003	0.000695 ± 0.000015	396 ± 3	−19.6 ± 0.5
11XL23-21	0.28233 ± 0.00006	0.00074 ± 0.00003	0.000748 ± 0.000019	421 ± 4	−6.5 ± 0.9
11XL23-22	0.28121 ± 0.00005	0.00155 ± 0.00003	0.001571 ± 0.000014	2643 ± 17	1.4 ± 0.8
11XL23-24	0.28164 ± 0.00015	0.00141 ± 0.00009	0.00143 ± 0.000082	266 ± 2	−34.5 ± 2.1
11XL23-25	0.28272 ± 0.00003	0.00077 ± 0.00002	0.000775 ± 0.000009	265 ± 2	3.9 ± 0.4

(continued)

Table C.1 (continued)

Sample	$^{176}Hf/^{177}Hf$	$^{176}Lu/^{177}Hf$	$^{176}Yb/^{177}Hf$	Age [Ma]	ϵ_{Hf}
11XL23-26	0.28253 ± 0.00003	0.00058 ± 0.00003	0.000589 ± 0.000015	271 ± 2	−2.7 ± 0.5
11XL23-28	0.2821 ± 0.00003	0.00085 ± 0.00003	0.000855 ± 0.000013	485 ± 3	−13.3 ± 0.4
11XL23-33	0.28271 ± 0.00006	0.00162 ± 0.00004	0.001637 ± 0.000036	297 ± 3	4 ± 0.8
11XL23-38	0.2811 ± 0.00004	0.0008 ± 0.00005	0.00081 ± 0.000041	2698 ± 20	0.1 ± 0.6
11XL23-39	0.28243 ± 0.00007	0.00131 ± 0.00004	0.001323 ± 0.000033	277 ± 2	−6.4 ± 1
11XL23-41	0.28231 ± 0.00008	0.00068 ± 0.00003	0.000684 ± 0.00002	470 ± 3	−6.1 ± 1.1
11XL23-43	0.28252 ± 0.00003	0.00069 ± 0.00004	0.000692 ± 0.000027	291 ± 3	−2.6 ± 0.5
11XL23-49	0.28251 ± 0.00003	0.0014 ± 0.00005	0.001411 ± 0.000042	274 ± 2	−3.4 ± 0.5
11XL23-50	0.28227 ± 0.00005	0.00137 ± 0.00004	0.001376 ± 0.000024	299 ± 3	−11.3 ± 0.7
11XL23-52	0.28251 ± 0.00003	0.00075 ± 0.00003	0.000751 ± 0.000017	269 ± 2	−3.6 ± 0.5
11XL23-54	0.28232 ± 0.00004	0.00068 ± 0.00003	0.000685 ± 0.000008	494 ± 4	−5.5 ± 0.6
11XL23-64	0.28255 ± 0.00003	0.00122 ± 0.00004	0.001229 ± 0.000033	279 ± 2	−2.1 ± 0.5
11XL23-66	0.2812 ± 0.00004	0.00089 ± 0.00003	0.000899 ± 0.000013	2733 ± 21	4.3 ± 0.6
11XL23-67	0.28258 ± 0.00003	0.00121 ± 0.00004	0.00122 ± 0.000025	449 ± 3	2.8 ± 0.5
11XL23-68	0.28226 ± 0.00008	0.00121 ± 0.00003	0.001216 ± 0.000011	263 ± 2	−12.5 ± 1.2
11XL23-69	0.28243 ± 0.00005	0.00145 ± 0.00003	0.001467 ± 0.000019	294 ± 4	−6 ± 0.8
11XL23-71	0.28245 ± 0.00004	0.00067 ± 0.00003	0.000677 ± 0.000015	443 ± 4	−1.9 ± 0.6
11XL23-73	0.2824 ± 0.00007	0.00153 ± 0.00005	0.001545 ± 0.000041	269 ± 3	−7.4 ± 1
11XL57-19	0.2827 ± 0.00003	0.00134 ± 0.00004	0.001217 ± 0.000028	265 ± 2	2.9 ± 0.5
11XL57-20	0.28269 ± 0.00004	0.00149 ± 0.00003	0.00135 ± 0.00001	265 ± 2	2.8 ± 0.5
11XL57-22	0.2827 ± 0.00004	0.0011 ± 0.00004	0.001 ± 0.000024	276 ± 2	3.3 ± 0.6
11XL57-24	0.2827 ± 0.00003	0.0012 ± 0.00003	0.001087 ± 0.000011	280 ± 2	3.3 ± 0.5
11XL57-25	0.28266 ± 0.00003	0.00189 ± 0.00004	0.001708 ± 0.000025	268 ± 3	1.7 ± 0.5
11XL57-30	0.28271 ± 0.00003	0.00092 ± 0.00005	0.00083 ± 0.000045	261 ± 2	3.4 ± 0.5
11XL57-32	0.28271 ± 0.00003	0.00157 ± 0.00003	0.001412 ± 0.000025	266 ± 3	3.2 ± 0.5
11XL57-34	0.28268 ± 0.00003	0.00139 ± 0.00002	0.001251 ± 0.000007	274 ± 2	2.5 ± 0.5
11XL57-37	0.28271 ± 0.00003	0.00142 ± 0.00003	0.001279 ± 0.000016	260 ± 2	3.2 ± 0.5
11XL57-39	0.2827 ± 0.00003	0.0011 ± 0.00002	0.001011 ± 0.000006	260 ± 2	2.9 ± 0.4
11XL57-42	0.28265 ± 0.00004	0.00414 ± 0.00028	0.003852 ± 0.000279	262 ± 2	0.6 ± 0.6
11XL57-43	0.28268 ± 0.00003	0.00113 ± 0.00002	0.001074 ± 0.000003	269 ± 2	2.5 ± 0.4
11XL57-45	0.28273 ± 0.00004	0.00247 ± 0.00003	0.002382 ± 0.000017	280 ± 2	4.3 ± 0.6
11XL57-46	0.28267 ± 0.00004	0.00152 ± 0.00004	0.001492 ± 0.000037	264 ± 2	2 ± 0.6
11XL57-48	0.28269 ± 0.00003	0.00088 ± 0.00002	0.000878 ± 0.000003	259 ± 2	2.7 ± 0.5
11XL57-49	0.28271 ± 0.00004	0.00119 ± 0.00013	0.001202 ± 0.000129	266 ± 2	3.5 ± 0.5
11XL57-52	0.28271 ± 0.00004	0.00146 ± 0.00003	0.001497 ± 0.00002	274 ± 3	3.7 ± 0.5
11XL57-53	0.28273 ± 0.00004	0.00224 ± 0.00006	0.002338 ± 0.000057	282 ± 2	4.3 ± 0.6
11XL57-54	0.28269 ± 0.00004	0.00171 ± 0.00004	0.001815 ± 0.000027	264 ± 2	2.6 ± 0.5

Appendix D
XRF Data

The first set of tables on the following pages comprise the results of all whole-rock major element analyses. The second set of tables comprise the results of all whole-rock trace-element analyses. All analyses were performed at the Chinese Academy of Sciences in Guangzhou during the four-year Ph.D. study period at The University of Hong Kong. Values for major elements are given in weight percentages, whereas those for trace elements are given in parts per million. For detailed methodological procedures please refer to Sect. 3.4 of this dissertation (Tables D.1 and D.2).

P. R. Eizenhöfer, *Subduction and Closure of the Palaeo-Asian Ocean along the Solonker Suture Zone: Constraints from an Integrated Sedimentary Provenance Analysis*, Springer Theses, https://doi.org/10.1007/978-981-32-9200-0

Table D.1 Major element data

Sample	Al_2O_3	CaO	Fe_2O_3	K_2O	MgO	MnO	NaO	P_2O_5	SiO_2	TiO_2
11xl001	17.00	4.11	5.96	1.07	4.58	0.13	2.73	0.19	61.40	0.51
11xl002-1	14.16	8.61	12.18	1.47	8.47	0.16	2.96	0.42	49.27	2.05
11xl002-2	14.07	7.42	12.65	2.60	3.56	0.16	3.84	0.75	51.43	3.34
11XL11	19.35	10.72	10.32	0.15	5.45	0.18	2.85	0.06	48.66	0.92
11XL12	14.49	0.66	3.47	5.38	0.35	0.16	4.06	0.12	69.69	0.56
11XL14-1	16.91	1.80	6.72	3.16	2.59	0.09	1.74	0.17	62.99	0.82
11XL14-2	15.81	1.72	3.17	0.85	1.26	0.04	6.28	0.11	68.82	0.39
11XL15-1	15.94	5.93	6.00	0.53	2.68	0.14	3.58	0.13	63.68	0.63
11XL15-2	16.03	3.83	5.10	0.91	2.37	0.09	4.50	0.13	65.39	0.60
11XL15-3	15.28	6.22	7.23	0.59	3.09	0.17	3.26	0.13	62.54	0.63
11XL17-1	11.00	6.10	4.76	1.21	1.70	0.09	1.93	0.08	71.60	0.41
11XL18-1	15.42	2.25	2.61	4.67	0.79	0.06	3.19	0.18	69.21	0.41
11XL18-2	16.37	1.02	1.47	6.89	0.41	0.02	3.65	0.08	69.01	0.22
11XL18-3	13.85	1.37	3.55	5.44	1.01	0.06	2.52	0.27	70.61	0.54
11XL18-4	16.95	1.48	1.45	7.06	0.43	0.02	3.12	0.08	68.40	0.22
11XL21-2	13.58	4.45	5.88	1.01	3.19	0.09	3.20	0.13	62.20	0.68
11XL21-3	14.37	4.04	5.93	1.36	2.53	0.13	3.30	0.13	62.33	0.68
11XL23	15.14	3.66	6.08	1.21	1.96	0.11	4.30	0.22	64.53	1.01
11XL24-1	15.33	1.99	4.72	1.11	2.71	0.06	5.37	0.24	65.42	0.75
11XL24-2	15.14	1.84	4.10	1.50	2.52	0.06	5.08	0.20	66.95	0.69
11XL25	12.49	3.92	5.14	1.66	2.51	0.09	2.91	0.14	63.19	0.64
11XL27	12.78	1.49	3.07	2.42	1.12	0.03	0.07	0.09	74.17	0.50
11XL28-2	15.61	2.37	7.36	3.02	2.07	0.14	4.31	0.34	61.98	0.91
11XL28-3	15.69	2.38	7.17	3.15	2.27	0.14	4.32	0.33	61.67	0.89
11XL29-2	16.42	5.42	9.93	1.47	4.85	0.15	1.58	0.21	53.59	0.63
11XL31	16.54	8.65	10.20	0.80	6.27	0.14	2.69	0.19	50.13	1.80
11XL32-1	14.07	1.34	6.27	1.57	2.10	0.20	4.33	0.23	66.69	0.86
11XL32-2	13.49	0.60	3.72	0.46	1.19	0.12	5.87	0.09	72.73	0.45
11XL33-2	13.23	1.51	4.59	1.07	1.47	0.15	4.71	0.13	71.02	0.60
11XL33-3	15.33	2.34	4.99	3.00	1.38	0.16	3.75	0.16	66.27	0.73
11xl33-4	12.69	1.17	4.40	1.13	1.40	0.12	4.35	0.12	72.66	0.55
11XL35-1	14.67	9.09	10.55	0.13	7.74	0.16	3.90	0.11	50.56	1.22
11XL35-2	14.79	9.99	10.81	0.14	8.50	0.17	3.38	0.10	48.84	1.18
11XL35-4	16.29	14.26	5.10	0.04	11.09	0.11	2.10	0.01	47.89	0.17
11XL36-1	0.57	0.09	9.08	0.01	39.00	0.10	−0.01	0.01	40.01	0.00
11XL36-3	0.83	0.69	7.64	0.01	39.30	0.12	0.01	0.01	39.46	0.00
11XL37-2	14.34	3.69	5.04	1.76	2.83	0.06	2.46	0.14	66.81	0.67
11XL38-1	12.25	1.85	3.94	3.11	2.52	0.07	2.57	0.11	71.20	0.56
11XL39-1	14.40	3.46	6.27	2.09	3.35	0.12	3.43	0.13	61.07	0.73
11XL40	14.40	2.19	3.15	4.47	1.24	0.06	2.84	0.09	69.24	0.42
11XL41-2	13.79	5.66	6.77	1.65	4.00	0.11	2.25	0.09	59.74	0.87
11XL41-3	13.21	9.14	6.15	1.69	3.76	0.12	2.00	0.09	55.74	0.83

(continued)

Table D.1 (continued)

Sample	Al_2O_3	CaO	Fe_2O_3	K_2O	MgO	MnO	NaO	P_2O_5	SiO_2	TiO_2
11XL41-4	15.65	3.20	7.47	1.93	3.66	0.09	2.12	0.09	61.06	0.94
11XL41-5	12.29	9.83	4.41	2.01	2.83	0.10	1.76	0.07	57.56	0.64
11XL42-1	15.41	5.58	8.30	2.22	2.93	0.20	2.19	0.19	58.75	0.85
11XL42-4	15.19	6.66	7.48	1.83	2.26	0.17	2.07	0.18	60.39	0.77
11XL43-1	0.56	0.26	7.37	0.01	40.83	0.12	0.06	0.00	36.35	0.00
11XL43-10	13.31	5.71	13.86	0.01	24.65	0.14	0.05	0.13	31.16	1.03
11XL43-11	12.73	7.80	14.24	0.02	23.22	0.13	0.06	0.14	31.85	1.09
11XL43-3	0.57	0.38	7.34	0.01	40.47	0.11	0.17	0.00	36.61	0.00
11XL43-4	0.59	0.53	7.43	0.01	40.15	0.11	0.06	0.00	36.58	0.00
11XL43-5	0.51	0.22	7.39	0.01	41.28	0.13	0.04	0.00	35.77	0.00
11XL43-7	0.58	0.39	7.31	0.01	40.22	0.11	0.06	0.00	36.91	0.00
11XL44-1	15.75	2.19	4.99	0.16	1.46	0.11	9.38	0.11	64.38	0.72
11XL44-2	9.08	12.11	12.81	0.02	21.55	0.16	0.05	0.10	35.70	0.94
11XL44-3	15.88	12.79	8.25	0.11	10.04	0.14	2.35	0.04	48.61	0.61
11XL45-2	9.31	1.41	2.40	1.79	0.50	0.03	1.64	0.12	79.92	0.43
11XL46-1	14.59	8.06	7.67	0.24	6.38	0.12	4.59	0.10	50.10	0.58
11XL47-1	8.08	2.17	1.95	1.13	0.86	0.05	2.07	0.08	80.47	0.30
11XL47-2	9.11	0.93	1.76	1.40	0.84	0.02	2.13	0.09	81.50	0.35
11XL48-1	16.28	3.02	8.80	1.98	5.21	0.12	2.65	0.20	54.79	1.18
11XL48-2	9.41	0.18	2.25	1.58	0.86	0.02	1.80	0.09	81.71	0.39
11XL49-1	15.10	1.86	4.64	4.20	1.38	0.11	3.22	0.15	66.30	0.65
11XL49-2	16.14	7.79	8.30	0.15	4.99	0.12	3.57	0.16	51.82	0.74
11XL50-2	12.61	1.43	4.95	2.05	1.68	0.03	0.37	0.11	71.83	0.56
11XL51-2	9.60	3.74	2.12	1.77	1.12	0.07	1.43	0.07	75.02	0.37
11XL52-2	16.04	7.57	9.98	0.76	4.58	0.15	2.90	0.77	53.15	1.61
11XL5-1	16.67	6.70	7.98	0.78	4.03	0.11	3.46	0.32	57.23	1.64
11XL5-2	15.93	5.29	7.00	2.51	3.55	0.09	4.04	0.53	58.69	1.26
11XL5-3	14.17	2.30	6.22	2.27	3.74	0.12	3.08	0.15	65.76	0.78
11XL5-4	12.91	5.62	4.93	1.54	2.76	0.14	2.29	0.11	67.58	0.65
11XL5-5	15.85	6.91	7.79	0.79	6.00	0.13	3.87	0.10	56.57	0.67
11XL5-6	14.94	8.22	9.57	0.86	8.65	0.21	3.23	0.07	51.83	0.81
11XL54-2	12.84	3.88	13.01	0.68	2.88	0.09	2.39	0.19	56.51	1.92
11XL55	15.51	5.34	8.24	0.65	5.56	0.28	2.86	0.15	58.10	0.88
11XL56-2	19.38	5.59	7.06	0.69	6.55	0.13	3.79	0.63	51.50	1.36
11XL58-1	18.54	3.44	6.05	4.24	2.25	0.09	2.85	0.10	60.67	0.65
11XL58-2	15.17	5.02	4.87	0.59	2.43	0.14	3.08	0.12	66.50	0.57
11XL58-3	17.45	6.15	6.77	0.77	3.71	0.12	3.47	0.15	58.69	0.76
11XL59-1	16.38	2.24	7.32	3.79	3.17	0.08	1.82	0.17	61.91	0.88
11XL63-1	14.41	6.90	5.87	2.27	2.54	0.08	2.42	0.19	57.69	0.72
11XL7-3	13.97	6.41	3.64	0.60	2.30	0.11	3.17	0.09	68.32	0.53
11XL7-4	13.21	6.54	5.17	0.99	2.84	0.11	2.97	0.10	66.69	0.53
11XL7-5	13.93	7.43	4.66	1.03	2.94	0.12	2.49	0.09	65.95	0.52
11XL7-6	13.47	6.12	4.20	1.10	2.32	0.10	3.03	0.12	68.37	0.51
11XL7-7	12.48	7.02	7.93	3.16	3.78	0.20	2.35	0.13	61.12	0.60
11XL9	17.65	4.40	7.65	2.35	1.58	0.16	4.82	0.40	59.11	1.23

Table D.2 Trace element data

Sample	V	Cr	Co	Ni	Cu	Zn	Rb	Sr	Zr	Ba	Y	Nb
11xl001	87.12	<20	<20	<20	<20	120.51	34.69	540.64	134.40	267.75	16.16	<5
11xl002-1	187.39	274.21	47.67	180.02	44.12	99.83	<20	529.63	160.33	389.94	23.21	25.97
11xl002-2	226.26	<20	26.70	25.55	67.45	115.87	28.31	477.09	280.99	632.46	34.36	46.68
11XL11	299.14	<20	28.67	<20	282.66	91.55	<20	879.77	<20	140.13	9.79	<5
11XL12	20.37	<20	<20	<20	<20	58.87	164.94	113.88	690.38	840.19	71.67	39.25
11XL14-1	147.16	65.18	<20	34.68	23.65	68.14	109.44	166.55	170.19	484.14	31.20	12.03
11XL14-2	48.10	26.55	<20	<20	41.53	62.42	24.17	373.29	128.98	253.35	11.45	<5
11XL15-1	115.80	47.64	<20	<20	<20	87.73	26.49	286.62	126.78	199.50	20.08	6.19
11XL15-2	102.57	38.72	<20	<20	<20	77.77	42.01	235.04	127.21	242.86	22.13	6.31
11XL15-3	109.96	54.34	<20	<20	32.23	101.03	28.18	280.20	124.35	186.48	19.14	5.59
11XL17-1	82.89	58.06	<20	20.88	<20	54.24	56.43	295.62	104.35	273.02	17.93	5.98
11XL18-1	37.05	<20	<20	<20	20.64	68.36	172.36	301.96	272.20	1189.24	20.93	14.82
11XL18-2	21.64	<20	<20	<20	<20	39.87	207.89	369.02	189.80	2704.33	6.60	<5
11XL18-3	49.88	<20	<20	<20	24.02	93.83	186.13	246.29	370.23	1312.74	25.45	14.60
11XL18-4	27.42	<20	<20	<20	<20	39.54	218.92	511.16	186.04	2585.59	8.14	<5
11XL21-2	104.11	66.89	<20	21.76	<20	69.96	34.29	286.51	116.70	1390.34	19.24	5.87
11XL21-3	135.56	74.38	<20	28.47	<20	78.14	48.76	289.11	114.21	471.73	17.32	6.08
11XL23	104.90	<20	<20	<20	<20	275.46	54.99	354.03	163.12	248.74	29.68	7.05
11XL24-1	97.34	36.25	<20	20.01	<20	77.49	22.89	654.89	156.08	607.23	20.28	6.99
11XL24-2	80.52	33.53	<20	<20	33.40	74.16	36.10	628.23	176.09	791.87	24.34	8.90
11XL25	116.28	139.16	<20	51.46	22.03	64.58	53.47	294.06	206.98	369.64	17.19	6.54
11XL27	54.69	41.58	<20	<20	<20	57.12	103.46	72.29	181.19	328.58	19.78	7.83
11XL28-2	93.77	<20	<20	<20	<20	88.06	68.69	506.89	161.03	866.16	38.56	6.13

(continued)

Table D.2 (continued)

Sample	V	Cr	Co	Ni	Cu	Zn	Rb	Sr	Zr	Ba	Y	Nb
11XL28-3	94.50	<20	<20	<20	24.17	96.22	62.76	456.29	158.70	871.68	37.50	5.79
11XL29-2	229.59	219.01	27.12	53.37	34.29	83.71	28.72	322.69	71.33	307.80	17.20	<5
11XL31	238.23	392.97	32.17	31.78	<20	46.11	25.93	169.89	129.67	164.20	33.02	<5
11XL32-1	111.73	52.60	<20	31.73	43.18	112.08	31.22	118.77	135.57	1195.14	40.79	9.24
11XL32-2	59.95	<20	<20	<20	41.20	77.63	<20	108.28	135.22	291.13	42.64	<5
11XL33-2	72.90	21.88	<20	<20	35.19	91.25	27.39	221.53	150.17	398.37	36.29	6.64
11XL33-3	96.50	<20	<20	<20	50.42	85.74	64.96	318.79	207.35	1184.54	36.40	8.78
11xl33-4	60.60	21.95	<20	<20	23.80	88.97	25.07	196.66	141.13	429.73	34.18	6.89
11XL35-1	288.08	238.20	36.19	60.98	51.84	72.93	<20	99.32	72.73	59.89	27.55	<5
11XL35-2	276.43	252.78	41.71	76.37	63.10	75.12	<20	106.38	63.48	<50	27.02	<5
11XL35-4	141.00	1279.09	30.81	174.43	50.30	31.71	<20	63.13	<20	<50	10.38	<5
11XL36-1	43.41	2884.84	86.67	2167.50	27.17	46.23	<20	<20	<20	<50	<5	<5
11XL36-3	48.64	2986.37	62.02	1323.20	<20	55.64	<20	<20	<20	<50	<5	<5
11XL37-2	85.91	62.23	<20	26.22	21.98	33.97	61.01	150.70	181.61	498.03	29.00	9.83
11XL38-1	91.21	51.74	<20	26.00	<20	57.56	71.94	105.65	161.98	606.78	28.07	7.79
11XL39-1	166.82	22.35	<20	<20	41.40	75.39	110.83	126.73	137.56	354.89	24.50	5.62
11XL40	67.81	<20	<20	<20	<20	35.95	153.65	233.84	177.63	551.18	21.67	5.52
11XL41-2	179.61	106.82	<20	41.07	35.57	75.54	67.94	205.81	113.08	270.14	18.92	7.29
11XL41-3	172.40	109.54	<20	41.91	33.41	65.13	63.59	222.18	110.58	242.86	23.33	6.51
11XL41-4	210.82	128.20	24.36	48.13	48.55	79.98	76.69	235.47	158.89	368.47	23.97	8.15
11XL41-5	115.34	82.41	<20	37.69	21.78	53.29	80.01	178.30	125.48	390.07	24.87	6.14
11XL42-1	151.07	<20	<20	<20	26.00	98.10	47.92	352.82	83.82	638.16	30.46	<5
11XL42-4	122.96	21.18	<20	<20	22.67	91.92	35.23	236.11	96.43	658.86	34.00	<5

(continued)

Table D.2 (continued)

Sample	V	Cr	Co	Ni	Cu	Zn	Rb	Sr	Zr	Ba	Y	Nb
11XL43-1	35.52	2728.63	99.76	2209.22	<20	46.16	<20	<20	<20	<50	<5	<5
11XL43-10	316.66	2343.39	84.96	745.65	<20	85.02	<20	<20	73.83	<50	19.68	<5
11XL43-11	335.23	2026.29	84.72	636.80	<20	76.20	<20	<20	79.04	<50	21.20	<5
11XL43-3	43.67	2620.32	94.15	2254.04	<20	48.10	<20	<20	<20	<50	<5	<5
11XL43-4	46.36	2964.90	94.68	2200.98	<20	52.37	<20	<20	<20	<50	<5	<5
11XL43-5	35.32	2895.39	97.76	2128.19	28.69	36.75	<20	<20	<20	<50	<5	<5
11XL43-7	41.92	2581.23	92.76	2144.39	<20	48.54	<20	<20	<20	<50	<5	<5
11XL44-1	71.66	<20	<20	<20	<20	80.09	<20	108.96	92.83	51.69	36.91	<5
11XL44-2	241.47	1644.00	64.55	503.25	43.09	42.94	<20	<20	61.71	<50	21.25	<5
11XL44-3	229.02	420.39	41.50	147.01	27.95	35.68	<20	133.18	<20	<50	18.18	<5
11XL45-2	60.28	47.52	<20	21.67	<20	34.73	64.31	112.53	239.77	473.44	21.81	9.36
11XL46-1	192.52	175.21	25.52	30.00	37.40	56.43	<20	262.68	53.18	220.82	16.19	<5
11XL47-1	36.64	35.33	<20	<20	<20	31.47	49.51	162.63	168.63	286.18	22.38	8.35
11XL47-2	61.25	35.79	<20	<20	<20	31.07	61.43	128.54	178.81	338.00	20.73	7.20
11XL48-1	228.27	142.63	27.30	72.90	73.23	85.10	96.01	305.30	81.10	312.77	17.08	<5
11XL48-2	64.92	42.18	<20	23.65	<20	42.31	82.39	68.44	177.40	393.41	21.00	7.81
11XL49-1	72.85	<20	<20	<20	35.15	89.42	100.55	290.19	239.29	1315.48	28.71	11.78
11XL49-2	274.23	147.71	26.97	29.36	55.23	87.30	<20	321.34	98.32	95.69	20.59	<5
11XL50-2	60.80	60.92	<20	20.97	<20	57.89	98.83	64.68	207.74	307.98	26.30	10.04
11XL51-2	50.35	74.09	<20	21.98	<20	45.92	67.83	166.56	185.43	272.05	21.11	6.15
11XL52-2	174.39	104.71	27.62	48.28	32.04	111.90	<20	966.18	202.98	657.15	24.01	13.15
11XL5-1	166.06	55.87	23.04	36.08	27.06	86.78	29.11	765.12	151.87	346.13	20.88	9.26
11XL5-2	107.24	77.61	<20	29.30	23.32	103.28	67.18	893.28	312.54	1228.79	21.67	16.66

(continued)

Table D.2 (continued)

Sample	V	Cr	Co	Ni	Cu	Zn	Rb	Sr	Zr	Ba	Y	Nb
11XL5-3	107.53	170.08	<20	100.78	50.24	83.51	115.33	271.99	158.45	549.63	28.19	8.88
11XL5-4	90.71	128.46	<20	64.29	33.63	78.24	66.88	401.56	148.04	564.51	23.75	8.67
11XL5-5	171.35	147.36	27.53	45.04	<20	67.34	34.80	273.32	98.83	134.59	25.50	<5
11XL5-6	226.95	278.25	34.83	60.18	<20	93.53	38.49	197.93	50.44	140.46	24.41	<5
11XL54-2	357.61	57.75	23.97	<20	30.22	152.21	24.00	199.61	234.22	342.28	20.64	9.96
11XL55	177.19	80.77	21.01	40.38	<20	143.79	22.56	437.40	143.61	335.75	24.54	8.52
11XL56-2	183.80	123.25	24.58	81.14	468.69	151.74	<20	2005.38	203.39	416.44	25.62	11.18
11XL58-1	112.73	33.35	<20	<20	<20	50.49	151.81	358.18	178.01	867.54	23.25	8.52
11XL58-2	97.02	47.91	<20	23.30	22.48	49.49	22.77	260.19	131.21	211.82	21.95	5.35
11XL58-3	132.06	80.92	<20	29.22	28.85	89.82	26.19	367.37	192.17	457.84	23.49	9.81
11XL59-1	148.94	79.39	<20	40.15	25.23	52.49	140.23	225.63	165.59	408.04	28.88	13.11
11XL63-1	93.73	47.72	<20	20.92	28.50	80.36	64.65	390.48	160.77	421.16	28.18	7.61
11XL7-3	95.80	76.34	<20	<20	<20	61.69	<20	267.65	130.02	274.52	18.79	6.35
11XL7-4	92.27	75.18	<20	43.33	25.24	70.22	25.72	254.24	121.44	402.21	18.01	<5
11XL7-5	92.72	66.25	<20	23.72	<20	75.84	20.66	262.31	124.33	401.12	16.84	<5
11XL7-6	98.03	43.91	<20	<20	<20	59.93	22.51	238.37	113.77	499.15	17.52	<5
11XL7-7	127.61	94.55	<20	37.42	<20	89.96	59.70	237.87	113.59	1882.28	20.36	5.48
11XL9	45.62	<20	<20	<20	<20	95.60	71.76	351.56	235.27	912.96	48.98	11.54

Appendix E
Whole-Rock Hf and Nd Data

The tables on this and the following page comprise the results of all whole-rock Hf and Nd isotope analyses. All analyses were performed at Northwest University, Xi'an during the four-year Ph.D. study period at The University of Hong Kong. Uncertainties are given at a 1σ level. Table columns correspond to rock samples, $^{176}Hf/^{177}Hf$ ratios and their uncertainties, and $^{143}Nd/^{144}Nd$ ratios and their uncertainties. For detailed methodological procedures please refer to Sect. 3.4 of this dissertation (Table E.1).

P. R. Eizenhöfer, *Subduction and Closure of the Palaeo-Asian Ocean along the Solonker Suture Zone: Constraints from an Integrated Sedimentary Provenance Analysis*, Springer Theses, https://doi.org/10.1007/978-981-32-9200-0

Table E.1 Whole-rock Hf and Nd data

Sample	$^{176}Hf/^{177}Hf$	$^{143}Nd/^{144}Nd$
11XL15-2	0.282648 ± 0.000007	0.511859 ± 0.000006
11XL17-1	0.282545 ± 0.000005	0.512057 ± 0.000007
11XL17-1R	0.282505 ± 0.000006	0.512204 ± 0.000005
11XL23	0.282751 ± 0.000006	0.512302 ± 0.000008
11XL24-1	0.282779 ± 0.000006	0.512151 ± 0.000005
11XL28-3	0.282819 ± 0.000005	0.512283 ± 0.000006
11XL31	0.283075 ± 0.000007	0.512867 ± 0.000005
11XL36-1	0.282981 ± 0.002060	0.512555 ± 0.000142
11XL36-1	0.282947 ± 0.000438	0.512363 ± 0.000090
11XL37-2	0.282593 ± 0.000006	0.511890 ± 0.000007
11XL39-1	0.282882 ± 0.000006	0.512183 ± 0.000009
11XL42-4	0.283200 ± 0.000007	0.512607 ± 0.000007
11XL44-1	0.283168 ± 0.000004	0.512610 ± 0.000005
11XL47-1	0.282291 ± 0.000005	0.511981 ± 0.000005
11XL47-1R	0.282311 ± 0.000006	0.511738 ± 0.000005
11XL51-2	0.282574 ± 0.000005	0.511862 ± 0.000008
11XL52-2	0.282768 ± 0.000006	0.512122 ± 0.000004
11XL54-2	0.282495 ± 0.000009	0.511731 ± 0.000006
11XL58-1	0.282593 ± 0.000004	0.511995 ± 0.000009
12XL14-2	0.282981 ± 0.000006	0.512692 ± 0.000007
12XL14-2R	0.282936 ± 0.000006	0.512646 ± 0.000005
12XL16-3	0.282995 ± 0.000005	0.512414 ± 0.000005
12XL16-3R	0.282987 ± 0.000005	0.512338 ± 0.000006
12XL17-2	0.282587 ± 0.000006	0.512068 ± 0.000006
12XL18-2	0.283054 ± 0.000008	0.512784 ± 0.000006
12XL19-2	0.283026 ± 0.000006	0.512615 ± 0.000007
12XL21-2	0.282578 ± 0.000005	0.512198 ± 0.000007
12XL22	0.282936 ± 0.000006	0.512524 ± 0.000012
12XL23-4	0.282738 ± 0.000015	0.512039 ± 0.000009
12XL24-2	0.282284 ± 0.000005	0.511688 ± 0.000005

Appendix F
Point-Counting Results

The table below summarises point-counting results on thin sections of clastic sedimentary rocks. All analyses were performed during the four-year Ph.D. study period at The University of Hong Kong. Table columns correspond to rock sample, number and percentage of counted quartz, feldspar grains, lithic fragments, and the total number of grains counted (Table F.1).

Table F.1 Point-counting data

Sample	Quartz	Feldspar	Lithic fragments	Grains
11XL7-2	46 (13.98%)	33 (10.03%)	250 (75.99%)	329
11XL13	93 (27.43%)	94 (27.73%)	152 (44.84%)	339
11XL15-1	77 (24.14%)	31 (9.72%)	211 (66.14%)	319
11XL16-1	43 (13.96%)	54 (17.53%)	211 (68.51%)	308
11XL17-2	59 (19.41%)	60 (19.74%)	185 (60.86%)	304
11XL23	25 (8.25%)	7 (2.31%)	271 (89.44%)	303
11XL24-1	127 (35.08%)	23 (6.35%)	212 (58.56%)	362
11XL25	105 (33.65%)	51 (16.35%)	156 (50.00%)	312
11XL26	62 (20.67%)	27 (9.00%)	211 (70.33%)	300
11XL27	71 (23.05%)	41 (13.31%)	196 (63.64%)	308
11XL51-1	87 (27.53%)	41 (12.97%)	188 (59.49%)	316
11XL54-1	74 (24.03%)	29 (9.42%)	205 (66.56%)	308
11XL57	145 (47.70%)	12 (3.95%)	147 (48.36%)	304
11XL41-2	38 (12.54%)	27 (8.91%)	238 (78.55%)	303
11XL42-1	12 (3.80%)	94 (29.75%)	210 (66.46%)	316
11XL45-2	161 (47.08%)	44 (12.87%)	137 (40.06%)	342

(continued)

P. R. Eizenhöfer, *Subduction and Closure of the Palaeo-Asian Ocean along the Solonker Suture Zone: Constraints from an Integrated Sedimentary Provenance Analysis*, Springer Theses, https://doi.org/10.1007/978-981-32-9200-0

Table F.1 (continued)

Sample	Quartz	Feldspar	Lithic fragments	Grains
11XL41-3	26 (8.72%)	24 (8.05%)	248 (83.22%)	298
11XL42-4	8 (2.67%)	107 (35.67%)	185 (61.67%)	300
11XL47-1	107 (34.97%)	44 (14.38%)	155 (50.65%)	306
11XL41-4	12 (3.99%)	30 (9.97%)	259 (86.05%)	301
11XL41-5	18 (5.96%)	23 (7.62%)	261 (86.42%)	302
11XL47-2	136 (45.33%)	38 (12.67%)	126 (42.00%)	300
11XL48-2	142 (46.41%)	18 (5.88%)	146 (47.71%)	306